SIMSG ISSMGE

International Society for Soil Mechanics and
Geotechnical Engineering
TC 302: Forensic Geotechnical Engineering

Fifth International Conference on
FORENSIC GEOTECHNICAL ENGINEERING

8-10 December, 2016 at Bengaluru, India

Organisers

INDIAN INSTITUTE OF SCIENCE

INDIAN GEOTECHNICAL SOCIETY

INDIAN GEOTECHNICAL SOCIETY Bangalore Chapter

Preface

The International Society for Soil Mechanics and Geotechnical Engineering (ISSMGE) constituted a Technical Committee (TC) on Forensic Geotechnical Engineering (FGE) in 2005. During the first four years it was designated as TC40 and is now designated as TC302. This committee has conducted four international seminars on FGE and the proceedings of the fifth conference held during December 8-10, 2016 at Bengaluru, India are presented herewith.

Forensic geotechnical engineering involves scientific, legalistic investigations and deductions to detect the causes as well as the process of distress in a structure, which are attributed to geotechnical origin. Such a critical analysis will provide answers to “what went wrong, when, where, why, how, and by whom”. Cases of remedied installations, particularly those which, fall under public / or government category, where the analysis and evaluation of adopted remedial measures with regard to their effectiveness and economy may be subjected to judicial scrutiny also, fall under this purview. It also gives strong inputs to improve designs. The normally adopted standard procedures of testing, analysis, design and construction are not adequate for the forensic analysis in majority of cases. The forensic investigations involve fresh field and laboratory tests apart from collection of all available data. The test parameters and design assumptions will have to be representative of the actual conditions encountered at site. While the designs are mostly stress based, the forensic analysis has to be deformation based. The forensic geotechnical engineer (who is different than the expert witness) has to be not only thorough in his field of specialization, but also be familiar with legal procedures. The proceedings of the International Conference highlight the principles of planning and executing a forensic investigation citing case histories. This is being organized by IGS Bangalore chapter, Indian Geotechnical Society (IGS), Indian Institute of Science Bangalore. American Society of Civil Engineers (ASCE), ASCE Forensic Engineering Division, Geotechnical Extreme Events Reconnaissance (GEER) Association (USA) and Deep Foundation Institute (DFI) are associated with organizing this event.

The organizers of the conference thank the keynote lecturers, invited lecturers, expert lecturers, and authors of contributed papers for their excellent contributions. We are sure that the deliberations at the conference will go a long way in addressing the needs of understanding failures of geotechnical origin and lead to better analysis and design procedures.

Prof. G L Sivakumar Babu
Chairman
International Conference of Forensic Geotechnical Engineering
Indian Institute of Science, Bangalore

CONTENTS

Invited and Expert Papers

Contributed Papers

Keynote Papers

Proposal of Japanese Geotechnical Society for More Reliable Installation of Prefabricated Piles

Ikuo Towhata[1] and Hiroshi Furuya[2]

[1]Former President of Japanese Geotechnical Society, 4-38-2, Sengoku, Bunkyo-Ku, Tokyo 112-0011 Japan; PH: (+81-3) 3946-8677; FAX: (+81-3) 3946-8678; e-mail: towhata.ikuo.ikuo@gmail.com

[2]Vice President of Japanese Geotechnical Society

ABSTRACT

The construction community in Japan has recently been jolted by tilting of one condominium building that is said to rest on insufficient length of prefabricated piles. Although the legal issue is unclear yet, the developer and the contractor decided to demolish the entire condominium complex, including four intact buildings, and reconstruct them on the companies' own expense. The governmental section in charge is calling on the importance of construction quality management. It is actually true that the extent of tilting is merely 2 to 3 cm over the building length of 56m but it stimulated the concern of the entire public. The Japanese Geotechnical Society established a special committee to shed light on the social aspect of this problem and has been discussing that the subsurface investigation needs to be conducted more elaborately in order to capture the non-uniform soil conditions. It deserves attention that the importance of geotechnical information is not understood by the society, resulting in many unnecessary troubles.

INTRODUCTION

This paper addresses an incident of a condominium building in Yokohama City, Japan, that was constructed in 2007, was of 10-12 stories and later subsided unexpectedly (Fig. 1). The differential subsidence was detected by residents in November, 2014. According to many public reports, differential settlement between two neighboring condominium buildings was about 2cm while the length of the affected building was 56 m. Thus, the gradient of tilting is 0.02m/56m = approximately 0.04 %. Although many discussion and documents have been published since then, no final conclusion has been reached yet. Hence, the present paper is of an intermediate nature and cannot provide sources of all information.

Figure 1. Subsided building in Yokohama

Situated upon very soft soil deposits along a river, the buildings were supported by prefabricated RC piles that were constructed by first drilling holes by augers down to the bearing layer (soft mud stone), embedding prefabricated piles and reinforcing soils around the pile tips by injection of cement slurry that is mixed with soil (Fig. 2). Note that the pile tip should be embedded in the bearing layer by 1 m or so. The depth of the bearing layer could be determined by monitoring electric current of the auger motor. It is suspected that some piles were not long enough to reach the bearing layer (8 out of 28 studied piles). The insufficient pile length requires additional piles to be designed, fabricated and connected to the lower pile, which takes additional days for pile completion. The problem was worsened when the urgent investigation detected that many construction records (electric current and flow amount of cement slurry) had been lost or replaced by irrelevant ones copied from other piles. Thus, the reliability of construction community was seriously affected. Although the final conclusion on the cause of settlement has not been drawn when this manuscript is written (November 2016), many discussion has been made on data abuse. The developer and contractors of the condominiums decided to reconstruct 5 buildings in the complex free of charge for the residents, although only one of them tilted.

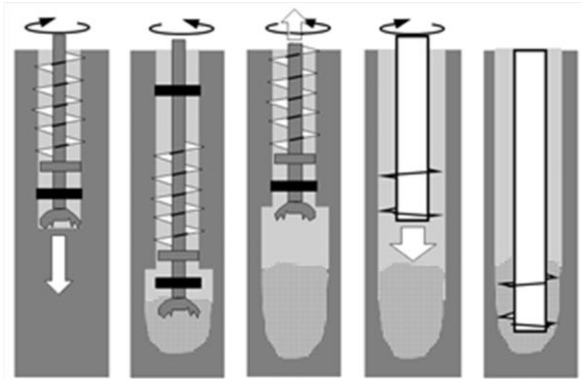

Figure 2. Construction sequence of prefabricated pile foundation (Drawn after JSCA)

In response to this problem, an intensive study was conducted by officials of the data recording practice and site engineers said that they had been copying data from other piles many times in the past due to inconvenient nature of the recording devices. The investigation, however, did not find any other building tilting in spite of construction by the same companies. The problem has been made more complicated by the multistoried structure of the project in which many companies are involved (Fig. 3). The real pile construction was conducted by two sub-companies while “Company A” did not play real role. Thus, apparently it is difficult to determine who is more responsible than others.

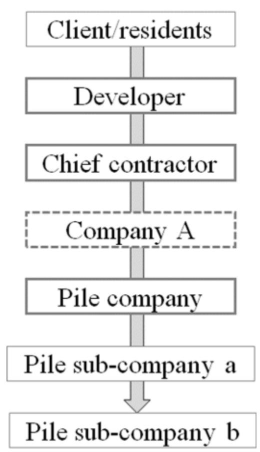

Figure 3. Multi-storied subcontract structure of project

The argument consists of two points which are 1) cause of tilting and 2) reasons why construction record are lost so often. So far, most arguments concerns 2) and many proposals have been made to solve this problem. However, the true cause of tilting has not been concluded yet.

REACTION OF GOVERNEMNT AND RELATED INSTITUTIONS

Although the chief issue in the problem is the unsatisfactory behavior (insufficient length?) of piles, no definite conclusion has been obtained to date or has not been open to the public. Most reactions so far published discuss the engineering ethics and reliable recording of construction procedure.

Ministry of Land, Infrastructure and Transport

This Ministry set up a special committee to investigate the problem and propose measures to improve the situation and its intermediate report was published in December 2015. According to this report, the developer reported to the committee that 28 piles were checked to find that possibly 6 of them did not reach the bearing layer and 2 were not sufficiently embedded in the bearing layer. There were 6 bore hole data obtained during the construction of a factory that existed in the same site in the past. The chief contractor conducted 10 bore hole investigations for design and additional 10 because of the non-uniform soil conditions. The committee states that, out of 810 piles, data abuse was found for auger drilling for 38 piles and 45 injection of cement slurry. Note that many of the abuse was caused by the inconvenient type of recording device. Importantly, a site engineer told the committee that he believed that piles reached the bearing layer according to his experience (although he did not touch upon the required embedment of piles in the bearing layer: remark by the first author).

The committee proposed measures to avoid repetition of the same problem in future. First, it was pointed out that the multi-storeyed structure of construction industry (Fig. 3) makes unclear the responsibility. The chief contractor should take the due responsibility of the entire construction procedure, including foundation. However, it was stressed that safety of buildings and abuse of data should be separately discussed. No final conclusion was reached on the situation of piles under the condominium building.

Japan Federation of Construction Contractors

A guide line for construction of prefabricated concrete piles was published in March, 2016. It puts emphasis on the responsibility of experts and site engineers in maintaining the good quality of pile foundations. It states that the depth of bearing layer has to be precisely captured in case that the depth is variable from place to place. It also states procedures that have to be taken when an installed pile does not reach a bearing layer at an expected depth. Also, it is stressed that construction procedure, such as energy for drilling and injection of cement slurry, has to be recorded in such a way that records may not be damaged by weather and also no human mistake may be possible. Thus, efforts were made to improve the construction procedure. Noteworthy is that the wrong practice in recording the construction procedure may not necessarily cause tilting of the building if piles are constructed in a reasonable way.

ON POSSIBLE CAUSES OF TILTING OF A BUILDING

This chapter addresses possible causes that have been discussed so far. It should be noted that no final conclusion has been drawn yet.

Insufficient pile length

The site is situated in a shallow valley near a hilly terrain (Fig. 4). The valley is filled with very soft alluvial soil that was deposited by a river (Fig. 5). Because of the ancient erosion procedure, the bearing layer, which continues to the nearby hill slope, is not horizontal. Its depth varies from place to place by the order of meters (Fig. 6). The data in this figure was obtained from a public data base but no bore hole data within the condominium site is released to the public.

Figure 4. View of the condominium site from nearby hill (tilted building shown by an arrow)

Figure 5. River whose soft sediments deposited in and filled the local valley

In principle, the depth of piles had to be determined by carrying out subsoil investigation. However, the pile company was asked by the chief contractor to prepare prefabricated piles of 14 meters in length (according to the pile company's own remark). It is argued nowadays that some piles were too short to reach the bearing layer and that the pile engineer could have noticed this problem to take necessary reactions. On the other hand, there had been a big electric factory prior to the construction of the condominium buildings and it is argued that the chief contractor had known upon demolition of the factory that the length of the end–bearing piles was 18 meters, which was 4 meters longer than the new piles. This may imply that 14 meters was an underestimation. If the previous bore hole data had been released to the public, the present pile company could have known more clearly the problematic nature of the subsoil. To see the argument on 14 m or 18 m, the first author feels that the depth of the bearing layer and the required length of piles (including necessary embedment in the bearing layer) may be confused.

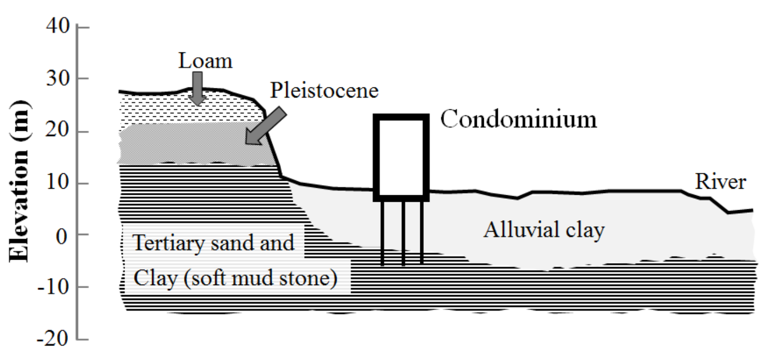

Figure 6. Conceptual sketch of the North-South cross section of the site

Choice of employed prefabricated pile

There is an argument that the selected type of prefabricated pile (Fig. 3) has been authorized only to sandy or gravelly bearing layers and not to soft mud stone which is the present case. However, the chief contractor carried out a pile loading test in the field to confirm the bearing capacity. Although the test result is not available to the public, the present paper trust this test and does not touch upon this issue.

ACTIVITY OF JAPANESE GEOTECHNICAL SOCIETY

The problem concerns not only the insufficient length and bearing capacity of pile foundations but also the serious practice of abusing of construction records. Because those records were intended to verify the good practice of pile construction, the construction community feared that its public fame might be seriously damaged. Several emergency actions were described in the former chapter. It appeared, however, that there were more problems to be solved. Therefore, as the President of the Japanese Geotechnical Society (JGS), the first author decided to take necessary actions.

At the beginning of the activity, it was agreed that the societal work would not hunt criminals. Also, detailed procedure of pile construction is not a matter of the society because the government (MLIT) and JFCC had commenced needed activities. Moreover, lawyers had been investigating this issue from their professional viewpoints. In this regards, JGS decided to pay its attention to the public background that could have led to the problem. The output from the activity is summarized in what follows.

Consideration on non-uniformity of subsoil condition

The depth of the bearing layer is an essential information for successful installation of prefabricated piles because, different from driven piles, it is difficult to directly confirm the existence of firm layer during pile construction (Fig. 2). Moreover, if the bearing layer is found deeper than the estimation during pile installation, additional pile has to be manufactured and connected to existing piles, which creates additional time and cost. Hence, care must be taken in advance of the depth of the bearing layer which may be different from pile to pile. This is particularly so near the hill slope where the soil profile is highly variable. In spite of these situations, the present practice does not pay sufficient attention to the importance of soil profile information. Efforts are needed to improve this unsatisfactory situation.

Need for more soil exploration technology

Ideally, soil condition should be explored at all sites of prefabricated pile locations. However, the Standard Penetration Test procedure, which is widely used and preferred in practice, requires time and cost. Hence, it is difficult to recommend to run it for all piles. Therefore, simplified and less time-consuming technology has to be introduced into practice so that soil profile can be interpolated between available SPT sites. The first author believes that this simplified technology does not have to be so advanced as to provide all the information for pile design because its aim is nothing more than interpolation. Interpolation, if conducted during the design stage, can demonstrate the variation of the depth of bearing layer in details. Even during construction, it helps urgent action be planned if installed pile is found too short.

Importance of open-access subsoil data base

There are open-access databases of existing bore holes. However, most of the data are from governmental infrastructure construction such as road and bridge, thus, the location of bore holes are limited along roads. This point will be shown later in Fig. 7. Although many more bore hole investigations have been conducted for design of pile foundation of private buildings, those data are scarcely included in the data base. If private bore hole data had been included, the present pile contractor could have studied it and understood that the “14 m” specification was nothing more than an idea and conducted more realistic pile design. JGS has been long insisting on the necessity of such an open-access bore hole data base, saying that the geo-space is a common property of the public and that its nature should be shared by the public as well. This point has not been understood generally. It is also a problem that existing open-access bore hole databases are not consistent with one another, using different data formats even including non-digital pdf format.

Need for involvement of good geotechnical experts

Buildings with very good design may fail if subsoil condition is bad. It is significantly important to capture the subsoil conditions precisely prior to design and it is particularly so when the local geology suggests non-uniformity. In this regard, good geotechnical experts should be involved in the design stage so that they can propose the needed amount and quality of soil investigations and interpret the obtained data. Those experts should be also involved in decision making during construction because unexpected soil condition may be encountered. Such a goal is not yet reached in the present practice.

Importance of geotechnical professional education

The recent development of science and technology has produced many "specialists" who have deep knowledge and experience in their fields of profession but are not familiar very much with other fields. This is not a good situation in a construction project which is an integration of different disciplines. In this respect the geotechnical education community should make efforts to produce experts of a wide scope. It is feared that design procedure will rely more on specified geotechnical design formulae and that engineers do not have to care their back grounds.

FIRST AUTHOR'S ADDITIONAL DISCUSSION

This chapter describes the first author's opinions on the problem and is not related with the JGS activity although relevant consistency is aimed.

Non-uniformity of subsoil condition

Figure 7 was drawn to show the locations of open-access bore hole data around the condominium site. All of them are located along roads, as mentioned before, and many of them (shown by ○) are limited within the surface soft soil only. Thus, less number of data help assess the depth of the bottom of soft soil (●) or the depth of the bearing layer (soft mud stone in general) (●).

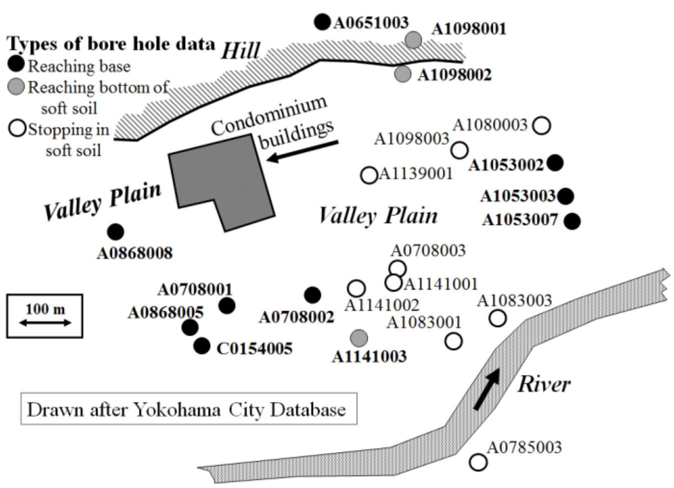

Figure 7. Location of subsoil data around the condominium obtained from a site of Yokohama City Government (http://www.asyura2.com/15/hasan104/msg/435.html)

According to Fig. 7 there is no open-access bore hole data, reaching the bearing layer, in and around the condominium site. This is a pity because there is a big shopping mall immediately to the east of the site and many bore hole investigations had been carried out for its pile foundations. Because of their private nature, their data are not open to the public. Hence, Fig. 8 plots the data at sites of ● symbol to the south and west of the condominium site in spite of the distance of hundreds of meters. Over a substantial depth, SPT- *N* was zero because of very soft clayey and organic soils. *N* value exceeding 50 is the idea of a bearing layer. Bore hole A1141003 (△) did not reach *N* = 50, and stopped at *N*=3 at the depth of 10 m. This figure implies that the data is classified into two groups shown by open symbols of □ and ○ at which the bearing layer was encountered at the elevation of -3 m and solid symbols (■, ▲ and ●) for which the bearing layer starts at -7 m. By comparing this data with Fig. 7, it is found that the bearing layer becomes lower towards the river. Moreover, Fig. 9 illustrates SPT-*N* profile reaching the bearing layer at three sites to the east of the condominium site. The elevation of the bearing layer is rather uniform here at -7 to -8 m but deeper than at sites in Fig. 8. This increased depth may be due to their more downstream locations.

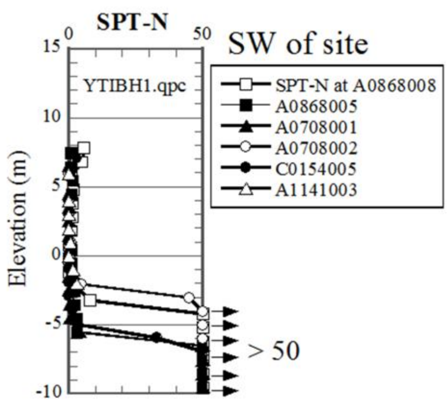

Figure 8. SPT-*N* profiles in soft soil area near the condominium site (SPT-*N* starts from 1 meter below the ground surface)

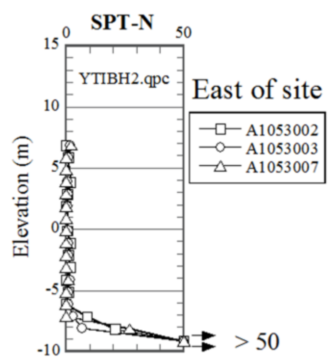

Figure 9. SPT-*N* profiles in soft soil area to the east of the condominium site (SPT- *N* starts from 1 meter below the ground surface)

Table 1 Depth of bearing layer (SPT-*N*>50) around the condominium site

Sites	Depth (m)
A0868008	13
A0868005	15
A0708001	14
A0708002	12
C0154005	15
A1053002	*17*
A1053003	*17*
A1053007	*17*

Table 1 compares the depth of first (shallowest) SPT-*N* greater than 50 at those sites. Herein depth means the distance from the local ground surface. It may be seen that the depth is variable to the west or south of the condominium site (first 5 sites) (12-15 m). If this extent of variation is the case at the condominium site as well, a constant length of pile is not a reasonable idea. Ignorance or insufficient attention to local soil conditions leads to a serious problem during construction and after completion.

Social pressure on geotechnical engineers

There are many uncertainties underground because we cannot directly see the subsoil. Even if many bore holes are drilled and other soil investigations (CPT etc.) are conducted, still there is a possibility to encounter unexpected soil conditions such as debris of former foundation, gravelly thin layer, locally deep bearing layer etc. As a consequence, auger drilling may be delayed or additional pile has to be manufactured. These situations result in delay of construction procedure and finally may affect the completion of the superstructure. Such a delay is blamed by the clients who is at the top of Fig. 3 and penalty may be claimed. Note that a delay is a significant problem to the clients because they have sold the present living places and need to move in to a new condominium on time; otherwise they have to arrange another tentative place to live with additional cost. To avoid such a situation, geotechnical engineers undergo significant pressure and stress. It seems that the construction of foundation should have reasonable flexibility in the work period as a provision for uncertainty. Such a delay is certainly reduced if more bore hole data is available through an open-access database.

On total demolition of buildings

As mentioned above, the detected differential settlement was 2 cm out of the building length of 56 m (0.04 %). According to the conventional liability rule, this range of tilting is not a legal fault of the contractor or even not detected by human sense. In the present case, however, the 2-cm differential subsidence was clearly visible at a joint of two buildings and the construction companies have been accused. It has been decided therefore that all five condominium buildings are demolished and rebuilt by the companies' own expense. There seems to be two points of discussion therein.

Significance of 0.04 % tilting

Because the differential settlement was probably (not yet concluded) caused by some deficit in pile foundation, residents were scared by the possible risk during future strong earthquake. This fear is understandable. Therefore, seismic resistance of the building was reconsidered and judged to be safe. Although details of this reconsideration are unknown to outsiders, the minor tilting suggests that there is no problem. It is desired that public sectors investigate many other buildings to show whether or not the 0.04 % tilting is exceptional.

Demolition of 5 buildings

It is very important nowadays to maintain the good fame of companies and industries among people. In this regard, the decision to demolish and rebuild the tilted building on the companies' own expense is not a bad idea. However, it is questionable to demolish and rebuild other 4 intact buildings. Now one building is going to be rebuilt by the companies because of 0.04 % tilting. If the same thing happens in other building projects in future, the present case may be used as a good reason to claim rebuilding. The first author is afraid that this very strict 0.04 % criterion will make the construction business very risky.

CONCLUSION

In response to a recent incidence of a condominium building, the Japanese Geotechnical Society established a special committee in order to publish a proposal from a society's viewpoint. The committee stated that the following 5 points deserve public attention which are

1. consideration on non-uniformity of subsoil condition,
2. need for more soil exploration technology,
3. importance of open-access subsoil data base,
4. need for involvement of good geotechnical experts and
5. importance of geotechnical professional education.

Moreover, the first author compared several bore hole data around the site and showed the possible range of variation in the depth of a pile bearing layer. He also pointed out that the significance of 0.04 % tilting should be discussed because this extent of tilting is very small.

ACKNOWLEDGMENT

The authors express their sincere gratitude to contributions made by members of JGS Committee members who are namely Messrs. K. Iwasaki, H. Ogura, J. Koseki, H. Nakamura, T. Hirade, M. Fujii and S. Yamato.

REFERENCES

Japan Federation of Construction Contractors (2016). A Guide Line for Construction of Prefabricated Concrete Piles (in Japanese).

Ministry of Land, Infrastructure and Transport (2015). Intermediate Report of Special Committee on the Problem Caused by Installation of Pile Foundation (in Japanese).

The Evolving Role of Information in Geotechnical Post-Disaster Reconnaissance and Forensic Investigations

J. David Frost[1], Ph.D., P.E., F.ASCE

[1] Elizabeth and Bill Higginbotham Professor, Sustainable Geotechnical Systems Laboratory, School of Civil and Environmental Engineering, Georgia Institute of Technology, Atlanta, GA, 30332, USA; e-mail: david.frost@ce.gatech.edu

ABSTRACT

The extraordinary volume of data that we can generate and access in support of geotechnical post-disaster reconnaissance and forensic investigations can be both awe-inspiring and overwhelming. To complement the ease of acquiring digital data, it is imperative that we develop and adopt parallel capabilities to synthesize and analyze this volume of data to transform it into information. The role and benefits of experience should not be disregarded in light of the unprecedented volumes of data but at the same time, experience should not inhibit our utilizing new information that can be gleaned from the volume of data we are now able to generate and access. This paper examines how information availability has evolved and may be used/abused. Specific examples of how the role of information in the study of geotechnical problems has evolved will be presented. A core tenet of the ideas presented in the paper is that both information quantity and quality have important roles to play.

INTRODUCTION

Irrespective of the scale of an event and whether it is a natural or human-induced, post-disaster reconnaissance and forensic investigations have a critical role to play in the practice as well as the continued advancement of geotechnical engineering as a profession. Observations and quantitative measurements of perishable data collected in the immediate aftermath of a disaster or failure are critical to both confirming existing knowledge and identifying factors likely to have contributed to the observed performance as well as identifying ill-understood phenomena worthy of additional study to prevent their occurrence in the future. These type of post-event forensic investigations are particularly critical in geotechnical engineering due to the natural variability that exists in the materials that geo-structures are built from and on.

In recognition of the importance of such reconnaissance activities, the US National Science Foundation supported the establishment of an entity, the Geotechnical Extreme Events Reconnaissance (GEER) Association that has responded to disasters and failures worldwide. Details of the association and its activities including reports describing the various reconnaissance activities it has undertaken are located at www.geerassociation.org . Throughout its existence, GEER has focused on the collection of data of the highest quality while at the same time, taking a leadership role in deploying new data collection technologies as they become available. This technology adoption culture is in particular driven by the desire to collect data without impacting the important rescue and recovery processes in the initial aftermath of a disaster or failure and at the same time recognizing that these critical activities can obscure perishable data that is critical to a robust engineering understanding of an event. In addition, GEER has a core focus of having all data geo-coded so that subsequent integration and use of the data by others is readily accomplished, if each piece of data has a unique latitude /longitude associated with it. Apart from the inherent value in the high-quality perishable data that is collected in GEER post-disaster and post-failure studies, it also serves as a basis for follow-on research studies to develop new knowledge and understanding of geotechnical phenomena.

DATA EVOLUTION

The past few decades have seen a dramatic change in the types and amount of data available for use in geotechnical studies. A significant factor in this has been the emergence of digital as opposed to analog data collection systems. This digital revolution has impacted the collection of geotechnical data of all types including from laboratory testing on specimens to site characterization using non-invasive and invasive methods to ground/airborne/satellite remotely sensed data collection methods. The result of this is that we have access to much larger volumes of data which, in general, should be of significantly higher quality and resolution than was available even three or four decades ago although the latter assertion related to quality is not always realized since the complexity of some of the data collection systems as well as the volume of data collected and thus required to be interpreted can exceed our capability to do so. These and similar considerations have led to a situation where the current state of practice can be summarized as follows:

- "Big Data" does not automatically lead to "Big Knowledge" – the trade-off between quantity and quality needs to be carefully managed.
- It is easy to generate and archive information – doing it well is significantly more difficult, particularly if it is to be retrieved and used by others at a later date.
- Data mining is currently an under-utilized technique – a number of useful tools have been developed for mining knowledge from large data sets but have yet to be adopted in main-stream geotechnical practice.
- There have been significant advances in the geospatial referencing and representation of geotechnical data but it is far from ubiquitous yet.
- There is an emerging interest in the collection of temporal data – change detection is being recognized as a powerful capability.
- Data quality evaluation protocols and metrics are still lacking – despite the advances in techniques to collect large volumes of data, little emphasis has been placed on end-use driven data quality. For example, a subsurface sounding may be of very high quality for geo-environmental purposes but may lack some critical information to allow it to be equally useful for geotechnical purposes.
- Data representation has not kept pace with the explosion in data quantity and types available.

The remainder of this paper presents some examples, at different scales, to illustrate some emerging data collection and information extraction capabilities and at the same time highlight the limitations and possible impediments to their adoption. Specifically, examples which illustrate regional landslide susceptibility, slope instability for an infrastructure component and challenges in merging historical and modern data sets in evaluating settlements for a site redevelopment are presented.

REGIONAL LANDSLIDE ASSESSMENTS

Recent major earthquakes around the world have highlighted the challenges of identifying geotechnical hazards as well as assessing damage and thus potential additional hazards immediately after the earthquake due to the scale of these events as well as the challenging topography in some earthquake regions. This is particularly important given that in many cases, even after the primary earthquake, significant new hazards are created due to secondary effects such as "quake lakes", tsunami and seasonal rainfall and these can produce additional catastrophic events. The availability of remotely sensed information from both before as well as immediately after natural disasters has opened up opportunities to address these challenges. In particular, this example shows how pre/post remotely sensed information from satellite, airborne and ground based imaging can be integrated to provide rapid assessment of continuing hazard. The technologies to be integrated range from high-resolution satellite imagery, rapidly deployed airborne photographic imagery as well as airborne laser imaging. A number of new GIS based analysis tools adapted or developed to facilitate these studies by allowing integration of information from the multiple platforms are also noted.

The availability of high resolution pre-post satellite imagery can allow for a much safer and more rapid assessment of conditions and future hazard. Figure 1 shows a pre/post high resolution image pair for the same area in a mountainous region near the epicenter of the May 12 Wenchuan, China event just north of the town of Yingxiu. Further, the availability of airborne LIDAR can enable geometric information such as slope angle and highway distance to be automatically determined thereby enabling a rapid assessment of future hazard. Figure 2 illustrates a recently developed method (Turel and Frost, 2011) for determining slope geometry from a Digital Elevation Model using hydrology tools within a GIS.

Image: Quickbird True Color Pan Sharpened Satellite Imagery
Acquistion Date: June 26, 2005
Spatial Resolution: 0.6 Meters

Image: Quickbird True Color Pan Sharpened Satellite Imagery
Acquisition Date: June 3, 2008
Spatial Resolution: 0.6 Meters

Figure 1. Pre and Post Earthquake Image Pair showing Landslide Occurrence near Epicenter

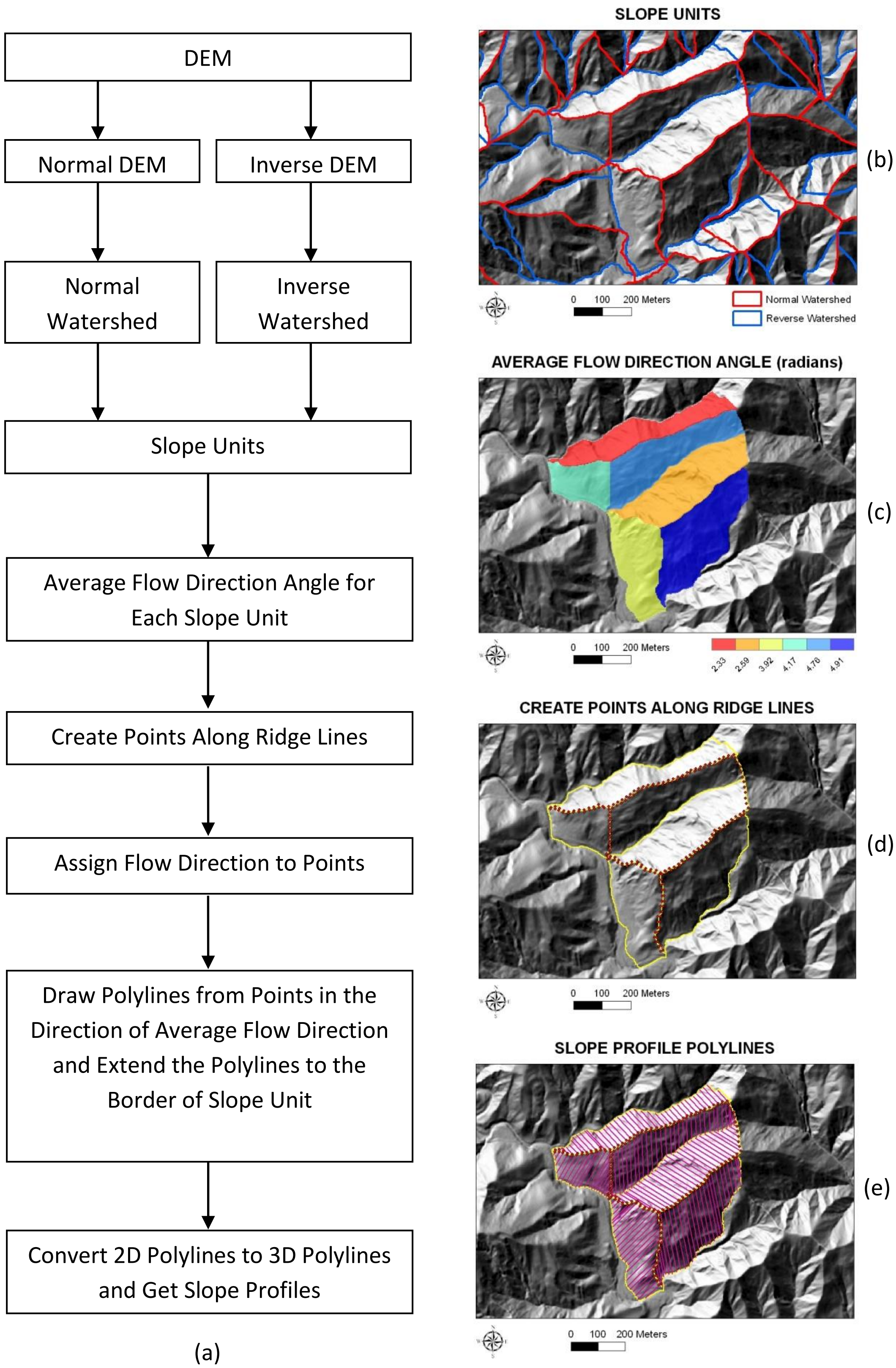

Figure 2. Slope Profile Delineation Using Slope Unit Approach

These and similar data tools allow for the engineer/scientist to conduct regional analysis "on a desktop". The ability to merge large data sets and conduct spatial/temporal analysis and visualization throughout project design, construction and performance phases is critical. Further, with the emergence of "unprecedented scenarios" catalyzed by climate change and associated events, our need to perform extensive parametric studies is becoming more critical since our ability to rely ono historical events is diminishing in the presence of "new normals".

INFRASTRUCTURE SYSTEM PERFORMANCE

Ensuring that major highway infrastructure routes remain functional following a major earthquake requires significant assessment of potential hazard and associated maintenance activities. At the same time, each earthquake provides the opportunity to gain new insights into how not only individual components of an infrastructure system performed but also how an entire system performs. In contrast to the impacts of the earthquake strong ground motions on highway infrastructure in Wenchuan following the May 12, 2008 event which predominantly impacted mountainous areas and thus produced many consequences associated with landslides, the strong ground motions following the February 27, 2010 event in Chile yielded equally significant impacts on the main highway which runs essentially North-South through the country yet much of it traverses terrain with low elevation changes. As the primary highway in that country, failures of a number of different elements severely impacted rescue and recovery efforts in the days immediately following the event. While relatively rapid highway service was re-established in the weeks following the event, the loss of sections of the highway due to embankment failures as well as the collapse of a number of bridge systems impacted post-earthquake response activities. As previously illustrated in this paper, the availability of high-resolution pre and post event satellite imagery along with ground based LIDAR and optical images can significantly enhance the insight into causative mechanisms and the guidance of future maintenance strategies.

To illustrate how satellite and ground based imagery can be effectively used in assessing not just the performance of an individual component of a highway system but a larger portion of such a system, a section of the major North-South Highway (Route 5) in Chile is considered. Pre and post satellite images for an approximately 8 km section of the highway were acquired. The highway in that region is a four-lane limited access divided highway (two lanes each direction) and while the highway grade is essentially flat, it does traverse a number of low lying areas where earth embankments were constructed and also a number of bridge structures that traversed rivers/ streams and a railway line. Available high resolution imagery for the study section ranged between 0.5 and 1.0 m resolution.

The similarity in location of embankment failure and embankment slumping sites suggests that 3-D effects may yield a lower factor of safety where a sharp corner exists. As seen in Figure 3, the embankment failure shows a lateral translation of a large mass of soil on the outside corner of a sharp curve.

Figure 3. Pre and Post Images Showing Failed Approach Road Overpass Embankment

The preceding assessment was based on a review of high resolution satellite images only. In addition, the failed overpass embankment was also imaged from the ground using both LIDAR and optical imaging techniques. The 3-D geometric model resulting from a LIDAR scan of the failed embankment is shown in Figure 4 (Bray and Frost, 2010). The lateral translation of the highway embankment is clearly evident in the LIDAR image. Further, the scarp formed during the translational spreading of the embankment is clearly evident in the ground based photo shown in Figure 5 while the availability of the 3-D geometric model obtained from the LIDAR images can be used to calculate lateral displacements as shown in Figure 6.

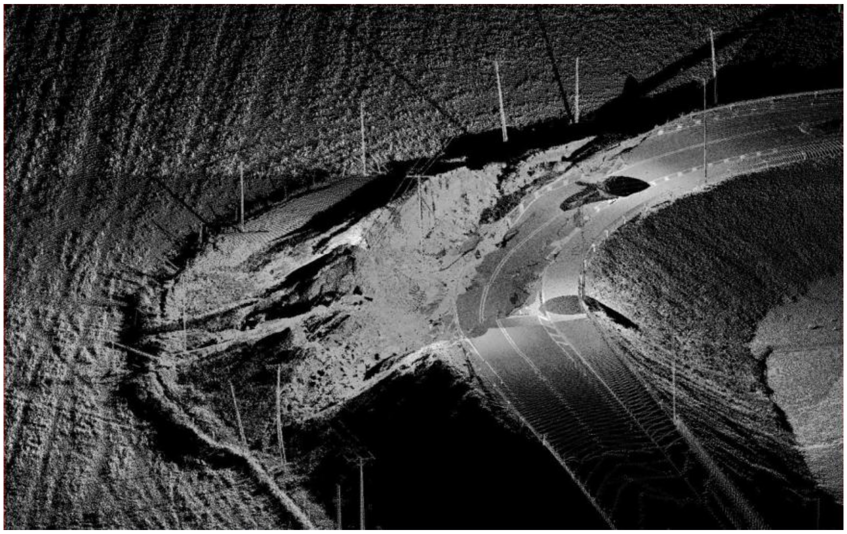

Figure 4. LIDAR Image of Failed Approach Embankment (courtesy Kayen)

Figure 5. Ground Based Optical Images of Failed Approach Embankment

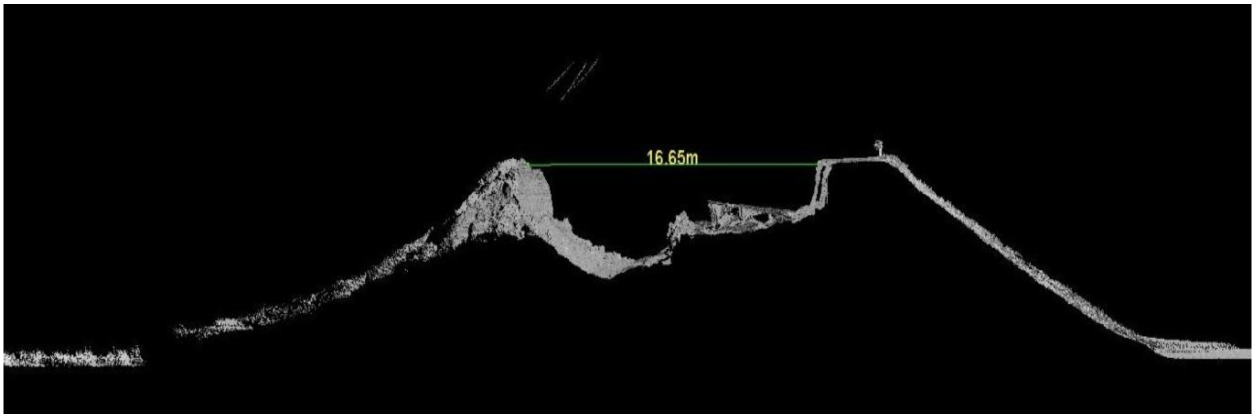

Figure 6. Interpretation of Translation from LIDAR Image of Failed Approach Embankment

SETTLEMENT EVALUATION

The redevelopment of a riverfront warehouse site for a new energy generation center provided a useful backdrop to evaluate the challenge in merging the results from laboratory specimen based consolidation settlement methods with more recent in-situ testing based approaches for estimating over-consolidation ratio and thus likely settlements. Of particular interest in this case was the relative amount of data and thus estimates of Over Consolidation Ratio (OCR) from laboratory testing (2 from oedometer tests) versus those from soundings (23,500 from CPT tests). Despite this overwhelming difference in number of estimates (Figure 7), the limited number from the laboratory testing dominated the decision making process in the original site investigation interpretation and ultimately the evaluation of likely settlement magnitudes.

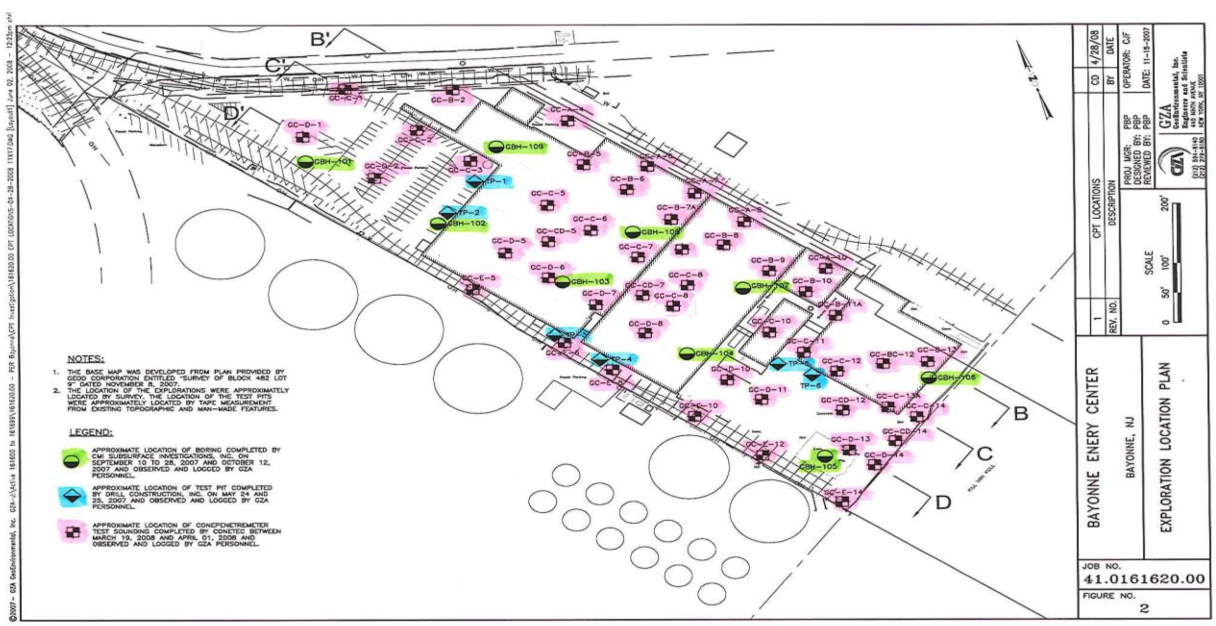

Figure 7. Locations of Test Pits, Borings and CPT Soundings

A review of the data from this example shows that amongst several factors contributing to the outcome, the sequencing of the site investigation phases, errors in initial interpretation of the limited laboratory based estimates, and lack of experience with the in-situ based methods, all contributed to a highly conservative decision to categorize the site as normally consolidated despite the overwhelming evidence to the contrary.

CONCLUSIONS

The preceding examples at multiple scales have sought to illustrate how the role of information is evolving in geotechnical post-disaster reconnaissance and forensic investigation. A number of observations are relevant:

- We are not lacking for information acquisition tools or quantity of information.
- We need improvements in how information quality is evaluated.
- We need to recognize that using bad information is detrimental to our assessments.
- We need to balance our respect for historical experience with the benefits of data gathered using new technologies.
- Post-disaster reconnaissance now involves the acquisition of a range of ground, airborne and satellite based techniques.
- Desktop tools for data mining, analysis, management and visualization provide us with exceptional opportunities to conduct parametric "what-if" simulations.
- We should not be afraid of new types of information which can lead to superior insights.
- We need to merge information from various sources in an unbiased approach.

ACKNOWLEDGMENTS

Much of the data presented in this paper was collected as part of GEER Association post-disaster study activities. The support of the US National Science Foundation under Grant CMMI #1265761 is gratefully acknowledged.

REFERENCES

Bray, J.D. and Frost, J.D., (2010), "Geo-Engineering Reconnaissance of the 2010 Maule, Chile Earthquake", Web Report, (Bray and Frost, Editors), http://www.geerassociation.org/administrator/components/com_geer_reports/geerfiles/Maule_Chile_2010/Ver2_Maule_Chile_2010_index.html

Turel, M., and Frost, J.D., (2011), "Delineation of Slope Profiles from Digital Elevation Models for Landslide Hazard Analysis", Proceedings of GeoRisk 2011 Conference, ASCE Geo-Institute, Atlanta.

Lessons about Managing Landslide Risk from the 2014 Oso, Washington Landslide

Robert Gilbert[1], David R. Montgomery[2], Joseph Wartman[2], Jeffrey R. Keaton[3], Scott Anderson[4], Jean Benoît[5] and John deLaChapelle[6]

[1]The University of Texas, Austin, Texas, USA
[2]University of Washington, Seattle, Washington, USA
[3]AMEC Americas, Los Angeles, California, USA
[4]BGC Engineering Inc., Golden, Colorado, USA
[5]University of New Hampshire, Durham, New Hampshire, USA
[6]Golder Associates, Redmond, Washington, USA

ABSTRACT

A landslide occurred in 2014 in Washington state, taking 43 lives and destroying a community of about 50 homes. Compared to three previous landslides at this location in the past 60 years, the 2014 event was about three times higher, involved ten times the volume of material and had a runout seven times further. In hindsight, the risk to people below this slope is above thresholds considered acceptable for landslides in other countries and major dams in the U.S.; however, the risk is similar to or even smaller than that associated with flooding from levees at multiple locations in the U.S. The following lessons about managing risk from natural landslides can be learned from this landslide: (1) History is not always the best guide to the future; (2) Many existing natural slopes are marginally stable and will only be a problem if they become destabilized in the future; (3) An early warning system may be helpful but not necessarily feasible; and (4) There is a need to improve the assessment and communication of risk.

INTRODUCTION

A landslide occurred on March 22, 2014 near Oso, Washington (Fig. 1), taking 43 lives and destroying the Steelhead Drive Community (Fig. 2). This paper summarizes the physical characteristics of the landslide and describes the risk management measures that were in place at the time of the landslide. The paper then provides a hindsight assessment of the risk and concludes with lessons that can be learned about managing risks from landslides.

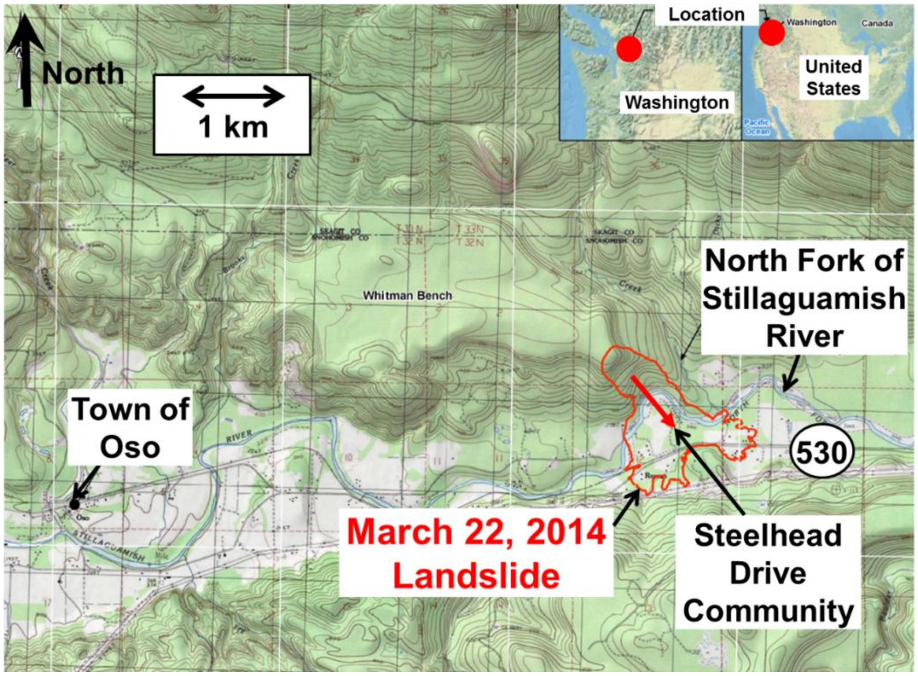

Figure 1. Site plan (adapted from Keaton et al. 2014).

Figure 2. Aerial photographs of Steelhead Drive Community before and after 2014 Landslide (photos from Google Earth®).

LANDSLIDE DESCRIPTION

Geology. The landslide occurred in glacial soils (Fig. 3) on the north side of the valley of the North Fork of the Stillaguamish River (Fig. 1). These soils were deposited in the most recent glacial period ending about 15,000 years before present. The 2014 event was preceded by three documented failures of the lower part of the slope occurring in 1949, 1967 and 2006 (Fig. 4). Compared to the three previous landslides, the 2014 event was about three times higher, involved about ten times the volume of material and had a runout of landslide debris about seven times further from the toe of the slope.

Hydrology: The weather was dry and clear when the 2014 landslide occurred. There was about 20 mm of precipitation 3 days before the landslide. In the year before the landslide, the only remarkable aspect of the hydrology was the cumulative precipitation for the period 21 days prior to the event; this 21-day cumulative precipitation has a return period of about 100 years based on historical records (Henn et al. 2015).

Stability: The documented landslides prior to the 2014 event were all within the glaciolacustrine clay (Fig. 4). A stability analysis of the 2006 event indicates one plausible hypothesis for this failure: the drained shear strength of the glaciolacustrine clay was mobilized, with a fully softened shear strength in the "intact" material and a shear strength between the fully softened and residual shear strengths in a zone of previous shearing from ancient 2014-like events that created the existing slope (ancient head scarp) above the glaciolactustrine clay (Fig. 5). A mobilized shear strength in the zone of ancient shearing that is 80-percent of the way between the residual and fully softened shear strengths gives a factor of safety of close to one for the 2006 slope (Fig. 5).

Following the same approach that gives a factor of safety of one for the 2006 event, the factor of safety with the topography at the time of the 2014 event (i.e., the post-2006 landslide topography) is also about one (Fig. 6). If the geometry of the head scarp in the lower slope was similar to what was produced by the 2006 event, then the factor of safety for the slope above the glaciolacustrine clay is well below one after a failure of the lower slope (Fig. 7). Therefore, one plausible hypothesis for the large 2014 landslide is that it was triggered by a smaller landslide similar to the 2006 event, which then caused a much larger failure that extended up nearly 200 m to the top of the valley side.

The runout of landslide debris from the 2014 landslide was the cause of the catastrophe for the community. The runouts from both the 1967 and 2006 landslides at this location did not impact homes and people in the Steelhead Drive Community (note that the community was not there prior to 1960). However, the community was destroyed by the 2014 landslide because the debris ran out all the way across the valley (Fig. 2). Field reconnaissance after the failure indicated there were two stages of run-out: the first stage was larger and likely responsible for destruction of the Steelhead Drive Community, while the smaller second stage came down onto the back side of the first stage (Wartman et al. 2016). Based on empirical correlations between the volume of debris and the height of the slope, the runout from the 2014 landslide is not surprising and consistent with other landslides in similar geologic settings (Fig. 8).

Consequences: The consequences of the 2014 landslide were catastrophic. Forty-three lives were lost, making it the deadliest landslide in the history of the United States. About 50 homes were destroyed. A major road, State Highway 530 (Fig. 1), was destroyed over a 600-m length. The North Fork of the Stillaguamish River was temporarily dammed by the landslide debris, causing upstream flooding.

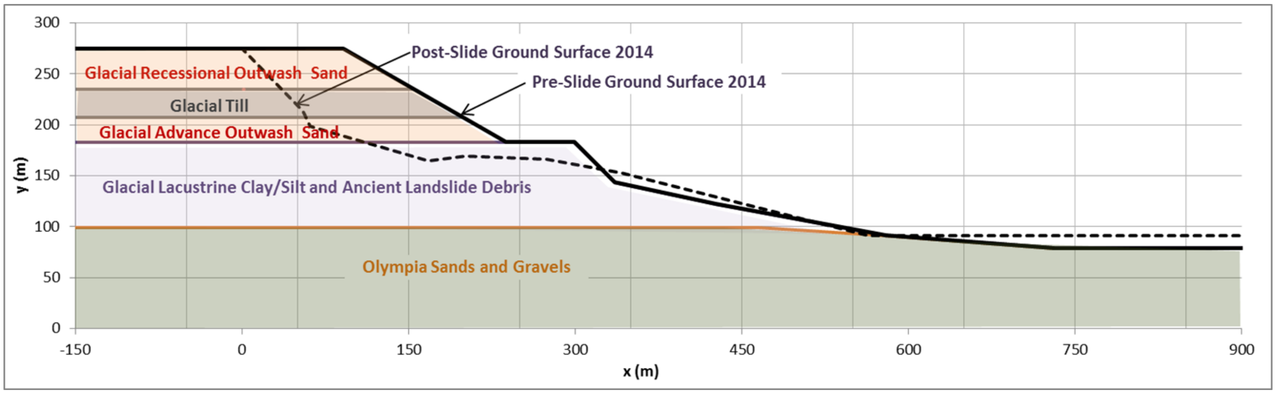

Figure 3. Cross-section from north to south of 2014 landslide.

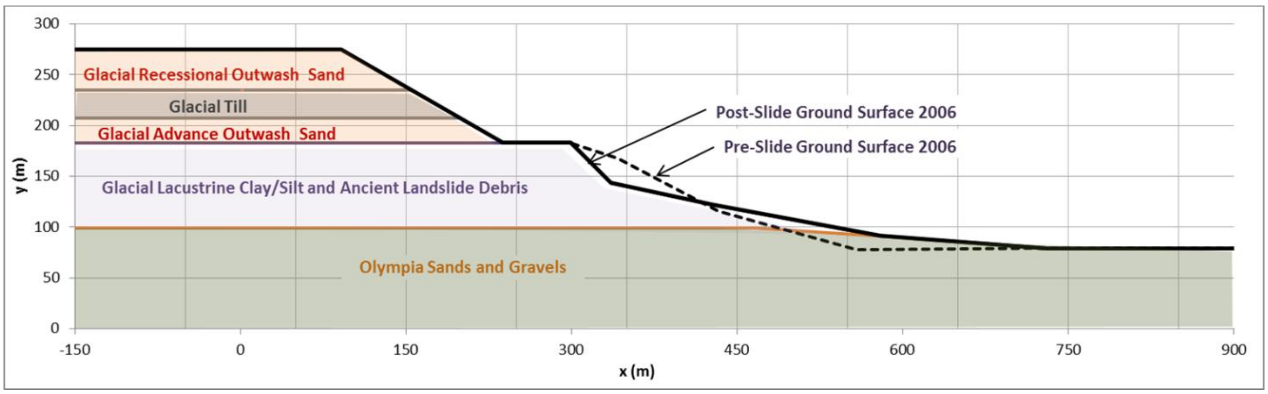

Figure 4. Cross-section from north to south of 2006 landslide.

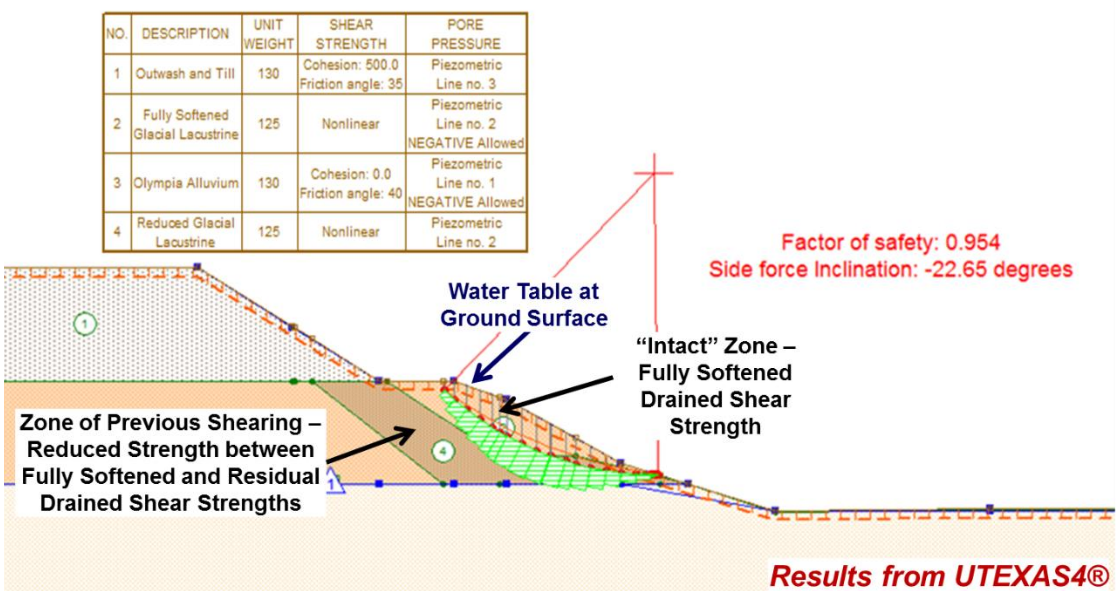

NO.	DESCRIPTION	UNIT WEIGHT	SHEAR STRENGTH	PORE PRESSURE
1	Outwash and Till	130	Cohesion: 500.0 Friction angle: 35	Piezometric Line no. 3
2	Fully Softened Glacial Lacustrine	125	Nonlinear	Piezometric Line no. 2 NEGATIVE Allowed
3	Olympia Alluvium	130	Cohesion: 0.0 Friction angle: 40	Piezometric Line no. 1 NEGATIVE Allowed
4	Reduced Glacial Lacustrine	125	Nonlinear	Piezometric Line no. 2

Figure 5. Stability analysis for 2006 landslide.

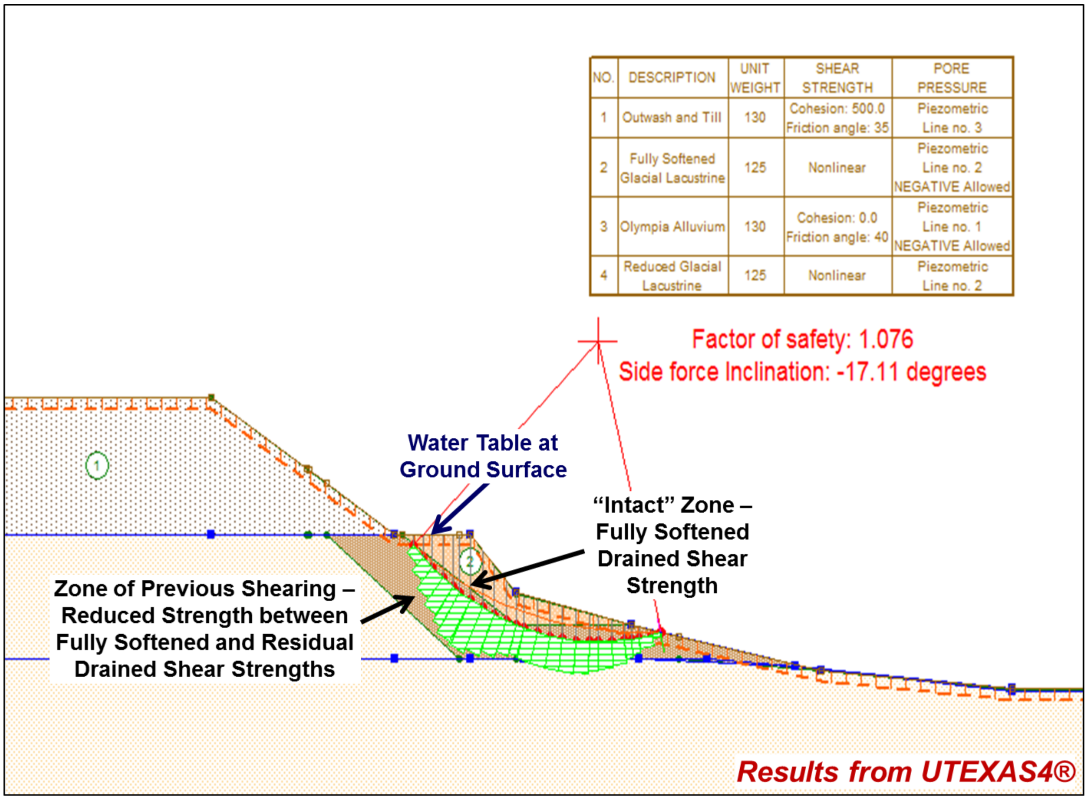

Figure 6. Stability analysis for 2014 landslide – initial condition.

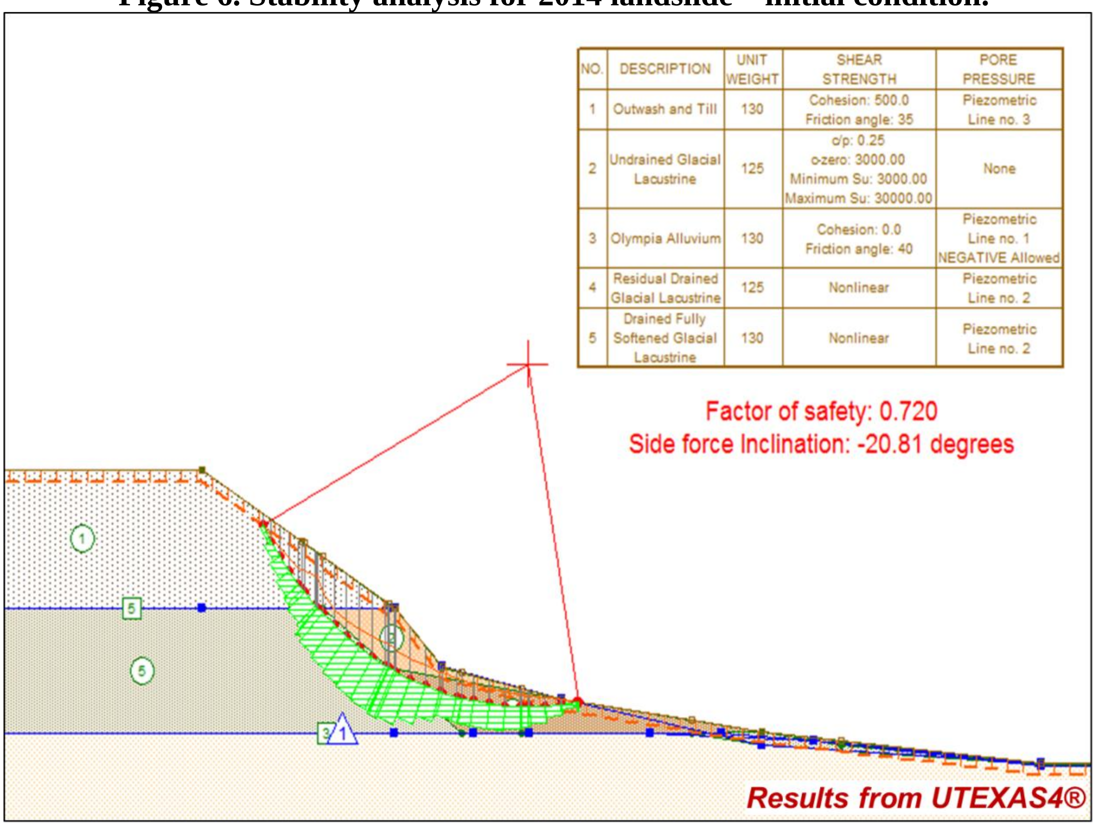

Figure 7. Stability analysis for 2014 landslide – post-failure of lower slope.

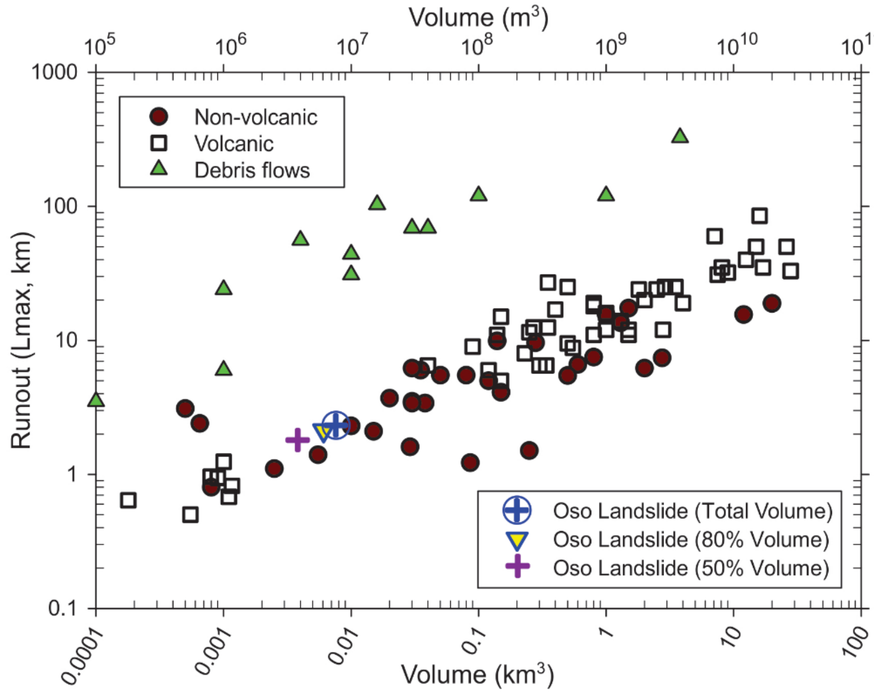

Figure 8. Comparison of runout from 2014 Oso landslide with other landslides (from Keaton et al. 2014).

RISK MANAGEMENT BEFORE EVENT

Risk Assessment: Risk is the possibility of suffering loss, and it is represented by the consequence and probability of a loss. Before the 2014 landslide, there were several studies of the landslide hazard at this location: Shannon and Associates (1952), Thorsen (1969), Miller (1999) and GeoEngineers (2001). All of these studies focused on the lower slope, which had failed several in the last century and most recently in 2006 (Fig. 4). Also, all of the studies were conducted with a focus on the river as a natural resource and a habitat for an endangered species, the Chinook Salmon. None of the studies explicitly assessed the probability of another failure. However, the GeoEngineers (2001) report included a statement that "Catastrophic failure potential places human lives and properties at risk." The maximum runout estimated in Miller (1999) is 275 m, which was larger than but similar to the runouts that had occurred in previous failures of the lower slope and larger than the runout in the 2006 failure.

Risk Management: The primary methods for risk management prior to the 2014 landslide were restrictions on land use. The entire slope above the Steelhead Drive Community was designated as a "Landslide Hazard Area" by Snohomish County (Fig. 9). This designation restricted development on the slope and within 90 m of the toe of the slope; the nearest home to slope before the 2014 landslide was 120 m away and outside of any land-use restrictions. The Washington Department of Natural Resources restricted logging activity on or above the slope.

In addition to people and property, the Chinook Salmon in the river were also at risk because continual erosion from the slope was fouling their habitat for spawning. In an attempt to minimize erosion from the river bank, the Stillaguamish Tribe of Indians (the entity responsible for the river as a resource) had constructed a 4.5-m high, 430-m long timber wall along the toe of the slope following the 2006 failure.

RISK ASSESSMENT IN HINDSIGHT

Studies since the 2014 landslide indicate that this type of a failure has occurred numerous times in this valley in the vicinity of the 2014 event (e.g., Fig. 10). Radiocarbon dating of buried trees in ancient landslide debris exposed by the scarp of the 2014 landslide indicates that the trees were killed 5,000 to 6,000 years before present (Keaton et al. 2014). Since this debris corresponds to the oldest mapped landslide unit in Figure 9, it is likely that all of the ancient landslides shown in Figure 9 occurred within the past 6,000 years.

Based on this post-landslide information, a rough assessment of the risk for landslides in this valley is as follows:

- Landslides with runouts of several hundred meters that are capable of pushing the river from the toe of the slope (like the previous landslides in 1949, 1967 and 2006) occur once every 10 to 100 years.
- Landslides with runouts of several thousand meters that are capable of covering the valley floor (and destroying people and property in their path) occur once every 100 to 1,000 years.

The risk of landslides to people in this valley, assuming that development is allowed as it has been in the past, is compared with several benchmarks for risk in Figure 11. The risk is above thresholds considered acceptable or tolerable for landslides in Australia and Hong Kong and major dams in the U.S. (Fig. 11). However, the risk is similar to that associated with flooding from levees in the Green River Valley, just south of Seattle and not far from Stillaguamish River Valley. Also, the risk is less than that associated with flooding from levees in the California Delta and New Orleans, which are both many orders of magnitude above what is considered acceptable for large dams in the United States (Fig. 11).

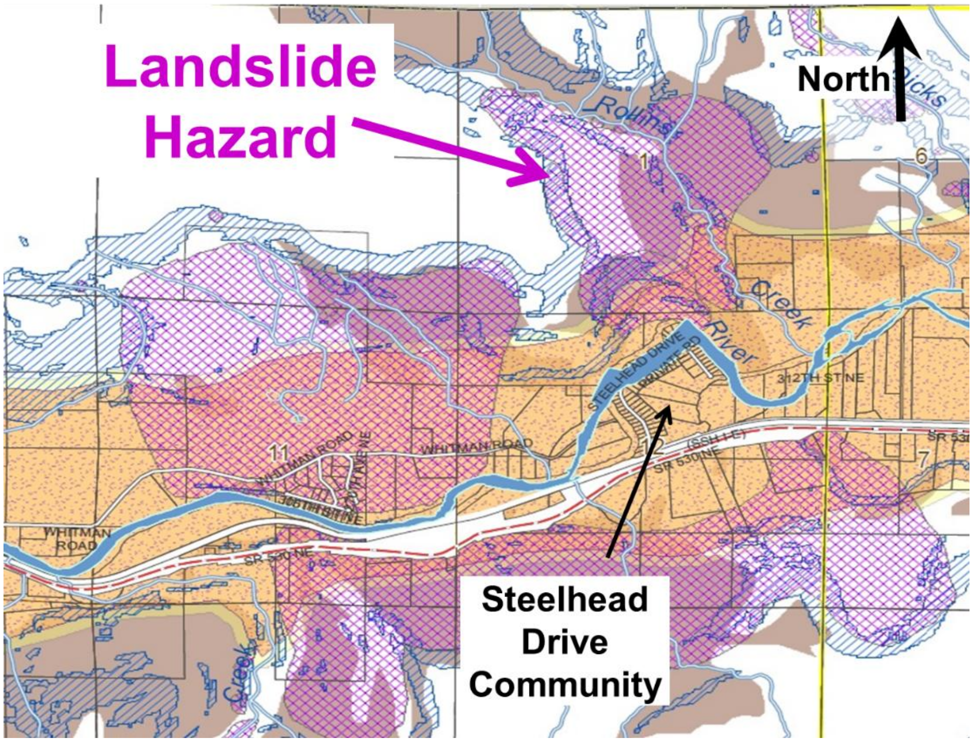

Figure 9. Designated Landslide Hazard Areas in Snohomish County Map dated 2007 (adapted from Keaton et al. 2014).

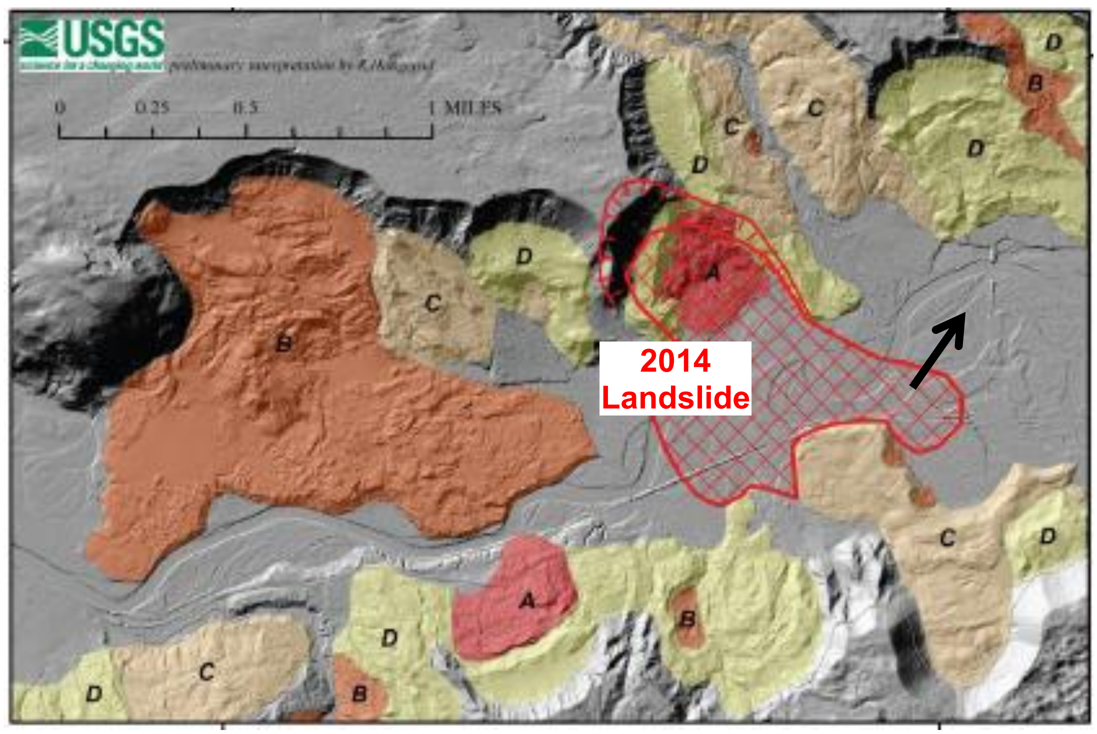

Figure 10. Relative age classes (A youngest to D oldest) of pre-2014 landslides in the immediate vicinity of the 2014 Oso Landslide (from Haugerud 2014).

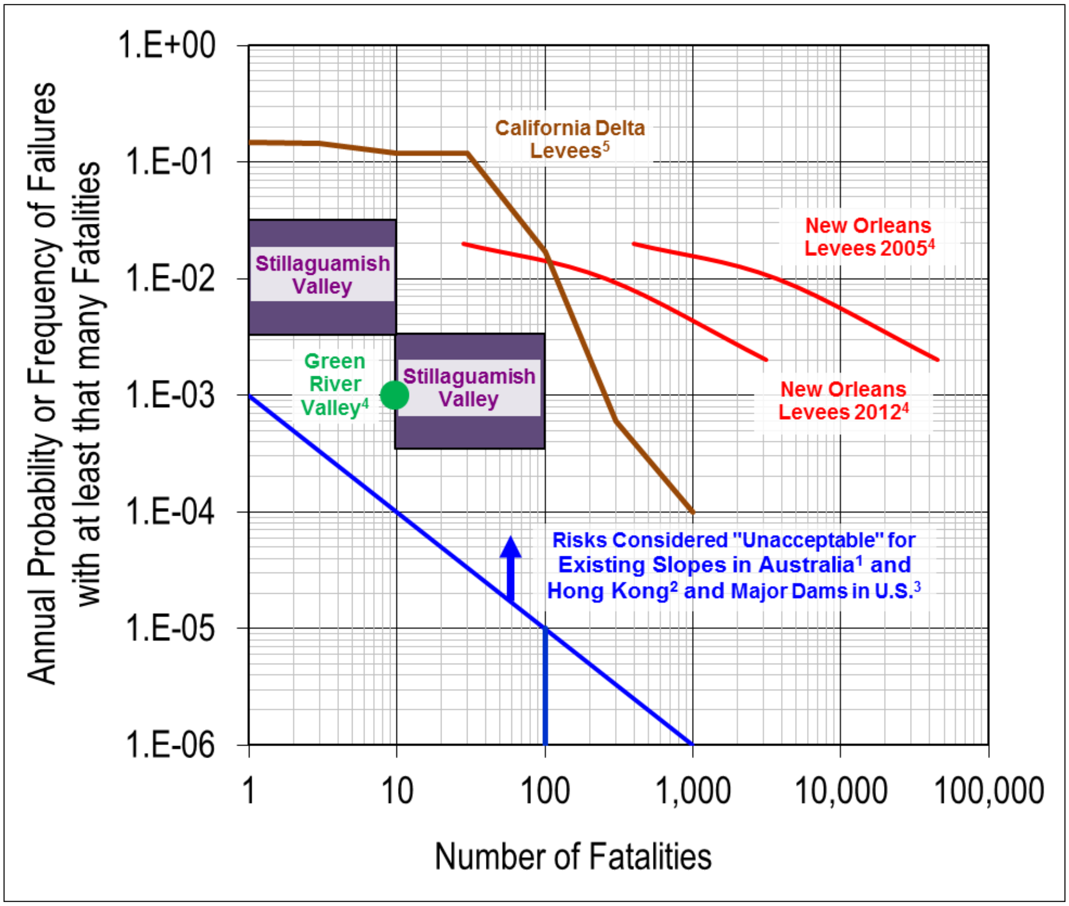

Figure 11. Comparison of rough assessment for risk from landslides in North Fork Stillaguamish River Valley with related benchmarks: [1]AGS 2000, [2]GEO 1998, [3]USACE 2014, [4]Gilbert 2013, [5]IPET 2009 and [6]DWR 2008 (adapted from Keaton et al. 2014).

LESSONS LEARNED ABOUT MANAGING RISKS FROM NATURAL LANDSLIDES

The following lessons about managing risk from natural landslides can be learned from the 2014 Oso landslide:

1. History is not always the best guide to the future. This slope had failed three times in the past 50 years, twice with homes just below it that were not impacted. Assessments of the stability and the potential for runout all focused on these types of failures and missed the potential for a larger failure with a much more significant runout.
2. The factor of safety for an existing natural slope can be very close to one. Many natural slopes are the remnants of previous failures and are just marginally stable. The challenge with these slopes is to assess the possibility and probability that the factor of safety will become less than one in the future either due to natural causes (such as dissipation of negative shear-induced pore water pressures from previous failures that relieved stresses or erosion) or man-made causes (such as changes to the hydrogeology through land use).
3. An early warning system may have been helpful here, but it may not have been feasible. First, it is not known if deformations or water pressures exhibited some type of signature in advance of the event indicating what was about to happen. With water pressures, it is possible localized measurements would have been required in the zone of shearing,

meaning that this zone would have to be known in advance. Second, it is not clear who would have been responsible for deciding to evacuate people from the community and what the criteria for deciding would have been. Last, it is not clear who would have been responsible for allowing people to return to their homes if the slope did not fail when they were evacuated.

4. There is a need to do better at assessing and communicating risk. The people living in the valley were not aware that a slope failure like this could occur, even though there was and is ample evidence that these failures have been happening every thousand years or so as the river has widened the valley since the last glaciation. However, the people also need to know how this risk compares to other risks, say from flooding in similar river valleys. Lastly, it is important that benefits, costs and risks all be considered collectively. There are many benefits to living in this beautiful valley, and there are limited resources available to minimize the risks.

ACKNOWLEDGEMENTS

Financial support for this work was provided by the United States National Science Foundation under grants CMMI-1266418 and CMMI-1636217. Steve Wright (Professor Emeritus, The University of Texas at Austin) was helpful in reviewing the stability analyses. Any opinions, findings, and conclusions or recommendations expressed in this material are those of the authors and do not necessarily reflect the views of the National Science Foundation or any collaborators.

REFERENCES

AGS (2000), "Landslide Risk Management Concepts and Guidelines," *Australian Geomechanics* 35/1, pp. 49-92.

DWR (2008), "Delta Risk Management Strategy Phase 1, Risk Analysis Report," California Department of Water Resources.

GEO (1998), "Landslides and Boulder Falls from Natural Terrain: Interim Risk Guidelines," Geotechnical Engineering Office Report 75, Government of Hong Kong.

GeoEngineers (2001), *Steelhead Haven Landslide Remediation Feasibility Study, Alternatives development and analysis and preliminary project designs, RM 20, NF Sillaguamish River*, Prepared for The Stillaguamish Tribe of Indians, Prepared by GeoEngineers Inc., April 26, 2001, 62 p.

Gilbert, R. B. (2013), "Expert Engineering Independent Third-Party Review, Briscoe-Desimone Levee Design, Green River Basin, State of Washington," Prepared for the King County Flood Control District, Prepared by R. B. Gilbert, February 16, 2013, 39 pp.

Haugerud, R. A. (2014), *Preliminary Interpretation of Pre-2014 Landslide Deposits in the Vicinity of Oso, Washington*, U.S. Geological Survey Open-File Report 2014-1065, U.S. Geological Survey, Reston, Virginia.

Henn, B., Cao, Q., Lettenmaier, D. P., Magirl, C. S., Mass, C., Bower, J. B., St. Laurent, M., Mao, Y., Perica, S. (2015), Hydroclimatic Conditions Preceding the March 2014 Oso landslide. *J. Hydrometeor*, V. 16, p. 1243–1249.

IPET (2009). "Performance Evaluation of the New Orleans and Southeast Louisiana Hurricane Protection System - Volume VIII Engineering and Operational Risk and Reliability

Analysis," Final Report of the Interagency Performance Evaluation Task Force, U.S. Army Corps of Engineers.

Keaton, J. R., Wartman, J., Anderson, S. A., Benoît, J., deLaChapelle, J., Gilbert, R., and Montgomery, D. R., *The 22 March 2014 Oso landslide, Washington*, Geotchnical Extreme Events Reconnaissance Association Report GEER-036.

Miller, D. J., (1999), Hazel/Gold Basin Landslides: Geomorphic Review Draft Report, Report to U.S. Army Corps of Engineers, 25 pp.

Shannon and Associates (1952), *Report on Slide on North Fork Stillaguamish River near Hazel, Washington*, unpublished report to the State of Washington Departments of Game and Fisheries, 18 p.

Thorsen, G. W. (1969), *Landslide of January 1967 which diverted the North Fork of the Stillaguamish River near Hazel*, Memorandum dated November 28, 1969, to Marshall T. Hunting, Department of Natural Resources, Geology & Earth Resources Division, Olympia, WA.

USACE (2014), "Safety of Dams – Policy and Procedures," ER-1110-2-1156, United States Army Corps of Engineers.

Wartman, J., Montgomery, D., Anderson, S., Keaton, J., Benoit, J., deLaChapelle, J. and Gilbert, R. (2016), "The 22 March 2014 Oso Landslide, Washington, USA," *Geomorphology*, Volume 253, pp. 275–288, Elsevier.

Vulnerability of Buildings to Landslides: Impact Loads and Failure Mechanisms

Limin Zhang[1], Liang Gao[2], and Hongxin Chen[3]

[1]Professor, The Hong Kong University of Science and Technology, Hong Kong, China; cezhangl@ust.hk
[2]PhD Research Assistant, The Hong Kong University of Science and Technology, Hong Kong, China; lgaoab@ust.hk
[3]Assistant Professor, Tongji University, Shanghai, China. Formerly, Post-doctoral Research Fellow, The Hong Kong University of Science and Technology, Hong Kong; chenhongxin@tongji.edu.cn

ABSTRACT

A large spoil slope in Shenzhen, China, failed on 20 December 2015. The landslide materials had a volume of approximately 2.6x10^6 m^3, travelled 1100 m and covered an area of 0.38x10^6 m^2. The landslide destroyed 33 buildings, leading to 73 deaths, 4 missing people, and 17 injuries. This was a rare landslide that occurred in a metropolitan setting and resulted in catastrophic consequences. Hence serious questions arose. What went wrong? Why did the debris travel so far and so fast? How were the buildings destroyed? What measures should be taken to present similar disasters in the future? This paper looks into the causes and mechanisms of the failure of the buildings by simulating the debris flow process, evaluating the impact pressures on the buildings, and exploring the failure mechanisms of the buildings. The history of the spoil soil slope is reviewed first. Then a digital elevation model of the slope, the terrain and the buildings prior to the slope failure is established using high-resolution satellite data. Subsequently, the flow process of the landslide material is simulated using a numerical program EDDA (Chen and Zhang 2015). Based on the simulations the impact pressures on the buildings are obtained. Finally, common failure mechanisms of buildings, i.e., column failure and foundation failure, are described, and the pertinent foundation failure mechanism for two buildings in the Shenzhen landslide event is analyzed in detail. The calculated flow depth and flow velocity at the distal end of the landslide are still far larger than the critical values for shear failure, so that the two buildings experienced large translational movements and collapsed.

INTRODUCTION

A large spoil soil slope in Shenzhen, China, failed on 20 December 2015. The landslide materials had a volume of approximately 2.6 x 10^6 m^3, travelled 1100 m and covered an area of 0.38 x 10^6 m^2. The landslide destroyed 33 buildings, leading to 73 deaths, 4 missing people, and 17 injuries. This was a rare landslide that occurred in a metropolitan setting and resulted in catastrophic consequences. Hence serious questions arose. What went wrong? Why did the debris travel so far so fast? How were the buildings destroyed? What measures should be taken to present similar disasters in the future?

Forensic geotechnical engineering involves scientific, legalistic investigations and deductions to detect the causes as well as the process of distress in a structural or geotechnical facility, which are attributed to geotechnical origin. This paper looks into the causes and mechanisms of the building failures in the Shenzhen landslide case by simulating the landslide debris flow process, evaluating the impact pressures on the buildings, and exploring the mechanisms of the failure of the buildings subject to impact. The causes of the failure of the spoil slope involved both technical and criminal investigations and are beyond the scope of this paper.

A number of studies have been performed to quantify the vulnerability of buildings to debris flow impacts in alpine areas (e.g., Lo 2000; Fuchs *et al*. 2007; Luna *et al.* 2011; Jakob *et al*. 2012). Lo (2000) reviewed empirical methods for estimating debris impact loads and design of natural terrain landslide debris-resisting barriers. Fuchs et al. (2007) conducted detailed site-specific analysis of the vulnerability of elements at risk to debris flows. Luna *et al.* (2011) generated three physical vulnerability curves that relate the intensity of debris flows to the economic losses. Jakob *et al*. (2012) reviewed 68 cases over the globe and classified four damage classes for building destruction. In the Shenzhen landslide case, the landslide and flow processes were well documented, and the failure mechanisms of several buildings were clearly exposed. The simulation of the landslide debris flow process and the impact pressures will further help reconstruct the failure process of the buildings.

FAILURE OF THE SPOIL SLOPE

The Hongao Spoil Soil Reception site is located at northwestern Shenzhen in Guangdong Province. The site was a quarry in late 1990's and was abandoned for some time. Figure 1(a) shows the quarry by the end of 2013, which was ponded with a reservoir volume of about 90,000 m^3. The quarry was late utilized as a spoil soil reception site, and was filled up rapidly in 2014 and 2015. Figure 1(b) shows the fill slope site in Sept. 2015, less than three months before the failure of the slope.

Figure 2 shows the geologic profile of the spoil soil slope. The bedrock consists of slightly to moderately decomposed granite on the back of the slope and slightly decomposed leptynite at the front of the slope. The elevation of the bedrock at the invert of the outlet of the quarry is about 60.6 m, where the elevation at the bottom of the quarry is about 44.3 m, leading to a maximum pond depth of 16.3 m. The pond was not drained before receiving soil fills hence the bottom of the spoil slope was fully saturated.

The spoil fill was stored in 9 stages and stages 7-9 were being filled and compacted before failure on the morning of 20 December 2015. The fill materials were primarily from basement and tunnel excavation, and may be classified as brown, fine to medium weak completely decomposed granite with some fill fragments. While the design slope crest elevation and the spoil soil volume were 95 m and 4.0 x 10^6 m^3, the actual highest elevation and soil volume reached 160 m and 5.83 x10^6 m^3, respectively,

Figure. 1. The spoil slope site as of (a) 25 Nov. 2013 and (b) 29 Sept. 2015.

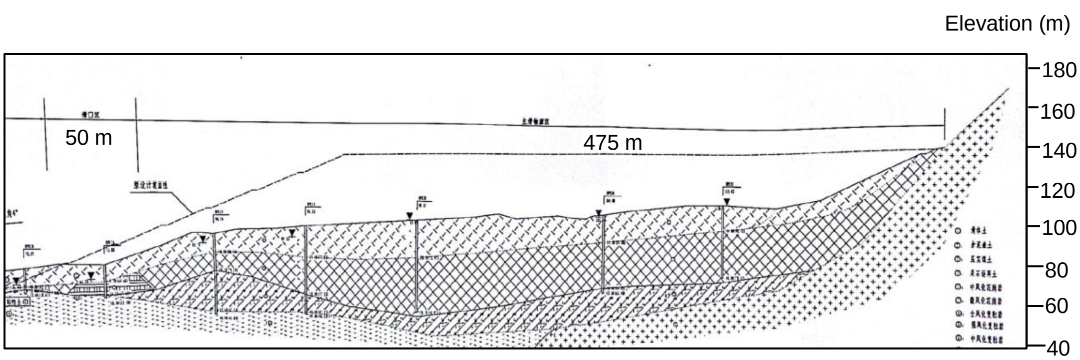

Figure. 2. Geologic profile of the spoil soil slope (after Shenzhen Geotechnical Investigation & Surveying Institute 2016).

before failure (State Council Shenzhen Landslide Investigation Panel (SCSLIP) (2016). According to SCSLIP, the failure of the spoil soil slope was caused by:

(1) No effective drainage. The quarry pond was not drained before filling spoil soils and no drainage blankets were designed inside the fill.

(2) Overloading. The fill height and volume were far larger than the design values so that the slope failed even at a relatively dry condition with only 1 mm of rainfall in the five days before the slope failure.

(3) Improper emergency management. The crest settled significantly and the slope bulged in the early morning of the failure day, showing signs of imminent failure. However the contractor failed to recognize such pre-failure signs. Rather the slope crest was filled up to compensate the settlement, accelerating the slope failure process.

ANALYSIS OF DEBRIS MOVEMENTS AND IMPACT PRESSURES

As shown in Figure 1(b), the proximity of the spoil soil slope endangers a large number of buildings downstream. In fact, the failure of the slope on 20 Dec. 2015 buried or destroyed 33 buildings as shown in Figure 3, including 24 industrial buildings, 3 residential buildings and 6 houses. To investigate the failure mechanisms of these buildings, it is essential to rebuild the landslide debris flow and building impact process. This paper reconstructs the process using numerical modelling.

A digital elevation model of the slope, the terrain and the buildings prior to the slope failure is established using high-resolution satellite data (Figure 4). Three-dimensional (3D) image analysis is also performed to rebuild the 3D images of some of the damaged buildings. Subsequently, the flow process of the landslide material is simulated using a quasi-three-dimensional depth-integrated numerical model, EDDA (Erosion–Deposition Debris flow Analysis) (Chen and Zhang 2015). EDDA simulates debris flow erosion, deposition and induced material property changes. In this model, the flow is driven by the potential energy of the landslide debris. The energy dissipation during the flow process is caused by frictional resistance, viscous energy loss and turbulence and particle interactions:

$$S_f = \frac{\tau_y}{\rho g h} + \frac{K\mu|v|}{8\rho g h^2} + \frac{{n_{td}}^2 |v|^2}{h^{4/3}} \tag{1}$$

where K is a resistance parameter for laminar flows; h is the flow depth; v is the flow velocity; τ_y is the yield stress; μ is the dynamic viscosity; n_{td} is an equivalent Manning coefficient. The determination of τ_y, μ and n_{td} has been described by FLO-2D Software Inc. (2009). The model considers changes in debris flow density, yield stress and dynamic viscosity during the flow process, and is applicable to both dry flows and wet flows. As the soil was wet, particularly the soil at the slip surface was nearly fully

Figure. 3. Buildings that faced the landslide.

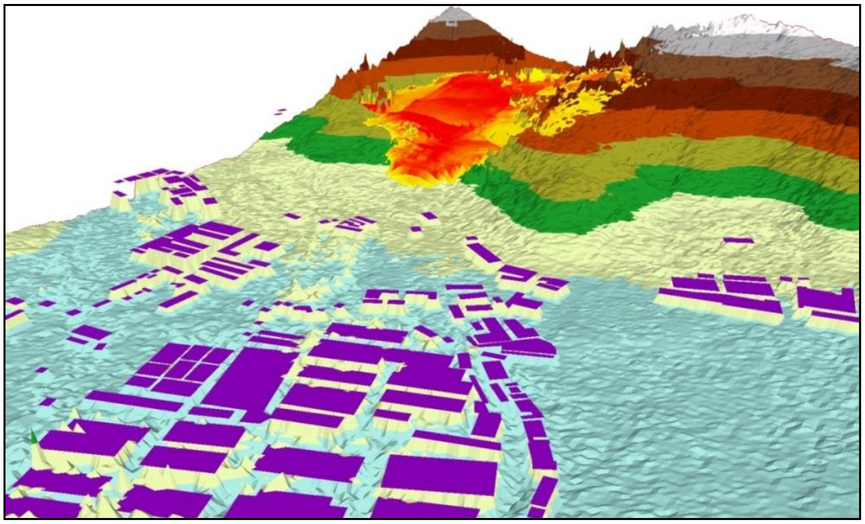

Figure. 4. Setting the flow model: the material above the slip surface is assumed fluid properties at time zero.

saturated, the flow was taken as a wet flow and typical values of the yield stress, dynamic viscosity and Manning's coefficient were assigned, as shown in Table 1. For comparison purposes, a dry flow case is also analyzed, assuming a yield stress based on a deposition angle of 12° as used for coal mining landslides by Hungr (1995). No viscous loss is present in the dry flow.

Table 1. Parameters for landslide debris flow analyses.

Flow type	Porosity	Density (kg/m^3)	Yield stress (kPa)	Dynamic viscosity (mPa.s)	Manning coefficient
Wet flow	0.37	2041	8.3	90*	0.06
Dry flow	0.37	1672	12**	0	0.06

* Water at 20 °C has a viscosity of 1.002 mPa·s.
** Based on Hungr (1995) for coal mine waste.

The soil volume above the slip surface was estimated as 2.4 x 10^6 m^3 based on post-failure field investigations. The model is set based on the filling geometry prior to the slope failure and the slip surface. At time zero, the material above the slip surface is set to flow. Figure 5 shows the impact areas and the maximum flow depths of the wet flow and the dry flow, as well as the actual landslide deposition area.

The debris flow impact force on buildings or any resistance structures may be composed into that from the impact of isolated boulders and that from the impact of the mixture. The impact force by a boulder can be expressed using the simplified Hertz equation:

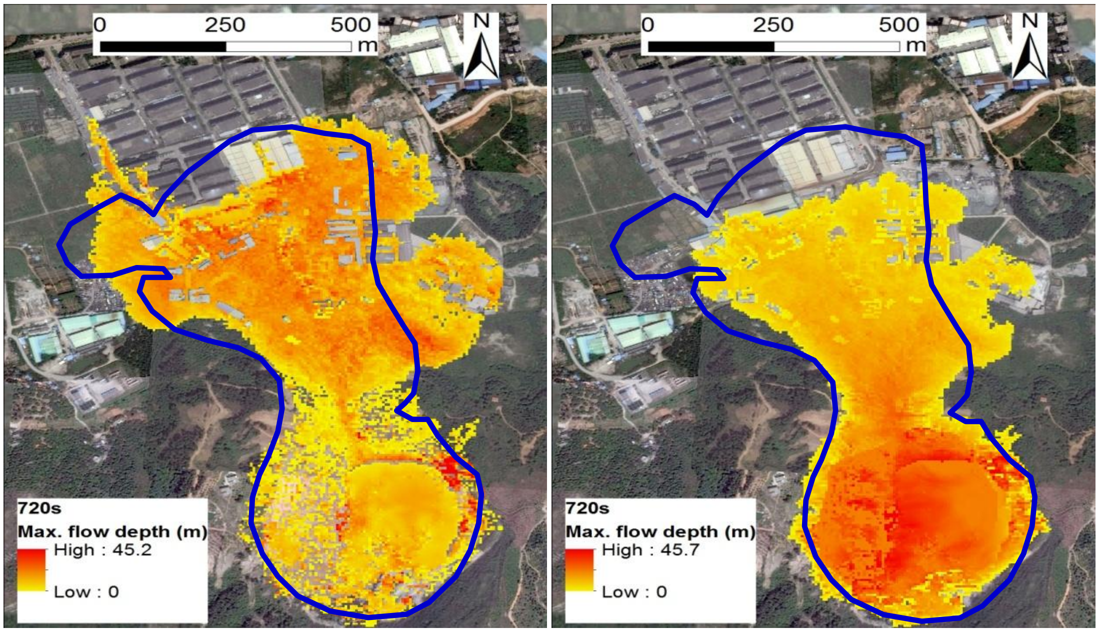

Figure. 5. Impact area and flow depth: (a) wet flow; (b) dry flow.

$$F_b = K_c\, 4000\, v^{1.2}\, r^2 \qquad (2)$$

where F_b is the impact force (kN); r is the radius of the boulder (m); v is the impact velocity normal to the resistance structure (m/s); and K_c is a coefficient accounting for the rigidity of the boulder and the medium and other factors.

The hydrodynamic debris flow impact pressure (Pa) on an idealized two- dimensional rigid barrier is:

$$p_{\mathrm{h}} = \rho v^2 \qquad (3)$$

where ρ is the density of the flow mixture (kg/m^3) and v is the flow velocity normal to the barrier (m/s). The impact pressure will be smaller if the barrier is flexible or if the barrier is not sufficiently large in the direction perpendicular to the impact direction (i.e., for a circular or square barrier). The total debris flow impact force on an obstacle, contributed from both the boulder impact pressure and the hydrodynamic pressure, is often expressed in a simplified form (Lo 2000; Kwan 2012):

$$F = \alpha\, \rho\, v^2 \sin \beta\, h\, w \qquad (4)$$

where F is the impact force (kN); α is the dynamic pressure coefficient considering the geometry and rigidity of the obstacle, boulder impact and other effects; h is the debris thickness (m), w is the debris width (m); and β is the angle between the impact face on the barrier and the debris motion direction. A design α value of 2.5 is recommended by Kwan (2012). In the Shenzhen soil slope case, the spoil soil was primarily silty or gravelly sand, hence the boulder impact effects were not considered and a theoretical α value of 1.0 was used.

Figure 6 shows the distributions of the flow velocity and impact pressure when the front of the flow reaches the building at the northwest corner. The depth-averaged flow velocity is still very high at the distal end of the debris flow, and the maximum depth-averaged impact pressure reaches 900 kPa.

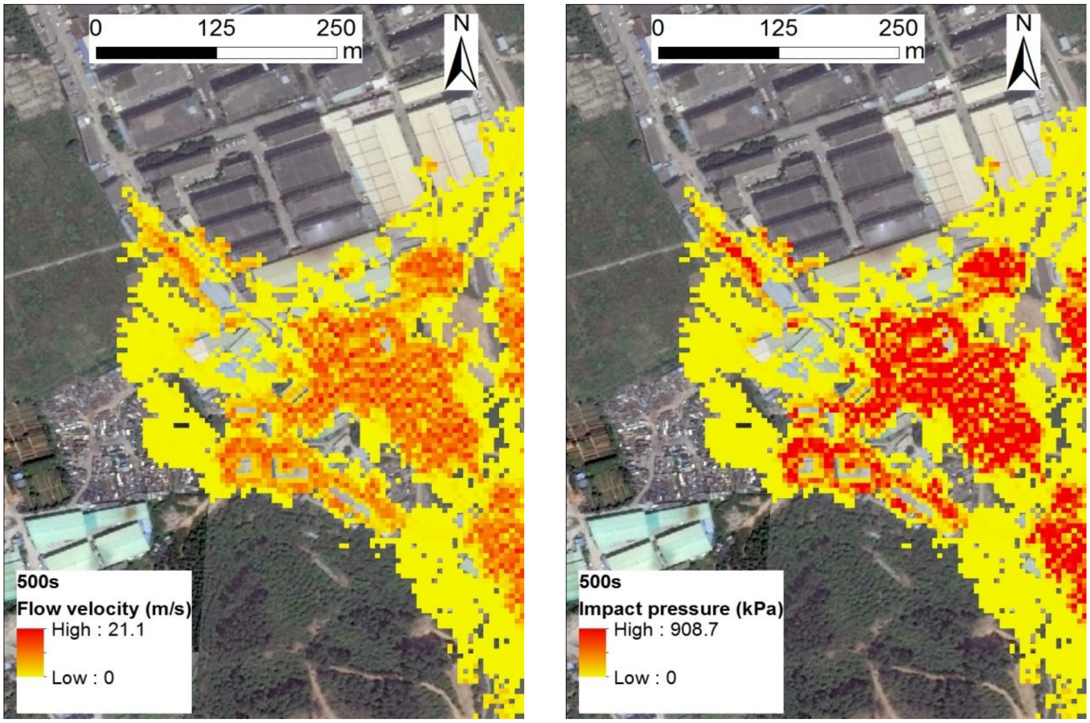

Figure. 6. Distributions of flow depth and impact pressure at northwest corner.

FAILURE OF THE BUILDINGS

The failure of a building due to debris flow impact can be divided into three damage modes:

(1) Burying damage. Burying refers to the debris flow destroying the ground floor external walls and breaking into the building interior. The building is basically intact but loses its intended function.

(2) Structural damage owing to the frontal impact of debris flow. This failure mode can result in the collapse of the entire structure if the main load-bearing components are seriously damaged and unable to resist the loads of the building. Moreover, damage can occur with the failure of only a few structural elements without the collapse of the whole structure.

(3) Damage to building foundations. The building foundations can be damaged due to soil erosion and bearing capacity failure in a sliding or bending mode.

Among the three failure modes, burying damage is the most common in small- scale debris flow events. Frontal impact often causes building collapses by structural damage or foundation damage in areas vulnerable to debris flows, and is thus a key element in engineering design.

In order to simplify the evaluation of the damage to reinforced concrete buildings under debris flow impact, a study of the critical velocity of debris flow and the diameter of large boulders is carried out considering two design scenarios:

(1) When a single column is damaged by a debris flow;

(2) Horizontal shear failure in the shallow foundation due to debris flow impact.

Column Collapse Mechanisms

The failure of a reinforced column can be described by the formation of plastic hinges. A design methodology of column failure analysis due to debris impact has been developed by Zeng *et al.* (2014). When the bending moment in the column caused by a debris flow reaches the ultimate moment of the column (M_u), plastic deformation of the column would be observed and plastic hinges would form at both ends of the column. If the column is a non-load-bearing element, another plastic hinge would also form in the mid-span of the column due to the continuous transfer of external bending moment. Therefore, the failure of the column can be classified into two types:

(1) Two-plastic-hinge collapse at the column ends (Figure 7(a)).

(2) Shear failure at location of direct impact (Figure 7(b)) or at the connections with horizontal structural component (Figure 7(c)).

The development of the plastic hinges is governed by the intensity of debris flow impact, the bearing capacity of the column and the impact condition between the debris flow and the column. The bearing capacity of the column is determined by its cross-sectional area, concrete and reinforcement strengths, the quantity of reinforcements, shear stirrups and the applied axial load in columns.

The study of Chan (2016) shows that the two-plastic hinge mechanism is more likely to occur than the shear failure mechanism. However, the column may fail easily by either mechanism when a boulder of 1 m diameter or larger impacts into the column. In fact, boulder impact is an important column failure mechanism.

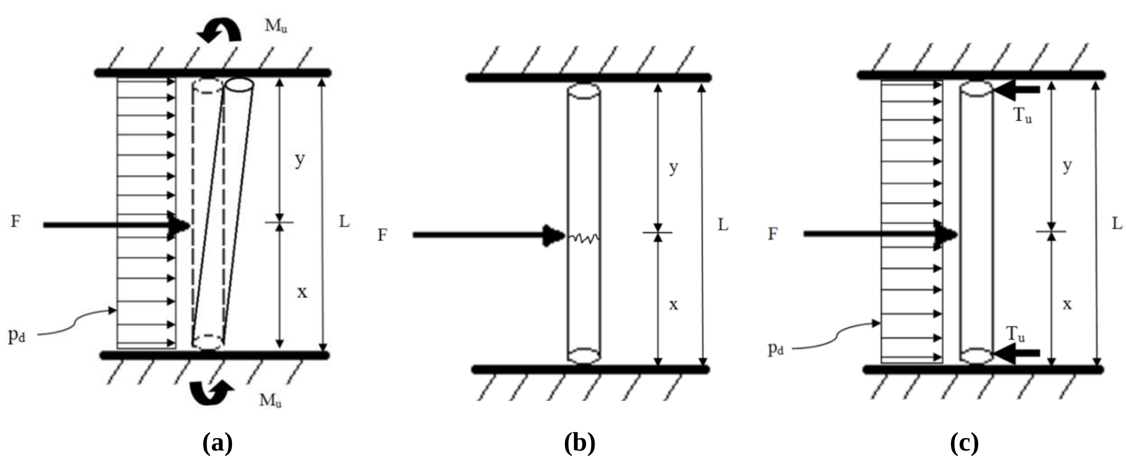

Figure. 7. Column collapse mechanisms under debris flow impact: (a) formation of two plastic hinges due to bending failure; (b) shear failure at impact location; (c) shear failure at end connections.

Foundation Shearing Failure Mechanism

Shallow foundations, where feasible, are generally more economical than deep foundations. Most shallow foundation failures are related to excessive movements rather than loss of load-carrying capacity. Under normal circumstances, the horizontal shear is small and the possibility of sliding is negligible. When stricken by a debris flow, the horizontal impact force brought by the debris flow may lead to sliding failure of the foundation. The friction between the base and the soil provides resistance to sliding, which depends on the axial load on the foundation, the self-weight of the foundation and the friction between the footing and the surrounding soil. The passive resistance of the soil in front of the foundation also plays an important role.

Consider a building on a level ground, supported by shallow foundations and subject to debris flow impact as shown in Figure 8. The impact load is resisted by the passive pressure on back side of the foundation (P_p), and the sliding resistance at the base of the foundation. At limiting equilibrium, the shear capacity, V_{fa}, is:

$$V_{fa} = (P + W_f + W_s)\,\mu + 0.5\,\lambda_a\,W\,D^2 \tag{5}$$

where P is the applied axial load from the column (kN); W_f is the total weight of the footing; W_s is the weight of the soil on the footing (kN), μ is the coefficient of friction between concrete and soil, λ_a is the net result of the active and passive pressures; W is the width of the footing and D is the depth of the footing. The coefficient of friction μ is given by

$$\mu = \tan\,(0.7\,\phi') \tag{6}$$

where ϕ' is the friction angle of soil. The value of μ is normally in the range of 0.3 to 0.7 depending on the soil characteristics (Coduto 2001). The net result of the active and passive pressures λ_a is given by

$$\lambda_a = \gamma\,[\tan^2\left(45° + \frac{\phi'}{2}\right) - \tan^2\left(45° - \frac{\phi'}{2}\right)] \tag{7}$$

where γ is the unit weight of soil. Suppose the building is impacted by n boulders of radius r and the debris mixture, and the boulders travel at the same velocity as the mixture. The critical velocity of the debris flow and the boulder size can be defined when the ultimate bearing resistance V_{fa} is reached:

$$400{,}000\,n\,v^{1.2}r^2 + \rho\,v^2\,W\,h = V_{fa} \tag{8}$$

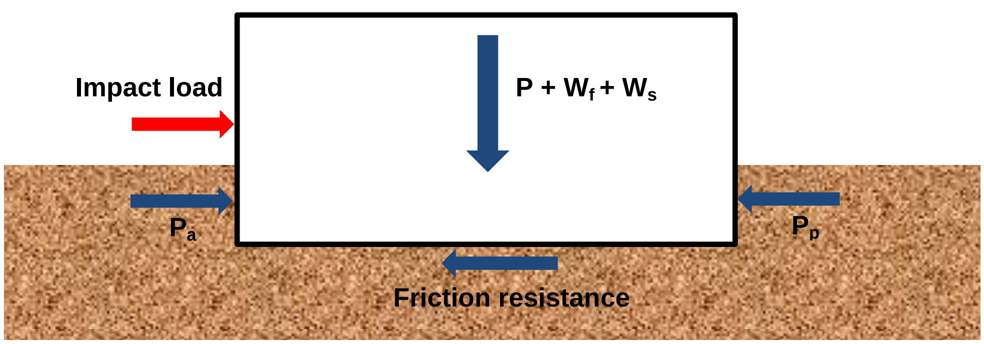

Figure. 8. Stability of building foundation under impact loading.

Foundation Shearing Failure Mechanism in the Shenzhen Spoil Landslide

In the Shenzhen spoil slope case, no large boulders were present as the spoil materials were sorted. Consider a building manhole of 3.0 m and an foundation embedment depth of 1.5 m. The density of the saturated spoil soil is taken as 2041 kg/m^3 and the unit weight of the foundation soil is taken as 20.0 kN/m^3. The friction angle of the completely decomposed granite soil is 30°-35°, corresponding to coefficients of friction between concrete and soil in the range of 0.384 to 0.455.

The vertical load on the foundation is the sum of the self-weight of the foundation and the superstructure load. The superstructure loading may be assumed to be 15 kPa per floor. The vertical pressures on the foundations of 3-, 5- and 10-storey buildings are shown in Table 2. Given the pressures and according to Equations (5) and (8), critical debris flow depth and velocity values are generated as shown in Figure 9.

Table 2. Footing dimensions and characteristics

Building storey	Vertical pressure (kPa)	Foundation width (m)	Foundation self-weight pressure (kPa)	Critical impact velocity at μ = 0.455 and h = 6 m (m/s)
3	45.0	3.0	30.0	3.87
5	75.0	3.0	30.0	4.29
10	150.0	3.0	30.0	5.19

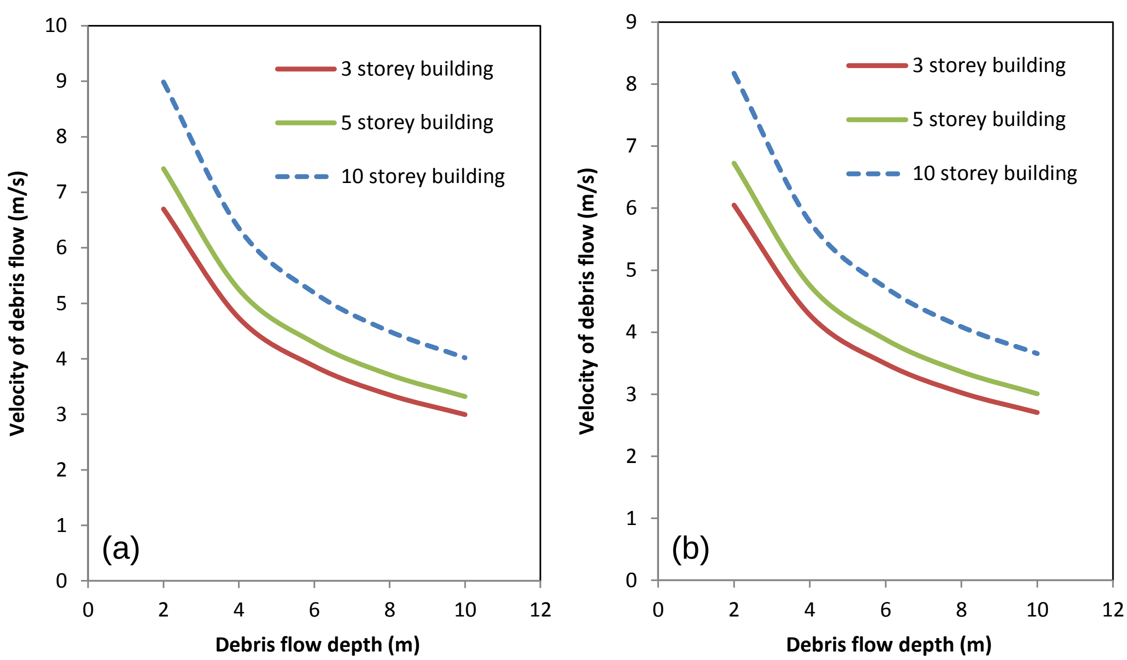

Figure. 9. Critical flow depth and flow velocity when no boulders are involved: (a) ϕ' =35° and μ = 0.455; (b) ϕ' =30° and μ = 0.384.

Figures 3 and 10 show the failure of several buildings at the front of the debris flow in the Shenzhen slope failure case. Two buildings (Buildings I and II in Figure 10(a)) exhibited a typical shear failure mechanism. Building I was sheared into two parts; the first part collapsed at place while the second part was sheared off its original location by about 50 m. The second building was sheared off site completely, and moved by more than 140 m.

The flow velocity in the frontal area is 5-7 m/s and the flow depth was about 6 m. The flow velocities are larger than those required to push over a 5 story building (e.g. 4.29 m/s). The flow velocities when the debris flow just arrived at the buildings in Area B in Figure 1(a) are estimated to be as large as 13 m/s and the flow depths are in the range of 7-13 m. These buildings might have been destroyed instantly.

FIG. 10. Front view of the building that was subject to sliding and overturning failure. (3D images with permission from Prof. Quan Long, https://www. altizure.com/project/567791fe9e0bd5b06ced19ba/model).

SUMMARY AND CONCLUSIONS

A large soil landslide in Shenzhen in Dec. 2015 caused 71 fatalities and destroyed 33 buildings. Detailed forensic investigations were conducted on geotechnical, operational, organizational and risk management aspects. This paper reproduces the landslide flow process and the distributions of debris impact velocity and pressure through numerical modelling, and evaluates the building failure mechanisms. The landslide debris travelled at a high speed of approximately 15 m/s when hitting the buildings, and slowed down as it swept over the building blocks. The flow velocity was still nearly 5 m/s at the distal end of the flow, sufficient to destroy the buildings.

Both the columns and the foundations of a building can fail under debris impact. A column can collapse in a two-plastic-hinge mechanism at the column ends or in a shear failure mechanism at the location of head-on impact or at the connections with horizontal structural component. The two-plastic hinge mechanism is more likely to occur than the shear failure mechanism. However, the column may fail easily by either mechanism when a boulder of 1 m diameter or larger impacts into the column. When a large debris flow impacts into a building, the impact load can be far larger than the horizontal resistance of the foundation; hence sliding failure can take place easily. The two buildings investigated in this paper were pushed off their original locations; one of them experienced a translational movement of approximately 140 m.

ACKNOWLEDGMENT

This research is substantially supported by the Research Grants Council of the Hong Kong SAR (Grants Nos. C6012-15G, T22-603/15N and 16212514). The technical assistance of Mr. K. C. Chan of the Hong Kong University of Science and Technology and Mr. A.G. Li of Shenzhen Geotechnical Investigation & Surveying Institute is also gratefully acknowledged.

REFERENCES

Chan, K.C. (2016). *Study of structure failure mechanisms under debris flow impact*. MSc Thesis, the Hong Kong University of Science and Technology, Hong Kong.

Chen, H.X., and Zhang, L.M. (2015). "EDDA 1.0: integrated simulation of debris flow erosion, deposition and property changes." *Geoscientific Model Development*, 8: 829–844.

Coduto D. (2001). *Foundation design*. Prentice Hall, New Jersey, 259-300.

FLO-2D Software Inc. (2009). *FLO-2D reference manual.* Nutrioso, Arizona, USA.

Fuchs, S., Heiss, K., and Hubl, J. (2007). "Towards an empirical vulnerability function for use in debris flow risk assessment." *Nat. Hazards Earth Syst. Sci.*, 7: 495–506.

Hungr, O. (1995). "A model for the runout analysis of rapid flow slides, debris flows, and avalanches." *Canadian Geotechnical Journal*, 32 (4): 610-623.

Jakob, M., Stein, D., and Ulmi, M. (2012). "Vulnerability of buildings to debris flow impact." *Nat. Hazards*, 60: 241–261.

Kwan, J.S.H. (2012). *Supplementary technical guidance on design of rigid debris-resisting barriers (GEO Report No. 270).* Geotechnical Engineering Office, Hong Kong, 91 p.

Lo, D.O.K. (2000). *Review of natural terrain landslide debris-resisting barrier design (GEO Report No. 104)*. Geotechnical Engineering Office, Hong Kong, 91 p.

Luna, B.Q., Blahut, J., van Westen, C.J., Sterlacchini, S., van Asch, T.W.J., and Akbas, S.O. (2011). "The application of numerical debris flow modelling for the generation of physical vulnerability curves." *Nat. Hazards Earth Syst. Sci.*, 11: 2047–2060.

Shenzhen Geotechnical Investigation & Surveying Institute (2016). *Shenzhen Guangming District landslide emergency geotechnical investigation report*. Shenzhen, China.

State Council Shenzhen Landslide Investigation Panel (2016). *Investigation of the disastrous landslide at Hongao Spoil Soil Reception Site of Shenzhen*. Shenzhen, Guangdong Province, China.

Zeng, C., Cui, P., Su, Z.M., Lei, Y., and Chen, R. (2014). "Failure modes of reinforced concrete columns of buildings under debris flow impact." *Landslides*, 12(3): 561-571.

Coal Ash Disposal Facilities: We have Come a Long Ways

Milind V. Khire, Ph.D., P.E.,[1]

[1]UNC Charlotte, Department of Civil and Environmental Engineering, 9201 University City Blvd., Charlotte, NC 28223, e-mail: mkhire@uncc.edu (Corresponding author)

ABSTRACT

Coal has been used for electrical power generation for decades. While the use of coal as a fuel for power generation has decreased in the U.S., it is growing in India and globally. There are several hundred unlined coal ash ponds and landfills in the U.S. due to the old regulations that had coal ash exempt from regulations which other streams of waste had to comply. However, coal ash spills from unlined ponds have had profound impact on the regulations in the U.S. While most developing countries currently do not have enforced regulations on air and water pollution from coal combustion plants, the case studies presented in this paper show that the human health and ecological cost is orders of magnitude greater after a spill compared to the cost of enforcing preventive measures. The new regulations in the U.S. have resulted in excavation and removal of unlined coal ash or in-situ capping. These heavy earth work activities have provided opportunities for research related to wet ash that has low strength to improve the strength and dewater or stabilize the moisture using innovative technics such as moisture absorbing polymers or electro-osmotically enhanced dewatering.

INTRODUCTION

Coal and oil lead the global sources of fuel used for energy production (at about 30% each). Coal while considered a “dirty” fuel due to the greenhouse gas (GHG) emissions and trace metals that it leaves behind in the combustion residue, it is the cheapest and easier to transport. Hence it is a popular fuel in China, U.S., and India, the three largest consumers of coal. The growth in the consumption of coal in China is tapering off as the country invests in alternative forms of energy. The consumption of coal in the U.S. has declined significantly in the last few years primarily due to relatively cheap natural gas from the fracking technology and stringent regulations for managing coal energy plants driving the cost up for energy from coal.

While China’s consumption of coal grew only by 17% from 2009 to 2014, due to strong economic growth, India’s consumption of coal increased by 44% to reach 360 million tons of oil equivalent. In addition to India, countries in the Asian continent are also increasing coal consumption, offsetting declines in Europe and USA. During the period 2009-2014, coal consumption rose by 83.3% in Indonesia, 75.4% in the Philippines and 78.5% in Vietnam (Euro monitor 2015).

Coal combustion is on a steady rise across the globe. Hence, it is vital to put in perspective the lessons learned from air and surface water and ground water pollution disasters. The developed countries made significant changes in the flue gas scrubbing system in the last few decades, which has significantly cleaned up the air emissions. However, the flue gas constituents those have been removed have moved to the fly ash and bottom ash depending on the air cleaning technology used by the plant. Hence, in the developed countries, the challenges lie in protecting surface and ground waters. In the developing countries including South Africa, not all coal energy plants use state-of-the-art scrubbing system to clean the flue gas and coal ash is seldom landfilled in lined facilities. In U.S., the new regulations came in effect in 2015 that will gradually move coal ash disposal from unlined ponds to lined landfills to protect the surface and ground waters. Developing countries, while behind on that front, will need to take actions to protect the air and waters.

This paper will focus on the two most recent key environmental disasters that changed the coal combustion product (CCP) regulations in the U.S. In addition, this paper will discuss the new CCP regulations and technological challenges and what research is in progress to make the transition to implementing new regulations cost effective and implementable on the tight schedule.

CCP GENERATION AND UTILIZATION

While CCP composition varies across coal power plants depending on the mineralogical composition of the coal, and the flue gas cleaning technology used, in the U.S., CCP contains the following fractions:

1. Fly ash: 80%;
2. Bottom ash: 15%; and
3. Boiler slag and flue gas desulfurization (FGD) residues such as gypsum: 5%

Figure 1 shows the global CCP production based on Heidrich et al. (2013). China, U.S., and India lead the production at approximately 300, 120, and 110 million metric tons, respectively. Figure 2, shows the percent of the produced CCP that is beneficially utilized. The percent utilizations in the U.S. and India are about 40% and 15%, respectively. Thus, remaining unutilized CCPs have been disposed in mostly unlined wet ponds or dry basins. These unlined facilities impose a long-term threat to the surface and ground waters. The risk is compounded due to oversight in routine inspections, structural and hydraulic maintenance of levees and storm water management system, and threat from natural hazards such as earthquakes.

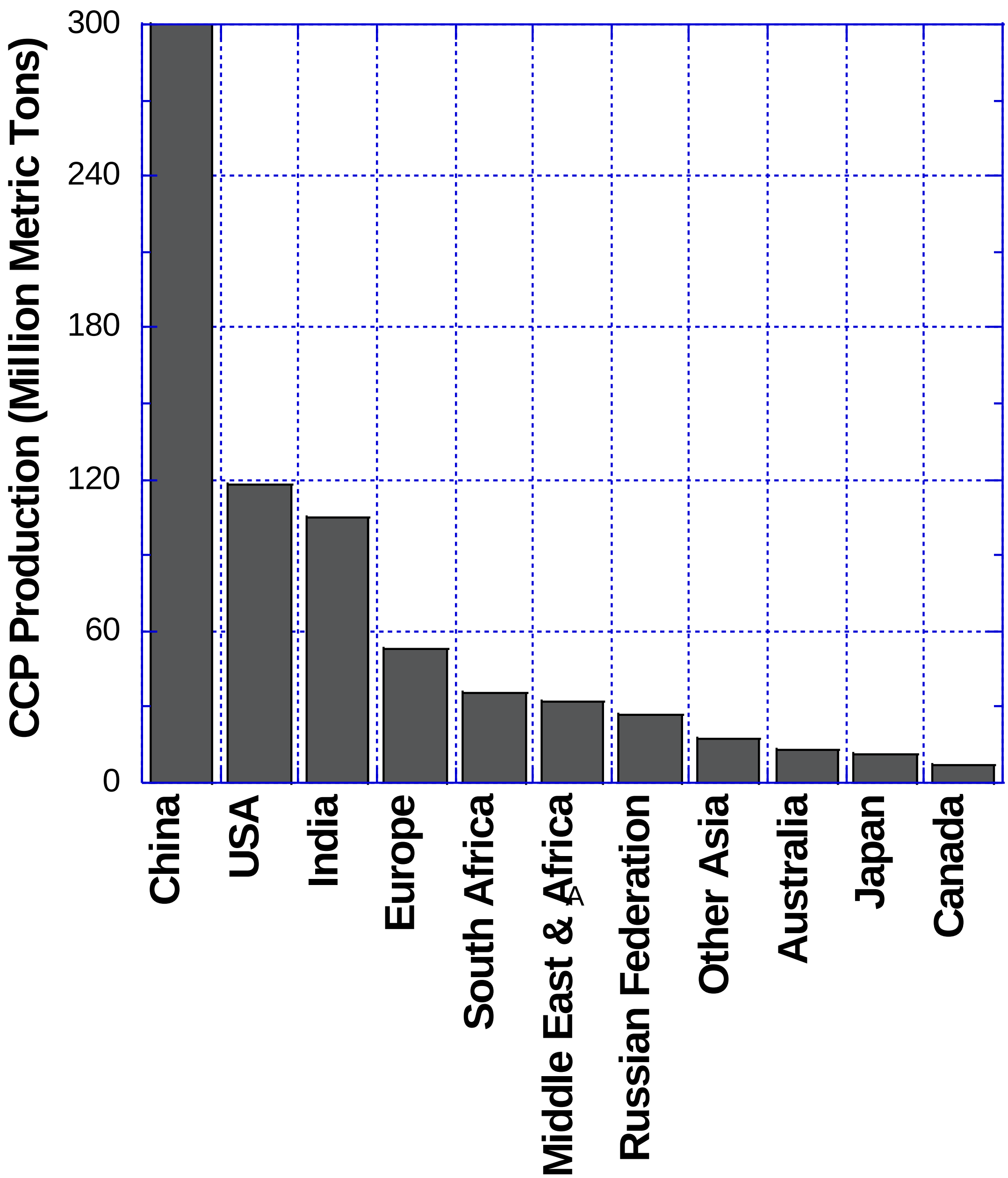

Figure 1. Global CCP Production

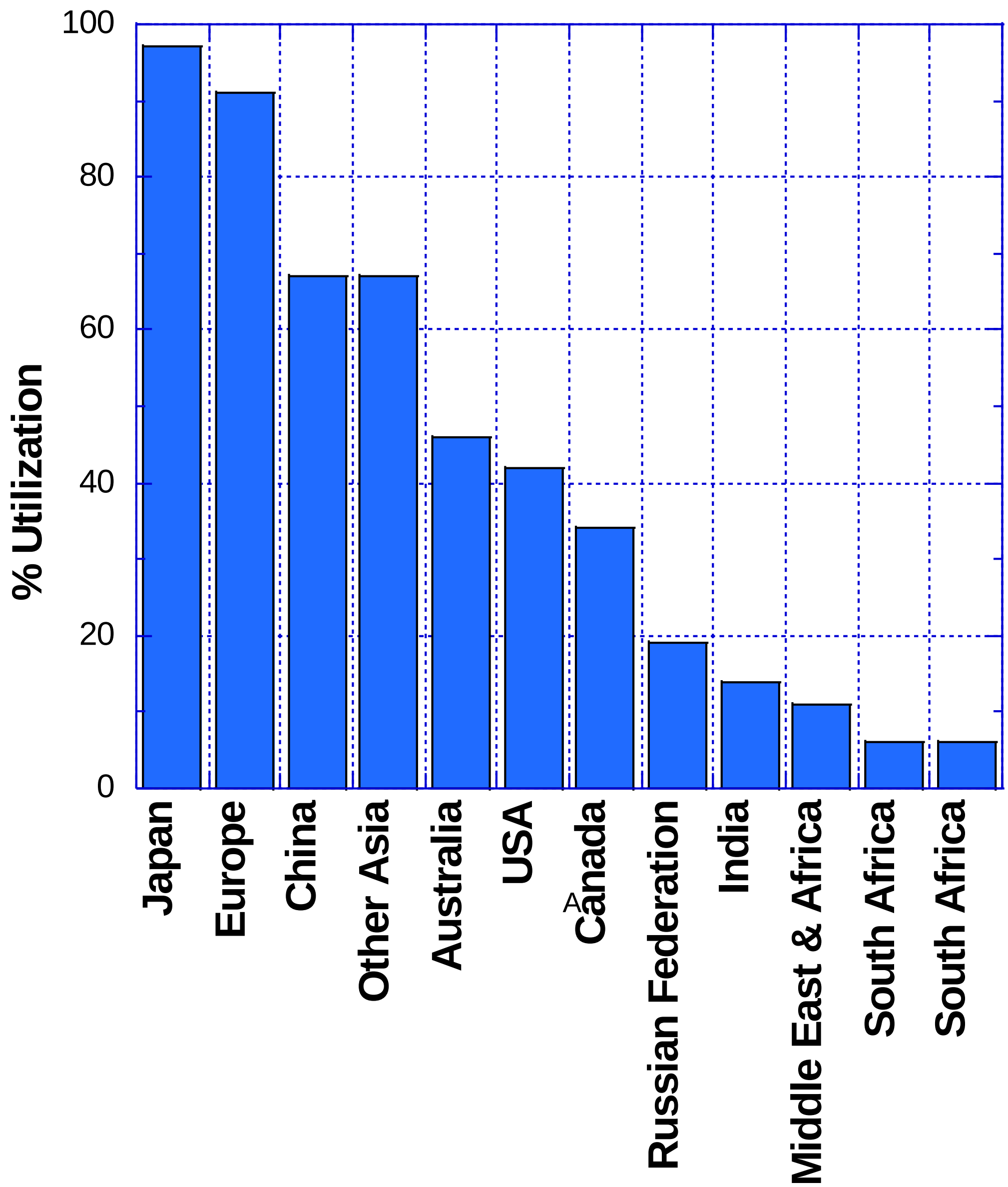

Figure 2. Global CCP utilization

CCP ENVIRONMENTAL ACCIDENTS

In the U.S. history, there have been three major reported accidents:

1. 2005: Pennsylvania Power & Light, Martins Creek Station, 380,000 m^3 of fly ash leaked into Delaware River;
2. 2008: Tennessee Valley Authority (TVA), Kingston Plant, 4 million m^3 of ash leaked into Emory and Clinch Rivers; and
3. 2014: Duke Energy, Dan River Steam Station, 35,000 metric tons of ash spilled into the Dan River.

In response to the TVA spill, the U.S. Environmental Protection Agency proposed final CCR rules in 2010 which impact surface impoundments at 480 coal-fired power plants in the U.S. (Daniels 2016). Similarly, the 2014 Dan River spill prompted the State of North Carolina (where Dan River Plant is located) to pass the Coal Ash Management Act (CAMA) in 2014. This is a unique situation where the state regulatory agency to initiate such counter measures to make sure this does not happen again within the state of North Carolina. Similar to EPA's CCR rules, CAMA sets out comprehensive requirements that dictate ash disposal, beneficial utilization, to happen in time frames that are shorter than EPA's CCR rules (Daniels 2016).

Dan River Coal Ash Spill (2014)

A 1.2 m diameter reinforced concrete pipe underlying a coal ash disposal impoundment at Duke Energy's Dan River Plant collapsed in February 2014. This pipe was there to carry the storm water up gradient of the impoundment to the Dan River located downgradient. When the pipe collapsed, the wet ash entered the pipe and resulted in a massive spill of approximately 35,000 metric tons of coal ash into the Dan River at Eden, North Carolina, U.S.A. Fig. 3 shows a schematic of the coal ash impoundment, the location of the broken pipe, and the river.

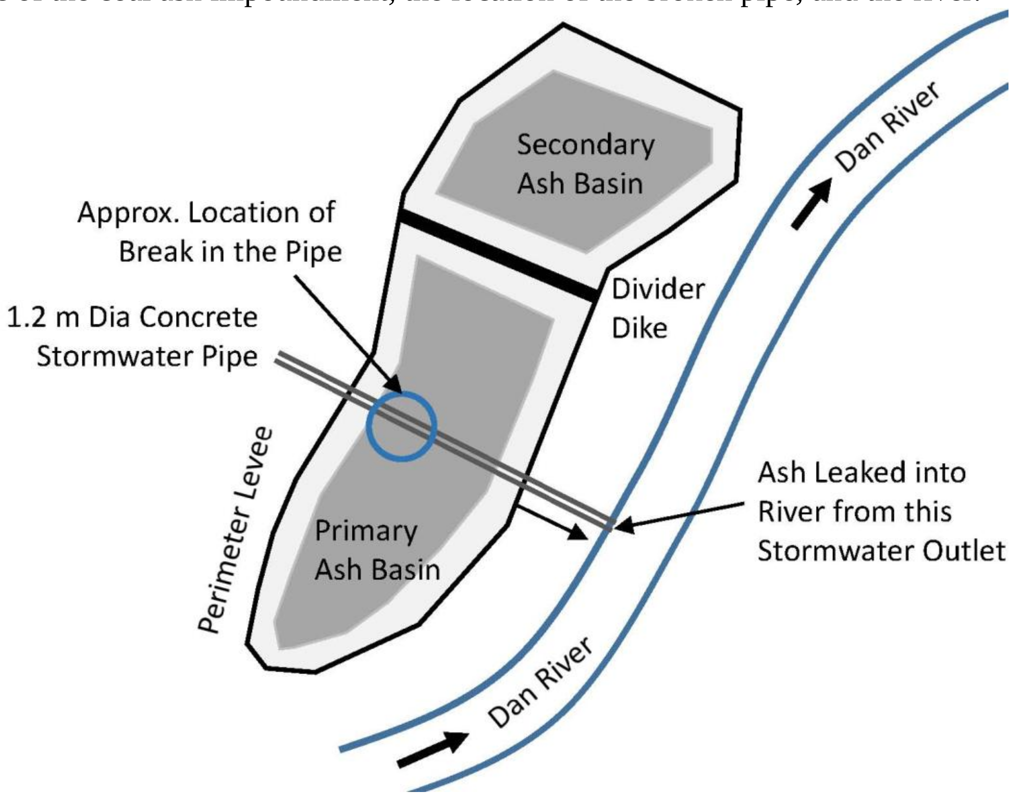

Figure 3. Schematic of Dan River CCP Spill in North Carolina, USA (modified version of schematic obtained from Duke Energy)

The spill coated the beds and the sides of the river channel with several-meter-thick ash deposits (Lemly 2015). It changed the water chemistry of the downstream segment of the river due to the release of heavy metals such as arsenic, selenium, manganese, chromium, and copper.

Lemly (2015) estimates about $300 million (U.S.) for short term impacts from this spill based on many factors including esthetics, ecological, recreational, and human health, and consumptive use. The author postulates that the costs will only increase due to the long-term nature of cleanup to bring the environment back to where it was before the spill. While the estimated damage amount may not be accurate because of the assumptions built in the analysis, it is clear than the cost to fix the environment after the spill is many orders more than the cost of preventive measures.

The volume of ash and porewater, and its rapid release, overwhelmed the river's natural flow and changed the chemistry of the entire flow of the river (Lemly 2015). Duke Energy temporarily fixed the leak by filling the leaky pipe with sand bags and rock and pumping water out of the pipe. The long-term solution implemented was to excavate the coal ash from the fill area and remove the pipe permanently and re-route the storm water. While much of the coal ash that went into the river was not captured due to the relatively high flow rates in the river transporting the ash over 110 km distance, hydraulic dredging was used to remove some of the ash that went into the river.

The key lessons learned from this spill are that any pipes that penetrate through a waste fill are pathways to carry the waste and pore fluids and it is just a matter of time when the physical integrity of these pipes is threatened. Hence, plugging or removal of the pipes and rerouting them around the waste is a better practice. If it is not possible to do that, routine inspections (using a video cam depending on the access) are critical to assess changes in the physical integrity of the pipe. However, it is often not possible to predict the rupture of an aging below grade pipe.

TVA Coal Ash Spill (2008)

A dike supporting a coal ash dredge fill of Tennessee Valley Authority's (TVA) coal fired power plant located in Kingston, Tennessee ruptured in 2008. It contained stored wet coal ash in an 84-acre containment area which leaked 4.2 million cubic meters of wet ash into the Emory river. This wet coal ash spill covered about 300 acres downstream and damaged waterways and personal property. This spill to date is considered the largest ash disaster in the U.S. history. The containment area has an average height of 20 m and is surrounded by a perimeter levee having an average height of 20 m. Leaks were detected in the levee few years prior to the rupture in 2008. The spill emptied 66% of the wet ash from the containment area. While the location of the spill is in a rural area, it damaged about 40 homes, power lines, water main, gas main, and downed many trees.

Ruhl et al. (2009) sampled the ash, sediments, and water from the upstream and downstream locations of the river and compared the concentrations to the background levels. The coal ash contained many heavy metals that were at higher concentrations than the background soil. However, strontium and arsenic levels in the ash were far great compared to the background soil. The authors also found a two-fold increase in mercury levels in the sediments downstream from the spill. River water samples had elevated heavy metal concentrations, especially arsenic. Shallow groundwater did not show any impacts in 2009. Thus, most impacts were confined to sediments and surface waters. All aquatic life near the plant downstream from the spill was buried and killed. Over a two-year period after the spill, almost 90% of the washed ash was dredged and removed from the river.

Regulatory Shift

Daniels (2016) point out that CCPs were regulated as per resource conservation and recovery act (RCRA) of 1976 in the U.S. However, CCPs were exempted as a special waste by amendment. Such amendments were possible when there was no history of major environmental disasters. Often the purpose of such exemptions was to reduce operational cost to the industry and consumers. However, in light of the coal ash disasters, to minimize the potential for such catastrophic environmental failures, the U.S. Environmental Protection Agency (EPA) approved final rules that establish a comprehensive set of requirements for the disposal of CCPs or coal ash in landfills and surface impoundments. These requirements have been finalized under the solid waste provisions, subtitle D, of the Resource Conservation and Recovery Act (RCRA). These regulations protect air and water. The rule establishes requirements for existing and new CCR landfills, surface impoundments and lateral expansion of an existing unit. The key requirements are focused on: (1) structural integrity; and (2) groundwater monitoring and corrective action. Because unlined CCP ponds or CCP disposal facilities leach CCP constituents to groundwater, the CCP Rules require comprehensive groundwater risk and hazard analysis. This requires simulating percolation of CCP leachate into the groundwater and predicting concentrations of CCP leachate constituents at the property boundary. If these concentrations exceed the maximum contaminant levels (MCLs) established for groundwater, corrective action is required.

RESEARCH NEEDS

The reported coal ash spills in the U.S. have triggered a strict schedule for coal energy plants to close the unlined ash ponds. Often these ash ponds contain saturated coal ash and handling the ash during excavation or grading is a challenge. The ash usually falls in the gradation of a silty soil. It has a much lower specific gravity than inorganic natural soils and relatively low strength when saturated. Often it weakens due to liquefaction when heavy equipment creates vibrations. Sinking of heavy equipment due to low strength is a real concern and often requires special technologies to dewater the ash in relatively short periods of time to allow the heavy equipment to move on the ash. It is also a need to classify the ash to predict at what water content it acts like a liquid. Traditional Atterberg limits tests used for natural soils do not seem to work well in predicting the behavior of coal fly ash. Thus, developing new dewatering technologies that would efficiently dewater the finer matrix of coal ash impoundments will be a valuable contribution. Alternatively, technologies that use moisture absorbing polymers which solidify the water fraction by reaction could be used to reduce the effect of moisture on the strength and handling of the ash in the field and eliminate the need to treat the pore water if dewatered. Thus, while the coal ash accidents had local environmental impacts, these disasters have resulted in good regulations and opportunities to do research so the industry can effectively implement the regulations.

ACKNOWLEDGEMENTS

The University of North Carolina at Charlotte, Department of Civil & Environmental Engineering provided the funding for the travel to Bengaluru, India to present this paper.

REFERENCES

Daniels, J. (2016). "Coal Ash and Groundwater: Past, Present, and Future Implications of Regulation," *Environmental Law and Policy Review*, 40,2, 535-555.

Duke Energy, http://www.coalashchronicles.com/tag/dan-river (Accessed 2016)

Euro monitor (2015). http://blog.euromonitor.com/2015/12/in-focus-which-countries-are-driving-global-coal-consumption-growth.html (Accessed 2016).

Heidrich, C. Feuerborn, H-C., and Weir, A. (2013). "Coal Combustion products: A Global Perspective," World of Coal Ash Conference, Lexington, KY, USA, April 22-25.

Lemly, D. (2015). "Damage Cost of the Dan River Coal Ash Spill," *Environmental Pollution*, 197, 55-61.

Ruhl, L., Vengosh, A., Dwyer, G., Kim, H-L., Deonarine, A., Bergin, M., and Kravchenko, J. (2009). "Survey of the Potential Environmental and Health Impacts in the Immediate Aftermath of the Coal Ash Spill in Kingston, Tennessee," Environmental Science & Technology, 43, 16, 6326-33.

Challenge in Geotechnical Engineering for Methane hydrate production in deep sea bed

Masayuki Hyodo[1], Yang Wu[2] and Shintaro Kajiyama[3]

[1] Graduate School of Sciences and Technology for Innovation, Yamaguchi University,
Email: hyodo@yamaguchi-u.ac.jp
[2] Graduate School of Sciences and Technology for Innovation, Yamaguchi University,
Email: yangwuuu0226@hotmail.com
[3] Graduate School of Science and Engineering, Yamaguchi University,
Email: u002wf@yamaguchi-u.ac.jp

ABSTRACT

Methane gas hydrates are clathrate solid constituted of methane gas tripped within the hydrogen-bonded of water molecules and expected to be a promising future energy source. The methane hydrate reservoirs are located in the deep sea bed at over 1000 m in sea depth. The investigation conducted in the Nankai Trough, Japan revealed that methane hydrate existed in the pore space in the sand and clay stratified layer. Well understanding the mechanical and dissociation properties of the methane hydrate-bearing sediments are significantly important to extract the methane gas from the marine ground. A series of triaxial compression tests were performed on the host sands containing different amounts of fines content and prepared with the similar grading curves and mineralogical compositions to those of the seabed sediment in Nankai Trough. The test results showed that the presence of methane hydrate increased the shear strength and stiffness and promoted the dilation behaviour. The normalized deviatoric stress of methane hydrate-bearing sands increased with the rise in methane hydrate saturation and fines content. Such increasing tendency became obvious as the methane hydrate saturation exceeding around 30%. An innovative high-pressure low-temperature plane strain testing apparatus equipped with an observation window was also employed to examine both the global stress-strain response and local deformation of methane hydrate-bearing granular materials in triaxial shearing test and dissociation test. The maximum shear strain of methane hydrate-bearing granular material was mostly concentrated near the shear band and the shear band became narrower once the methane hydrate was formatted. An elasto-plastic constitutive model with the capacity of predicting the shear strength and deformation behaviour of methane hydrate-bearing sands over a wide range of methane hydrate saturations and confining pressures had been proposed.

KEYWORDS: Methane hydrate-bearing sands, High pressure, Temperature, Dissociation behaviour, Local deformation, Constitutive model

INTRODUCTION

Methane hydrate (MH) is a solid compound in which a large amount of methane is trapped within a crystalline structure of water, forming a solid similar to ice. It is known to exist in a stable condition under certain temperature and pressure conditions. Its existence has been confirmed in permafrost layers and in deep ocean floors. Recently there has been much research on MH in the deep seabed as a developable material. MH is believed to exist in various forms, such as massive structures within muddy layers or at the surface of deep seabed, or embedded within the pores of sandy layers (Waite, *et al*. 2009). In Japan, an MH rich layer was found in the Nankai Trough and production tests was performed in March 2013 (Japan Oil, Gas and Metals National Corporation, 2013). MH in the deep sea bed can exist at certain water pressure and temperature conditions. It exists in the pore space of the sandy sediments, bonding the grain particles. The MH rich layer is located around 100 m-300 m beneath the seabed, in deep seas with depths of over 1000m. As MH is formed in such uncemented sandy sediments, there are many geotechnical-engineering related problems in order to confirm the stability of the production well and the marine grounds in its vicinity (Yamamoto, 2009).

Currently, the method proposed for abstracting methane in the Nankai Trough is by drilling a rig into the MH-rich layer, and heating, depressurizing, or inserting hydrate inhibitors, causing the dissociation of MH into methane and water after which the gas could be collected (Yamamoto, 2009). Among them the depressurization method is going to be introduced as the most suitable production method. Using these methods, the solid MH existing in the pores within the soil is transformed into gas for collection; in the process, complex physical events, such as changes in the soil structure and thermal conductivity, pore fluid and gas migration, and other complicated phenomena require further consideration. It is predicted that a combination of such phenomena could cause consolidation and shear deformation of the ground due to changes in the effective stress and decrease in soil particle strength. Therefore, it is important to investigate the mechanical and dissociation properties of MH-bearing sediments, for safe and economical exploitation.

A series of mechanical tests were performed on MH bearing sediments with various host sands containing different amounts of fines content and prepared with the similar grading curves and mineralogical compositions to those of the seabed sediment in Nankai Trough using a temperature-controlled high pressure triaxial shear testing apparatus. An innovative high-pressure low-temperature plane strain testing apparatus equipped with an observation window was also developed for visualizing the deformation of methane hydrate bearing sand due to methane hydrate production. Using this testing apparatus, plane strain compression tests and dissociation tests induced by depressurization method were performed with the measurement of localized deformation. On the basis of the experimental results, an elastoplastic constitutive model for methane hydrate-bearing sands was developed using the sub-loading theory. The bonding effect due to the cementation by methane hydrate was introduced into the model. The simulation values agree well with the measured results for the shear behaviour of methane-hydrate bearing sand in triaxial test at a wide range of confining pressure and methane hydrate saturation.

HISTORY OF MECHANICAL TESTS ON MH BEARING SEDIMENTS

Based on the author's experiences of triaxial testing of sand specimens (Yasufuku, *et al*., 1991), the investigation of the mechanical behavior of MH- bearing sediments was started using a triaxial compression test apparatus equipped with a high-pressure cell inside a freezer by the authors in 1996. Unconsolidated and undrained triaxial compression tests were performed on specimens consisting of granulated MH and sand prepared by mixing and compacting mixture of MH powder and sand to investigate the effects of temperature and confining pressure on the strength characteristics of MH and sand mixtures (Hyodo, *et al*., 2002; 2005). The development of a testing apparatus which could more accurately reproduce the deep seabed temperature and pressure conditions was initiated and a triaxial compression testing apparatus was developed that could simulate predicted temperature changes in-situ and during the MH production process. The testing apparatus could apply high back (pore water) pressure and confining pressure corresponding to those existing in-situ. The dissociation of MH by heating and depressurization method could be reproduced and the investigation on the deformation behaviour of MH-bearing sands during the MH dissociation process became possible (Hyodo, *et al*., 2007, 2008, 2013; Yoneda, *et al*., 2007). Using this apparatus, methane gas could be injected into moist sand within the cell to produce MH dispersed around the soil particles which was similar to the process of methane hydrate formation in deep seabed conditions. The authors performed consolidated drained triaxial compression tests on MH-bearing sediments under a similar physical environment to that found in-situ and an empirical equation for predicting strength of MH-bearing sediments associated with temperature, water pressure and MH saturation has been proposed (Yoneda, *et al*., 2007; Hyodo, 2013). K_0 consolidated drained triaxial compression tests were also performed on undisturbed sediments from the Nankai Trough. These showed the mechanical properties of undisturbed sediments and artificially prepared sediments were quite similar (Yoneda, *et al*., 2010).

Miyazaki, et al. (2007) performed triaxial compression tests with varying strain rates to investigate the shear strength characteristics and shear rate dependency for medium and large-strain ranges. They performed triaxial compression tests on dense specimens with varying confining pressures, and an empirical equation for predicting shear strength of MH-bearing sediments related to confining pressure was proposed. In addition, employing a comparatively low pressure to generate hydrate from THF (tetrahydratefuran), Yun, *et al*. (2005) formed hydrate within sand, silt and kaolinite using THF-saturated water and carried out compression tests on hydrate-bearing sand with 0 to 100 % of hydrate saturation. The results indicated that the increase in shear strength was small for THF-hydrate saturation ratios less than 40% but a marked increase in shear strength was observed when the saturation ratios exceeded 40%.

For the consideration of deformation due to MH production, a one dimensional cylinder type experiment is commonly used. Sakamoto *et al*. (2008) used the depressurization method to dissociate the hydrate in MH-bearing sand and based on the observed one-dimensional compression behavior, they examined the changes in the seepage characteristics. Lee *et al*. (2010) also investigated volume change of sediments by hydrate formation and dissociation within sand, silt and kaolinite using THF under various confining pressures. These results are valuable for predicting settlement simply due to depressurization.

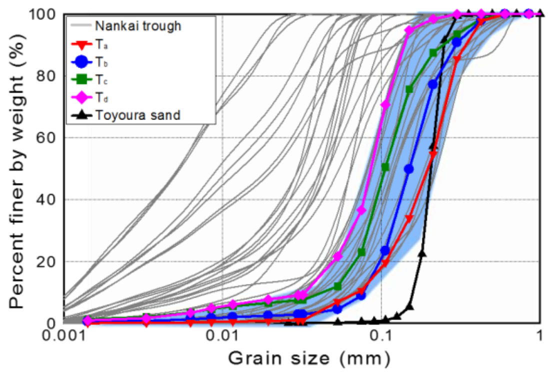

Figure 1. Grain size distribution curves (Nankai Trough and artificial samples)

A high-pressure low-temperature plane strain testing apparatus was developed by the authors (Yoneda, *et al*. 2013) for visualizing the deformation of methane hydrate-bearing sand due to methane hydrate production. Using this testing apparatus, plane strain compression tests were performed on MH-bearing sands with localized deformation measurements. Localized shear strain and volumetric strain were monitored during the compression tests. The contours of the maximum shear strain and the volumetric strain at each strain level, seen on the intermediate principal stress plane of each specimen, defined for the initial dimensions of each specimen. The shear bands appeared when strain softening occurred. Thus, it seems that the stresses are concentrated inside the shear band.

To investigate the intact strength of natural gas hydrate-bearing sediments in the eastern Nankai Trough pressure coring using a hybrid pressure coring system (hybrid-PCS) was undertaken in 2012. Recovered pressure cores were subsampled using the pressure core analysis and transfer system (PCATS) and subsequently transported to the laboratory within hydrate stability pressure temperature conditions to avoid dissociation of natural gas hydrates. Then the triaxial compression shear tests were performed on natural gas hydrate-bearing sediments at in situ pressures without any hydrate dissociation using a transparent acrylic cell triaxial testing system (TACTT system) (Yoneda, *et al*., 2015).

MATERIALS USED IN EXPERIMENTS

Grain size distribution curves for samples from Nankai Trough and the reconstituted granualar materials prepared in this study are shown in Fig. 1. The sediments in Nankai Trough's seabed soil constituted turbidite and show stratified layers with wide grain distribution curves, with contents ranging from sand to clay. The grain size distribution for the MH rich layer in Nankai Trough is shown in grey. It is the sandy sediments containing fines content. In order to simulate the grain size distribution and mineralogical composition of this layer, silica sand, kaolin and mica were mixed and four kinds of simulated sands T_a, T_b, T_c, T_d were prepared as host sands. The fines content increases in order of T_b, T_a, T_c, T_d and the mean particle size decreases in order of T_a, T_b, T_c, T_d.

TESTING EQUIPMENT AND SAMPLE PREPARATION

Triaxial testing apparatus

The temperature-controlled high pressure triaxial testing apparatus was developed such that the back pressure and confining pressure could be controlled under various temperature and high pressure conditions in order to examine the mechanical behaviour of MH-bearing sand specimens under deep seabed stress and temperature conditions (Hyodo, *et al.*, 2007, 2008, 2013). The maximum permissible load was 200 kN. To remove the influence of piston friction, a cylindrical-shaped loading cell that was not affected by temperature and pressure was set up in the cell pressure could be increased up to 30 MPa. To reproduce back pressure associated with this high pressure condition, a syringe pump was installed. By using incompressible solution in the cylinder, the measurement of volume change of the specimen was enabled by calculating the amount of penetration of the piston in the cylinder. To measure the volumetric change of partially saturated soil during dissociation, an inner cell was installed, with a mechanism similar to the syringe pump for back pressure. Temperature was controlled by a system which circulated the cell fluid from a low temperature water tank set up outside allowing the temperature to be adjusted from -35^{o}C to +50^{o}C.

Specimen Preparation

Based on visual observation of the undisturbed core samples obtained from the Nankai Trough (Suzuki, 2006), it is believed that MH in-situ is buried within the pores between grains of the sand. Based on this, MH-bearing sand was artificially produced using the grain size distribution curves of the undisturbed core sample (Suzuki, 2009) and Toyoura sand was also chosen as the host material for a comparison. First, the amount of water for the target MH saturation was mixed with sand whose volume corresponded to a target density. The moist soil was placed in 15 layers in a mold measuring 30 mm in diameter and 60 mm high, with each layer compacted by a tamper 40 times. In order make the specimen to stand by itself, the mold containing the sand was placed in a freezer. The frozen specimen was then removed from the mold and placed on the pedestal, and the membrane was installed. Because the specimens in the tests were subjected to low temperature and high pressure, rubber membranes conventionally used in triaxial tests were avoided. Instead, silicon-type membranes were used because of their flexibility under low temperature/high pressure conditions and butyl rubber was used in long term tests, such as MH dissociation because silicone is to some degree permeable to methane gas.

Generation of MH and Experimental Procedure

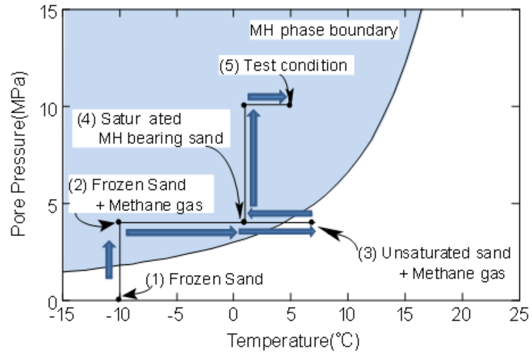

Figure 2. State paths for pressure and temperature to produce MH-bearing sand

After forming the specimen, it was subjected to a series of processes under specific temperatures and pressures, as depicted in Figure 2. First of all, the frozen specimen (1) was thawed to room temperature inside the triaxial cell (2). Then, the back pressure was gradually increased to 4MPa while methane was injected into the specimen (c) by filling the pores of the specimen with methane. (3) To smoothly form the methane hydrate in specimen, the temperature was increased to the outside of methane hydrate phase boundary and terminally reduced to 1.0 MPa where the MH was stable. (4) The pore pressure and temperature were kept constant in the entire hydrate formation process and this procedure last 24 hours to 36 hours according to the property of host sand. By keeping the gas pressure constant in the connection between the specimen and the syringe pump and by observing the amount of gas flowing at various times, the transformation of water within the pores into hydrate was judged to be complete if there was no marked change in the amount of gas, as indicated in the figure.

After the hydrate was generated, water under constant pressure was allowed to infiltrate the specimen. Then, the pore water pressure was applied and the temperature was adjusted to the prescribed test condition (5). While keeping the pressure constant, consolidation was carried out until the specified effective stress was reached and shearing was conducted with a strain rate of 0.1%/min. After shearing, the temperature in the specimen was increased and MH dissociated; the amount of gas was measured using the gas mass flow meter. The amount of gas measured was then converted into MH saturation, (assuming the density of MH was 0.912 mg/m^3).

SHEAR CHARACTERISTICS OF MH-BEARING SANDS BY TEMPERATURE-CONTROLLED HIGH-STRESS TRIAXIAL TESTING

Production of MH-bearing sands and their shear tests were conducted using the temperature-controlled high pressure triaxial testing apparatus (Hyodo, *et al*. 2008). For the reconstituted granular material, MH was formed in these host sands with 50%, 30% and 0% degree of MH saturation. From the results of density tests on natural cores from Nankai Trough, the porosities of the reconstituted materials were set as n=40% and 45% (Hyodo, *et al*. 2014). In this paper, only

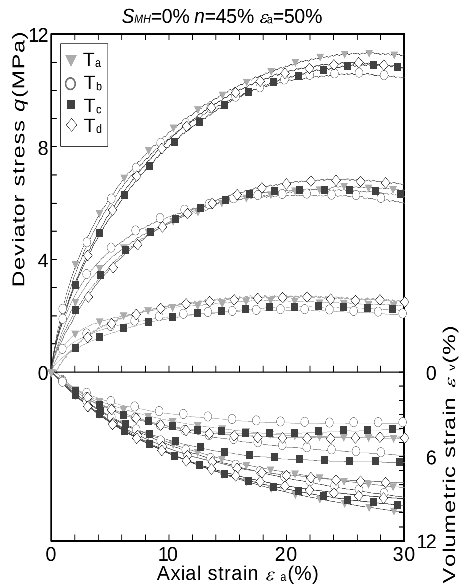

Figure 3. Variation of deviator stress and volumetric strain against axial strain for host sands

the results of n = 45% are presented. The triaxial test results for reconstituted host sands T_a, T_b, T_c and T_d with an initial porosity of n =45%, under an effective confining stresses of 1MPa, 3MPa and 5MPa are presented in Fig. 3. The initial stiffness and shear strength at critical state slightly decreases with increasing fines content, however there is no marked difference. Volumetric strain induced by shearing stress appears in the contractive side and the contraction tendency increases with increasing fines content and confining stress. Figure 4 shows the variation of the secant modulus at 1% axial strain against fines content for each material with each confining stress. It can be seen that there is a trend for the secant modulus to decrease with increasing fines content at all confining stresses. However, this is not true for T_a and T_b, due to the effect of their mean particle size. Fig.5(a)-(c) show the shear testing results for MH-bearing sands prepared with T_a, T_b and T_c

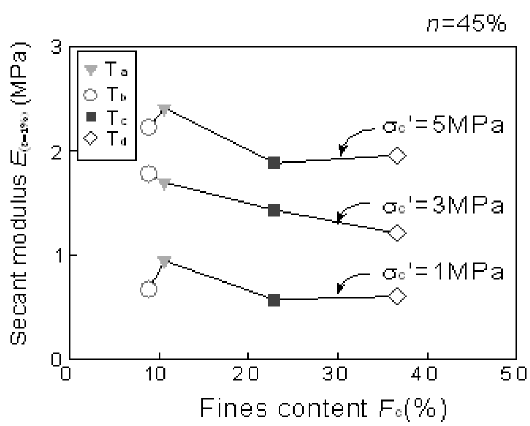

Figure 4. Relationship between secant modulus and fines content

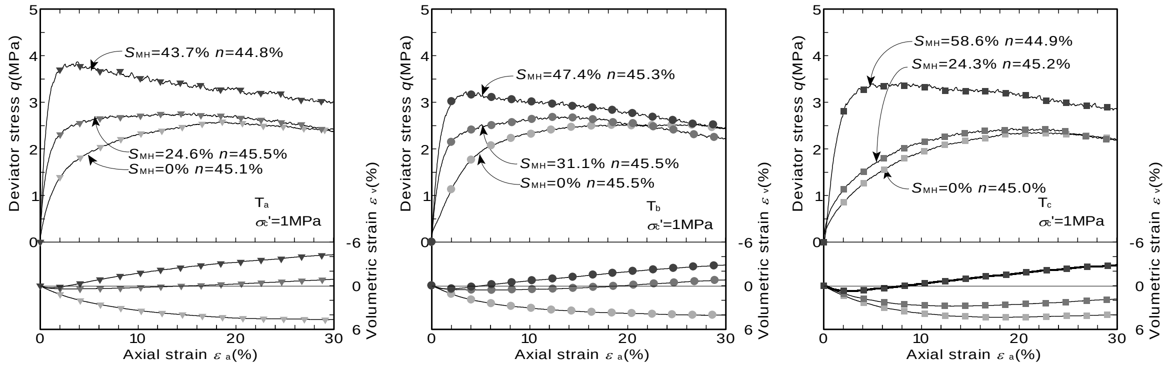

(a) Ta (b) Tb (c) Tc

Figure 5. Variation of deviator stress and volumetric strain against axial strain for methane hydrate-bearing sands

as host sands. Tests were performed at a porosity of n = 45% with effective confining stress of 1MPa at various MH saturations. It is observed that initial stiffness and the shear strengths at both peak and critical states increased with the rise in MH saturation. The presence of the methane hydrate promotes the dilation behaviour and the dilation tendency became obvious with the increasing MH saturation. In Figure 6, the difference between the peak shear strength of MH-bearing sand and the shear strength of the corresponding host sands are normalized by effective confining stress and then plotted against the degree of MH saturation. It can be observed that the normalized deviatoric stress difference increased with the level of MH saturation and this increasing tendency accelerated when the MH saturation was in excess of 30%. At lower MH saturation, the variation in the normalized deviatoric stress difference for T_c with the largest amount of fines content was the smallest. The rate of increasing tendency of the curves for T_c exceeded the other two sands T_a and T_b at some MH saturation between 20% and 30% and kept this position at higher MH saturation.

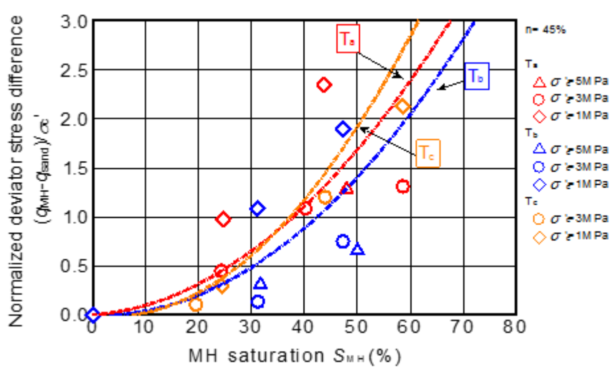

Figure 6. Variation of normalized deviator stress difference against degree of MH saturation for T_a, T_b and T_c

SHEAR CHARACTERISTICS OF MH- BEARING SANDS BY HIGH-STRESS PLANE STRAIN SHEAR TESTING

An overview of the testing equipment (Yoneda, *et al*. 2011, 2013) is shown in Fig. 7. This apparatus can control temperatures and pressures equivalent to an MH reservoir in deep seabed. Additionally, observation windows are installed in front of and behind the specimen in order to allow the local deformation of the specimen during shear tests to be measured. The specimen is a cuboid with 80 mm width, 60 mm thickness and 160 mm height. A 5 mm x 5 mm mesh was drawn on the membrane in front of the observation window. The observation was performed using a digital camera(g), which took pictures according to a timer controlled by a remote system. An LED (h) was installed to brighten the pressure cell (i), which allowed the specimen(e) to be observed. Local deformation analysis was performed by observing the cross-points of the mesh during shear tests and using this data in PIV analysis. Thermocouples(k,l) were installed at 60mm and 30mm from the bottom of the specimen in order to measure the variation of the temperature during the dissociation of MH. Glass beads and Toyoura sand were the materials used for comparison. Specimens were prepared with water contents equivalent to given degrees of MH saturation and tamped in 12 layers to give a porosity of n = 45%. Formation of MH was performed using the same method as in the triaxial compression tests. The specimens were saturated by filling the pore water and consolidated at given effective confining stress and then subjected to shear tests under drained conditions. The speed of shear was 0.1%/min. Also, in order to understand the behavior during MH production, MH was dissociated by decreasing pore water pressure by 7 MPa under constant cell pressure and observing the behavior. After finishing MH dissociation, the pore water pressure again rises and the behavior was also investigated. The rate of depressurization during dissociation of MH and re-pressurization was 0.5MPa/min.

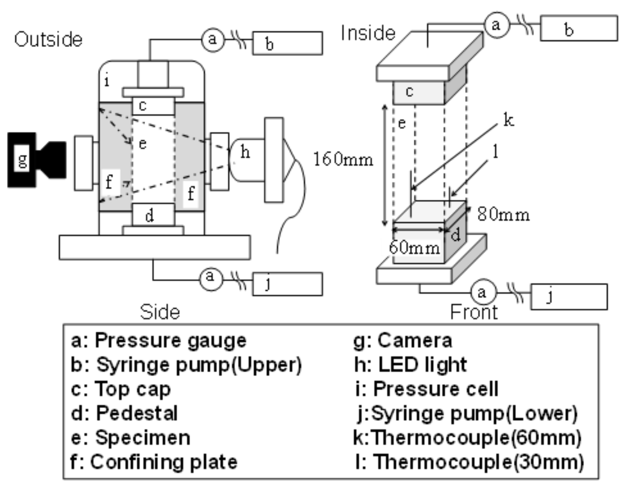

Figure 7. Schematic overview of the high-pressure low-temperature plane strain testing apparatus

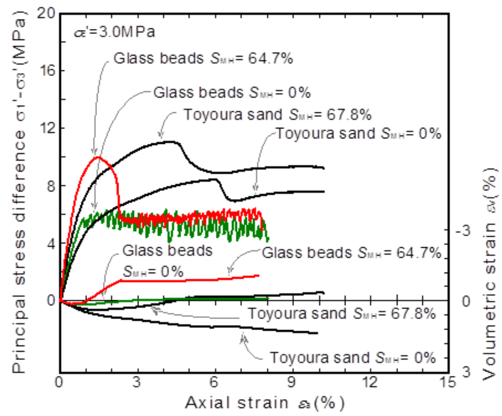

Figure 8. Variation of principal stress difference and volumetric strain against axial strain for methane hydrate-bearing sands

Figure 8 shows the shear test results for glass beads and Toyoura sand with and without MH. A marked increase in the strength and stiffness due to the cementation of MH are observed in both specimens. Methane hydrate-bearing glass beads owned a larger initial stiffness and attained its peak shear strength at a smaller axial strain. A marked post-peak strain-softening behaviour and remarked dilation behaviour of methane hydrate-bearing glass beads could be seen and the shear strength of methane hydrate-bearing glass beads approach to that of pure glass beads

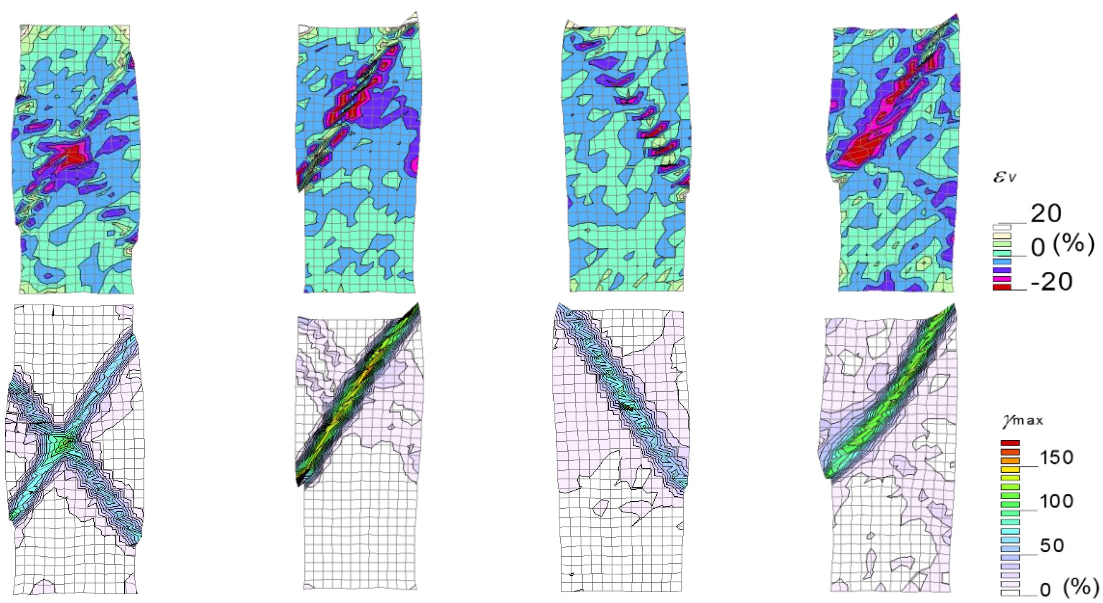

Glass beads S_{MH}=0%, ε_a= 8% | Glass beads S_{MH}=64.7%, ε_a= 8% | Toyoura sand S_{MH}=0%, ε_a= 10% | Toyoura sand S_{MH}=67.8%, ε_a= 10%

Figure 9. Volumetric strain and maximum shearing strain contours after failure by PIV analysis

after the peak strength as the axial strain progressed. Figure 9 shows the results of the PIV analysis during shear for the specimens with and without MH. The upper part shows the volumetric strain and the lower part shows shear strain contour at axial strain of 8% for glass beads and 10% for Toyoura sand. The shear bands can be observed for glass beads and Toyoura sand with and without MH. The shear band of Toyoura sand and glass beads became narrower and clearer once the MH was formed within the specimens.

Next, in order to simulate the production of MH, pore water pressure was decreased whilst keeping constant initial shear stress, MH was dissociated and the deformation behavior of loss of cementation was investigated. Specimens which had cell pressure 10MPa, pore water pressure 7MPa and consolidated at effective stress 3MPa had their pore water pressure decreased by 7MPa. Stress and temperature conditions were set outside of the MH stability state line and MH was dissociated. Figures 10 and 11 show effective stress paths applied to the experiments. In these figures, only the results for Toyoura sand are shown. Failure envelopes for Toyoura sand with and without MH are shown by broken and solid line, respectively. The dissociation tests were performed in two cases. In Case 1, after the specimens were isotropically consolidated, depressurization was conducted at a rate of 0.5MPa/min. Then, re-pressurization was performed at the same speed after finishing MH dissociation. These pore water pressure histories correspond to real production of MH in recovering pore water pressure after production. In Case 2, after specimens were isotropically consolidated, initial shear stress was applied at an amount greater than the host sand but less than MH bearing sand. Depressurization is then conducted in the same way as Case 1 and at the same speed. After finishing MH dissociation, pore water pressure was increased at the same rate. This test was done to simulate the element in the vicinity of the production well, where the stress condition is close to failure. In Fig. 11, the specimen failed during re-pressurization when the stress path reached the failure line of the host sand. In Fig. 12, the relationship between the temperature and pore water pressure during the depressurization process is shown. As can be seen, temperature decreased suddenly when the pore pressure was decreased to the value of the state boundary curve. This is due to the temperature absorption phenomena of MH during dissociation. Also, at a pressure of 3 MPa dissociation and reformation repeats, and when dissociation is complete the temperature of the specimen rises to room temperature. Figure 13 shows the relationship between the effective stress ratio and active strain during dissociation tests of MH for Case 2. Point (a) corresponds to the point before dissociation, where initial shear stress has been applied. Point (b) corresponds to the point where pore water pressure was decreased from 10MPa to 3MPa. Point (c) corresponds to the point where MH is dissociated. Point (d) corresponds to the point where the specimen failed due to an increase in pore water pressure (re-pressurization). In Case 2, the specimen failed during re-pressurization when the stress path reached the strength of the host sand. From the photo, it can be seen that from point (d) a shear band appeared in the specimen and failure occurred. Figures 14 and 15 show the volumetric strain and maximum shear stress contour obtained by Photo 1. From point (a) to (c) the specimen was consolidated and the volume was compressed. At (d), volumetric dilation occurred in the shear band and local deformation was observed clearly.

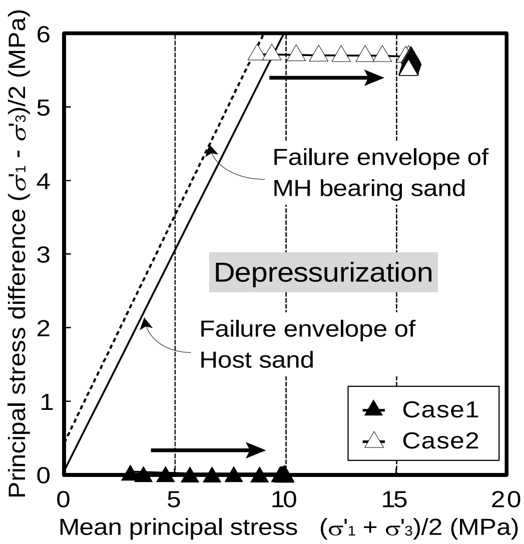

Figure 10. Stress path in depressurization test

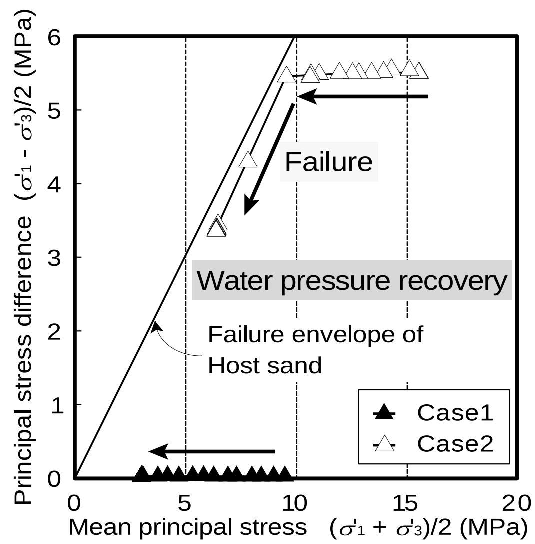

Figure 11. Stress path in repressurization test

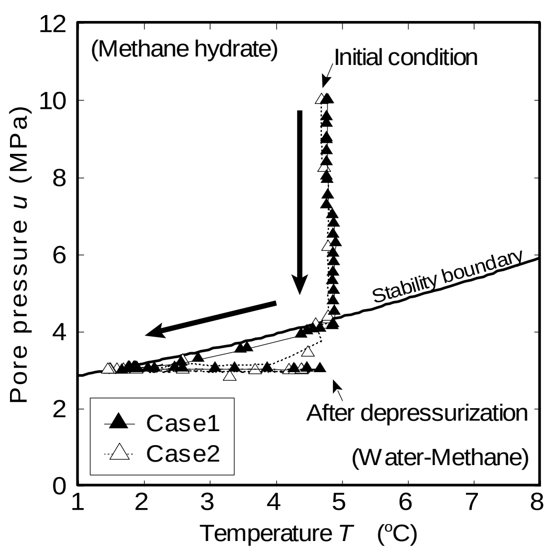

Figure 12. Temperature and pore pressure path in depressurization test

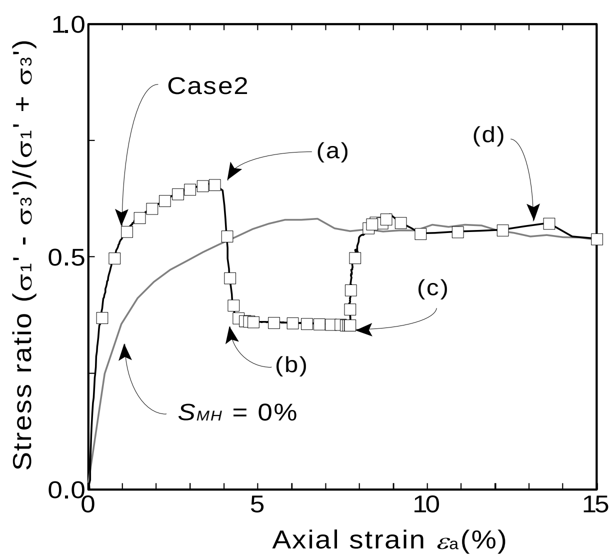

Figure 13. Relationship between stress ratio and axial strain (Case2)

CONSTITUTIVE MODEL FOR METHANE HYDRATE BEARING SAND

Framework of constitutive model

Researchers have discussed the obtained relationships of dilatancy with mobilized shear strength and stiffness; in particular, Yun *et al*. (2005) and Waite *et al*. (2009) proposed a possible micro-mechanical model for hydrate-bearing sediment. Then, several constitutive models (e.g., Hyodo,

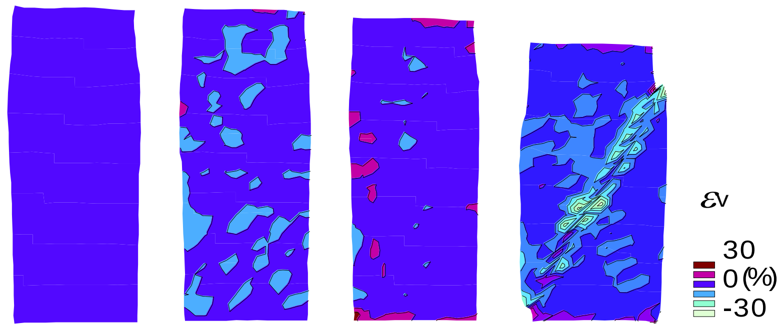

(a) ε_a= 3.5% (b) ε_a= 4.0% (c) ε_a= 7.2% (d) ε_a= 12.7%

Figure 14. Contour of volumetric strain at each axial strain (Case2)

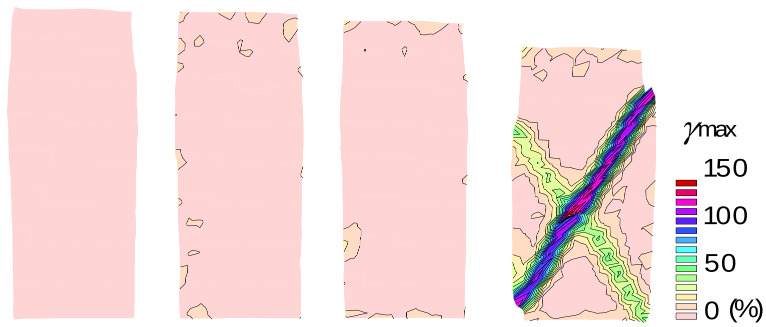

(a) ε_a= 3.5% (b) ε_a= 4.0% (c) ε_a= 7.2% (d) ε_a= 12.7%

Figure 15. Contour of maximum shear strain at each axial strain (Case2)

et al. 2008; Uchida, *et al*. 2012) have been proposed on the basis of their idea, and seabed deformation due to MH exploitation was predicted (Kimoto, *et al*. 2007; Klar, *et al*. 2010; Yoneda, *et al*. 2011).

Previous experimental study demonstrated that methane hydrate (MH) bearing sand owned larger peak strength and initial stiffness and displayed much more obvious dilatancy behaviour in comparison with pure sand. An internal stress representing the strength enhancement by hydrate is employed. An elasto-plastic constitutive model incorporating the internal stress and the subloading surface concept has been proposed to describe the shear behaviour of MH bearing sand in deep seabed. The validity of the constitutive model has been examined by comparing the predicted values with the experimental results in triaxial test.

Normal-yield surface and evolution of internal stress

Figure 16 shows the normal-yield surface of host sand, normal- yield surface of MH bearing sand and the subloading surface on *p*-*q* plane. The normal-yield surface of host sand takes the same form as the modified Cam-clay model (Roscoe and Burland 1968) represented in Eq. (1).

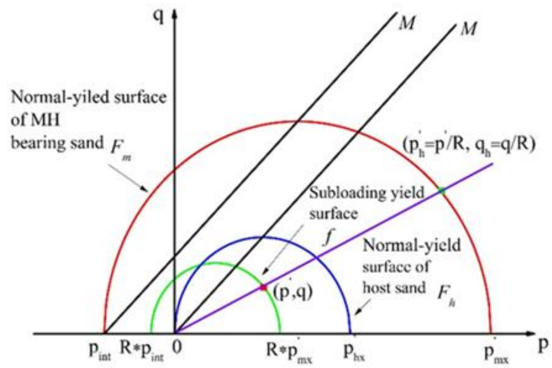

Figure 16. The normal-yield surface of host sand, normal-yield surface of methane hydrate bearing sand and subloading surface

$$F_h = (p_h')^2 - p_h' p_{hx}' + \frac{q_h^2}{M^2} = 0 \tag{1}$$

where p_h' and q_h are the mean and deviatoric stress on the normal-yield surface of host sand Fh, p_{hx}' is the yield stress for host sand. The stress in the constitutive model refers to the effective stress. M is the stress ratio at critical state. A stress variant p_{int}, the internal stress, is added into the modified Cam-clay model to consider the cementation force among the particles formed by the hydrate. The yield surface F_h expands toward both the left and right sides with the addition of the internal stress p_{int}. The normal-yield surface of MH bearing sand F_m is obtained in Eq. (2).

$$F_m = (p_h' + p_{\text{int}})^2 - (p_h' + p_{\text{int}})(p_{mx}' + p_{\text{int}}) + \frac{q_h^2}{M^2} = 0 \tag{2}$$

where p_{mx}' is the yield stress for MH bearing sand. The dependence of the yield stress p_{mx}' on the yield stress p_{hx}' as well as the internal stress p_{int} is explained in the hardening rule part.

The initial internal stress of MH bearing sand p_{int0} is greatly dependent on the degree of hydrate saturation and the existence conditions of MH including the pore pressure and temperature. Thus, the determination of the internal stress at initial state is given in Eq. (3).

$$p_{\text{int}0} = \xi L S_{MH} \tag{3}$$

where ξ is the material parameter and S_{MH} is the degree of hydrate saturation. Herein, L is the parameter indicating the distance from the point which initial state for the given pore pressure, degree of hydrate saturation and the temperature corresponds to the phase equilibrium curve.

Kasama *et al*. (2000) proposed the expression of the internal energy dissipation for the cement treated soil in Eq. (4).

$$dW_{\text{in}} = (p' + p_{\text{int}})\sqrt{(d\varepsilon_v^p)^2 + (Md\varepsilon_d^p)^2} - p_{\text{int}} d\varepsilon_v^p \tag{4}$$

The degradation of the internal stress is considered to be determined by the internal energy dissipation and the rate of internal stress dp_{int} is defined in Eq. (5). Besides, dp_{int} should also fulfill the following three conditions (a) $p_{int}=0, dp_{int}=0$; (b) $d\varepsilon_v^p\neq 0, dp_{int}<0$; (c) $d\varepsilon_d^p\neq 0, dp_{int}<0$. Here, $d\varepsilon_v^p$ and $d\varepsilon_d^p$ are the plastic volumetric and deviatoric strain increment.

$$dp_{\mathrm{int}} = -\chi dW_p \tag{5}$$

where χ is the degradation coefficient of internal stress and only the internal energy dissipation induced by the internal stress is accounted in the definition. Therefore, the rate of internal stress is specified in Eq. (6).

$$dp_{\mathrm{int}} = -\chi p_{\mathrm{int}} \sqrt{(d\varepsilon_v^p)^2 + (Md\varepsilon_d^p)^2} \tag{6}$$

Subloading surface

To predict the plastic strain rate induced by the stress ratio inside the normal-yield surface, the subloading surface concept proposed by Hashiguchi (1989) is integrated with the expression of Eq. (2). The subloading surface f in Eq. (7) is derived by replacing the stress $(p_h^{'}, q_h)$ on the normal-yield surface F_h in Eq. (2) with the current stress ($p^{'}/R = p_h^{'}$, $q / R = q_h$). The subloading surface keeps the similarity to the normal-yield surface of MH bearing sand and passes through the current stress $(p^{'}, q)$.

$$f = (p^{'} + Rp_{\mathrm{int}})\left[1 + \frac{q^2}{M^2(p^{'} + Rp_{\mathrm{int}})^2}\right] - R(p_{mx}^{'} + p_{\mathrm{int}}) = 0 \tag{7}$$

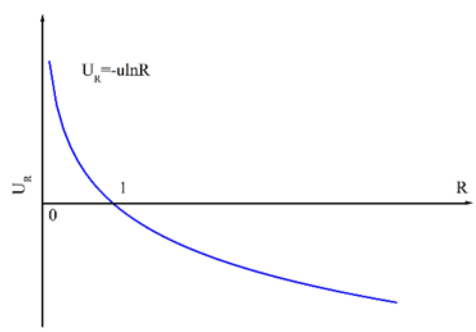

Figure 17. Evolution law of the normal-yield ratio R

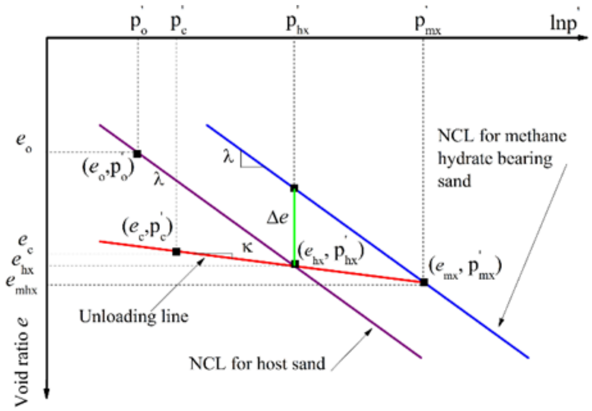

Figure 18. Relationship between the yield stress of host sand and the yield stress of MH bearing sand

where the normal-yield ratio R ($0<R<1$) expresses the approaching degree of the subloading surface to the normal-yield surface. The rate of the normal-yield ratio dR is defined in Eq. (8).

$$dR = U_R \times \|d\boldsymbol{\varepsilon}^p\| \tag{8}$$

where U_R is the monotonically-decreasing function of R as shown in Fig.17. The specific expression of U_R is expressed in Eq. (9).

$$U_R = -u \ln R \tag{9}$$

Hardening rule

The normal consolidation line (NCL) of host sand and MH bearing sand are assumed to be two parallel straight lines on e-ln$p$ plane as shown in Figure 18. The NCL of MH bearing sand shifts to the right due to the addition of internal stress formed by hydrate. e_{hx} and e_{mx} are the void ratio in corresponding to the yield stress of host sand p'_{hx} and yield stress of MH bearing sand p'_{mx}. The yield surface p'_{hx} is employed as the hardening parameter for the normal-yield surface of host sand. It can be expressed by the plastic volumetric strain increment $d\varepsilon_v^p$ as given in Eq. (10).

$$dp'_{hx} = \frac{1+e_o}{\lambda - \kappa} p'_{hx} \cdot d\varepsilon_v^p \tag{10}$$

where λ is the compression index and κ is the swelling index decided from the isotropic loading and unloading test, respectively. p'_o is the reference consolidation stress on NCL of host sand, and e_o is the void ratio in corresponding to the reference consolidation stress p'_o.

For the yield stress p'_{hx}, the difference Δe in the void ratio on the NCL of MH bearing sand and NCL of host sand in Figure 18 can be calculated by Eq.(11). This difference in void ratio for MH bearing sand and host sand is believed to be caused by the existence of internal stress p_{int}. Therefore, Δe is assumed to be expressed using the internal stress p_{int} by Eq. (12). The Eq. (13) is obtained by the combination of Eqs. (11) and (12).

$$\Delta e = \lambda \times \ln \frac{p'_{mx}}{p'_{hx}} - \kappa \times \ln \frac{p'_{mx}}{p'_{hx}} \tag{11}$$

$$\Delta e = \frac{p_{\text{int}}}{\alpha + \beta p_{\text{int}}} \tag{12}$$

where α and β are the parameters about the effect of the variant of internal stress p_{int} on the yield stress p'_{mx}.

$$p'_{mx} = \exp\left\{ \ln p'_{hx} + \frac{p_{\text{int}}}{(\alpha + \beta p_{\text{int}})(\lambda - \kappa)} \right\} \tag{13}$$

p'_{mx} is adopted as the hardening parameter for MH bearing sand and its increment dp'_{mx} in Eq. (14) can be obtained by the partial differential form of the Eq. (13).

$$dp'_{mx} = \frac{\partial p'_{mx}}{\partial p'_{hx}} dp'_{hx} + \frac{\partial p'_{mx}}{\partial p_{\text{int}}} dp_{\text{int}} \tag{14}$$

Calculation of the plastic strain

This constitutive model takes the associated flow rule. The expression of the plastic potential g is equal to the yield surface function *f*. The volumetric and deviatoric plastic strain increment can be calculated by Eqs. (15) and (16).

$$d\varepsilon_v^p = \Lambda \frac{\partial g}{\partial p'} \tag{15}$$

$$d\varepsilon_d^p = \Lambda \frac{\partial g}{\partial q} \tag{16}$$

where Λ is the plastic multiplier

The consistency condition of the subloading surface f in Eq. (7) is shown in Eq. (17).

$$\frac{\partial f}{\partial p'} dp' + \frac{\partial f}{\partial q} dq + \frac{\partial f}{\partial p'_{mx}} dp'_{mx} + \frac{\partial f}{\partial R} dR + \frac{\partial f}{\partial p_{\text{int}}} dp_{\text{int}} = 0 \tag{17}$$

$$\frac{\partial f}{\partial p'} = 1 - \frac{q^2}{M^2 (p' + R p_{\text{int}})^2} \tag{18}$$

$$\frac{\partial f}{\partial q} = \frac{2q}{M^2 (p' + R p_{\text{int}})} \tag{19}$$

$$\frac{\partial f}{\partial p'_{mx}} = -R \tag{20}$$

$$\frac{\partial f}{\partial R} = -\frac{q^2 p_{\text{int}}}{M^2 (p' + Rp_{\text{int}})^2} - p'_{mx} \tag{21}$$

$$\frac{\partial f}{\partial p_{\text{int}}} = -\frac{q^2 R}{M^2 (p' + Rp_{\text{int}})^2} \tag{22}$$

$$\Lambda = \frac{\frac{\partial f}{\partial p'} dp' + \frac{\partial f}{\partial q} dq}{H} \tag{23}$$

$$H = -\frac{1+e_0}{\lambda - \kappa} p'_{hx} \cdot \frac{\partial f}{\partial p'} \frac{\partial f}{\partial p'_{mx}} \frac{\partial p'_{mx}}{\partial p'_{hx}} + u \ln R \cdot \left| \frac{\partial f}{\partial \sigma'} \right| \frac{\partial f}{\partial R} + \chi p_{int} \sqrt{\left(\frac{\partial f}{\partial p'}\right)^2 + \left(M \frac{\partial f}{\partial q}\right)^2} \left(\frac{\partial f}{\partial p'_{mx}} \frac{\partial p'_{mx}}{\partial p_{int}} + \frac{\partial f}{\partial p_{int}} \right) \tag{24}$$

The plastic multiplier Λ in Eq. (23) can be calculated by inputting the Eqs. (6), (8), (10), (18), (19), (20), (21), (22) into Eq. (17). H in the Eq. (24) is the hardening modulus.

The elastic volumetric and deviatoric strain increment can be calculated by Eqs. (25) and (26).

$$d\varepsilon_v^e = \frac{dp'}{K} \tag{25}$$

$$d\varepsilon_d^e = \frac{dq}{3G} \tag{26}$$

where K is the bulk modulus and G is the shear modulus.

Table 1. Parameters of constitutive model for MH bearing sands

Parameters	Value	Illustration
λ	0.1460	Compression index
κ	0.0016	Swelling index
p_i	1.2	Reference consolidation stress on NCL (MPa)
e_i	0.973	Void ratio corresponds to the reference consolidation stress p_i
M	1.2	Stress ratio at critical state
u	10	Material parameter associated with the magnitude of plastic strain increment
α	10	Parameters about the effect of the variant of internal stress p_{int} on the yield stress p'_{mx}
β	10	
χ	20	Degradation coefficient of the internal stress p_{int}
ξ	0.1	Parameter of the pore pressure and temperature for deciding the initial internal stress

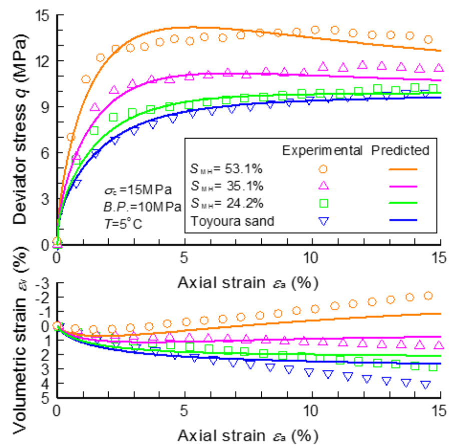

Figure 19. Predicted and numerical relationships between the axial strain with the deviatoric stress and volumetric strain of MH bearing sand with different MH saturations

From the unloading line in Figure 18, the elastic volumetric strain increment can also be expressed by Eq. (27). Thus, the bulk modulus K in the constitutive model can be deduced as Eq. (28).

$$d\varepsilon_v = \frac{\kappa}{1+e_o}\frac{dp'}{p'} \tag{27}$$

$$K = \frac{1+e_o}{\kappa} p' \tag{28}$$

Prediction versus experimental results

Figure 19 shows that the predicted values of the proposed constitutive model agree well with the experimental results not only for host sand but also the MH bearing sand with different degrees of hydrate saturation in drained triaxial compression test. The ten parameters included in the constitutive model are shown in Table 1.

The constitutive model is capable of predicting the increasing peak strength and initial stiffness as well as remarkable positive dilatancy for MH bearing sand with the increasing degree of hydrate saturation. Numerical results exhibit from the strain softening behavior for host sand to the strain softening behaviour for MH bearing sand with a larger degree of hydrate saturation.

CONCLUSIONS

The research was conducted in order to understand the fundamental mechanical and dissociation properties on MH-bearing sands. The following conclusions were drawn:

(1) In triaxial shear tests on host sands, initial stiffness and peak shear strength decreased with increasing fines content and there was a strong trend for volume contraction.

(3) Artificially prepared samples containing MH were successfully produced by controlling stress and temperature conditions. For all specimens with MH, the presence of MH increased the initial stiffness and peak shear strength of specimens due to MH's cementation force and promoted the dilation behaviour. However, both initial stiffness and strength decreased with increasing fines content of host sands.

(4) The normalized deviatoric stress difference increased rapidly when the degree of MH saturation exceeded 30%. At lower MH saturation, the variation in the normalized deviatoric stress difference for T_c with the largest amount of fines content was the smallest. The rate of increasing tendency of the curves for T_c exceeded the other two sands T_a and T_b at some MH saturation between 20% and 30% and kept this position at higher MH saturation.

(5) Due to the existence of MH, initial stiffness and strength increased for MH-bearing glass beads and MH-bearing Toyoura sand in plane strain test. MH-bearing glass beads owned a higher initial stiffness and exhibited remark post-peak strain-softening behaviour.

(6) The shear band of specimens became much clearer and narrower for Glass beads and Toyoura sand once the MH was formed. During depressurization, marked deformation was not observed, because of an increase of effective stress. However, after depressurization, repressurization caused the specimen to fail in the case of high initial shear stress conditions.

(7) The bonding effect due to the cementation by methane hydrate was introduced into the elastoplastic constitutive model. The bonding force was correlated with the pressure and temperature according to the experimental results.

(8) The constitutive model was capable of predicting the increasing peak strength and initial stiffness as well as remarkable positive dilatancy behaviour of MH-bearing sands over a wide range of confining pressures and MH saturations.

ACKNOWLEDGEMENTS

The present work was done as the activity of Research Consortium for Methane Hydrate Resources in Japan (MH21 Research Consortium) by the Ministry of Economy and Industry and the part of the work was supported by KAKENHI 25249065 by the Ministry of Education and Science in Japan. The authors would like to express their sincere thanks to their supports

REFERENCES

Hashiguchi, K. (1989): Subloading surface model in unconventional plasticity, International Journal of Solids and Structures, 25, 917-945.

Hyodo, M., Hyde, A. F. L., Nakata, Y., Yoshimoto, N., Fukunaga, M., Kubo, K., Nanjo, T., Matsuo, T. and Nakamura, K. (2002). Triaxial compressive strength of methane hydrate, Proc. of 12th Int. Offshore and Polar Engrg. Conf., pp. 422-428.

Hyodo, M., Nakata, Y., Yoshimoto, N., Ebinuma, T. (2005). Basic research on the mechanical behavior of methane hydrate-sediments mixture, Soils and Foundations, Vol. 45, No. 1, pp.75-85.

Hyodo, M., Nakata, Y., Yoshimoto, N. and Yoneda, J. (2007). Mechanical behavior of methane hydrate-supported sand, Proc. of Int. Symp. on Geotechnical Engineering, Ground Improvement and Geosynthethics for Human security and Environmental Preservation, pp.195-208.

Hyodo, M., Nakata, Y., Yoshimoto, N. and Yoneda, J. (2008). Shear strength of methane hydrate bearing sand and its deformation during dissociation of methane hydrate, Proc. of 4th Int.Symp. on Deformation Characteristics of Geomaterials, pp.549-556.

Hyodo, M., Yoneda, J., Yoshimoto, N., Nakata, Y. (2013):Mechanical and dissociation properties of methane hydrate-bearing sand in deep seabed, Soils and Foundations, 53(2), 299-314, http://dx.doi.org/10.1016/j.sandf.2013.02.010 .

Hyodo, M., Kajiyama S., Yoshimoto, N., Nakata, Y.(2014):Triaxial behaviour of methane hydrate bearing sand , Proceedings of 10th Int. ISOPE Ocean Mining & Gas Hydrate Symposium OMS-2013, Szczecin, Poland, 126-134.

Japan Oil, Gas and Metals National Corporation (2013). Gas Production from Methane Hydrate Layers Confirmed. News Release, 12.03.13, pp. 1e3. https://www. jogmec.go.jp/english/news/release/release0110.html.

Kasama, K., Ochiai, H. and Yasufuku, N. (2000): On the stress-strain behaviour of lightly cemented clay based on an extended critical state concept, Soils and Foundations, 40(5), 37-47.

Kimoto, S., Oka, F., Fushita, T., Fujiwaki, M. (2007). A chemo-thermo-mechanically coupled numerical simulation of the subsurface ground deformations due to methane hydrate dissociation, Computers and Geotechnics, 34 (4), pp. 216-228.

Klar, A., Soga, K., Ng, M.Y.A. (2010). Coupled deformation–flow analysis for methane hydrate extraction, Geotechnique, 60(10), pp. 765-776.

Kvenvolden, K.A., Ginsburg, G.D. and Soloviev, V.A., (1993). Worldwide distribution of subaquatic gas hydrates, Geo-Marine Letters, Vol.13, pp.32-40.

Lee, J.Y., Carlos Santamarina, J., Ruppel., C. (2010). Volume change associated with formation and dissociation of hydrate in sediment. Geochemistry Geophysics Geosystems 11, Q03007.

Roscoe, K. H. and Burland, J. B. (1968): On the Generalized Stress-strain Behaviour of “Wet” Clay, Engineering plasticity, Cambridge University Press, Cambridge, UK, 535-609.

Sakamoto, Y., Shimokawara, M., Oga, H., Miyazaki, S., Komai, T., Aoki, K., Yamaguchi, T., (2008): Laboratory tests on the consolidation behavior and seepage characteristics of methane hydrate during dissociation by depressurization method. Journal of MMIJ 124 (8), 498–507 (in Japanese).

Suzuki, K., Ebinuma, T. & Narita, H.(2009) : Features of methane hydrate-bearing sandy-sediments of the Forearc Basin along the Nankai Trough: Effect on methane hydrate-accumulating mechanism in turbidite, Journal of Geography, 118 (5) : 899-912 (in Japanese).

Suzuki, K., Ebinuma, T., Narita, H. (2009). Features of methane hydrate- bearing sandy-sediments of the forearc basin along the Nankai trough: effect on methane hydrate-accumulating mechanism in turbidite. Journal of Geography 118 (5), 899–912 (in Japanese).

Uchida, S., Soga, K., Yamamoto, K. (2012). Critical state soil constitutive model for methane hydrate soil, Journal of Geophysical Research, Vol. 117, B03209, 13 pp, doi:10.1029/2011JB008661.

Waite,W. F., Santamarina, J. C., Cortes, D. D., Dugan, B. Espinoza, D. N., Germaine, J., Jang, J., Jung, J. W., Kneafsey, T. J., Shin, H., Soga, K., Winters, W. J., and Yun, T.-S. (2009). Physical properties of hydrate-bearing sediments, Reviews of Geophysics, 47, RG4003.

Yamamoto, K. (2009). Production techniques for methane hydrate resources and field test programs. Journal of Geography,Vol.118, No. 5, 913-934. Japan

Yasufuku, N., Murata, H. and Hyodo, M. (1991). Yield characteristics of anisotropically consolidated sand under low and high stresses, Soils and Foundations, Vol. 31, No. 1, pp. 95-109

Yoneda, J. and Nakata, Y. (2011). Deformation of deep seabed during dissociation of methane hydrate. Proc. The 14th Asian Regional Conference on Soil Mechanics and Geotechnical Engineering. ISSMGE. Paper ID290. China.

Yoneda, J., Hyodo, M., Nakata, Y., Yoshimoto, Orense, R. (2011). Deformation of seabed due to exploitation of methane hydrate reservoir, Frontiers in Offshore Geotechnics II, pp. 245-250, doi: 10.1201/b10132-18.

Yoneda, K. (2011):Examination of strength characteristics of the cement treated soil, Geotech Forum 2011, Kyoto, Japan, No.88 (in Japanese).

Yoneda, J., Hyodo, M., Yoshimoto, N., Nakata, N., Kato, A. (2013a): Development of high-pressure low-temperature plane strain testing apparatus for methane hydrate-bearing sand, Soils and Foundations, 53(5), 774-783, http://dx.doi.org/10.1016/j.sandf.2013.08.014.

Yoneda, J., Masui, A., Konno, Y., Jin, Y., Egawa, K., Kida, M., Ito, T., Nagao, J. and Tenma, N. (2015): Mechanical behavior of hydrate-bearing pressure-core sediments visualized under triaxial compression, Marine and Petroleum Geology, http://dx.doi.org/10.1016/j.marpetgeo.2015.02.028

Yun, T.S., Francisca, F.M., Santamarina, J.C., Ruppel, C., (2005): Compressional and shear wave velocities in uncemented sediment containing gas hydrate, Geophys. Res. Lett., 32, L10609, doi:10.1029/2005GL022607.

Causes of Cyclic Shear Failure at Lokanthali of Araniko Highway after Mw7.8 2015 Gorkha Earthquake

Binod Tiwari, Ph.D., P.E.[1] Beena Ajmera, Ph.D.[2] , and Brian Yamashiro[3]

[1]Professor, Civil and Environmental Engineering Department, California State University, Fullerton, 800 N State College Blvd., E-419, Fullerton, CA, 92831.
[2]Assistant Professor, Civil and Environmental Engineering Department, California State University, Fullerton, 800 N State College Blvd., E-318, Fullerton, CA, 92831.
[3]Graduate Student, Civil and Environmental Engineering Department, California State University, Fullerton, 800 N State College Blvd., Fullerton, CA, 92831.

ABSTRACT

The M_w 7.8 2015 Gorkha Nepal Earthquake was one among the most devastating earthquakes in in the history. It left close to 9,000 people dead, 22,000 people injured and caused over $5B loss of properties. The earthquake triggered over 15,000 co-seismic landslides. Although the major highways and bridges performed well, majority of the hydropower projects located within the earthquake-affected area sustained different types of damages. A few dozens buildings, including several modern constructions, collapsed in Kathmandu due to the earthquake shaking, killing thousands of people. The earthquake also caused cyclic shear failure of a sector of Araniko Highway at Lokanthali, Kathmandu. This highway is very important trade route to China. A 250 m long stretch of the highway collapsed with vertical movements of more than a meter and lateral displacements of approximately 0.5 m. The landslide seriously damaged dozens of buildings and displaced a few of them by approximately 1 m. To investigate the causes of ground failure, the authors performed site investigation including subsoil exploration, in-situ tests and laboratory tests on the slope forming materials in addition to topographic mapping. Additionally, deformation and limit equilibrium analyses were also performed using the laboratory and field data. The study revealed that earthquake induced shaking in combination with post-cyclic strength degradation of the lacustrine deposit, locally named *Kalimati*, caused the cyclic shear failure although the site has gentle slopes and the earthquake main shock produced relatively moderate ground accelerations at this location.

INTRODUCTION

The Mw = 7.8 2015 Gorkha earthquake was one among the deadliest earthquakes in the South Asian region. It killed close to 9,000 people and injured more than 22,000, displaced millions of residents, and left hundreds of thousands of people homeless. Estimated economic loss resulted due to the earthquake is over $5B (almost 25% of the Nepalese GDP). The epicenter of the Gorkha earthquake is located at Barpak, Gorkha, approximately 80 km northwest of Kathmandu. The hypocenter of the earthquake is estimated at a shallow depth of 15 km (Hashash et al., 2015). The first author co-lead the NSF funded 15-member GEER team for post-earthquake reconnaissance immediately after the earthquake and spent 30 days in the field to collect perishable geotechnical information. Despite the large magnitude of earthquake, the observed peak ground accelerations, recorded at very few locations in and around Kathmandu valley were relatively small. As such, the damage caused by this earthquake was much less than expected for an earthquake with this magnitude. However, at clustered locations, significant damage was observed. There was very limited ground motion information that could be useful to analyze and assess the individual damage. One among those limited information was the ground motions (Figure 1) recorded in Kathmandu Valley at the KATNP station, which is located about 6.3 km north-west from the site. USGS released the ground motion data recorded at this station immediately after the earthquake. Both the north-south and east-west components of the peak ground accelerations (PGA) recorded at this station were surprisingly low, at the order of 0.16g. Dixit et al. (2015) analyzed the records from the main shock, as well as additional recordings from aftershocks and microtremors, and reported a dominant period of about 5 seconds for the main shock. Although majority of the highways and bridges performed well during and immediately after the earthquake, several mountain roads including the access roads to hydropower projects were fully damaged at hundreds of locations, completing blocking the through traffic. One among the spectacular damage along the roads in Kathmandu Valley was Lokanthali Cyclic shear failure. This road was widely covered in media and reconnaissance reports. The GEER team mapped the damage, performed open cuts for soil exploration, and performed a few laboratory experiments on the field samples collected during the field visit (Hashash et al. 2015; Moss et al. 2015).

The first author made three more trips to Nepal in addition to the month-long field reconnaissance with the GEER team. The latest trip was in August 2016, to collect post-earthquake field information. Detailed topographic survey, in-situ soil tests, and soil sampling were performed at Lokanthali cyclic shear failure area to evaluate the cause of failure. The subsequent section includes details of those investigation and the results of stability and deformation analyses performed.

EXTENT OF DAMAGE

The 2015 Gorkha Earth caused a significant damage to building structures in Kathmandu and other moderately large towns located in the eastern side of the main shock. Although the level of damage was much less than expected with such large magnitude earthquakes, a few dozen of modern structures were fully or partially damaged, killing hundreds of people (Figure 2). Moreover, majority of the other damaged buildings were constructed with brick masonry structures on mud mortar. Aerial reconnaissance with helicopter revealed that hundreds of buildings located on the ridge of the slopes within the rupture surface were fully collapsed. Dozens of cultural heritage sites and temples were either fully or partially damaged due to the earthquake induced ground shaking.

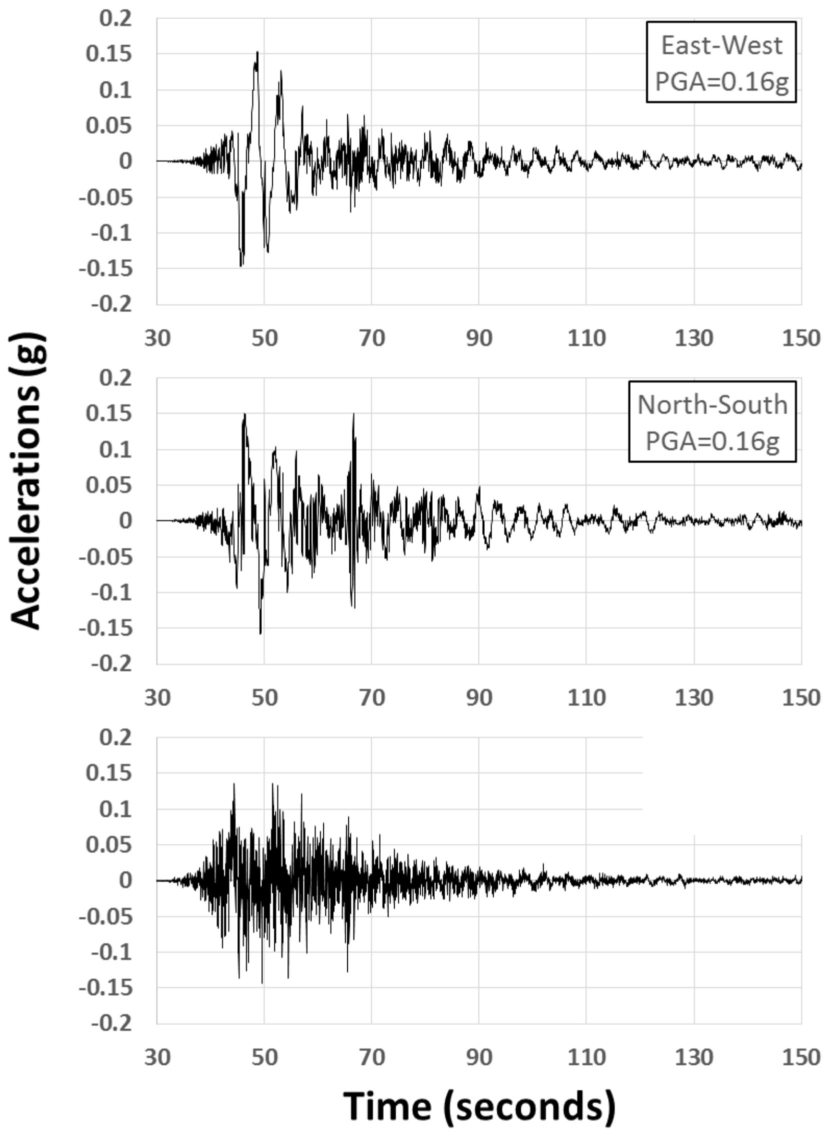

Figure 1. Ground accelerations recorded at the KATNP station during the April 25, 2015 Gorkha earthquake (CESMD, 2015).

The 2015 Gorkha earthquake triggered liquefaction at more than 15 locations (Figure 3). At those locations, traces of liquefied sand ejecta were observed. Some of those ejecta were in significantly large in quantity and the others were clearly visible traces, but not in abundant quantity. The field observation showed that the earthquake shaking was just enough to liquefy the soil, but was not sufficient to cause a massive damage to structures.

Figure 2. Extent of structural damage observed in Kathmandu Valley due to the 2015 Gorkha Earthquake. Majority of the damage were soft-story collapses.

The 2015 Gorkha earthquake significantly affected the hydropower projects. While majority of the damage was observed in the dams, penstocks and powerhouses due to landslides and rock falls, 19 cm of seismically induced settlement was observed on the dam body of the Upper Tamakoshi Hydropower project, the largest Hydropower Project of the nation, which was under construction at the time of earthquake (Figure 4).

As expected, the 2015 Gorkha earthquake triggered approximately 15,000 co-seismic landslides (Figure 5). Approximately 3,500 of these landslides were larger than 100 m^2 in area. Tiwari et al. (2016) correlated those landslides with terrain slope, geology, and peak ground acceleration (PGA) and reported that slope inclination and PGA were the most influencing factor in triggering those landslides. More than 99% of those triggered landslides were disruptive landslides. Although very small in number, the coherent landslides triggered by the earthquake caused significant damage to structures and killed hundreds of people. Two among those landslides are Langtang Debris Avalanche and Lokanthali cyclic shear failure. Description of Langtang Debris Anavalche and other valley blocking landslides are available in Hashash et al. (2015), Moss et al. (2015) and Collins and Jibson (2015). This article discusses in detail about the Lokanthali cyclic shear failure site.

Figure 3. Sand ejecta observed at the edges of Kathmandu Valley due to liquefaction. The liquefaction sites, although were wide spread, did not damage structures.

Figure 4. 19 cm settlement observed at the main dam of Upper Tamakoshi Hydropower project due to seismically induced settlement of the foundation material.

Lokanthali cyclic failure site is located about 1 km east of Kathmandu airport in Nepal (27°40'28.1"N, 85°21'44.6"E). Hashash et al. (2015) and Moss et al. (2015) mapped this failure site. Field evidence of ground failure was observed along a ridge for a distance of about 1 km. At different locations, fissures larger than 2 m and tension cracks with vertical offsets larger than 1.4 m along the top of the ridge, were observed (Figure 6). The surprising feature of this cyclic failure was that the ground slope was very gentle and such failure was not expected at this newly renovated highway.

Figure 5. Typical co-seismic landslides observed in various parts of the country due to the 2015 Gorkha Earthquake.

The authors conducted post-earthquake field investigation to evaluate the damage condition and potential cause of ground failure. The cyclic failure caused three major types of damage – a) partial collapse and major settlement of approximately 250 m length of Araniko Highway (Figure 7), b) partial or complete damage of many modern structures (Figure 8), c) development of tension cracks and settlement at 300 m x 300 m plan area (Figure 9).

Major portion of the settled highway is presented in Figure 7. This portion of the highway was constructed during the recent road improvement and includes an engineered fill within MSE walls (that can be seen in Figure 9). Figure 9 shows a few cracks observed along the eastern and western boundaries of the landslide. More than 1 m of vertical drop was observed at different locations within the residual area in the southeastern side of the distressed highway. Several buildings, located in the unstable side of the slope, were observed to have moved by 0.5-1.0 m along with their foundations without having a noticeable tilt in the building. Settlement occurred on both east and west sides of the highway ends near the creek, presented in Figure 10. This creek, which accumulates a large amount of surface run-off during the rainy season (that the authors observed during their field investigation during mid-monsoon period), is currently channelized with approximately 60 cm. diameter concrete pipes.

Figure 6. Observed main distress features at Lokanthali site and locations of in-situ investigation performed for this study (indicated by points "B").

Figure 7. Overall view of distressed portion of Araniko Highway at Lokanthali, Left: North side of the highway; Right: South side of the highway.

INVESTIGATION AND SHEAR TESTING

The Kathmandu valley was formed during the Pliocene to Pliostecene geologic eras by draining the lake water form an outlet point (Yoshida and Gautam, 1988). The subsurface materials in the Kathmandu valley consist mainly of deep lacustrine deposits, which locally are on the order of 600 m thick (Piya 2004). River incisions and excavation activities for different purposes such as highway and building construction locally expose these lacustrine deposits throughout the valley.

Where observed, the deposits consist mainly of poorly consolidated plastic clays and silts, locally interlaid by thin sandy layers.

Figure 8. Typical structural damage observed during the field investigation.

Tiwari and Pradel (2016) conducted field investigation of the study area in August 2015. They explored the subsurface conditions at six locations in the vicinity of Araniko Highway, in the area where seismic ground movements were most prevalent (Figure 6). The most prevalent material at Lokanthali, was a dark grey to black plastic clay, locally known as “Kalimati”, i.e., “black cotton clay” (Figure 11). Later, the authors of this article collected soil samples from the study area and conducted various soil tests at California State University Fullerton. Based on the laboratory test results, the natural moisture content, fine content, clay fraction, liquid limit, plasticity index, and USCS classification of these soft clays were 30-36%, 80-85%, 10-26%, 32-46, 12-17, and ML, respectively. The x-ray diffraction of the separated clay fraction from the soil collected showed dominance of illite with significant proportions of kaolinite.

To assess the strength of this material, Tiwari and Pradel (2016) conducted Swedish Cone Tests (SCT, also commonly known as the Swedish Weight Sounding tests), and in-situ Vane Shear Tests (VST). The undrained shear strengths obtained from both VST and SCT tests are available in Tiwari and Pradel (2016). The effects of near surface desiccation were apparent near ground surface. However, below a depth of 2.5 m, the clays at Lokanthali generally became saturated and were found to be extremely soft. The VST residual strength tests showed that Kalimati clay has high sensitivity. Hence, that its strength is expected to drop rapidly and significantly during cyclic shearing.

Figure 9. Left: Observed tension cracks and settlements throughout the study area.

Figure 10. Concrete pipe and open culvert that used to drain the water from the study area.

Figure 11 (Left). Left: Typical soil profile observed near the main scarp location; Center: Lacustrine deposits exposed along road cut (27°40'30.6"N, 85°21'42.4"E), composed of plastic clay beds separated by very thin sand layers (light grey in the photo); Right: Type of material observed during subsoil exploration.

DYNAMIC STRENGTH PROPERTIES OF SOIL FROM LOKANTHALI SITE

Soil samples were collected from BH 2 of the study area (Figure 6) from four different depths ranging from 0.5 m to 3.0 m. The soil samples were reconstituted at the liquidity index of 1 and consolidated in a constant volume simple shear device at effective normal stresses ranging from 25 to 800 kPa to measure undrained shear strength and corresponding fully softened shear strengths. The laboratory shear test results (Figure 12) shows the undrained strength ratios of 0.25 to 0.47. The fully softened shear strength was obtained from the effective stress analysis of the constant volume direct simple shear device, as presented in Figure 12. The secant fully softened friction angles ranged from 21.5^{o} to 37.5^{o}.

Soil samples collected from the study area was reconstituted at liquidity index of 1 and consolidated in cyclic simple shear device and cyclically sheared at different cyclic stress ratios (CSRs) until 2.5%, 5%, and 10% double amplitude shear strains were observed. The methodology for the cyclic shear tests are similar to that explained in Ajmera et al. (2015). Shown in Figure 13 are the cyclic strength curve and backbone curve of Lokanthali Soil Sample No. 1. Likewise, G/Gmax as well as damping ratio vs shear strain plots are presented in Figure 14. Considering the CSRs of the tested soil, the CSRs of the soil for 5% double amplitude strain is about 0.15 only. Likewise, the test results show that the soil significantly drop its stiffness with an increase in shear strain. Moreover, the soil exhibit over 50% damping at 1% shear strain. The result of monotonic simple shear test immediately after the cyclic loading showed a post-cyclic strength degradation of 71%. This amount of reduction is close to the reduction amount proposed by Ajmera et al. (2015), as shown in Figure 15.

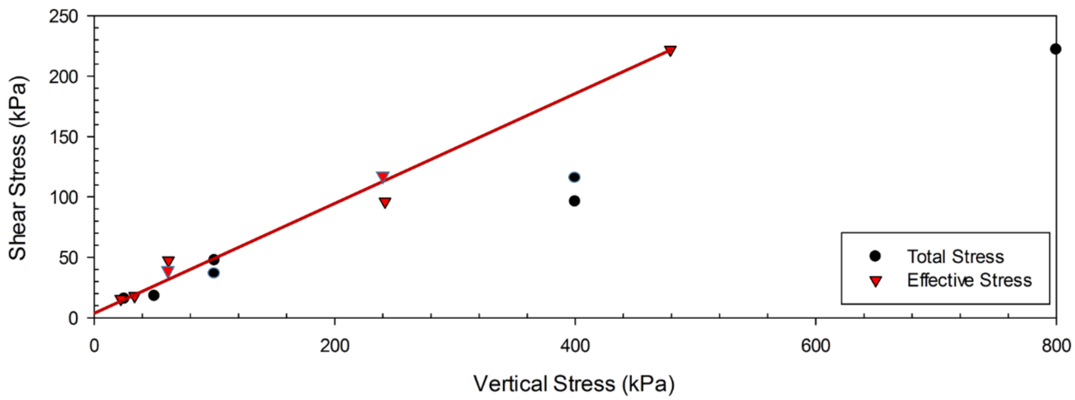

Figure 12. Total and effective shear envelopes obtained from the constant volume monotonic direct simple shear tests for Lokanthali soil Sample 1.

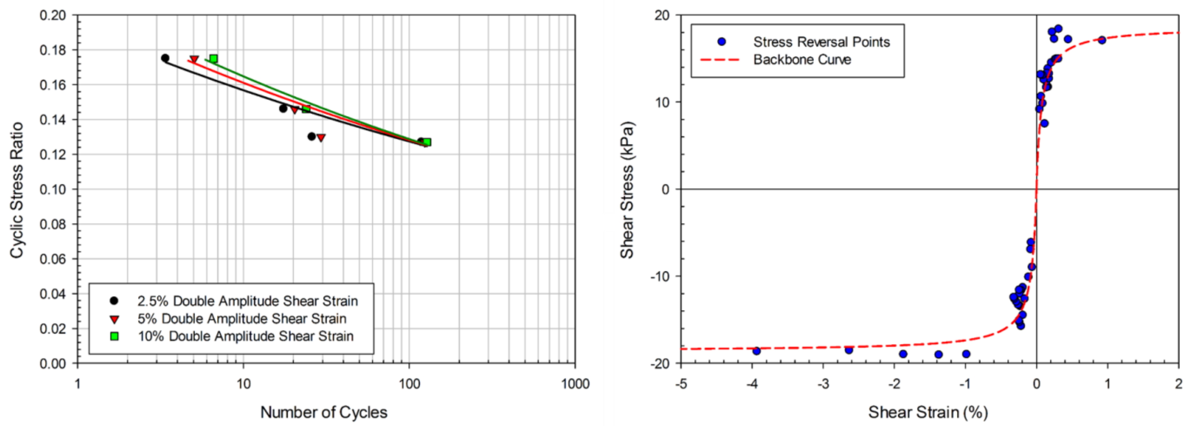

Figure 13. Cyclic stress curves and backbone curves for Lokanthali soil Sample 1.

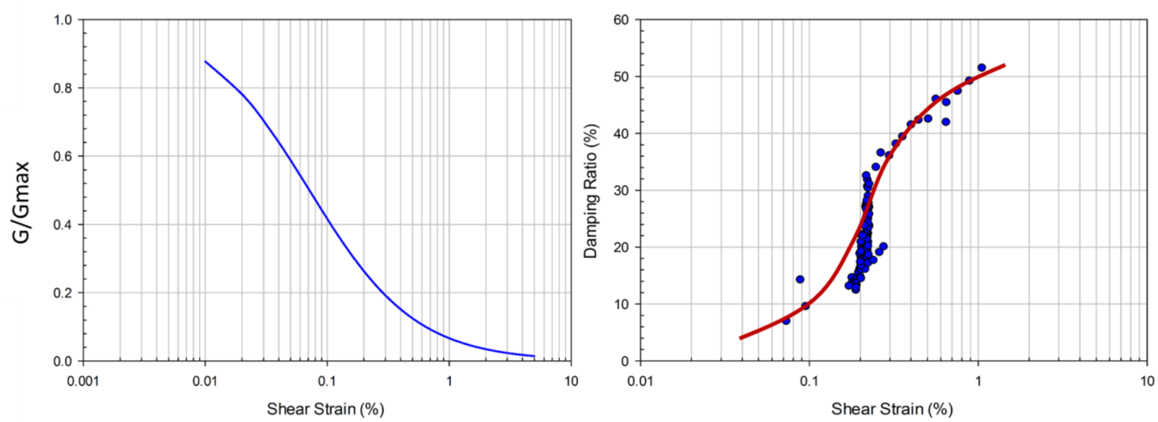

Figure 14. G/Gmax and damping curves for Lokanthali soil Sample 1.

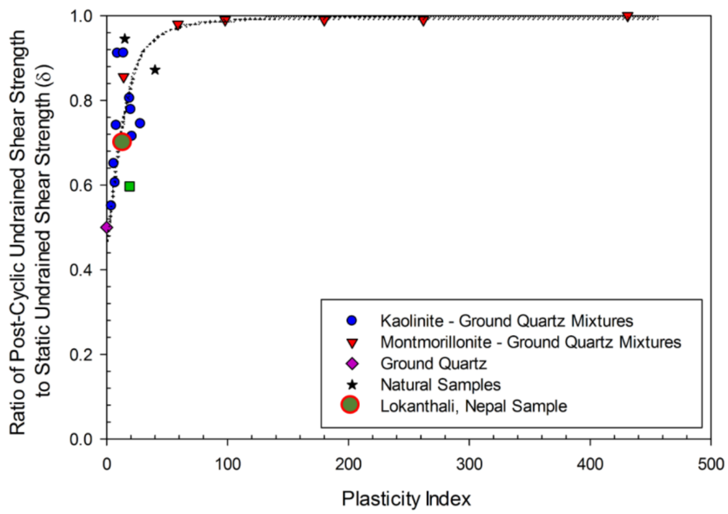

Figure 15. Post-cyclic strength degradation for Lokanthali soil Sample 1, plotted in the strength degradation chart proposed by Ajmera et al. (2015).

DEFORMATION ANALYSIS RESULTS AND POSTULATED FAILURE MECHANISMS

Considering the clays to be very soft and having very small undrained strength ratios depicted both by the laboratory tests and the in-situ measurements, the slope failure at Lokanthali can be considered as a result of seismic activities. Based on the plasticity indices of the materials obtained from the laboratory tests, liquefaction is not considered to be the cause of failure. However, the strongest possible cause of failure could be the reduction in undrained shear strength in combination of seismic force induced by the earthquake. The authors conducted deformation analyses using Phase^{2}v8 (RocScience, 2016) for the cross-section geometry of the Lokanthali ground profile (that was obtained from the field investigation) and the undrained shear strength parameters obtained from the laboratory tests and the strong motion data recorded at the KATNP station, which is close to the study area.

Results of the deformation analyses after the earthquake without and with strength degradation are presented in Figures 16 and 17, respectively. As can be observed from Figure 16, the slope was stable prior to the earthquake and after the earthquake considering the shear strength of soil prior to earthquake. When a strength degradation of 70% (which was obtained from the laboratory test) was applied, maximum horizontal displacements of approximately 1.2 m was observed. Magnitude and amount of those deformations are close to that observed in the field. When the ground motion after the major aftershock of Mw7.3 was applied, the slope did not show any additional deformation. The first author was at Lokanthali site at the time of the Mw 7.3 earthquake and confirmed that the earthquake did not trigger any further movements of the slope. The numerical study result shows that the shear strength degradation in combination with the seismic loading were responsible for the cyclic shear failure at Lokanthali.

Tiwari and Pradel (2016) performed non-linear dynamic geomechanical numerical analyses using deconvoluted ground motions from the recordings at KATNP using the lower and upper bound strengths obtained from in-situ tests. They performed numerical analyses using the computer program FLAC version 7.0 (Itasca, 2011). Their numerical analysis result shows the the vertical and horizontal displacements of 1.0 m and 0.5 m, respectively, which is close to the results obtained from this study.

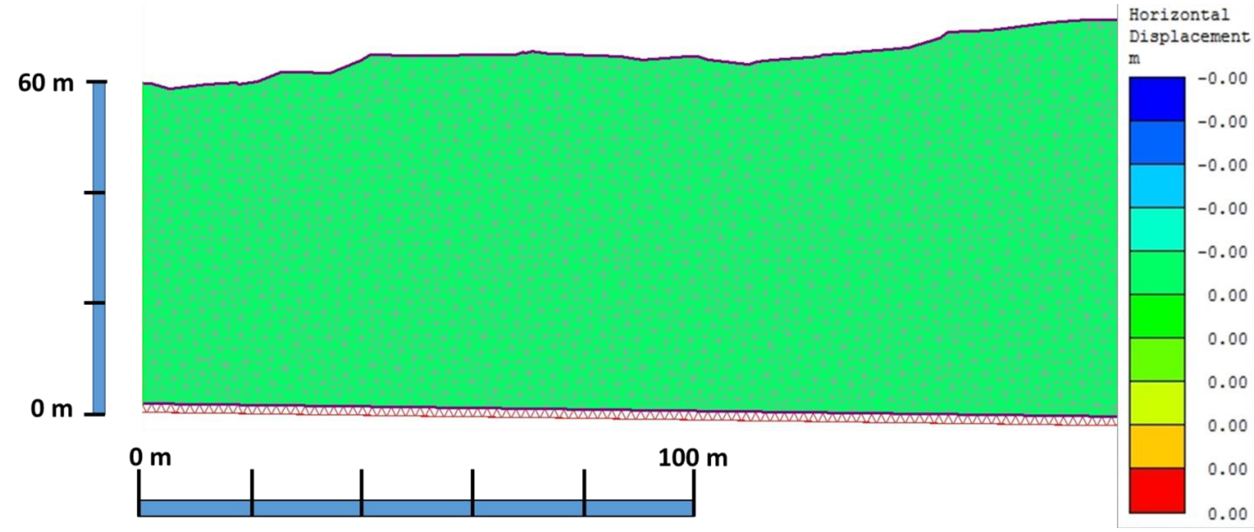

Figure 16. Horizontal displacement of slope obtained after earthquake load without strength degradation, as calculated from numerical analysis

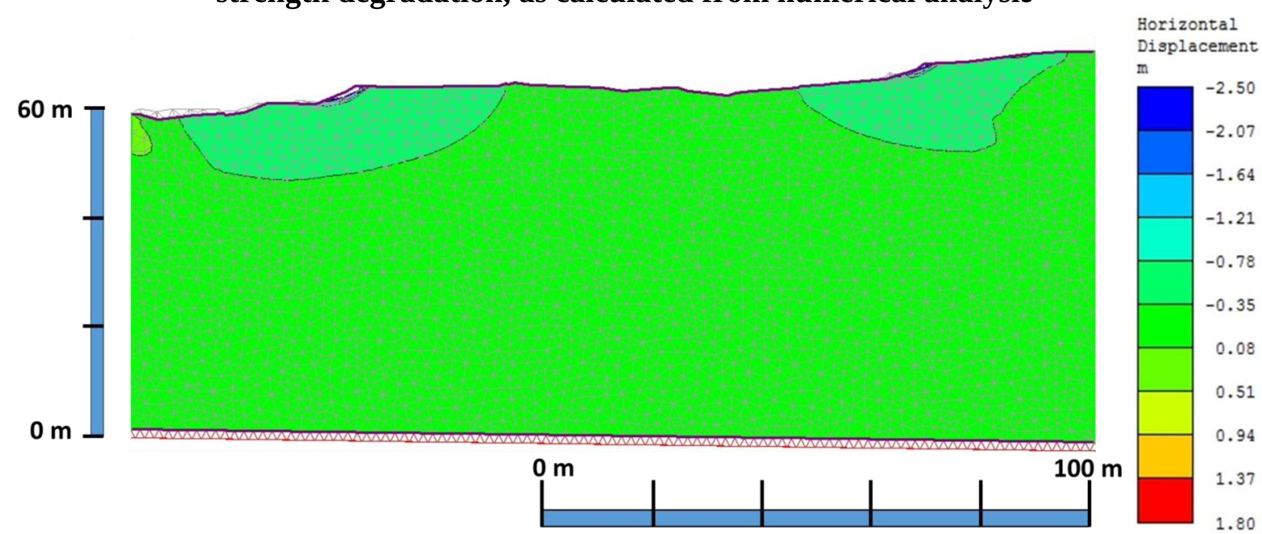

Figure 17. Horizontal displacement of slope obtained after earthquake load with strength degradation, as calculated from numerical analysis

CONCLUSION

Lokanthali cyclic shear failure was one among the major geotechnical damages caused by the 2015 Gorkha Earthquake. In-situ Vane Shear and Swedish Cone Tests conducted on the site revealed that the site is underlain by very soft, plastic lacustrine clays that have very low shear strength and high sensitivity, which are highly vulnerable to seismically induced sliding. The laboratory test results conducted on the soil collected from the site revealed post-cyclic strength degradations of 70%. The numerical analyses conducted by the authors show that the cyclic failure would not occur with earthquake induced ground motion if the shear strength would not have degraded after the earthquake shaking. The horizontal and vertical displacements obtained from the numerical analyses were consistent observed values in the field. Thus Lokanthali cyclic shear failure is attributed to combination of the cyclic loading and associated shear strength degradation.

REFERENCES

Ajmera, B., Brandon, T., and Tiwari, B. (2015). "Cyclic Strength of Clay-Like Materials," Proceedings of 6th International Conference on Earthquake Geotechnical Engineering, Christchurch, New Zealand.

ASTM (2008), "Standard test method for field vane shear test in cohesive soil. ASTM standard D2573-08", ASTM International, West Conshohocken, Penn.

CESMD (2015), "Center for Engineering Strong Motion Data record of USGS Station KATNP on April 25, 2015.

Collins B.D. and Jibson R.W. (2015), "Assessment of Existing and Potential Landslide Hazards Resulting from the April 25, 2015 Gorkha, Nepal Earthquake Sequence", USGS Open-File Report 2015-1142.

Dixit A.M. et al. (2015), "Strong-motion observations of the M 7.8 Gorkha, Nepal, earthquake sequence and development of the N-SHAKE strong-motion network." Seismological Research Letters 86.6 1533-1539.

ENV 1997:3-2000, (2000), Euro Code 7: Geotechnical Design Assisted by Field Testing, 146.

GEER (2015) "Geotechnical Field Reconnaissance: Gorkha (Nepal) Earthquake of April 25 2015 and Related Shaking Sequence", Geotechnical Extreme Event Recon. Report No. GEER-040.

Itasca (2011), "FLAC (Fast Lagrangian Analysis of Continua) Version 7.0," Minneapolis, USA, www.itascacg.com.

JGS (2004), Japanese Standards for Geotechnical and Geoenvironmental Investigation Methods, Standards and Explanations (in Japanese), p.125.

Moss, R. et al. (2015). Geotechnical Effects of the 2015 Magnitude 7.8 Gorkha, Nepal Earthquake and Aftershocks, Seismological Research Letters, 86, 1514-1523.

Piya (2004), "Generation of a geological database for the liquefaction hazard assessment I Kathmandu Valley, Natural Hazard Studies, Enschede, The Nethelands, ITC.

RocScience (2016), "Phase^2 v8"

Seed H.B. and Idriss I.M. (1970), "Soil Moduli and Damping Factors for Dynamic Response Analyses," Report No. UCB/EERC 70/10, Earthquake Engineering Research Center, University of California, Berkeley.

Tiwari, B., Ajmera, B., Dhital, S., and Sitoula, N. R. "Geological, Topographical and Seismological Control on the Co-Seismic Landslides Triggered by the 2015 Gorkha Earthquake," Geotechnical Special Publication2017 (In Press).

Tiwari B. and Pradel D. (2016) "CASE STUDY: Landslide Movement at Lokanthali during the Mw = 7.8 Gorkha (Nepal) Earthquake of April 25 2015", Geotechnical Special Publication, ASCE Press, in press.

Yoshida M. and Gautam P. (1988), "Magnetostratigraphy of Plio-Pleistocene lacustrine deposits in the Kathmandu Valley, central Nepal." Proceedings of Indian National Science Academy A 54 (1988): 410-417.

Lessons Learned From Field Instrumentation and Remote Sensing Studies of Instrumented Pavement and Bridge Infrastructure

Anand J. Puppala[1], Ujwalkumar D. Patil[2] and Tejovikash Bheemasetti[3]

[1]Distinguished University Professor, University of Texas at Arlington, anand@uta.edu
[2]Research Associate, University of Texas at Arlington, ujwalkumar.patil@uta.edu
[3]Research Associate, University of Texas at Arlington, tejovikash.bheemasetti@mavs.uta.edu

ABSTRACT

This keynote paper presents lessons learned from several field-based research studies conducted on pavement and bridge approach sites that were built on various treated materials, lightweight materials, and foundation systems. Field instrumentation, elevation surveys, and remote sensing studies, including terrestrial-based LiDAR studies, are described and analysed to give insight into the performance monitoring of these structures. Some of the data are compared with numerical analysis results to illustrate the benefits of using treated and lightweight materials to reduce pavement distress, such as rutting and differential cracking.

INTRODUCTION

Transportation infrastructure plays a prominent role in a nation's development, and over the years, several noteworthy innovations have taken place. These include new construction materials and procedures, and advanced methods of evaluating field performance. The most important evolutions pertain to the techniques employed to identify the distress patterns on pavements and bridge infrastructures.

Traditional surveying methods, such as robotic total station, tacheometry, 3D scanners, GPS, and others are labor intensive, costly, and very often time-consuming. However, under most conditions, particularly for a large area, a combination of remote sensing, using satellites and unmanned aerial vehicle systems (UAVs), and photogrammetric techniques has proven to be an inexpensive and viable alternative to conventional land surveying techniques (Mills and Newton, 1996; Ahmad, 2006; Uddin and Ahmad, 2014; Room and Ahmad, 2014; Siebert and Teizer, 2014).

Remote sensing techniques, such as synthetic aperture radar (SAR), interferometric synthetic aperture radar (InSAR), Johnson satellite differential interferometry (DInSAR), satellite thermal imagery, light detection and ranging (LIDAR), and unmanned airborne vehicles (UAVs) are used to collect sophisticated data on various infrastructures (Tripolitsiotis et al., 2014; Oscar et al., 2013; Tronin, 2010; Rathje et al., 2006). This data can be analyzed to assess the performance of the civil infrastructure.

The utilization of UAVs is gaining momentum due to their role in civil missions, such as aerial photography, surveillance and control of maritime traffic, fishing and farming surveillance, detection and control of coastal hazards, flood monitoring, terrain mapping, fire disasters, reconnaissance surveys, remote data acquisition of existing pavement conditions, and earthquake damage assessment (Adu-Gyamfi et al., 2014; Shamsabadi et al., 2014; Oscar et al., 2013; Tahar and Ahmad, 2012; Pereira et al., 2009; Rathje et al., 2006).

The first section of this paper briefly introduces remote sensing technology, using an unmanned aerial vehicle system (UAV) and its application to monitor pavement and bridge infrastructures. The second section introduces various materials used in soil treatment, especially chemical treatments for ground improvement, and briefly discusses a case study related to the performance of geofoam material in embankments to reduce pavement distress. In addition, the field instrumentation implemented at this site and the data obtained from it are discussed. The following sections present the details of these studies.

UNMANNED AERIAL VEHICLE SYSTEMS (UAVs)

Rotor wing and fixed wing are the two types of UAV units. Studies suggest that the difference is small between the photogrammetric output obtained from a fixed platform and mobile platform, such as a light-weight rotary wing UAV; hence, the unmanned aircraft system (UAS) can be used for large-scale mapping of aerial terrain (Tahar and Ahmad, 2012).

Close Range Photogrammetry

UAVs have become a popular tool in the past decade due to their versatility. Photogrammetry, using UAVs, can provide a digital elevation model (DEM) and a good quality digital terrain model (DTM) in a short period. The main advantage of UAS technology over traditional surveying techniques is its capability to capture direct, rapid, and detailed images of the study area. The adoption of UAVs for photogrammetry comes under the category of close-range photogrammetry (CRP) (Siebert and Teizer, 2014; Colomina and Molina, 2014). In this paper, this technology is referred to as UAS-CRP.

The three main components of UAS and CRP are the unmanned aerial vehicle, the ground control station, and the communication data link. The system can be controlled from the ground control station (GCS). The availability of GPS and gyroscope technology allows the UAV to precisely deliver the digital camera to the best location and altitude to capture the environment. In photogrammetry, it is a common practice for the ground control point (GCP) to be established after the aerial photography session. There are several methods that can be used to establish the GCP, such as traversing and the Global Positioning System (GPS) (Cesetti et al. 2011).

Rotary and Fixed Wing Type UAV

Fig. 1 shows commercially-available rotary-type UAV (Aibotix X6 multi-rotor) and fixed wing (UX 5) type UAV, both of which are available from Leica Geosystems. Aibotix X6 is a versatile UAS, best suited for acquiring data over relatively small areas. The hovering capability of the aircraft provides a unique data collection platform that can be applied to many areas. The Aibotix X6 multi-rotor UAS can be adopted for small-scale investigations, and the UX5 fixed wing UAS can be adopted for large-scale environments. The Aibotix X6, with an on-board RTK GPS receiver, allows the UAS to communicate and use real-time kinematic positioning provided by the existing TxDOT VRS network.

Fixed wing aircraft systems are better suited for collecting data in remote areas far from roadways with limited access. UX5 is a high-performance system with 50 minutes of flight time per battery charge and a 50 mile per hour cruise speed. This allows rapid collection of data over large areas. At a 2-inch pixel resolution, the UAS can cover 541 acres per charge; at a 4-inch resolution it can cover over 1200 acres per charge.

Application of UASs in Pavement Monitoring

Distress in pavement surfaces usually manifests in the form of surface cracking, roughness, rutting, permanent deformation, or bumps and is caused by its interaction with vehicular traffic, thereby affecting the functional and structural performance of the pavement (Adu-Gyamfi et al., 2014).

a

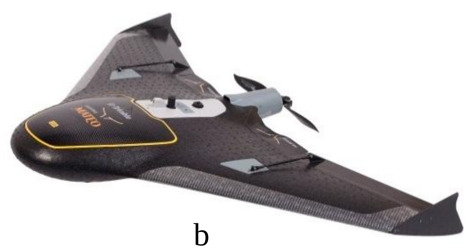

b

Fig. 1 a) Aibotix X6 rotary-type UAS; b) UX 5 fixed wing UAS (Leica Geosystems)

Currently, various departments of transportation (DOTs) conceptualize existing road conditions based on their own pavement distress databases, wherein data is gathered either via physical inspection by engineers/expert technicians or by using road vehicles mounted with optical sensors.

Such traditional methods are expensive, collect only localized data, have poor repeatability due to surveys conducted by different operators, can endanger the safety of personnel involved due to traffic accidents, and may cause delays in processing data (Oh, 1998; Mustaffar et al., 2008). This makes it difficult for the decision-making managers to achieve cost-effective road maintenance plans while staying within budgetary constraints (Shamsabadi et al., 2014). In addition, there is a growing need to perform continuous health monitoring of complete road networks rather than doing repairs for localized patches. Incorporation of accurate data regarding present pavement conditions, along with models predicting the rate of deterioration within the management frameworks, identifies and prioritizes future maintenance and improves the management plan for maintenance, rehabilitation, and/or reconstruction (Adu-Gyamfi et al., 2014). AASHTO defines "physical failure (deterioration)" as one of the major types of risks, reinforcing the importance of continuing health monitoring (AASHTO 2011).

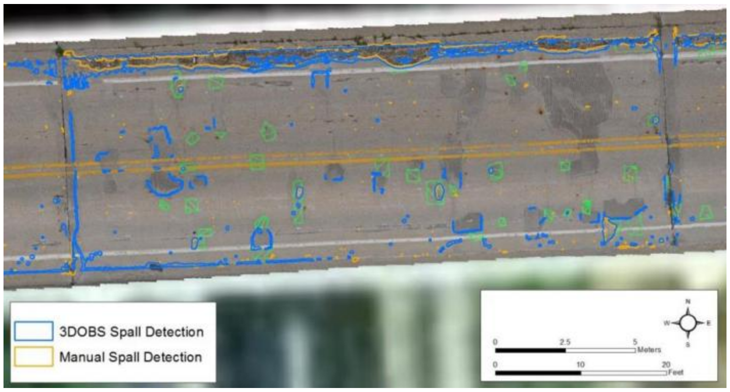

Fig. 2. Manual and automated detection of pavement distress (spalls) at Willow Road Bridge near Milan, MI (Brooks et al., 2015; MTRI 2016).

Fig. 2 depicts a reconstructed orthophoto that was created from a series of photos with a Nikon D5000 camera at Willow Road Bridge near Milan, Michigan. It shows pavement distress, in the form of spalls, detected both manually and through image analysis (Brooks et al., 2015; MTRI 2016). Recent developments in digital photogrammetric technology have provided a low-cost and nearly real-time geometrical imaging technique that can be performed without physically invading the pavement. Mustaffar et al. (2008) used a digital photogrammetric system, combined with an automated pavement imaging program (APIP), to measure pavement distress, such as longitudinal, transverse, and alligator cracking. Accuracy was approximately 90 percent that of traditional methods.

Fig. 3a shows the rotary-type UAV (Berger Tazer 800 helicopter), with a camera attached, employed by Michigan Technological University for aerial surveys of pavements and bridges. Fig. 3b shows the captured high resolution image from a Tazer 800 UAV that was fitted with a Nikon D800 DSLR camera (Brooks et al. 2015).

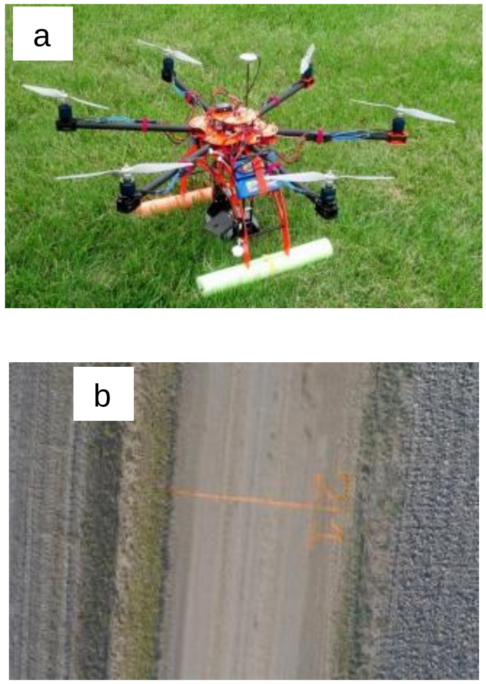

Fig. 3 a) Bergen Tager 800 helicopter UAV (rotary wing) with digital camera; b) High-resolution image collected from Tager 800 UAV camera (Brooks et al. 2015)

Application of UASs in Bridge Monitoring

Recently, the DJI Phantom 2 UAV (quadcopter), which can fly in relatively challenging areas such as beneath bridges and inside confined spaces, was employed for aerial surveys during a research program conducted jointly by the Michigan Tech Research Institute and Michigan Tech Transportation Institute (Brooks et al., 2015). The camera, which has the capacity to take pictures and record video to micro SD cards with a real-time video link of up to 900 feet, was mounted on the DJI Phantom Vision 2 UAS. It was used to create photographic inventories of study sites, such as bridges with hard-to-reach areas, and to look for damage on the inside of a pump station. Fig. 4 shows the same DJI Phantom Vision 2 UAS, with a small (GoPro) camera mounted on its top to shoot photos of the underside of bridges.

Fig. 4. DJI Phantom Vision 2 quadcopter UAS performing under-bridge inspection (Brooks et al., 2015; www.mtri.org).

Photogrammetric output, such as digital maps and orthophotos, can be successfully obtained from small-format cameras. Once analyzed, the data can be used to compare and assess any changes in the infrastructure.

Ground Improvement with Chemical Stabilization

Chemical Stabilizers

Lime reduces the swelling potential, liquid limit, plasticity index, and maximum dry density of the soil and increases its optimum water content, shrinkage limit, and strength (Croft, 1967). It improves the workability and compaction of subgrade soils (Jung et al., 2008). When clay soil is treated with lime and reacts in the presence of water, new compounds are formed through the processes of cation exchange, flocculation, carbonation, and pozzolanic reaction (Al-Rawas et al., 2005). The length of time required for these processes to be completed can vary, depending on the type of clay being treated. Therefore, lime-treated soil is allowed one to four days for mellowing, which helps to establish a consistent or homogeneous mixture (Al-Rawas et al., 2005; Puppala et al., 2006; Chittoori et al., 2013).

Lime stabilization is a widely-used means of chemically transforming unstable soils into structurally sound foundations. Lime stabilization enhances engineering properties in soils by improving strength; improving resistance to fracture, fatigue, and permanent deformation; improving resilient properties; reducing swelling; and enhancing resistance to the damaging effects of moisture. The most substantial improvements in these properties are seen in moderately-to-highly plastic clays (Little, 1999; Puppala et al., 2006, 2013). When lime is combined with water and the soluble silica and alumina present in clay, a chemical reaction occurs, resulting in the formation of new compounds. During this reaction, the primary function of lime is to alter the particle structure and increase resistance to shrink-swell behavior and moisture susceptibility.

A secondary result is an increase in strength caused by the binding of particles through chemical gels, including formed tobermorite gels (Al-Rawas et al., 2005). Tobermorite gels are typically formed due to hydration of calcium silicates and result in the hardening of treated soils. Since alteration of particle structure occurs slowly, depending upon the type of clay present, a mellowing period of one to four days can produce a homogeneous, friable mixture. Many researchers successfully use lime as a stabilizer to modify soils and enhance the soil’s properties.

Soils that have a plasticity index (PI) value higher than 30 are not typically used for stabilization or mixed with cement. To bypass this issue, lime can be added prior to adding the cement, which will keep the soil more pliable (Hicks, 2002). Many researchers have successfully treated subsoils with a mixture of lime and cement. Sirivitmaitrie et al. (2008) studied a combined lime-cement stabilization method performed on several soils from Arlington, Texas, USA. Laboratory tests, including Atterberg limits, unconfined compressive strength (UCS) tests, resilient modulus (MR), vertical swell, and linear shrinkage bar tests were conducted on untreated soils, lime-treated soils (lime making up 12% by dry weight of soil), and lime-and-cement treated soils (6% lime and 6% cement). The resilient moduli test results showed that the moduli were significantly higher for lime-cement treated soils. After laboratory studies, several pavement test sections were built on lime-cement treated soils, and the performance data indicated that these treatments provided effective stabilization of soils in Arlington, Texas. Based upon this study, Sirivitmaitrie et al. (2008) recommended that the stabilizer dosage be reduced from a total of 12% to 8%, which may provide stable and uniform support to pavements.

Fly ash is one of four coal combustion products (CCPs) that are produced as a byproduct of burning coal for generating electricity in the United States. The remaining three types are bottom ash, boiler slag, and flue gas desulfurization byproduct material (i.e., gypsum). Fly ash makes up 58% of CCPs; of this 58%, only 32% is reused in construction. Its primary construction application is its use as part of the base material in highways. Another benefit of its use in civil applications is that less fly ash will be placed in a landfill, thereby reducing landfill costs and mitigating environmental impacts (Arora and Aydilek, 2005).

Coal burning power plants do not produce the same types of fly ash since each plant is operated differently and may use a different type of coal. Two major groups of fly ash are produced: Class C and Class F. Burning lignite and subbituminous coal produces Class C fly ash, whereas burning anthracite, also known as bituminous coal, produces Class F fly ash (Çokça, 2001). Although there can be multiple variations of the chemical additive, fly ash particles generally consist of hollow spheres of silicon, aluminum, iron oxides, and carbon, all of which make both classes of fly ash pozzolans-siliceous or siliceous and aluminous materials. Class F fly ash is not used as often as Class C because it is not a self-cementing material and requires an activator, either lime or cement, to form pozzolanic stabilized mixtures (PSMs) (Arora and Aydilek, 2005).

A combination of lime and fly ash is effective for stabilizing silty and sandy soils because it drastically increases the stiffness of the final product. Bergeson and Barnes (1998) used Class C fly ash with lime to develop guidelines for determining the structural layer coefficient for the base layer of flexible pavement, and showed that the required base-layer thickness decreases with the addition of both additives. Although lime, cement, and fly ash are commonly-used stabilizers, there are many other options in the market, such as cement bypass dust (CBPD), also known as cement kiln dust (CKD); lime kiln dust (LKD); blast furnace slag; and others (Al-Rawas et al., 2002). These are supplementary and secondary stabilizers that do not work well alone. They require a primary stabilizing agent, such as lime or cement additives, to initiate the stabilization reactions (Chittoori et al., 2013; Puppala, 2016).

Lightweight Materials in Infrastructure

Various lightweight materials have been used in earthworks construction, including EPS (expanded polystyrene) geofoam, foamed Portland cement concrete, wood fibers, shredded tires, expanded shale and clays, boiler slag, air-cooled blast furnace slag, fly ash, and expanded blast furnace slag. The following section discusses the use of EPS geofoam as a partial substitute material in road embankments.

Project Description

The bump at the end of a bridge is a pervasive problem that is common to most bridge infrastructures. It is frequently encountered in Texas and many other states, and transportation agencies spend millions of dollars annually to repair them. The major cause of the problem is the settlement of the backfill materials and foundation soils, as well as the erosion of the backfill, and is due to the settlement of the approach slabs with reference to the bridge deck level. Several technologies to solve this problem have been tried by various organizations; however, the settlement issue of the approach slabs on high embankments seems to persist.

A site in Johnson County, Texas, USA experiences huge settlements and was the focus of a research project launched at the University of Texas at Arlington. It is located on US 67 over SH 174 in Cleburne, Texas. The bridge is 12.2 m (40 ft.) high, and in the 16 years since its construction, the approach slab has experienced more than 16 in. of settlement, as shown in Fig. 5. One of the primary causes of the settlement is the self-weight of the 40-ft high embankment fill material which undergoes self-consolidation, inducing large stresses and settlement to the underlying foundation subgrade. To mitigate the settlement, several treatment methods were applied, including hot mix overlays, grout injections, soil nailing, and others; however, they were not effective.

Laboratory studies were conducted on the basic properties of the soil, including compressibility characteristics and shear strength, and on the properties of the EPS 22 geofoam. Field monitoring studies were also conducted at regular time intervals to study the performance of the EPS geofoam under live traffic. Modeling studies were conducted, using the PLAXIS program, to predict the long-term performance of the test section.

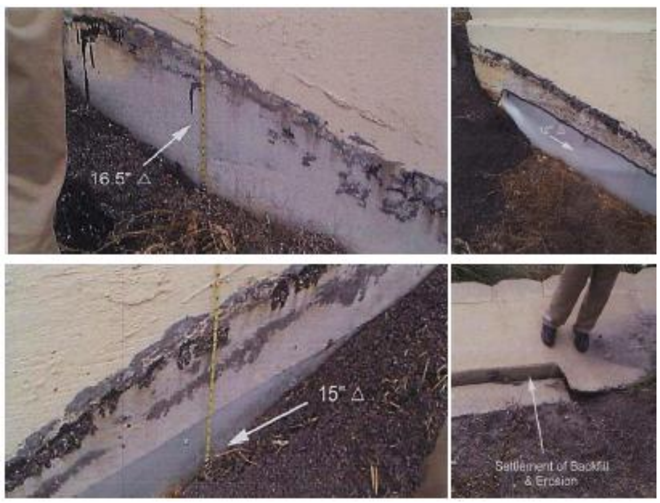

Fig. 5 Bridge approach slab settlement in Johnson County, Texas, USA

The Texas Department of Transportation (TxDOT) considered several lightweight fill materials to reduce the self-weight of the soil, and selected EPS geofoam as an embankment fill material. The lightweight and compact EPS geofoam material has specific advantages, such as ease of construction, lighter weight (at least 20 to 30 times lighter than other lightweight fill alternatives), ability to reduce the lateral stresses on retaining walls, limited labor costs, and an expedited construction schedule, which reduces the overall cost of the structures (Archeewa, 2010).

The embankment was reconstructed, replacing the top of the existing fill soil with lightweight EPS 22 geofoam blocks to reduce the loads imposed on the underlying subgrade and to reduce the magnitude of settlement due to the consolidation phenomenon. Because of the huge settlements, the quality assurance studies of the performance of the geofoam approach slab was the key aspect of this study. The following sections discuss the site location and quality assurance studies conducted for this project. The research is ongoing to achieve the final objective, which is to develop design and construction guidelines, for future use, on other geofoam-related construction.

Site Description

The test site was located at the intersection of US 67 and State Highway 174 in Johnson County, Texas USA, as illustrated in Fig. 6. The bridge was designed for two-lane traffic, and both ends of the bridge were placed on abutments supported by drilled shaft foundations. Approach embankments were built adjacent to the bridge abutments to support the interfacing bridge approach slabs and roadways. The embankment fill soils were classified as clayey sand (SC), and the foundation soils were classified as clays of low plasticity (CL), as per the USCS classification.

Fig. 6 Test site location

Construction with EPS Geofoam

The rehabilitation of the test site began in January 2012. The test site was constructed with EPS 22 geofoam, which has unit weight of 24.35 kg/m^3 (1.52 pcf) and unconfined compressive strength of 152 kPa (3174 psf). The embankment soils were first excavated to a depth of about 2.74 to 3.04 m (8 to 10 ft.).

A sand layer was put in place to provide a proper leveling base before the installation of the EPS geofoam. The geofoam blocks were then placed on top of the sand layer to a height of 1.83 m (6 ft.) and were connected, using a barbed plate, and encapsulated in a geotextile membrane, which protected the geofoam blocks from the infiltration of any fluids and termite infestations. Fig. 7 illustrates the construction process of the EPS geofoam. Different sizes of the geofoam blocks were used in this construction to fill all the narrow spaces. A pavement structure of 0.61 m (2 ft.) was placed on top of the geofoam blocks, using a flex base and hot mix asphalt concrete (HMAC) pavement surface.

Fig. 7 Construction of EPS Geofoam

Instrumentation Details

The test site was instrumented to monitor the settlement and pressure that was exerted on the structure. Horizontal inclinometers, which measured the displacement of the subsurface layers in a direction perpendicular to the axis of a flexible plastic casing, were used to monitor the settlement. Four small trenches were excavated in the top geofoam blocks in accordance with the size of the inclinometer casing, as shown in Fig. 8.

Long PVC casing pipes of about 7.9 m (24 ft.) were installed in the trenches, and the extended ends of the casings were fastened with cast-in-place concrete bases. Four earth pressure cells, made of two circular stainless steel plates welded together to form a sealed cavity, were installed in the embankment to monitor the pressures exerted on the structure. The cavity was filled with a non-compressible fluid, and a pressure transducer was connected to the cell. Fig. 9 depicts the installation of the pressure cells in the embankment. A Quattro Logger, a compact data logger, was used to monitor the four installed pressure cells. The logger was automated to record the pressures at 15-minute intervals. The recorded data was retrieved after every site visit.

Fig. 8 Horizontal inclinometers installation

Fig. 9 Pressure cell installation

Results and Analysis

The horizontal inclinometer and pressure cell readings were taken monthly to evaluate the performance of the geofoam block structure. Fig. 10 presents the plot of the cumulative settlement of the embankment along the inclinometer casing at one station.

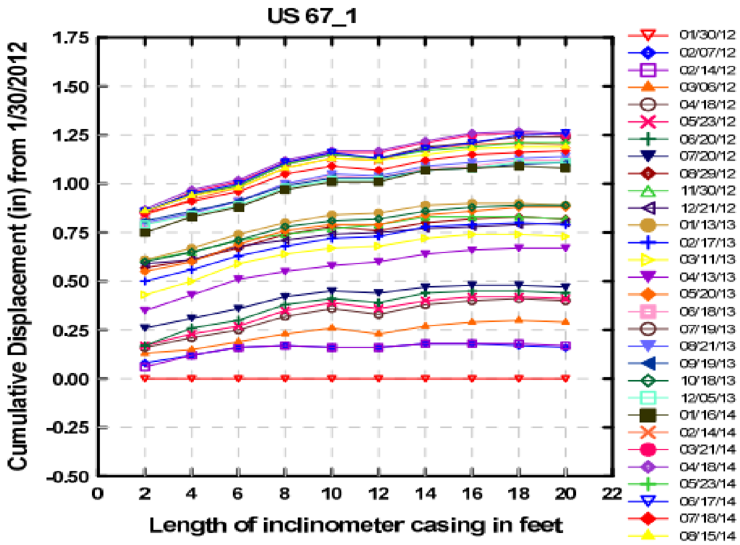

Fig. 10 Horizontal Inclinometer readings

The data was collected in January 2012, immediately after the installation. From the plots, it can be observed that the maximum displacement was less than 33 mm (1.5 in.). This means that the geofoam blocks can sustain the traffic load effectively and can mitigate the settlements (Ruttanaporamakul 2014), thus assuring the quality of the geofoam blocks' performance in the bridge approach slabs.

The data recorded from the pressure cells depicted an average vertical pressure of 33.8 kPa (4.9 psi) and 12.4 kPa (1.8 psi) from pressure cells 1 and 2. The pressure cells, that were installed to measure the lateral pressures, provided negative values due to the loss of contact of the pressure cell to the EPS geofoam layer and abutment walls.

Summary and Conclusions

Based on the studies discussed in the first section of this paper, a combination of the UAV system and photogrammetry seems to be a promising technology. However, its performance in the transportation arena and in the geotechnical environment has been minimally explored, and more research is needed.

The second case study evaluated the performance of the geofoam blocks used as fill material in the embankment to arrest settlement of the approach slab. The use of instrumentation, such as horizontal inclinometers and pressure cells, provided the real field settlements and pressures that were occurring in the bridge approach slabs.

Additional studies using remote sensing equipment, such as the terrestrial Lidar and UAVs mounted with cameras, are ongoing at the University of Texas at Arlington. In the future, this data will be compared with that of the conventional instruments that was presented in this study.

ACKNOWLEDGEMENTS

The author would like to acknowledge Mr. David Marshall, Ms Shelly Hattan, and Mr. Richard S. Williammee for their valuable assistance and cooperation throughout the research.

REFERENCES

Adu-Gyamfi, Y.O., Teenaah, T., Attoh-Okine, N. O., and Kambhamettu, C. (2014). "Functional evaluation of pavement condition using a complete vision system." J. Transp. Eng., vol. 140 (9), ASCE, pp. 1-10.

Ahmad. A. (2006) "Digital photogrammetry: An experience of processing aerial photograph of UTM acquired using digital camera." In AsiaGIS, 3-5 March; UTM Skudai, Johor, Malaysia, pp. 1-11.

Al-Rawas, A. A., Hago, A. W., and Al-Sarmi, H. (2005). "Effect of lime, cement and Sarooj (artificial pozzolan) on the swelling potential of an expansive soil from Oman." Build. Environ., 40(5), 681-687.

American Association of Highway and Transportation Officials (AASHTO) (2011). AASHTO transportation asset management guide: a focus on implementation. Washington, D.C.: AASHTO, 2011.

Archeewa, E. (2010). "Comprehensive studies on deep soil mixing and lightweight aggregates application to mitigate approach slab settlements." Dissertation submitted in partial fulfilment of the requirements for the degree of the Doctor of Philosophy, the University of Texas at Arlington, Arlington, Texas.

Arora, S., and Aydilek, A. (2005). "Fly-ash amended soils as highway base materials." J. Mater. Civ. Eng., ASCE, 17(6), pp. 640-649.

Bergeson, K. L., and Barnes, A. G. (1998). "Iowa thickness design for low volume roads using reclaimed hydrated class C fly ash bases." USUERI-Ames 98401, Iowa State University, Ames, Iowa, pp. 253-258.

Brooks, C. N., Oommen, T., Havens, T. C., Ahlborn, T. M., Zhang, K., Mukherjee, A., and Dobson, R. (2015). "Implementation of unmanned aerial vehicles (UAVs) for assessment of transportation infrastructure – Phase II." Prepared by Michigan Technological University for MDOT, 68 pgs., www.mtri.org.

Brooks, C., Dobson, R. J., Banach, D. M., Dean, D., Oommen, T., Wolf, R. E., Havens, T. C., Ahlborn, T. M. and Hart, B. (2015). MDOT: "Evaluating the use of unmanned aerial vehicles for transportation purposes." Michigan Tech Research Institute and Michigan Tech Transportation Institute, Final report No. RC-1616, Revised version April 7, 2015, www.mtri.org.

Cesetti A., Frontoni E., Mancini A., Ascani A., Zingaretti P. and Longhi S. (2011). "A visual global positioning system for unmanned aerial vehicles used in photogrammetric applications." Journal of Intel Robot systems, vol. 61, pp. 157-168.

Chen F. H. (1988). Foundations on expansive soils. 2nd ed. New York: Elsevier Science Publications.

Chittoori, B. C. S., Puppala, A. J., Wejrengsikul, T., and Hoyos, L. R. (2013). "Experimental studies on stabilized clays at various leaching cycles." ASCE, J. Geotech. Geoenviron. Eng., 139(10), 1665-1675.

Cokca, E. (2001). "Use of class C fly ashes for the stabilization of an expansive soil." J. Geotech. Geoenviron. Eng., 127(7), pp. 268-273.

Colomina I., and Molina P. (2014). "Unmanned aerial systems for photogrammetry and remote sensing: a review." ISPRS Journal of Photogrammetry and Remote Sensing, vol. 92, pp.79-97.

Croft, J. B. (1967). “The influence of mineralogical composition on cement stabilization.” Geotechnique, 17: 119-135.

De Bel R., Correia, A. G., Verbrugge, J. C. (2009). “Contribution of loamy soil treatment to improve embankments performance.” Geotech. Spec. Publ., 189, pp. 186-191.

Hicks, R. G. (2002). Stabilization design guide. FHWA_AK_RD_01-6B, Oregon State University., Corvallis, Oregon, TRB: 2002.

Jung, C., Bobet, A., Siddiki, N. Z., and Kim, D. (2008). “Long-term performance of chemically modified subgrade soils in Indiana.” Transp. Res. Rec., 2059, 63-71.

Little, D. N. (1999). “Evaluation of structural properties of lime stabilized soils and aggregates: Vol. 1, Summary of Findings.” National Lime Association Publication.

Mills, J.P. and Newton, I. (1996). “Aerial photography for survey purposes with a high resolution small format digital camera.” Photogrammetric Record, vol. 15(88), pp. 575-587.

Mustaffar, M., Ling, T. C., and Puan, O. C. (2008). “Automated pavement imaging program (APIP) for pavement cracks classification and quantification – A photogrammetric approach.” The International Archives of the photogrammetry. Remote sensing and spatial information science, 37(B4): pp. 367-372.

Nelson J. D., and Miller J. D. (1992). Expansive soils: Problems and practice in foundation and practice in pavement engineering. Wiley, New York: Colorado State University.

Oh, H. (1998). “Image processing technique in automated pavement evaluation system.” University of Connecticut: Ph.D. Dissertation.

Oscar, E. S., Ellen, M. R., and Buckely, S. M. (2013). “Deformation of a rapidly moving landslide from high-resolution optical satellite imagery.” Geo-Congress 2013, ASCE, San Diego, CA, March 3-7, 2013, GSP 231, pp. 269-278.

Pedarla, A., Chittoori, B. C. S., Puppala, A. J. (2011). “Influence of minerology and plasticity index on the stabilization effectiveness of expansive clays.” J. Transp. Res. Board, Nat. Acad. Sci., Transp. Res. Board, 2212: 91-99.

Pereira, E., Bencatel, R., Correia, J., Felix, L., Goncalves, G., Morgado, J., and Sousa, J. (2009). “Unmanned air vehicles for coastal environmental research.” Journal of Coastal Research, SI 56 (Proceedings of the 10th International Coastal Symposium), 1557-1561, Lisbon, Portugal, ISSN 0749-0258.

Puppala, A. J. (2016). “Advances in ground modification with chemical additives: From theory to practice.” Transportation Geotechnics, 9, 123-138.

Puppala, A. J., Chittoori, B. C. S., Talluri, N., Le, M., Bheemasetti, T., and Thomey, J. (2013). “Stabilizer selection for arresting surficial slope failures: A sustainability perspective.” ASCE GeoCongress, San Diego, California, pp. 1465-1474.

Puppala, A. J., Kadam, R., Madhyannapu, R., and Hoyos, L. R. (2006). “Small strain shear moduli of chemically stabilized sulphate-bearing cohesive soils.” J. Geotech. Geoenviron. Eng., 1(32), 322-336.

Rathje, E. M., Woo, K., and Crawford, M. (2006). “Spaceborne and airborne remote sensing for geotechnical applications.” GeoCongress 2006: Geotechnical Engineering in the Information Technology Age, Atlanta, Georgia, US, February 26-March 1, 2006, pp.1-19.

Ruttanaporamakul, P. (2014). Evaluation of lightweight geofoam for mitigating bridge approach slab settlements. Doctoral dissertation, The University of Texas at Arlington, Texas, USA.

Room, M.H.M., and Ahmad, A. (2014). “Mapping of river using close range photogrammetry technique and unmanned aerial vehicle system.” 8th International Symposium of the Digital Earth, Earth and Environmental Science, vol. 18, pp. 1-6.

Shamsabadi, S. S., Wang, M., and Birken, R. (2014). “PAVEMON: A GIS-based data management sysytem for pavement monitoring based on large amounts of near-surface geophysical sensor data.” 27th Symposium on the Application of geophysics to engineering and environmental problems *2014*, pp. 130-133, Red Hook, NY, Curran.

Siebert, S., and Teizer, J. (2014). “Mobile 3D mapping for surveying earthwork projects using an unmanned aerial vehicle system.” Automation in Construction, vol. 41, pp. 1-14.

Sirivitmaitrie, C., Puppala, A. J., Saride, S., and Hoyos, L. R. (2008). “Combined lime and cement treatment of expansive soils.” ASCE, Geotechnical Special Publication, 178, Geo-Congress, New Orleans, Louisiana, pp. 646-653.

Tahar, K. N., and Ahmad, A. (2012). “A simulation study on the capabilities of rotor wing unmanned aerial vehicle in aerial terrain mapping.” International Journal of Physical Sciences, 7(8), pp. 1300-1306.

Tripolitsiotis, A., Chrysanthos, S., Eirini, P., Zacharias, A., Stelios, M., and Panagiotis, P. (2014). “Complementing geotechnical slope stability and land movement analysis using satellite DinSAR.” Central European Journal of Geosciences, Ist International Conference on Remote Sensing and Geoinformation of Environment, vol. 6, No. 1, pp. 56-66, March 2014.

Tronin, A. A. (2010). “Satellite remote sensing in seismology – A review.” Remote Sensing, vol. 2, pp. 124-150, doi: 10.3390/rs2010124.

Udin, W. S. and Ahmad, A. (2014). “Assessment of Photogrammetric Mapping Accuracy Based on Variation Flying Altitude Using Unmanned Aerial Vehicle.” 8th International Symposium of the Digital Earth, Earth and Environmental Science, vol. 18, pp. 1-7.

Yi, Y., Liu, S., and Puppala, A. J. (2016) “Laboratory modeling of T-shaped soil-cement column for soft ground treatment under embankment.” Geotechnique, 66(1), 85-89.

Some applications of the mechanics of unsaturated soils in forensic geotechnical engineering

S.K. Vanapalli, Z. Han, S. Qi & Y. Liu

Department of Civil Engineering, University of Ottawa, Ottawa, ON, K1N 6N5, CANADA

ABSTRACT

Present understanding of the mechanics of unsaturated soils has advanced significantly in recent decades for proposing useful tools in the rational design and analysis of the geotechnical infrastructure. Such design approaches are suitable in semi-arid and arid regions where soils are typically found in a state of unsaturated condition. This paper highlights the need for extending the mechanics of unsaturated soils for forensic geotechnical engineering investigations. Focus of these studies has been mainly directed to expansive soils investigations which are typical examples of unsaturated soils and are challenging to the geotechnical engineers. Forensic investigations are widely extended in expansive soils regions because of extensive and expensive failures to the constructed infrastructure in comparison to other conventional soils. Examples summarized include the design of slopes in expansive soils taking account of the influence of infiltration, the design and analysis of the failure of retaining walls and piles in expansive soils taking account of the influence of swelling pressure and the design of pavements considering the influence of the variation moisture content. The rationale and the feasibility of using the mechanics of unsaturated soils in the forensic geotechnical engineering investigations are highlighted in this paper.

Keywords: unsaturated expansive soils, suction, forensic geotechnical engineering, slopes, retaining walls, piles, pavements.

INTRODUCTION

Forensic geotechnical engineering involves scientific and legalistic investigations to determine the failure or distress of a structure that is likely attributed to incomplete soil investigations, interpretation of soil properties or fallacies associated with the geotechnical design procedures or other unforeseen reasons. Forensic geotechnical engineering is gaining increasing importance in many countries as geotechnical failures may lead to litigation and even criminal action (Poulos 2016). Carper (1986) has summarized various lessons and other valuable information that facilitates geotechnical engineers to learn from failures. Day (1999) introduced valuable forensics guidelines that can be extended in geotechnical and foundation engineering area. Most of the forensics investigations presently used in geotechnical engineering practice is based on conventional soil mechanics principles assuming that the failure or distress to the infrastructure occurs only when the soil is in a state of saturated condition. In other words, soil is assumed to be a two phase material with soil and water constituting the solids and liquid, respectively. The forensic foundation of geotechnical investigations uses the effective stress equation, $(\sigma - u_w)$, which is a single stress state variable, as a key tool.

Geotechnical problems for reliable interpretation, particularly in arid and semi-arid regions where the soils are typically found in a state of unsaturated condition, have to consider the influence of matric suction. The matric suction is the negative pore-water pressure with respect to pore-air pressure, which is considered to be atmospheric. In unsaturated condition, soil is a three phase material with air as an additional gaseous phase. Two stress states variables; namely the net normal stress, $(\sigma - u_a)$ and the matric suction, $(u_a - u_w)$ are required (where σ is the total stress, u_a is the pore air pressure and u_w is the pore water pressure) for interpretation of unsaturated soils behavior (Fredlund and Rahardjo 1993). For rigorous forensic analyses of the failure of geotechnical infrastructure, it is important for engineers to take into account the contribution of the external environmental factors (i.e. flux boundary conditions) such as the infiltration and evaporation. The influence of environmental factors can be well interpreted using the mechanics of unsaturated soils. This paper highlights rational design principles for some routine geotechnical infrastructure using the mechanics of unsaturated soils from recent literature. The illustrated cases include the assessment of the slope stability of expansive soils upon infiltration, the analysis of the failure of retaining walls and piles in expansive soils and pavements. The critical role of the mechanics of unsaturated soils in the failure and distress analysis of common geotechnical infrastructure considering the influence of the external environmental factors is highlighted for these infrastructures. Focus of these studies has been mainly directed to expansive soils investigations which are typical examples of unsaturated soils. More forensic investigations are likely because of extensive and expensive failures to the infrastructure constructed in expansive soils in comparison to other conventional soils. The rationale and the feasibility of using the mechanics of unsaturated soils in the forensic geotechnical engineering are succinctly summarized in this paper.

THE VOLUMETRIC BEHAVIOR OF EXPANSIVE SOILS AND THE ASSESSMENT OF THE SLOPE STABILITY OF EXPANSIVE SOILS UPON INFILTRATION

Expansive soils are widely distributed in semi-arid and arid regions of the world; including, Argentina, Australia, Burma, Canada, China, Cuba, Ethiopia, Ghana, Great Britain, India, Iran, Kenya, Mexico, Morocco, Rhodesia, South Africa, Spain, Turkey, USA, and Venezuela (Fredlund and Rahardjo 1993, Chen 2012). Expansive soils that contain active clay mineral such as the montmorillonite imbibe significant amount of water. The clay mineral montmorillonite has a high water retention capacity that contributes to dramatic swell characteristics. The volume increase of an expansive soil element can reach 30% or even more for expansive soils with montmorillonite. This process is only partially reversible when water content decreases due to evaporation or desiccation. During this period, expansive soil contracts contributing to the development of cracks and fissures. The shrinkage and swelling associated with drying and wetting cycles of expansive soils significantly alter their structure characteristics promoted by the development of fissures and cracks and weakened shear strength resistance. Due to this reason, slope failures are often triggered by a wetting process: such as rainfall or snow melting.

Post-failure investigations (including laboratory and field studies) have shown that the physical reactions of expansive soil upon wetting are mostly responsible for the eventual catastrophic collapse, including:

- Initial suction decrease leads to significant amount of loss in soil shear strength.
- The stress regime changes associated with water infiltration in the shallow layer of expansive soil contributes to the swelling potential. The stress redistribution might be responsible for the observed irrecoverable displacements due to plastic straining at yielding.
- Expansive soil is usually over consolidated and exhibits softening behavior both under constant suction and infiltration conditions.

Failures to account for the above processes contribute to an inaccurate design of slope when they are based on conventional saturated soil mechanics, which typically assume constant values for soil parameters (Duncan 1996). However, in reality the soil parameters are not constant and are influenced by the flux boundary conditions of water infiltration and other precipitation activities (Zhang et al. 2010). For this reason, stability investigations in expansive soils from back calculations suggest stable state condition of the slope in spite of their failure (Widger and Fredlund 1979). Rigorous slope stability analysis and appropriate slope mitigation procedures can be achieved by extending soil mechanics of unsaturated soils. In other words, this understanding can also be extended in forensic investigations. In this section, advanced methodologies are highlighted by considering soil behaviour with varying saturation conditions during a wetting process. Some examples are illustrated using numerical techniques.

Numerical techniques are valuable for providing quick comparative studies using unsaturated soil mechanics by selecting appropriate unsaturated soil properties for evaluation of expansive soil slope that is subjected to wetting process associated with infiltration. Qi and Vanapalli, (2015a,b,c,d) have undertaken several studies in this direction which provide new insights for understanding the most fundamental physical process of interaction between water and soil phases leading to eventual collapse. The methodologies and most important findings from these studies are summarised here from two aspects, including (i) effects of cracks (Qi and Vanapalli, 2015a,b,c); and (ii) role played by swelling behaviour (Qi and Vanapalli, 2016d).

Effect of cracks

The effect of cracks on the slope stability of expansive soils is investigated by Qi and Vanapalli (2015a) using a failed slope for illustration purposes. This slope is located in Regina, Canada and failed in the spring of 1973, which was triggered by infiltration from snow melting 6 years after construction. The cyclic environmental changes during the period between construction and failure led to an abundant of cracks and fissures within the surficial layer where the failure mass is located. The effect of fissures and cracks is considered through use of the bimodal (Soil Water Characteristic Curve (SWCC) and bimodal permeability function with an increased saturated coefficient of permeability, assigned to the surficial layer of numerical model for a slope shown in Figure 1.

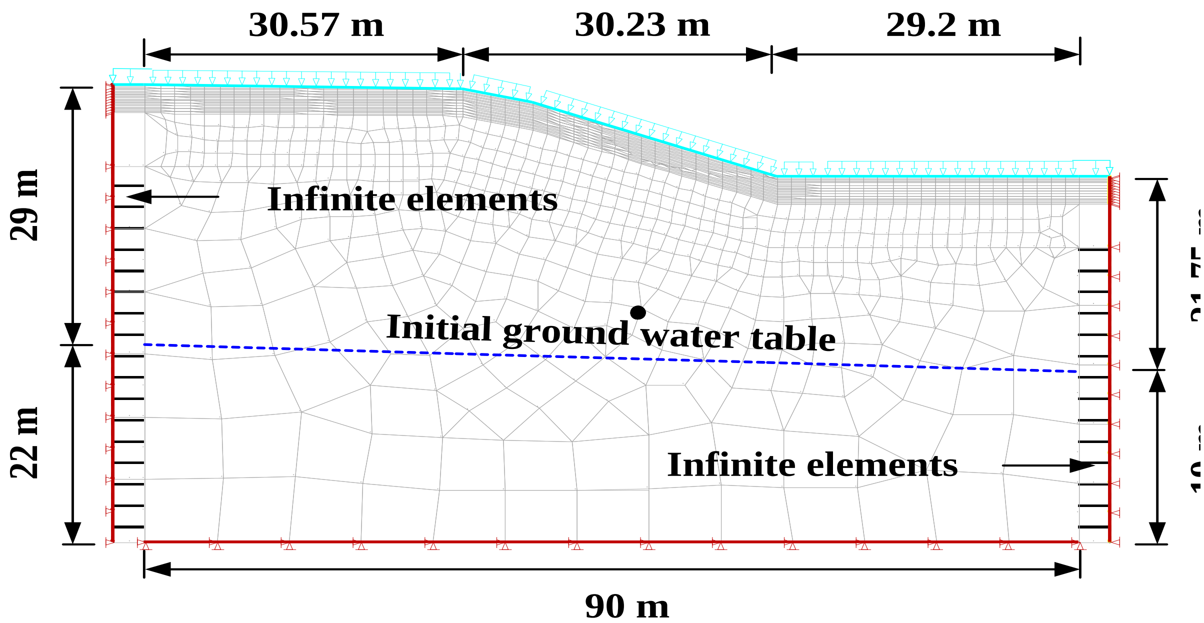

Figure 1 Finite element method based computational model (modified after Qi and Vanapalli 2015a)

The permeability coefficient at saturated state for cracked soil can increase significantly due to the influence of cracks and fissures; however, it is difficult to be determined. For this reaon, parametric analysis is undertaken by Qi and Vanapalli (2015a): six cases (i.e. different saturated coefficient of permeability values for cracked soil by 0.5, 1, 1.5, 2, 2.5, and 3 of magnitudes, respectively in comparison to laboratory measured value of permeability coefficient) are assumed for analysis.

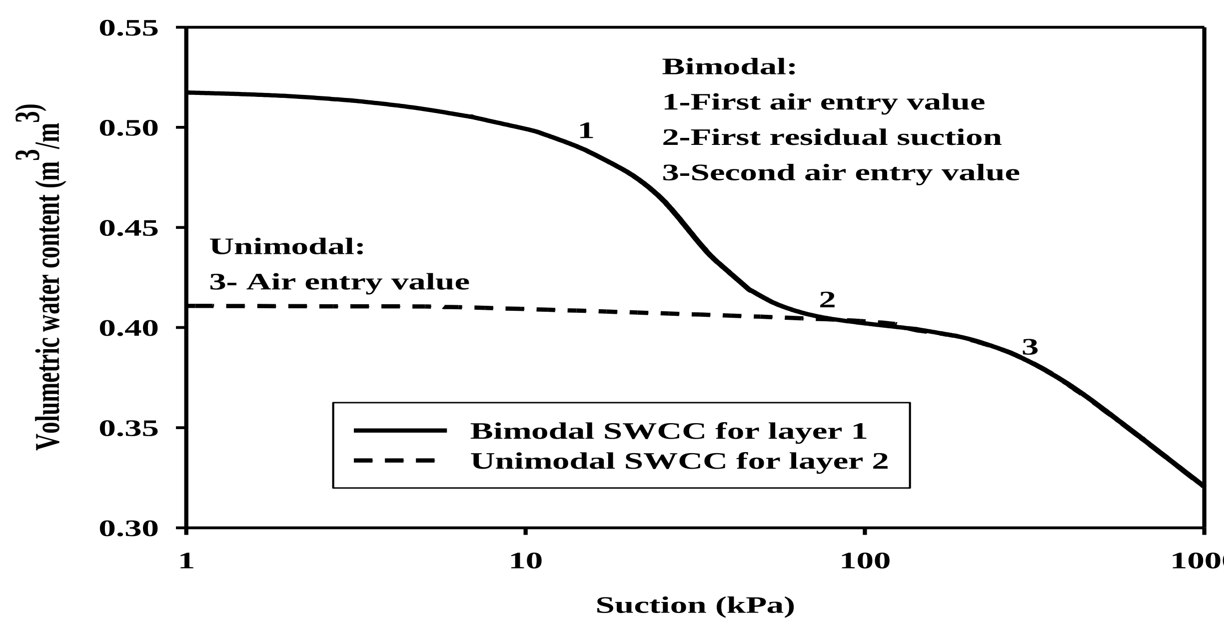

Figure 2 SWCCs of Regina clay

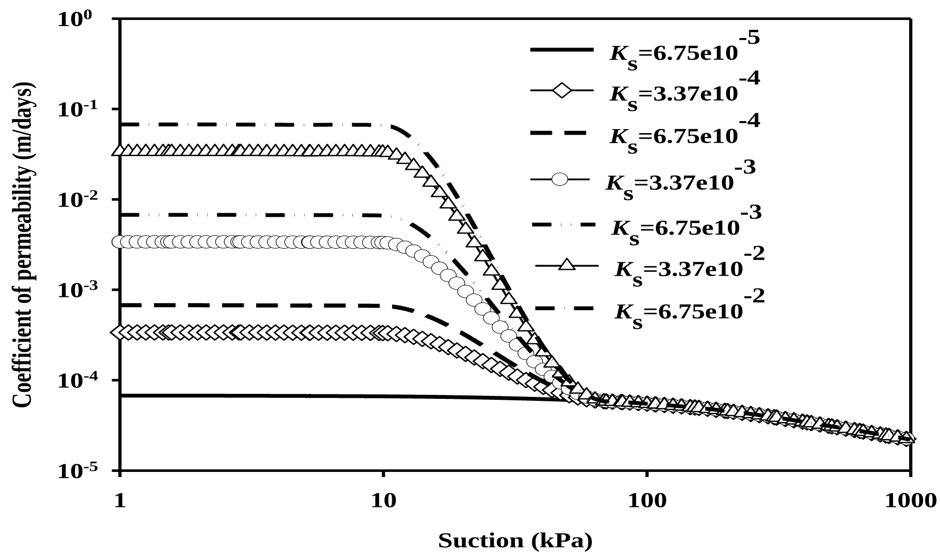

Figure 3 Permeability functions for Regina clay

Figure 2 and 3 summarize the hydraulic properties and hydraulic response taking account of influence of suction of the slope for different infiltration rates (estimated from the environmental data). A slope stability analysis is carried out using the positive or negative pore water pressure from the transition seepage analysis. Figure 4 summarizes the variation of factor of safety with time is illustrated which shows that the slope failures (observed during the two months of snow melting) can only be predicted by increasing the saturated coefficient of permeability by 2-3 orders of magnitudes in comparison to the laboratory measured value.

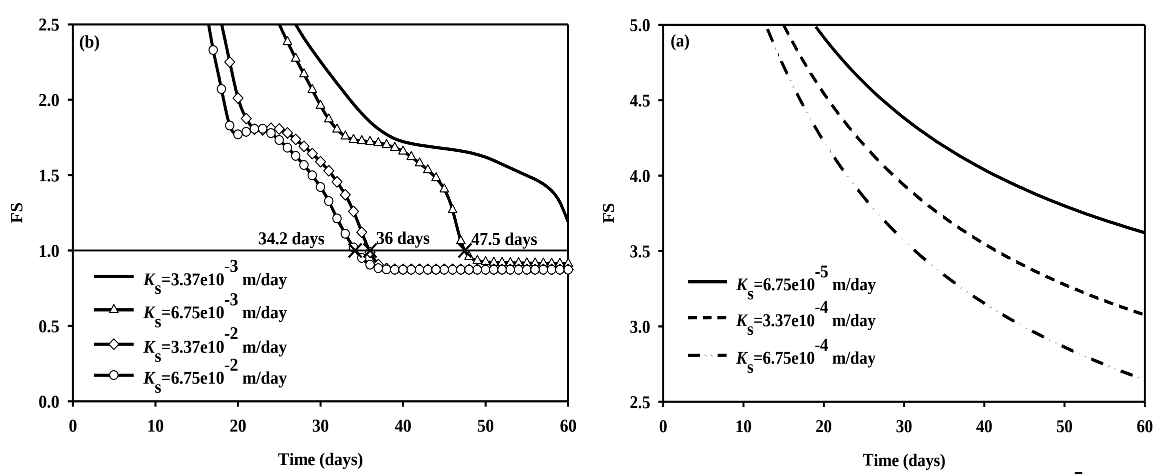

Figure 4 Variation of FS for peak shear strength parameters: (a) K_S= 6.75×10^{-5}, 3.37×10^{-4}, 6.75×10^{-4} m/days; (b) K_S=3.37×10^{-3}, 6.75×10^{-3}, 3.37×10^{-2}, 6.75×10^{-2} m/day

Role associated with the swelling behaviour of expansive soils

The role associated with the swelling behaviour of expansive soils in initiating the slope failure is investigated by Qi and Vanapalli (2016d), who developed an infinite slope formation, in which the soil is modeled using the extended Mohr-Coulomb elasto-plasticity taking into account the strain-softening behaviour. The infinite slope formulation is shown in

Figure 5.

The fundamental physical process that occur in an infinite slope formulation subjected to wetting is postulated based on the following observations (e.g. Ng et al. 2003) as: with a decreasing suction, the normal stress, σ_η will increase due to that soil swelling potential is restrained in this direction. However, it cannot increase to a value beyond soil shear strength described using the extended Mohr-Coulomb model. Once the stress state due to increasing σ_η reaches the soil's strength, plastic straining develops. When the plastic strain accumulates to a certain value, the expansive soil shear strength starts to decrease. The variation of strength with accumulated plastic strain is assumed as shown in Figure 6, including the decrease of ϕ^b (accounting for the suction contribution to shear strength of unsaturated soils) with plastic straining. The physical process is divided into three phases by Qi and Vanapalli (2016d): (i) pure elastic phase; (ii) perfectly plastic phase; (iii) strain softening phase. The stress-strain relationship was solved using respective elastic/plastic matrices with a specifically developed program by Qi and Vanapalli (2016d).

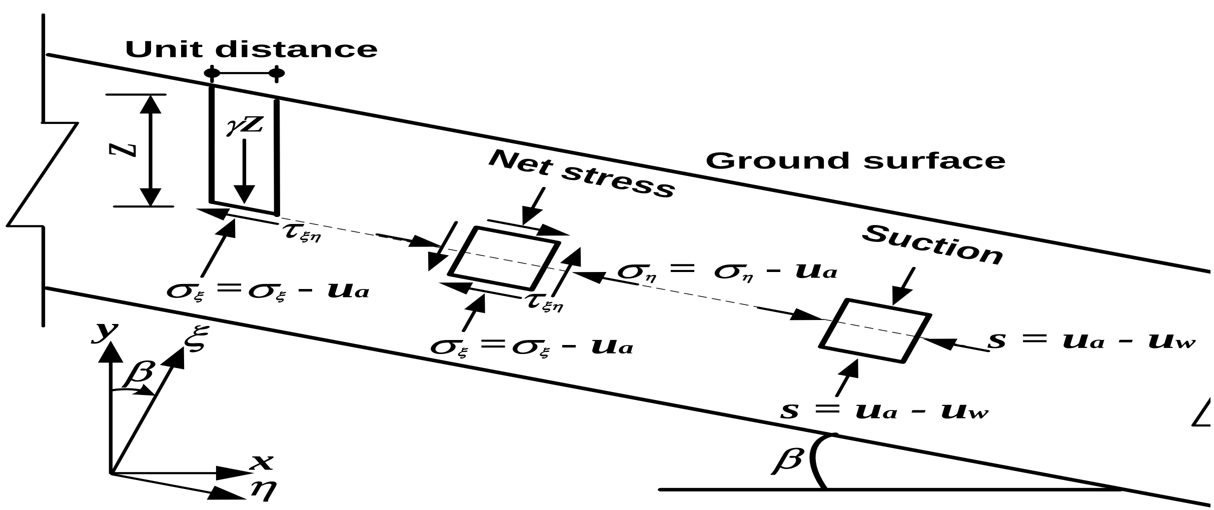

Figure 5. Geometrical scheme of the infinite slope.

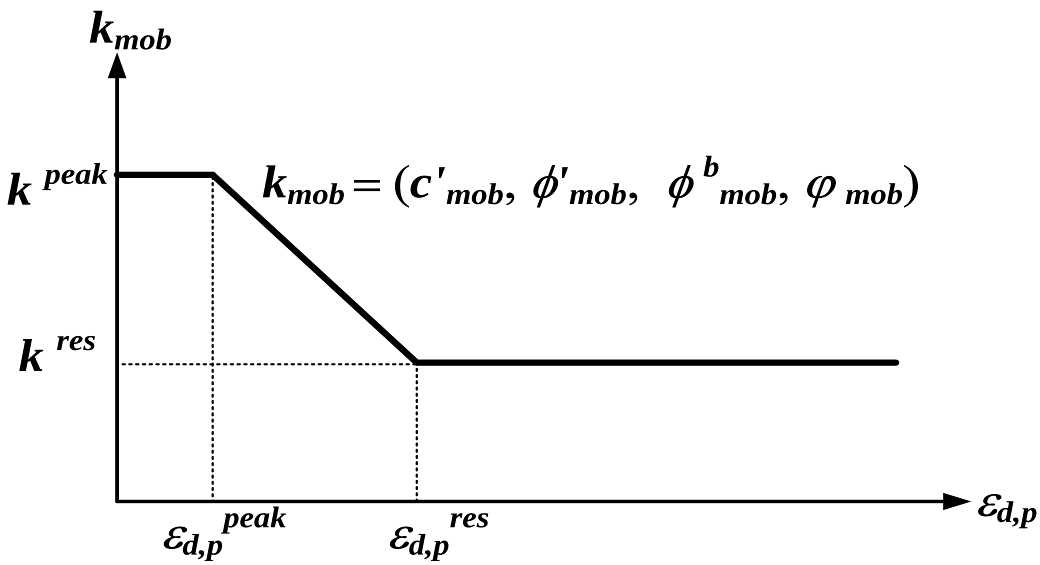

Figure 6. Variation of mobilized material parameters with plastic deviatoric shear strain.

The numerical analysis using the developed code is performed with reference to slopes using Regina clay soil properties. The variation of factor of safety profiles obtained by Qi and Vanapalli (2016d) with and without consideration of the strain softening behaviour is shown in Figures 7 and 8, respectively. For the softening analysis, the Factor of Safety at depth of 0.9 m first decreases to 1, while no failure is observed in the non-softening analysis. This shows the methods that neglect softening behavior (using peak shear strength parameters assuming saturated soil condition in traditional analysis framework) may result in an unsafe design of the unsaturated expansive soil slopes. Detailed analyses presented in Qi and Vanapalli (2016d) showed that the initial stress ratio, softening rate and slope angle all have significant influence on the failure depths and time. A gentle slope typically assures stability and hence used as a widely accepted conclusion based on the traditional saturated soil mechanics; however, the studies summarized in this paper highlight the need for considering soil softening process for unsaturated expansive soils.

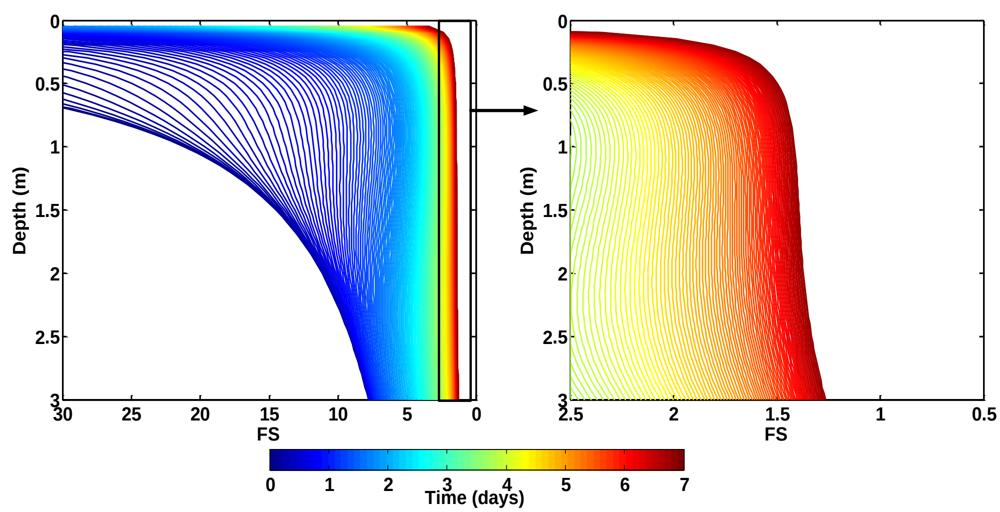

Figure 7. Variation of FS profile from non-softening analysis

Significance of proposed model on the forensic analysis on the failure of retaining wall and pile foundation in expansive soils

From the above summarized discussions, underground infrastructures constructed in expansive soils have a greater possibility to suffer failure during their design life period, if they are not based on rational design methods. For retaining walls constructed in expansive soils, most failures can be attributed to the lack of shear strength resistance and increasing total LEP upon infiltration.

In forensic investigations to assess the failure, several simple laboratory tests can be conducted to determine the key properties and estimate the magnitude of the LEP that contributed to the failure of the retaining wall using the proposed model. In many scenarios, pile foundation failure in expansive soils can be attributed to the upward movement induced by water infiltration. The model proposed in this paper provides a useful tool to evaluate this value. In addition, this approach can also be used as a safety assessment tool and for proposing remediation works to alleviate retaining wall failures.

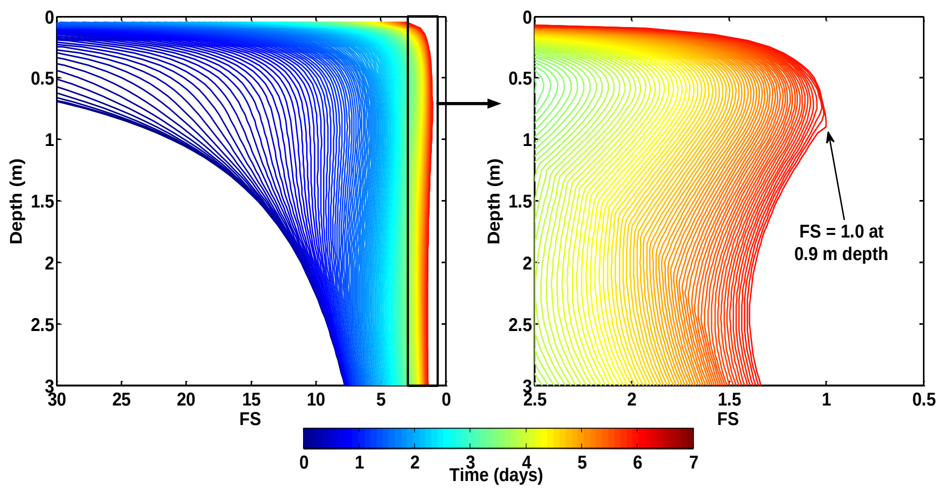

Figure 8. Variation of FS profile from softening analyses.

INFLUENCE OF LATERAL SWELLING PRESSURE ON THE RETAINING WALL AND PILE FOUNDATION FAILURE IN EXPANSIVE SOILS

Upon infiltration, lateral swelling pressure (LSP) acts as an additional stress on the geo-infrastructure along with the lateral earth pressure (LEP), which is typically associated with soil unit weight and/or surcharge. The increased LEP can be significant (as shown in Table 1) in certain scenarios and likely contributes to various problems to geo-infrastructure such as the retaining walls and pile foundations within or adjacent to expansive soils (Ruwaih, 1987; Chen, 1988; Nelson and Miller, 1997).

Possible vulnerable area within geotechnical infrastructure in expansive soils is shown in Figure 9. For retaining structures, increased LEP associated with the LSP can contribute to the development of cracks in basement walls, pipe lines, tunnels and sewers. In certain scenarios, failure of these structures is also likely (for example, Kassiff and Zeitlen 1962).

Typically, it reduces the factors of safety against overturning and sliding failure for retaining walls or slopes with a higher possibility of failure during the period of rainfall (Ng et al. 2003). For pile foundations, increased LEP contributes to the development of uplift friction along the pile shaft in the active zone. After analyzing several case studies of pile failures in expansive soils, Chen (1988) pointed out that additional design checks are necessary to take into account the tension capacity of the pile as well as the stability of superstructures with respect to the ground heave. This part sets out a relatively simple framework for investigating the possible causes of retaining walls and pile foundation failures in expansive soils.

Table 1. Ratio of LEP considering LSP to vertical pressure

References	Ratio of LEP considering LSP to vertical pressure
Richards and Kurzeme (1973)	1.3 to 5
Lytton (2007)	4
Moza et al. (1987)	10
Joshi and Katti's (1980)	10
Mohamed et al. (2014)	10

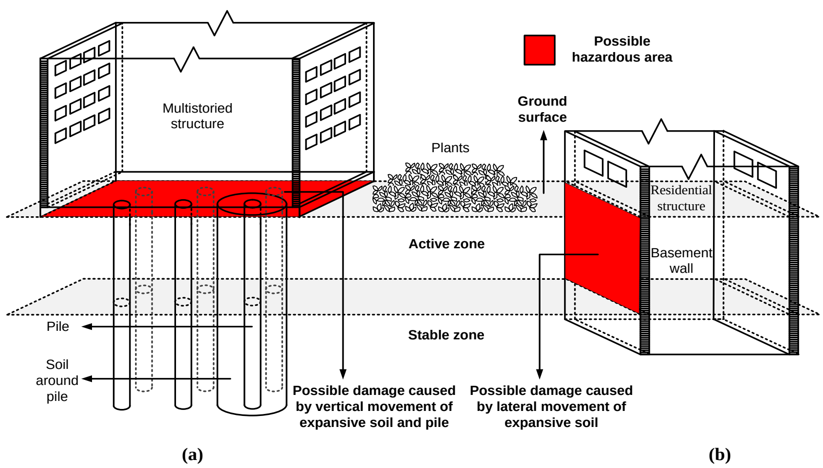

Figure 9. Possible hazardous area within retaining wall and pile foundation in expansive soil

Analytical method for estimation of the lateral earth pressure (LEP) considering the influence of lateral swelling pressure (LSP)

Expansive soils exhibit swell when there is a water content increase; however, if this volume expansion is restricted, swelling pressure develops. Figure 10 highlights the LSP development against retaining structure and around pile upon wetting which contributes to development of the at-rest LEP in the active zone due to soil unit weight and/or surcharge. For retaining structure without surcharge, LEP from LSP contributes in addition to the LEP that typically arises due to soil unit weight and other structural surcharge loads. For piles buried in expansive soils, in several scenarios, enough crawl space is not provided between ground surface and structure to accommodate the ground heave. In such scenarios, restricted vertical heave translates into vertical load and acts on the ground surface together with surcharge due to the superstructure loads.

As shown in the Mohr-circle below (Figure 11), when there is a suction decrease, LSP can be considered as an additional part to the at-rest earth pressure. A theoretical model (Eq. 1) is proposed by Liu and Vanapalli (2016) to calculate the total lateral earth pressure (LEP) behind a retaining structure with expansive soils as backfill material considering the influence of LSP. The proposed LEP estimation method considering the influence of LSP is validated using the experimental data collected from the literature; namely, a large scale test conducted by Katti et al. (1983) and a centrifuge test on a model retaining wall conducted by Gu (2005). There is a good comparison between experimental data and estimations using the proposed methods. More details are discussed in Liu and Vanapalli (2016).

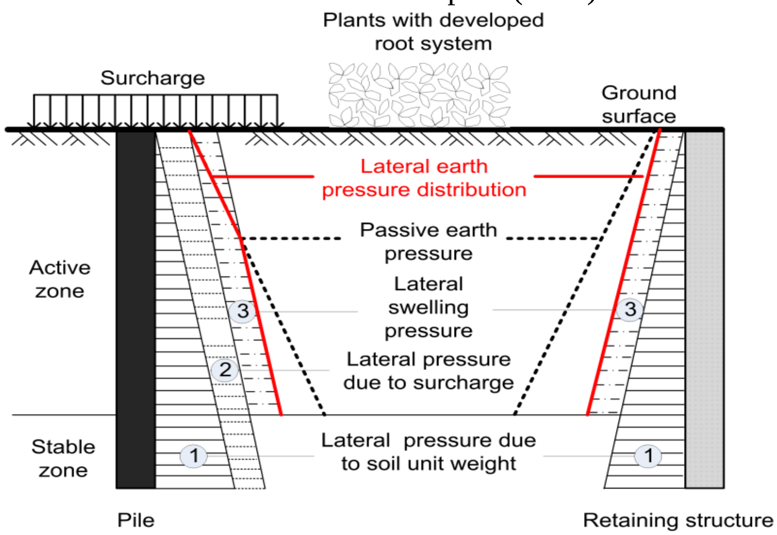

Figure 10. Distribution of lateral earth pressure behind retaining wall and around the single pile upon infiltration (after Liu and Vanapalli 2016)

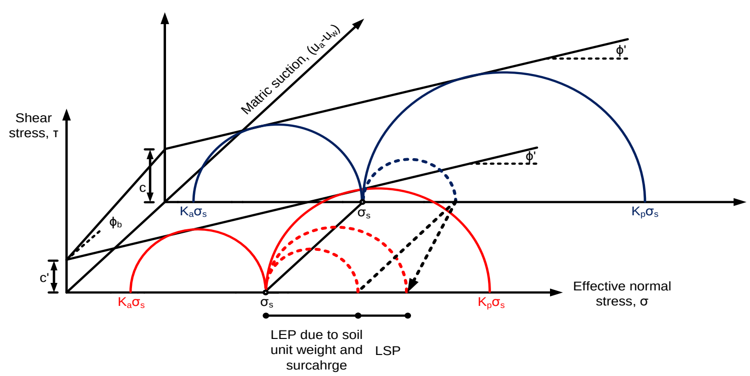

Figure 11. Variation LEP in expansive soils upon wetting and drying

$$P_{LS} = \frac{(1-\upsilon-2\upsilon^2)P_s}{1-\upsilon^2-\dfrac{P_s}{E_a}(1+\upsilon)(1-\upsilon-2\upsilon^2)} + \frac{\upsilon}{1-\upsilon}\sigma_s \qquad (1)$$

where P_s = VSP from free swell-load back test; VSP from constant volume swell test or swell under surcharge test also can be used as an approximation; E_a = average value of various E_{unsat} calculated over the range of matric suction variation; ν = Poisson's ratio.

$$E_{unsat} = E_{sat}[1+\alpha\frac{(u_a-u_w)}{P_a/100}S^{\beta_1}] \qquad (2)$$

where E_{unsat} = the elastic modulus of unsaturated expansive soil; E_{sat} = elastic modulus of saturated expansive soil;α and β_1 = fitting parameters, Adem (2015) calculated E_{unsat} for five different expansive soils and suggested that β_1 = 2 typically and α varies from 0.05 to 0.15 for expansive soils. In this study, an average value, α equals to 0.1 is used; P_a = atmospheric pressure, S = degree of saturation.

$$\upsilon = \frac{K_0}{1+K_0} \tag{3}$$

$K_0 \approx 1-\sin\varphi'$ for normally consolidated soil (Jaky 1944)

$K_0 = (1-\sin\varphi')OCR^{\sin\varphi'}$ for over consolidated soil (Mayen and Kulhawy 1982)

where K_0 = at rest earth pressure coefficient; ϕ' = effective soil internal friction angle; OCR = over consolidation ratio.

Limitation for the development of lateral earth pressure (LEP) considering the influence of lateral swelling pressure (LSP)

However, the development of LSP has a limiting value. From Figure 11, along with the mobilization of LSP, the diameter of the Mohr circle keeps increasing until it touches the shear strength failure envelop defined by Rankine's theory. Traditional Rankine's theory is only suitable for saturated soils against frictionless surface of a structure. In engineering practice, there can be scenarios where the roughness of the structure surface cannot be neglected (e.g. drilled pier). In many scenarios, even after water infiltration, expansive soils may still not attain fully saturated condition. In such situations, both the friction of the soil-structure interface and suction present within the expansive soils can significantly influence the LEP that develops. Wang et al. (2008) extended Rankine's earth pressure taking account of the frictional influence between back-surface of vertical retaining works and soils into consideration. Rankine's theory was extended for the calculation of passive earth pressure (Eq. 4) and active earth pressure (Eq. 5) against rough back-surface of retaining works.

$$\sigma_{hp1} = \sigma_s \frac{1+\sin\varphi'\cos 2\alpha_p}{1-\sin\varphi'\cos 2\alpha_p} + c'\frac{2\cos\varphi'\cos 2\alpha_p}{1-\sin\varphi'\cos 2\alpha_p} + p_0 \tag{4}$$

$$\alpha_p = \frac{1}{2}\arcsin\frac{C}{\sqrt{A^2+B^2}} - \frac{1}{2}\arctan\frac{B}{A}$$

$$\sigma_{ha1} = \sigma_s \frac{1-\sin\varphi'\cos 2\alpha_a}{1+\sin\varphi'\cos 2\alpha_a} - c'\frac{2\cos\varphi'\cos 2\alpha_a}{1+\sin\varphi'\cos 2\alpha_a} + p_0 \tag{5}$$

$$\alpha_a = \frac{1}{2}\arcsin\frac{C}{\sqrt{A^2+B^2}} + \frac{1}{2}\arctan\frac{B}{A}$$

$$\begin{cases} A = \sigma_s\sin\varphi' + c'\cos\varphi' \\ B = c_a'\sin\varphi' - \sigma_s\sin\varphi'\tan\delta' - 2c'\cos\varphi'\tan\delta' \\ C = \sigma_s\tan\delta' + c_a' \end{cases}$$

where σ_s = the vertical stress due to unit weight of upper soil layers and surcharge; p_0 = the pore water pressure; ϕ'= effective soil internal friction angle; c' = effective soil cohesion; c_a' = effective pile-soil interface cohesion; δ' = effective pile-soil interface friction angle.

The unsaturated soil-structure interface shear strength can be determined from a series of direct shear tests considering different roughness conditions at different degrees of saturation of the soil. Hamid and Miller (2009) suggested that the shear strength of the pile-structure interface can be modelled as Eq. 6 and Eq. 7.

$$\tau_f = c'_a + (\sigma_{nf} - u_{af})\tan\delta' + (u_{af} - u_{wf})\tan\delta^b \quad (6)$$

$$\tau_f = c'_a + (\sigma_{nf} - u_{af})\tan\delta' + (u_{af} - u_{wf})\tan\delta^b\left(\frac{\theta-\theta_r}{\theta_s-\theta_r}\right) \quad (7)$$

where δ' = the interface friction angle with respect to net normal stress, δ_b = the interface friction angle with respect to matric suction; θ = volumetric water content; θ_s = volumetric water content at a saturation of 100%; θ_r = residual volumetric water content.

The modified Rankine's theory proposed by Wang et al. (2008) can be extended to include the influence of the matric suction to the soil shear strength and soil-structure interface shear strength. Figure 12 illustrates the development of the passive earth pressure against rough and frictionless retaining structures under both saturated and unsaturated conditions. From Figure 12 it can be derived that during the desaturation process, both the passive earth pressure against rough retaining surface and frictionless retaining surface increases. Passive earth pressure against frictionless retaining surface always has a value higher than rough retaining surface neglecting the degree of saturation for constant vertical stress. The passive earth pressure for saturated soil against rough surface (σ_{hp1}), saturated soils against frictionless surface (σ_{hp2}), unsaturated soil against rough surface (σ_{hp3}) and unsaturated soils against frictionless surface (σ_{hp4}) are given in Eq. 4, Eq. 8, Eq. 9 and Eq.10, respectively.

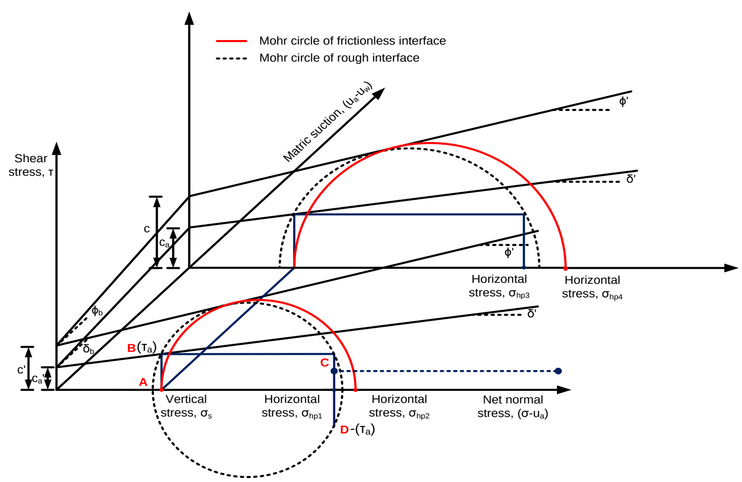

Figure 12. Development of Rankine's passive earth pressure at different degree of saturated against frictionless and rough surface (modified after Liu and Vanapalli 2016)

$$\sigma_{hp2} = \frac{\sigma_s(1+\sin\varphi')}{1-\sin\varphi'} + \frac{2c'\cos\varphi'}{1-\sin\varphi'} \quad (8)$$

$$\sigma_{hp3} = \sigma_s\frac{1+\sin\varphi'\cos2\alpha_p}{1-\sin\varphi'\cos2\alpha_p} + [c' + (u_{af} - u_{wf})\tan\varphi^b]\frac{2\cos\varphi'\cos2\alpha_p}{1-\sin\varphi'\cos2\alpha_p} \quad (9)$$

$$\alpha_p = \frac{1}{2}\arcsin\frac{C}{\sqrt{A^2+B^2}} - \frac{1}{2}\arctan\frac{B}{A}$$

$$\begin{cases} A = \sigma_s \sin\varphi' + [c' + (u_{af} - u_{wf})\tan\varphi^b]\cos\varphi' \\ B = [c'_a + (u_{af} - u_{wf})\tan\delta^b]\sin\varphi' - \sigma_s \sin\varphi' \tan\delta' \\ \quad -2[c' + (u_{af} - u_{wf})\tan\varphi^b]\cos\varphi' \tan\delta' \\ C = \sigma_s \tan\delta' + [c'_a + (u_{af} - u_{wf})\tan\delta^b] \end{cases}$$

$$\sigma_{hp4} = \frac{\sigma_s(1+\sin\varphi')}{1-\sin\varphi'} + \frac{2[c' + (u_{af} - u_{wf})\tan\varphi^b]\cos\varphi'}{1-\sin\varphi'} \tag{10}$$

Similarly, the active earth pressure for saturated soil against rough retaining surface (σ_{ha1}), saturated soils against frictionless surface (σ_{ha2}), unsaturated soil against rough retaining surface (σ_{ha3}) and unsaturated soils against frictionless surface (σ_{ha4}) are given in Eq. 5, Eq. 11, Eq. 12 and Eq. 13 respectively.

$$\sigma_{ha2} = \frac{\sigma_s(1-\sin\varphi')}{1+\sin\varphi'} - \frac{2c'\cos\varphi'}{1+\sin\varphi'} \tag{11}$$

$$\sigma_{ha3} = \sigma_s \frac{1-\sin\varphi'\cos 2\alpha_a}{1+\sin\varphi'\cos 2\alpha_a}$$

$$-[c' + (u_{af} - u_{wf})\tan\varphi^b]\frac{2\cos\varphi'\cos 2\alpha_a}{1+\sin\varphi'\cos 2\alpha_a} \tag{12}$$

$$\alpha_a = \frac{1}{2}\arcsin\frac{C}{\sqrt{A^2+B^2}} + \frac{1}{2}\arctan\frac{B}{A}$$

$$\begin{cases} A = \sigma_s \sin\varphi' + [c' + (u_{af} - u_{wf})\tan\varphi^b]\cos\varphi' \\ B = [c'_a + (u_{af} - u_{wf})\tan\delta^b]\sin\varphi' - \sigma_s \sin\varphi' \tan\delta' \\ \quad -2[c' + (u_{af} - u_{wf})\tan\varphi^b]\cos\varphi' \tan\delta' \\ C = \sigma_s \tan\delta' + [c'_a + (u_{af} - u_{wf})\tan\delta^b] \end{cases}$$

$$\sigma_{ha4} = \frac{\sigma_s(1-\sin\varphi')}{1+\sin\varphi'} - \frac{2[c' + (u_{af} - u_{wf})\tan\varphi^b]\cos\varphi'}{1+\sin\varphi'} \tag{13}$$

Analytical method for estimation of the uplift friction surrounding the pile upon water infiltration

For piles buried in expansive soils, special attention is required with respect to the uplift friction generating along the pile shaft in the active zone due to increasing normal stress on the pile shaft. Figure 13 (a) shows a pile buried in expansive soil without surcharge applied on the surrounding soil. For such a scenario, prior to water infiltration associated with rainfall or flood, positive friction is developed along the entire length of the pile. The applied load is typically carried by shaft friction with some contribution arising from the pile tip. However, as water infiltrates into the active zone, expansive soil swells. Positive friction increases in the active zone while negative friction arises in the stable zone [as shown in Figure 13 (b)]. The net contribution that arises from the negative shaft friction, tip or end bearing capacity and surcharge combine to balance the increased uplift friction. When the positive friction exceeds the resisting force, the pile tends to move upward. The positive friction that generates in the active zone upon water infiltration is referred to as uplift friction.

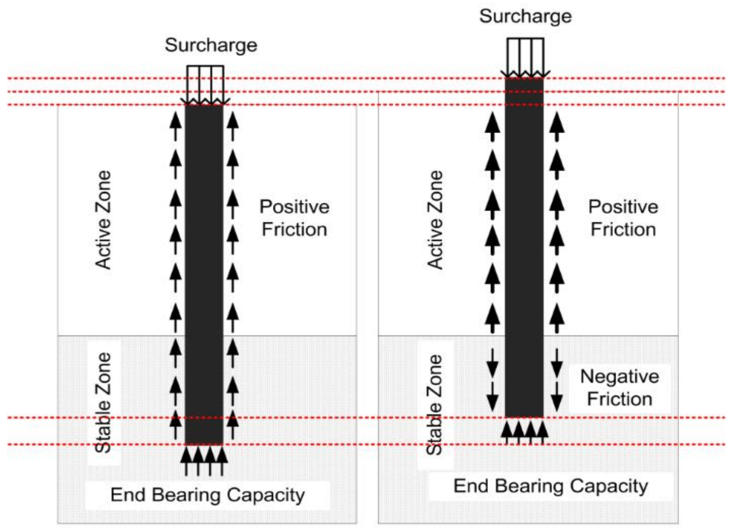

Figure 13. Distribution of shaft friction along a pile before and after infiltration

Based on Eq. (1), Liu and Vanapalli (2016) further proposed a model for the calculation of uplift friction around the pile considering both the increasing normal stress and matric suction [Eq. (14)]. Eq. (14) can be expressed in another form as shown in Eq. (15) if the information of entire SWCC (i.e. from 0 to 10^6 kPa) is available for the expansive soil, which facilitates estimation of the residual volumetric water content, θ_r. The fitting parameter κ in Eq. (14) can be replaced in Eq. (15) using the approach suggested by Vanapalli et al. (1996). The proposed uplift friction estimation method is validated on a model pile placed in an expansive soil tank with infiltration tests (Fan 2007). More detailed discussions are presented in Liu and Vanapalli (2016).

$$f = c'_a + \tan\delta'\{\frac{(1-\upsilon-2\upsilon^2)P_s}{1-\upsilon^2-\frac{P_s}{E_a}(1+\upsilon)(1-\upsilon-2\upsilon^2)} + \frac{\upsilon}{1-\upsilon}\sigma_s + (u_a-u_w)_r S^\kappa\} \tag{14}$$

$$f = c'_a + \tan\delta'\{\frac{(1-\upsilon-2\upsilon^2)P_s}{1-\upsilon^2-\frac{P_s}{E_a}(1+\upsilon)(1-\upsilon-2\upsilon^2)} + \frac{\upsilon}{1-\upsilon}\sigma_s + (u_a-u_w)_r(\frac{\theta-\theta_r}{\theta_s-\theta_r})\} \tag{15}$$

where S = degree of saturation; κ = fitting parameter for shear strength calculation.

SIGNIFICANCE OF PROPOSED MODEL ON THE FORENSIC ANALYSIS ON THE FAILURE OF RETAINING WALL AND PILE FOUNDATION IN EXPANSIVE SOILS

From the above summarized discussions, underground infrastructures constructed in expansive soils have a greater possibility to suffer failure during their design life period, if they are not based on rational design methods. For retaining walls constructed in expansive soils, most failures can be attributed to the lack of shear strength resistance and increasing total LEP upon infiltration.

In forensic investigations to assess the failure, several simple laboratory tests can be conducted to determine the key properties and estimate the magnitude of the LEP that contributed to the failure of the retaining wall using the proposed model. In many scenarios, pile foundation failure in expansive soils can be attributed to the upward movement induced by water infiltration. The model proposed in this paper provides a useful tool to evaluate this value. In addition, this approach can also be used as a safety assessment tool and for proposing remediation works to alleviate retaining wall failures.

DESIGN OF PAVEMENTS CONSIDERING THE INFLUENCE OF SEASONAL MOISTURE CONTENT VARIATION

Unsatisfactory design of pavements may result in poor performance and reduce the service life of pavements or contribute to excessive rehabilitations works which can be very expensive. Accidents and associated litigation or law suits are also likely if pavements are not properly designed. Reliable methods are necessary to serve the rational pavement design all seasons. Such methods can also be useful for undertaking remediation measures and use them in the forensic investigations.

Pavements are layered structures typically formed with compacted granular materials placed over compacted subgrade soils and sealed with flexible and / or rigid surfacing. The development in the understanding of the pavement failure mechanism over the past 50 years has greatly contributed to the pavement design methods.

The original pavement design methods, which were developed during the phase of extensive infrastructure development prior to World War II, were predominantly empirical. Unfortunately, some of these methods are still used in practice in various countries. These methods focussed on limiting shear failure/deflection of pavements which is not the major failure mechanism for pavements. Remarkable progress has been achieved since then and had advanced throughout the 1980s. Empirical methods were gradually replaced by mechanistic-empirical design methods in most of the developed countries. Modern mechanistic-empirical methods have the following advantages: (i) improvement in the design reliability as they take into account of the influence of external environment; (ii) ability to predict the various types of distress; (iii) feasibility to extrapolate from limited field and laboratory data; and (iv) ability to provide cost-effective design and lower the life-cycle cost (Huang 2004).

The mechanistic design methods for flexible pavements focus on the serviceability of the pavements for estimating the service life and failure of the pavement structure. The two major failure criteria, including the fatigue cracking that initiates at the bottom of the surfacing layer and the rutting that happens at the surface of the surfacing layer, are therefore recommended in the design stage.

The fatigue cracking is related to the local tensile strain and the elastic modulus of the surfacing materials (Huang et al. 2004). For example, Eq. 16 is used in mechanistic pavement design methods to determine the allowable number of load repetitions (N_f) based on the fatigue cracking criterion:

$$N_f = f_1(\varepsilon_t)^{-f_2}(E_1)^{-f_3} \tag{16}$$

where ε_t is the tensile strain at the bottom of the asphalt layer and E_1 is the elastic modulus of the asphalt layer. The f_1, f_2 and f_3 are material constants. Tensile strain (ε_t) at the bottom of the surfacing layer due to the formation of the deflection basin under wheel loads is calculated using elastic theory by assuming that the base, subbase and subgrade layers are essentially elastic. The resilient modulus (M_R) represents the material stiffness under cyclic loadings conditions and is defined as the ratio of the cyclic deviator stress (σ_d) to the resilient strain (ε_r). The M_R is practically used as the elastic modulus of pavement materials and therefore is the key material property required in the mechanistic pavement design methods for determining the deformation of pavement layers and the resulting tensile strain at the bottom of the surfacing layer.

Pavement base course materials and subgrade soils are typically compacted at optimum moisture content (w_{opt}, subscript opt hereafter is used to indicate the corresponding soil properties or physical states at optimum moisture content condition) to achieve maximum dry density (ρ_{dmax}) that assures better engineering performance such as the higher stiffness and shear strength (Khoury and Zaman 2004, Azam et al. 2013, Li et al. 2016). Due to this reason, the M_{Ropt} of pavement materials is conventionally determined and used in the design of pavements. Moisture content of compacted pavement materials during their service life would fluctuate seasonally upon impacts of environmental factors such as the surficial infiltration and evaporation, freeze-thaw cycles and the variation of the ground water table. Figure 14 shows typical evolution of pavement capacity, which is mainly determined by the M_R of pavement layers, during a period of one year. Soil starts to freeze in late fall and typically remains in frozen condition during most of the winter (Line AB in Figure 14). The M_R can increase 20 to 120 times during the freezing process (Bosscher and Nelson 1987, Bigl and Berg 1996, Zapata et al. 2007). The volume of frozen soil increases due to the formation of the ice lenses, which decreases the soil's dry density and cohesion, and increases its moisture content. The pavement capacity and M_R reduce dramatically during the spring thaw period, which begins in late winter or early spring (Line BC in Figure 14). Decrease in the M_R is mainly caused by (i) the weakened soil structure and (ii) the increase in the moisture content after thawing. Several studies suggest that the M_R of the post-thawing soil can be 50% - 40% less than the M_R of the same soil that is never frozen (Mahoney et al. 1985, Lee et al. 1995, Jong et al. 1998, Li et al. 2016). Pavement capacity and M_R gradually recover during the summer and fall period (Line CD and Line DE in Figure 14) due to the drainage and evaporation that lead to decrease in the soil moisture content.

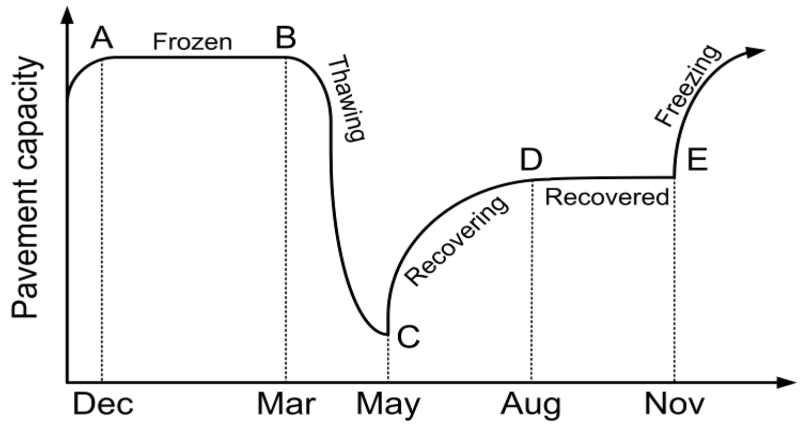

Figure 14. Pavement capacity evolution (modified after Jong et al. 1998)

Moisture changes significantly influence the M_R of compacted pavement aggregate materials and subgrade soils. Typically, the M_R increases with decreasing moisture content and decreases with increasing moisture content (Li and Selig 1994, Tian et al. 1998, LeKarp et al. 2000, Bilodeau and Doré 2012, Khoury et al. 2013, Li et al. 2015, Zou et al. 2015, Han and Vanapalli 2016a). Due to these reasons, the reliable determination of (i) moisture content distribution and changes associated with various environmental factors and (ii) the resulting changes in M_R of pavement materials is required in the mechanistic pavement design methods. As can be seen from Figure 14, the M_R varies significantly during the year with temperature and moisture content. For this reason, it is important to model the seasonal variation of the M_R rather than to only use a constant M_R value at saturated condition or optimum moisture content condition for pavement design and its service life estimation. The use of single M_R value or the erroneous estimation of the significant variation of the M_R with temperature and moisture content will result in the discrepancies in the service life of the pavement structure and could possibly lead to law suits.

As-compacted soils are typically in a state of unsaturated condition. Their hydraulic and mechanical behaviors should be interpreted within the framework of the mechanics of unsaturated soils using suction (s) as the primary state parameter (Fredlund 2006, Sheng 2011). Moisture migration within unsaturated pavement layers can be analyzed using numerical methods by applying different hydraulic boundary conditions to simulate the respective environmental factors (Zapata et al. 2007). Soil-water characteristic curve (SWCC), which defines the relationship between the moisture content and suction, is the fundamental constitutive relationship for the hydraulic analysis of unsaturated soils (Fredlund 2006, Qi and Vanapalli 2015a). On the other hand, variation in the M_R with moisture content can be interpreted and predicted by establishing the M_R - s relationships. Such an approach has been successfully used by several researchers for various pavement materials (Caicedo et al. 2009, Abu-Farsakh et al. 2015, Zou et al. 2015, Han and Vanapalli 2015, Coronado et al. 2016).

Han and Vanapalli (2015) proposed Equation 17 to relate the MR to the s, Sr and w using one model parameter ξ.

$$\frac{M_R - M_{Rsat}}{M_{Ropt} - M_{Rsat}} = \frac{s}{s_{opt}}\left(\frac{S_r}{S_{ropt}}\right)^{\xi} = \frac{s}{s_{opt}}\left(\frac{w}{w_{opt}}\right)^{\xi} \qquad (17)$$

In Eq. 17, a model parameter ξ value of 2.0 has been found suitable for different types of cohesive fine-grained soils which are typically used as subgrade soils (Han and Vanapalli

2015, Han and Vanapalli 2016b). If the ξ is assumed to be 2.0 for all cohesive fine-grained soils and the s corresponding to the S_r or w is estimated from the SWCC, Equation 15 can predict the M_R - S_r or M_R - w relationships using only the experimental data of M_{Rsat}, M_{Ropt}, s_{opt} and S_{ropt} or w_{opt}.

Figure 15 shows the measured SWCCs (shown in symbols) and the fitted SWCCs (shown in continuous line) using Fredlund and Xing (1994) equation for five subgrade soils collected from different highway locations in Ontario, Canada (i.e. Kincardine lean clay, KLC; Sudbury lean clay, SLC; Toronto silty clay, TSC; Toronto lean clay, TLC; Ottawa lean clay, OLC).

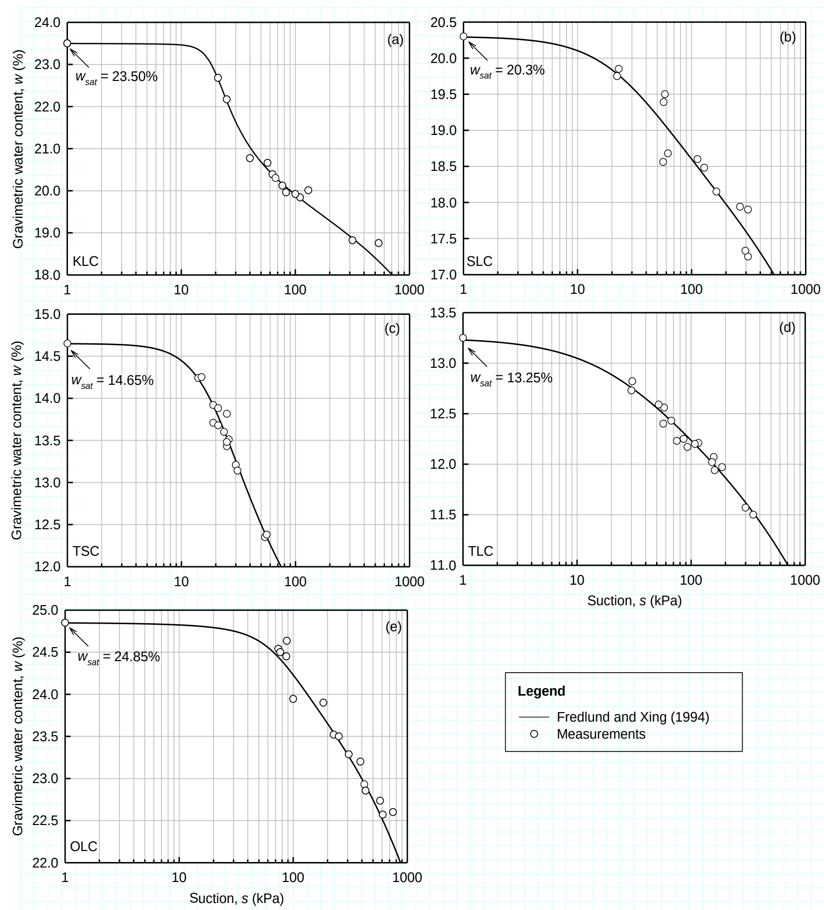

Figure 15 Measured and fitted SWCCs for (a) KLC, (b) SLC, (c) TSC, (d) TLC and (e) OLC

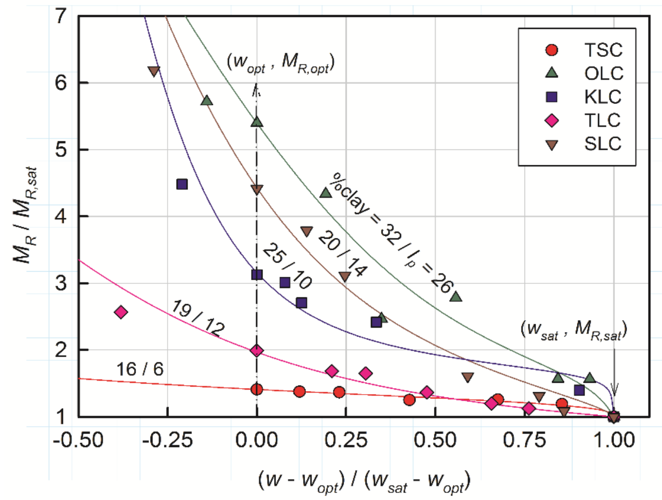

Figure 16 Sensitivity of M_R to w for the five subgrade soils

Figure 16 shows in symbols the variation of the measured M_R with gravimetric water content (w) for the five soils measured at the cyclic stress (σ_d) of 48.2 kPa and the confining stress (σ_c) of 27.6 kPa following AASHTO T307-99 (AASHTO 2003) testing protocol. Figure 16 is shown as a relationship between the (M_R / $M_{R,sat}$) versus ($w - w_{opt}$) / ($w_{sat} - w_{opt}$) relationships along with the soils' plasticity information (i.e. %clay and plasticity index I_p). The predicted M_R - w relationships using Equation 17 and the fitted SWCCs in Figure 16 are shown in solid lines. The measured M_R - w relationships are generally non-linear and sensitive to soils' clay content and I_p. The sensitivity of the M_R to the w increases with an increase in the clay content and the I_p. For example, the M_R increases only 50% from w_{sat} to w_{opt} (i.e. $M_{R,opt}$ = 1.5 $M_{R,sat}$) for the low plastic TSC. However, this increase is greater than 200% for the medium plastic TLC (i.e. $M_{R,opt}$ > 3 $M_{R,sat}$) and is approximately 450% for the high plastic OLC (i.e. $M_{R,opt}$ = 5.5 $M_{R,sat}$). These observations are consistent with results of other studies on the stiffness parameters reported in the literature (e.g., Drumm et al. 1997, Khoury et al. 2013, Hoyos et al. 2015). The predicted lines using Equation 17 closely describe the non-linear evolution of the M_R with w for all the soils. It should be noted that the predicted non-linearity bounded by the measurements of $M_{R,sat}$ and $M_{R,opt}$ is defined by Equation 17 using only the SWCC and fitting parameter $\xi = 2$.

Equation 17 only requires limited and easy-to-obtain experimental data for predicting the variation of the M_R with w and s and hence are simple and encouraging for use in the mechanistic pavement design. In addition, they can be used in the forensic geotechnical investigations to assess the mechanical behavior of unsaturated pavement materials considering the influence of seasonal moisture content variation.

SUMMARY AND CONCLUSIONS

This paper illustrates the importance of using the mechanics of unsaturated soils for the rational design and analysis of geotechnical infrastructure including slope, pile, retaining wall and pavement considering the influence of the environmental factors. The importance of using the mechanics of unsaturated soils as a tool in the forensic geotechnical engineering is highlighted. The following conclusions can be drawn from the studies summarized in this paper:

• The first numerical case study illustrates the effect of cracks on slope stability and also highlights the importance of selecting appropriate hydraulic properties. The approach presented is valuable in understanding how FS of a slope can vary with time taking account of the interaction between soil and environmental conditions (particularly wetting and drying)

• The second numerical case study highlights the effect of swelling behaviour on slope stability shows. The study shows the shear strength properties vary consistently during a hydraulic and mechanical process. Analysis relying on a single pair of shear strength parameters from saturated soil specimens in the laboratory may not be sufficient in engineering design. For this reason, in forensic analysis the pre-failure hydro-mechanical process should be taken into account using unsaturated soil mechanics.

• A simple framework is highlighted for failure of retaining walls and pile foundations in expansive soils are established in this paper. Using the proposed model, reasonable evaluation of the total lateral earth pressure acting on the retaining wall considering lateral swelling pressure and uplift frictions generating along the pile shaft is possible. The proposed approach can be valuable tool in forensic investigations. In addition, this approach can be used for providing remediation measures to alleviate likely failures.

• Moisture content variation has a significant influence on the resilient modulus of pavement materials. A simple approach is introduced in this paper for predicting the variation of the resilient modulus with moisture content and suction (i.e. taking account of the environmental factors). This approach only requires limited and easy-to-obtain experimental data for prediction and can be used for the rational design of pavements. The proposed approach can also be used in the failure assessment of the pavement structure for forensic investigations.

REFERENCES

Aashto. (2003). Designation T307-99: Determining The Resilient Modulus Of Soils And Aggregate Materials. American Association Of State Highway And Transportation Officials. Washington, D.C.

Abu-Farsakh, M. Y., Mehrotra, A., Mohammad, L., and Gaspard, K. (2015). “Incorporating The Effect Of Moisture Variation On Resilient Modulus For Unsaturated Fine-Grained Subgrade Soils.” Transportation Research Record, 2510, Transportation Research Board, Washington, D. C., 44-53.

Adem, H. H. (2015). "Modulus Of Elasticity Based Method For Estimating The Vertical Movement Of Natural Unsaturated Expansive Soils." PhD Thesis, University Of Ottawa, Ottawa, Canada.

Azam, A. M., Cameron, D. A., and Rahman, M. M. (2013). “Model For Prediction Of Resilient Modulus Incorporating Matric Suction For Recycled Unbound Granular Materials.” Canadian Geotechnical Journal, 50(11): 1143-1158.

Bigl, S. R., and Berg, R. L. (1996). Material Testing And Initial Pavement Design Modeling: Minnesota Road Research Project. Crrel Report 96-14, USACE Cold Regions Research And Engineering Laboratory, Hanover, N.H., USA.

Bilodeau, J. P., and Doré, G. (2012). “Water Sensitivity Of Resilient Modulus Of Compacted Unbound Granular Materials Used As Pavement Base.” International Journal Of Pavement Engineering, 13(5): 459-471.

Bosscher, P. J., and Nelson, D. L. (1987). “Resonant Column Testing Of Frozen Ottawa Sand.” Geotechnical Testing Journal, 10(3):123-134.

Caicedo, B., Coronado, O., Fleureau, J. M., and Correia, A. G. (2009). "Resilient Behaviour Of Non-Standard Unbound Granular Materials." Road Materials And Pavement Design, 10(2): 287-312.

Carper, K. L. (1986) Forensic Engineering - Learning From Failures. ASCE, New York.

Chen, F. H. (2012). Foundations On Expansive Soils (Vol. 12). Elsevier.

Chen, F. H. (1988). Foundations On Expansive Soils, Elsevier, New York.

Coronado, O., Caicedo, B., Taibi, S., Correia, A. G., Souli, H., and Fleureau, J. M. (2016). "Effect Of Water Content On The Resilient Behavior Of Non-Standard Unbound Granular Materials." Transportation Geotechnics, 7: 29-39.

Day, R. W. (1999) Forensic Geotechnical And Foundation Engineering. Mcgraw Hill, New York.

Drumm, E. C., Reeves, J. S., Madgett, M. R., and Mrolinger, M. D. (1997). "Subgrade Resilient Modulus Correction For Saturation Effects." Journal Of Geotechnical And Geoenvironmental Engineering, 123(7): 663-670.

Duncan, J. M. (1996). State Of The Art: Limit Equilibrium And Finite-Element Analysis Of Slopes. Journal Of Geotechnical Engineering, 122(7), 577-596.

Fan, Z. H. (2007). "Research On Swelling-Shrinkage Characteristic And Pile-Soil Interaction Of Expansive Soil Foundation." Phd Thesis, Central South University, Changsha, China. (In Chinese)

Fredlund, D. G., and Rahardjo, H. (1993). Soil Mechanics For Unsaturated Soils. John Wiley And Sons.

Fredlund, D. G., and Xing, A. (1994). "Equations For The Soil-Water Characteristic Curve." Canadian Geotechnical Journal, 31(4): 521-532.

Fredlund, D. G. (2006). "Unsaturated Soil Mechanics In Engineering Practice." Journal Of Geotechnical And Geoenvironmental Engineering, 132(3): 286-321.

Gu, X. W. (2005). "Study On The Interaction Between Unsaturated Expansive Soils And Structure." MS Thesis, Nanjing Hydraulic Research Institute, Nanjing, China (In Chinese).

Hamid, T. B. and Miller, G. A. (2009). "Shear Strength Of Unsaturated Soil Interfaces." Canadian Geotechnical Journal, 46 (5), 595-606.

Han, Z., and Vanapalli, S. K. (2015). "Model For Predicting The Resilient Modulus Of Unsaturated Subgrade Soil Using The Soil-Water Characteristic Curve." Canadian Geotechnical Journal, 52(10): 1605-1619.

Han, Z., and Vanapalli, S. K. (2016a). "State-Of-The-Art: Prediction Of Resilient Modulus Of Unsaturated Subgrade Soils." International Journal Of Geomechanics. Doi: 10.1061/(Asce)Gm.1943-5622.0000631.

Han, Z., and Vanapalli, S. K. (2016b). "Stiffness And Shear Strength Of Unsaturated Soils In Relation To Soil-Water Characteristic Curve." Géotechnique. Doi: 10.1680/Geot./15-P-104.

Hoyos, L. R., Suescún-Florez, E. A., and Puppala, A. J. (2015). "Stiffness Of Intermediate Unsaturated Soil From Simultaneous Suction-Controlled Resonant Column And Bender Element Testing." Engineering Geology, 188(7): 10-28.

Huang, Y. H. (2004) Pavement Analysis And Design (Second Edition). Prentice Hall: New Jersey.

Jaky, J. (1944). "The Coefficient Of Earth Pressure At Rest." Journal Of The Society Of Hungarian Architects And Engineers, 78(22), 355–358.

Joshi R. P., and Katti, R. K. (1980). "Lateral Pressure Development Under Surcharges." Proceedings, 4th Intemational Conference On Expansive Soils, Denver, Co, 227-241.

Jong, D. T., Bosscher, P., and Benson, C. (1998). "Field Assessment Of Changes In Pavement Moduli Caused By Freezing And Thawing." Transportation Research Record: Journal Of The Transportation Research Board, (1615): 41-48.

Katti, R. K., Bhangle, E. S., and Moza, K. K. (1983), "Lateral Earth Pressure Of Expansive Soil With And Without A Cohesive Non-Swelling Soil Layer- Applications To Earth Pressures Of Cross Drainage Structures Of Canals And Key Walls Of Dams (Studies Of K0 Condition)." Central Board Of Irrigation And Power. Technical Report No. 32, New Delhi, India.

Khoury, C. N., Brooks, R., Boeni, S. Y., and Yada, D. (2013). "Variation Of Resilient Modulus, Strength, And Modulus Of Elasticity Of Stabilized Soils With Postcompaction Moisture Contents." Journal Of Materials In Civil Engineering, 25(2): 160-166.

Khoury, N. N., and Zaman, M. M. (2004). "Correlation Between Resilient Modulus, Moisture Variation, And Soil Suction For Subgrade Soils." Transportation Research Record, 1874, Transportation Research Board, Washington, D.C., 99-107.

Lee, W., Bohra, N. C., Altschaeffl, A. G., and White, T. D. (1995). "Resilient Modulus Of Cohesive Soils And The Effect Of Freeze-Thaw." Canadian Geotechnical Journal, 32(4): 559-568.

Lekarp, F., Isacsson, U., and Dawson, A. (2000). "State Of The Art. I: Resilient Response Of Unbound Aggregates." Journal Of Transportation Engineering, 126(1): 66-75.

Li, D., and Selig, E. T. (1994). "Resilient Modulus For Fine-Grained Subgrade Soils." Journal Of Geotechnical Engineering, 120(6): 939-957.

Li, Q., Ling, X., and Sheng, D. (2015). "Elasto-Plastic Behaviour Of Frozen Soil Subjected To Long-Term Low-Level Repeated Loading, Part I: Experimental Investigation." Cold Regions Science And Technology, 125: 138-151.

Liu, Y. and Vanapalli, S. K. (2016) Influence Of Lateral Swelling Pressure On The Geotechnical Infrastructure In Expansive Soils. Journal Of Geotechnical And Geoenvironmental Engineering (In Press).

Lytton, R. (2007). "Design Of Structures To Resist The Pressures And Movements Of Expansive Soils." Texas A and M University.

Mohamed, O. Z., Taha, Y. K. and El-Aziz, E. M. (2014). "Field Study Of The Distribution Of Lateral Swelling Pressure Of Expansive Soil On Retaining Structure." Journal Of Engineering Sciences, 42(2): 289-302.

Kassiff, G. and Zeitlen, J.G. (1962). "Behaviors Of Pipes Buried In Expansive Clays." Proc. ASCE, Journal Of Soil Mechanics And Foundation Engineering, Sm 2, No. 3103.

Mahoney, J. P., Lary, J. A., Sharma, J., and Jackson, N. (1985). "Investigation Of Seasonal Load Restrictions In Washington State." Transportation Research Record: Journal Of The Transportation Research Board (1043): 58-67.

Mayne, P. W., and Kulhawy, F. H. (1982). "K0–OCR Relationships In Soil." Journal Of The Geotechnical Engineering Division, ASCE, 108(Gt6), 851–872.

Moza, K. K., Katti, R. K. and Katti, D. R. (1987). "Active Pressure Studies In Saturated Expansive Soil." Proceedings Of The Eighth Asian Regional Conference On Soil Mechanics And Foundation Engineering, Kyoto, Japan, 189-192.

Nelson, J. D. and Miller, J. D. (1997). "Expansive Soils, Problems And Practice In

Foundation And Pavement Engineering." Wiley Press, New York.

Ng, C. W. W., Zhan, L.T., Bao, C. G., Fredlund, D. G., and Gong, B. W. (2003). Performance Of An Unsaturated Expansive Soil Slope Subjected To Artificial Rainfall Infiltration. Géotechnique, 53(2), 143-157.

Poulos, H. G. (2016). A Framework For Forensic Foundation Engineering. In Forensic Geotechnical Engineering (Pp. 1-15). Springer India.

Qi, S., and Vanapalli, S. K. (2015a). Rainfall-Induced Shallow Failure In Expansive Soils: A Case Study In Regina, Canada. International Journal Of Geohazards And Environment,1(1):7-19.

Qi, S., and Vanapalli, S. K. (2015b). Hydro-Mechanical Coupling Effect On Surficial Layer Stability Of Unsaturated Expansive Soil Slopes. Computers And Geotechnics, 70, 68-82.

Qi, S., and Vanapalli, S. K. (2015c) Numerical Study On Expansive Soil Slope Stability Considering The Effect Of Swelling Behaviour And Cracks. In Proceedings Of The 2015 Asia-Pacific Conference On Unsaturated Soils, Guilin, China.

Qi, S., and Vanapalli, S. K. (2016d). Influence Of Swelling Behavior On The Stability Of An Infinite Unsaturated Expansive Soil Slope. Computers And Geotechnics, 76, 154-169.

Richards, B.G. and Kurzeme, M. (1973). “Observations Of Earth Pressures On A Retaining Wall At Gouger Street Mail Exchange, Adelaide.” Australian Geomechanics Journal, G3 (1): 21-26.

Ruwaih, I.A., (1987). "Experiences With Expansive Soils In Saudi Arabia." Proc., Of The 6th Int. Conf. On Expansive Soils, New Delhi, India, 317–322.

Sheng, D. (2011). “Review Of Fundamental Principles In Modelling Unsaturated Soil Behaviour.” Computers And Geotechnics, 38(6): 757-776.

Tian, P., Zaman, M. M., and Laguros, J. G. (1998). “Gradation And Moisture Effects On Resilient Moduli Of Aggregate Bases.” Transportation Research Record, 1619, Transportation Research Board, Washington, D. C., 75-84.

Vanapalli, S.K., Fredlund, D.G., Pufahl, D.E., and Clifton, A.W. (1996). “Model For The Prediction Of Shear Strength With Respect To Soil Suction.” Canadian Geotechnical Journal, 33: 379–392.

Wang, C.H., Liu, Q.C. and Li, B. (2008). "Rankine's Earth Pressure Theory Considering Roughness Of Wall Back Surface." Chinese Journal Of Geotechnical Engineering, 30(Supp), 129-133. (In Chinese)

Widger, R. A., and Fredlund, D. G. (1979). Stability Of Swelling Clay Embankments. Canadian Geotechnical Journal, 16(1), 140-151.

Zapata, C. E., Andrei, D., Witczak, M. W., and Houston, W. N. (2007). “Incorporation Of Environmental Effects In Pavement Design.” Road Materials And Pavement Design, 8(4): 667-693.

Zhang, L. L., Zhang, J., Zhang, L. M., and Tang, W. H. (2011). Stability Analysis Of Rainfall-Induced Slope Failure: A Review. Proceedings Of The Ice-Geotechnical Engineering, 164(5), 299.

Zou, W. L., Zhang, J. F., Li, Y. L., Vanapalli, S. K., Tu, H. Y., and Zhang, J. (2015). “Comparisons Between The Measured And Predicted Resilient Modulus Of Subgrade Red Clay Using A SWCC Based Model.” In Proceedings Of The 6th Asia-Pacific Conference On Unsaturated Soils, Guilin, China, 743-748.

Failure analysis of Malin Landslide

G L Sivakumar Babu[1] and Pinom Ering [2]

[1]Professor, Geotechnical Engineering division, Department of Civil Engineering, Indian Institute of Science, Bangalore -560012, Karnataka, India; Email: gls@civil.iisc.ernet.in, glsivakumar@gmail.com
[2]Research Scholar, Geotechnical Engineering division, Department of Civil Engineering, Indian Institute of Science, Bangalore -560012, Karnataka, India; Email: pinom@civil.iisc.ernet.in, pinom432@gmail.com

ABSTRACT

A recent slope failure in India which resulted in the burial of a village called Malin and claimed large number of lives is presented. In this study, Forensic analysis is conducted which focuses on understanding what went wrong, what could have happened and how failure can be prevented using engineering analysis principles. The analysis helps identify the causative factors of slope failure. The paper discusses various lessons learnt from the slope failure, which might help to foresee and mitigate such failures in the future.

INTRODUCTION

Forensic geotechnical engineering is an emerging discipline with a focus on understanding what went wrong, what could have happened and how failures can be prevented using engineering analysis principles in the case of failures of geological/geotechnical origin. It involves scientific investigations and deductions to detect the causes as well as the process of distress in a structure. The standard procedures of testing, design and analysis are not adequate for forensic analysis. It requires detailed investigation of failure incident that results in uncovering the probable causes of failure and answer to questions like “What happened”, “Why did it happen”, “Whose fault it is” and “How can it be fixed”.

In this study, a slope failure which occurred on 30 July 2014 in western India and led to about 160 deaths is investigated. The causative factors of slope failure are investigated. The mechanisms responsible for initiation of landslide are also identified. The investigation involves following steps: collection of data, distress characterisation, development of failure hypothesis, field and laboratory tests, and back analysis. Probabilistic back analysis is performed in the study, it has the ability to diagnose failure mechanism while considering uncertainty. It is important to consider uncertainty in the analysis because uncertainty arises at all stages in the resolution of the problem, from material property evaluation to analysis and consequent assessment.

This paper presents a case study of Malin landslide where Forensic geotechnical engineering is effectively utilized to investigate the failure mechanism. Important lessons learnt from the failure incident are also discussed, which is essential to mitigate landslide risk in the future and for remediation of the problem.

SITE DESCRIPTION

Fig. 1 shows the site located in the Malin village of Pune District in western Maharashtra, India. The area is located about 95 km away from Pune city at an elevation of 760 m (Ering et al., 2015). A devastating landslide occurred in the area on 30 July 2014 and claimed 160 lives

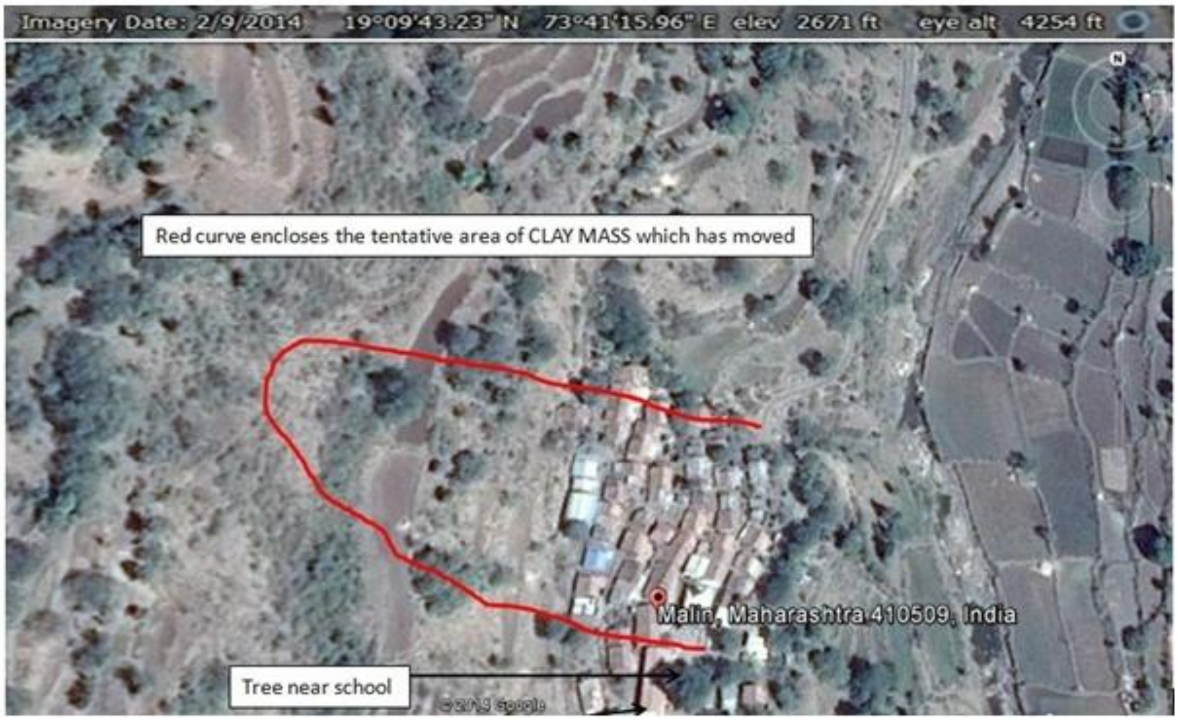

Figure 1: Landslide area

METHODOLOGY

The methodology involved in Forensic analysis consists of six stages. This kind of methodology is required to provide rational explanations for failure incident.

Collection of data

↓

Distress characterisation

↓

Development of failure hypothesis

↓

Field and Laboratory tests

↓

Back analysis

Figure 2: Different stages in failure analysis.

These stages are discussed in the following sections.

Stage 1: Collection of Data

A post-failure investigation was conducted around the Malin landslide area. The findings of the investigation are the basis of this study. A site investigation was carried out to obtain representative information about the landslide area. The hill slope where the slide occurred, was divided into four zones: Zone 1, 2, 3 and 4. The site consisted of thin forest in pre-slide scenario. These trees may have played a role in restricting the lateral extent of the landslide and spread of its debris. A longitudinal section A-A' is drawn on the southern side of the slide from across the ground level up to the crown level of landslide and this section reveals the pre-slide slope configuration of the slided area. Different zones in the section have different slope angles as shown in Table 1.

Table 1: Slope angles in different zones

Zone 1	Zone 2		Zone 3	Zone 4		
20°	10°	25°	30°	18°	25°	50°

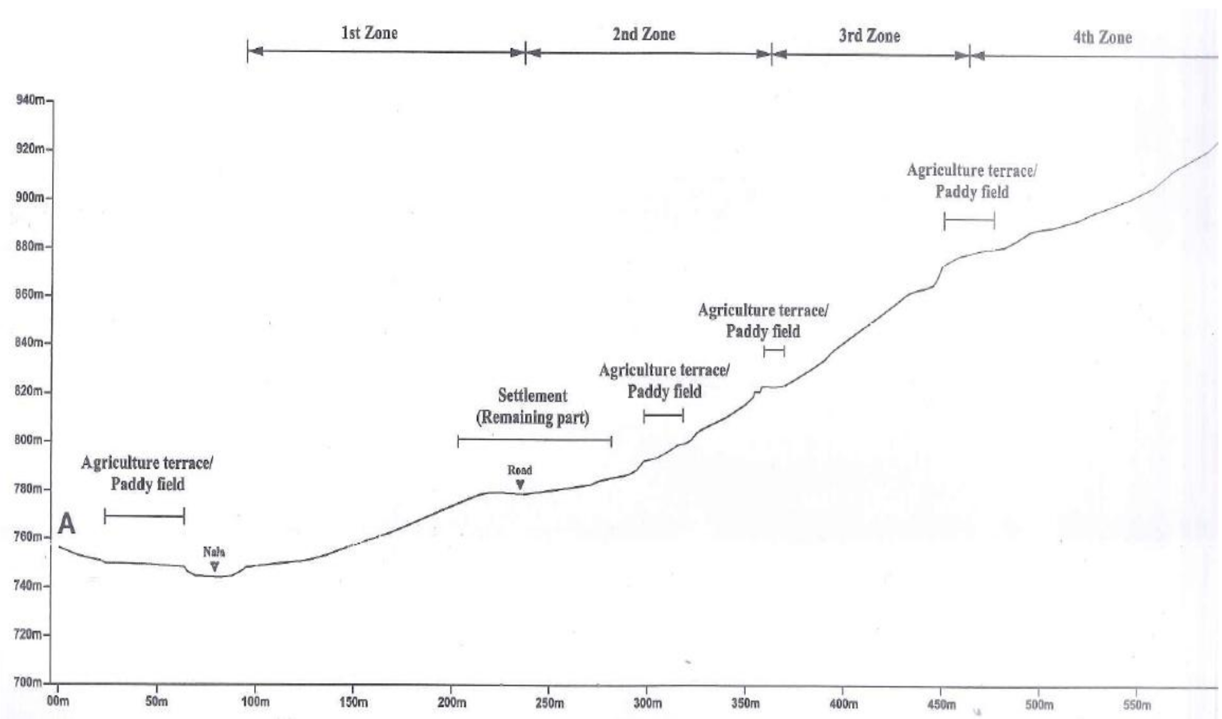

Figure 3: **Longitudinal section**

First zone has fairly uniform slope angle of 20°, zone 2 comprises of two local slopes: the lower part shows 10° while the upper part shows 25°. Zone 3 represents a uniform slope which measures 30°. Zone 4 can be roughly divided into three parts: the lowermost part shows 18°, while the middle and top part shows 25° and 50°. The slope length of zone 1 is 142 m while that of zone 2, 3 and 4 are 130 m, 80 m and 137 m respectively.

The urgency to clean up the failed site limits the time available for investigation and makes it essential that all relevant data are recorded before the evidence is removed. Representative soil samples are collected inside and outside the distressed zone of failed slope to determine their geotechnical properties.

Based on site investigation and discussion with the public it was learnt that landslide occurred after three days of high intensity rainfall. Hence, rainfall data of Malin area was collected from the nearby rain gauge station.

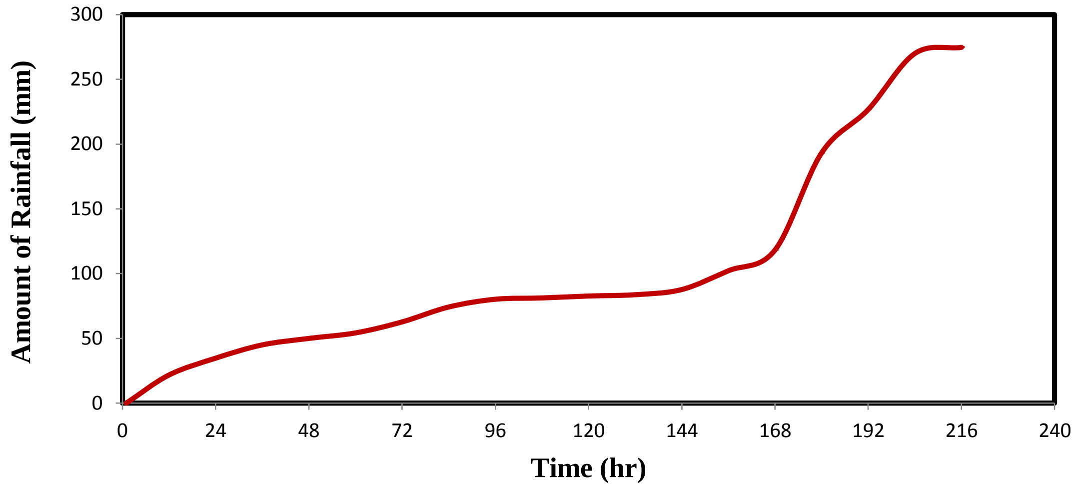

Figure 4: Rainfall data

It can be noted that during previous few days i.e from July 22 to 28, the antecedent rainfall was nothing extraordinary. However the rainfall record for 29th July i.e after 168 hours shows high amount of rainfall (108 mm). This may have played a significant role in slope instability.

Stage 2: Distress characterisation

A decade earlier (in 2003) signs of distress were witnessed by some NGOs in the region (Ramasamy et al. 2015). The villagers also observed appearance of cracks in the hills. Due to such signals indicating possible landslides, the villagers were evacuated to the adjacent area and housed in specially erected shelters; but they returned to Malin village which led to the large-scale causalities.

From the field observations, height of the landslide is roughly estimated as 190 m while the width of the slide varied from 45 m to 134 m (Ering et al., 2015). The entire length of the slide from crown to toe is 514 m. The landslide affected area is 44245 m^2 . Part of zone 4, entire zone 3 and maximum part of zone 2 are depleted by the landslide. A zone of accumulation was formed by the lowest part of zone 2 and zone 1, unfortunately this zone of accumulation is the settlement area of Malin village. The approximate thickness of slided material in the zone of accumulation is 7 m.

Stage 3: Development of failure hypothesis

Development of failure hypothesis is important to identify all the possible causes of failure. Failure analyses are usually carried out to find evidence in support of the hypothesis.
From the field observations, heavy rainfall over three days seem to have triggered the landslide in the area. This rainfall infiltration might have decreased the mobilized shear strength in soil below the threshold value required to maintain equilibrium in the slope.

Stage 4: Field and Laboratory tests

Failure analysis requires fresh field and laboratory tests apart from collection of all available data. Soil samples collected from the slided area are tested in laboratory to determine their geotechnical properties. Grain size analysis, moisture content, dry density and consistency limits are determined. Laboratory shear tests are performed to evaluate shear strength parameters of the soil samples. Table 2 shows the result of geotechnical tests.

Table 2: Geotechnical parameters of soil samples

Parameter	Value
Moisture content (%)	27.3
Dry density (kg/m^3)	1336
Bulk density (kg/m$^{3)}$	1700
Specific Gravity	2.56
Grain Size analysis	Silty clay
Liquid limit (%)	52
Plastic limit (%)	29
Plasticity Index	23
Cohesion (kPa)	36
Friction angle (°)	22

Field tests were not performed as the slided area was the settlement area of Malin village, in addition most of the nearby areas were converted to paddy fields making it more difficult to carry out geotechnical investigations.

Stage 5: Back analysis

Landslide initiation is a complex problem and it is important to understand the relevant physics behind it. For this purpose, back analysis is carried out on the failed slope in Malin. The analysis carried out to identify the cause of slope failure is known as back analysis. It can be utilized to determine the shear strength parameters, pore water pressure and other conditions at the time of failure. It is an effective approach to provide an insight into the underlying failure mechanism. While majority of hill slopes are in unsaturated state, the conventional methods of stability analysis are performed based on assumptions of saturated behaviour. Slope failures triggered by rainfall infiltration essentially occurs in unsaturated slopes. Hence, an extensive and detailed saturated-unsaturated transient seepage analysis is required for such case.

In this study, a systematic methodology is presented to explain the mechanism of rainfall-induced landslide initiation in unsaturated slopes. Transient seepage and stability analyses are combined with probabilistic back analysis to provide rational explanations to landslide initiation. Numerical analyses using FLAC (Fast Langrangian analysis of continua) are performed based on the actual rainfall data, saturated-unsaturated seepage theory and the mechanical theory of unsaturated porous media to simulate the slope in Malin that failed during rainfall infiltration. The results of deterministic analyses in FLAC are used as input for the probabilistic back analysis of the slope. The two phase flow option in FLAC is used and it enables numerical modeling of flow of two immiscible fluids (air and water) through porous media. In FLAC, soil water characteristic curve and relative permeability of fluids are built-in and based on the empirical laws of the van Genuchten form (van Genuchten, 1980). The slope is composed of silty clay which is modeled as Mohr-coulomb material with cohesion 36 kPa and friction angle 22°.The soil and fluid properties used in the analysis are given in Table 2 and 3.

Table 3: Fluid properties

Parameter	Value
Wetting fluid density (kg/m3)	1000
Non-wetting fluid density (kg/m3)	0.0
van Genuchten parameter, *a*	0.281
van Genuchten parameter, *b*	0.0
van Genuchten parameter, c	0.5
van Genuchten parameter, P_0 (Pa)	4350
Wetting fluid modulus (MPa)	1.0
Non-wetting fluid modulus (Pa)	1.0
Mobility coefficient (m^2/ Pa-sec)	$7.074*10^{-11}$

The van Genuchten parameters a, b, c for a typical silty clayey soil are taken from Leij et al. (1996). The FLAC model is 340 m wide and the highest elevation from the base is 180 m as given in Figure 5. Zone 1 is not included in the model since it was not depleted during the landslide and only formed the zone of accumulation.

The slope is analysed for two successive rainfall events of increasing intensity and decreasing duration. The rainfall data is divided into two parts: 1) First rainfall event in which 260 mm of rain accumulates in a period of 57 days (1st June to 27th July) and 2) Second rainfall event in which 182 mm of rain accumulates in three days (28th July to 30th July). The numerical simulation is run in two stages: first rainfall event has intensity of $5.192*10^{-8}$ m/sec and second rainfall event has intensity of $7.05*10^{-7}$ m/sec.

Probabilistic back analysis is used in the study as it has the ability to determine numerous sets of stability parameters with uncertainty. The method acknowledges that there could be various combinations of parameters that can result in slope instability, but their relative likelihoods are different and can be quantified by probability distributions. Probabilistic method used in the analysis is based on Bayesian analysis. The method uses the measurements of observable parameters to infer the values of the parameters that characterize the system. Detailed explanation of this back analysis method is given Ering and Babu (2016).

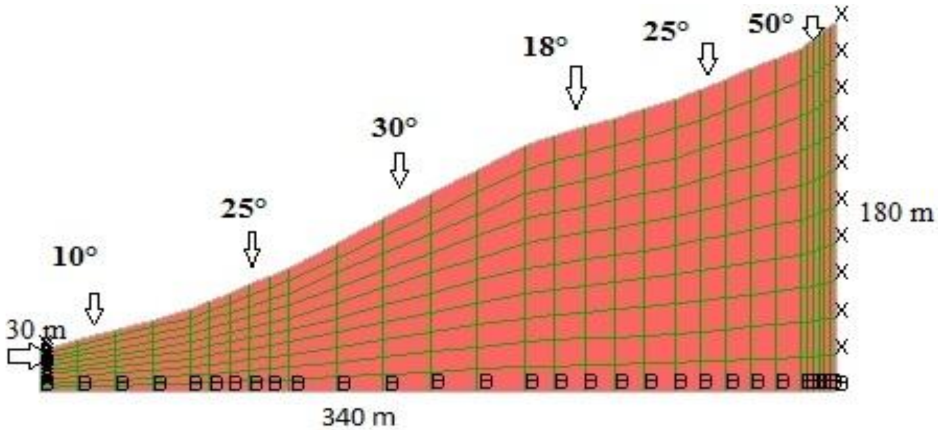

Figure 5: Slope geometry

Tarantola (2005) provided a probabilistic method to back analyze the slope stability parameters. A slope stability model is represented by R(x) and x is the set of uncertain input parameters. The uncertain input parameters used in this study are cohesion, friction angle and pore water pressure or matric suction. The probabilistic back analysis approach updates the probability distribution of x based on the observed slope behavior. A multivariate normal distribution with mean μ_x and covariance matrix $\mathbf{C}_x$ is employed to represent the prior probability distribution of x. The prior distribution as given by (Tarantola, 2005) is:

$$f(x) = const.\ \exp\left[-\frac{1}{2}(x-\mu_x)^T C_x^{-1}(x-\mu_x)\right] \tag{1}$$

Where a normalization constant is required to make the probability density function f(x) valid. The actual response (y) of the system is different from the observed one (y_{obs}) because of observational uncertainty. The probability density function of y given y_{obs} as given by Tarantola (2005) is

$$f(y|y_{obs}) = const.\exp\left[-\frac{1}{2}(y-y_{obs})^T C_y^{-1}(y-y_{obs})\right] \tag{2}$$

In addition, model uncertainty induces difference in the predicted response R(x) and the actual response y of the system. To incorporate the model imperfection effect in the system response, the model uncertainty can be assumed as a random variable z with mean μ_z and covariance matrix C_z

$$z = y - R(x) \tag{3}$$

Incorporating model uncertainty in the analysis, the probability density function of y given x is

$$f(y|x) = const.\exp\left[-\frac{1}{2}\left(y-R(x)\right)^T C_z^{-1}\left(y-R(x)\right)\right] \tag{4}$$

Based on these assumptions, the improved distribution of x considering the prior distribution f(x) and observed data y_{obs} can be described as:

$$f(x|y_{obs}) = const. f(x)\exp\left[-\frac{1}{2}(R(x)-y_{obs})^T C_M^{-1}(R(x)-y_{obs})\right] \tag{5}$$

Expanding f(x) in the above equation, the posterior distribution of x given y_{obs} becomes

$$f(x|y_{obs}) = const.\exp\{[R(x)-y_{obs}]^T C_M^{-1}[R(x)-y_{obs}] + (x-\mu_x)^T C_x^{-1}(x-\mu_x)\} \tag{6}$$

Where y_{obs} is the observed data; C_x is the prior covariance matrix of x; $C_M = C_y + C_z$, C_y is the covariance of actual system response (y) and C_z is the covariance of model uncertainty (z).

From equation (6), the posterior density function follows a Gaussian distribution so there must be a point such that the posterior density function can be written as:

$$f(x|y_{obs}) = const. \exp\left[-\frac{1}{2}\left(x - \mu_{x|y}\right)^T C_{x|y}^{-1}\left(x - \mu_{x|y}\right)\right] \quad (7)$$

Tarantola (2005) postulated that for a linear prediction model, the solution for the above equation is a closed form one and is given by:

$$\mu_{(x|y)} = \mu_x + C_x G^T (G\, C_x G^T + C_M)^{-1} (y_{obs} - G\, \mu_x) \quad (8)$$

$$C_{(x|y)} = (G^T C_M^{-1}\, G + C_x^{-1})^\wedge - 1 \quad (9)$$

$$G = \frac{\partial\, R(x)}{\partial x}\Big|_{x=\mu_x} \quad (10)$$

Where R(x) = G μ_x is a linear prediction model; G is the row vector which describes the sensitivity of *R* (x) with respect to x at point μ_x; $\mu_{x|y}$ and $C_{x|y}$ are the posterior mean and covariance of x respectively. In equation (8), R(x) = G μ_X is a biased model with mean model uncertainty μ_z hence an unbiased prediction model can be written as R(x) = G μ_x + μ_z. The unbiased posterior mean can be determined as (Tarantola, 2005):

$$\mu_{(x|y)} = \mu_x + C_x G^T (\, G\, C_x G^T + C_M)^{-1}\, (y_{obs} - G\, \mu_x - \mu_z\,) \quad (11)$$

Back analysis is required to provide technical evidence to prove or to disprove the hypotheses made on the cause of failures and to establish scenarios of failure. The objective of back analysis in this case study is to identify triggering factors of slope failure and to investigate the mechanisms which initiated landslide. Although from the previous studies, it has been concluded that rainfall infiltration in unsaturated slopes reduces matric suction or shear strength which leads to failure. However, till date it has not been establish how much decrease in matric suction can initiate landslide.

RESULTS

Heavy rainfall over three days before the slope failure is identified as the triggering factor for landslide because seismic activities were not recorded in the area. From numerical analysis, it is observed that the factor of safety of slope decreases from 1.475 in its initial state to 1.46 after the first rainfall infiltration. The stability further decreases and failed after the second rainfall infiltration. Figure 6 and 7 shows the state of slope after first rainfall and second rainfall event respectively. This reduction in factor of safety can be attributed to the lowering of shear strength of soil due to changes in pore water pressure and saturation contours in the slope during rainfall infiltration.

Figures 8, 9 show the saturation and pore water pressure at different depths. The depth zero corresponds to the top surface of the slope. It is observed that the saturation of the slope increases due to rainfall infiltration. During the second rainfall infiltration, the slope becomes fully saturated upto some decent depth as saturation increases from 0.55 to almost 1. The pore pressures generated in the slope changes from negative to positive values due to rainfall infiltration. During the second rainfall infiltration, the pore water pressures in the upper layers become positive. This is due to the complete saturation of the soil particles. From the results it can be concluded that rainfall infiltration did affect the stability of slope and the slope eventually failed. Rainfall infiltration increased the saturation in the slope and decreased negative pore water pressure or matric suction. This type of deterministic analysis is helpful in providing insights of the failure mechanism.

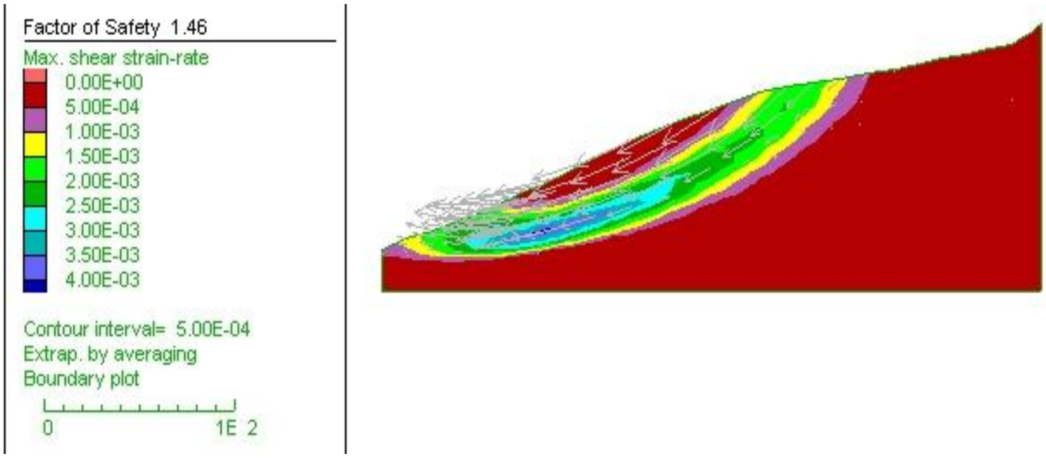

Figure 6: Factor of safety after First rainfall event

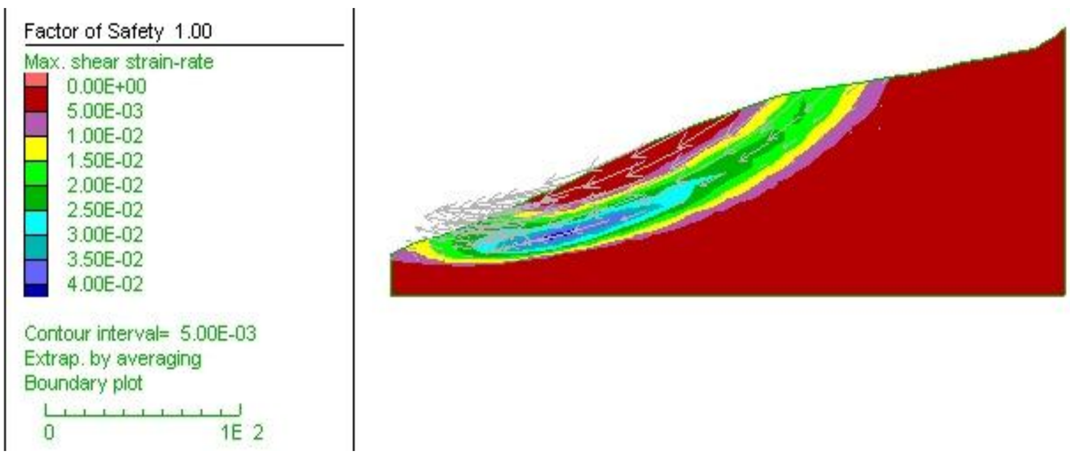

Figure 7: Factor of safety after second rainfall event

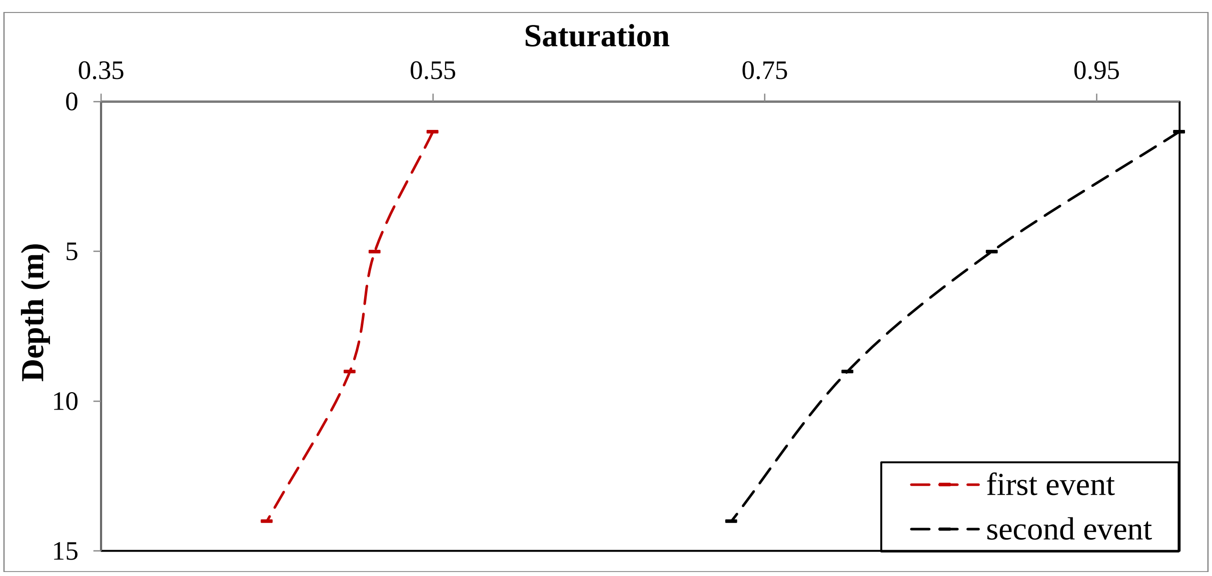

Figure 8: Saturation contours

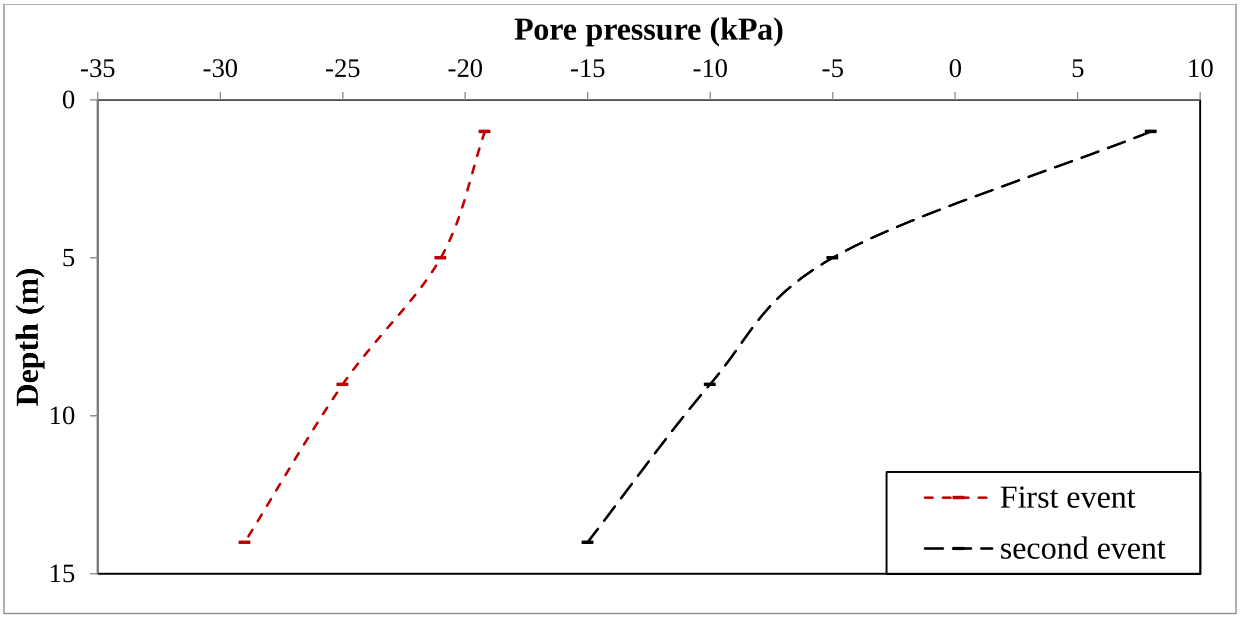

Figure 9: **Pore water pressure contours**

However, slope stability problems are dominated by uncertainty and this uncertainty arises at all stages in the resolution of the problem. Hence, it is important to incorporate uncertainty in the analysis.

Probabilistic back analysis based on Bayesian method is employed to incorporate uncertainties in the analysis. The input parameters (c, φ, ψ) are assumed to be statistically independent and a multivariate normal distribution with mean $\mu_x = \{36, 22, 19.5\}^T$ describes the prior distribution of x. The coefficient of variation of input parameters is given in Table 4. These values are taken from Babu and Murthy (2005).

Table 4: Coefficient of variation of parameters

Parameter	Mean value	COV (%)
Cohesion	36 kPa	10
Friction angle	22°	10
Matric suction	19.5 kPa	40

The covariance matrix of multivariate normal distribution is

$$C_x = \begin{bmatrix} 3.6^2 & 0 & 0 \\ 0 & 2.2^2 & 0 \\ 0 & 0 & 7.8^2 \end{bmatrix} \qquad (12)$$

The model uncertainty of slope stability model can be assumed as a random variable with mean (μ_z) 0.05 and standard deviation (σ_z) 0.07 (Zhang et al., 2010a). The analysis is conducted in two stages: first, to obtain posterior distributions of x due to first rainfall infiltration during which the slope is stable and second, to obtain posterior distributions of x due to second rainfall event during which the landslide occurred. From the field observations, the slope was stable during and after the first rainfall event. Hence, the observed data or observed factor of safety (y_{obs}) can be taken as 1.5. The posterior mean of x can written as:

$$\mu_{(x|y)} = \mu_x + C_x G^T (G\, C_x G^T + \sigma_z^2)^{-1} (1.5 - R(x) - \mu_z) \quad (13)$$

Where μ_x, C_x are prior mean and covariance of x; G is a row vector which describes the sensitivity of R(x) w.r.t x at μ_x; G^T means transpose of G; σ_z^2 and μ_z are the covariance and mean of model uncertainty.

$$\mu_{(x|y)} = \mu_x + C_x G^T (G\, C_x G^T + 0.07^2)^{-1} (1.5 - R(x) - 0.05) \quad (14)$$

Posterior covariance of x can be obtained by

$$C_{(x|y)} = \left(\frac{G^T\, G}{\sigma_z^2} + C_x^{-1}\right)^{-1} \quad (15)$$

Sensitivity G of R(x) at μ_x is obtained by running (2n+1) numerical analysis where n is the number of input parameters. R(x) is computed with respect to change in an individual input parameter while keeping all other parameters same. The samples of input parameters are generated in MATLAB with mean and standard deviation obtained from the analysis. Field observations revealed that the slope failure occurred after the second rainfall event. Hence y_{obs} is 1 in this case. The improved mean based on updated information is given as:

$$\mu_{(x|y)} = \mu_x + C_x G^T (G\, C_x G^T + 0.07^2)^{-1} (1 - R(x) - 0.05) \quad (16)$$

The prior mean and covariance for this analysis is the same as posterior mean and covariance obtained from the previous analysis or first rainfall event. Given the prior mean, covariance of x; model uncertainty mean and covariance, the posterior mean and covariance of x can be obtained. The first stage involves updating the probability distributions of x based on the first rainfall event. The value of R(x) at this stage is 1.475 which is evaluated from the FLAC analysis. The sensitivity G is [0.029 0.131 0.004] where the first value is the sensitivity of cohesion, second is that of friction angle and the last is that of matric suction. Solving equations (14) and (15), we get posterior mean and covariance as

$$\mu_{(x|y)} = \begin{bmatrix} 35.9059 \\ 21.8412 \\ 19.4391 \end{bmatrix} \quad (17)$$

$$C_{(x|y)} = \begin{bmatrix} 11.5451 & -2.3870 & -0.9162 \\ -2.3870 & 0.8132 & -1.5456 \\ -0.9162 & -1.5456 & 60.2468 \end{bmatrix} \quad (18)$$

Equation (18) gives covariance matrix of correlated normals. Hence, to generate the samples of input parameters or x, Eigen value transformation is performed to convert correlated normals to uncorrelated normals in MATLAB. Figures 10, 11 and 12 shows the improved distributions of cohesion, friction angle and matric suction respectively.

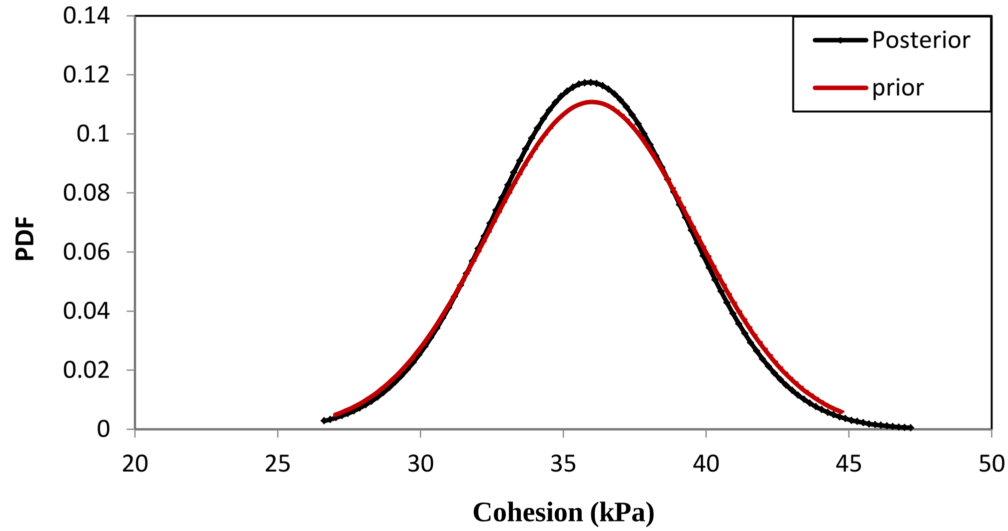

Figure 10: **Probability distribution of cohesion**

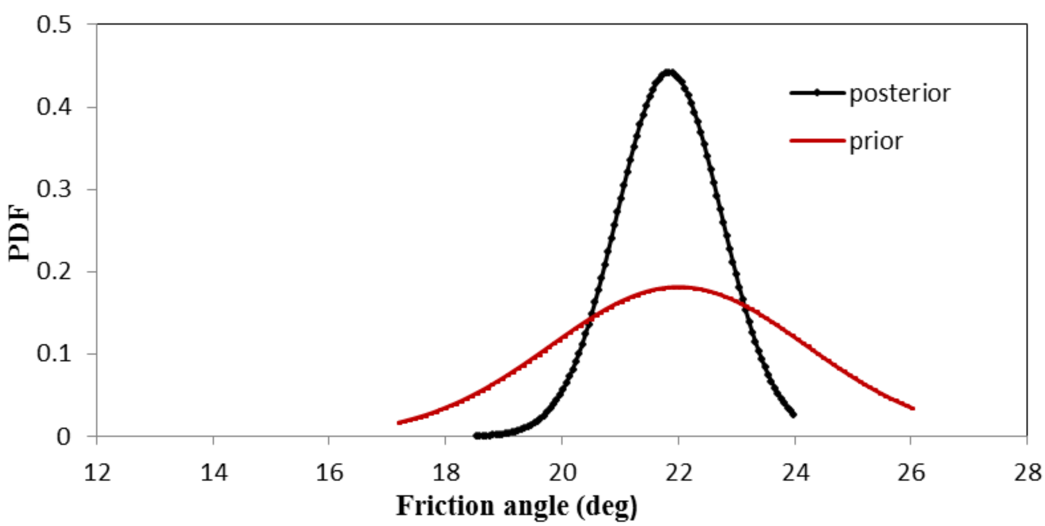

Figure 11: **Probability distribution of friction angle**

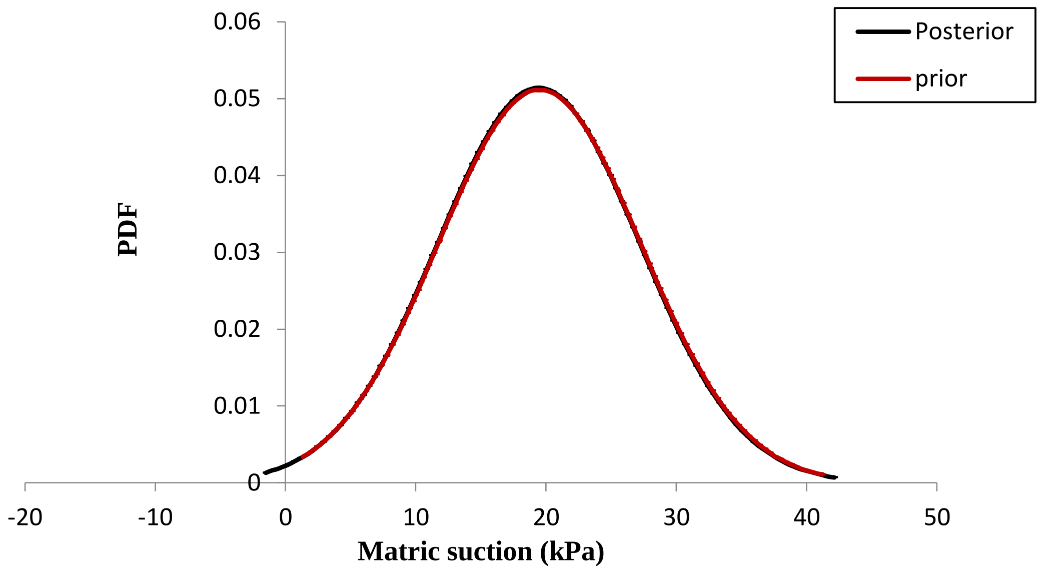

Figure 12: **Probability distribution of matric suction**

It is observed that the cohesion remains almost the same before and after the first rainfall event. The mean value of friction angle remains same but the coefficient of variation is less in the posterior distribution. The improved distribution of matric suction coincides with the prior distribution which indicates that there is no significant reduction in matric suction due to first rainfall event. These results explain that since shear strength parameters and matric suction did not change after the first rainfall event, the slope remains stable during and after the first rainfall event.

The second stage involves updating the above distributions of x based on the second rainfall or slope failure information. The prior mean and covariance of x is same as (17) and (18). At this stage, the value of R(x) is 1.46, observed slope data is 1 and the sensitivity is [0.002 0.002 0.012]. Solving equations (16) and (15), the improved or posterior mean and covariance is obtained. The improved mean and covariance at second stage are:

$$\mu_{(x|y)} = \begin{bmatrix} 35.6290 \\ 22.6615 \\ -7.7115 \end{bmatrix} \tag{19}$$

$$C_{(x|y)} = \begin{bmatrix} 11.5451 & -2.3752 & -1.3060 \\ -2.3752 & 0.7783 & -0.3906 \\ -1.3060 & -0.3906 & 22.0210 \end{bmatrix} \tag{20}$$

Equation (19) implies that after second rainfall event, friction angle increases and matric suction becomes negative. Figures 13, 14 and 15 shows the posterior distributions of cohesion, friction angle and matric suction. From Figure 15 it is observed that the pore pressures in the slope changed from negative to positive values or matric suction values changed from positive to negative. This reduction in matric suction values along the slip circle to about 100% can be attributed to the rainfall infiltration.

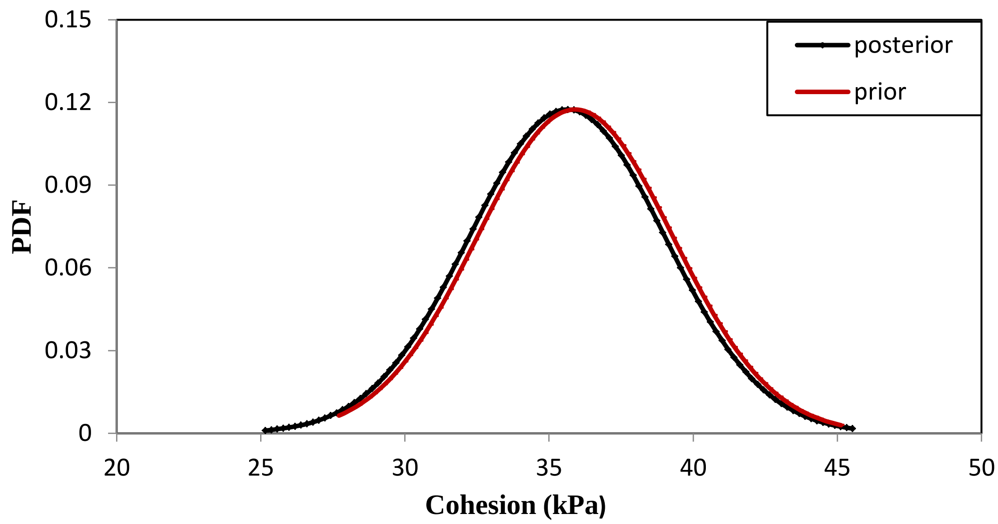

Figure 13: **Probability distribution of cohesion**

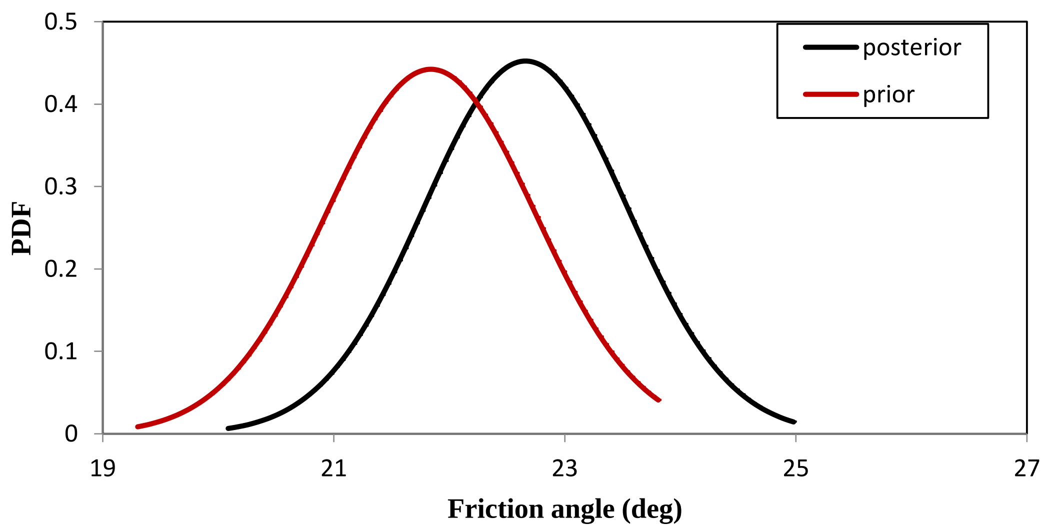

Figure 14: **Probability distribution of friction angle**

The matric suction is reduced to such a value that it no longer provides additional cohesion or strength to the soil slope and the development of positive pore pressures increase the stresses induced in the slope such that equilibrium can no longer be maintained in the slope. Hence, the reduction in matric suction to about 100% and the development of positive pore pressures together has caused the landslide in Malin area.

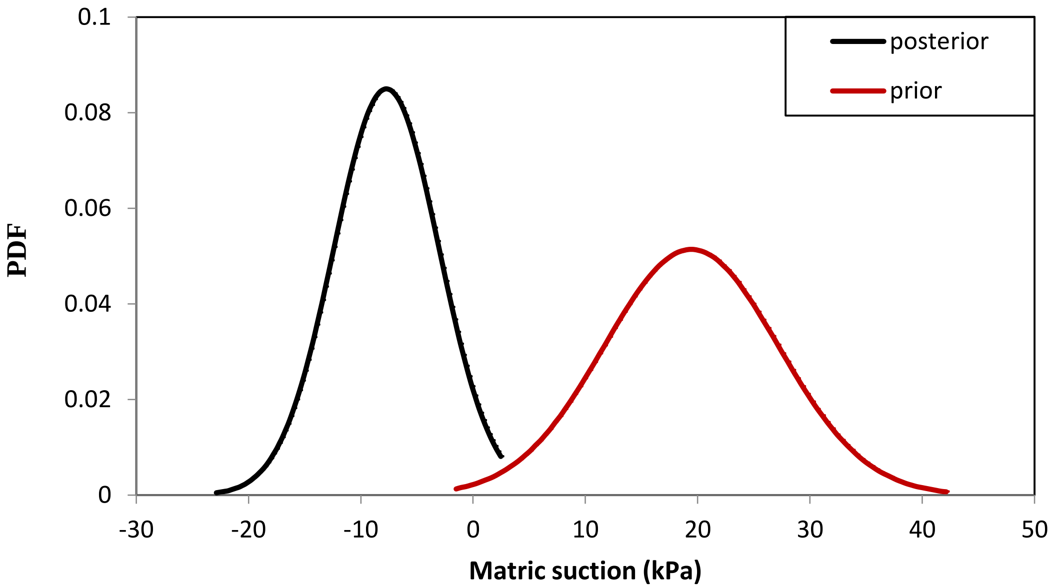

Figure 15: **Probability distribution of matric suction**

CONCLUDING REMARKS

The disaster in Malin has taught us lessons especially in Indian scenario that we are yet to evolve comprehensive, protective and predictive mitigation strategies for such disasters. It is time to start working on strategies to prevent such costly disasters in the future rather than leaving everything to the heroic deeds of National Disaster Response Force (NDRF). Following are some of the important points derived from the failure incident in Malin:

1. The results of failure analysis reveal that landslide initiation is a complex problem. To understand the physics behind or to answer the question “why did it happen”, it is essential to investigate the disaster to the last detail. Different stages of investigation are employed to give rational explanations to the failure. For landslide analysis, it is important to develop a framework which incorporates unsaturated soil mechanics into the traditional slope stability analyses. Conventional stability analysis which assumes saturated behaviour of soils underestimate the soil strength and might give misleading failure scenarios.
2. Uncertainty is inherently present at all stages in the resolution of problem, from the material property evaluation to analysis and consequent assessment. Hence, it is essential to involve uncertainty in failure analysis. Probabilistic back analysis was carried out on the failed slope in Malin and all the possible combinations of parameters that can result in slope instability are determined. Although there can be various failure scenarios but it is observed that the reduction in matric suction value of about 100% and development of positive pore water pressure was the most probable failure mechanism**.**
3. Heavy rainfall is considered as the triggering factor for the disaster but the fact is rainfall has always been a seasonal visitor in the area. Human activities such as deforestation, improper land use planning also have contributed to the slope failure. Amongst all other factors which trigger landslide, rainfall is the easiest one to quantify correctly. Rainfall induced landslides can be prevented by formulating a relationship between rainfall intensity, duration and occurrence of landslides. Though global rainfall thresholds for

landslide occurrence are developed but these types of thresholds should also be developed for regional scales.

4. As discussed earlier, signs of distress and cracks were witnessed by the villagers but they chose to move back to the village without understanding the risk associated with it. It is important to perform risk assessment of the area which involves characterisation of consequence scenarios, determining elements at risk and their vulnerability, evaluate probability of landsliding and severity of consequences. Such assessment or zoning may help people in avoiding those danger areas.
5. The disaster in Malin could have been avoided if efficient early warning systems were used. It is important to monitor inclinations, deformations and pore water pressures in the slopes among others. Slope health monitoring is essential to reduce the risk of landsliding in the area. It is only a matter of time that the slope will fail because all slopes which look like they are about to fail will eventually fail and all slopes which look stable will also eventually fail due to the effect of gravity and other factors. Hence, installation of early warning system become essential to mitigate slope failures in the future.
6. It is important to develop people-centred early warning system. As it is observed from the Malin incident that people were warned of the risk of landslide but they moved back in the area. Communication or dissemination of alerts and warnings should be efficient such that the local bodies should respond to the warnings. People living in landslide risk zones should be educated about the risk of landslide and their consequences.

REFERENCES

Ering, P., Kulkarni, R., Kolekar, Y., Dasaka, S.M., and Babu, G. L. S. (2015). "Forensic analysis of Malin landslide in India." *Proc. IOP Conf. Series: Earth and Environmental Science*, 26, 012040**.**

Ering, P., and Babu, G. L. S. (2016). "Probabilistic back analysis of rainfall induced landslide- A case study of Malin landslide, India." *Engineering Geology*, 208, 154-164.

Leij, F.J., Alves, W.J., van Genuchten, M.Th., and Williams, J.R. (1996). *The UNSODA unsaturated hydraulic database*. EPA/600/R-96/095, U.S. Environmental Protection Agency, Cincinnati, OH.

Ramasamy, S.M., Muthukumar, M., Subagunasekar,M., and Subagunasekar, M. (2015). Malin-Maharashtra landslide: a disaster triggered by tectonics and anthropogenic phenomenon. *Current Science, Vol. 108, No.8, 25 April 2015.*

Tarantola, A. (2005). *Inverse problem theory and methods for model parameter estimation*. 2nd Edition, Elsevier Science, New York.

Van Genuchten, M.T. (1980). "A closed-form equation for predicting the hydraulic conductivity of unsaturated soil." *Soil Sci. Soc. Am. J., 44(5), 892-898.*

Failure of Coal Ash Containment Facilities: Causes, Impacts, Remediation, and Lessons Learned

Girish Kumar[1], Iziquiel Cecchin[2], Antonio Thomé[2] and Krishna R. Reddy[1]

[1]University of Illinois at Chicago, USA and [2]University of Passo Fundo, Brazil

ABSTRACT

Coal ash, in conjunction with other coal combustion residuals (CCR), constitutes the second largest waste stream in the United States. The major concern with the coal ash is its safe storage and disposal, as it contains trace contaminants that could migrate into the environment (air, soil, surface water and groundwater) posing risk to public health. The coal ash disposal facilities should be engineered for adequate structural integrity and waste containment to prevent contaminants spreading into the environment. However, until recently regulations allowed for coal ash disposal in unlined surface impoundments. This paper describes the failure of two recent coal ash disposal facilities, specifically the TVA Kingston Fossil Plant Coal Fly Ash Slurry Spill and the Dan River Coal Ash Spill. The aim of this study is to identify the causes for these failures, assess their impact on public health and the environment, and summarize the measures taken to remediate the spills. Overall, this study emphasizes the need for evaluating the geoenvironmental risk associated with the existing coal ash/waste disposal facilities and implementing sustainable closure/remedial measures. Besides maximizing innocuous beneficial reuse, the study underscores the need for design and operation of safe and effective containment systems for newly generated coal ash and other waste streams such as mine waste.

1 INTRODUCTION

Coal has been one of the primary sources of energy for generating power since ages. In 2015, about 33% of the total U.S. electricity generation was derived from burning coal (US EIA). In addition to generating electricity, combustion of coal produces several by-products called coal combustion residuals (CCRs). CCR includes bottom ash, fly ash, boiler slag and flue-gas desulfurization material. Coal ash consists primarily of oxides of silica, aluminum and iron and can further be classified based on particle size, chemical composition and other physical properties.

Over the decades, coal-fired power plants have been generating large amounts of coal ash and traditionally the coal ash was mixed with water to facilitate pumping it to large open pits usually regarded as ash basins. As the ash settles down in the basin the water that remains over the ash is released into the nearby surface water systems, subject to applicable discharge permitting criteria. This has been practiced as a part of coal ash storage and management over the years by most power generating facilities (Daniels, 2016). The storage of coal ash in an unlined disposal facility poses a threat to the groundwater, as the ash-laden water can leach out heavy metal contaminants and percolate into the subsurface.

Current coal ash disposal practices can pose a risk to the public health and environment. In addition, the inappropriate containment and storage of coal ash without adequate engineering inspection and safety measures increases the risk of facility failure. This study focuses on two of the most recent well publicized failures in the United States namely, the TVA Kingston Fossil Plant Spill that occurred in 2008 and the Dan River Coal Ash Spill in 2014. This study discusses the causes for these failures, outlines their impacts and enumerates the restoration plan with an engineering perspective. Finally, some of the major lessons learned from the investigation of these failures are highlighted.

2 TVA KINGSTON FOSSIL PLANT COAL ASH SPILL

2.1 Site Background

The Kingston Fossil Plant is a property of Tennessee Valley Authority (TVA) that generates power from coal combustion. The plant is located in Roane County, near the city of Kingston and the Watts Bar Lake coast in the state of Tennessee. Its construction started in 1951, and was considered to be the largest coal combustion energy plant, when it started its activities in 1955 (TVA, 2016). Since 1950's, the Kingston plant has been storing coal ash in containment ponds next to its headquarters near the Emory River. The containment ponds were initially built on the former flood plain of Swan Pond Creek.

In 1965, the initial provision pond had already reached its capacity and the new ponds were built for settling and storage of ash by subdividing the initial cell into smaller cells (Moore, 2009). The ash was mixed with water and sluiced to the sedimentation tank and thereafter the settled ash in the pond was dredged and transported to the storage cell. The dam safety monitoring system at the site performed visual inspection regularly and provided a detailed survey of the plant evaluating the safety issues, annually. In 2003 and 2006, a consulting company noted small slope failures in some of the containment dikes (Moore, 2009). The last inspection by the Tennessee Department of Environment and Conservation was held in August 2008, four months before the dike broke down. Interestingly, the last visual inspection of the containment pond was held a few hours before the failure, indicating no apparent problem (Moore, 2009).

2.2 Coal Ash Spill and Impacts

The incident at the TVA Kingston Fossil Plant occurred on December 22, 2008. The dike that held the disposed ash collapsed, causing the release of coal ash material to an area of about 300 acres in the Roane County, Tennessee, USA. An aerial survey of the affected area presented an estimate that more than tripled the first estimate of spill provided by TVA and EPA (1.3 million cubic meters), reaching over 4 million cubic meters (TVA, 2012). After the failure, the stored coal ash slurry crossed the Emory River, reaching the opposite shore of it covering about 1.2 square kilometers of the surrounding area, damaging the residences and the flowing watercourses nearby.

The mudflow caused by containment dike breakdown covered 12 homes stripping them completely of their foundation and causing damage to at least 42 other residential properties. The accident resulted in breaking a natural gas line that crossed the area, blocked a railway line, and destroyed one of the water supply systems and electricity supply lines. This incident was the largest coal ash spill in the history of US, exceeding by more than 3 times the sludge spill in Martin County in 2000, which shed 1.16 million cubic meters of coal ash slurry (TVA, 2012). A picture of the TVA incident is shown below.

Figure 1: Failure of the dike causing coal ash spill at Kingston fossil plant (Source: TVA, 2011)

2.3 Factors Influencing the Failure

The failure involved a number of contributing factors. In the EPA final report, the factors that promoted the failure of the dike that collapsed are listed. The dikes were built under the wet ash with a high void ratio and on a sensitive silt layer (slime) causing instability in the new dikes built over the existing dikes (TVA, 2012). The dredge cell area for the additional coal ash produced became smaller by introducing dikes one over the other. In order to fit the same volume of coal ash produced the height of the dike had to be increased. This increased the load on wet ash at the lower layers that rested on weak slime layer contributing to the failure of the dike. Several creep failures were also observed due to reduction in available strength in slimes.

The old ash disposed in the cell had high water content in the system, an unusually high liquid limit and relatively low undrained shear strength (TVA, 2012). In addition, the ash sent to the dredge cell had a high void ratio and low consolidation or densification by the weight of the ash from the upper layers (Walton and Buttler, 2009). Thus, the ash became highly compressible, leading to low resistance. The same report noted that TVA could have prevented the spill at Kingston Fossil Plant if it had made the recommended corrective actions as observed during the regular inspections.

2.4 Remediation/Restoration Plan

2.4.1 Infrastructure Repairs: Shortly after the rupture of the dike, the first measure adopted by the TVA was to remove the material from roads and railways, opening different ways to enter into the area. The damage caused to more than 900 meters of the railway has been rebuilt, reaching its original alignment and was released for traffic in January 2009. The electricity, water and gas systems that had been affected by the accident were restored in the same year (2008) (TVA, 2012).

2.4.2 River Flow and Ash Migration Control: After the failure of the dike, the migration of ash in the river was controlled by the construction of a barrier system. This reduced the flow of water in the spill area and prevented the migration of ash to downstream areas of the river. After few days following the failure, a provisory containment dike, using boulders as the main material was built. The main purpose of this dike was to avoid migration of the ash to the canal of the Emory River. In addition to its containment function, this dike was built to serve as a functional road during the process of removing the ash (TVA, 2012).

2.4.3 Dredging: The dredging of coal ash was performed in two stages during the remediation process. The Phase-1 was to remove the ash deposited in the riverbed by combined mechanical and hydraulic dredging methods to reduce possible flooding and migration of the ash to the downstream. An estimated 1.76 million cubic meters of coal ash was withdrawn. The Phase 2 of the dredging process was to remove the remaining ash in the river as well as reduce the impacts of coal ash along the natural river sediment. The volume of ash removed in this stage was 596,000 cubic meters and soon after the completion of this process, the Emory River was reopened to the public (TVA, 2012).

2.4.4 Dewatering Process of Ash: The process of dewatering the ash was performed simultaneously with the dredging process of the riverbed. The ash collected by hydraulic dredging was forwarded to the Rim Ditch, Sluice Trench and Ash Pond, so that ash could settle under gravity. After sedimentation, the material was excavated to Ball Field for air drying. After drying, the material was temporarily stored near the site before it was transported to the landfill. The excess water from the hydraulic dredging process was initially forwarded to the Rim Ditch. However, the excess water carried certain ash into the Rim Ditch. So, in January 2010 the water with some ash in it was forwarded to a filter press system for dewatering. It is estimated that at its peak operation, it dewatered about 635 m^3 of ash water (TVA, 2012).

2.4.5 Loading, Transportation and Final Disposition: The loading of dry material began in June 2009 through the railway system near the site. The ash was sent to the State of Alabama and disposed in the Arrowhead Landfill in Perry County. The transport and disposal continued until approximately 4 million tons were transported to the Arrowhead landfill. Although the destination was already set, the daily removal rate of ash (7650-15300 m^3) was higher than the daily rate of transport (6120-7650 m^3), and this required a temporary storage for the ash in stable cells near the power plant (TVA, 2012).

2.4.6 Containment and Removal of the Cenospheres: The management of contamination of cenospheres (floating ash) was initially performed with containment floats, and was suctioned with the help of truck mounted pumps. Approximately 52,000 cubic meters of liquid cenospheres was removed from the area (TVA, 2012).

2.4.7 Dust Control: Considering the problems that the air loaded with silica can cause on human health, a dust control system was immediately implemented in the impacted area. In the area of dredged stable cell, vinyl-acrylic solution was sprayed to suppress the generation of dust on site. For the rest of the area, TVA held aerial seeding of several species of grass, as well as application of fertilizers, to establish a temporary vegetation cover for about 86 hectares and helped reduce erosion in the impacted area (TVA, 2012).

2.4.8 Reconstruction of the Cell and Disposal of Ash: Due to the fast recovery of the impacted area, the disposal of the ash was initiated even before the stabilization of surrounding area. The maximum inclination adopted in the cell was 6H: 1V in order to provide greater stability to it (TVA, 2012). Due to concerns about the stability of underground already affected by the former failure, several monitoring systems (piezometers, slope inclinometers and settlement plates) were implemented to check the safety and stability of the cell. The ash was compressed to 90% of the maximum dry density with its moisture ranging from -2 to +6 of the optimum moisture content. During the construction phase in the winter period, problems in moisture control were observed during the compaction process (TVA, 2013). Accordingly, it was thought to incorporate 2 to 3% (by weight) of lime to the ash deposited in the cell, causing the lime hydration by consuming the excess water, and also enhancing the geotechnical properties of the soil (TVA, 2012).

2.4.9 Stabilized Containment Wall: To increase the stability of the landfill from seismic events, a soil berm was designed around the perimeter of the site, built over a system of stabilized bentonite-cement walls. The walls were built perpendicular to the perimeter of the landfill, with a function to transfer the impulses generated by a possible earthquake to the underlying bedrock (Kilgore, 2009; Bussey et al., 2012; Dotson et al., 2013). All foundation walls were embedded in shale from 0.6 to 2 meters, depending on location. The width of the stabilized area ranged from 15 to 30 meters, the walls being spaced 4.5 to 6.2 meters and with depths ranging from 12 to 21 meters. High performance backhoes were used for the construction of stabilized walls. The slurry used for the construction of walls was a mixture of slag cement and hydrated bentonite (cement-bentonite), which gains strength over time (Dotson et al., 2013).

2.4.10 Cover/Capping of Cell: The cover/capping was performed using a high capacity geocomposite (LLDPE) and 30 cm of cover soil. The use of this system was due to shortage of clayey soil for a compacted soil layer of low permeability. The cover system and the effects of its interface with the ash were analyzed to assess the drained and undrained static stability as well as the pseudo-static seismic conditions (Dotson et al., 2013). The surface drainage was addressed by grading the surface appropriately, allowing the rainwater drained to river (Dotson et al., 2013).

2.4.11 Surface Water Quality Control: A channel system was built around the impacted area to prevent the clean rainwater from entering into the contaminated area and become polluted. In order to avoid the entrainment of materials into the channels, daily cleaning was performed using backhoes. In addition, several monitoring programs were implemented to evaluate the river water, drinking water, air and soil quality near the affected area throughout the restoration period (TVA, 2012; Dotson et al., 2013).

3 DAN RIVER COAL ASH SPILL

3.1 Site Background

Duke Energy, headquartered in Charlotte, North Carolina (NC) is one of the largest electric power holding companies in the United States. In North Carolina itself Duke Energy owns 14 coal-fired power plants, one of which is the Dan River Steam Station (DRSS) located by Dan

River in Rockingham County near Eden, NC. The DRSS began its operation as a coal-fired power generating station in 1949 and was retired from service in April 2012. A natural gas power generating facility was constructed at the same site, few hundred yards away and began operations in 2012. The coal ash residue from DRSS was disposed of in the ash basin system located adjacent to the Dan River.

The primary ash basin was constructed in 1956 and was extended in length approximately 1200 feet east along the Dan River over two existing stormwater pipes in 1968. An intermediate dike was constructed on existing ash deposits in 1976, bisecting the basin into primary and secondary ash basins. The primary ash basin received sluiced ash from pipes through the plant. The secondary basin received decanted flow from the primary ash basin and the flows exit the basin through a decant structure in the secondary basin. The ash basin systems are unlined and are operated as an integral part of site's waste water treatment system. The flow from the secondary ash basin is controlled by National Pollutant Discharge Elimination System (NPDES) Permit. Two dry ash stacks are located to the north of the primary and secondary ash basins. These ash stacks consist of coal ash material dredged from the primary ash basin. Stormwater run-off from the ash stacks is contained within the ash basin system and flows to the secondary ash basin. The ash stacks are unlined and have a vegetative soil cap.

3.2 Coal Ash Spill

On February 2, 2014, a section of the 48 inch diameter stormwater pipe partly made of corrugated metal that ran beneath the primary ash basin collapsed releasing around 39,000 tons of coal ash and 27 million gallons of contaminated water into the Dan River (Duke Energy, 2014a). This coal ash spill was reported to be the third largest coal ash spill in the history of U.S. In a report, the United States Fish and Wildlife Service (USFWS) reported that the coal ash and ash like material were mixed with the sediments as much as 5 feet deep in places and as far as 70 river miles downstream within days following the spill. An immediate action was taken to stop the release and begin assessment of the environmental impact. A concrete plug was placed permanently at the outlet of both the stormwater pipes where the stormwater discharged into the Dan River. The ash deposits were removed from the immediate vicinity of the pipe failure and other downstream locations. Once the ash settled, few locations wherever identified, the ash was successfully removed.

On February 8, a coal ash bar about 75 feet long and 15 feet wide which had as much as five feet of ash or ash/sand mix over the natural stream bottom was identified and was subsequently removed resulting in the recovery of 15 tons of coal ash and native sediment. On July 7, Duke Energy recovered a coal ash deposit (258 tons of a coal ash/sediment mixture) at a site approximately two miles downstream from the steam station on a native sandbar delta at the mouth of Town Creek. The removal of around 2,500 tons of coal ash mixed with native sediment was performed by vacuum dredging at the Schoolfield Dam in Danville, VA in July 2014. In addition to these removal actions, a total of about 466 cubic yards of ash/sediment mix was removed from the water treatment plants at Danville and South Boston and properly disposed of along with dredged material from the Dan River (Dan River, 2014, 2015). A picture of the Dan River coal ash spill is shown below.

Figure 2: Coal ash spill at Dan River due to stormwater pipe collapse (Source: Duke Energy)

3.3 Impacts

The impacts of the Dan River coal ash spill on the natural resources and services were assessed as discussed below.

3.3.1 Surface Waters: The release of coal ash and contaminated water into the Dan River has significantly influenced the water quality. The evaluation of contaminant concentrations in the surface waters downstream showed an increase in the concentrations of copper, selenium, zinc, arsenic and lead exceeding the water quality standards and thresholds, in the days following the spill (Dan River, 2014). However, the risk associated with the contaminated water in the downstream for drinking purposes was mitigated soon.

3.3.2 Geological Resources: Geological resources include the soils and sediments located in upland and wetland areas closely associated with Dan River. The initial screening of sediment also indicated arsenic and selenium as a potential concern for sediments based on the exceedance of the threshold levels. The surveys between the release site and Kerr Lake headwaters indicated ash deposits of sufficient depth overlying native sediments to potentially impact stream habitats (Dan River, 2015). In addition, contaminated sediments serve as a source of continuing releases of hazardous substances to the water column.

3.3.3 Fish and Aquatic Wild Life: The aquatic habitat and wild life that includes fish, migratory birds, and aquatic plants that are dependent on the Dan River have been investigated by the release. The possible pathways for the exposure of aquatic biota to ash-related hazardous substances include direct contact with suspended or dissolved contaminants in the water column, direct contact with contaminated sediments, ingestion of contaminated sediment during foraging or feeding, and indirect contact through ingestion of contaminated prey species, including bioaccumulation (Dan River, 2015). The coal ash released into the aquatic environment can result in injury mainly by burial of native habitats and through destruction of habitat during removal actions to address larger depositional areas. The ash can coat the bottom in depositional areas, burying animals and their food; accordingly, there is a potential for physical burying of habitat that is important for aquatic life. Moreover, the concentrations of hazardous substances in surface water and sediments have been sufficient to cause injury to fish and other aquatic biota as well. It was also learnt that the ecological impact of the coal ash release towards the aquatic life was driven by the burial of aquatic habitat under coal ash rather than the contamination of surface waters due to heavy metals (Dan River, 2015).

3.4 Remediation/Restoration Plan

The disastrous coal ash spill into the Dan River spurred the state of North Carolina (NC) to impose strict regulations for coal ash management and its safe disposal. As per the Coal Ash Act in 2014, Duke Energy is required to close the coal ash impoundments at the DRSS no later than August 1, 2019. In this regard, Duke Energy has come up with a coal ash excavation plan that would assist in its work to close the ash basins at Dan River.

3.4.1 Excavation Plan: Phase I of the plan includes the excavation and removal of 1.2 million tons of ash from the ash stacks or the ash basins at Dan River Steam Station (Duke Energy 2014b). The Maplewood Landfill in Virginia located around 120 miles from DRSS has been identified as the ash storage site. The subsequent phase(s) of the coal ash management plan at DRSS would remove the remaining ash at the site and place it in a fully lined on-site landfill near the existing ash stacks, to facilitate the safe disposal of remaining ash (Duke Energy, 2016). Duke Energy has recently (10/26/2016) received the relevant permit from the NC state department for environmental quality to go ahead with the construction of a lined landfill at DRSS.

3.4.2 Dewatering Plan: The Dan River ash basins will be dewatered to facilitate the removal of ash and transport it to a lined landfill. The lowering of water level within each basin will improve safety factors of the dams by reducing the driving force on the upstream face of the dam (Duke Energy, 2015a). Similarly, dewatering will improve the physical properties of the retained ash, making it less susceptible to flow. The primary ash basin contains an undetermined amount of water which will be pumped to the secondary ash basin at a maximum drawdown rate of one foot over seven days. Following free water removal, vacuum well points will be installed in the ash along the dam to draw down entrapped water in the vicinity of the dam. The dewatering of secondary ash basin that contains approximately 20.7 million gallons of free water will be done similarly as done for primary ash basin (Duke Energy, 2015a).

3.4.3 Safe Basin Closure/Final Cap: The final measure to contain coal ash basins is to construct a final cap that prevents water from entering the system and leaching hazardous contaminants. Duke Energy considers the closing of ash basins by either placing the cap/final cover onto the dewatered ash or excavating the ash from the basin and placing it in a lined landfill. Both of these methods involve safe disposal of water from the basin without affecting the water quality of the water resources. Capping in place involves placing an engineered synthetic cover system over the dewatered ash in the basin with layers of soil and vegetation placed on top. The final cover prevents the rain water from entering into the basin. In fact this method would prevent the need for additional disposal locations, lowers transportation emissions and reduces other impacts on communities. If the excavation of ash is sought then, the feasibility of an on-site landfill is evaluated to help minimize community impacts. If the ash needs to be relocated off-site, the material is excavated, transported by truck or train and stored in a lined landfill that is sealed with a synthetic cover and a layer of protective soil and vegetation (Duke Energy, 2015b). However, in any case a regular monitoring of groundwater is essential in the vicinity of the basin or the landfill to check for the contaminant concentrations in groundwater.

3.4.4 Erosion and Sediment Control (E&SC) Plan: It is important to minimize the impacts to the community while excavating and relocating the ash off-site. Several measures are undertaken to control the dust at the site, including wetting exposed surface areas and maintaining ash at the proper moisture content to prevent dust. The transportation of coal ash to the off-site landfill is predominantly done by rail cars. The approved contractor will install the E&SC measures indicated in the plan such as site preparation activities, including mobilization, installing required site haul roads, installing rail load out spur for rail transportation, and install truck load out and truck wash for truck transportation (Duke Energy, 2015b).

3.4.5 Recycling of Coal Ash: Coal ash has some beneficiary aspects that provide a great opportunity to use it as a construction material. The pozzolanic nature of coal ash (particularly fly ash) makes it a good alternative for cement in construction materials. It is estimated that more than half of the concrete produced in U.S. contains coal ash for construction of structures such as roads, bridges and buildings and make them more durable. In this regard, Duke Energy has been contemplating several avenues for beneficial reuse of coal ash. In fact, Duke Energy had recycled around 63 percent of the coal ash produced in 2015 for beneficial reuse. The company continues to review other innovative technologies and conduct a comprehensive study to evaluate coal ash recycling market and available technologies (Duke Energy, 2016b).

4 Lessons Learned

The catastrophic failures discussed in this study are by no means natural hazards but are induced by some factors. There are many such un-engineered coal ash impoundments which are at a potential risk of failure. The failures discussed in this study set a good example for what needs to be accounted while managing and disposing of coal ash efficiently and safely. There are significant differences between the TVA and Dan River incidents, but there are also similarities that the agencies can utilize in channelizing their efforts to manage coal ash efficiently. The following are some of the important lessons learnt from the two incidents:

- Poorly maintained infrastructure was one of the main reasons for the failure of both the coal ash spills. In Dan River coal ash spill, there is an evidence of the failure of the stormwater pipe in the portion built of corrugated metal. Similarly, in the case of TVA facility the physical instability of the slope and the dikes were overlooked. Hence, it is imperative to check and assess for physical safety in terms of the integrity and stability of the containment system by performing static and seismic analyses to avoid such failures. Structural stability of the impoundments could be maintained by strengthening the containment features (e.g. dikes, MSE berms), and solidifying the load bearing ash to support the overlying load. Although the system is designed for a design life, there could be several factors during the course of its operation which can cause failures and hence timely inspection is indispensable.
- The Dan River spill is a prime example to show that, even without generating new coal ash, the coal ash left behind from decades of operation with inadequate storage can be

disastrous. The ash basins close to the surface waters could pose threat to the water quality in several ways. Firstly, direct discharge of contaminated water from the basin into the river can have adverse effect on the ecosystem of the river and could be carried over to humans. Secondly, the storage of coal ash without any containment barrier would pose threat to the groundwater quality with the leaching of heavy metal contaminants into the groundwater. Hence contaminant migration needs to be properly assessed based on seepage and contaminant fate and transport analysis to check for groundwater contamination. The major intervention in assessing these failures is possible by holistically evaluating the system based on risk associated with the system.

- Proactive remediation strategies which are cost effective and sustainable have to be employed to restore from the damages caused by these failures. Employing energy intensive remediation techniques would however solve the problem but adds greatly to other existing problems and exacerbates the situation. This would involve dewatering and clean-up of the affected site (sediments) using passive technologies and employing alternate sustainable materials in place of traditional materials during the process.
- It is necessary to consider the issues associated with coal ash impoundments based on the broader social, economic and environmental impacts. The environmental impacts shall be assessed in terms of the effects that the facility could have to the surrounding surface water systems, groundwater systems, soil and air. The contaminant transport needs to be assessed with an engineering perspective and needs to be minimized causing no risk to the environment and public health. The economic impacts of these facilities would sometimes be due to their influence on the surrounding property or the real estates. In addition, the economic impacts could also be from the use of materials for closure of the impoundments. Hence, the choice of materials can influence the cost and thereby the economic aspects associated with the facility. Finally, it is quite important to consider the community education and participation in decision-making.
- The end use of these coal ash impoundments should be planned similar to engineered landfills as there is a great opportunity for beneficial reuse of the land for several commercial and recreational purposes. Unlike MSW landfills, the surface impoundments provide great opportunity for reuse of space without posing any significant concerns with regards to the stability of the structures or the services built over it. However, there needs to be adequate monitoring employed at these sites to check for instabilities or any threat to the beneficiaries.
- Coal ash is a promising material in terms of its use in construction material, after being processed, to build more strong and durable structures. The encapsulated coal ash when used as a construction material can help reduce GHG emissions, diverge waste from going into landfill thereby reducing the need for landfill space, alleviates the need for primary raw materials preserving the natural resources. The recycling of coal ash has the most significant environmental benefits and it needs to be leveraged by innovative and technological systems.

The coal ash storage and disposal has been a concern to environmentalists for decades. However, it seems that these failure events made this problem gain adequate attention and the political momentum to create some new regulations for coal ash management. With the advent of NC Coal Ash Management Act, the US Environmental Protection Agency (EPA) has also imposed final rule providing a comprehensive set of requirements for regulating the safe disposal of CCRs (USEPA 2016). The final rule is based on extensive study on the effects of CCRs to the environment and public and the risks associated with them. The rule emphasizes on the structural integrity of surface impoundments to prevent any catastrophic failures experienced earlier. The rule also supports recycling of coal ash for beneficial reuse (USEPA 2016). The lessons learned and the new regulations would not only help US but other countries to develop such strategies for safe and effective management of coal ash.

References

Bussey, K. R., Jr., Steele, M. J., and Smiley, P. B. (2012). "Quality Control Program for the Construction of Cement-Bentonite Slurry Walls at the Kingston Coal Ash Landfill Facility." Proc., Ohio River Valley Soils Seminar, Lexington, Kentucky

Duke Energy (2014b). "Coal Ash Excavation and Removal-Fact Sheet" https://www.duke-energy.com/ash-management/#news-center (October 24, 2016)

Dan River Coal Ash Spill: Natural Resource Damage Assessment Plan (2015) https://www.fws.gov/northeast/virginiafield/pdf/contaminants/20150616_Draft_DAP_with_Appendices.pdf (October 24, 2016)

Dan River (2014) "NRDAR Scoping Document" http://ncdenr.s3.amazonaws.com/s3fs-public/CoalAsh/documents/CoalAsh/DanRiverCoalAshScopingDocument_10012014_Final.pdf (October 24, 2016)

Daniels, J. (2016), "Coal Ash and Groundwater: Past, Present and Future Implications of Regulation", 40 Wm. & Mary Envtl. L. and Pol'y Rev. 535, http://scholarship.law.wm.edu/wmelpr/vol40/iss2/6 (November 3, 2016)

Dotson, V.; Herron, D; Rauch, A.F; Steele, M.J. (2013) "Closure of the Failed Ash Dredge Cell at Kingston – The Engineering Challenge" 2013 World of Coal Ash (WOCA) Conference. Lexington, KY.

Duke Energy (2014a). "Dan River Response: Important Information" http://www.duke-energy.com/Dan-River/ (October 24, 2016)

Duke Energy (2015a). "Dan River Steam Station-Coal Ash Excavation Plan" https://www.duke-energy.com/ash-management/#news-center (October 24, 2016)

Duke Energy (2015b). "Safe Basin Closure Update" https://www.duke-energy.com/ash-management/#news-center (October 24, 2016)

Duke Energy (2016a). "Interim Semi-Annual Report on Closure and Excavation" https://www.duke-energy.com/pdfs/Duke-Energy-Semi-Annual-Report-Closure-Excavation.pdf (October 24, 2016)

Duke Energy (2016b) "Recycling and Reusing Coal Ash" https://www.duke-energy.com/ash-management/#news-center (October 24, 2016)

Kilgore, T., Tennessee Valley Authority (2009), "Testimony to United States Senate", Com. on Environment and Public Works.

Lemly, A. D. (2015). "Damage Cost of the Dan River Coal Ash Spill". Environmental Pollution, 197, 55-61

Moore, R.W. (2009). "Final Report - Review of the Kingston Fossil Plant Ash Spill Root Cause Study and Observations about Ash management". http://oig.tva.gov/re ports/09rpts/2008-12283-02.pdf (October 19, 2016)

Rauch, A. F., McAffee, R. P., Wu, Y., and Arduz, L. J. (2013). "Seismic Design of Perimeter Slurry Walls for the Kingston Coal Ash Pond Closure." Proc., USSD Annual Conference, Phoenix.

The Coal Ash Management Act (2014), North Carolina General Statutes §130A-309.200. www.ncleg.net/Sessions/2013/Bills/Senate/PDF/S729v6.pdf (October 24, 2016)

TVA (2011). "TVA Kingston Fossil Fuel Plant Release Site On-Scene Coordinator Report for the Time-Critical Removal Action May 11, 2009 through December 2010. https://www.tva.gov/file_source/TVA/Site%20Content/About%20TVA/Guidelines%20and%20Reports/Kingston%20Recover%20Project/OSC%20Report%202011-03-31%20FINAL.pdf (October 19, 2016)

TVA (2012). "TVA Kingston Fossil Fuel Plant Release Site On-Scene Coordinator Report Addendum for the Time-Critical Removal Action Addendum No. 01 Harriman, Roane County, Tennessee" https://www.tva.gov/file_source/TVA/SiteContent/AboutTVA/GuidelinesandReports/KingstonRecoverProject/EPA-AO-030A-Approved-TC-OSC- ReportAddendum.pdf (October 19, 2016)

TVA (2016). "Kingston Fossil Plant" https://tva.com/Energy/Our-Power-System/Coal/Kingston-Fossil-Plant (October 19, 2016)

U.S. EPA (2016), "Final Rule: Disposal of Coal Combustion Residuals from Electric Utilities". https://www.epa.gov/coalash/coal-ash-rule#summary (October 24, 2016)

Walton, W. H., and Butler, W. (2009). "Root Cause Analysis of TVA Kingston Dredge Pond Failure on December 22, 2008." http://www.greenenvironmentnews.com/feed_images/6953de52-791e-43d2-937e-021944b861df.pdf (October 19, 2016)

Invited and Expert Papers

A Forensic Investigation on Sinkhole Formation in Urban Area

Albert T. Yeung, PhD, FASCE, FICE, FHKIE, RPE (CIV, ENV, GEL), CEng, PE[1]

[1]Department of Civil Engineering, University of Hong Kong, Pokfulam, Hong Kong; e-mail: yeungat@hku.hk

ABSTRACT

The formation of sinkholes in urban areas in different geologic topographies results in sudden ground collapse. People, properties and/or moving vehicles fall into these sinkholes without any warning. The sinkhole is often developed from an enlarging underground cavity progressively and unnoticeably until the occurrence of sudden ground collapse. The sudden ground collapse can cause personal injuries and loss of properties. Although the sinkhole or ground collapse occurs suddenly without any warning, the underground cavity may develop suddenly or through a prolonged period depending on the underground cavity formation mechanism. The forensic investigation on the formation of a sinkhole in the urban area of Hong Kong is presented in this paper.

INTRODUCTION

The sudden occurrences of sinkholes or ground collapse in urban areas, such as Hong Kong, can be disastrous (Friend 2002). The sinkhole can be dry or submerged in water. People, properties, and/or moving vehicles can fall into sinkholes suddenly without any warning as shown in Figures 1 & 2, resulting in personal injuries and/or property damage.

Most sinkholes are developed from existing underground cavities. Although the sinkhole occurs suddenly, the underground cavity can be developed suddenly or through a prolonged period depending on the formation mechanism. Underground cavities and the subsequent sinkhole can be developed rapidly by bursting of water-carrying utilities. Such formation mechanism is obvious and a forensic investigation is thus not necessary.

However, the cause for sinkhole formation initiated by an underground cavities developed through a prolonged period requires a forensic investigation to allocate the responsibility of the incident and to prevent the formation of such underground cavity in urban area in the future, thus preventing the occurrence of sinkhole and personal and property damage. The forensic investigation of a real-life case in Hong Kong is presented in this paper.

Figure 1. Falling of people into a sinkhole.

Figure 2. Falling of a drinking water delivery truck into a sinkhole.

POSSIBLE MECHANISMS OF SINKHOLE FORMATION

Formation of sinkhole occurs in stages. However, the duration of each stage may vary depending on the formation mechanism. These different stages are outlined as follows:

Sinkhole or Sudden Ground Collapse. A sinkhole or ground collapse occurs suddenly without any warning. The ground surface suddenly cracks and the surface materials collapse into an underground cavity, resulting in the formation of an opening on the ground surface. The sinkhole may be dry or submerged in water. In most cases, the sudden ground collapse is triggered by the application of additional load on the ground surface, such as the weight of a pedestrian walking by or that of a vehicle driving by, resulting in the falling of the pedestrian or vehicle into the sinkhole as shown in Figures 1 & 2.

Sinkholes can also occur when the load imposed on the ground surface is substantially increased. For example, the substantial weights of industrial or runoff-storage ponds constructed on ground surface can trigger an underground collapse of supporting materials, thus forming a sinkhole. However, such sinkhole formation mechanism is beyond the scope of this paper.

Formation of Soil Arch. The formation of a sinkhole is often initiated by the existence of an underground cavity. As the underground cavity is being developed, the ground surface is supported by the arching effect of the soil spanning across the underground cavity. Terzaghi discovered the existence of arching effect in soil and described the soil arching process as the transfer of pressure from a yielding mass of soil onto adjacent stationary parts (Terzaghi *et al*. 1996). Two conditions are considered essential for the generation of the soil arching effect depending on the assumed soil arching pressure distribution: (1) an uneven or relative displacement of soil mass; and (2) the existence of arch springing (Handy 1985; Harrop-Williams 1989).

Nonetheless, the practical effect of soil arching is that the load imposed on the ground surface above an underground void is temporarily supported by the soil arch. As the underground cavity is being enlarged by erosion progressively, the span of the soil arch is increased gradually and the load-carrying capacity of the soil arch is diminishing accordingly. When the load imposed on the ground surface eventually exceeds the load-carrying capacity of the soil arch, the soil arch fails suddenly and the surface materials collapse into the underground cavity, resulting in the formation of the sinkhole.

Formation of Underground Cavity. A sinkhole is often initiated by the development of an underground cavity. However, there are different possible mechanisms for the formation of the underground cavity.

It may involve natural processes of erosion or gradual removal of slightly soluble bedrock (such as limestone) by percolating water, the collapse of a cave roof, or a lowering of the groundwater table. Underground cavities in karst topography can also develop through the process of suffosion which occurs when loose cohesionless materials are overlying a limestone substratum containing fissures and joints. Rain and surface water gradually wash these materials through the fissures into caves beneath. The process creates a depression on the landscape of varying depth. Moreover, groundwater may dissolve the carbonate cementing sandstone particles together and then carry the loosen particles away, gradually forming an underground cavity.

Underground cavities can also develop from abandoned mines and salt cavern storage in salt domes in places such as Louisiana, Mississippi and Texas of the United States by intentional human activities.

Underground cavities can also develop when natural water-drainage patterns are changed and new water-diversion systems are developed. The changes can be caused by temporary dewatering for the construction of underground structures, such as basements and foundations. However, more commonly, underground cavities occur in urban areas as a result of soil erosion caused by water main bursts or sewer collapses when old pipes deteriorate with time. They can also occur from the over-pumping and extraction of groundwater and subsurface fluids.

Because of the many possible mechanisms for underground cavity formation, forensic studies are often required to identify the mechanism for the particular case and to allocate the responsibility of the damage so caused.

THE INCIDENT

The ground surface adjacent to a construction site fell into an underground cavity forming a sinkhole abruptly. A pedestrian fell to the bottom of the sinkhole and suffered multiple injuries. The sinkhole of approximately 3.5 m long, 2.5 m wide and 3.7 deep with the formation of an opening of approximately 1 m by 1 m formed at the paving blocks of the pedestrian pavement.

The construction site in question was located in the downtown area of Hong Kong where foundation and excavation & lateral support works were being constructed for a hotel development project during the occurrence of the sinkhole. The foundation works included large-diameter bored piles. The excavation and lateral support works included a cofferdam enclosing the four sides of the site made of pipe piles and grout curtain and the associated strutting system constructed to facilitate the excavation for the construction of pile cap and basement. The forensic investigation was conducted to determine whether or not the sinkhole was caused by the construction activities at the site.

THE FORENSIC INVESTIGATION

Available Information. Available information of the project including: (1) borehole logs obtained from the ground investigation program specifically designed for the project; (2) geotechnical engineering design parameters and design assumptions adopted for the analyses and design of the project; (3) design calculations; (4) design drawings of the foundation and excavation and lateral support; (5) results of the pumping test after completion of the cofferdam; (6) site monitoring records of groundwater levels, settlements of adjacent ground, settlement of nearby utilities, tilting of adjacent buildings, and ground vibration during construction; (7) construction and maintenance records of nearby water-carrying utilities; (8) records of routine inspections by government officials; (9) statements of eye witnesses of the incident; etc.; were scrutinized for its validity. More importantly, the information was used to conduct the forensic study for the incident.

Field Investigation. A specifically designed field investigation program was conducted for the forensic study. The field investigation program included: (1) observations made during backfilling of the sinkhole; (2) field inspection of the cofferdam; (3) surveying of existing water-carrying utilities and detection of potential subsurface cavities around the site; and (4) GCO probe tests, and Standard Penetration Tests (SPTs) and soil sampling at locations around the site.

The GCO Probe is a dynamic probing tool comprises of a sectional rod with a cone of 25 mm in diameter fitted at the end. The diameter of the base of the cone is 12 mm larger than that of the rod. It is driven into the ground by a 10-kg mass falling through a distance of 300 mm. Probe results are normally reported as number of blows per 100 mm penetration. They are very useful for assessing the depth and degree of compaction of buried fill, making comparative qualitative assessments of ground characteristics, and supplementing the information obtained from trial pits and boreholes (Geotechnical Engineering Office 1987). In particular, the GCO Probe test may be a very effective way to locate any underground cavities around the site.

FORENSIC ANALYSES

Assumption. The sinkhole was not formed by the process of dissolution or suffosion as it was not located in karst topography. The underground cavity causing the formation of the sinkhole was thus not developed by natural processes but by artificial activities that might include construction activities at the site.

Hypothesis. The sinkhole was initiated by an existing underground cavity. The underground cavity was formed by removal of subsurface soil. Therefore, the soil particles must have migrated somewhere. The subject of investigation is to investigate whether or not the removal of subsurface soil was caused by construction activities at the site.

Review of the Statements of Eye Witnesses. The statements of eye witnesses were carefully reviewed, in particular, the statement of the victim who fell into the sinkhole. He did not notice anything abnormal near the sinkhole on the pedestrian pavement, in particular, he did not notice any bumps or depressions prior to his fall. His observations were supported by the site monitoring data collected prior to the incident. He fell almost 4 m to the bottom of the sinkhole and he sank only to his ankles, indicating the layer of loose soil was very thin. He did not feel any stagnant or flowing water in the sinkhole.

It should be noted that he remained atop the paving blocks and the arching soil supporting the paving blocks prior to the incident. Therefore, he was supported on a mat of paving blocks mixing with soil originally located at the crown of the sinkhole when he reached the floor of the sinkhole. As a result, he felt that the soil was loose. It should be noted that the soil he touched was not the soil originally on the floor of the sinkhole. His observation cannot be relied on to locate the groundwater level in the sinkhole prior to the incident.

Observations made during backfilling of the sinkhole. The sinkhole was backfilled immediately by six trucks of concrete for public safety. The volume of concrete, approximately 42 m^3, used to backfill the sinkhole gave a good estimate of the actual volume of the sinkhole. It is very likely that the volume of concrete was slightly larger than the actual volume of the sinkhole as the loose soil in the sinkhole might have been compacted by the wet concrete. More importantly, the excavation was carefully observed during backfilling to observe whether or not any wet concrete might emerge into the excavation. No trace of concrete was found in the excavation, indicating the sinkhole was not directly connected to the excavation.

Review of the Cofferdam Design. The design of the cofferdam, in particular the seepage analyses, was carefully scrutinized for its adequacy. There were lateral earth pressures and water pressures acting on the cofferdam from outside and inside the excavation. As the ground level and groundwater level outside the cofferdam were higher than those inside the cofferdam, there was a net lateral earth pressure and a net water pressure acting on the cofferdam from the outside. The cofferdam was designed to withstand the net lateral earth pressures and the net water pressures acting on it for the structural stability of the excavation. Moreover, it was designed to control the seepage force induced by groundwater flow on the soil to prevent piping and heaving of the excavation floor for hydraulic stability of the excavation as shown in Figure 3. It was also designed to control the volumetric seepage flow rate into the excavation to acceptable levels as shown in Figure 4 so that it was possible to maintain dry working conditions in the excavation by pumping.

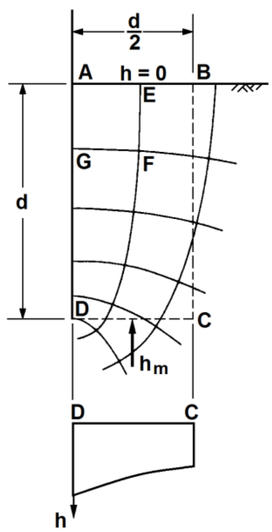

Figure 3. Analysis of heaving.

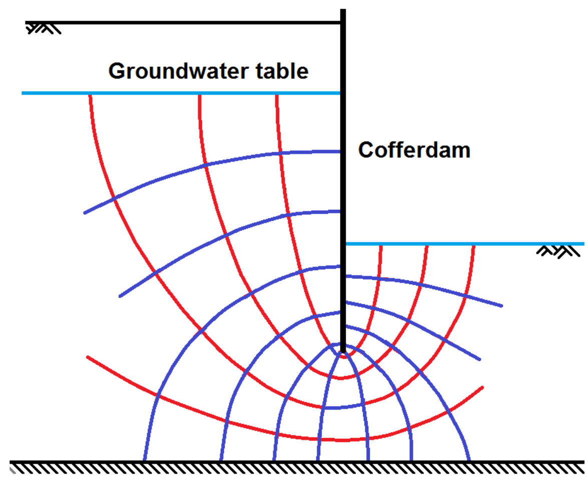

Figure 4. Analysis of groundwater seepage into excavation.

Basically, the inside and outside of the cofferdam was separated by a cofferdam built of pipe piles together with grout curtain and steel lagging plates. It was a steel box surrounding the excavation. Even if there were any cracks in the grout curtain, it was not probable that such a large amount of soil (a three-phase material containing air, water and solids) could pass through such a completely sealed structure and totally unnoticed by full-time resident site staff. The integrity of the grout curtain was substantiated by the results of the pumping test conducted upon completion of the cofferdam.

Review of Probing Test Results. The purposes of conducting the GCO Probe tests and SPTs around the Site were: (1) to identify and locate any existing cavities around the Site, if any; and (2) to reveal any concrete fragment so as to identify any connection between the sinkhole and the excavation. Many GCO probe tests could not penetrate to the toe level of pipe piles due to the presence of underground obstructions at shallow depths. As a result, SPTs were used to continue the investigation. No concrete fragment identifying any connection between the sinkhole and the excavation was found. The *in-situ* measurements of soil strength indicate the soil around the site has not been loosened by the construction works at the site.

Another underground cavity was discovered farther away from the site during the field investigation. If the underground cavity is allowed to grow unnoticed by erosion, it may eventually develop into a sinkhole similar to the sinkhole of the Incident, indicating the possibility of underground cavity formation without any involvement of construction activities at the site. It can be observed in Figure 5 that there are utilities and water in the underground cavity.

Review of Site Monitoring Data and Inspection Reports. All the site monitoring data, including ground settlements, utility settlements, building tilting, ground vibrations and groundwater levels, recorded from the commencement of the project did not exceed their respective alert levels stipulated in approved drawings. As revealed in the inspection reports submitted by government officers, there were no irregularities on the monitoring check points.

There was no observation in the site monitoring data on groundwater levels to justify any drawdown of groundwater table caused by the excavation and lateral support works at the site. However, the groundwater table may be drawn down locally in the underground cavity prior to the formation of the sinkhole as shown schematically in Figure 6 if the underground cavity was connected to somewhere thus providing a conduit for drainage of groundwater. The phenomenon explains why the victim did not feel any water in the sinkhole in addition to the fact that he was standing atop the paving blocks that fell with him into the sinkhole.

Figure 5. Utilities and water in the other underground cavity.

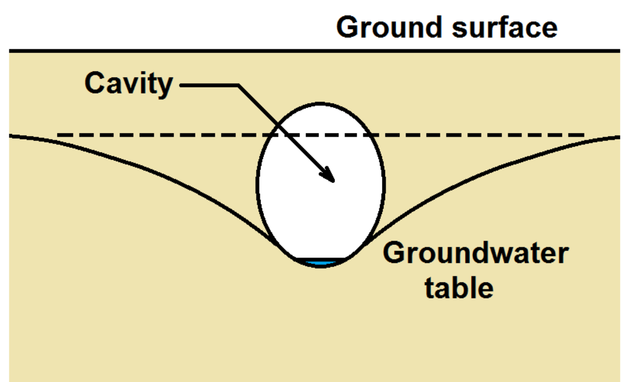

Figure 6. Local drawdown of groundwater in the underground cavity.

Review of Construction and Maintenance Records of Water-carrying Utilities. The results of the review reveal there were many water-carrying utilities near the sinkhole. Moreover, it was revealed in the maintenance records that these water-carrying utilities were leaking continuingly and maintenance was consistently required. It can be inferred that water is continuingly leaking into the subsurface and causing subsurface erosion.

Review of Utility Survey Results. The results of the utility survey indicate there are many leaking drains and manholes. Moreover, many manholes are blocked by soil, indicating soil particles are being migrated from the subsurface into these manholes through broken drains. The results are consistent with the maintenance records of water-carrying utilities.

Other Field Observations. Two sudden ground subsidence incidents occurred in the proximity of the site shortly before the occurrence of the sinkhole. When the two sinkholes were backfilled, no connections between the sinkholes and the excavation were identified. Moreover, government officers inspected the incidents did not attribute the causes of these incidents to the construction activities at the site.

Results of the Forensic Investigation. The results of the forensic investigation indicate the formation of the sinkhole in the urban area of Hong Kong is not related to the construction activities in a nearby site. The evidence also reveals that the formation of the underground cavity was probably caused by the leakage of water-carrying utilities. Therefore, it is necessary to develop reliable non-destructive methods to locate these underground cavities prior to the formation of sinkhole to protect public safety (Yeung and Ng 2009; Lam *et al*. 2011).

CONCLUSIONS

A forensic investigation was conducted on the sinkhole or sudden ground collapse occurred in the urban area of Hong Kong. Having scrutinized all the available information and conducted a specifically formulated field investigation program, it can be concluded that the formation of sinkhole in urban area of Hong Kong is probably caused by leakage of water-carrying utilities. Research on non-destructive technologies on the detection of underground cavities should be conducted to protect public safety.

REFERENCES

Friend, S. (2002). *Sinkholes*. Pineapple Press Inc., Sarasota, Florida.

Geotechnical Engineering Office (1987). *Guide to Site Investigation*. Geoguide 2, Geotechnical Engineering Office, Civil Engineering and Development Department, Hong Kong SAR Government, Hong Kong.

Handy, R. (1985). "The arch in soil arching." *Journal of Geotechnical Engineering*, ASCE, 111(3), 302-318.

Harrop- Williams, K. (1989). "Arch in soil arching." *Journal of Geotechnical Engineering*, ASCE, 115(3), 415-419.

Lam, S.S.S., Yeung, A.T., and Ng, A.K.L. (2011). "Field-scale evaluation of non-destructive underground void detection techniques." *Proc., 2nd International Conference on Utility Management and Safety*, Hong Kong.

Terzaghi, K., Peck, R.B., and Mesri, G. (1996). *Soil Mechanics in Engineering Practice*, 3rd Edition. John Wiley & Sons, New York, New York.

Yeung, A.T., and Ng, A.K.L. (2009). "Non-destructive detection of underground voids." *Proc., 1st International Conference on Utility Management & Safety*, Hong Kong, 253-260.

Influence of Hydraulically Deposited Layer at Downstream Side on Stability of an Embankment

Manoj Datta[1], G.V. Ramana[1], Jyoti K.C[2] and Garima Gupta[3]

[1]Professor, Department of Civil Engineering, Indian Institute of Technology Delhi, New Delhi; e-mail: mdatta@civil.iitd.ac.in, gvramanaiitdelhi@gmail.com
[2]M.Tech student, Department of Civil Engineering, Indian Institute of Technology Delhi, New Delhi; e-mail: kc.jyoti10@gmail.com
[3]Research scholar, Department of Civil Engineering, Indian Institute of Technology Delhi, New Delhi; e-mail: gamma840@gmail.com

ABSTRACT

A study was undertaken to analyze the cause of failure of an embankment of an impoundment holding slurry deposited waste. Three causes of instability were identified, namely, deposition of a layer of slurry deposited waste on the downstream side, low unit weight of the deposited material and the high level of water in the waste. Stability analysis was conducted to identify the role of each cause. It was observed that larger thickness of waste, lower unit weight of waste and higher water level in waste layer resulted in factor of safety falling to a level lower than acceptable. The study shows that the stability of embankments of slurry deposited wastes, which are incrementally raised by the downstream method of construction, can be severely compromised by indiscriminate deposition of the waste outside the ponded area.

BACKGROUND

An impoundment, approximately 1000 m x 1300 m in plan, as shown in Fig. 1, is used to store slurry-deposited coal combustion residuals. The waste is transported in the form of a slurry and the excess water is decanted after deposition of the waste in the impoundment. The main perimeter embankment of the impoundment has been designed with a 8 m high starter dyke of local soil and is raised incrementally in stages of 5 m (using the downstream method) as the impoundment fills up. Over the design life, seven or more raisings are anticipated. The main perimeter embankment underwent base failure at the end of second stage of filling up of the impoundment. A study was undertaken to analyse the cause of failure and recommend remedial measures. This paper reports an extension of the study and highlights how variations in some critical parameters influence the stability of the incrementally raised embankments.

AS-DESIGNED EMBANKMENT

Fig. 2 shows the cross-section of the as-designed embankment. The starter dyke comprises of compacted local soil (sandy clay). The raisings are constructed using compacted waste with a soil cover and an internal chimney drain and blanket drain. The outer slopes of the starter dyke are 2H:1V and of the raisings are 3H:1V with berms at height intervals of 5m.

AS-BUILT EMBANKMENT

During the filling operations, some waste was also discharged briefly on the downstream side of the starter embankment under emergency condition as the capacity of the impoundment had been exceeded. This was possible because a low-height outer dyke had been constructed 200 m away from the main perimeter embankment in the very beginning to prevent encroachments into the acquired land area for subsequent raisings and also to keep surface water out of the low-lying ground surface of the site. (This was a unique feature.) Thereafter, subsequent raisings were constructed on the deposited waste and all subsequent waste material was deposited on the upstream side. Fig. 3 shows the as-built embankment at the end of second stage of raising. Two important observations can be made from Fig. 3. One, that the raisings are resting on slurry deposited waste on the downstream side (the thickness of the deposited material varies from 2 m depth to 6 m depth depending on the undulations in the original ground level). The second important observation is that the level of water in the slurry deposited waste is at the surface of the waste material. This results from the fact that water seeping through the raised embankments accumulates on the downstream side due to poor drainage and due to the presence of a low-height outer dyke constructed well away (200m) from the downstream toe.

EMBANKMENT FAILURE

The embankment underwent failure when the impoundment was full of waste after the second raising and the slurry water was close to the top of the crest of the second raising. The breach occurred along a length of about 100 m of the embankment and it caused the waste to flow towards the downstream side. Damage to property and crops was minimal as the length of travel of the waste was limited to about 150 m. Post failure inspections revealed that the failure was akin to a slope-cum-base failure of low depth with the failure surface passing through the slurry deposited waste on the downstream side and not below the original ground surface. The toe drain moved horizontally by a distance of a hundred metres. ‘Sand boils’ were observed in the loose waste indicating that upward flow of seepage water had a major role in causing the instability. An estimate of the probable failure surface established by post failure visual inspections and subsurface investigations is shown in Fig. 4.

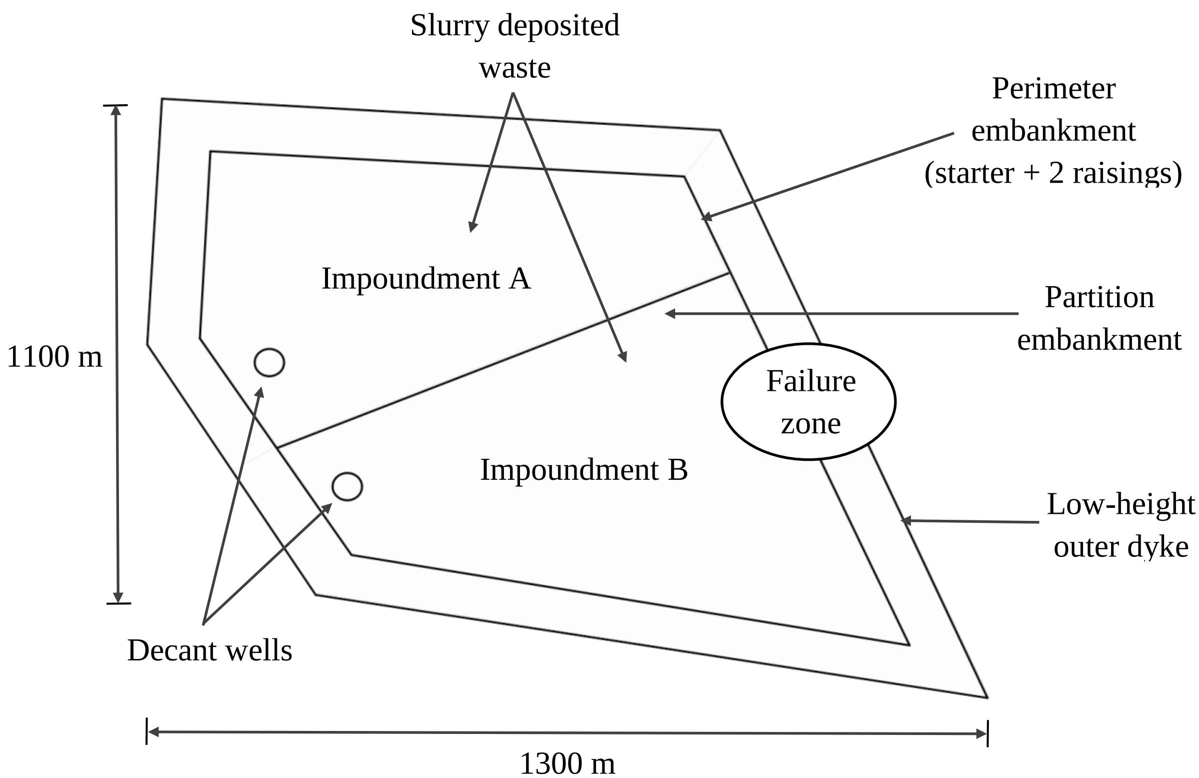

Figure 1. Schematic (plan) view of impoundment with slurry deposited waste

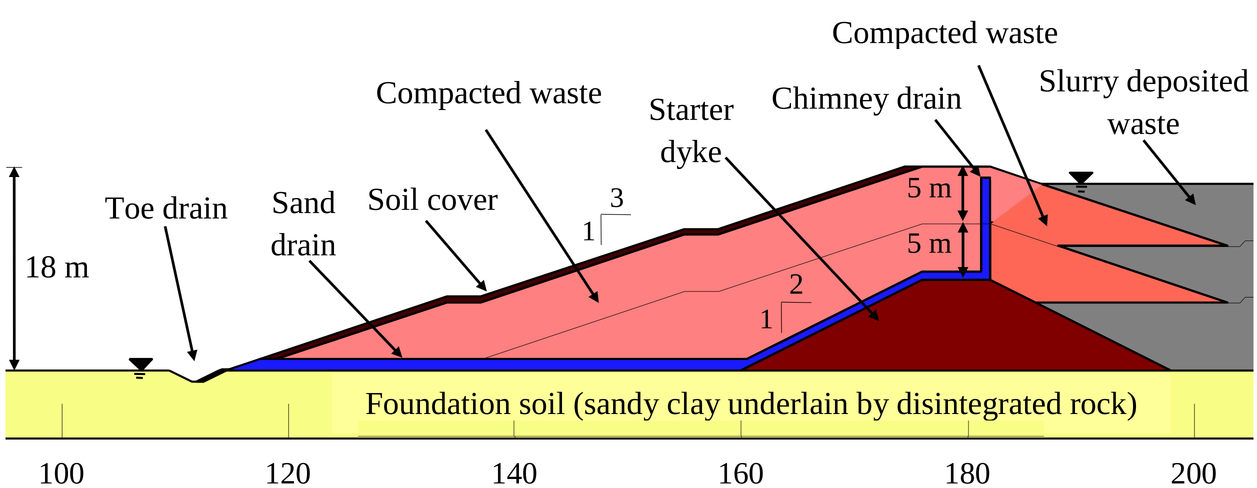

Figure 2. As-designed embankment

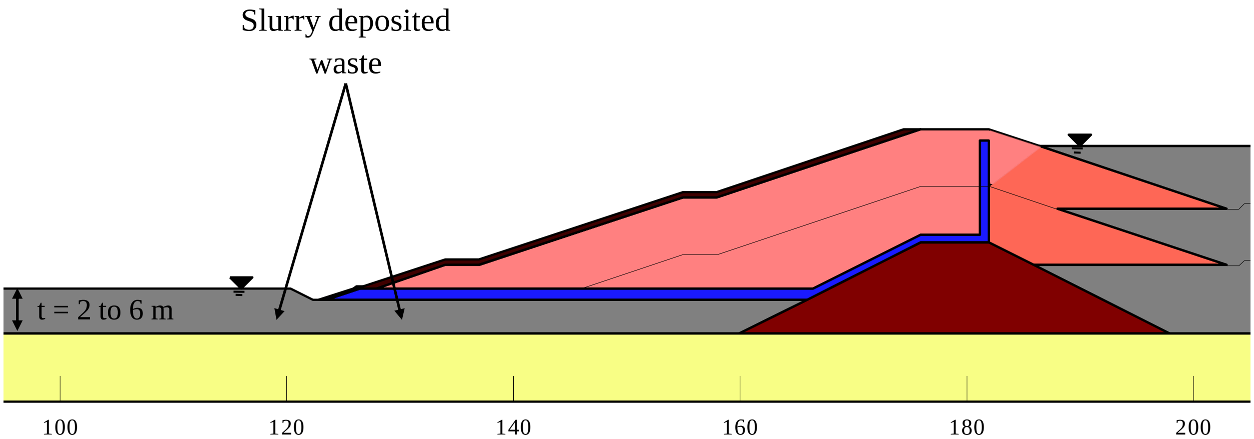

Figure 3. As-built embankment

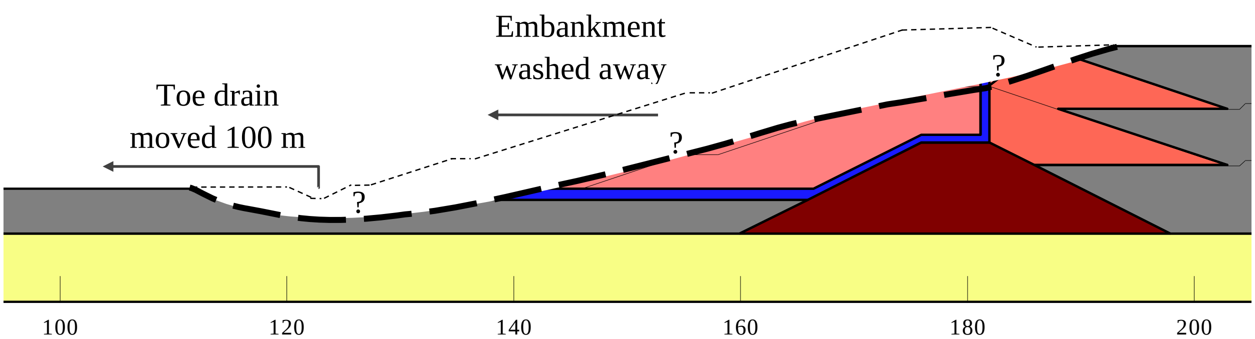

Figure 4. Probable failure surface in as-built embankment

GEOTECHNICAL PROPERTIES

Table 1 lists the geotechnical properties of the embankment materials and the foundation soil obtained from site investigations and laboratory tests. The foundation soil comprises of sandy clay with small quantities of gravel sized material. It is underlain by weathered rock at 6 to 10 m depth. The foundation soil has also been used to construct the starter embankment by excavating it from a local nearby area. The waste material has grain size in the range of sandy silt; it is non plastic and has low specific gravity. The geotechnical properties of the waste material are similar to those reported by Datta et.al (1996), Sridharan et.al. (1996), Datta (1998) and Jakka et al. (2010). The shear strength and permeability values of all materials are listed in Table 1.

Table 1. Geotechnical properties of soil and waste

Material	w_L	w_P	G_s	γ_d (kN/m^3)	γ_{sat} (kN/m^3)	c' (kPa)	ϕ' (°)	k (m/s)
Foundation soil (sandy clay, medium to stiff, underlain by disintegrated rock)	26	14	2.65	20.0	16.4	5	28	1.00e-08
Embankment soil (compacted local sandy clay)	26	14	2.65	200	16.4	5	28	1.00e-08
Sand drain	-	-	2.65	20.0	20.0	0	36	1.00e-03
Compacted waste (sandy silt)	-	-	2.17	12.5	16.5	0	35	1.00e-06
Slurry deposited waste (sandy silt)	-	-	2.17	9.0	14.7	0	25	5.00e-06

SEEPAGE ANALYSIS

Seepage analysis was done using standard available software SEEP/W (GeoStudio 2007). Fig. 5 shows the flowlines under reservoir full condition at the end of second raising. One notes that most of the seepage water is intercepted by the internal drains of the raisings. The presence of the layer of slurry deposited waste on the downstream side causes the water to flow through and below the blanket drain resulting in outward and upward movement of water in the loose waste.

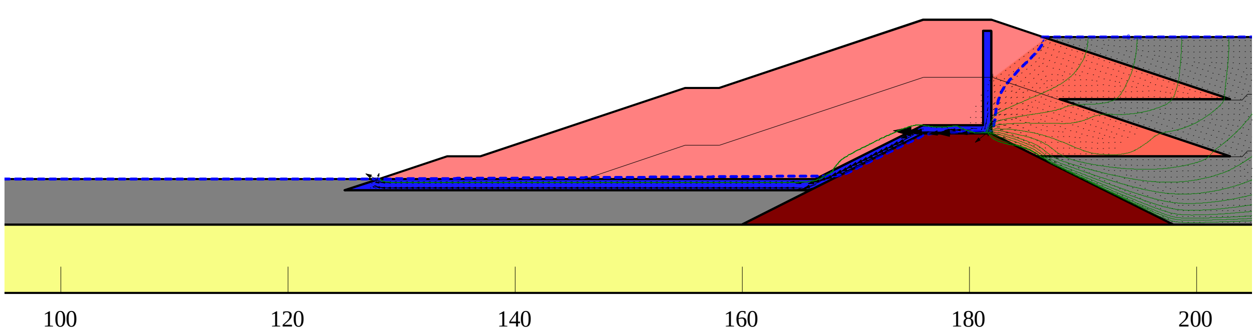

Figure 5. Flow lines in as-built embankment

STABILITY OF AS-DESIGNED EMBANKMENT

Fig. 6 and Fig. 7 show the minimum factors of safety and the critical failure surfaces obtained for the as-designed embankment by the Ordinary method of slices (Fellenius 1936) and the Bishop's simplified method (Bishop 1955) using SLOPE/W (GeoStudio 2007) for the reservoir full condition. The embankment slopes are stable with factor of safety being well above 1.5. The values of the factor of safety are similar by both methods but the shapes of the failure surfaces are different – one being base failure and the other being slope failure.

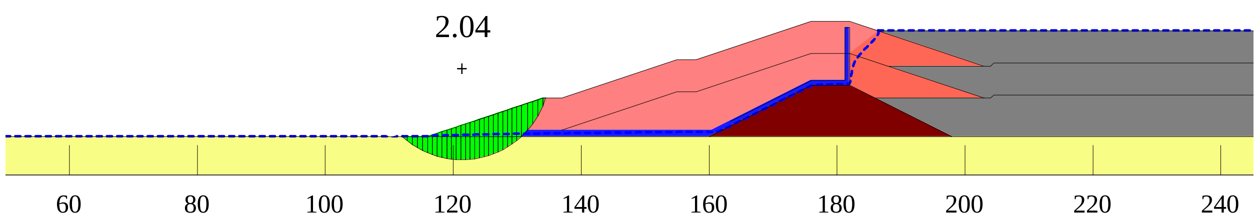

Figure 6. Stability analysis of as-designed embankment by Ordinary method of slices

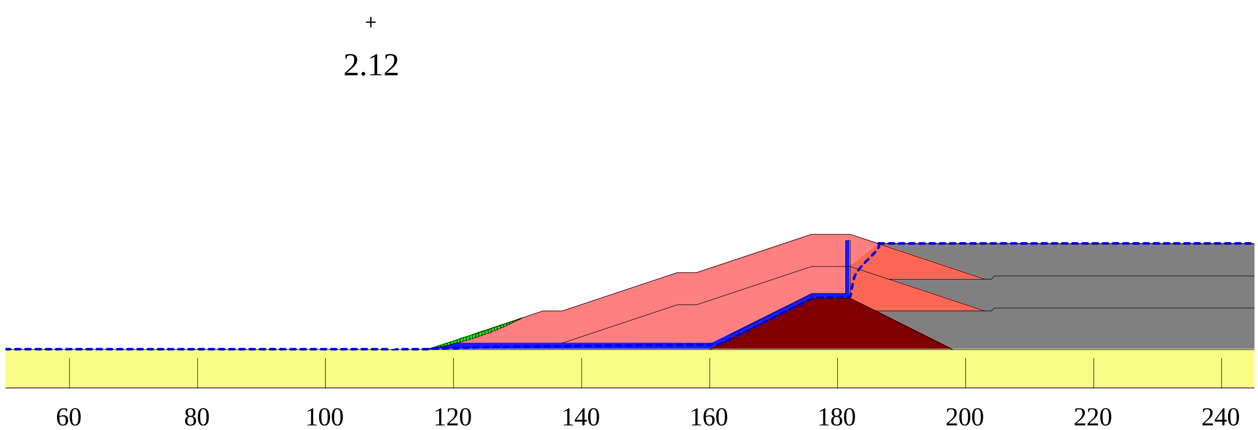

Figure 7. Stability analysis of as-designed embankment by Bishop's simplified method

STABILITY OF AS-BUILT EMBANKMENT

Fig. 8 shows the minimum factor of safety and critical failure surface obtained by the Ordinary method of slices for the reservoir full condition for as-built embankment with saturated unit weight of slurry deposited waste being 14.7 kN/m^3, waste thickness of 4 m and tail water level (TWL) at surface of waste. The presence of slurry deposited layer of waste causes the factor of safety to fall below the acceptable level of 1.5 and the critical failure surface passes primarily through the waste beyond the embankment toe. The low factor of safety is a result of the low shearing resistance offered by the loosely deposited waste and the influence of pore water pressures induced by the seepage flow.

While conducting the stability analysis, it became apparent that three parameters had a critical influence on the factor of safety, namely the unit weight of the waste (being light weight material with low specific gravity (see Table 1)), thickness of the deposited waste and the level of the tail water. The influence of these parameters is discussed hereafter.

INFLUENCE OF UNIT WEIGHT

The waste material has a low specific gravity and a low unit weight when it is in the loose state after hydraulic deposition on the downstream side of the embankment. The influence of variation in unit weight on the factor of safety of the downstream slope and the critical failure is brought out in Fig. 8 and Fig. 9 and is summarised in Table 2. One notes that as the unit weight decreases, the factor of safety falls. This appears to be on account of the reduced shearing resistance offered by the waste material due to lower value of the effective normal stress resulting from low unit-weight.

Table 2. Influence of unit weight of waste on stability

Case	Fig.	t (m)	TWL	γ_d (kN/m^3)	γ_{sat} (kN/m^3)	FOS
I	8	4	At surface	9	14.7	1.01
II	-	4	At surface	8	14.1	0.94
III	-	4	At surface	10	15.2	1.10
IV	9	4	At surface	11	15.7	1.20

INFLUENCE OF WASTE THICKNESS

Fig. 10, Fig. 11 and Table 3 show the influence of waste thickness deposited on the downstream side on the failure surface on the factor of safety. As the depth of deposited waste increases, the failure surface passes deeper through the loose slurry deposited waste and the factor of safety falls. It appears to reach its lowest value for deposition depth of 6 m.

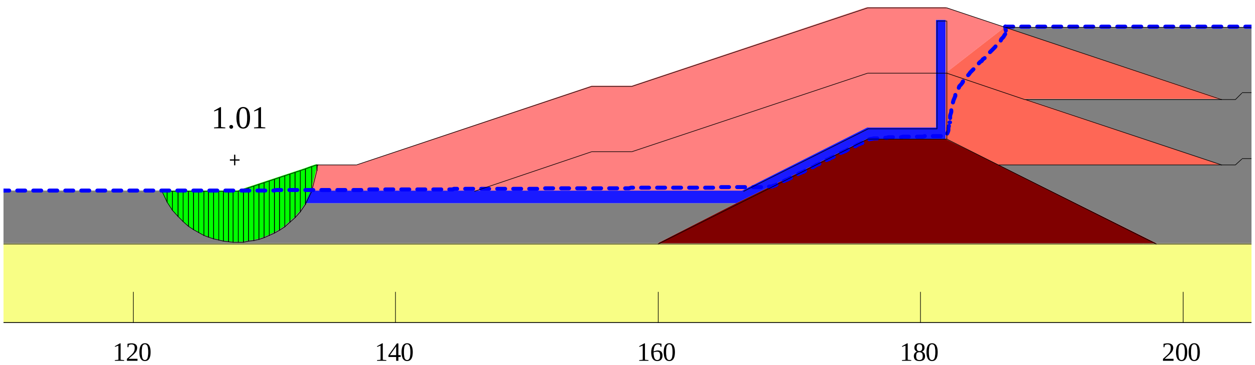

Figure 8: Stability analysis of as-built embankment (γ_{sat} = 14.7 kN/m^3) by Ordinary method of slices (Case I: t = 4 m, TWL at surface)

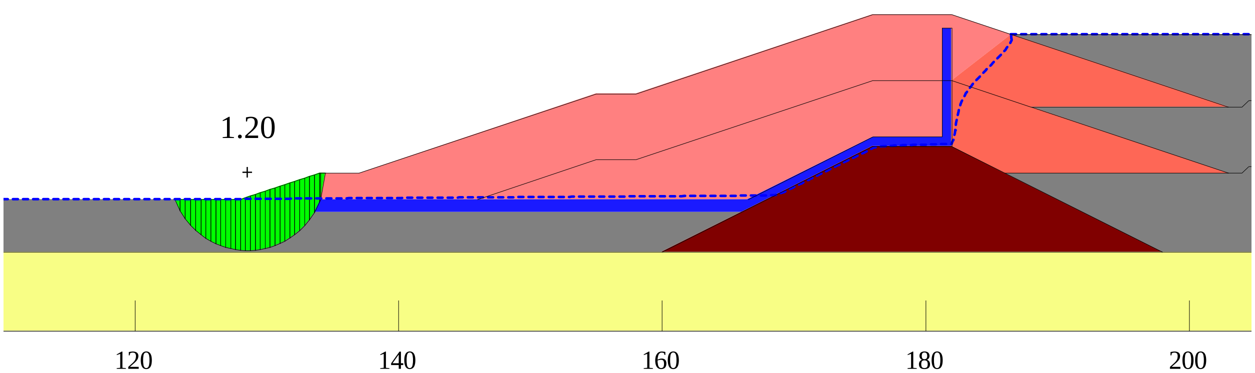

Figure 9. Stability analysis of as-built embankment (γ_{sat} = 15.7 kN/m^3) by Ordinary method of slices (Case IV: t = 4 m, TWL at surface)

Table 3. Influence of thickness of waste on stability

Case	Fig.	γ_{sat} (kN/m^3)	TWL	t (m)	FOS
V	10	14.7	At surface	2	1.21
I	8	14.7	At surface	4	1.01
VI	11	14.7	At surface	6	0.98

INFLUENCE OF TAIL WATER LEVEL

Tail water level plays an important role in the stability of the downstream slope. Fig. 12, Fig. 13 and Table 4 highlight this aspect. For higher tail water level the stability is lower. This is to be expected as the strength of the material beyond the toe reduces with increase in pore water pressure.

Table 4. Influence of tail water level on stability

Case	Fig.	γ_{sat} (kN/m^3)	t (m)	TWL	FOS
I	8	14.7	4	At surface	1.01
VI	12	14.7	4	2 m below	1.74
VII	13	14.7	4	4 m below	1.74

INFLUENCE OF METHOD OF ANALYSIS

One of the unexpected findings of the study is that change in method of stability analysis results in very different factors of safety. It is normal to expect 10 to 20 % variations in results by different methods. However, Table 5 show that the difference in results is unusually high when stability analysis is performed by three different methods. The Ordinary method of slices yields significantly lower results in comparison to the results by Bishop's simplified and Morgenstern and Price (1965) method which produce results similar to each other. The reason for this can be attributed to the manner in which inter-slice forces are handled by each method and the way in which equilibrium equations are set up. This aspect needs further study.

It is noted that a for a combination of low unit weight, high thickness of waste and high tail water level, the embankment has lower than acceptable factor of safety of 1.5 by all three methods.

Table 5. Influence of method of stability of analysis

Case	Fig.	γ_{sat} (kN/m^3)	t (m)	TWL	Method of analyses	FOS
I	8	14.7	4	At surface	Ordinary	1.01
I	-	14.7	4	At surface	Bishop's simplified	1.81
I	-	14.7	4	At surface	Morgenstern-Price	1.80

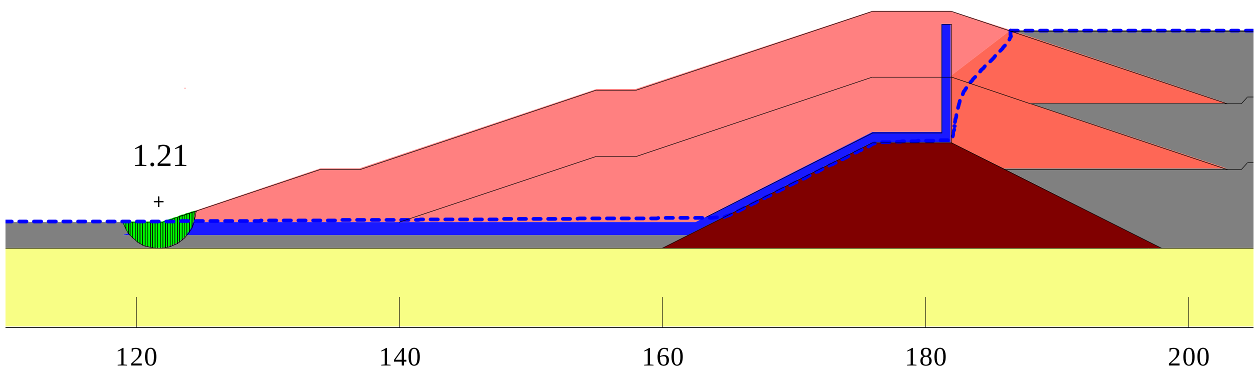

Figure 10. Stability analysis of as-built embankment (t = 2 m) by Ordinary method of slices (Case V: γ_{sat} = 14.7 kN/m^3, TWL at surface)

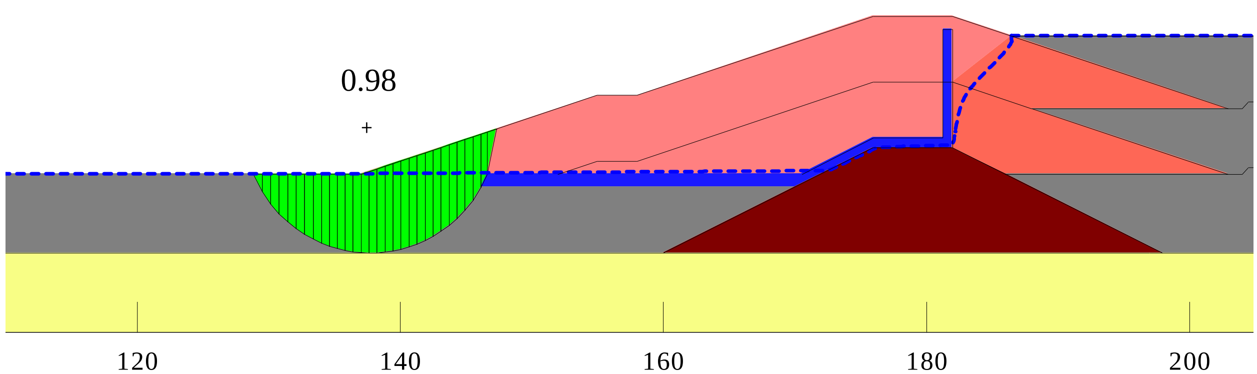

Figure 11. Stability analysis of as-built embankment (t = 6 m) by Ordinary method of slices (Case VI: γ_{sat} = 14.7 kN/m^3, TWL at surface)

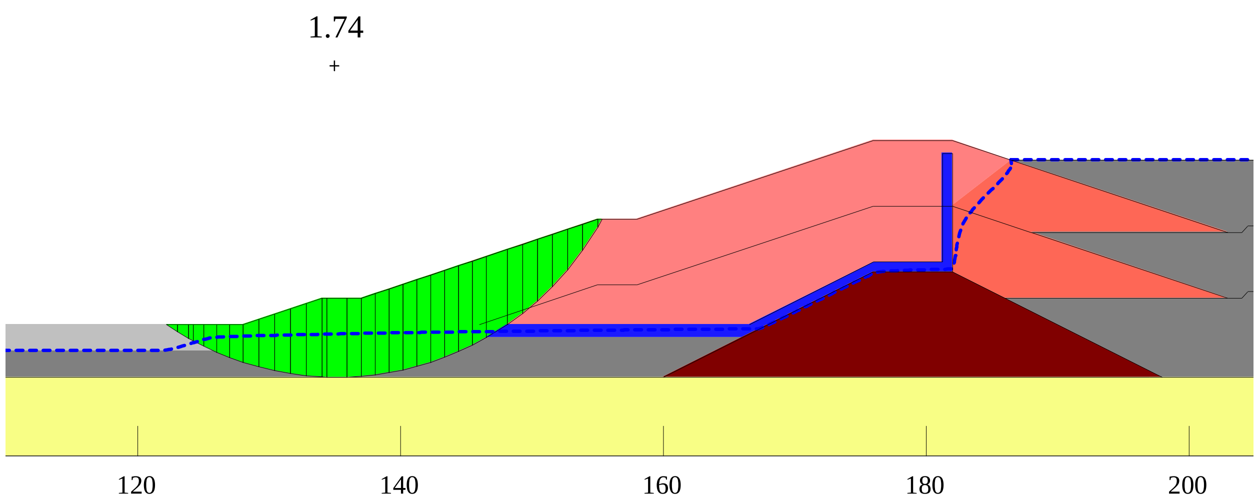

Figure 12. Stability analysis of as-built embankment (TWL 2 m below surface) by Ordinary method of slices (Case VII: γ_{sat} = 14.7 kN/m^3, t = 4 m)

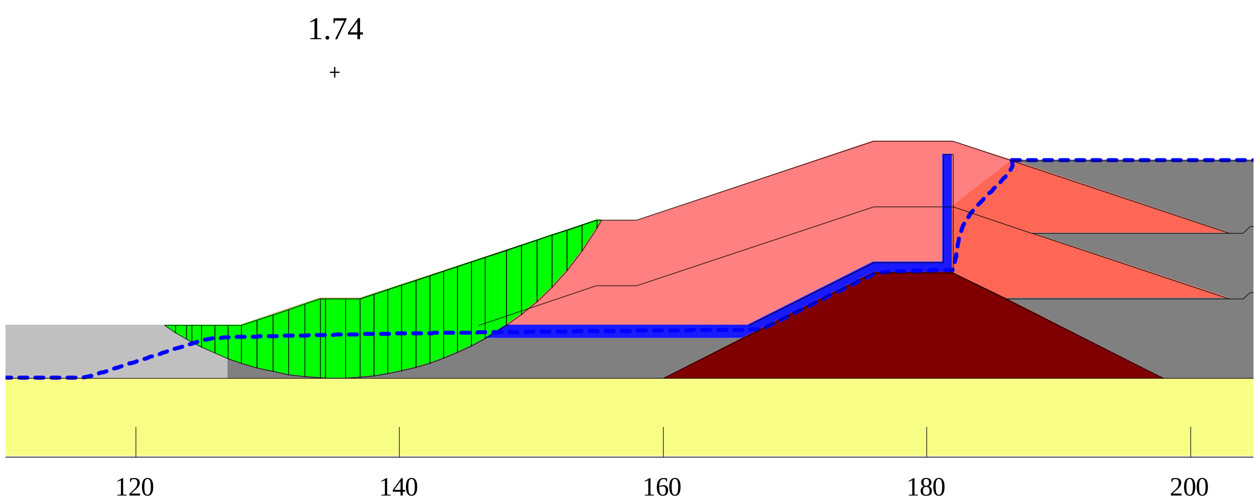

Figure 13. Stability analysis of as-built embankment (TWL 4 m below surface) by Ordinary method of slices (Case VIII: γ_{sat} = 14.7 kN/m^3, t = 4 m)

OPTIONS FOR REMEDIATION

Based on the results of the study, three options were considered for remediation, namely (a) removal of waste from downstream side; (b) provision of a stabilizing berm; and / or (c) lowering of tail water level. No single method was found feasible alone and a combination of (b) and (c) was considered feasible and economical.

CONCLUDING REMARKS

Low-weight wastes with shear strength parameters akin to soils are often preferred in earthworks for replacement of soil since they induce lower stresses for the same height of earth filling. The present study brings out a new aspect relating to reduced stability of an embankment on account of indiscriminate deposition of low-weight material on downstream side by hydraulic deposition. Even though the angle of shearing resistance of the material in the loose state is not low, the shearing resistance offered against slope stability is inadequate due to the lower effective normal stress induced along the failure surface on account of low specific gravity of the waste material and the high tail water level. This aspect is of importance in design of embankments resting on slurry deposited wastes.

REFERENCES

Bishop, A.W. (1955). "*The use of the slip circle in the stability analysis of slopes*." Géotechnique, 5(1), 7-17.

Datta M. (1998). *"Engineering properties of coal ash."* Proceedings of Indian Geotechnical Conference, New Delhi, India, 2, 41-46.

Fellenius, W. (1936). *"Calculations of the stability of earth dams."* Transaction of the 2nd Congress on Large Dams, Washington, D.C., 4, 445-463.

GeoStudio (2007), Version 7.23, Build 5099. Geo-Slope International Ltd., Calgary, Canada.

Jakka, R. S., Ramana, G. V., Datta, M. (2010). *"Shear behaviour of loose and compacted pond ash."* Geotechnical and Geological Engineering, 28(6), 763-778.

Morgenstern, N.R., Price, V.E. (1965). *"The analysis of the stability of generalised slip surfaces."*
Géotechnique, 15(1), 79-93.

Sridharan, A., Pandian, N. S., Rajasekhar, C. (1996). *"Geotechnical characterization of pond ash."* Ash Ponds and Ash Disposal Systems. Raju, V.S., Datta, M., Seshadri, V., Agarwal, V.K., Kumar, V. (eds). Narosa Publishing House, New Delhi, India, 97–110.

Inclination of a condominium building caused by inadequate bearing capacity of piles - Disguise of piling records and what geotechnical engineering should involve -

Yoshinori Iwasaki, Ph.D., Dr.Eng., PE

Geo Research Institute, Osaka

ABSTRACT

Tilting of an 8floor condominium building in Yokohama was found and it was reported by shorter pile length than required. The technical standard of piling in Japan had been established and practiced at every piling site in Japan. How the shortage of the pile took place? It turns out the site report of construction was revealed as disguised. There was no original record of driving pile but only a copy of record for another pile.

Japanese Government created a special investigation committee on "Disguised report of piling and improvement of piling standard." Japan Geotechnical Society also organized a task committee on the problem. The association of piling business in Japan responded the problem and published "The comment of the disguised report and revised standard of the new procedure of piling in Japan."

However, none of these reports did not explore the fact that had introduced the shortage of the pile at Yokohama site. The author describes the fact on this problems based upon another source of document report and show the real reason and propose the similar problem in the future in this paper.

INTRODUCTION

In October 2015, newspapers and TV stations in Japan reported tilting of an 8floor condominium building in Yokohama site was found and it was resulted with the disguise of the site report of piling construction. The fact of the disguised report in piling construction in Yokohama triggered the further study of the piling reports in the past. The disguised records were revealed not only by the piling company at the Yokohama but also were widely spread to almost all piling company in Japan.

People in the country were so shocked and the government of Japan had organized a special investigation committee on "How to control the quality of pile and pile supported building." The members of the committee include professors of civil, architectural, and geotechnical engineering, as well as lawyer. The reliability was lost for piling business as well as geotechnical engineering in Japan.

The author recommended Japan Geotechnical Society to set a special committee to create a recommendation on “Quality control of piling foundation and their technical standard.” JGE also organized a special task committee on this problem.

This paper deals with the how the disguise was performed under the existing technical standard and the author’s view to solve the problem.

The Prolog, the troubled condominium in Yokohama

Construction of the condominium was started on November 30, 2005 and completed in November 2007 as shown in Photo-1.

“Park-city LaLa Ykohama” consists of four buildings with 12 floors and 705 residential homes.

In October 2015, residents found a small difference of heights between two handrails at the connecting floor between buildings of west and central units.

As shown in Fig.1, the end of the hand trail of the connecting floor was found settled and 24mm lower than that on the central unit.

Sumitomo Mitsui Construction Co., Ltd. (SMC) that constructed the buildings began investigation of the foundation of the inclined west building. At the initial phase it was explained that the settlement was due to the great East Japan earthquake of 2011 of M9.

The long width of the west unit is about 60m and the inclination of the building is 24mm/60m=$0.4x10^{-3}$.

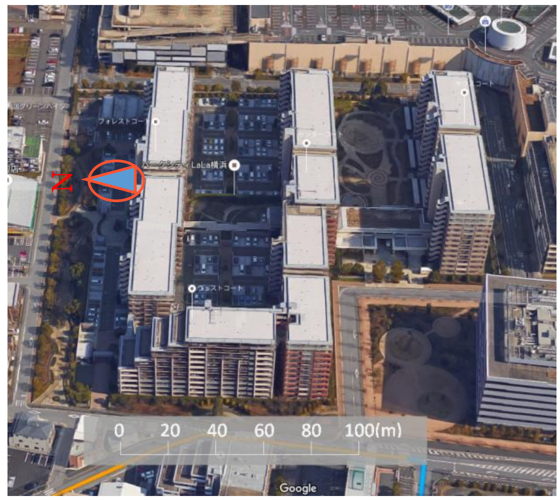

Photo-1 Park-city LaLa Yokohama

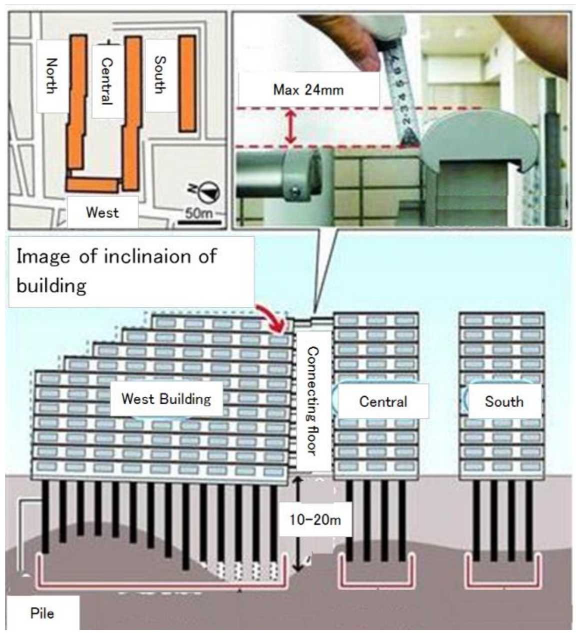

Figure 1 vertical gap between adjacent hand rails of west and central units

The inclination was classified as less than the critical limit of 5x10-3, suggested by Ministry of Construction of Japanese Government.

Pile foundation

Based on the notice by the residents, the SMC surveyed the inclination of the building and began investigation of the reason of the inclination of the west unit in November 2014. The building was designed to be supported by 52 piles. The MSC made a survey of the piles of the foundation with boring study. Comparison between boring results and the length of the pile, the SMC reported the shortage of the length of the eight piles as to have caused the inclination in October 2015. The SMC further disclosed the disguise of the piling records by a subcontractor that had carried out piling for the building.

Ministry of Land and Transportation of Japanese Government organized a special committee to discuss the disguise piling problem for improving the construction practice.

Disguised problem of piling records

At the Lala port Yokohama site, Asahi Kasei Company performed the piling as the 2ndary sub-contractor. The installation of concrete pile is illustrated as in Fig.2.

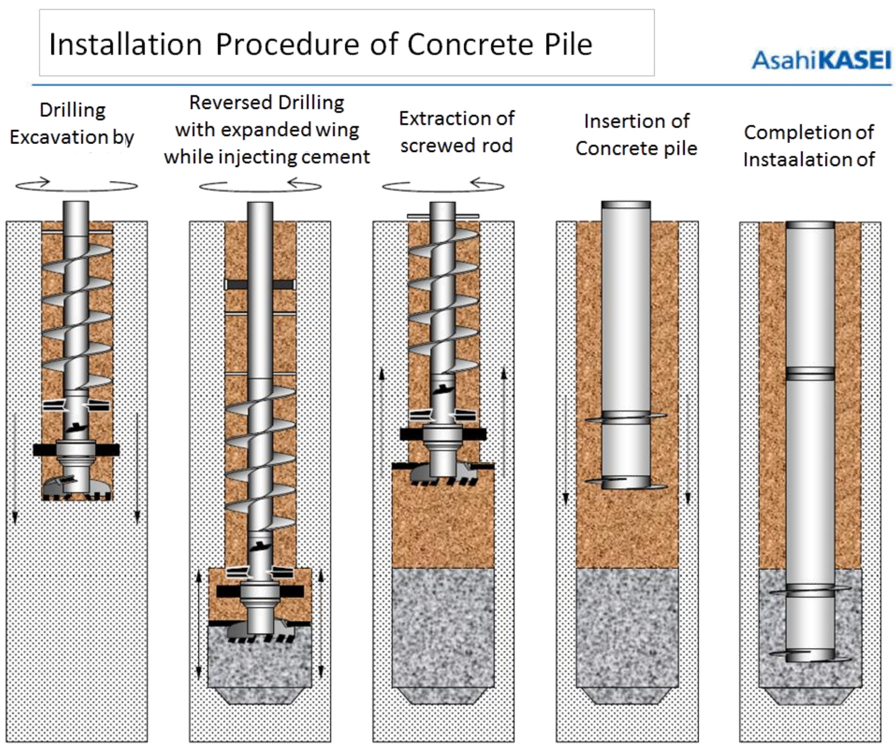

Figure 2 Installation of concrete pile by Asahi Kasei Co

The piling procedure consists from five steps as follows,

1. A hole in the ground is excavated by drilling rod until arriving at the supporting layer with monitoring electric currency that was consumed for drilling. The sudden increase of the currency is usually experienced and rather easy to be notified.
2. A wing at the bottom of the screw edge is expanded and widening the diameter of the hole

with rotation of reverse direction while the cement mortar is injected from the ground surface to the excavated space of the bottom.

3. Extraction of the screwed rod
4. Insert of concrete pile
5. Completion of insert of concrete pile rod

The above procedure is monitored with the change of the currency of the drilling machine and the monitored record at site that is printed at the site or stored in electric file that should be submitted as construction record.

An example of recording of performance of piling is shown in Fig.4.

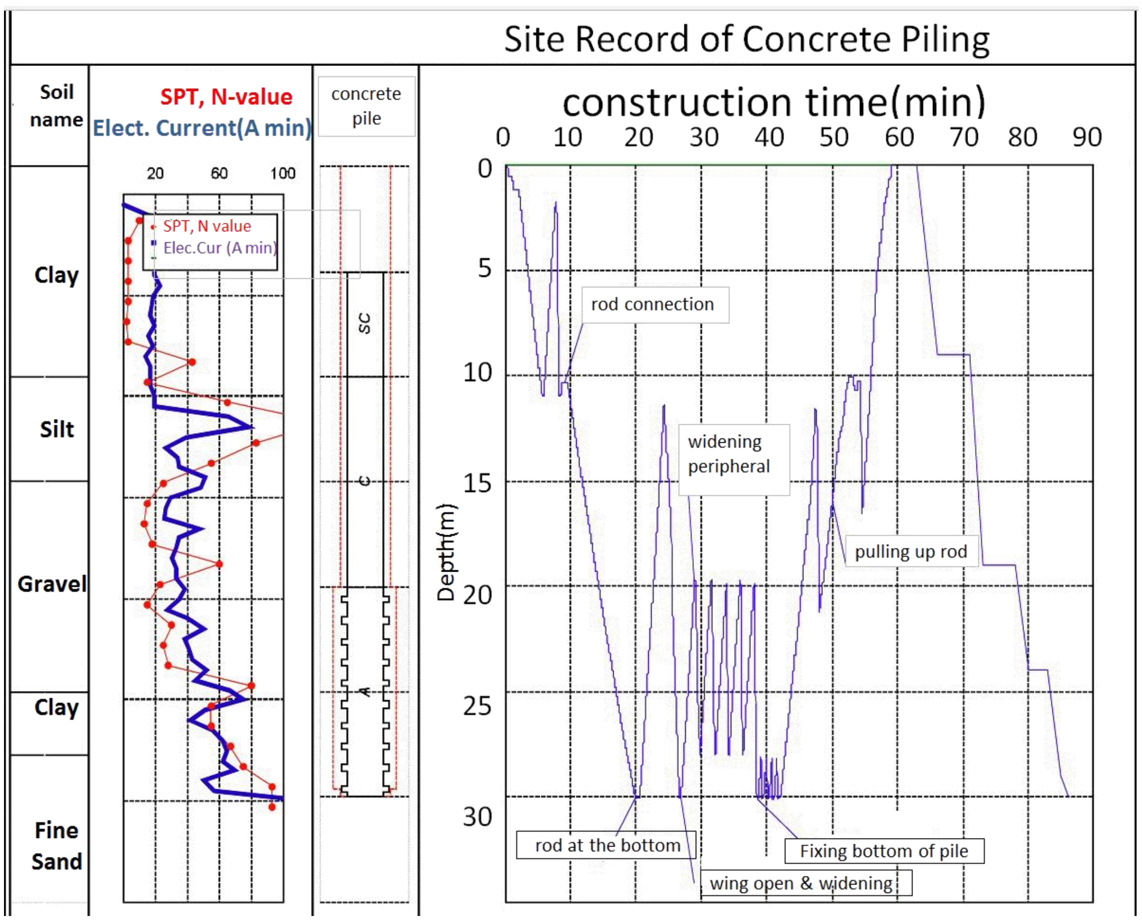

Fig.2 shows an example of record of piling sequence for concrete pile, which consists of several phases of 1.) drilling rod to the supporting layer, 2.) widening peripheral of the rod, 3) fixing the bottom of the pile, 4) pulling up the rod, and 5) insertion of concrete pile. The record contains change of electric current (A min) with depth, which is the resistance of ground against drilling of rod into the ground and relatively good correspondence with SPT N-values.

Such a record of piling is accepted as a positive proof of the execution of the pile construction.

During the investigation step, it was found that some of these records were disguised by copying the records of nearby piles.

At this step of October, 2015, Ministry of Land and Transportation of Government of Japan decided to organize a special committee on "Technical Guideline of Pile Construction."
Such committees on disguised report of piles and how to improve the present problem were organized in professional association of concrete piling as well as Japanese Geotechnical Engineering. After several months later, each committee opened the results of their discussions and conclusions. These committees did not explore the real problem what happened in the piling construction.

The facts of the design and the construction control of piling for the building

A report by a non-engineer who had investigated the disguised site report of piling at Yokohama disclosed in a monthly magazine "Bungei-Shunjyu," January 2016. I had read the report that contains important contents of the difference of the lengths of piles between the designed stage and the required length that was opened after the occurrence of the problem.

The troubled piles were identified as 6 piles that were installed to all the same length of 14m. The SMC reported the length of 2piles out of the six should be 16m after the trouble, which meant the designed length of the piles is 16m and the sub-contractor for piling ignored the design.

If the statement is wrong, SMC should have brought the magazine to legal issue, however, no action was taken.

Another important fact was the construction site was not green site but had been used as to build a housing that had been supported by piles of 18m in length. These piles had been pulled up and mortar cement had been filled up in the void of ground.

When the subcontractor started the piling work, no information of the history of the site but only the designed length of the pile was given by SMC of the main contractor.

Recommendations by several advisory committees

As referred earlier, the Ministry of Land and Transportation organized the special committee to prevent disguising the piling records. The committee opened their results after several meetings in May.

The Ministry prohibited three contractors that constructed the building to bit the construction projects funded by the government for six months from January 2016.

The committee also expresses the need of strengthening the legal aspect to avoid disguising the records.

The legal system of civil engineering works in Japan has been built upon the engineers and technicians are reliable and expected to behave as procedure that are described in the guidelines.

The Japanese Geotechnical Society also organized a task force committee on the problem and issued the statements that are similar with other committees.

The Key Issues of the Disguised Piling Report

The real situation that the pile technician who told what was the truth to the rupo writer was as follows,

1. The length of the six piles in the questioned area was designed as a constant length of 14 meters, in which two piles were claimed to be 16m by the contractor MSK.
2. The pile technician was not used to handle the new model of pile recording system and encountered in difficulty to keep the formatted records of piling. However, the piling work was simple and straight forwards and completed without any doubt.
3. The geotechnical condition of the site was rather simple as shown in Fig.3

The top surface is soft soil with N-values less than 5 with thickness of 10-15m followed by hard stiff clay of SPT N-values of greater than 50. The change of SPT-N values at the ground near the site is shown in Fig.3.
The technical staff for the piling told “It was very clear to identify when it arrived at the supporting base layer.”
The fact that the site was once used for building that was supported by piles of 18m in length was not informed to the site technical staff.
The injected mortar may be either not very hard or may have hardened at the piling period.

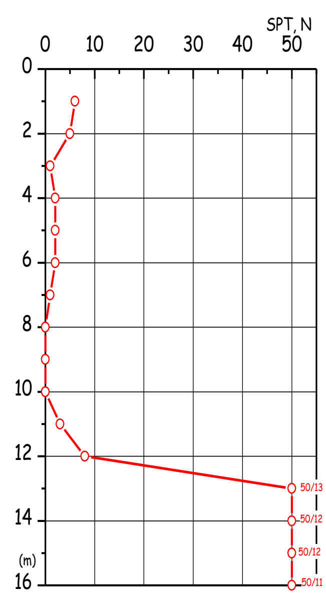

Figure 3 SPT N-value

The site where the condominium was constructed was in northern Yokohama city and some building that was supported by piles of 18m in length had been used by an electric company. The existing building had been demolished and the concrete piles of 18m in length were completely removed and replaced with cement mortar as shown in Fig.4.

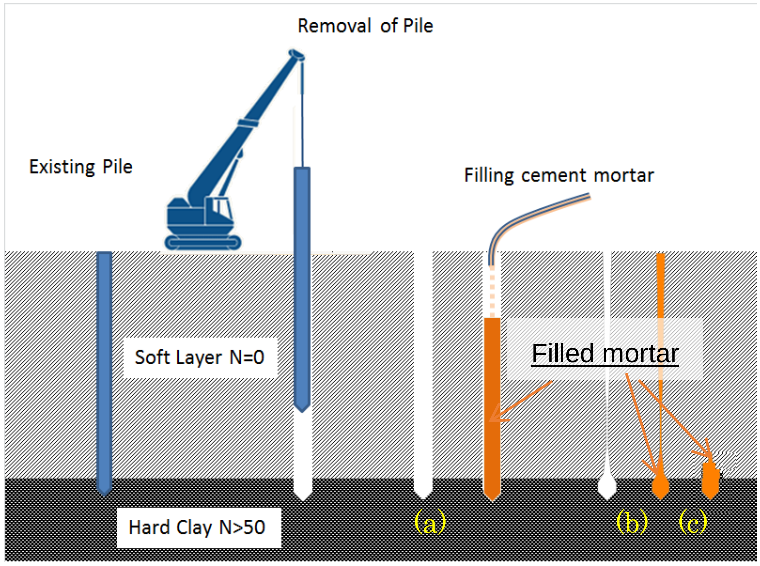

Figure 4

Removal of pile and filling the remaining void with mortar

In conventional practice of removal and replacement with mortar, filling step is followed after removal of pile. When the layer above the supporting ground is such a very soft state of SPT N=0, the ground hole in the soft layer after the removal of pile is very easy to collapse and tends to close the hole. As shown in Fig.4, it may be impossible to keep the void shape as it was as case (a) in Fig.4 and most likely to become as case (b) or (c) and the mortar became to form unexpected shape in the deep ground.

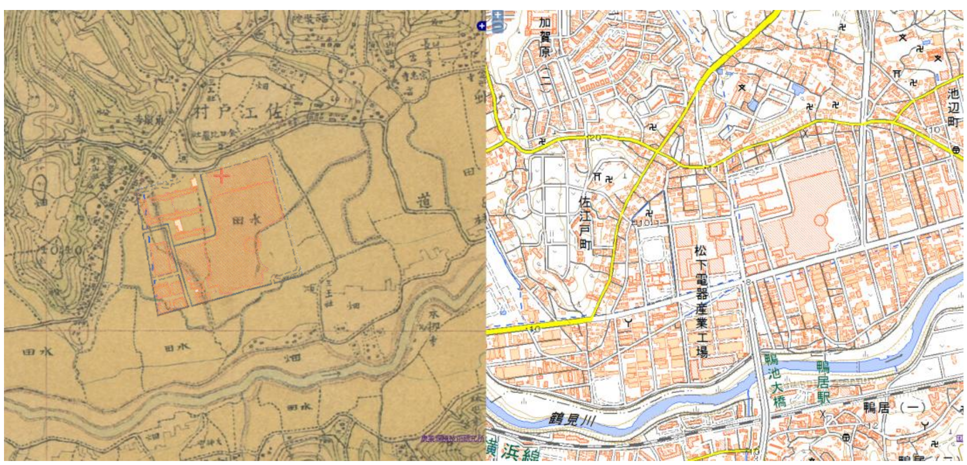

Map in 1886 Map at present (2016)

Figure 5 Comparison of maps in past and present

SITE HISTORY

These ground conditions were not informed to the site engineer; it was very easy to be trapped to make wrong judgment to arrive the hard clay layer if the driving pile has reached at the top of the mortar as a case of (c).Yokohama city provides various map information including historical changes of the city area back to 1886 when the precise survey became to be available.

The site was known as paddy field in 1886 and became to be developed as residential area.

CONCLUSIONS

Construction records of piling were revealed disguised in 20015 in Yokohama, Japan and became a big issue of the reliability of construction business especially to the geotechnical engineering. Legal system was reviewed and revised by the Ministry of Land and Transportation of Japanese Government.

Based upon the case study of Disguise of piling record in Yokohama, it turned out that the site technician had no intention to disguise the piling records, instead, they had just followed what they have been taught and what they have learnt.

What was wrong was inadequate guidance to help them from the professional geotechnical engineering on key issues including

A. Site history of the land use,

B. Available all geotechnical boring information should be transferred,

C. When the site is not a green, the information of foundations of the existing or existed structure should be given to the piling team,

D. Technical guidelines for the site where the piles are removed and replaced by cement mortar.

Since the situation changes from site to site, each geotechnical society should try to disclose the special issues for each region to help these technicians for piling.

REFERENCE

Revised guidelines for concrete piling, Ministry of Land and Transportation, Government of Japan, March 4, 2016 (in Japanese)

Shuntaro Yuri(2016), “Disguised problem of pile report,”Bungei-Shunjyu,Vol.1, 2016, pp.158-167 (in Japanese)

http://www.mlit.go.jp/report/press/totikensangyo13_hh_000403.html

Back calculation of a flow slide in sensitive clays

V. Thakur[1]

[1]Norwegian University of Science and Technology, *E-mail*: vikas.thakur@ntnu.no

ABSTRACT

Natural hazards in the form of massive flow slides in sensitive clay deposits have been responsible for the loss of human lives and damage to nearby infrastructure. Therefore, an accurate assessment of runout is an essential part of the hazard assessment of flow slides in sensitive clays. An understanding of flow behavior of sensitive clays is important input in calculation of runout of landslides. However, limited knowledge available regarding the flow behavior of sensitive clays has resulted in little guidance available today on the calculation of the landslide runout in such material. An approach to deal with situation is to study the historical landslides, numerically, and understand the parameters that govern the runout. Accordingly, this work presents a back calculation of runout of Byneset flow slide that took place in Norway in 2012.

INTRODUCTION

Highly sensitive clays are mainly found in Canada, Norway, and Sweden. Sensitive clays are often categorized using the term sensitivity (S_t), which is the ratio between the undrained shear strength (c_u) measured in the intact state (c_{ui}) and the remolded (c_{ur}) sensitive clay using the fall cone method. Rosenqvist (1953) demonstrated that the sensitivity of Norwegian marine clays is related to the leaching of salts by fresh groundwater within the grain structure. Bjerrum (1955, 1961) demonstrated that highly sensitive clays may have salt contents as low as 0.5%, whereas marine clays commonly have salt contents of 3% or more.

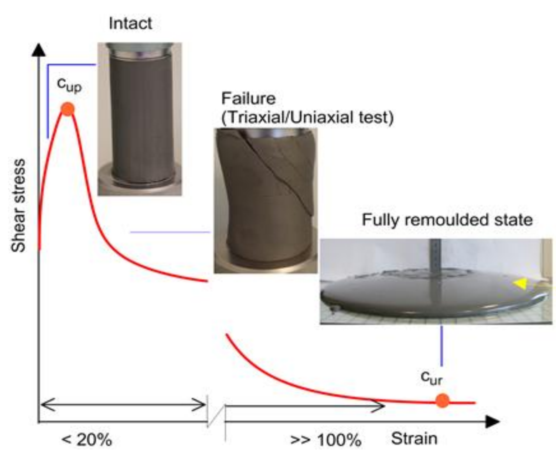

Figure.1. **Disintegration of a sensitive clay sample with increased shearing (Thakur et al. 2017)**

Transformation from an intact material to a fully remolded state at their natural water content is a typical characteristic of highly sensitive clays (Figure 1). Such peculiar behavior is mainly responsible for the large run-out of the debris involved in flow slides in sensitive clays. To understand this aspect, a brief review of literature on the prediction of run-out distances and the characteristics of sensitive clays in their intact and remolded states is presented in the later part of this paper.

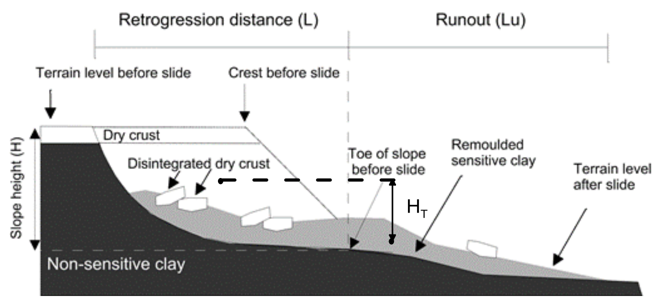

Figure 2. Flow slides in sensitive clays (Strand et al. 2017)

Rapidly developing flow slides in sensitive clay deposits possess substantial destructive capabilities, resulting in the loss of life and destruction of surrounding properties (Fig. 2). In the last 40 years, there have been one or two sensitive clay landslides per decade with volumes exceeding 500,000 m3. In Norway alone, several hundred people have died in such landslides in sensitive soft clay slopes, and as recently as 1893, the Verdal landslide killed 116 people (Furseth, 2006; Walberg 1993; Issler et al. 2012; Oset et al. 2014; Thakur et al. 2014). Geotechnical assessments of such flow slides include an estimation of the retrogression and prediction of the run-out of the slide debris. Although the estimation of landslide retrogression in sensitive clays has received considerable attention (*e.g.*, Lebuis and Rissmann 1979; Tavenas et al. 1983; Karlsrud et al. 1985; Trak and Lacasse 1996; Leroueil et al. 1996; Vaunat and Leroueil 2002; Thakur and Degago 2012), an appropriate method for investigating the run-out of sensitive clay debris remains the focus on ongoing research (*e.g.*, Mitchell and Markell 1974; Karlsrud 1979; Edger and Karlsrud 1982; Norem et al. 1990; Trak and Lacasse 1996; Locat and Leroueil 1997; Hutchinson 2002; Vaunat and Leroueil 2002; Hungr 2005; Locat and Lee 2005; Khaldoun et al. 2009; L'Heureux 2012; Issler et al. 2012; Thakur et al. 2013 & 2014).

The run-out of sensitive clay debris is dependent on several factors, including the thickness of the dry crust, sensitive clay layers, boundary conditions, and topographical aspects that may allow sensitive clays to 'escape' from the slide scarp (Mitchell & Markell 1974; Lebuis and Rissmann 1979; Tavenas et al. 1983; Karlsrud et al. 1985; L'Heureux 2012; Thakur et al. 2012, 2013 & 2014). However, the ability of the clay debris to disintegrate and thus flow is one of the decisive factors in determining the run-out. Recent studies by Thakur et al. (2012), Thakur and Degago (2012), and Thakur et al. (2013, 2014 & 2017) have shown that seemingly small variations in the remolded shear strength (c_{ur}) have significant effects on the flow behavior of sensitive clays. Over the past three decades, a large number of numerical models have been developed for other landslide types or snow avalanches. However, none of these tools and the implement analytical models/rhehologies were developed specifically for the landslides in sensitive clays. One alternative is to study the historical landslides apply the existing tools and gain the knowledge. By doing so, one can lay a solid basis for a tool that suitable for sensitive clays. Accordingly, in this paper an attempt has been made study a flow slide in Norway using a numerical tool. Intention has been to study the suitability of the implemented analytical model in the numerical tool.

STATE OF KNOWLEDGE

Rapid debris flows, debris avalanches, earth flows, sensitive clay slides, rock avalanches and failures of loose fill and mining waste are among the most dangerous and damaging of all landslide phenomena. Their runout determines the consequences and the risk associated with the landslides. Runout parameters include the maximum distance reached, flow velocities, thickness and distribution of deposits, as well as the behaviour in bends and at obstacles in the flow path. (Rickenman 2005; Hungr 2005; Hungr 2016; Lacasse 2013, Crosta 2005; 2016). Several references, e.g. Mitchell and Markell (1974); Corominas (1996); Rickenmann 1999); Fell et al. (2000); Fannin & Wise (2001); Legros (2002); Vaunat & Leroueil (2002); Bathurst et al. (2003); Crosta et al. (2003); Hungr 2005; Locat & Lee (2005); L'Heureux (2012); Thakur & Degago (2013), pro-posed different analytical and empirical models to estimate *L* and *Lu*. These prediction methods are based on travel distance (*L+Lu*) and event magnitude, volume balance, mass point methods, remoulding energy, or some limiting criteria such as critical slope angle. However, continuum based simulation models to calculate *Lu* have so far received limited focus. Some approaches and methods have been developed in the past for a quantitative risk analysis using dynamic runout models for debris flows and avalanches such as BING (Imran et al. 2001) and NIS (Norem et al. 1987), and quasi-three-dimensional models such as DAN3D (Hungr 1995; McDougall & Hungr 2004), MassMov2D (Beguería et al. 2009), LS-RAIPD (Sassa 1988) and RAMMS (Christen et al. 2002). Depending on the characteristics of slide debris, Bingham, plastic, frictional or Voellmy rheology is used. It is worth mentioning that none of these models is specifically developed for sensitive clay slides. However, efforts are being made in this direction by Grue (2017), Tran et al. (2017), Yifru (2017) and Turmel et al. (2017), but there is still a lot of research to be done.

Empirical relationships are the most commonly adopted techniques for estimating the run-out distance of slide debris. Among others; Mitchell and Markell (1974), Hsü (1975), Karlsrud (1979), Edger and Karlsrud (1982), Karlsrud et al. (1985), Cannon (1993), Corominas (1996), Locat and Leroueil (1997), Rickenmann (1999), Fell et al. (2000), Fannin and Wise (2001), Legros (2002), Hutchinson (2002), Vaunat and Leroueil (2002), Bathurst et al. (2003), Crosta et al. (2003), Hungr (2005), Locat and Lee (2005), L'Heuruex (2012), and Thakur and Degago (2013 & 2014) have reported empirical correlations for estimating the run-out distance for various geomaterials, including sensitive clays.

Rickenmann (1999) proposed an expression (Eqn 1) based on a worldwide dataset including 154 debris flow events. This function suggests that the maximum run-out distance (L_u) is mainly linked with the vertical drop (H_T) and the debris-flow volume (V). Here H_T is the vertical distance between the center of gravities of the soil body subject to landslide and the deposit of slide debris in the downstream side.

$$L_u = 1.9\, V^{0.16}\, H_T^{0.83} \tag{1}$$

Corominas (1996) compared a dataset of 52 debris flows, debris slides, and debris avalanches that occurred in the Pyrenees to 19 worldwide events and proposed the following relationship:

$$L_u = 1.03\ V^{-0.105}\ H_T \qquad (2)$$

Locat et al. (2008) proposed a correlation between the run-out distance and normalized slide volume for Canadian sensitive clays based on collected landslide data. A unique empirical relation could not be derived due to scatter in the data; instead, upper and lower limits were suggested. The upper limit is given as follows:

$$L_u = 1.3 \left(\frac{V}{W_{avg}}\right)^{0.73} \qquad (3)$$

Similarly, L’Heureux et al. (2012) suggested the following relationship for Norwegian sensitive clays:

$$L_u = 9 \left(\frac{V}{W_{avg}}\right)^{0.73} \qquad (4)$$

Equations 3 and 4 suggest that the run-out distance for sensitive clays generally increases with an increasing volume of the slide debris (V) per unit width (W_{avg}).

Another important relationship that has been noted is that the run-out distance in sensitive clays is closely related to the retrogression distance (L_R). Locat et al. (2008) suggested a maximum run-out distance for Canadian landslides as:

$$L_{FL} = 8.8\ L_R^{0.8} \qquad (5)$$

Recently, Strand et al. (2017) proposed the following relationships based on the data from 51 landslides in Norway. The recommendations are based on landslide types and the terrain in the downhill side. See Fig. 3. The recommendations are for estimating the *retrogression distance, Lu* of onshore landslides in sensitive clay deposits

Flow slide in channelized terrain:

$$Lu = 3.0\ L \qquad (6)$$

Flow slide in open terrain:

$$Lu = 1.5\ L \qquad (7)$$

Flakes or rotational landslides:

$$Lu = 0.5\ L \qquad (8)$$

The major advantage of these empirical relationships is their simplicity. The only required input data are the longitudinal profile of the flow path and the landslide volume. In contrast, empirical relationships are often established using large datasets of observed debris flows without considering the specific characteristics of the sliding debris or topographical aspects that may influence the dynamic behavior and trajectory.

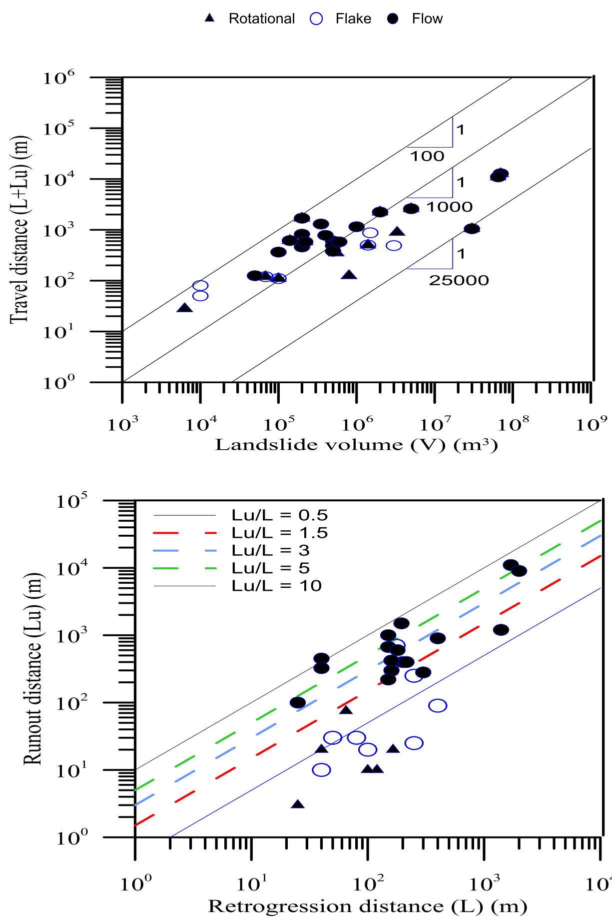

Figure 3. Relationships between (above) travel distance (*L*+*Lu*) and landslide volume and (down) runout distance (*Lu*) and retrogression distance (L), landslides in Norwegian sensitive clays (Strand et al. 2017)

The limitations of the empirical approach are often compensated for using analytical models. Analytical approaches have been developed for rock avalanches *e.g.*, Körner (1976); Hungr et al. (2005), flow slides *e.g.*, Hutchinson 1(986), snow avalanches *e.g.*, Voellmy (1955), Perla et al. (1980), and debris flows *e.g.*, Rickenmann (1990). Sassa (1988) proposed an analytical model so called the friction or sled model. The landslide is represented by a mass concentrated at one point, and the total vertical drop and the total horizontal travel distance of the mass are respectively noted *H* and *L*. The sliding resistance *T* obeys the law:

$$T = \mu N \tag{9}$$

where μ is the friction coefficient, *N* is the normal force exerted by the mass on the sliding surface. The loss of potential energy to the energy dissipated by friction was considered equal. Accordingly:

$$H/L = T/N = \mu \quad (10)$$

μ is usually consider to be equal to the tangent of the friction angle φ of the material. Scheidegger (1973) proposed to estimate the run-out distance of rock falls:

$$L_u = L_T\,(1 - H_T\,L_T^{-1})\tan\varphi_m \quad (11)$$

Here, the reach angle (φ_m) is expressed by arctan ($H_T\,/L_T$). H_T and L_T are respectively the vertical and horizontal distances from the head of the landslide source to the distal margin of the displaced mass.

An approach based on the energy balance is suggested by *e.g.,* Scheidegger (1973); Hsü (1975); Sassa (1988); Vanaut and Leroueil (2002); Thakur and Degago (2013) for the estimation of run-out in sensitive clay debris. The approach by Thakur and Degago (2013) suggests, in flow slides of sensitive clays, the change in potential energy before and after the slide is transformed to a different form of energy that results in disintegration of the soil to its remolding state and slide movement (kinetic and frictional energy). The available potential energy is a function of slope geometry and soil density. The available potential energy to be transformed and the disintegration energy have huge significance in deciding the extent of landslides in sensitive clays. It also implies that, for a given change in potential energy, sensitive clays with higher disintegration energy result in smaller slide movement than sensitive clays with lower disintegration energy. The slide movement is characterized by the run-out distance and the retrogression distance, which is controlled by the amount of energy transferred to kinetic and frictional energy during the slide process. Thakur and Degago (2013) proposed this equation to calculate runout using the concept of remolding energy;

$$Lu = \left(\frac{24}{c_u I_p}\right)^2 \quad (12)$$

where *cu* is the fall cone shear strength of sensitive clays and *Ip* is the plasticity index.

BYNESET FLOW SLIDE

The Byneset flow slide took place on 1st January 2012 in a highly sensitive clay deposit. The slide is located in the central part of Norway. The actual reason for the initiation of the flow slide is unknown but it is believed that the slide was initiated due to natural erosion at the toe of the slope. The slide area was approximately 150 m in width. The flow slide retrogressed backward to a distance approximately 450 m from the toe of the slope. The slip surface was located between 10-12 m below the terrain. The volume of the slide debris was estimated to be approximately 3 – 3.5 × 10^5 m^3. Photos taken immediately after the flow slide illustrate that the slide masses evacuated the slide scar almost completely (Fig. 4). The slide debris followed a dry water canal, having a modest downstream slope of around 3^o, over a distance of approximately 870 m. Due to low discharge in the canal in the winter season, water is not expected to have played an important role in the run-out of the slide debris. Completely remoulded sensitive clay debris were observed along the entire flow path (Figs 5, 6).

Figure 4. The Byneset flow slide (Source NVE, 2012). A closer view of the slide area and the gate

A detailed site investigation was carried-out beside the area where the Byneset flow slide took place. Several total soundings, pore pressure measurements, CPTU and samplings were done. A representative cone penetration test result (CPTU) is shown in Figure 7. A representative undrained triaxial test results on a block sample is shown in Figure 8. The sample was extracted from depth 7.5 m below the ground level. Table 1 provides an executive summary over the engineering properties of the material. The overconsolidation ratio of the tested material varied between 1.1 and 3.3, and the soil sensitivity was in the range of 4 to 400. Since the investigations were carried out on the same soil deposit once can assume that the properties represented in Table 1 is representative to the material involved in the Byneset flow slide

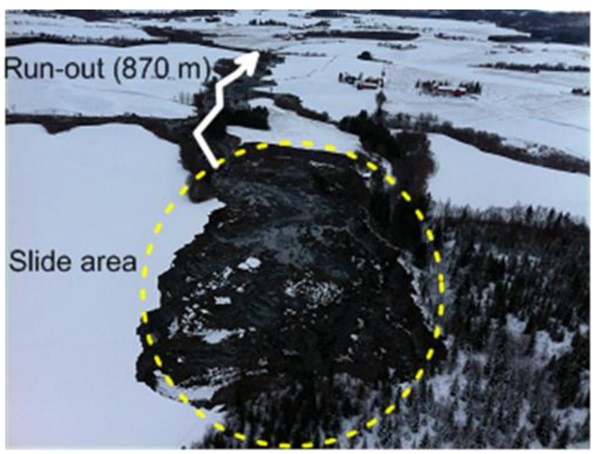

Figure 5. The extent of the Byneset flow slide (Source NVE, 2012)

Figure 6. The remolded sensitive clay debris along the flow path. (Source NVE, 2012)

Table 1 Engineering characterization of the tested material

Properties	**Byneset**
Sampling depth (H) [m]	4 – 12
Clay fractions (< 2 μm) [%]	30 – 55
Water content (w) [%]	27 – 48
Plasticity index (I_P) [%]	3 – 15
Liquidity index (I_L) [-]	0.9 – 5.4
Undisturbed undrained shear strength (c_{ui}) [kPa]	5.2 – 72
Remolded shear strength (c_{ur}) [kPa]	0.1 -1.0
Sensitivity (S_t) [-]	4 – 400
Over consolidation ratio (OCR) [-]	1.1 – 3.3
Salinity (g/l)	0.6 – 0.74

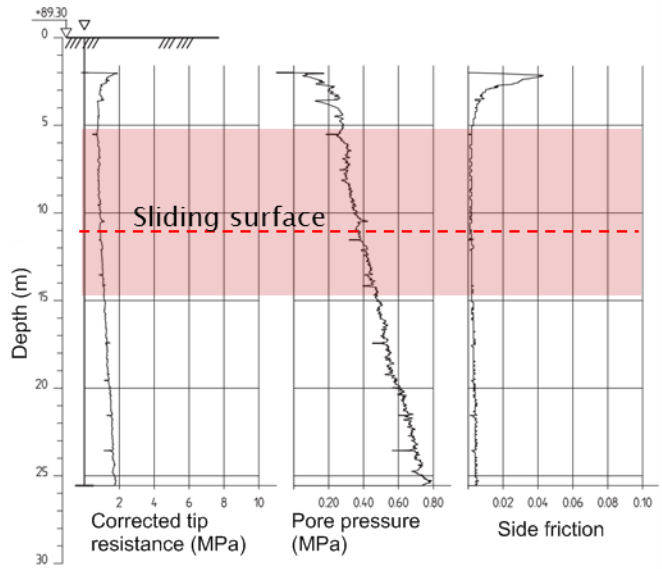

Figure 7. A CPTU result. The sensitive clay layer was located between 5-15 meters.

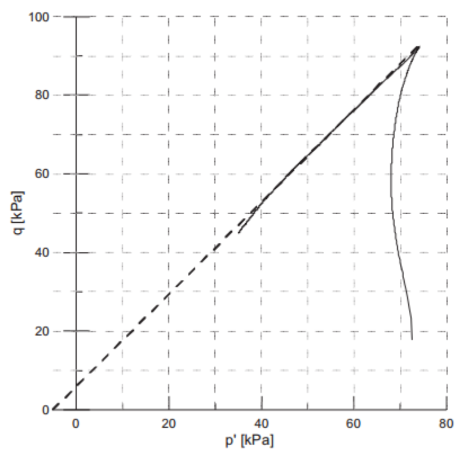

Figure 8. A undrained triaxial test result in a block sample extracted from 7.5 depth. Here *P'* is the mean effective stress and *q* is the deviator stress. The sample was anisotropically consolidated. The cohesion is about 6 kPa and the friction angle found to be 30^{o}

CALCULATION TOOL AND THE AVAILABLE RHEHOLOGIES

In this study a tool called Dynamic Analysis of Landslides (DAN) in 3D, also known as DAN3D is used. This tool has been progressively developed by Hungr (1995), McDougall & Hungr (2004), McDougall (2006), DAN3D is designed to predict the velocity and extent of motion of rapid landslides such as debris flows and avalanches, flow slides and rock avalanches. The software has been extensively tested by various researchers for different types of landslide run-out except for sensitive clay landslide. The origin and description of DAN3D can be found in Hungr (1995), McDougall & Hungr (2004), McDougall (2006). DAN3D uses a semi-empirical approach based on the concept of “equivalent fluid” (see Figure 9), as defined by Hungr (1995).

The heterogeneous and complex landslide material is modelled as a hypothetical material, which is governed by simple internal and basal rheological relationships (Thakur et al. 2013).

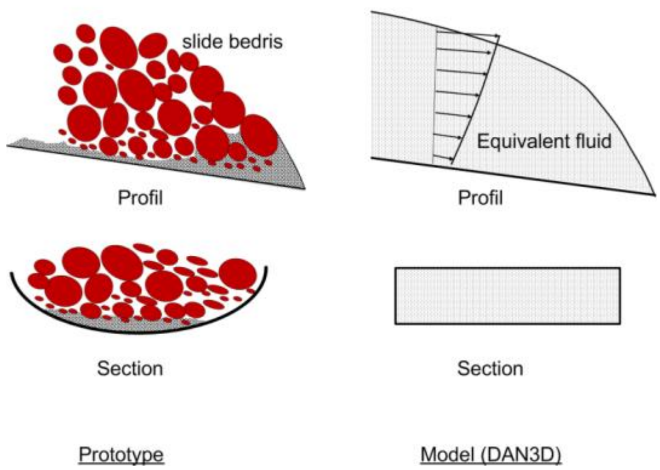

Figure 9. Equivalent fluid concept in DAN3D (Hungr, 1995)

The internal rheology is assumed to be frictional and is governed by one parameter, the internal friction angle, φ_i. In contrast, a single basal rheology is not imposed. Instead, to allow the simulation of different types of rapid landslides involving different geological materials, a variety of basal rheological relationships can be implemented in DAN3D, including laminar, turbulent, plastic, Bingham, frictional and Voellmy rheologies. The user can change the basal rheology along the path or within the slide mass. Readers are encouraged to refer to a PhD thesis by McDougall in 2006 to obtain complete information regarding the DAN3D program, its governing equations and corresponding numerical solution method. Two basal rheological models, available in DAN3D, have been used in this study and they are briefly discussed here below.

The plastic rheology is related with a pseudo-static motion of liquefied debris, the base shear resistance (τ) is assumed equivalent to a constant yield strength (c_{ur}) value.

$$\tau = -c_{ur} \tag{13}$$

The yield strength (c_{ur}) of sensitive clays in this case is fully remolded shear strength obtained using the fall cone test.

The Voellmy rheology was proposed by Voellmy (1955) for snow avalanche modelling. The rheology is a two parameters mode, which combines turbulent and frictional behaviour of sliding mass. The basal resistance is given by:

$$\tau = -\left(\sigma f + \frac{\gamma v^2}{\xi}\right) \tag{14}$$

where f is the friction coefficient; ξ is so-called turbulence parameter; γ is the unit weight σ is stress normal to the bed. The first term on the right side accounts for any frictional component of resistance (f is analogous to $\tan\varphi$). The second term was originally introduced by Voellmy (1955) to account for the velocity-dependent influence of air drag on snow avalanches. Here, ξ is analogous to the square of the Chézy coefficient. The rheological models discussed above require a set of input parameters. Some parameters e.g. remoulded shear strength, internal friction angle, viscosity and soil unit weight can be obtained from the laboratory testing. Whereas the other parameters e.g. friction coefficient and turbulence coefficient are usually obtained from back-calculation of landslides. Hungr (1998), McDougall & Hungr (2004), McDougall (2006) suggest that f may range from 0.08 to 0.1 and ξ may range from 200 to 1,000 m/s^2. It must be noted that these value of f and ξ may not necessarily be representative for sensitive clay debris. Therefore, a rough estimation can be made using

$$\xi = K_s^2 R^{1/3} \tag{15}$$

where K_s is the inverse value of Gauckler–Manning coefficient and R is the hydraulic radius, which depends on the cross section of the flow path and the peripheral contact between the slide debris and terrain.

CALCULATION PROCEDURES AND APPROXIMATIONS

The analysis in DAN3D requires a grid terrain model which designate the pre-slide topography and release area (the area where the slide mass evacuates from). After placing the terrain model, the computation of run-out relies on the selection of basal rheological model and parameters associated with the selected basal rheological relationship that will govern the flow. The parameters depend on the type of rheology selected, thus, appropriate parameterization is important. Once the topography and flow behaviour are defined, the simulation starts by distributing the particles over an interpolated surface in accordance with the selected rheological model. Each computation step generates a grid file that shows the flow deposit depths, velocity of the debris and discharge at the grid nodal points. The flow deposit depths plotted in grid files shows the thickness of the flow deposit along the flow path. (McDougall, 2006)

The Byneset flow slide was back-calculated using DAN3D. Several simple approximations were made to back-calculate the flow slide:

(1) The slide debris obeys either plastic basal rheology or the Voellmy rheology.

(2) The effects of bed friction along the contact surface between the flow path and slide debris were neglected in the plastic rheology.

(3) External factors, such as the effects of vegetation and water or snow along the flow path, were not considered in the model.

(4) It was assumed that the run-out is solely controlled by the flow behavior of sensitive clays and topography of the area.

RESULTS AND DISCUSSIONS

Sets of numerical calculations were carried-out using the plastic and Voellmy rheologies. These parameters are selected based on the site investigation report (Table 1) and using values suggested in the literature. In doing so, the selected geotechnical parameters have been varied in order to back calculate the Byneset flow slide and also to study sensitivity of parameters. Accordingly, the impact and the significance of these input parameters are discussed in light of the numerical results.

The plastic rheology is found to be the simplest among all the rheological models implemented in DAN3D. The rheology required only γ and c_{ur} values, which are easily obtainable. The flow deposit contours obtained from the plastic rheology, with c_{ur} = 0.1 kPa, are shown in Figure 10. The total run-out of the slide debris obtained at the end of the simulation (Figure 10) is quite similar to that observed in the field.

The run-out distance decreased with the increasing value of c_{ur} . The runout distance became zero when c_{ur} was greater than 1 kPa. This observation is in line with Thakur et al. (2014). The Vollemy rheology is used with various combination of friction coefficient (*f*) and turbulence coefficient (ξ). In adopting the rheology, a decrease on *f* and an increasing on ξ show an increase on the estimate of the run-out distance (Figure 11).

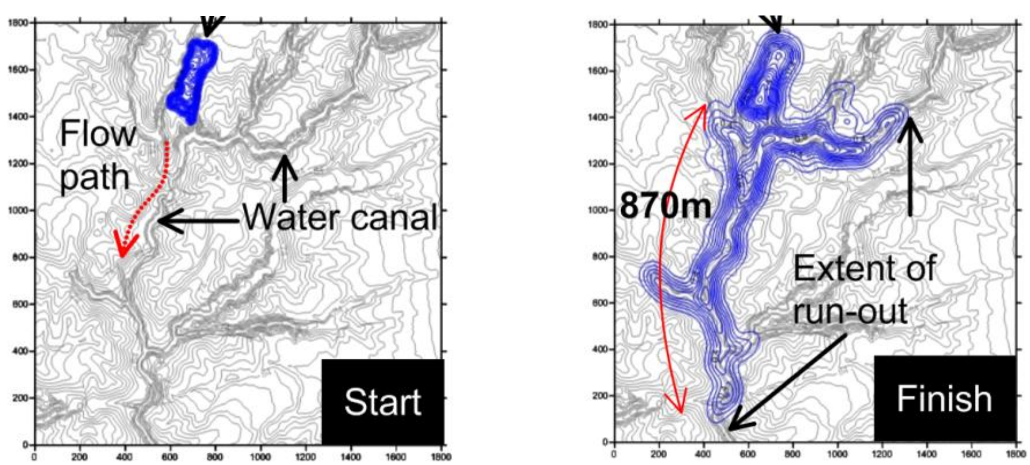

Figure 10. Flow contours obtained from the plastic rheology with c_{ur} = 0.1 kPa

Based on back-analyses of various debris flows using DAN3D, calibrated values of *f* typically range between 0.01 and 0.2, while values of ξ range between 100 and 600 m/s^2 (Hungr et al. 2005). Use of Equation 13 to estimate ξ for Byneset slide yielded range 100-200. Despite this, ζ was varied to a very high value up to 5000 in the analyses. The actual runout observed out in the field was able to be back calculated for a combination of the input parameters i.e. f = 0.005 and ξ = 4000. It was also found that influence of ζ was lesser compared to *f*. This makes sense because sensitive clay debris usually are dominated by clay contents allowing the debris to behave like thick viscous material. From this simple study, it is clear that *f* is the dominating and important parameter compared to ξ in case of sensitive clay debris. The velocity of the slide debris was between 15 and 20 m/s, which is a relatively high velocity for such sub-aerial flow slides. It is difficult to verify the obtained velocity, as actual measurements are not available. However, slide debris involved in the Rissa landslide (1978) in Norway also had a velocity of approximately 11-12 m/s. Therefore, it is possible to conclude that the obtained velocity for the Byneset flow slide is reasonable.

In summary, the back- calculated run-out distance is in agreement with the field evidences. The major challenge with the use of Voellmy rheology for the calculation of runout of sensitive clays is related to the fact that the input parameters are not based on the standard geotechnical parameters e.g. remolded shear strength, viscosity, liquidity index etc. Therefore, usefulness of the Voellmy rheology is limited until a connection between the model's input parameters and the standard geotechnical parameters are not on place.

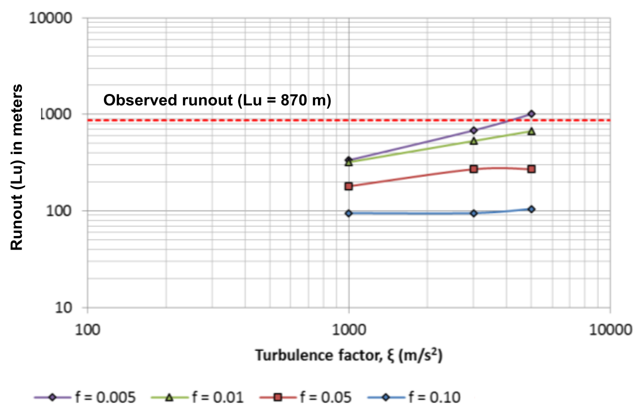

Figure 11. Calculated runout using various combination of the input parameters.

CONCLUSIONS

This paper uses a simplified approach to look into a very complex problem, which is yet to be fully understood. Therefore, several simple approximations were necessary in order to focus on the role of certain parameters governing the rheology on run-out of sensitive clay debris. Based on the back-calculation of a flow slide in a sensitive clay deposit, it was found that the plastic rheology and seems to predict the run-out distance of the flow slide in Byneset reasonably well. It is also worthwhile to appreciate that this rheology requires only one parameter, which are obtainable from the laboratory tests. However, the Voellmy rheology, which are sophisticated models, require more parameters, which are not readily available for sensitive clays. Hence, it was difficult to adopt the rheologies In general; the work presented in this study demonstrates that with further validation of input parameters for sensitive clays, the approach offers an appealing numerical tool. Currently, an experimental study is planned to initiate to establish some of the parameters for Norwegian sensitive clays.

REFERENCES

Bathurst, J.C., Burton, A., and Ward, T.J. (2003) "Debris flow run-out and landslide sediment delivery model tests". Journal of Hydraulic Engineering, 123-5, pp410–419.

Begueria, S., Van Asch, Th.W.J., Malet, J.P., and Gröndhal, S. (2009) "A GIS-based numerical model for simulating the kinematics of mud and debris flows over complex terrain". Natural Hazards and Earth System Sciences 9, pp1897-1909.

Bjerrum, L. (1955) "Stability of natural slopes in quick clay". Géotechnique, issue 5-1, pp 101–119.

Bjerrum, L., (1961) "The effective shear strength parameters of sensitive clays", Proc. 5th International Conference Soil Mechanics Foundation Engineering Paris, pp23–28.

Bjerrum, L., and Kjærnsli, B. (1957) "Analysis of the stability of some Norwegian natural clay slopes". Géotechnique, issue 7-1, pp1–16.

Burland, J. B. (1990) "30th Rankine Lecture: on the compressibility and shear strength of natural clays". Géotechnique, issue 40-3, pp329–378.

Cannon, S.H. (1993) "An empirical model for the volume-change behavior of debris flows", In: Shen, H.W., Su, S.T., Wen, F. (Eds.), National Conference on Hydraulic Engineering. ASCE, San Francisco, pp1768–1773.

Christen, M. Bartelt, P., and Gruber, U., (2002) "AVAL-1D: An Avalanche Dynamics Program for the Practice", In: International Congress Interpraevent 2002 in the Pacific Rim - Matsumo, Japan, Congress publication, 2, pp715-725.

Corominas, J., (1996) "The angle of reach as a mobility index for small and large landslides". Canadian Geotechnical Journal, 33-2 , pp 260–271.

Crosta, G.B., Cucchiaro, S., and Frattini, P., (2003) "Validation of semi-empirical relationships for the definition of debris-flow behavior in granular materials", In: Rickenmann, D., Chen, C. (Eds.), 3rd Int. Conf. on Debris-Flow Hazards Mitigation. Millpress, Davos, pp821–831.

Dai, F.C., Lee, C.F., and Ngai, Y.Y., (2002) "Landslide risk assessment and management: an overview". Engineering Geology, 64-1, pp65–87.

Edgers L., and Karlsrud, K., (1982) "Soil flows generated by submarine slides", NGI Publication 143.

Fannin, R.J., and Wise, M.P., (2001) "An empirical–statistical model for debris flow travel distance". Canadian Geotechnical Journal, 38, pp982–994.

Fell, R., Hungr, O., Leroueil, S., and Reimer, W., (2000) "Keynote Lecture – Geotechnical engineering of the stability of natural slopes, and cuts and fills in soil", GeoEng 2000, issue 1, p21–120.

Furseth A (2006). Skredulykker i Norge. Tune Forlag, Oslo.

Grue R, Issler D, L'Heureux JS, Thakur V (2017) Viscometric tests of sensitive clay from Byneset, Norway, and fit to the Herschel–Bulkley model Second International Workshop on landslides in sensitive clays. June 2017. Springer book series Advances on natural and technological hazards research.

Hsü, K., (1975) “Catastrophic debris streams (Sturzstroms) generated by rock falls”. Geological Society of America Bulletin, 86, pp129–140.

Hungr O (2016). A Review of landslide hazard and risk assessment methodology. Landslides and Engineered Slopes. Experience, Theory and Practice: Proceedings of the 12th International Symposium on Landslides (Napoli, Italy).

Hungr, O. (2005) “Classification and terminology”. Debris-flow hazards and related phenomena. Springer. ISBN 3-540-20726-0, pp9–24.

Hungr, O., Corominas, J., and Eberhardt, E., (2005) “Estimating landslide motion mechanism, travel distance and velocity”, In: Hungr, O., Fell, R., Couture, R., Eberhardt, E. (Eds.), Landslide Risk Management. Taylor & Francis Group, Vancouver, pp99–128.

Hutchinson, J. N. (2002) “Chalk flows from the coastal cliffs of northwest Europe, Catastrophic landslides: Effects, occurrence, and mechanism”s. Geol. Soc. of Ame. Reviews in Eng. Geo., pp257–302.

Hutchinson, D. J. (1961) “A landslide on a thin layer of quick clay at Furre, central Norway”. Geotechnique, issue11-2, pp69–94.

Hutchinson, J.N., 1986. A sliding-consolidation model for flow slides. Canadian Geotechnical Journal 23, 115–126.

Imran, J., Parker, G., Locat, J., and Lee, H., (2001) “1D numerical model of muddy subaqueous and subaerial debris flows”. Journal of Hydraulic Engineering, 127-11, pp959–968.

Issler, D., Cepeda, J.M., Luna B.Q. and Venditti, V., (2012) “Back-analyses of run-out for Norwegian quick-clay landslides”. NIFS report. Available at www.naturfare.no

Karlsrud, K. (1979) “Skredfare og planlegging”, Lecture notes NIF-Course, Hardanger.

Karlsrud, K., Aas, G., and Gregersen, O. (1985) “Can we predict landslide hazards in soft sensitive clays? Summary of Norwegian practice and experience”. NGI Publication nr 158.

Karlsrud, K., Lunne, T., and Brattlien, K., (1996) “Improved CPTU interpretation based on block samples”, In Proceedings of the 12th Nordic Geotechnical Conference, Iceland, issue 1 pp195–201.

Khaldoun, A., Moller, P., Fall, A., Wegdam, G., De Leeuw, B., Méheust, Y., Fossum, J. O. and Bonn, D., (2009) “Quick clay and landslides of clayey soil”. Phys. Rev. Lett. 103, 188301.

Körner, H.J., (1976) “Reichweite und Geschwindigkeit von Bergstürzen und Fliessschneelawinene”. Rock Mechanics, 8, pp225–256.

L’Heureux, J. S., (2012) “A study of the retrogressive behaviour and mobility of Norwegian quick clay landslides”, Proc. 11th INASL, Banff, Canada, issue 1, pp981–988.

Lacasse, S., Berre, T., and Lefebvre, T., (1985)” Block sampling of sensitive clays”, International Conference of Soil Mechanics and Foundation Engineering, issue 2, pp887–892.

Lebuis. J., and Rissmann, P., (1979) “Les coulées argileuses dans le région de Québec et de Shawinigan. In: Argiles sensibles, pentes instables, mesures correctives et coulées des régions de Québec et Shawinigan”, Geo. Assoc. of Canada Guidebook, pp19–40

Legros, F., (2002) “The mobility of long-runout landslides”. Engineering Geology, 63, pp301–331.

Leroueil, S., Locat, J., and Vaunat, J., (1996) “Geotechnical characterisation of slope movements”, Proceedings of the 7th International Symposium on Landslides, pp53–74.

Leroueil, S., Tavenas, F., and Le Bihan, J.P. (1983) “Propriétés caracteristiqués des argiles de I’est du Canada”. Canadian Geotechnical Journal, issue 20, pp681–705.

Locat, A., Leroueil, S., Bernander, S., Demers, D., Locat, J., and Ouehb, L., (2008) “Study of a lateral spread failure in an eastern Canada clay deposit in relation with progressive failure: The Saint-Barnabé-Nord slide”, Proceedings of the 4th Canadian Conference on Geohazards : From Causes to Management, pp89-96.

Locat, J., and Demers, D. (1988) “Viscosity, yield stress, remolded strength, and liquidity index relationships for sensitive clays”. Canadian Geotechnical Journal, issue 25, pp799–806.

Locat, J., and Lee, H. J. (2005) “Subaqueous debris flow”. Debris-flow hazards and related phenomena. Springer. ISBN 3-540-20726-0, pp203–246.

Locat, J., and Leroueil, S. (1988) “Physicochemical and mechanical characteristics of recent Saguenay Fjord sediments”. Canadian Geotechnical Journal, issue 25, pp382–388.

Locat, J., and Leroueil, S., (1997) “Landslide stages and risk assessment issues in sensitive clays and other soft sediments”, Proc. International Workshop on Landslide Risk Assessment, (Cruden and Fell ed.) Hawaii, Balkema, Rotterdam, pp261-270.

Locat, P., Leroueil, S., and Locat, J., (2003) “Characterization of a submarine flow-slide at Pointe-du-Fort, Saguenay Fjord, Quebec, Canada”, Proceeding of the 1st Symposium on Submarine Mass Movements and their Consequences, pp521–529.

Locat, P., Leroueil, S., and Locat, J., (2008) “Remaniement et mobilité des débris de glissements de terrain dans les argiles sensible de l’est du Canada”, Proceedings of the 4th Canadian Conference on Geohazards: From Causes to Management. Presse de l’Université Laval, Québec, pp97–106.

Lunne, T., Berre, T., and Strandvik, S., (1997) “Sample disturbance effects in soft low plastic Norwegian clay”, In Proceedings of the Conference on Recent Developments in Soil and Pavement Mechanics, pp81–102.

McDougall, S., (2006). “A new continuum dynamic model for the analysis of ex-tremely rapid landslide motion across complex 3D terrain”. PhD thesis, University of British Columbia, Vancouver, Canada.

McDougall, S., and Hungr, O., (2004) “A model for the analysis of rapid landslide motion across three-dimensional terrain”. Canadian Geotechnical Journal, 41, pp1084–1097.

Mitchell, R.J., and Markell, A.R. (1974) “Flow slides in sensitive soils”. Can. Geot. Journal, issue 11-1, pp11–31.

NGF (1974). Guidelines by Norwegian Geotechnical Society.

Nordal, S., Alen, C., Emdal, A. Madshus, C., and Lyche E. (2009) Landslide in Kattamrka in Namsos 13. March 2009. Transportation Ministry, Norway, 2009, Report ISBN 978-82-92506-71-4.

Norem, H., Irgens, F. and Schieldrop, B., (1987) “A continuum model for calculating snow avalanche velocities”, In: Avalanche formation, movement and effects, Proceedings of the Davos symposium, September 1986. IAHS publication no. 162, pp 363-379

Norem, H., Locat, J., and Schieldrop, B. (1990) “An approach to the physics and the modeling of submarine flowslides”. Marine Geotechnology, 9, pp93–111.

NVE (2012). Kvikkleireskred ved Esp, Byneset I Trondheim. Norwegian Water and Energy Directorate (NVE), Oslo, Norway. NVE Report no. 1-2012 prelim-inary version 2012-01-09, 79 pp.

Oset, F., Thakur, V., Dolva, B. K., Aunaas, K., Sæter, M. B., Robsrud, A., Viklund, M. Nyheim, T., Lyche, E. and Jensen O. A. (2014) "Regulatory framework for Regulatory framework for road and railway construction on the sensitive clays of Norway". Natural Hazards book: Advances in Natural and Technological Hazards Research, ISSN: 1878-9897 (Print) 2213-6959 (Online), pp 343-354.

Perla, R., Cheng, T.T., and Mc Clung, D.M., (1980) "A two parameter model of snow avalanche motion". Journal of Glaciology, 26-94, pp197–208.

Rickenmann, D., (1990) "Debris Flows 1987 in Switzerland: modelling and fluvial sediment transport". In: Sinniger, R.O., Monbaron, M. (Eds.), Hydrology in Mountainous Regions; Lausanne Symposium. IAHS, Lausanne, pp371–378.

Rickenmann, D., (1999) "Empirical relationships for debris flows". Natural hazards, 19-1, pp47–77.

Rickenmann, D., (2005) "Run-out prediction methods", In: Jakob, M., Hungr, O. (Eds.), Debris-flow Hazards and Related Phenomena. Springer, Berlin, pp305–324.

Rickenmann, D., (2005) Hangmuren und Gefahrenbeurteilung. Kurzbericht für das Bundesamt für Wasser und Geologie. Unpublished report, Universität für Bodenkultur, Wien, und Eidg. Forschungsanstalt WSL, Birmensdorf, 18p.

Rickenmann, D., Laigle, D., McArdell, B., and Hübl, J., (2006) "Comparison of 2D debris-flow simulation models with field events". Computational Geosciences 10-2, pp241–264.

Rickenmann,D., and Koch, T.,(1997) "Comparison of debrisflowmodeling approaches", In: Chen, C. (Ed.), 1st Int. Conf. on Debris-Flow Hazards Mitigation, San Francisco, pp 576–585.

Rosenqvist, I. T. (1953) Considerations on the sensitivity of Norwegian clays. Geotechnique 3, 195–200.

Sassa, K. (1988) "Special lecture: Geotechnical model for the motion of landslides", In: C. Bonnard (ed.), Proc. of 5th Symp. on Landslides, Balkema, Rotterdam, pp37–55.

Scheidegger, A. E. (1973) "On the prediction of the reach and velocity of catastrophic landslides". Rock Mechanics, 5, pp231–236.

Strand, SA, Thakur V, J S L'Heureux, S Lacasse, K Karlsrud, T Nyheim, K Aunaas, H Ottesen, V Gjelsvik, O A Fauskerud, R Sandven, A Rosenquist6trand (2017) Runout of landslides in sensitive clays. Second International Workshop on landslides in sensitive clays. June 2017. Springer book series Advances on natural and technological hazards research.

SVV (2009). Technology report 2425 by the Norwegian Public Roads Authority.

Tavenas, F., Flon, P., Leroueil, S., and Lebuis, J., (1983) "Remolding energy and risk of slide retrogression in sensitive clays", Proceedings of the Symposium Slopes on Soft Clays, Linköping, pp423–454.

Thakur V (2012) Landslide at Byneset. NIFS report. ISBN nr 978-82-410-0822-1. Available at www.naturfare.no

Thakur V, Degago S, Selänpää J, Lansivaara T (2017) Remoulding of sensitive clays. Second International Workshop on landslides in sensitive clays. June 2017. Springer book series Advances on natural and technological hazards research.

Thakur, V., and Degago, S.A. (2012) “Quickness of sensitive clays”. Géotechnique Letters, issue 2-3, pp87–95.

Thakur, V., and Degago, S.A. (2013) “Disintegration of sensitive clays”. Géotechnique Letters, issue 3-1, pp20–25.

Thakur, V., Degago S, Oset, F., Dolva, B. K., Aabøe, R., Aunaas, K., Nyheim, T., Lyche, E., Jensen O. A. Viklund, M., Sæter, M. B., Robsrud, A., Nigguise, D., and L’Heureux J.S. (2013) “Characterization of post-failure movements of landslides in soft sensitive clays”. Natural Hazards book: Advances in Natural and Technological Hazards Research, ISSN: 1878-9897 (Print) 2213-6959 (Online), pp 91-104.

Thakur, V., Oset, F., Aabøe, R., Berg, P. O., Degago, S. A., Wiig, T., Lyche, E., Haugen, E. E. D., Saeter, M. B., and Robsrud, A. (2012) “A critical appraisal of the definition of Brittle clays (Sprøbruddmateriale)”, Proc. 16th Nordic Geotechnical Meeting Copenhagen, issue 1, pp 451– 462.

Trak, B., and Lacasse, S., (1996) “Soils susceptible to flow slides and associated mechanisms”, Proceedings of the 7th International Symposium on Landslides, Trondheim, issue 1, pp 497–506.

Tran, QA, Solowski, W, Thakur V, Karstunen M (2017). Modelling of the quickness test of sensitive clays using the generalized interpolation material point method. Second International Workshop on landslides in sensitive clays. June 2017. Springer book series Advances on natural and technological hazards research.

Turmel D, Locat J, Locat P, Demers D (2017) Parametric analysis of the mobility of debris from flow slides in sensitive clays. Second International Workshop on landslides in sensitive clays. June 2017. Springer book series Advances on natural and technological hazards research.

Vaunat, J., and Leroueil, S. (2002) “Analysis of Post-Failure Slope Movements within the Framework of Hazard and Risk Analysis”. Natural Hazards, issue 26, pp83–102.

Voellmy, A., 1955. Über die Zerstörungskraft von Lawinen. Schweizerische Bauzeitung 73, 212–285.

Yifru A, Degago S, Thakur V (2017) Back-calculation of the Byneset sensitive clay slide using the modified Voellmy rheology. Second International Workshop on landslides in sensitive clays. June 2017. Springer book series Advances on natural and technological hazards research.

Perspectives in Forensic Geotechnical Engineering

M.R. Madhav, Ph.D., D.Sc., FNAE[1] and S.V. Abhishek, M.E., S.M.ASCE[2]

[1]Professor Emeritus, JNT University & Visiting Professor, IIT, Hyderabad 500034, India; e-mail: madhavmr@gmail.com
[2]Ph.D. Student, Lyles School of Civil Engineering, Purdue University, West Lafayette, IN 47907, USA; e-mail: vsaklesh@purdue.edu

ABSTRACT

The paper presents some perspectives in forensic geotechnical engineering with respect to (i) structural vs. geotechnical engineering, (ii) bearing capacity vs. leaning instability, (iii) linear vs. non-linear and thin vs. thick layer responses. Traditional approaches for the estimation of ultimate bearing capacity of shallow foundations use limit equilibrium methods that are based only on soil strength apart from the geometry of the foundation element. However, the effect of the height of the structure on its stability is ignored. Tall structures, particularly towers, resting on or in soft ground, could lean or fail by a mechanism called leaning instability due to the compressibility of the ground rather than its strength. Terzaghi's one-dimensional consolidation theory is based on a linear void ratio–effective stress relationship, and is applicable for thin layers only. The differences between the linear theory and a theory of non-linear consolidation of a thick clay deposit considering linear void ratio–log effective stress relationship are highlighted. Some parallels are drawn between geotechnical engineering and the practice of medicine.

INTRODUCTION

Structural vs. Geotechnical Engineering. Structural engineers work with engineered materials such as concrete and steel that possess unique and well-defined properties of density, elastic modulus, compressive/tensile strengths, and flexural stiffness among others. On the other hand, geotechnical engineers deal with soil, a material made by Nature/God with highly variable spatial and temporal properties. Structural designs are code-based since theoretical closed-form solutions are derived based on the given geometry, material properties, and loading. However, geotechnical designs are judgement-based due to highly variable geometry, complex loading, and material properties that are not precisely determinable. According to Gray (1992), "Men are from Mars and Women are from Venus"; extending the analogy, indeed "Structural engineers are from Mars and Geotechnical Engineers are from Venus".

Stress–Strain Relationships. Figure 1(a) and (b) show the stress–strain curves of various civil engineering materials in linear and log-log scales, respectively. Soils are so weak and highly deformable that their stress–strain curves are not visible on the linear scale in comparison with those of steel (Fe250 and Fe415) and concrete (M50 and M15) but become discernable if plotted on a log-log scale. The ultimate strength and stiffness of steel are 415 MPa and 210 GPa, respectively, while those of soils range from about 10 kPa (soft clay) to 400 kPa (dense sand) and 0.5 to 10 MPa, respectively. Thus, these plots contrast the significantly large differences in the strength and stiffness of soils in comparison with those of steel and concrete. Soils are generally subjected to much higher strains at failure (of the order of about 15 to 20% for loose sands and soft clays, and 5 to 10% for dense sands and stiff clays) when compared to concrete (0.3%) or steel (about 0.2 to 0.4%)

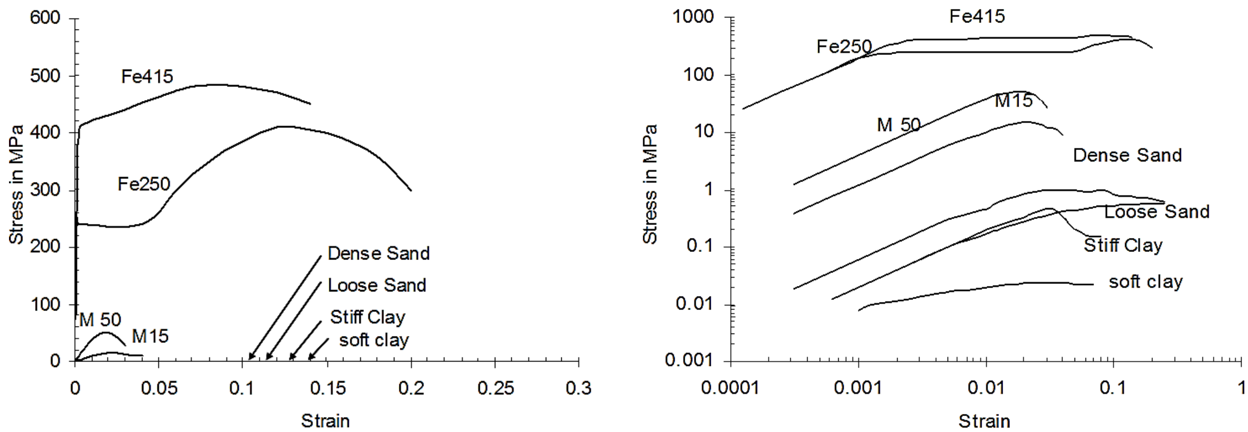

(a) (b)

Figure 1. Stress-strain relations for various materials: (a) natural scale and (b) log-log scale

BEARING CAPACITY vs. LEANING INSTABILITY

Bearing Capacity of Shallow Foundations. Prandtl's theory is the starting point for the estimation of bearing capacity of shallow foundations. Terzaghi (1943) modified the same and proposed his theory for a strip footing resting on a cohesive–frictional (c–ϕ) soil (Figure 2). The slip mechanism consists of an active rigid/elastic wedge defined by the angle of shearing resistance ϕ, a fan region of continuous plastic deformation (distortion+rotation), and the passive wedges defined by the angle ($\phi/4$-$\pi/2$) with respect to the horizontal. Prandtl's solution modified for c–ϕ soils (c being the cohesion component) with the active wedge defined by ($\phi/4$+$\pi/2$) instead is adopted as appropriate for geotechnical applications. Soils do not fail in 'general shear' and a new failure mode termed 'local shear failure' was identified as a possible alternative. The ultimate bearing capacity of shallow foundations for local shear failure is estimated using the general shear failure equation but with both the strength parameters, c and tan ϕ, reduced to two-thirds of their corresponding values (Terzaghi and Peck 1967). Vesic (1973) extended this concept and identified a third failure mode, 'punching shear failure', occurring in loose soils at shallow depths and at depth in case of dense soils. Figure 3 classifies the three failure modes as dependent on both the relative density of granular soils and the relative depth D/B of the footing. Vesic (1973) proposed a general expression for the ultimate bearing capacity of shallow foundations based on cavity expansion analysis accounting for the compressibility of ground through a rigidity index $I_r = G/s_u$, the ratio of the shear stiffness to the undrained shear strength of ground. Unlike in structural engineering where ultimate capacity is based on the ultimate strength of the material, geotechnical designs are governed by both the strength as well as the compressibility of the ground.

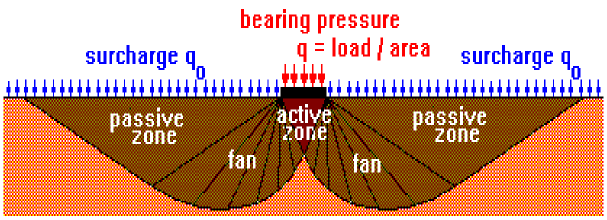

Figure 2. General shear failure for *c*–ϕ soil (Terzaghi 1943)

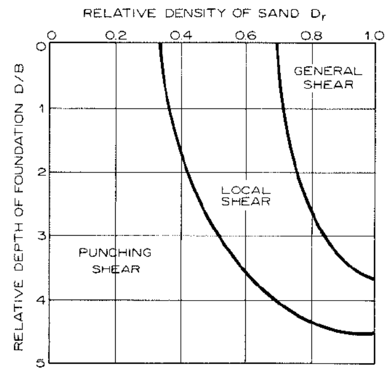

Figure 3. Modes of failure of shallow foundations in sand (after Vesic 1973)

Structure-Foundation-Ground Interaction (Leaning Instability). In traditional design, the influence of the height of the structure on its stability is ignored, while only foundation–ground interactions are considered. However, the height of a tall structure plays an important role in the overall behaviour of the system and leads to a different failure mechanism, termed 'Leaning Instability', examples of which are the famous Leaning Tower of Pisa and the more recent case of a 58-storey condominium in San Francisco. Leaning instability occurs at a critical height to width ratio when the overturning moment caused by a small inclination cannot be compensated by the corresponding resisting moment mobilized by the foundation (Hambly 1985, 1990). Leaning instability is due to the high compressibility of the ground and is not dependent on the strength. Figure 4 depicts (i) a structure whose height H is ignored (H = 0), (ii) a medium to low rise structure with H/B<1 and (iii) a high rise structure with H/B>1, where B is the width or diameter of the footing. It can be shown experimentally and analytically that the ultimate capacity of the footing decreases with increased height of the structure.

Studies by Hambly (1985, 1990), Cheney et al. (1991), Lancellotta (1993) and Potts (2003) quantify the effect of the height of the structure on its stability as somewhat akin to that of buckling of long columns. Incidentally, the buckling of long slender columns is controlled by the flexural stiffness of the structure and not by the strength of the material. Figure 5 illustrates a leaning instability model with the ground represented by a series of Winkler springs. In advanced mechanical modelling, the time-dependent response of the ground is represented by a Kelvin–Voigt model as shown in Figure 6.

Potts (2003) models a simple tower of 60 m height and 20 m diameter with an initial tilt of 0.5^0 , resting on a uniform deposit of clay with s_u of 80 kPa and G of 10, 100 and 1000 times s_u. The clay was modelled as a linear-elastic Tresca material. Conventional theory predicts identical bearing capacities of the tower for all the three cases. However, if the rotation of the tower is plotted against its weight, the effect of G/s_u becomes significant (Figure 7). The weights of the tower at failure are 60, 110 and 130 MN for G/s_u of 10, 100 and 1000, respectively. Failure is abrupt for very stiff soils when compared to that of relatively softer soils.

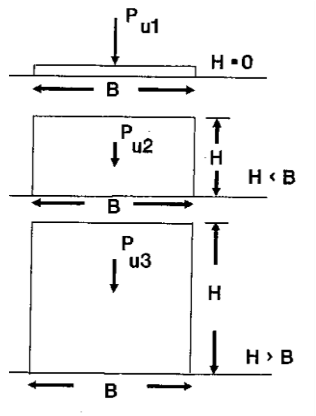

Figure 4. Structures with different heights *H* relative to their width/diameter *B*

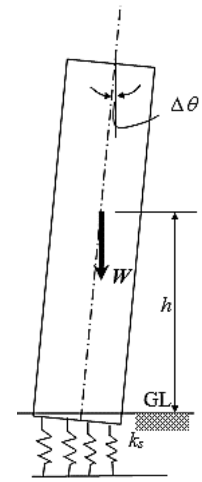

Figure 5. Model for leaning instability

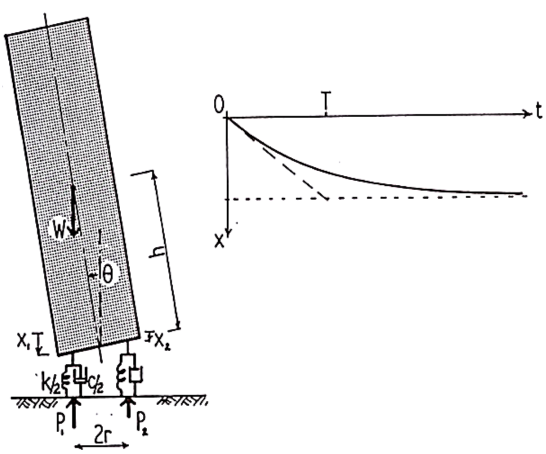

Figure 6. Kelvin–Voigt model for time-dependent behaviour of ground

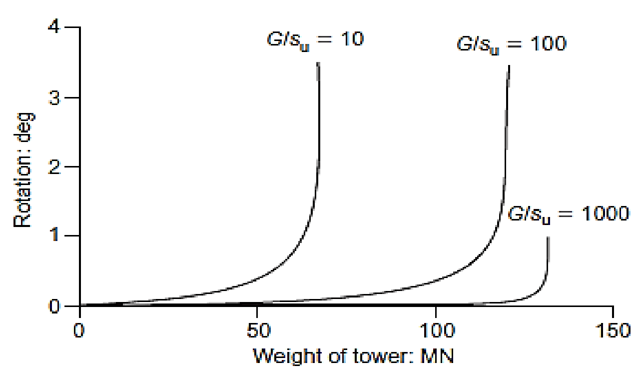

Figure 7. Rotation of tower with increase in its weight (Potts 2003)

THIN vs. THICK LAYER RESPONSES

Vertical Consolidation. Terzaghi's one-dimensional consolidation theory neglects the effect of self-weight of soil, assumes infinitesimal strain, linear relationship of void ratio and effective stress, and is valid for thin layers only. A theory of non-linear consolidation was proposed by Khan et al. (2010a) for a thick clay layer considering void ratio–log effective stress relationship by assuming (i) constant coefficient of consolidation (Madhav and Miura 2004) (the coefficient of hydraulic conductivity and the coefficient of volume change are inversely proportional to the vertical effective stress), (ii) constant thickness of clay layer, and (iii) constant initial void ratio with depth, but accounting for the variation of initial vertical effective stress with depth as an extension of the thin layer non-linear theory of consolidation developed by Davis and Raymond (1965). In the linear theory, the void ratio–effective stress relationship is considered to be bilinear with respective coefficients of volume change representing the slopes of the recompression and virgin compression lines. However, in the non-linear theory, the void ratio–log effective stress relationship is considered to be bilinear with the recompression index C_r and the compression index C_c representing the slopes of the recompression and virgin compression lines, respectively.

Figure 8(a) shows the average degree of settlement for the entire thickness of the clay layer U_s versus the time factor for vertical flow T_v (= $c_v.t/H_{dr}^2$) where c_v is the coefficient of consolidation for vertical flow, t is the time needed to complete the required degree of consolidation, and H_{dr} is the length of the drainage path (= H/2 for the case of double drainage or pervious top and pervious bottom PTPB, where H is the thickness of the clay layer). The results from the thick layer theory tend to those from the conventional thin layer theory for normalized load intensity q^* (= $q/(\gamma' H)$) $\geq$ 10,000 (i.e., for H tending to zero, thin layer). For T_v of 0.197, the degree of consolidation increases from 51% to 60% for q^* decreasing from 10,000 to 1. Thus, the theory of consolidation for thin layers underestimates the degree of settlement.

Figure 8(b) presents the average degree of dissipation of excess pore pressures for the entire thickness of the clay layer U_p versus T_v. The degree of dissipation of excess pore pressure from the non-linear theory is slower than the degree of settlement. While the degree of settlement is 51% (Figure 8(a)), the corresponding degree of dissipation of excess pore pressure is only 8% for q^* of 10,000 in thick layers, against a value of 50% from the thin layer theory, for T_v of 0.197. Thus, the conventional thin layer theory overestimates the degree of dissipation of excess pore pressures.

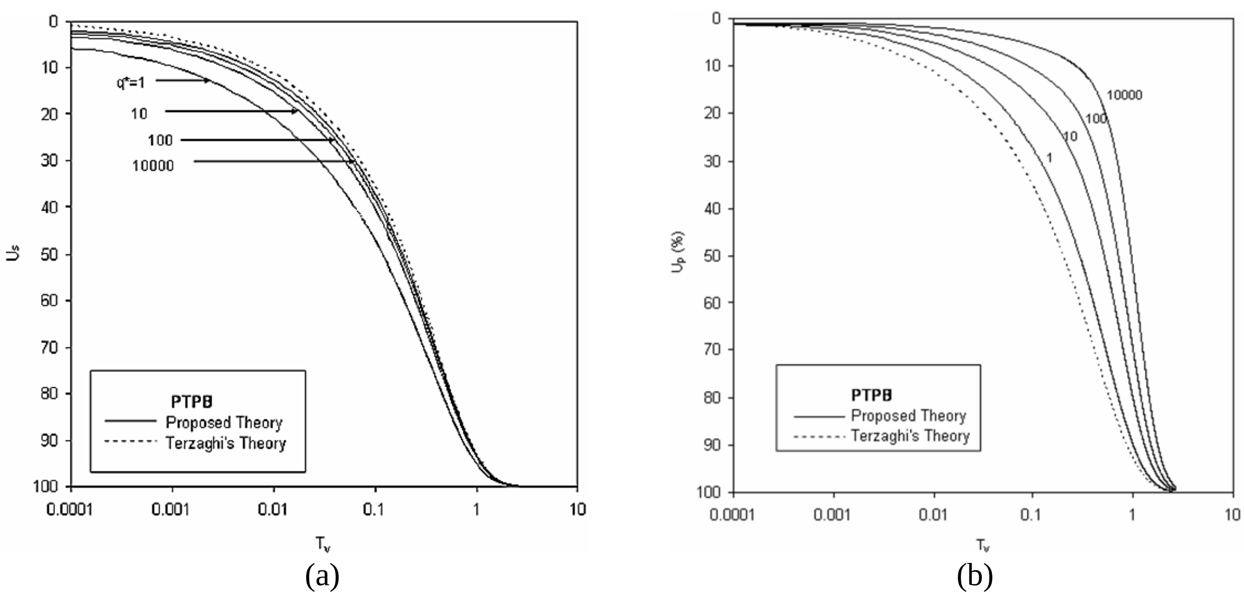

Figure 8. PTPB results: (a) degree of consolidation vs. time factor and (b) average degree of dissipation of excess pore pressures vs. time factor (Khan et al. 2010a)

Radial Consolidation. Preloading with prefabricated vertical drains (PVDs) is one of the most effective methods of soft ground improvement. The classical theory of Barron (1948) is based on the assumptions of small strains, a linear void ratio–effective stress relationship and constant coefficients of volume compressibility m_v and hydraulic conductivity in the horizontal direction k_h. However, for a relatively large applied stress range, void ratio is not proportional to vertical effective stress and the coefficients of compressibility and hydraulic conductivity decrease during consolidation. Khan et al. (2010b) developed a theory of non-linear consolidation for radial flow around a PVD in a thick deposit of clay based on the non-linear theory of consolidation for vertical flow presented by Davis and Raymond (1965). Both initial and final (initial+applied load) vertical effective stresses were considered to vary linearly with depth.

Figure 9(a) depicts the variation of σ'_f/σ'_0, the ratio of the final to the initial vertical effective stress, with normalized depth Z (= z/H) for different values of q^*. The vertical effective stress ratio σ'_f/σ'_0 decreases sharply from values as high as 21–121 near the ground surface (Z = 0.025) to 6.3–33 at Z = 0.1 for values of q^* increasing from 0.5 to 3.0. The sharp decrease of σ'_f/σ'_0 is due to the low initial vertical effective stress near the ground surface.

The decrease of σ'_f/σ'_0 with depth is significant for Z = 0.1–0.4, but is negligible for $Z > 0.4$. Hence, the effect of non-linear consolidation in a thick clay layer by PVD is pronounced at shallow depths compared to that at deeper depths. Figure 9(b) illustrates the excess pore pressure variation with radial distance at different depths for q^* = 1, n = 15 and T_h = 0.2, where $n = d_e/d_w$ (d_e is the equivalent diameter of the zone of influence of the PVD and d_w is the equivalent diameter of the PVD) and T_h is the time factor for horizontal flow.

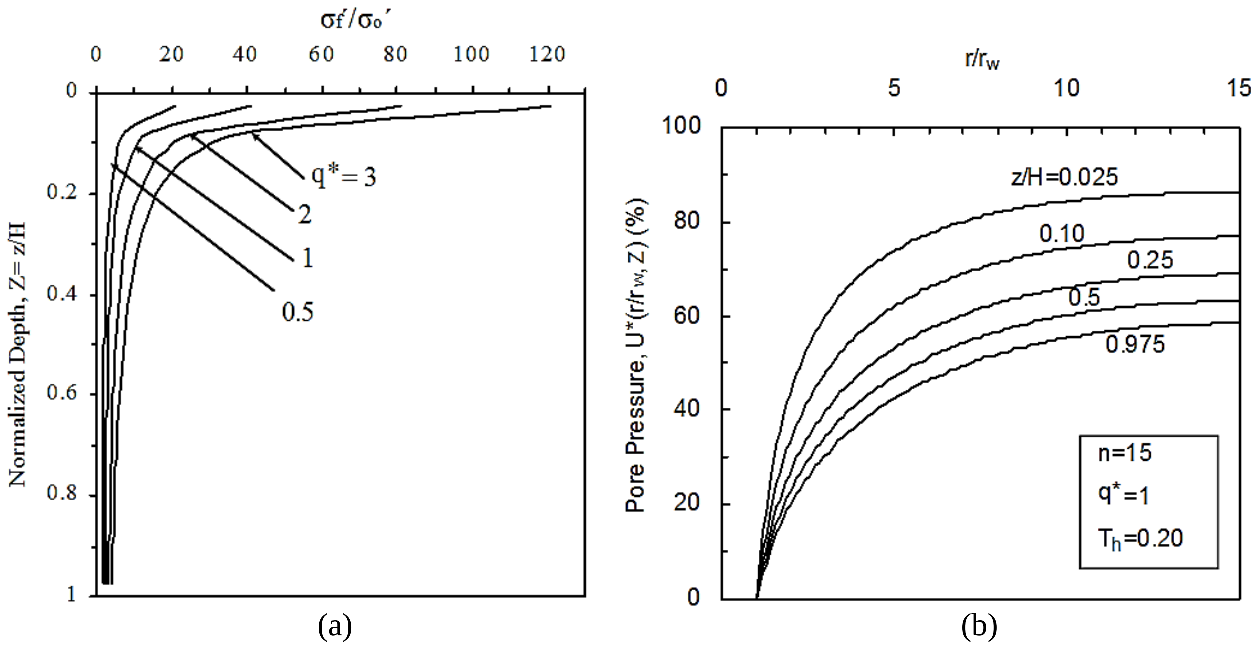

Figure 9. Results for non-linear thick layer consolidation by PVD: (a) variation of σ'_f/σ'_0 with depth (Khan et al. 2009) and (b) variation of excess pore pressures with radial distance – effect of depth (Khan et al. 2010b)

r/r_w = 1 corresponds to the edge of the PVD while r/r_w = 15 corresponds to the edge of the unit cell. The normalized excess pore pressure U^* (= u/u_0, where u_0 is the initial excess pore pressure) is relatively large at shallow depths where σ'_f/σ'_0 is extremely large, but decreases with depth since σ'_f/σ'_0 also decreases. The excess pore pressure variation with radial distance r is relatively more significant in the upper half of the deposit compared to that in the lower half. At the edge of the unit cell (r/r_w = 15) and for T_h of 0.2, U^* decreases from about 87% near the ground surface to 63% at Z = 0.5 and to about 58% near the bottom of the deposit (Z = 0.975).

GEOTECHNICAL vs. MEDICAL PRACTICES

Several similarities can be observed between the practices of medicine that deals with the human body and geotechnical engineering that deals with the ground. Firstly, both are not manufactured to specifications, though off late, cloning is becoming possible. Secondly, both the human body and the ground have evolved over long periods of time, by natural evolution in the case of the former, and by geological processes in the case of the latter. A human being has the usual set of organs, limbs, bones, and muscles. While these features appear to be the same for most human beings, however, each human is very different from another because of genetics, pedigree, upbringing, parental care, and environment. Thus, we have extroverts or introverts, traits such as sad/happy, helpful (friendly), neutral or unfriendly, and positive or negative attitudes. Likewise, soil can be characterized as porous, saturated/unsaturated, non-homogeneous, anisotropic, inelastic (elasto-viscoplastic), dilatant, sensitive, with failure state varying from brittle to ductile, and a material with memory (preconsolidation stress, overconsolidation ratio).

While there are several parallels between the practices of medicine and geotechnical engineering (Madhav and Abhishek 2016), there are, however, some major differences:

1. In medicine, the patient goes to a doctor, whereas, a geotechnical engineer has to go to the site to diagnose the problem.
2. The patient talks to the doctor, whereas, a geotechnical engineer listens to the ground.
3. The failures of doctors are often buried or cremated in the ground, whereas, the successes of geotechnical engineers get buried and failures show up glaringly.
4. Doctors are paid much more handsomely than geotechnical engineers.

CONCLUDING REMARKS

Some perspectives in forensic geotechnical engineering that need to be considered are presented. Consideration of the height of a tall structure rather than just the bearing capacity of the foundation leads to an interesting failure mechanism termed leaning instability that is governed by the compressibility of the ground rather than its strength. The non-linear, thick layer theory of consolidation indicates that the conventional linear, thin layer theory underestimates the degree of consolidation and overestimates the degree of dissipation of excess pore pressures. The non-linear theory for radial flow into PVDs has similar effects on the degree of settlement, degree of dissipation of excess pore pressures and variation of excess pore pressures with respect to time, radial distance and depth. An interesting outcome is the induced vertical flow in a radial flow problem. In sum, if important mechanisms or responses are not taken into account during a forensic geotechnical investigation, then the predicted cause of failure would be completely different to what the real cause actually might have been.

REFERENCES

Barron, R. A. (1948). “Consolidation of fine-grained soils by drain wells.” *Transactions, ASCE*, 113(1), 718–742.

Cheney, J. A., Abghari, A., and Kutter, B. L. (1991). “Stability of leaning towers.” *Journal of Geotechnical Engineering, ASCE*, 117(2), 297–318.

Davis, E. H., and Raymond, G. P. (1965). “A non-linear theory of consolidation.” *Geotechnique*, 15(2), 161–173.

Gray, J. (1992). *Men are from Mars, Women are from Venus*. Harper Collins, London.

Hambly, E. C. (1985). “Soil buckling and leaning instability of tall structures.” *The Structural Engineer*, 63A(3), 77–85.

Hambly, E. C. (1990). “Overturning instability.” *Journal of Geotechnical Engineering, ASCE*, 116(4), 704–709.

Khan, P. A., Madhav, M. R., and Reddy, E. S. (2009). “Non-linear theory of consolidation of thick clay layer by PVD.” *International Symposium on Ground Improvement Technologies and Case Histories*, Singapore, 337–344.

Khan, P. A., Madhav, M. R., and Reddy, E. S. (2010a). “Simplified non-linear theory of vertical consolidation of thick clay layers.” *Indian Geotechnical Conference*, Mumbai, 921–924.

Khan, P. A., Madhav, M. R., and Reddy, E. S. (2010b). “Consolidation of thick clay layer by radial flow − non-linear theory.” *Geomechanics and Engineering*, 2(2), 157–160.

Lancellotta, R. (1993). “Stability of a rigid column with non-linear restraint.” *Geotechnique*, 43(2), 331–332.

Madhav, M. R., and Abhishek, S. V. (2016). “Ground versus soil: a new paradigm in geotechnical engineering education.” *International Conference on Geo-Engineering Education (TC 306) - Shaping the Future of Geotechnical Education (SFGE)*, Belo Horizonte, Brazil, DOI:10.20906/CPS/SFGE-09-0002.

Madhav, M. R., and Miura, N. (2004). “Phase transition effect on preconsolidation stress of soils.” *Indian Geotechnical Journal*, 34(1), 80–95.

Potts, D. M. (2003). “Numerical analysis: a virtual dream or practical reality?” *Geotechnique*, 53(6), 535–573.

Terzaghi, K. (1943). *Theoretical soil mechanics*. John Wiley & Sons, New York.

Terzaghi, K., and Peck, R. B. (1967). *Soil mechanics in engineering practice*. Wiley, New York.

Vesic, A. S. (1973). “Analysis of ultimate loads of shallow foundations.” *Journal of The Soil Mechanics and Foundations Division*, 99(1), 45–73.

Deployment of civil engineering expertise during crises – Experiences in the Netherlands

Ton Peters and André Koelewijn.[1]

[1]Deltares, Department of Geo-Engineering, P.O. Box 177, 2600 MH, Delft, the Netherlands;
E-mail addresses: ton.peters@deltares.nl and andre.koelewijn@deltares.nl

ABSTRACT

Modern societies are complex and depend largely on the proper functioning of the Critical Infrastructure (CI). A crisis is an unpredictable event that can lead to a disruption of CI and the functioning of society. In order to save lives and limit damage, decisions have to be taken under stress and time pressure while the situation is still very uncertain and so require a special approach to answering the relevant civil engineering questions. In the Netherlands, Deltares is on 24/7 stand-by to provide this technical assistance. The introduced SQD procedure is an approach for crisis management meetings that makes it possible to quickly get a mobilized expert team into the action phase to answer these questions. This is illustrated by two examples. The main conclusion is that deploying civil engineering expertise rapidly, as part of the crisis management, contributes significantly to limit the consequences for society.

INTRODUCTION

Modern societies are complex and depend largely on the proper functioning of the Critical Infrastructure (CI). A nation's CI provides the essential services that underpin society and serve as the backbone of the economy, security and health. Overall, 16 types of CI sectors can be delineated that compose of assets, systems and (physical and virtual) networks. The interdependencies between CI can cause so-called cascading effects, where for example a disaster like a local dike failure results in flooding of a high voltage transformer unit which then causes power blackout in a whole region leading to disruptions of telecommunication, transport and public services.

In this paper, the focus will be on four sectors that show the most civil engineering challenges, i.e. the water, energy, urban and transport sectors. These CI are all either built on the subsurface or in the subsurface and often also use material from the subsurface as building material. The subsurface itself can also be part of potential hazards, e.g. in case of landslides and earthquakes.

Table 1 presents an overview of the CI considered and the possibility of impact of natural disasters, extreme weather events and man-made hazards.

Table 1. Possibility of impact (x) of hazards on Critical Infrastructure

		Natural disasters			Extreme weather events			Man-made hazards		
	Critical Infrastructure (CI):	Flooding	Landslides	Earthquakes	Coldwaves, icing, snow	Heat waves, droughts	Storms, tornadoes	Fire and explosion	Crime and terrorism	Construction failure
Energy	Oil and gas production	X	X	X			X	X	X	X
	Electricity generation and transmission	X	X	X			X	X	X	X
	Distribution electricity, oil, gas	X	X	X			X	X	X	X
Water	Drinking-water and sewage system	X	X	X	X	X	X	X	X	X
	Surface waters	X	X	X	X			X	X	X
Urban	Public buildings, offices	X	X	X				X	X	X
	Monuments, historic buildings	X	X	X	X	X	X	X	X	X
	Resident housing	X	X	X				X	X	X
	Underground construction	X	X	X				X	X	X
Transport	Road & Rail	X	X	X	X	X	X	X	X	X
	Airports	X	X	X	X	X	X	X	X	X
	Ports and inland waterways	X	X	X	X	X	X	X	X	X
	Pipelines	X	X	X				X	X	X

The water, energy, urban and transport sectors are essential for the quality of life and vital for the competitiveness of Europe. In 2006 the European Commission adopted the European Program for Critical Infrastructure Protection (CIP), to support the member states in building a more resilient society and to improve on contingency planning. This resulted in 2008 in the Council Directive on the identification and designation of the European critical infrastructures and the assessment of the need to improve their protection. Building a more disaster resilient society is a major task for the European countries. For example the Netherlands alone are already planning to invest € 20 billion in the next 30 years (Delta Program) to maintain safety against flooding.

In order to stimulate knowledge development on Critical Infrastructure Protection, the European Commission has developed research programs on this topic. In several of these projects Deltares is involved, one of them being the INTACT project (2014-2017). INTACT addresses these challenges and demonstrates in five countries, methods to assess the impact of natural disasters and extreme weather events, the design of protective measures and the crisis response & recovery capabilities. Findings of the project will accumulate in the INTACT Reference Guide, that will support decision makers, owners and operators to protect their CI.

These ongoing developments increase not only the need to mitigate the impact of hazards but also require capabilities for immediate action in case of an emergency in order to save lives, limit the damage and return to the normal operational state effectively and as soon as possible.

CRISIS MANAGEMENT

A crisis can occur as a result of an unpredictable event (e.g. a natural disaster) that within a small time frame leads to a disruption of the functioning of society. It requires decisions on remedial actions to be taken quickly to save lives, to limit the damage and return to the normal state effectively. These decisions are taken under stress and time pressure, while the situation is still very uncertain and only limited information is available. Technical expertise is needed to answer the civil engineering questions, which are often very relevant during a crisis caused by a natural disaster, extreme weather event or failure of a construction.

Crisis management is the application of strategies designed and prepared to help an organization deal with a sudden and significant negative event. In crisis management theory, four stages are delineated, see Figure 1:

1. ***Mitigation***: this is the stage where measures are designed and implemented to prevent a crisis from happening, thus increasing societal resilience.
2. ***Preparedness***: during this stage the responsible organization develops effective action plans to execute when a disaster strikes. The action plans are based on scenarios describing possible crises and are detailed accordingly to support the staff during the crisis situation. Crisis response (mock up) exercises are also important for this stage to train staff and to test and improve the action plans. Details (e.g. alarm procedures, names of key staff, telephone numbers and access codes to information) in the action plans are aging so regular updating is required to stay prepared.
3. ***Response***: in this stage one responds to a crisis by mobilizing key resources, emergency services and first responders to deal with the situation, focusing on saving lives and limiting damage. Each team has specific tasks at different levels in the crisis management organization and is led by a team leader. Especially the collaboration between different response teams from different organizations and adequate communication of information is crucial and challenging given the stress and (time) pressure the teams face.
4. ***Recovery***: after response, this stage deals with restoring the original situation. In practice the distinction between the response and recovery stage can be vague. Many issues can come up during the recovery stage involving many more parties, for example because of investigation into the cause of the incident, liability issues and the cost of recovery. While response is often a fast stage, the recovery stage may take a long time depending on the scale and complexity of the crisis at hand.

Figure 1. Four stages of crisis management

24/7 EMERGENCY RESPONSE

As part of an agreement with the Dutch Ministry of Infrastructure and the Environment, Deltares is on 24/7 stand-by for emergency response. Should a crisis arise within the Deltares fields of expertise (i.e. water, subsurface and infrastructure), experts are available to provide technical assistance. The Deltares team is part of a much larger crisis management organization that, depending on the scale of the crisis, is activated on a local, regional or national level.

Within an hour after the alarm, a small Deltares team is formed consisting of a team leader, a department manager, a communication officer and a supporting secretary. This small team performs a first assessment of the situation and the questions that need answering. In the next phase the team is scaled up bringing in Deltares staff that has the expertise and (local) experience to deal with the identified civil engineering questions and recommend on measures to be taken. In a crisis, several groups of experts can be mobilized to work simultaneously on different questions. The team leader is responsible for the organization of this process and delivering results (i.e. advice on technical questions) within the given time period, sometimes only a few hours. The major dilemma is that on the one hand the results needs to be accurate and boundary conditions well defined but on the other hand the given time deadline has to be met under all circumstances. Each year several mock exercises are conducted to train Deltares staff and maintain a sense of vigilance.

One of the facilities used during crisis is the iD-lab (see Figure 2), an interactive data research laboratory, which combines and displays big amounts of data and brings together models, visualization techniques and expert knowledge. A major advantage is that the available information can be presented quickly to the whole team for a common analyses of the situation.

Figure 2. The iD-Lab: a Deltares facility on handling big data and operational forecasting

Next to that, the team uses the practical **SQD** procedure: a 3-step method of **S**ituation assessment, **Q**uestion analyses and **D**ecision taking. The SQD procedure is our standard approach for a crisis management meeting that, when trained well, makes it possible to get a mobilized expert team into the action phase within 30 minutes. In the action phase the team will work out advices on the formulated civil engineering questions and report about that. After quality control this advice is communicated to the crisis management organization.

In the SQD meeting the team will (i) acquire a **common** understanding of the crises situation based on controlled information, (ii) identify and prioritize the civil engineering questions and (iii) the team experts will know when they have to deliver advice about these questions. The Deltares team consists, next to the team leader, of a plotter, a communication officer and several experts. The team is arranged in the meeting in a half circle setting that allows easy contact between team members while facing the iD-lab screens and three white boards, entitled: **S**ituation, **Q**uestions and **D**ecision. The iD-lab screens are used to display maps, weather and flood forecasting and a communication channel with the crisis management organization (InfraWeb).

In Table 2 the main discussion items for the meeting are presented. During the meeting chaired by the team leader, the plotter will visualize the information on the appropriate whiteboard to help create a common understanding, to structure the discussion and to focus towards the goal of the meeting. The communication officer will keep a log, monitor incoming information and after the meeting prepare outgoing communication with the team leader.

Table 2. SQD procedure for a crisis management meeting

Situation assessment	Question analyses	Decision taking
▪ Current and expected situation (including timeline) ▪ Network analyses (who is involved?) ▪ Problem definition and prioritization ▪ Immediate no-regret measures	▪ Question 1 (facts, measures) ▪ Question 2 (facts, measures) ▪ Question 3 (facts, measures) ▪ …….. ▪ Resources check: do we need more experts, information, etc.?	▪ What questions to answer? ▪ Remaining questions ▪ Actions ▪ Communication ▪ Team check: does everybody know what to do next?

CASE HISTORIES

From the various crisis situations of the past years that have helped to shape and improve the presented SQD procedure and iD-Lab, two are highlighted here.

Flooding of an urban area at Wilnis.

On the 26th of August 2003, in the middle of the night, a sudden breach occurred in a regional dike in the village of Wilnis, close to Amsterdam. The failure of this 6 m high dike, mainly consisting of peat, flooded an urban living area and emptied the canal in front of the dike. By rapid response, a dam was constructed by dumping clay from a nearby bridge, within two hours after the breach. This prevented the inflow of some 250,000 m^3 of water from a nearby lake, which would have caused much more damage and also casualties, which were now prevented. At daylight, the following morning, the damage caused by the breach became more clear (Figure 3).

Figure 3. Aerial view of the dike breach at Wilnis

Over a length of about 1 km, the canal had been emptied, resulting in secondary stability failures towards the canal along the sides and on-going settlements in the area. This area is highly sensitive to even subtle changes in the groundwater table because of the thick underlying peat layer. The settlement process endangered further the already damaged gas and electricity utilities. After the immediate response to close the canal as quickly as possible, the emergency team therefore decided to:

- Monitor deformations and pore water pressures on both sides of the breach 24/7 to detect any impending additional failures;
- Cut off gas and electricity along the damaged canal section, investigate local damages and restore services as quickly as safely possible;
- Close the breach with a temporary measure to enable the safe restoration of the water level in the canal, mitigating further settlements;
- Investigate the root cause of this sudden breach.

Within a few days, a supporting bank was raised behind the dike sections next to the breach location. In about one week time, a sheet pile wall was constructed alongside the breach and the canal could be carefully refilled while monitoring deformation and pore water pressure. No further damages occurred. The cause of the breach turned out to be an exceptional dehydration of the peat dike during the previous extremely dry period and the complex geo-hydrological situation. Details on the root cause analysis are given by Bezuijen et al. (2005).

Piercing a naphtha pipeline near a canal

In the late afternoon of August 6, 2013, a drilling rig used for soil investigations near the village of Born pierced an underground naphtha pipeline between the Port of Rotterdam and a large chemical plant in the south of the Netherlands. This 10 bar pressure pipeline was not in use at that time because of maintenance, but it still contained naphtha, which is a poisonous fluid. A vapor of naphtha escaped to the surface, creating a dangerous situation in the immediate area around the rig. After several hours of deliberations on how to handle this situation, with a pressing economic damage in mind because management of the chemical plant demanded repair of the pipeline within 48 hours, claiming millions of euros of damage per day, the authorities realized that the incident location was very close to a canal. This canal, the Julianakanaal, is constructed above the original surface level, with steep embankments on both sides. Repair works planned could undermine the embankments and cause a flooding of the area. Next, an emergency response team was called for, which was formed according to the SQD procedure described.

A member of the team investigated the situation at the location (Figure 4), which was complicated by the presence of the vapor and the brushwood, obstructing a clear view on the situation, including lack of information on the actual distance from the incident to the dike. Yet, the information that could be obtained was sufficient to enable a supporting team to quickly perform stability calculations, indicating how to proceed with this situation. Another supporting team gave advice on how to deal with the environmental issues, affecting a large area because of the high velocities in the groundwater in the gravel layers, presumably reached already by the naphtha.

Within the required time period a practical advice could be given on how to proceed with this situation: a phased excavation of the affected area after removal of the rig by heavy lift equipment operating from outside of the vapor-affected area, repair of the pipeline and backfilling including periodic 24/7 visual inspection of the embankments. Meanwhile, an alternative route had been found to provide the chemical plant with naphtha.

Afterwards, it was found out that the rig had been operating outside its designated area: the drilling location actually used, about 10 m away, allowed for much easier access.

Figure 4. Location of the incident showing the drilling rig and the brushwood (left) and an aerial overview after clearing during refilling (right)

CONCLUSIONS

Natural disasters, extreme weather events and man-made hazards can disrupt the Critical Infrastructure and the functioning of society. It is shown that deploying civil engineering expertise rapidly, as part of the crisis management, contributes significantly to limit the consequences for society. In the Netherlands, the 24/7 stand-by of technical assistance by Deltares provides support during the response and recovery stage of a crisis. From the cases the following lessons are learned:

- Crisis management procedures are important, but also improvisation capacity is needed.
- Preparation (action plans) and training is very important to maintain vigilance.
- During a crisis, many organizations with different interests become involved. A clear mandate and proper communication is crucial.

REFERENCES

Bezuijen, Adam, Kruse, Gerard A.M., and Van, Meindert A. (2005). "Failure of peat dikes in The Netherlands", *Proc., 16th Int. Conf. on Soil Mech. and Geot. Eng.,* Osaka, Millpress, Rotterdam, 1857-1860.

European Commission – Migration and Home Affairs http://ec.europa.eu/dgs/home-affairs/what-we-do/policies/crisis-and-terrorism/critical-infrastructure/

Government of the Netherlands – Delta Program https://www.government.nl/topics/delta-programme

INTACT (2014-2017) http://www.intact-project.eu/ this project receives funding from the European Union Seventh Framework Program (FP7/2007-2013).

US Department of Homeland Security https://www.dhs.gov/what-critical-infrastructure

CAPWAP Complexities and Case Studies for Pile Foundation Testing in India

Ravikiran Vaidya[1], and Sujan Kulkarni[2],

[1]Principal Engineer, Geo Dynamics, 49, Atmajyoti Nagar Society, Ellora Park, Vadodara, India; e-mail: ravikiran@geodynamics.net
[2]Senior Manager (Technical), Geo Dynamics, 49, Atmajyoti Nagar Society, Ellora Park, Vadodara, India; e-mail: sujan@geodynamics.net

ABSTRACT

Bored pile foundations typically range from 300mm to 2m diameter and are installed in a variety of soils. Since they are under-ground and are installed with various techniques, methods and with fast track construction being a norm, QA/QC becomes a vital requirement for bored piles before acceptance. In addition to conventional static load tests which yield little information on failures, High Strain Dynamic Pile Testing (HSDPT), Low Strain Integrity Testing (LSIT), Cross Hole Sonic Logging (CSL), Parallel Seismic Method provide substantial information on quality and capacity of bored piles. The methods have also been extensively used for forensic engineering purposes to investigate the quality, reasons for failure, and also when no prior information is available about the depth or capacity of pile foundations.

Case Pile Wave Analysis Program (CAPWAP®) analysis is an integral part of High Strain Dynamic testing for bored piles. However, there is not much awareness of the complexity of the CAPWAP analysis in India, and generally, it is assumed that the initial findings as seen on field are close to the final result for the pile. CAPWAP and high strain testing require knowledge of geotechnical and structural behavior pile, soil and importantly also knowledge of wave mechanics.

This paper briefly describes the fundamental features of CAPWAP and complexities associated with it. The paper includes several case studies where HSDPT, CAPWAP and PIT were used not only for QA/QC, but also as forensic tools for pile foundations to identify failures causes. One case wherein pile foundations that were thought to be suspect were actually proven to be of good quality because of forensic engineering is also described.

INTRODUCTION

HSDPT with the Pile Driving Analyzer® (PDA) was first offered by Pile Dynamics in 1972 following a decade of pioneering research at Case Western Reserve University. Later low strain integrity testing using Pile Integrity Tester, Cross Hole Sonic Logging, and Thermal Integrity Profiling was also popularized by PDI worldwide. Today, these methods are used across six continents and in more than 90 countries.

The original research on dynamic pile testing began at Case Western Reserve University more than 55 years ago (Eiber, 1958). The Ohio Department of Transportation (ODOT) and Federal Highway Administration (FHWA) subsequently funded a project starting in 1964 for further development of the technology (FHWA Ref. Manual – Vol. 2, 2006). A detailed historical development of these technologies has been documented by Hussein (2004).

High Strain Dynamic Pile Testing along with CAPWAP was introduced to India in the later part of eighties and subsequently the first author (Vaidya, 2001, 2004) for the first time in 1998 successfully demonstrated its reliability and use for major infrastructure and real estate projects. The entire process of dynamic testing involves three phases. The first step is selection of hammer for bored piles. The second step is actual field-testing which also requires an experienced engineer to monitor the tests. If the data collection is poor and yet an output is generated then the final results have no relevance. The significance of data collection and data interpretation is adequately described by the first author and various papers as per mentioned references. The third step is post processing of data by CAPWAP analysis. For bored piles, it is mandatory that the data is further analyzed by CAPWAP to evaluate correct damping, pile profile, friction distribution etc. and only then can the correct capacity and load settlement curve is possible.

The HSDPT and CAPWAP requires expertise and practice which can generally be only obtained with dedicated analysis, sound understanding of the subject and importantly sound integrity of the engineer doing the analysis. Any intentional or unintentional error can lead to an incorrect end result, which in some cases can be significant; in many cases, data distortion or manipulation leads to loss of trust in a well developed technology. Although lots of literature is available on HSDPT, there is limited information about CAPWAP particularly in the Indian context. Hence, an effort is being made in subsequent section to elaborate the CAPWAP analysis and complexities associated with it as this has a large implication when these methods are used for forensic engineering purposes.

CAPWAP ANALYSIS AND COMPLEXITIES

CAPWAP (CAse Pile Wave Analysis Program) is signal matching procedure in which force and velocity data collected during HSDPT is imported in CAPWAP software, iterative analysis is performed to derive pile capacity, and pile profile viz. bulges, defects etc. It is standard program worldwide for the prediction of simulated static load test curve from HSDPT data. The analysis consists of adjustment of various soil parameters until measured and calculated pile top variables such as force and velocity reach a reasonable match. In other words, the method computes static and dynamic soil resistance parameters for pile along the depth and at the toe. The analysis is continued until a best possible match between computed pile top variable such as force or velocity and its measured equivalent is obtained. This can only be obtained by changing soil resistances along the pile depth based on the wave profile. Such an analysis of changing soil parameters and resistances can only be done by an engineer familiar with the pile behavior under impact. The CAPWAP is based on the wave equation model, which analyses the pile as a series of elastic segments and the soil as a series of elasto-plastic elements with damping characteristics, where the stiffness represents the static soil resistance and the damping represents the dynamic soil resistance. CAPWAP separates static and damping soil characteristics and allows for an estimation of the skin friction distribution and the end bearing component of pile. Following sections elaborate the CAPWAP in detail along with complexities associated with it.

CAPWAP performs actual calculations by dividing the pile into series of segments which are individually of uniform properties. The pile is divided into N_p segments of uniform cross section with normally ΔL = 1m length (which can be changed by user if required) such that the wave travel time of all segments is equal. The soil resistance is also divided into N_s shaft resistance forces. Refer to Figure 1 for schematic of CAPWAP model.

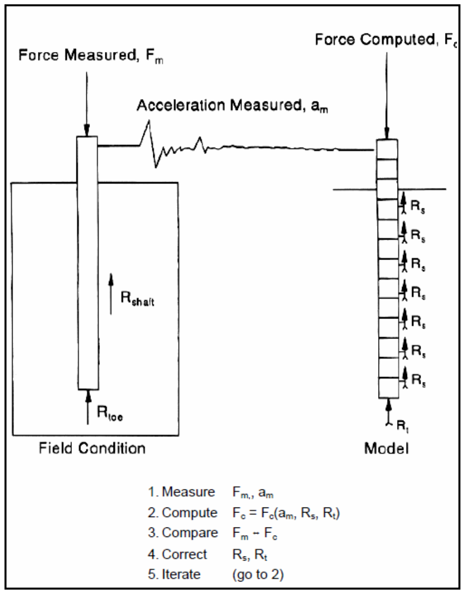

Figure 1 Schematic of CAPWAP model

The CAPWAP modeling consist of following elements: Pile profile, Slacks, Pile and soil Damping, Impedance, Toe Gap, Plugs, Radiation damping etc. These parameters are briefly explained below. Because of so much inputs and variables the analysis becomes quite complex and results in non-unique solution. However, if two individual experts perform the analysis then often it is seen that their solutions are very close and similar if not identical.

The first basic step before starting the CAPWAP program is to select a correct blow for analysis that depicts the pile behavior wherein either the pile has reached the required test load during field testing or has shown a permanent set of 4mm per blow or more possibly implying ultimate pile capacity. Once the selected blow is imported into the program the CAPWAP generated a computed force or wave-up curve based on the measured velocity curve. The program should typically be continued by adjusting the damping parameters so as to ensure that the measured and computed forces and velocity curves match reasonably. The Case skin damping is specified by Js and the Case toe damping is defined as Jt. These are related to the Smith soil damping parameters Ss and St and are provided as the original model was based on the Smith damping parameters. The analyst may also choose shaft and toe damping type options and they can be linearly viscous, smith or combination of both.

Note that an increase in damping during analysis results in a reduced capacity estimate and vice versa. There is a guideline for damping parameters and they depend more on the grain size. However, since actual pile behavior is complex and is tested generally for proof loads only, these parameters should carefully be selected based on engineering judgment and geotechnical behavior during field pile testing. The quakes also need to be computed and this requires trial and error inputs of skin quake Qs and toe quake Qt. The skin quake does not to vary too much and generally ranges from 1mm to 4mm. However, the toe quake may range from 1mm to 50mm based on pile movement and soil type.

Once the damping and quakes are modeled, it is sometimes recommended to look at confining soil resistance on the pile which can be adjusted with the radiation damping option Sk inside the software. Broadly if the pile is uniform and with no major defects, bulges or cracks, the above parameters maybe produce a good output which the CAPWAP defines in terms of Match Quality. Typically, Match quality is a number generally atleast less than 3 or 5 (Vaidya, GL, 2013). However, bored piles are rarely like pre-cast or steel piles with uniform profile and uniform material properties. In several cases, the piles may have bulges or hard layers of soil, defects or hairline cracks. The quality of the pile head may also require extensive proper modeling.

Once the soil modeling is complete, based on the understanding of wave mechanics and wave profiles, it may be required to model the pile profile by changing the pile area or elastic modulus, also called pile impedance. These parameters are useful not only in obtaining the pile profile but they also affect the unit resistance calculations. It is recommended that before changing the pile profile, information like concrete pour card, bore log data, tremie choke, delay in concrete, etc. should be reviewed. This will help better model bulges and also provide information not only about defect but the magnitude of defect inside the pile. The pile model may include tension or compression slacks to model splices or cracks. Modelling cracks or splices with slacks is not a simple task because two models exists and each model involves two unknowns. The appropriate slack model and its location has to be found by trial and error input of slack values at various elements. A typical input screen is shown below as Figure 2 and Figure 3 highlights the primary input parameters of the CAPWAP analysis.

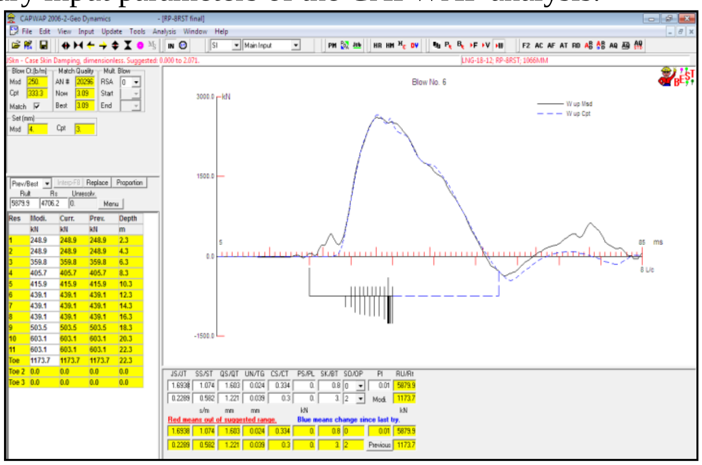

Figure 2 Typical CAPWAP input screen

JS/JT	SS/ST	QS/QT	UN/TG	CS/CT	PS/PL	SK/BT	SO/OP	PI
1.6938	1.074	1.603	0.024	0.334	0.	0.8	0	0.01
0.2289	0.582	1.221	0.039	0.3	0.	3.	2	Modi.
	s/m	mm	mm		kN			

JS/JT – Case skin and Case toe damping parameter; QS/QT – Skin and toe quakes
SS/ST – Smith skin and Smith toe damping parameter; UN – skin friction unloading limit
TG – Toe gap; CS/CT – Skin and toe unloading to loading quake ratio; PS/PL – Soil Plugs
SK/BT – Radiation damping and skin and toe; SO/OP – Skin and toe damping selection;
PI – Pile damping

Figure 3 Primary input parameters

For piles on a very hard end bearing layer, a gap beneath the pile toe sometime exists just before the pile toe starts to move downwards, which is known as toe gap and can be modeled in CAPWAP. Furthermore, the inertia force may be caused by the mass of the soil sticking to the pile trapped underneath or to the sides which is known as soil plug (acceleration dependant resistance) and can be modeled in the analysis if required. Other input parameters include unloading and reloading multipliers, skin and toe unloading quake multipliers etc., which make the analysis more complicated.

Thus, it is evident that CAPWAP analysis comprises of several variables for each segment of the pile that need to be modeled. . It is extremely important to keep these parameters within specified range as provided by the software based on the measured force curve, so that a meaningful and acceptable output is obtained. Each one of these parameters has certain limitations and its application directly affects the match between measured and computed wave and eventually match quality.

The effort of the analyst should be directed towards obtaining an acceptable match quality without compromising on the geotechnical or the structural behavior of the pile and this must reflect in the analysis. The CAPWAP also offers an auto match that may produce a good match quality but is not recommended for bored piles due to the complexities involved. Results with higher match quality may be acceptable with valid justifications. Thus, the CAPWAP analysis if done correctly provides useful information not only on the load settlement curve but also about friction and end bearing, hammer performance, soil behavior, pile integrity, pile stresses etc. A good forensic investigation thus will require a sound knowledge of CAPWAP in addition to field data collection with Pile Driving Analyzer. A few case studies of using the PDA/CAPWAP and other tools to investigate pile foundations are summarized below.

CASE STUDIES FOR PILE FOUNDATION TESTING IN INDIA

A project site in Cochin

For a project site located in Cochin, the subsurface conditions consist of layers of sand and clay. A generalized subsurface condition is presented as Table 1. Bored concrete piles having diameter of 800mm upto 48m length, and 1200mm upto 75m length were installed at the site. The design loads were ranged from 500tons to 1100tons depending upon diameter and depth. There were apprehensions about 75m length of pile with 1200mm as this was the first time such a long pile was installed in India.

PIT was performed on around 500 piles. PIT graph for a 75m long pile is presented in Figure 4. Generally, no major problems were reported with the PIT tests. Although L/D ratio for these long piles was quite high (i.e. around 62), satisfactory data was collected using PIT. Here it is important to note that it is possible to test long piles with PIT even though old literature suggests that testing is possible upto an L/d ratio of 25-30. There is no rule of thumb for L/d ratio and it depends on the soil and pile profile. Soils with high resistance and/or piles with major bulges are difficult to evaluate even for low L/d ratio of 20, whereas uniform piles with low resistance for significant depth can be evaluated even for longer lengths as seen in the current case.

Table 1 Generalized Subsurface Profile – A project site in Cochin

Layer No.	Soil Type	Depth (m)		Layer No.	Soil Type	Depth (m)
1	Fill	0-0.75		7	Medium Stiff Clay	33-41
2	Soft Clay	0.75-11		8	Dense Sand	41-45
3	Soft Sandy Clay	11-20		9	Clayey Sand	45-57
4	Sand	20-28		10	Silty Clay	57-59
5	Very Stiff Clay	28-31		11	Hard Clay	59-62
6	Medium Sand	31-33		12	Clayey Silt	62-68

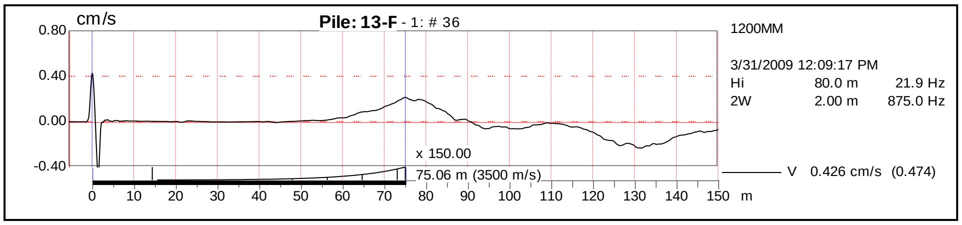

Figure 4 PIT data collected at a site in Cochin

HSDPT was also performed on 15 piles having 1200mm diameter after establishing its reliability with static load test. The reliability study was obtained by testing the same pile statically first and then with HSDPT. The study is presented as Figure 5. Eventually, HSDPT was conducted using 10.5 tons, 14tons & 22tons hammers depending on test loads and pile lengths. A photo showing HSDPT in progress is shown in Figure 6. The graphical output of CAPWAP performed on the one of the routine pile is shown in Figure 7.

All the tested piles were able to achieve the required test load. Thus, it was proved that testing of long piles is possible with the non destructive testing methods. Correlations validated the results. The methods also helped prove that the piles were of acceptable quality and capacity. There was significant savings in time with the use of High Strain Dynamic testing instead of conventional static load testing.

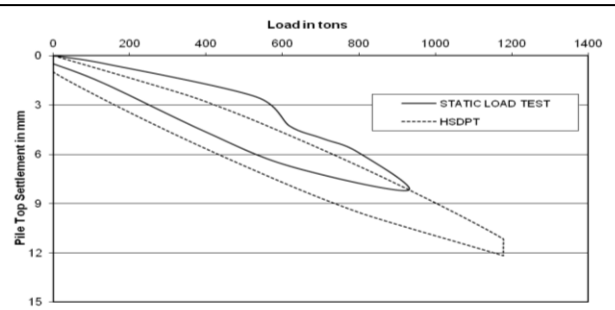

Figure 5 Correlation Study

Figure 6 HSDPT in progress

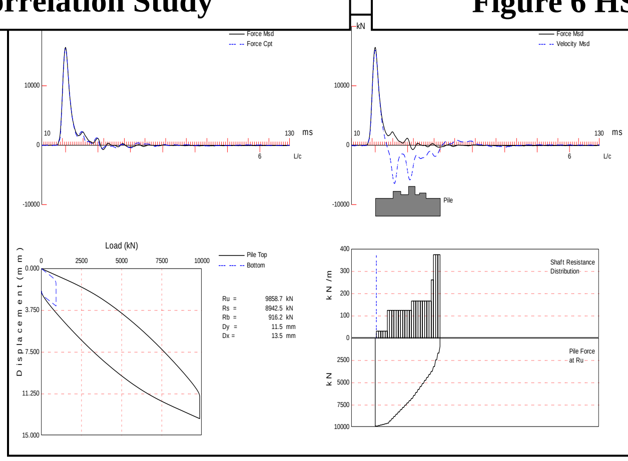

Figure 7 CAPWAP output for typical pile

Testing of Pile Foundations at a site near Vadodara, Gujarat

More than 500 piles were installed at a project site near Vadodara, Gujarat. About 98 sets of the cube test results for the piles passed 7 day tests but failed 28 day tests. The design concrete grade was M30. Results of 9 sets were in the range of 19-22N/mm^2. Results of 36 sets were in the range of 23-25N/mm^2. Results of remaining 53 sets were >25N/mm^2 but <30N/mm^2. Hence, pile concrete quality was questioned and client wanted to evaluate the matter further. The objective was to assess pile foundations due to inconsistent cube test results. The authors were engaged as experts to provide inputs and to help the contractor correctly assess the piles.

Since large number of cubes failed 28 days test, the authors suspected several issues rather than mere focus on concrete quality. Some of the issues were a) Test results depend on proper representative sampling, 2) Handling, 3) Curing, 4) testing procedure, 5) size and shape of mould etc. It was also observed that not all the cubes in a batch had failed but only certain cubes in each batch failed.

Hence, High Strain Dynamic Testing and PIT was suggested to evaluate the concrete and the piles. Thirteen piles were tested using HSDPT followed by CAPWAP. The pile design load was 150 tons and the piles were tested to more than 375 tons to be sure that concrete was acceptable. The CAPWAP showed uniform pile profile and a minimum wave speed of 3400m/sec. Thus, no structural or geotechnical failure was noticed at more than 2.5 times the design load indicating the piles and the concrete was within acceptable range. The maximum stresses in the piles at design load and test load of 375 tons was 5Mpa and 13Mpa. This was much lower than the worst cube test results even assuming concrete was of lower quality. The wave speed although did not indicate any lower quality concrete. The concrete consumption record for the piles indicated overpore and the ratio was 1 to 1.2. Thus under-consumption was not an issue. Static load tests also showed acceptable piles.

Thus all available information and investigations indicated acceptable concrete and acceptable piles. The results of testing were also validated by a reputed European testing company. It was proved failed cube test results does not imply poor pile concrete and vice versa is also true. Cubes test results only provide information about consistency of concrete obtained from batch mix plant and preliminary information on concrete quality. It should be noted that for piles, cube test results are not sufficient to evaluate pile quality but their integrity and capacity are the most important considerations. Inspite of all these supporting facts, client asked contractor to prove that the grade of concrete is M30 up to pile bottom for all the piles. The client then rejected all the piles. This adamant approach by client resulted in huge delays and expenses for the contractor. It also resulted in huge waste of precious natural resources inspite of all the forensic investigations

A Project in Northern India

At a project site in Northern India 1500mm and 1600mm diameter piles were installed. The depth of the piles ranged from 40m to 48m. The proposed construction method was top down construction and after the piling was completed, piles were partially exposed in order to serve as building columns. As described in geotechnical report, the soil at the site consists of alternating layers of clayey silt and sandy silt up to the exploration. A plot indicating variation of SPT along the depth is shown as Figure 8.

The design loads on the piles were 1250tons and 1425tons for 1500mm and 1600mm piles respectively. Since this was a fast track project and only had 54 piles, the contractor was not keen to conduct any testing and representations were made accordingly. An opinion was sought from the first author who recommended that atleast 2 load static or dynamic load tests and few integrity tests should be conducted as there was no such precedence in the region of such large diameter and large ultimate load of 3000 tons or more. Hence it was agreed to conduct tests eventually. . The first author team conducted PIT on all the piles and also three dynamic load tests. From the data, it was apparent that some of the piles have defects. A typical PIT data for a defective pile and confirmation of defect after excavation is shown in Figure 9.

Three piles of 1600mm diameter and two piles of 1500mm diameter were selected for dynamic testing. Four pairs of strain gages and accelerometers were attached to the pile head at 90^0. A 35ton hammer was used for testing. A picture showing HSDPT in progress is shown in Figure 10. All the tested piles were unable to achieve the required test load and settlement of piles were more than 3mm per blow for several blows indicating piles have reached ultimate capacities. Three of the piles did not achieve even design load, also showed major defects, and may have been one of the causes of failures. A third party also validated the CAPWAP test results as the report had huge cost and time implications to the project. A typical graphical output of CAPWAP is shown as Figure 11. A static load test also indicated similar results.

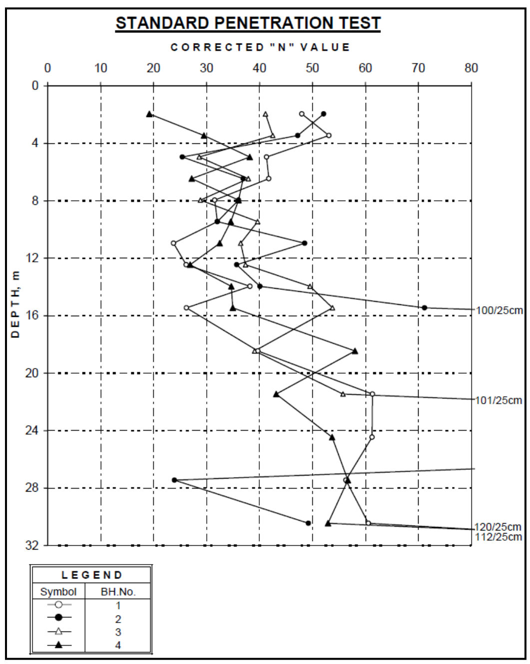

Figure 8 Variation of SPT along the depth

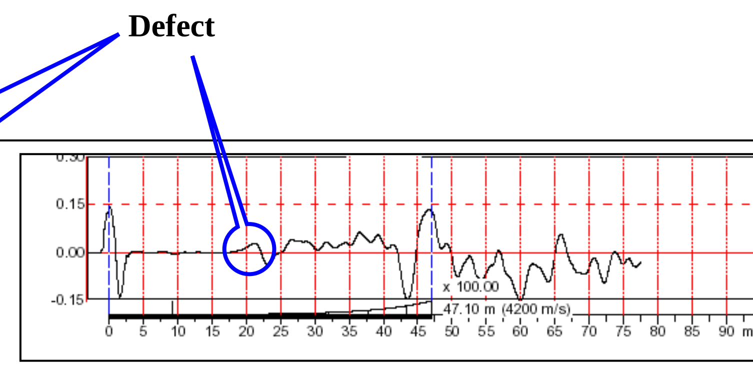

Figure 9 PIT data collected and exposed defect at a site in Northern India

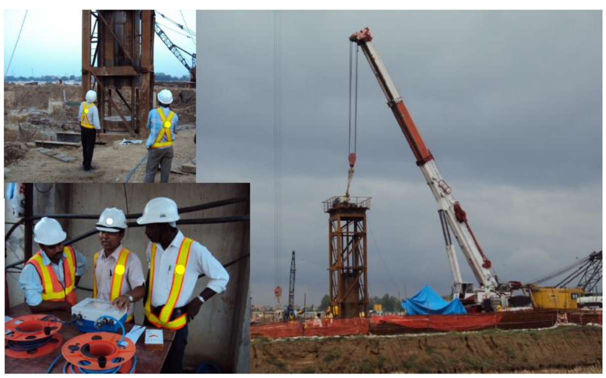

Figure 10 HSDPT using 35ton hammer

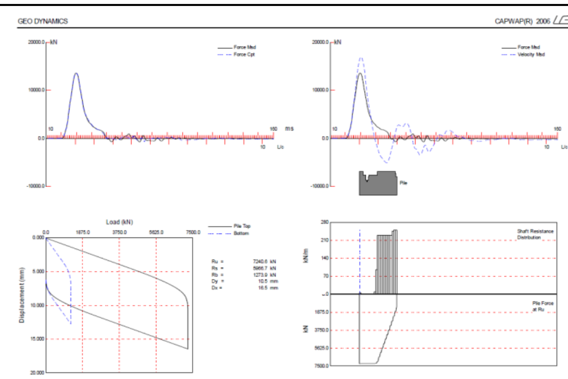

Figure 11 CAPWAP output

Since piles were unable to carry required load, safe load carrying capacity was revised and conservatively considered to be around 450tons – 500tons and the foundation type was changed to piled-raft type. The piles were exposed upto 16m and defects were visible as seen in Figure 9 and matched the PIT, HSDPT findings. . The entire project was like forensic investigation as initially not only the results were in question, eventually it was required to identify even the reasons of failure. Validation by excavation proved the findings and saved a very important structure.

A Project Site in Gujarat

For a project site located in Gujarat, it was proposed to construct residential buildings for an important government organization. . Pile foundations were adopte as the subsurface conditions consist of filled up soil up to upper 4m below which silty sand was encountered up to boring termination depth. In a central portion of the site the depth of fill was found to be as deep as 9m because a presence of a sewer line. The silty sand was loose to medium dense up to around 15m below which the silty sand was dense to very dense. A plot of SPT blowcount along the depth of exploration is presented as Figure 12. The subsurface conditions were similar across the site and soil consistency was increasing along the depth. R.C. bored piles having diameter of 400mm, 500mm and 600mm were installed at the site using truck mounted rig. The lengths of most of the piles were around 18m. The design loads were around 39tons for 400mm, 53tons for 500mm, and 68tons for 600mm piles.

This was again a project where the client had a very limited budget. So it was decided to execute the foundations without any testing. Thus cube tests, bentonite consistency tests, static or dynamic tests, PIT were all removed from the scope of the work.

After completion of piling, in some piles concrete was missing at cut-off level and sound concrete could not be located even after excavating additional 1.5m. The matter was then referred to the authors who suggested PIT on few piles including some piles that were assumed to be acceptable. The PIT results indicated several defective piles and piles with possible soft material at bottom. HSDPT was also conducted on some of the piles and the results confirmed PIT findings with several piles unable to achieve the require test load. The PIT for a typical defective pile is presented in Figure 13 and the CAPWAP results for the same pile are presented in Figure 14.

Almost 30% piles were unable to achieve required test load and most of the piles had defects from 10m-16m depth. Subsequent investigation by the first author proved that truck mounted rotary machines with wash boring is not a suitable equipment for piling in the current form. Since no bentonite consistency was maintained, slush may have remained at the bottom resulting in soft material at pile bottom. It was reported that there were water currents during piling and this might be due to the old sewerage line at 8m-9m and may also have caused subsidence of concrete at top. . The soil profile showed no specific issues and the failure was largely due to poor workmanship and poor selection of machinery for piling. Thus the complete forensic investigations including testing helped the consultants arrive at the possible causes of failure and saved a possible catastrophe.

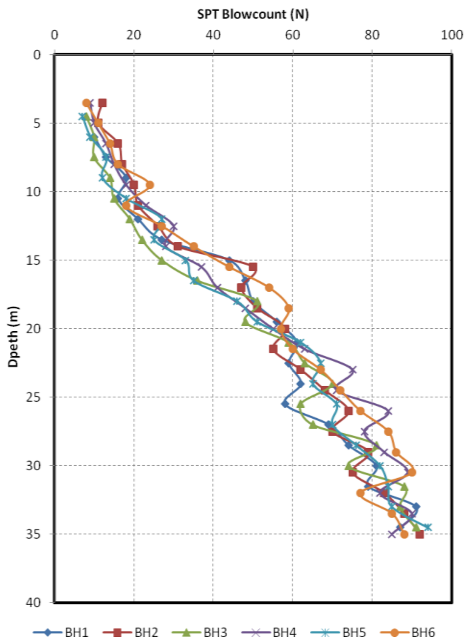

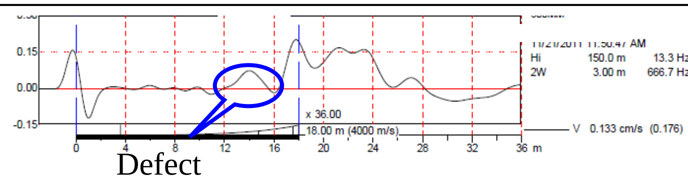

Figure 13 PIT data collected at a site in Gujarat

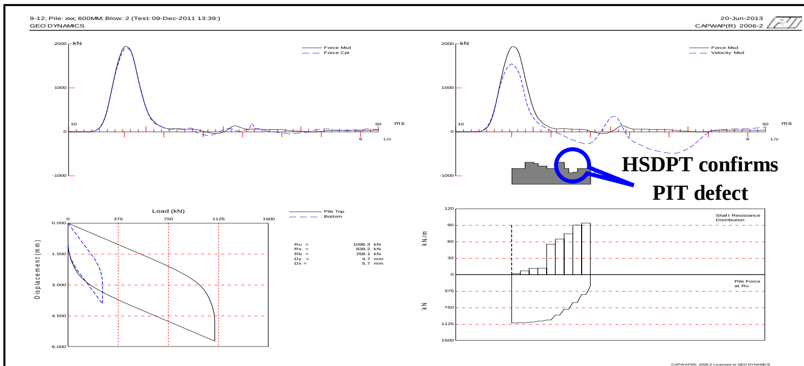

Figure 14 CAPWAP output
HSDPT confirms defect by PIT

Figure 12 SPT blowcount along the depth

A Project Site in Mumbai

At another project site located in Mumbai where rock socketed piles were proposed, the site consists of shallow rock (basalt) which was varying significantly across the site. The top of rock was varying from 4.5m to 10m. The upper soil consists of filled up material up to 2-3m followed by silty sand of varying consistency upto top of the rock. A subsurface profile is presented as Figure 15.

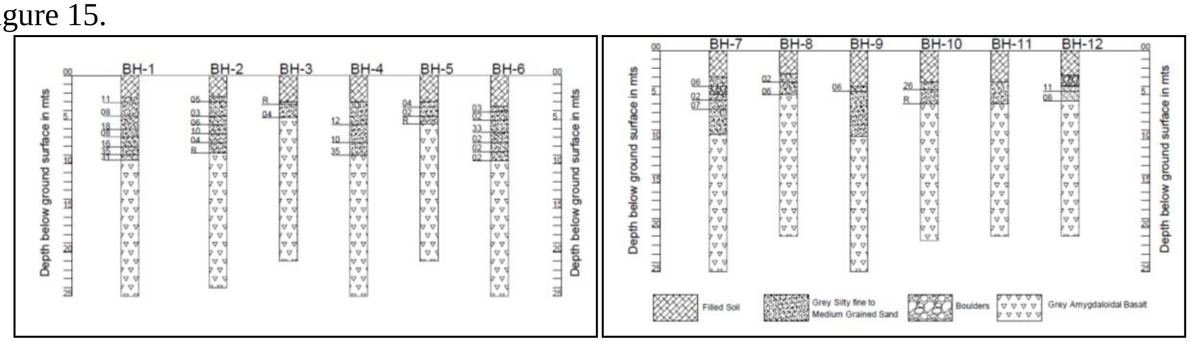

Figure 15 Subsurface profile – A site in Mumbai

Bored concrete rock socketed piles having diameter of 750mm were installed for this 45 storey tower project. The lengths of piles were varying significantly depending on depth of rock. The design load was 280tons and the test load was 420 tons for these piles. The authors were engaged at the jobsite only at the insistence of the consultants as the contractors wanted their own expert. Eventually it was agreed that the authors will perform 50% of the PIT tests. The PIT results showed soft material at pile bottom for several piles. Two such piles is presented as Figure 16. Short and defective piles were also reported. Hence, High Strain Dynamic tests were conducted on 24 piles, and for 15 piles the permanent sets ranged from 4mm to 12mm per blow and the average ultimate capacity ranged from 100 tons to 200 tons against a requirement for 420 tons.

It was then concluded that these piles are not sufficiently socketed or some collapse may have taken place after boring and before concreting and hence may not be able to achieve required capacity.

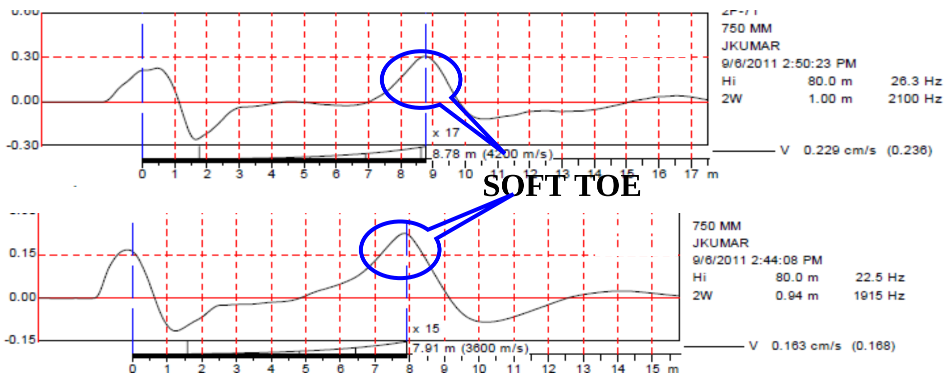

Figure 16 Soft Toe – PIT data for piles tested at a site in Mumbai

The report and findings were contested and it was agreed to core through the centre of the pile. Core test results revealed sand instead of rock. The contractor's consultants then explained that problems in the piles maybe due to soil contamination and the damage was due to Ryznar's index. The Ryznar's index was broadly explained as sudden chemical attack on concrete and subsequent deterioration. This was also contested by the first author and the independent geotechnical engineer employed by the client. It was eventually agreed to install new piles with proper rock socketing at the same site ignoring contamination issues. The additional cost of rectification exceeded Rs. 20 million. The new piles showed good integrity. Due to shortage of space, the design load was revised to 440 tons and all the new piles showed a capacity more than 700 tons with nominal permanent set. Thus forensic investigation helped prove that poor workmanship, inadequate flushing of pile bottom and perhaps termination of piles at inadequate depths during pile installation and was a major reason for failure at the jobsite.

CONCLUDING REMARKS

PIT, HSDPT, CAPWAP analysis etc. are proven tools when it comes to QA/QC practices and for forensic engineering of pile foundations. In all cases the CAPWAP was useful in evaluating actual pile capacities, pile profiles, friction, end bearing components and establishing correlations with static load tests for validation. Thus although CAPWAP theory and analysis is complex, it can also provide solutions when used effectively. There is a huge benefit to the industry if these methods are used properly. However, misuse and abuse of these methods may result in substandard foundations and loss of faith. Thus it is essential that clients and consultants understand the complexity of pile foundation and testing before using them at the project site.

The methods are almost a pre-requisite for forensic investigations in case of pile foundations. It is also important that when such an investigation is under-taken, other data like piling method, soil profile, concrete pour card, source of concrete, structural and geotechnical capacity, and any other allied information in addition to findings from HSDPT, PIT etc. be taken into account before arriving at conclusions.

REFERENCES

Alvarez C., Zuckerman B., and Lemke J. (2006).“Dynamic Pile Analysis Using CAPWAP and Multiple Sensors” ASCE GEO Congress: Atlanta, Georgia.

CAse Pile Wave Analysis Program (CAPWAP) Background Report – 2006.

Eiber, R.J. (1958). “A Preliminary Laboratory Investigation of the Prediction of Static Pile Resistances in Sand”. Master’s Thesis, Case Institute of Technology, Cleveland, Ohio.

Federal Highway Administration Reference Manual – Volume II. April 2006. Design and Construction of Driven Pile Foundations. Publication No. FHWA NHI-05-043.

Hussein, M.H., Goble, G. G., (2004). “A Brief History of the Application of Stress-Wave Theory to Piles”. Current Practices and Future Trends in Deep Foundations, Geotechnical Special Publication No. 125, DiMaggio, J. A., and Hussein, M. H., Eds, American Society of Civil Engineers: Reston, VA; 186-201.

Rausche, F., Robinson, B., and Liang, L., (2000). “Automatic Signal Matching with CAPWAP”. Proceedings of the Sixth International Conference on the Application of Stress-wave Theory to Piles: São Paulo, Brazil; 53-58.

Vaidya Ravikiran & Shah D.L.(2001), “Pile Diagnostics By Low Strain Integrity Testing”, IGC 2001, “The New Millenium Conference”, Indore, India.

Vaidya, R., (2004). “Low Strain Integrity & High Strain Dynamic Testing of Piles - an Indian Overview”. Proceedings of the Seventh International Conference on the Application of Stress Wave Theory to Piles 2004: Kuala Lumpur, Malaysia.

Vaidya, R., Likins, G.E., December (2014). “Guidelines for successful High Strain Dynamic Load Tests & Low Strain Integrity Tests for Bored Piles”. Proceedings of the Indian Geotechnical Conference 2014: Kakinada, India.

Contributed Papers

The Cause of the Collapse of Yeager Airport Extended Runway

A. S. S. Raghuram[1], S.M. ASCE, B. Munwar Basha[2], M. ASCE

[1]Research Scholar, Dept. of Civil Engineering, Indian Institute of Technology Hyderabad, Kandi, Sangareddy, 502285, Telangana, India, Email: raghuram.ammavajjala@gmail.com
[2]Assistant Professor, Dept. of Civil Engineering, Indian Institute of Technology Hyderabad, Kandi, Sangareddy, 502285, Telangana, India, Email: basha@iith.ac.in

ABSTRACT

Yeager Airport was constructed near Charleston, West Virginia, USA in the 1940's on the top of mountainous terrain. The purpose was to create an even site for the runways. The construction comprised of excavating 7 hilltops and filling nearby valleys. The airport was extended the runway to meet safety regulations. The tallest green faced geosynthetic reinforced slope (GRS) was constructed for this purpose. The geosynthetic reinforced structure is 74 meters high having a slope of 1H: 1V. A portion of the mechanically stabilized earth retention structure failed on 12th March 2015 and the spectacular slide has occurred in the Yeager Airport Expansion Runway. The slide occurred in the south side of the slope. In this paper, an outcome of the forensic analysis of an extended runway is presented. The factors of safety against overstressing and pullout failures are calculated for checking internal stability of reinforced soil slope. By using logarithmic spiral failure mechanism, the tensile strength of reinforcement necessary to maintain the stability was calculated. The possible failure mechanisms considered are: tension failure and pullout failure of the reinforcement. The field data of reinforced, retained and bearing soil zones were collected from the published literature. The paper presents noticeable reasons of failure of reinforced soil retaining wall. From the results of the analysis, it was observed that the considered long term design strength of the reinforcement (T_{all}) was more than adequate to resist the tensile failure. The results also revealed that the available length of the reinforcement was adequate to maintain stability against pullout failure.

INTRODUCTION

Steepened slopes with height more than 70 m have the benefit of increasing land usage, whereas the slope inclination is limited by the characteristics of the in situ soil shear strength. Ground improvement techniques using geosynthetics allow for the construction of slopes with steeper inclination than a natural soil slope through tensile reinforcement and geosynthetic/soil interactions. Extensive use of geosynthetics for more than 20 years to reinforce soil slopes all over the world is clearly visible. The better understanding of the mechanical behaviour of geosynthetically reinforced soil (GRS) slopes which are constructed over different types of foundation soils is necessary. This paper presents a history and forensic analysis of a spectacular slide which has occurred in the Yeager Airport Expansion Runway.

HISTORY, CONSTRUCTION AND COLLAPSE OF YEAGER AIRPORT EXTENDED RUNWAY

Yeager Airport, (formerly Kanawha Airport), construction was completed in 1947 which is present in Charleston, West Virginia. To construct a new airport in Charleston, a committee was setup to evaluate the probable site locations. Due to space constraints, the committee was decided to construct the airport on hilltops as shown in **Fig. 1**. The construction of the new airport began in October 1994. In order to get the large flat site for the airport, it required excavating 7 hilltops and filling the surrounded valleys. Finally, earthwork was completed in 1947. Behind the Panama Canal, it was reported as the second largest earth-moving project in the world at that time. The earthwork consisted of moving more than 6,881,000 m^3 of earth and rock. It required more than 907,000 kilograms of explosives for the earthwork. The project cost approximately $4.5 million, which is more than 34 times the cost of the site.

Figure 1. Yeager Airport situated on series of semi-connected hill tops know as “Coonskin Ridge. (Courtesy Google Earth, downloaded on Sep 20, 2016)

Due to the dramatic slopes of 91 m height around the airport, they could not meet with the Federal Aviation Administration (FAA) safety regulations and a few concessions were made. Finally, the airport was completed in 1947 and came into operational on December 01. Moreover, the committee decided to upgrade the Yeager airport facilities in order to meet the FAA safety regulations. For this upgradation to meet FAA safety regulations, Runway 5 required a 150 m extension as the previous runway did not include the emergency stopping area. Lostumbo (2010) reported that reinforced steepened slope was determined to be the best option for the project as it offered an economical solution. In addition, Lostumbo (2010) reported that the construction of the 1:1 reinforced slope was completed in just under 2 years, starting in the late summer of 2005 and finishing in spring 2007. On, 11th Mar 2015, the Charleston Daily Mail reported that six residents were moved out of their houses below the slope as the movement of the slope was detected. On, 12th Mar 2015, this quickly developed into a very large-scale landslide as shown in **Figs. 2, 3** and **4**. Formation of fissures before failure was shown in **Fig. 3(a)** and **3(b)**.

This paper mainly focuses on the collapse of Yeager airport extended runway. In an attempt to recognize probable causes for the collapse, a broad analytical investigation was carried out by computing the internal stability against tensile failure and pullout failure, based on the current design approaches. For the internal stability of GRS structure, safety against tension and pullout failure should be ensured for the satisfactory design. The factors of safety against overstressing and pullout failures are calculated for checking the internal stability of GRS. By using logarithmic spiral failure mechanism as reported by Basha and Babu (2012), the tensile strength of reinforcement necessary to maintain the stability was calculated. The field data of reinforced, retained and bearing soil zones were collected from published literature (Lostumbo 2010). The most likely causes about the collapse of the slope are provided at the end of the paper.

Figure 2. The failure of Yeager airport expansion runway as reported by Charleston Gazette-Mail on 12 Mar 2015
(http://www.wvgazettemail.com/article/20150312/DM05/150319672)

(a) At the base of the slope (b) Close view of the fissures

Figure 3. Formation of fissures at the bottom of the slope
(Source: Geotechpedia blog, March 20, 2015. http://blog.geotechpedia.com/index.php/2015/03/what-could-have-gone-wrong-in-yeager-airport-expansion-slide/)

Subsurface Exploration

As reported by Lostumbo (2010) the site consisted of fill, colluvial and shallow rock. Slope bearing area mainly consisted of weathered sandstone underlain by shale.

Table 1. Geotechnical properties of soil as reported by Lostumbo (2010)

Property	Value
Sand stone and Sand material Maximum Dry Density Optimum Moisture Content	 19.2 to 20.9 kN/m^3 8.3 to 11.8 %
Clay with rock fragments Maximum Dry Density Optimum Moisture Content	 17.9 to 18.8 kN/m^3 12.1 to 12.6 %
Internal friction angle of weathered sandstone	38.9^o to 39.6^o
Compressive strength of weathered sandstone	30,405 to 97,630 kPa

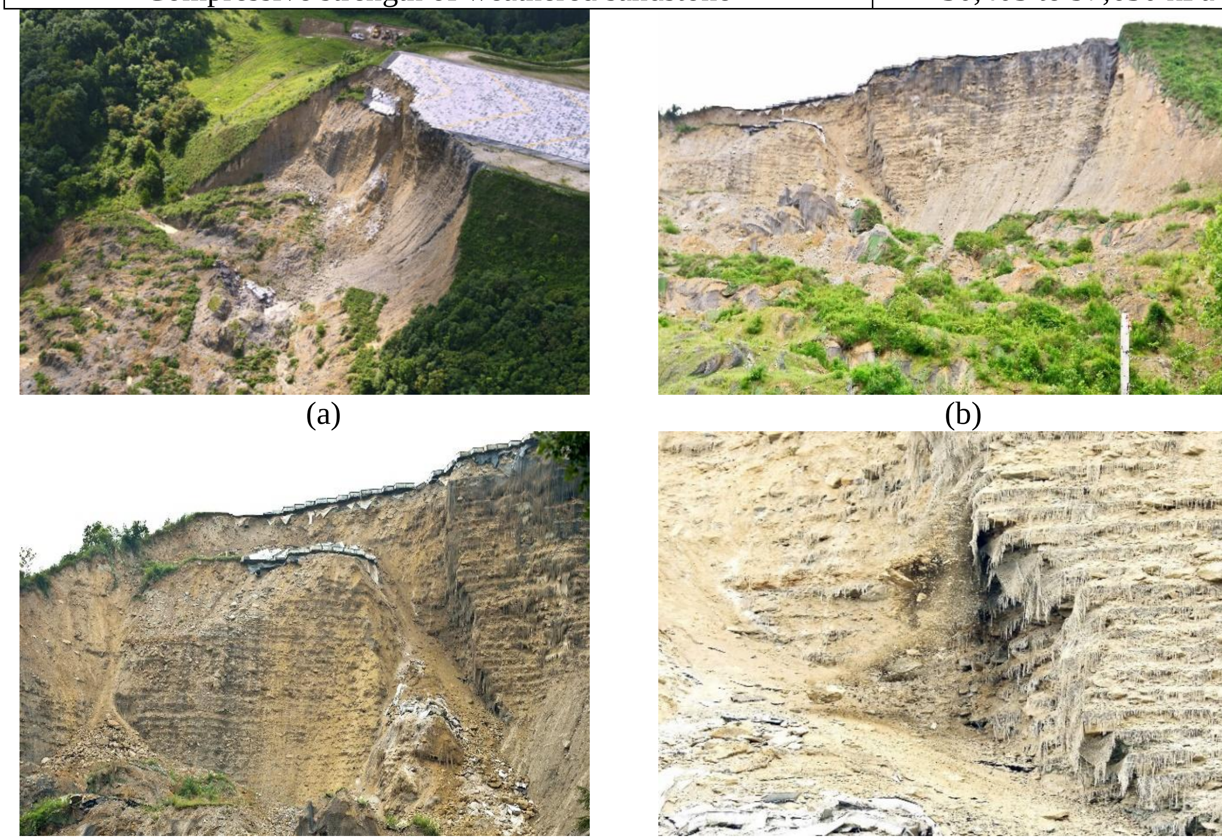

(a) (b) (c) (d)

Figure 4. Collapse of extended runway (a) View from top, (b) Long front view, (c) Close front view, (d) Failure of reinforcement

(Source: (a) Charleston Gazette Mail, Feb 24-2016, http://www.wvgazettemail.com/news/20160224/yeager-chairman-says-rebuilding-collapsed-safety-zone-airports-top-priority , (b), (c), and (d) Charleston Gazette Mail, July 15-2015, http://www.wvgazettemail.com/article/20150715/DM01/150719584/200404251)

Table 1 summarizes the geotechnical properties of the soil.

Design Considerations

The soil properties that are used in the design was categorized into three zones namely reinforced soil, retained soil, and bearing soil zones. The unit weights for the above respective zones are

18.1, 18.1, and 22.0 kN/m^3. The cohesionless is considered for all the three zones. The internal frictional angle varied as 36^o, 36^o, and 40^o respectively for reinforced, retained and bearing soil zones. Three different types of primary and secondary reinforcement of different strengths as provided by Lostumbo (2010) are adopted for the design. The long term design strength (T_{all}) of the reinforcements which are used for the design are provided in **Fig. 5.** The geogrids used were woven polyester uniaxial geogrids coated with PVC. As shown in the Fig. 3, the length of the geogrid varied from 44 m in the top 37 m segment at a spacing of 0.9 m and 53 m in the bottom 37 m of the segment at a spacing of 0.45 m. The minimum ultimate tensile strength of the geogrid reinforcement (T_{ult}) used in the three zones are 160.1, 154.5, and 123.2 kN/m respectively. The actual values of T_{ult} in the three zones are 187.9, 187.9 and 145.2 kN/m respectively. **Fig. 5** clearly shows the arrangement and placement of geogrid layers as reported by Tencate.

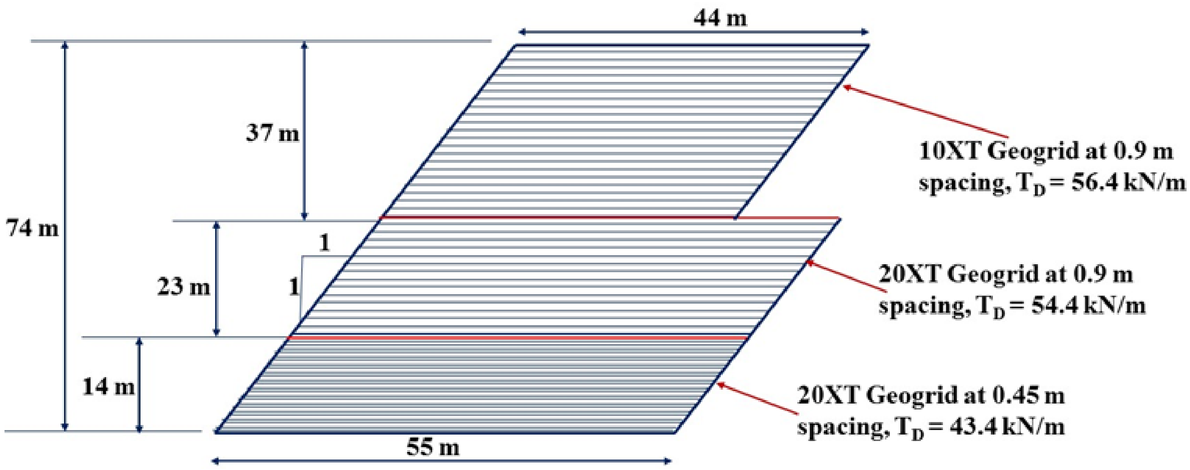

Figure 5. Cross section of Yeager airport extended runway slope (as reported by Tencate).

INTERNAL STABILITY ANALYSIS

Limit equilibrium approach is used as suggested by FHWA (2001). The analysis developed by Basha and Babu (2012) is used to calculate reinforcement force coefficient (K) to stabilize the slope. The factors of safety against tension and pullout failure modes are provided in the following sections.

Factor of Safety against Tension Failure

For the slope to be stable, the main criterion is the maximum load in the reinforcement layers ($T_{i\max}$) should be less than the design tensile strength of the reinforcement layer (T_D). The factor of safety against tension (FS_t) is given by Eq. 1.

$$FS_t = \frac{T_D}{T_{i\max}} \tag{1}$$

where $T_{i\max}$ can be calculated by using the following equation.

$$T_{i\max} = (z\gamma + q)K(S_v \times S_h)$$

Where S_v = vertical spacing $= H/n$, S_h = horizontal spacing = 1m, n = number of reinforcement layers and z = depth of layer of reinforcement.

The number of geogrid layers of reinforcement was 98 (i.e. n = 98) as reported by Tencate. As shown in Fig. 3, the spacing of reinforcement in the top 60 m portion is 0.9 m. For the remaining 14 m height of slope, the spacing is 0.45 m.

Factor of Safety against Pullout Failure

For the slope to be stable, the maximum load in the soil reinforcement ($T_{i\max}$) should be less than available resisting force (P_{ri}) on the embedded reinforcement length (L_{ei}) of the layer. The factor of safety against tension (FS_{po}) is given by

$$FS_{po} = \frac{P_{ri}}{T_{i\max}} \tag{2}$$

where $\mathrm{P}_{ri} = 2\sigma_{vi} L_{ei} \tan\delta$, $\sigma_{vi} = z\gamma$ is the effective vertical stress and δ is interface friction angle between soil and reinforcement. The available resisting force P_{ri} depends on embedded length of reinforcement as shown in Fig. 5

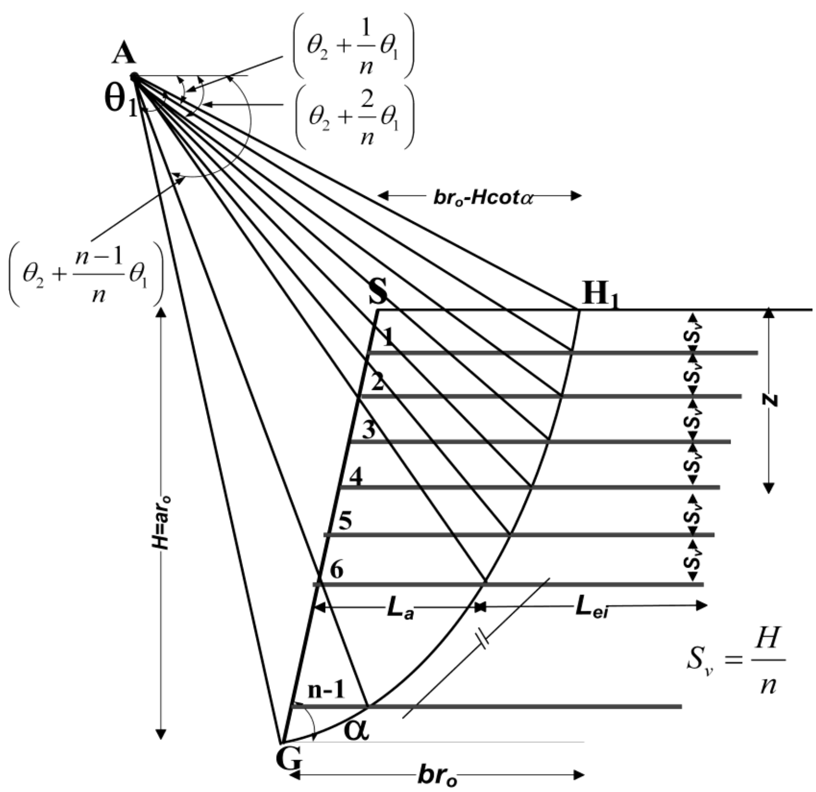

Figure. 6(a) Calculation of L_a and L_t for all layers (Basha and Babu 2012)

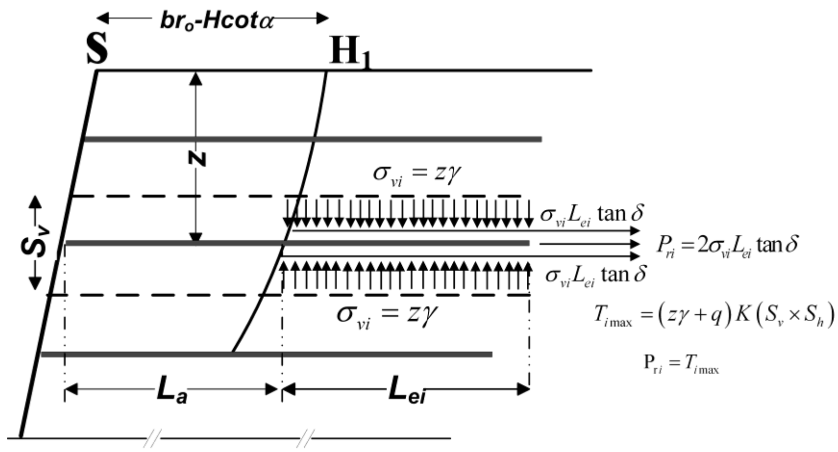

Figure. 6(b) Calculation of pullout length of reinforcement (Basha and Babu 2012)

Estimation of Total Length of Reinforcement

In the analysis logarithmic spiral failure mechanism was used. The total length of reinforcement is divided in to two parts, when the log spiral failure surface passes through the toe of the reinforced wall as shown in **Fig. 6(a)** and **6(b)**. From **Fig. 6(a)** the total length of reinforcement can be written as

$$L_t = L_a + L_{ei} \quad (3)$$

where

$$L_a = br_o - L_s - L_b,\ L_s = (H - Z)\cot\alpha \qquad \text{and } L_b = r_o \cos\theta_2 - r\cos(\theta_2 + \theta)$$

The active length of reinforcement (L_a) is obtained by maximizing the reinforcement force coefficient (K) required to stabilize the wall and it can be calculated using.

$$\frac{L_a}{H} = \frac{1}{a}[e^{\theta\tan\phi}\cos(\theta_2 + \theta) - e^{\theta_1\tan\phi}\cos(\theta_1 + \theta_2)] - (1 - \frac{Z}{H})\cot\alpha \quad (4)$$

where $\frac{Z}{H} = \frac{1}{a}[e^{\theta\tan\phi}\sin(\theta_2 + \theta) - \sin\theta_2]$ and $\theta = i(\theta_1 / n)$, i = 1 to n-1

RESULTS AND DISCUSSIONS

Checking Adequacy of Safety against Internal Stability Modes

The results of the stability analysis on the collapsed Yeager Airport extended runway are presented here. The magnitudes of FS_t and FS_{po} are computed for three different reinforcement strengths, γ = 18.1 kN/m^3, K = 0.025 (which is obtained from Basha and Babu, 2012), S_h = 1 m, tanδ = 0.486, α = 0.8, pullout factor = 0.61, ϕ = 36^o and reported in Tables 2(a) and 2(b). It can be noted from **Tables 2(a)** and **2(b)** that magnitude of FS_t with respect to depth decreases due to increase in $T_{i\max}$. Moreover, the magnitude of FS_{po} increases with depth due to increase in P_{ri} value. The increase in P_{ri} is more due to effective overburden pressure. An important observation that can be made from **Tables 2(a)** and **2(b)** that the GRS constructed for extension of Yeager

Airport runway ensures stability against tension and pullout failure modes as both factors of safety are more than 1.5 (recommended by FHWA, 2001) for all 98 layers of reinforcement from top to bottom of the slope. The magnitudes of factors of safety indicate that the reinforced soil slope is overly safe for the values reported by Lostumbo (2010). Therefore, the failure cannot be attributed to the internal stability modes. Now, the cause of collapse may be due to inadequate external stability.

Effect of Reduction in Friction Angle of the Reinforce Soil on Internal Stability

Fig. 8(a) shows the variation of a factor of safety against tension failure (FS_t) of 98 layers of reinforcement along the depth of wall for ϕ = 36^o, 34^o, 32^o, 30^o, 28^o and 26^o and typical values mentioned in the above sections. For the top layers where an axial tensile force in the geosynthetic layer is significantly less, a very high value (i.e. 118.41) of factor of safety is observed. It can be observed from the figure that the bottom layers of reinforcement from the top of the wall are more critical to the tension mode of failure due to overburden pressure and generally have a lower factor of safety values for $\phi \leq$ = 30^o. The results presented in **Fig. 8(b)** show the variation of factor of safety against pullout failure (FS_{po}) of 98 layers of reinforcement along the depth of wall for ϕ = 36^o, 34^o, 32^o, 30^o, 28^o and 26^o. It can be noted from **Fig. 8(b)** that the upper layers of reinforcement from the top of the wall are more critical to the pullout mode of failure and slope does not have adequate pullout length to maintain the factor of safety against pullout failure (FS_{po}) more than 1.5 for $\phi \leq$ = 28^o.

Table 2(a). Factors of safety against tension and pullout failure modes

Layers No	depth, Z (m)	S_v (m)	$T_{i\max}$ (kN/m)	FS_t	L_a (m)	L_{ei} = (m)	P_{ri} (kN/m)	FS_{po}
1	0.90	0.9	0.37	118.41	15.77	28.23	218.45	595.99
2	1.80	0.9	0.73	59.20	15.68	28.32	438.25	597.84
3	2.70	0.9	1.10	39.47	15.59	28.41	659.43	599.72
4	3.60	0.9	1.47	29.60	15.50	28.50	882.05	601.63
5	4.50	0.9	1.83	23.68	15.41	28.59	1106.12	603.57
6	5.40	0.9	2.20	19.73	15.32	28.68	1331.68	605.54
7	6.30	0.9	2.57	16.92	15.22	28.78	1558.77	607.55
8	7.20	0.9	2.93	14.80	15.12	28.88	1787.42	609.58
9	8.10	0.9	3.30	13.16	15.03	28.97	2017.68	611.65
10	9.00	0.9	3.67	11.84	14.93	29.07	2249.57	613.76
11	9.90	0.9	4.03	10.76	14.83	29.17	2483.12	615.89
12	10.80	0.9	4.40	9.87	14.72	29.28	2718.39	618.05
13	11.70	0.9	4.76	9.11	14.62	29.38	2955.39	620.25
14	12.60	0.9	5.13	8.46	14.51	29.49	3194.17	622.48
15	13.50	0.9	5.50	7.89	14.41	29.59	3434.76	624.74
16	14.40	0.9	5.86	7.40	14.30	29.70	3677.20	627.04
17	15.30	0.9	6.23	6.97	14.19	29.81	3921.53	629.37
18	16.20	0.9	6.60	6.58	14.08	29.92	4167.77	631.72
19	17.10	0.9	6.96	6.23	13.96	30.04	4415.97	634.12
20	18.00	0.9	7.33	5.92	13.85	30.15	4666.16	636.54
21	18.90	0.9	7.70	5.64	13.73	30.27	4918.38	639.00
22	19.80	0.9	8.06	5.38	13.61	30.39	5172.66	641.49

23	20.70	0.9	8.43	5.15	13.49	30.51	5429.04	644.01
24	21.60	0.9	8.80	4.93	13.37	30.63	5687.55	646.56
25	22.50	0.9	9.16	4.74	13.25	30.75	5948.24	649.15
26	23.40	0.9	9.53	4.55	13.13	30.87	6211.13	651.77
27	24.30	0.9	9.90	4.39	13.00	31.00	6476.27	654.42
28	25.20	0.9	10.26	4.23	12.87	31.13	6743.69	657.11
29	26.10	0.9	10.63	4.08	12.74	31.26	7013.43	659.82
30	27.00	0.9	11.00	3.95	12.61	31.39	7285.52	662.58
31	27.90	0.9	11.36	3.82	12.48	31.52	7560.00	665.36
32	28.80	0.9	11.73	3.70	12.35	31.65	7836.90	668.18
33	29.70	0.9	12.10	3.59	12.21	31.79	8116.27	671.03
34	30.60	0.9	12.46	3.48	12.08	31.92	8398.14	673.91
35	31.50	0.9	12.83	3.38	11.94	32.06	8682.55	676.82
36	32.40	0.9	13.19	3.29	11.80	32.20	8969.53	679.77
37	33.30	0.9	13.56	3.20	11.66	32.34	9259.13	682.75
38	34.20	0.9	13.93	3.12	11.51	32.49	9551.37	685.77
39	35.10	0.9	14.29	3.04	11.37	32.63	9846.29	688.82
40	36.00	0.9	14.66	2.96	11.22	32.78	10143.94	691.90
41	36.90	0.9	15.03	2.89	11.08	32.92	10444.35	695.01
42	37.80	0.9	15.39	3.53	10.93	42.07	13672.31	888.16
43	38.70	0.9	15.76	3.45	10.78	42.22	14047.98	891.34
44	39.60	0.9	16.13	3.37	10.62	42.38	14426.52	894.55
45	40.50	0.9	16.49	3.30	10.47	42.53	14807.98	897.80
46	41.40	0.9	16.86	3.23	10.32	42.68	15192.37	901.08
47	42.30	0.9	17.23	3.16	10.16	42.84	15579.76	904.40
48	43.20	0.9	17.59	3.09	10.00	43.00	15970.16	907.75
49	44.10	0.9	17.96	3.03	9.84	43.16	16363.62	911.13

Table 2(b). Factors of safety against tension and pullout failure modes

Layers No	depth, Z (m)	S_v (m)	$T_{i\max}$ (kN/m)	FS_t	L_a (m)	L_{ei} (m)	P_{ri} (kN/m)	FS_{po}
50	45.00	0.90	18.33	2.97	9.68	43.32	16760.17	914.54
51	45.90	0.90	18.69	2.91	9.51	43.49	17159.86	917.99
52	46.80	0.90	19.06	2.85	9.35	43.65	17562.72	921.48
53	47.70	0.90	19.43	2.80	9.18	43.82	17968.79	925.00
54	48.60	0.90	19.79	2.75	9.01	43.99	18378.11	928.55
55	49.50	0.90	20.16	2.70	8.84	44.16	18790.71	932.13
56	50.40	0.90	20.53	2.65	8.67	44.33	19206.64	935.75
57	51.30	0.90	20.89	2.60	8.50	44.50	19625.92	939.40
58	52.20	0.90	21.26	2.56	8.33	44.67	20048.61	943.09
59	53.10	0.90	21.62	2.52	8.15	44.85	20474.73	946.81
60	54.00	0.90	21.99	2.47	7.97	45.03	20904.33	950.56
61	54.90	0.90	22.36	2.43	7.79	45.21	21337.44	954.35
62	55.80	0.90	22.72	2.39	7.61	45.39	21774.11	958.18
63	56.70	0.90	23.09	2.36	7.43	45.57	22214.37	962.03
64	57.60	0.90	23.46	2.32	7.24	45.76	22658.25	965.92
65	58.50	0.90	23.82	2.28	7.06	45.94	23105.81	969.85
66	59.40	0.90	24.19	2.25	6.87	46.13	23557.07	973.81

67	60.30	0.90	24.56	2.22	6.68	46.32	24012.07	977.80
68	60.75	0.45	12.37	4.56	6.49	46.51	24290.93	1963.66
69	61.20	0.45	12.46	4.53	6.30	46.70	24572.12	1971.79
70	61.65	0.45	12.55	4.49	6.10	46.90	24855.66	1979.98
71	62.10	0.45	12.65	4.46	5.91	47.09	25141.57	1988.24
72	62.55	0.45	12.74	4.43	5.71	47.29	25429.88	1996.58
73	63.00	0.45	12.83	4.40	5.51	47.49	25720.61	2004.98
74	63.45	0.45	12.92	4.37	5.31	47.69	26013.76	2013.45
75	63.90	0.45	13.01	4.33	5.11	47.89	26309.37	2021.99
76	64.35	0.45	13.10	4.30	4.91	48.09	26607.46	2030.60
77	64.80	0.45	13.19	4.27	4.70	48.30	26908.03	2039.28
78	65.25	0.45	13.29	4.24	4.49	48.51	27211.12	2048.02
79	65.70	0.45	13.38	4.22	4.28	48.72	27516.75	2056.84
80	66.15	0.45	13.47	4.19	4.07	48.93	27824.92	2065.73
81	66.60	0.45	13.56	4.16	3.86	49.14	28135.67	2074.68
82	67.05	0.45	13.65	4.13	3.65	49.35	28449.02	2083.71
83	67.50	0.45	13.74	4.10	3.43	49.57	28764.98	2092.81
84	67.95	0.45	13.84	4.08	3.21	49.79	29083.58	2101.97
85	68.40	0.45	13.93	4.05	3.00	50.00	29404.83	2111.21
86	68.85	0.45	14.02	4.02	2.78	50.22	29728.76	2120.52
87	69.30	0.45	14.11	4.00	2.55	50.45	30055.38	2129.89
88	69.75	0.45	14.20	3.97	2.33	50.67	30384.72	2139.34
89	70.20	0.45	14.29	3.95	2.10	50.90	30716.80	2148.86
90	70.65	0.45	14.39	3.92	1.88	51.12	31051.63	2158.45
91	71.10	0.45	14.48	3.90	1.65	51.35	31389.25	2168.10
92	71.55	0.45	14.57	3.87	1.42	51.58	31729.66	2177.83
93	72.00	0.45	14.66	3.85	1.19	51.81	32072.89	2187.63
94	72.45	0.45	14.75	3.82	0.95	52.05	32418.96	2197.50
95	72.90	0.45	14.84	3.80	0.72	52.28	32767.89	2207.44
96	73.35	0.45	14.94	3.78	0.48	52.52	33119.70	2217.46
97	73.80	0.45	15.03	3.75	0.24	52.76	33474.41	2227.54
98	74.25	0.2	15.12	3.73	0.00	53.00	33832.05	2237.69

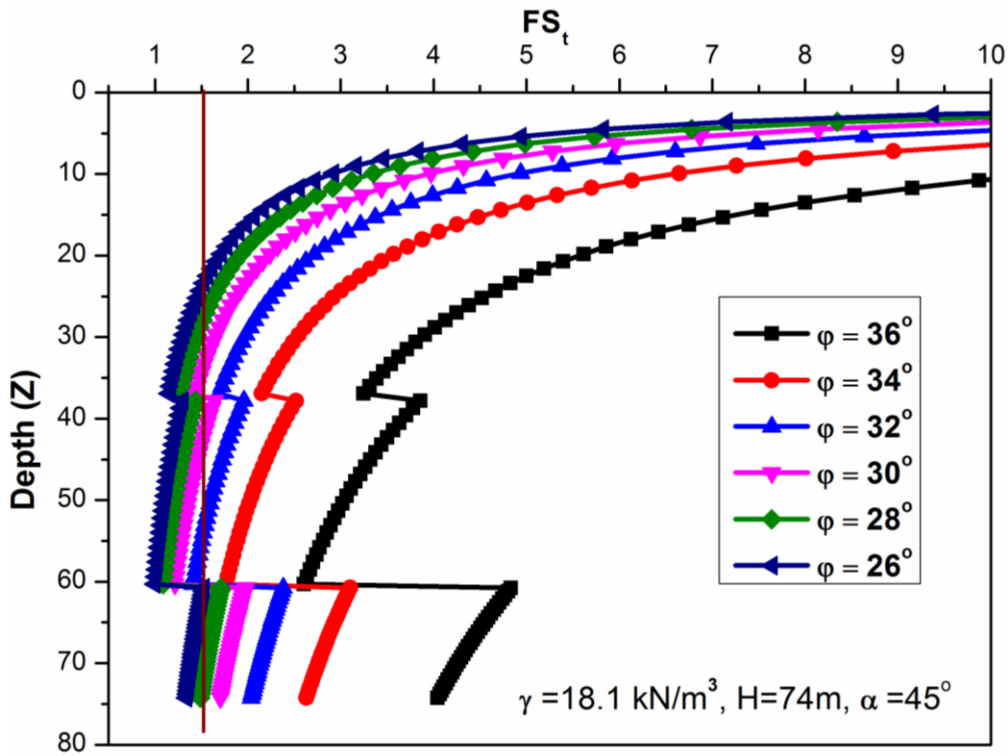

Figure 8(a). Factors of safety against tension failure for different values of ϕ

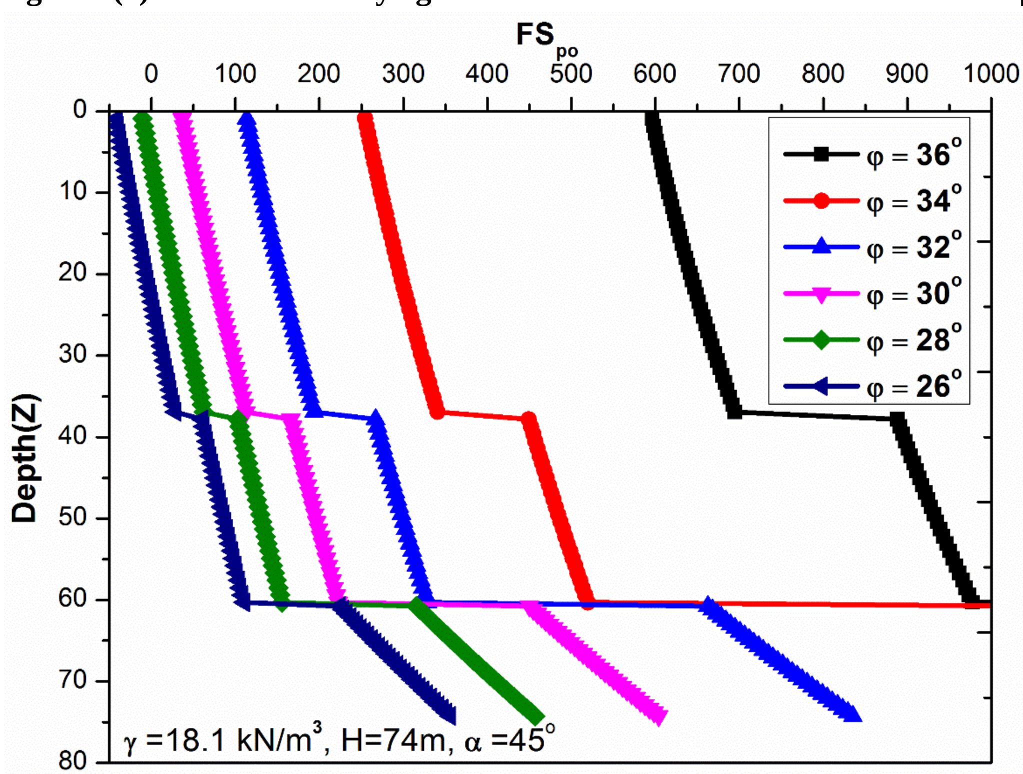

Figure 8(b). Factors of safety against pullout failure for different values of ϕ

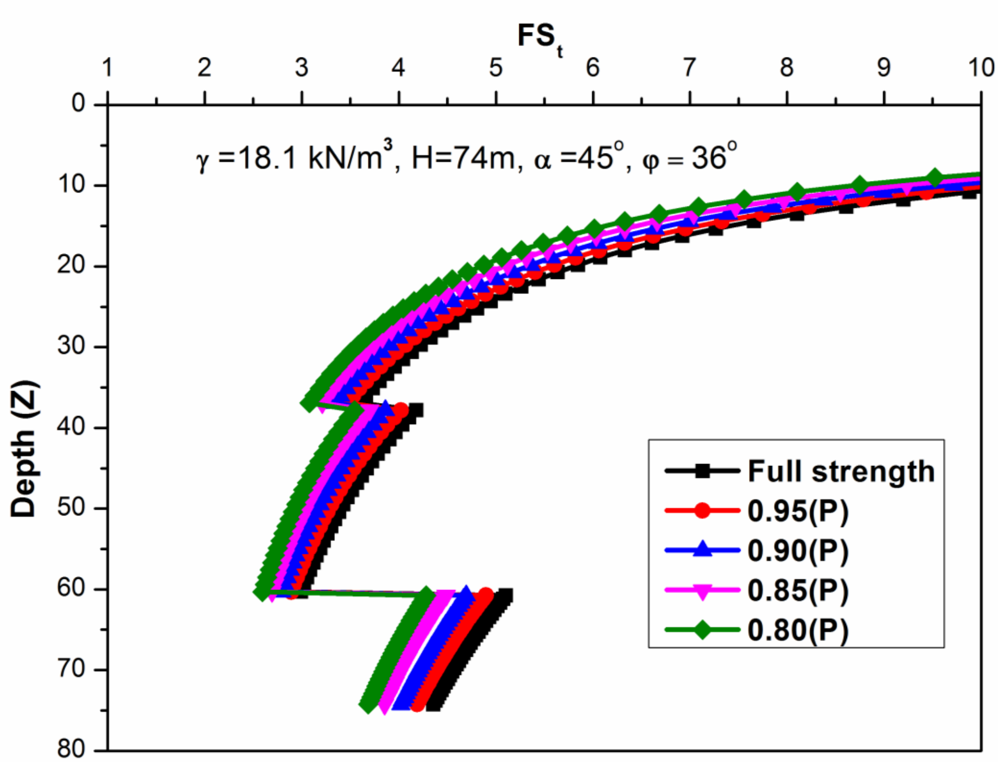

Figure 9. Factor of safety against tension for different values of reinforcement strengths

An important conclusion that can be made from this section that the reduction in friction angle from 36^o to 26^o could have made the GRS critical to tension and pullout failures. However, the failure images as shown in **Figs. 2, 3** and **4** do not show any signs of either overstressing or pullout failures. Therefore, a significant reduction in friction angle is highly unlikely.

Effect of Reduction in Design Strength of the Geogrids on Internal Stability

The reduced reinforcements strengths may be expected as there is a chance for the reinforcement to encounter the creep and biodegradation in the field. Therefore, results presented in **Fig. 9** shows the variation of a factor of safety against tension failure (FS_t) of 98 layers of reinforcement along the depth of wall for different reduced reinforcement strengths, 0.95T_{all}, 0.9 T_{all}, 0.85T_{all} and 0.8T_{all} and typical values adopted in the above sections. It may be noted from **Fig. 9** that the bottom layers of reinforcement from the top of the wall are not critical to the tension mode of failure due to reduction in design strength of the reinforcement from 100 to 80%. Hence, the assumption of reduction in design strength of the reinforcement is not realistic.

Cause of the Collapse of Reinforced Soil Slope

Figs. 2 and **3** shows that the reinforced soil zone sheared where the reinforcement ended, and the reinforced soil as a whole is sliding down the hillside. The reinforcement is visible in the top layers, but not at the bottom. The fact is that it is at the base where the initial failure might have occurred, as this looks to be a rotational slide. The road embankment at the base of the slope as shown in **Fig. 3(a)** appears to be quite soft, with electricity poles leaning down the hill. Further, it can also be noted that the area of bedrock exposure as shown in **Fig. 3(b)** shows flat lying sedimentary rock. It appears to include a competent pale sandstone over a greyish shale.

Another interesting observation that can be made from **Figs. 3(a)** and **3(b)** that the excavation and foundation of the GRS did not go to the base of the hill. The bedrock is visible in the back and presence of some moisture can be observed at somewhat higher in the slope. Lostumbo (2010) reported that foundation soil below the base of the GRS consists of “sandstone and some shale”. The small intercalations of shale material can produce enormous bearing capacity problems. The low value of bearing capacity of shale can be attributed to lower compressive strength but more importantly significantly lower friction angle. Finally, an important conclusion that can be drawn from the study is that the founding bedrock failure is the most likely the cause of the collapse.

CONCLUSIONS

In an effort to recognize the potential causes of the failure of Yeager airport runway extension, the investigation is carried out for internal and external stability analysis. The findings of this forensic geotechnical investigation warrant the following conclusions.

1. It is observed that the considered long term design strength of the reinforcement and available length of the reinforcement are more than adequate to resist the tensile and pullout failure modes.
2. The failure cannot be attributed to either reduction in the friction angle due to improper compaction or reduction in the long term design strength of the reinforcement due to creep and biodegradation.
3. An important conclusion from the forensic investigation is that the founding bedrock failure is the most likely the cause of the collapse.

REFERENCES

Basha, B.M. & Babu, G.L.S. (2012). “Target reliability-based optimisation for internal seismic stability of reinforced soil structures.” *Geotechnique*, No. 1, Vol. 62: 55–68.

FHWA (2001). *Mechanically stabilized earth walls and reinforced soil slopes: design and construction guidelines*, FHWA NHI-00- 43. Washington, DC: Federal Highway Administration and National Highway Institute.

Lostumbo, J.M. (2010). “Yeager Airport Runway Extension: Tallest Known 1H:1V Slope in U.S.” *Proc. of GeoFlorida, 2010: Advances in Analysis, Modeling & Design*, GSP 199, 2010 ASCE.

Tencate, http://www.tencate.com/amer/Images/Reinforced%20Soil%20Case%20Studies_tcm29-19401.pdf

Determination of soil deformations using gpr under bridge approach slabs

Sireesh Saride[1], Vinay Kumar V[2] and Maheshbabu Jallu[3]

[1]Associate professor, Department of Civil Engineering, Indian Institute of Technology Hyderabad, Kandi, Sangareddy, Telangana- 502205; e-mail: sireesh@iith.ac.in
[2] Doctoral student, Department of Civil Engineering, Indian Institute of Technology Hyderabad, Kandi, Sangareddy, Telangana- 502205; e-mail: ce13p1003@iith.ac.in
[3] Doctoral student, Department of Civil Engineering, Indian Institute of Technology Hyderabad, Kandi, Sangareddy, Telangana- 502205; e-mail: ce15resch11014@iith.ac.in

ABSTRACT

Ground penetrating radar (GPR) is one of the non-destructive technics that provide high-resolution information to a greater depth of soil strata. It works on the principle of reflection/refraction of an electromagnetic wave that occurs when there is a change in dielectric properties of two adjacent layers across a soil boundary, or a material interface. GPR is an effective tool for subsurface inspection and quality control, whose applications are very wide and include locating buried objects, detection of voids or cavities, locating re-bars in concrete slabs and applications in archaeological surveys.

The objective of this study is to determine the subsurface soil deformations under a bridge approach slab using GPR. Multiple GPR surveys were performed over a bridge section on a national highway near Hyderabad. The aim of this study is to detect the layers of low-density soil located at different regions throughout the bridge approach embankment and quantify the volume of road material involved in the settlements. A broad range antenna of 500MHz frequency having highest signal-to-noise ratio has been employed to generate a wave with a controlled velocity of 0.15m/ns. The radargrams were analyzed along with an image processing software to explore the defective ground pockets and soil deformations with a great success. The total volume of soil deformed under the bridge approach slabs were found to be as high as 72 m^3. The qualitative data obtained from the GPR radargrams were verified with the lightweight deflectometer (LWD) data.

INTRODUCTION

Bridge approach slabs are the structures constructed to provide a ramp or a gradual transition between the bridge superstructure and the pavement embankment. The approach slabs are constructed in order to reduce the abrupt bump created at the end of the bridge. The approach slabs along with the approach embankment often tend to settle or heave with respect to the bridge deck. The amount of approach embankment settlement along with various other distresses caused has to be determined to avoid further damage to the service life of the bridge structure. In addition, the bump at the end of the bridge not only leads to damage of the deck but also cause severe inconvenience to the users and responsible for frequent vehicle maintenance. The estimated maintenance cost of bridges with the bump issue sums upto $ 6.3 million per year (2001) in Texas alone in USA and over $100 million in the entire country (Ha et al. 2002). Quantification of the bump or distress is a crucial parameter in retrofitting the structure. There are number of destructive and non-destructive testing (NDT) techniques including profilometers, radar technics etc. available to determine the fault locations in the approach embankment and pavement structure. The NDT methods are generally preferred over the conventional destructive techniques as they are advantageous in evaluation of the subsurface conditions of the structure without causing any damage to the structure (Chen & Scullion, 2006). Ground penetrating radar (GPR), falling weight deflectometer (FWD), profilometers are few such NDT methods employed to check for the subsurface conditions and merging of their test data can be useful for pavement condition assessment (Scullion & Saarenketo, 2000).

The GPR technique applies a short pulse of energy in the form of radio waves into the material from the antenna and the waves are reflected from the materials or layers below to the antenna (Maser, 2000). The arrival time and the amplitude of the reflected waves depend upon the dielectric constants of the materials and the subsurface pavement conditions are evaluated based on these reflected waves (Chen & Wimsatt, 2010). For a typical pavement survey with the ground coupled antenna, the transmitter sends the waves through the layers and a part of the waves are reflected back, when it hits the interface as shown in Fig. 1 and they are recorded as two way travel time and the amplitude of the wave. The thickness of the pavement layers can be determined using the velocity and the two-way travel time of the radar wave through a given layer using Eq. 1.

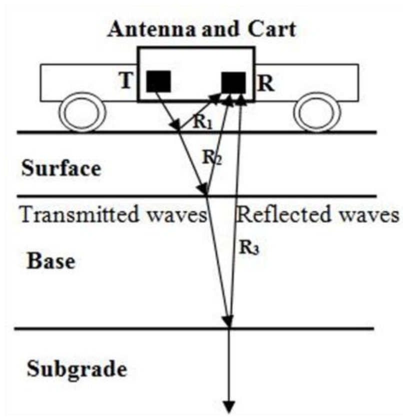

Figure 1. Principle of GPR

$$H = \frac{\Delta t \times c}{2\sqrt{\varepsilon_r}} \qquad (1)$$

Where, H is the layer thickness, c is a speed constant (speed of light in air = 0.3m/ns), Δt is the two-way travel time through the layer i.e. the time difference between the reflected wave (R_1) and the reflected wave (R_2) as seen in Fig. 1 and ε_r is the relative dielectric constant of the material or layer.

BACKGROUND

The NDT methods generally consist of applying electromagnetic radiation, ultrasonic pulse and radio waves to evaluate the condition of the material. NDTs provide instant solution to the problems and due to this reason; they have various applications in the field of concrete structures and pavements.

Among the various non-destructive test methods referred above, various researchers have identified anomalies in the sub-soil structures and pavements have adopted GPR successfully.

According to Miller (1996), GPR is an efficient, precise, non- destructive tool, which is effective in determining the human made subsurface subsidence along with its shape, its precise location and the depth of distress. A void under continuously reinforced plain concrete pavements in an Interstate Highway was identified by Chen and Scullion (2007) using the GPR technology. Besides, Uddin and Hudson (1994) evaluated the performance of various NDT methods like dynamic deflectometer, proof roller, Benkelman beam, GPR, FWD and transient dynamic response (TDR) to determine the voids under concrete pavements and advocated that the GPR technic is most useful in determining the location and extent of the voids precisely. Chen and Wimsatt (2010) have made a similar observation when they detected various anomalies and the presence of moisture in the flexible pavements along with the voids detected using GPR technic.

Besides, Park (2004) and Scullion, and Saarenketo (2000) have advocated that the GPR technic have a potential to evaluate the structural performance of the pavements and FWD to re-estimate the stiffness of the pavements after identifying the distresses. The distress locations estimated using GPR were cross-checked by coring and found that the GPR results correlated well with the cores excavated with an average error of less than 2.5% (Samer and Al-Qadi 2007). Maierhofer (2003) used GPR for the evaluation of the concrete infrastructure, whereas Chen et al. (2007) used GPR to determine the various causes for the failure of bridge embankment with cracked approach slabs. Similarly, Rister and Hopwood (2008) reported the use of GPR to investigate the presence of voids and cracks on the Interstate highway-275 twin bridges over the Ohio river in Kenton county.

The literature suggests that the NDT methods, especially GPR, would provide a clear information about the distresses and their location in various civil engineering projects spanning from pavements to embankments when used with care. To date, the NDT methods were used mostly for qualitative analysis of the projects. However, to quantify these destresses, one needs to compliment the NDT methods with other technics. The objective of this study is to investigate the causes of the soil deformations under a bridge approach slab along National Highway near Hyderabad, India and to quantify the zone of distress and using GPR, LWD and high definition image processing technics.

SITE LOCATION AND GPR SURVEY DETAILS

Severe bridge approach embankment settlements are noticed on either side of a bridge along Hyderabad - Pune highway near Hyderabad, which are causing intolerable discomfort to the users. It is a two span 60m long bridge with 6.0m high approach embankments, crossing a creek, oriented towards East-West directions. To plan on appropriate maintenance activities and remedial measures, it is necessary to understand the problems and accurately estimate the deformed zones of embankment. To avoid any traffic congestions along the highway, non-destructive test methods are proposed to employ to map the distresses. A 100 m long stretch of the embankment has been considered to cover the undisturbed zones of embankment on either side of the bridge deck, zones covering the settled approach slabs and the firm bridge section. It has been physically noticed that the pavement was settled for about 10.0m long on either side of the approach slabs. The Google image of the bridge site and the test sections are presented in Fig. 2, which includes the west side approach embankment (0.0 to 17.0 m), approach slab (17.0 to 21.5 m), bridge deck (21.5 to 78.5 m) and approach slab and embankment portion on the east side (78.5 to 100.0 m). The stretch of the approach slab from 20m to 21.5m rests on the wing wall and the bridge abutment and the remaining length rests over the embankment soil. The bridge deck spans from 21.5m to 78.5m with three expansion joints present at 21.5m, 50m and 78.5m, respectively. The whole stretch is symmetrical about the centrally located expansion joint as shown in Fig. 2. To investigate, identify and quantify the soil deformations in each layer accurately, a series of GPR surveys were conducted on the test stretch using a 500 MHz frequency ground coupled antenna along both directions i.e. west to east and east to west with a radar wave velocity of 0.15m/ns. Along the GPR survey track, lightweight deflectormeter (LWD) tests were also carried out to verify/quantify the in-situ deformation modulus of the test sections. The LWD data would provide the reduced modulus of the deformed stretches. The GPR surveys and LWD tests were repeated for three times to avoid errors in the measurement. Important physical features of the test section viz., start and end points of approach slabs, expansion joints, start and end points of bridge deck were marked on the ground and cross verified during the GRP surveys. These marks as flags can be seen in the radargrams (Fig. 3), which validates the survey data.

ANALYSIS OF RESULTS AND DISCUSSION

The series of radargrams obtained from the GPR surveys are first filtered to minimize the unwanted disturbances and noise caused due to the ringing effect of radar waves. In the current study, background removal, static correction, F-K filter with migration algorithm and linear gain function filters are adopted. Figure 3 presents the typical processed radargram of the test stretch after adopting the appropriate noise filtering techniques. A series of strong kinks noticed in the radargram are due to strong reflection of electro-magnetic waves from the iron sections placed at the expansion joints i.e. at 21.5m, 50m and 78.5m. The bridge deck spanning from 20m to 80m has shown strong reflections compared to the other areas owing to its stiff and dense material nature (Fig. 3). The rebars along the length of the bridge deck can also be visualized in the radargram if an appropriate high frequency antenna (about 1 to 2 GHz) is employed (Ha et al. 2002, Chen and Wimsatt, 2010, Chen and Scullion, 2006). However, the antenna used in this study is a 500 MHz medium range frequency antenna and hence, the rebars could not be traced with high resolution. The depth of the study depends upon the frequency range of the antenna used. Greater the depth of interest, lesser should be the frequency of the antenna and vice-versa.

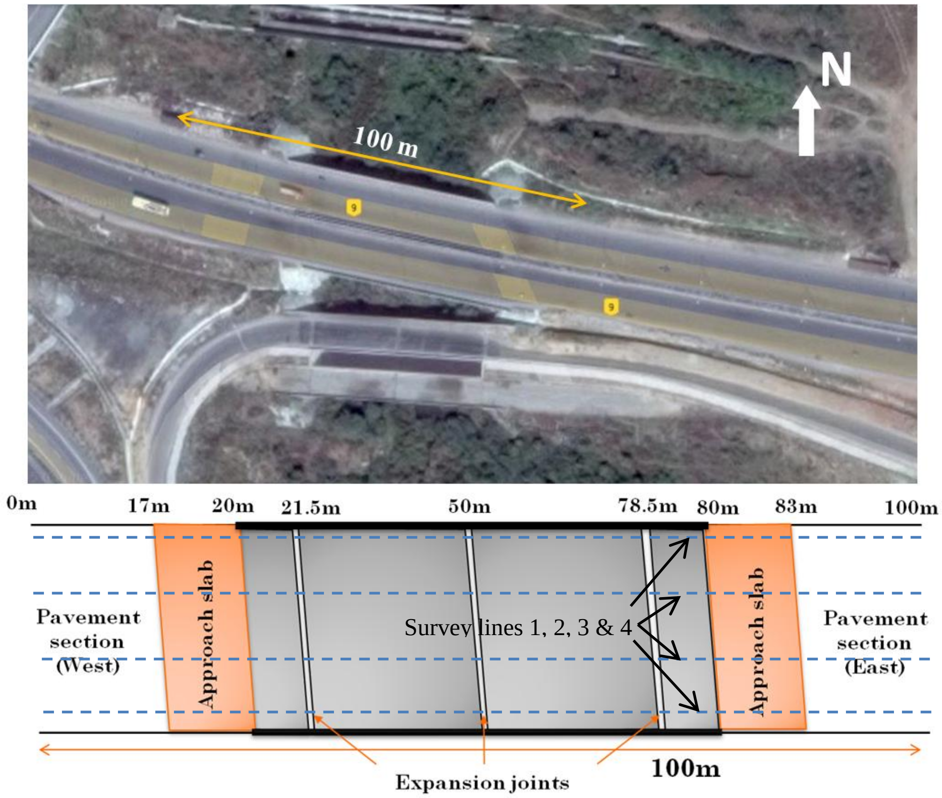

Figure 2. Google Image and plan view of the test location.

It is now important to identify the thickness of each pavement layer that would provide more information about the anomalies and distresses in the compacted embankment material. The thickness of the bound pavement layer i.e. asphalt concrete, can be calculated using ASTM D4748-10, a standard test method to determine the thickness of bound and unbound pavement layers using short pulse radar. The thickness of asphalt concrete layer can be calculated from Eq. 1 using the velocity and two way travel time of the radar wave. From the radargram, the two-way travel time of the radar wave is found to be 2ns and hence, the thickness is found to be 0.175m approximately. The thickness of the bridge deck excluding the asphalt surface is approximately 0.25m to 0.30m. The bottom of the bridge can be seen in Fig. 3 at a depth of about 0.4m to 0.45m. The thickness of the unbound pavement layers are found to be 0.275m total thick, which can be visualized from Fig. 3 that these layers are compacted in two lifts of 0.15m and 0.125m, respectively. It can be clearly seen that the compacted soil has extensively disturbed/deformed stretches between 15m and 17.5m and between 83m and 91m. Further, multiple surveys were carried out along these deformed stretches to quantify the distresses/settlements. Figure 4 shows a processed radargram of the deformed test stretch from 100m to 78.5m traversed from east-west direction. The reasons for the soil settlement under the approach slabs may be attributed generally to inadequate compaction of the embankment material and specifically the adopted lift thicknesses in this region. It can be observed that the lifts are of unequal depths especially under approach slabs. It is also noticed that an asphalt overlay was placed over the deformed test sections on either side of the approach slabs as a measure to retrofit the sections and improve the ride quality (Figs. 3 and 4).

A void was also detected underneath the approach slab on the test stretch between 81.5m to 83m, as visualized in Fig. 4. Chen and Scullion (2006) and Chen and Wimsatt (2010) observed similar type of voids under the continuously reinforced plain concrete pavements in IH 40, IH 35 and IH 90 respectively. Rister and Hoopwood (2008) reported the possibility of a void approximately one or two inch in depth under the approach slab of a bridge on I-275 in Kenton County, USA. Based on thorough analysis of various radargrams from these studies and the present study, a void is identified in the Fig. 4, which is denoted by a clear change in the radargram near the void location, due to the change in the dielectrics of the material. The extent of voids formed and the volume of the deformed soil are quantified using an image processing and analysis software as presented in Fig. 5. The procedure consists of converting the high-resolution processed radargram into grey scale (Fig. 5a) and then marking the region to be measured with the help of editing tools (Fig. 5b). The number of black square pixels are measured after filling the marked region using fill command (Fig. 5c). Similarly, the total number of square pixels covering the entire image is also measured (Fig. 5d). The procedure is repeated for several times to check for the repeatability of the technic and found to be accurate with a COV of about 0.025. Now, the area of distress is calculated in mm^2 from the number of square pixels measured, based on the known dots per inch (dpi) information of the image, using a conversion formula given by Jones (internet content, 2016). Although, the area (length and depth) of the distress can be calculated from this method, the volume of distress is calculated by determining the settlements along the width of the pavement through multiple GPR surveys as shown in Fig. 2). Table 1 gives the volume of deformed soil and the volume of voids calculated in the stretch 100m-78.5m. Similarly, the deformed soil zones and potential voids on the west side of the bridge stretch between 16m to 18m were also observed in the radargram of test stretch 21.5m to 0m (east-west) and the data is presented in Table 1.

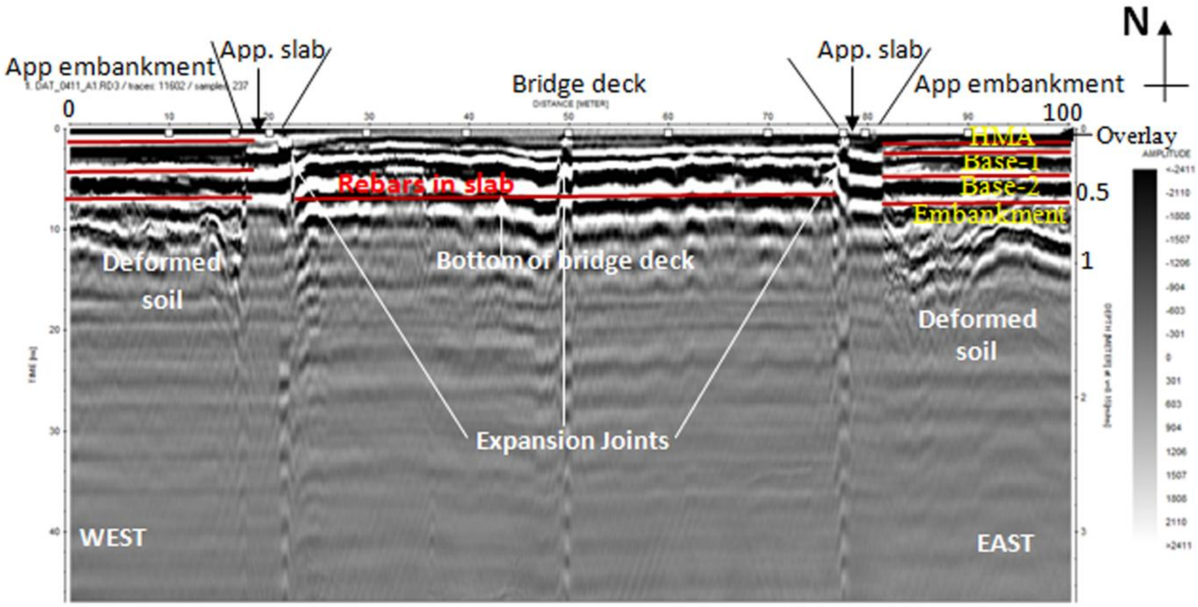

Figure 3. Processed radargram of the complete test stretch (West-East)

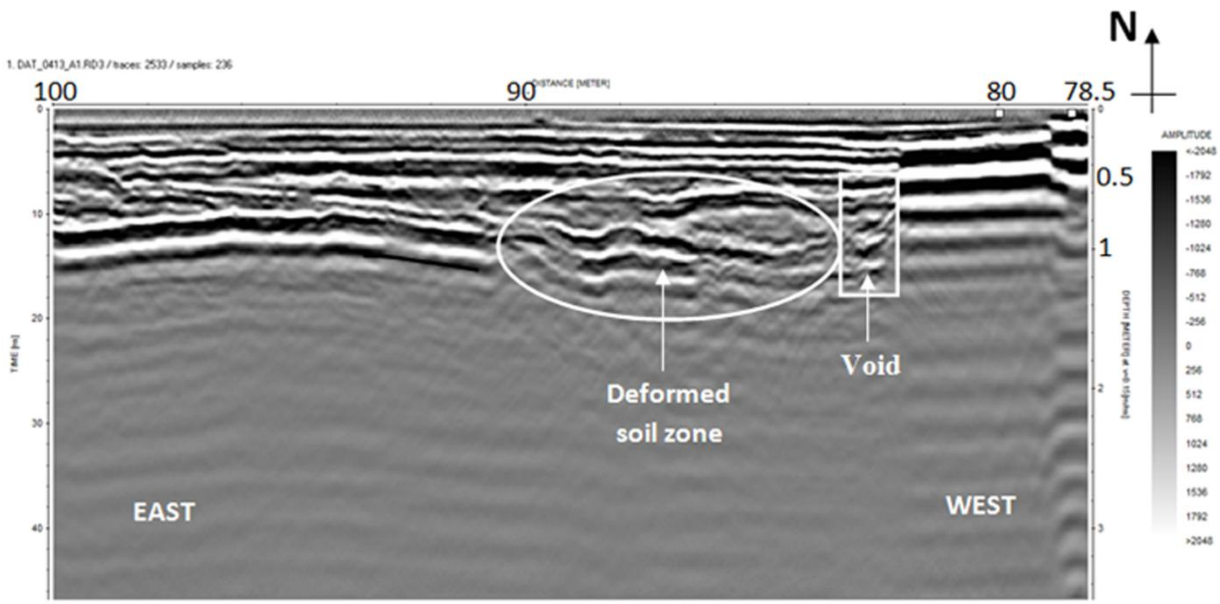

Figure 4. Processed radar gram of the test stretch from 100m to 78.5m (East- West)

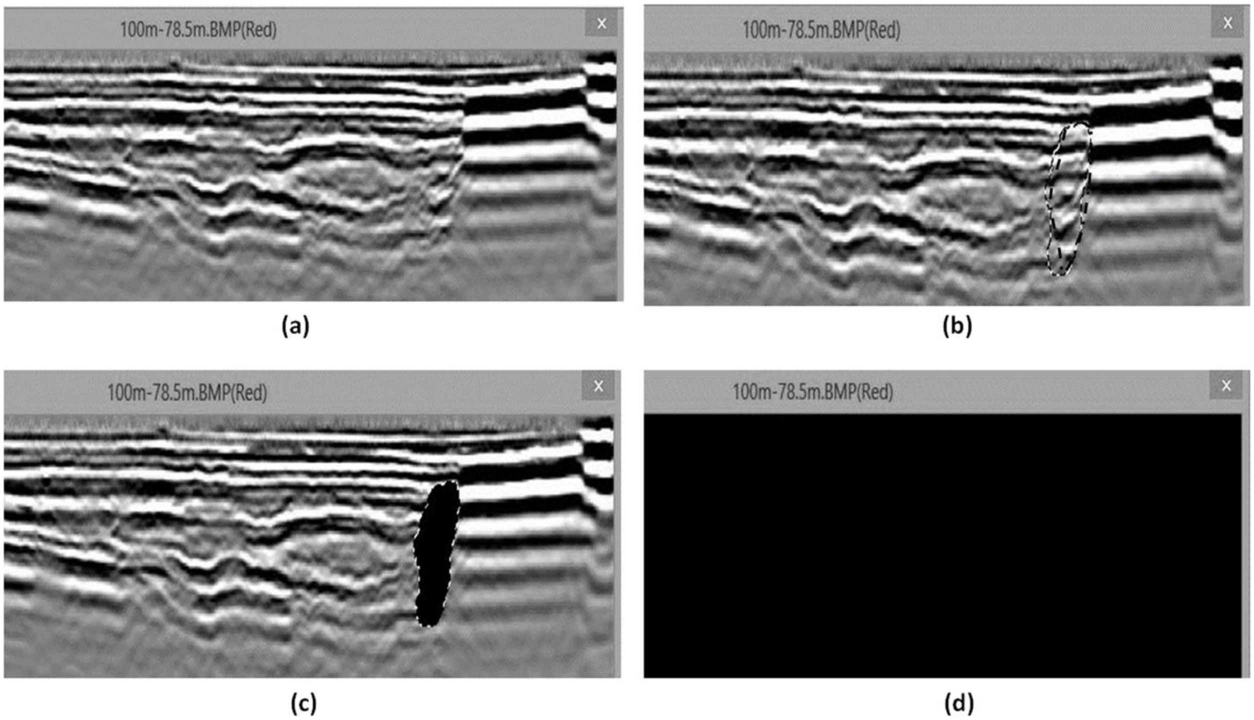

Figure 5. (a) Original image, (b) area of distress is marked using editing tool, (c) darkened distress area, and (d) fully darkened image.

Table 1**:** Summary of distress locations in the test stretch

S/l No.	**Total Image area (m^2)**	**Total Image area in sq. pixels**	**Distress Area in sq. pixels**	**Distress area (m^2)**	**Distress Volume (m^3)**	**Remarks**
1	75.25	306400	2913	0.72	7.56	Void (100m-78.5m)
2	75.25	306400	22950	5.64	59.22	Settlement (100m-78.5m)
3	75.25	306400	3883	0.95	4.98	Void (21.5m-0m)

In continuation in analyzing the distresses, LWD testing has been performed on the pavement test stretch at chainages 0m, 15m, 25m, 75m, 85m, 100m along the west to east directions and vice-versa. The chainages were selected such that the LWD test is conducted on the approach embankment section, settled approach slab and the bridge deck on both west and east directions. The deflection and deformation modulus values along the test stretch are presented in Table 2. It was observed that the deformation modulus values were about 271.08 MPa and 284.81 MPa at 0m and 100m, respectively where there were no soil deformations were identified in the GPR radargrams. Adjacent to the approach slab, where severe deformations were identified in the radargrams, very low deformation Moduli of 135.5 MPa and 132.4 MPa were recorded at 15m and 85m, respectively. The deformation Moduli of the bridge deck were recorded as 218.45 MPa and 220.35 MPa at 25m and 75m respectively. It is very clear that the

LWD test results correlate well with the radargrams obtained by the GPR surveys, thus validating the GPR analysis.

Table 2: LWD test results

Location	Chainage (m)	D_{Avg} (mm)	Deformation Modulus (MN/m^2)
Pavement	0	0.083	271.08
	100	0.079	284.81
Approach pavement	15	0.166	135.54
	85	0.17	132.35
Bridge deck	25	0.103	218.45
	75	0.105	220.35

CONCLUSION

Non-destructive testing methods can be effectively used to identify the distress locations in the approach embankments, pavements and other concrete infrastructure very quickly without causing any inconvenience to the traffic. A series of non-destructive tests viz., ground penetrating radar (GPR) and lightweight deflectometer (LWD) were adopted to identify and quantify the anomalies and distresses of a bridge approach embankment on a national highway near Hyderabad city. The following conclusions are drawn from the study:

A series of ground penetrating radar surveys using a 500 MHz mid frequency antenna was adopted to determine the thickness of various bound and unbound layers of the flexible pavement structure. It can also be used to determine the thickness of concrete structures in pavements like cement concrete pavements and bridge decks to the nearest possible extent.

The radargrams were analyzed to quantify the distresses such as voids beneath the approach slabs and soil deformations. The voids were identified using the change in dielctrics of the compacted soil. With the assistance of image processing software, the total volume of the soil involved in the approach embankment settlement was quantified, which amounts to about 72 m^3. In addition, LWD tests were used to determine the approach embankment and pavement condition through deformation modulus. The LWD test results seem to correlate well with the GPR results obtained in the current study.

Overall, the NDT test methods along with advanced image processing technics assist in estimating the anomalies accurately to adopt appropriate maintenance operations, hence, these methods can be adopted in forensic investigations.

REFERENCES

Al-Qadi, I.L. (1990). "*Detection of Moisture in Asphaltic Concrete by Microwave Measurements*," Ph.D. Thesis, The Pennsylvania State University, College Park, PA.

ASTM D4748-10 (2010). "*Standard Test Method for Determining the Thickness of Bound Pavement Layers using Short-Pulse Radar*," ASTM International, Conshohocken, PA.

Chen, D.H, and Scullion, T. (2006). "Using Non-destructive Testing Technologies to Assist in Selecting the Optimal Pavement Rehabilitation Strategy," *JTEVA*, Vol. 35, No. 2.

Chen, D.H, and Scullion, T. (2007). "Detecting Subsurface voids using Ground-Coupled Penetrating Radar," *Geotechnical Testing Journal*, ASTM, Vol. 31, No. 3.

Chen, D.H., Hong, F., and Zhou, F. (2007). "Premature Cracking from Cement-Treated Base and Treatment to Mitigate Its Effect," *J. Perform. Constr. Facil.*, 25(2), 113–120.

Chen, D.H, and Wimsatt, A. (2010). "Inspection and Condition Assessment using Ground Penetrating Radar," *Journal of Geotechnical and Geoenvironmental Engineering*, ASCE, Vol. 136, No. 1.

Ha, H.S., Seo, J., and Briaud, J.L. (2002). "*Investigation of settlement at bridge approach slab expansion joint: Survey and site investigations,"* Report No. FHWA/TX-03/4147-1, Texas Transportation Institute, Texas A&M.

Jones, D http://www.dallinjones.com/2008/07/how-to-convert-from-pixels-to-millimeters/ Accessed on 08-01-2016.

Maierhofer, C. (2003). "Non-Destructive Evaluation of Concrete Infrastructure with GPR," *Journal of Materials in Civil Engineering*, ASCE, Vol. 15, No. 3.

Maser, K.R. (2000). "Pavement Characterization Using Ground Penetrating Radar: State of the Art and Current Practice," *Non-destructive Testing of Pavements and Back calculation of Moduli: Third Volume*, ASTM STP 1375.

Miller, E.S. (1996). "Disturbances in the Soil: Finding Historical Background Buried Bodies and Other Evidence Using Ground Penetrating Radar," *Journal of Forensic Sciences, JFSCA,* Vol. 41, No. 4, pp. 648—652.

Park, S. (2004). "Load Limits Based on Rutting in Pavement Foundations," *KSCE Journal of Civil Engineering,* Vol. 8, No. 1, pp. 23-28.

Rister, B., and Hopwood, T. (2008). *"Investigations of voids/cracking on the I-275 twin bridges over the Ohio river in Kenton county-Phase 1,"* Report No. KTC-08-07/KH-60-07-IF, Kentucky Transportation center.

Samer, L., and Al-Qadi, I.L. (2007). "Automatic detection of multiple pavement layers using GPR data," *NDT&E International*, 41, pp. 69–81.

Scullion, T., and Chen, D.H. (2009). "Forensic studies: A key tool for directing future research," *Road Pavement Material Characterization and Rehabilitation, GeoHunan International Conference, China, pp. 87-95.*

Scullion, T., and Saarenketo, T. (2000). "Integrating Ground Penetrating Radar and Falling Weight Deflectometer Technologies in Pavement Evaluation," *Non-destructive Testing of Pavements and Back calculation of Moduli: Third Volume*, ASTM STP 1375, West Conshohocken, PA.

Uddin, W., and Hudson, R. (1994). "Evaluation of NDT Equipment for Measuring Voids under Concrete Pavements," *Non-destructive Testing of Pavements and Back calculation of Moduli (Second Volume)*. ASTM STP 1198, Philadelphia.

Behavior of Monopile Supported Offshore Wind Turbines in Clay due to Long term Dynamic Loads

Swagata Bisoi[1] and Sumanta Haldar[2]

[1]Research Scholar, Department of Civil Engineering, School of Infrastructure, Indian Institute of Technology Bhubaneswar, Jatni, Khordha, Orissa 752050, India, E-mail: sb17@iitbbs.ac.in
[2]Associate Professor, Department of Civil Engineering, School of Infrastructure, Indian Institute of Technology Bhubaneswar, Jatni, Khordha, Orissa 752050, India, E-mail: sumanta@iitbbs.ac.in

ABSTRACT

Design of offshore wind turbine (OWT) is primarily driven by serviceability limit state. The fundamental frequency of OWT shall be placed far from rotor frequency and wave frequency. The fundamental frequency and response alters due to long term cyclic load and soil stiffness degradation. Current design codes advocate beam on Winkler model using American Petroleum Institute (API) based cyclic *p-y* curves. Major drawback of *p-y* model is that it cannot capture cyclic degradation of soil due to cyclic loading. This study examines the response and fundamental frequency of OWT based on model experiments. Experimental observations show that the fundamental frequency of OWT system decreases due to increase in load cycles and amplitude. A rational soil-pile interaction model is developed using Winkler's hypothesis which is capable of predicting the fundamental frequency and response under long term loading. Finally limitations of *p-y* analysis is outlined with respect to a 5 MW OWT.

INTRODUCTION

Offshore wind turbine (OWT) is a tall flexible structure supported on monopile foundation installed at shallow water depth (20 - 30 m) (DNV-OS-J101, 2010). Design of OWT structure requires estimation of the fundamental frequency to avoid resonance due to rotor frequency (1P), blade passing frequency (3P) and wave frequency (Bhattacharya 2014). Dynamic response of the monopile-tower system and stability of the structure are of great importance to an OWT system in the current design paradigm (Feld 2001, GWEC 2011). The serviceability limit state (SLS) of excessive rotation at monopile head at mud line also governs the design (Lesny et al. 2004). Prediction of responses and the fundamental frequency of OWT system requires appropriate soil-structure interaction model. In general, API (2011) based cyclic *p-y* curves are widely used to model soil resistance (Andersen et al. 2012, API 2011, Damgaard et al. 2013, DNV-OS-J101 2010, Mostafa and El Naggar 2004). However, API based cyclic *p-y* curves were developed for small diameter flexible piles. It has been observed that, it overestimates the soil reaction at greater depth and underestimates at the top of large diameter monopiles (Bekken 2009, Lombardi et al. 2013). Moreover, the cyclic *p-y* curves were proposed for less than 200 cycles of loads (Achmus et al. 2009). However, OWT is subjected to millions cycles of loading and extreme wind and wave loading which is not considered in the development of cyclic *p-y* curve (Lombardi et al. 2013). Based on field and experimental observations it was reported that the foundation stiffness of OWT structure changes due to cyclic loading which cannot be captured in the *p-y* model (Lombardi et al. 2013, Li et al. 2010, LeBlanc 2009). Various design codes recommended *p-y* curves for the estimation of ultimate pile capacity, however no explicit guideline is yet available in recent design codes to predict the change of the soil stiffness under long term loading. Several previous studies also used *p-y* based Winkler foundation model for the prediction of the fundamental frequency of OWT (Carswell et al. 2015, Damgaard et al. 2013, Andersen et al. 2012).

Based on scaled model tests several researchers investigated the change in the fundamental frequency of OWT system due to long term cyclic loading (Lombardi et al. 2013, Bhattacharya et al. 2011, Bhattacharya and Adhikari 2011). It has been observed that the fundamental frequency of the system changes with foundation flexibility (Martinez-Chaluisant 2011). Guo et al. (2015) verified the dynamic response of OWT in sand. They observed that the increasing trend of natural frequency up to certain load cycles and beyond which it decreases. The variation in natural frequency and damping is evaluated due to change in strain level surrounding the pile in kaolin clay considering a group of similitude relationships for different loading conditions (Lombardi et al. 2013). They observed that the fundamental frequency of monopile supported wind turbine foundation on clayey soil changes with load cycles.

In this study, a Winkler based soil-pile interaction model is proposed that captures the changes in fundamental frequency and responses of OWT founded in clay due to long term cyclic loading. Dynamic response of monopile supported offshore wind turbine in clay is examined considering a scaled model OWT. The numerical model is calibrated with respect to the measured fundamental frequency and lateral deflection for different number of load cycles from the experimental observations. The results from numerical model is also compared with conventional *p-y* model. Degraded stiffness model is proposed in this study to incorporate the change in the fundamental frequency and rotation with number of cycles. The results are also compared with API based model. Finally limitations of *p-y* analysis is shown considering a real 5 MW OWT.

EXPERIMENTAL MODEL

A 5 MW monopile supported prototype OWT structure is selected in this study. Monopile and tower is modelled using 1:100 scale model for experimental tests. Table 1 shows the selected parameters for prototype and model structure. Scaling laws are used in a non-dimensional form for prototype and model to develop the similitude relationships. Kaolin clay is used to prepare the soil bed which is widely used in experimental study (Lombardi et al. 2013). Liquid limit and plastic limit of the soil are 49% and 27% respectively. Compression index is evaluated as 0.05 for kaolin clay and saturated density is 1450 kg/m^3. The natural frequency, damping, shear modulus and stiffness of soil-pile are measured in every load cycles. The shear modulus is also measured initially for different depth at 3 locations in kaolin clay bed. A photograph of experimental program and schematic diagram are shown in Figure 1. The cyclic loading is applied using vibration shaker to the OWT system which having different load amplitudes, frequencies (2 Hz and 5 Hz) and cycle number (50000 cycles). Load amplitude is measured by force sensor. The responses are measured considering two LVDTs attached to the tower-monopile system. Rotor nacelle mass is presented as lumped mass as shown in Figure 1. The tower and monopile are considered as hollow cylindrical section with uniform diameter and thickness.

Table 1. Selected parameters for prototype and model

Parameter	Symbol	Prototype	Model
Tower height (m)	H_t	100	1
Tower diameter (m)	D_t	7	0.07
Tower thickness (m)	t_w	0.07	0.005
Monopile length (m)	L_p	50	0.5
Monopile diameter (m)	D	7	0.07
Monopile thickness (m)	t_w	0.07	0.005
Monopile mass (kg)	M_p	598164.7	1.35
Tower mass (kg)	M_{Tower}	1195723	2.71
RNA mass (kg)	M_{RNA}	310000	0.70
Young's modulus of tower and pile (N/m^2)	E	2.1×10^{11}	7×10^{10}
Material	-	Steel	Aluminium
Density of tower and pile (kg/m^3)	ρ	7850	2656
Unit weight of tower and pile (N/m^3)	γ	77008.5	26055.36
Yield stress of tower and pile (N/m^2)	σ_y	5.50×10^8	2.50×10^8
Shear modulus (Pa)	G	8.00×10^7	5.33×10^6
Undrained shear strength of clay (kPa)	s_u	14	14
Coefficient of permeability (m/sec)	k_h	1.00×10^{-9}	1.00×10^{-10}
Point of application from soil bed (m)	y	65.7	0.78
Total horizontal load (N)	P	2.63×10^6	2000
Loading frequency (Hz)	f	0.25 Hz	5 Hz

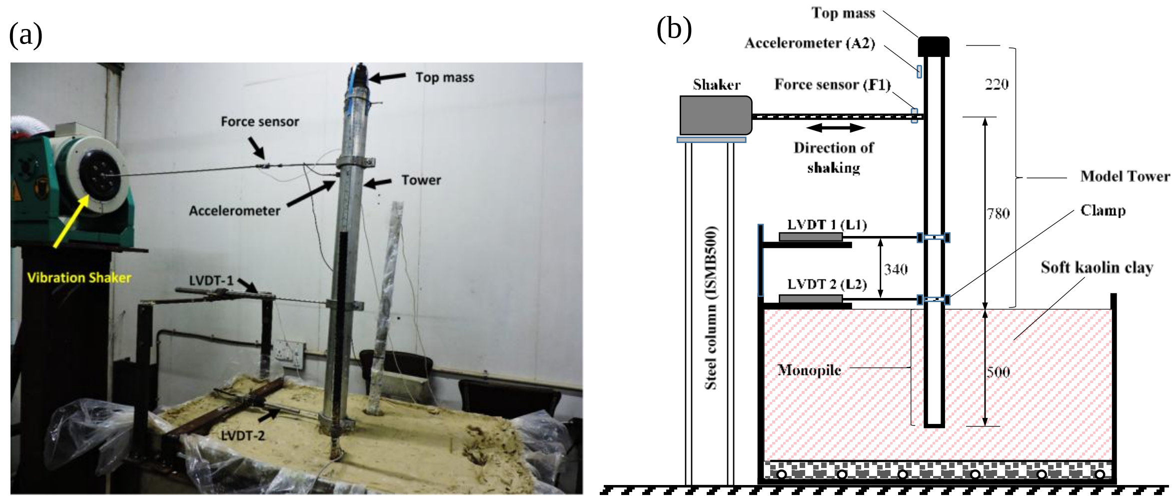

Figure 1. (a) Photograph of experimental program and (b) Schematic diagram of test set-up.

METHODOLOGY

API based *p*-*y* model

API (2011) and DNV-OS-J101 (2010) based cyclic *p*-*y* curve is used as the soil resistance in this present study to verify the response of OWT in a conventional method. The tower and monopile are considered as Euler-Bernoulli beam element where soil resistance is considered as nonlinear Winkler spring element. The discretized soil spring element is assumed to be attached with each beam element of monopile in which the lateral resistance (p) against pile deflection (y) is generated. A tubular uniform cross section of tower-monopile structure is assumed. The rotor-nacelle mass is considered as point mass attached on the tower top of the structure. The end of the monopile is assumed to be supported on a roller to prevent the vertical movement and allow the horizontal movement.

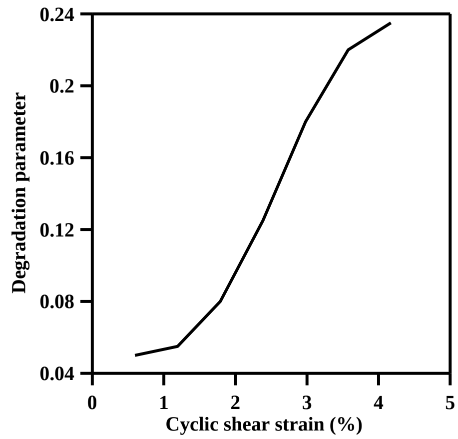

Figure 2. Relationship between degradation parameter and strain (reproduced from Idriss et al. 1978).

Proposed numerical model

Degradation of shear modulus is modeled according to Idriss et al. (1978) in which shear modulus of soil degraded with increasing number of cycles. The degradation can be evaluated with number of cycle as follows:

$$\delta = \frac{k_N}{k_{initial}} = N^{-m} = \left(\frac{t}{T}\right)^{-m} \text{; if } t/T < 1,\ \delta = 1 \qquad (1)$$

where k_N is the soil spring stiffness after N cycles of loading, k_{initial} is the initial stiffness of soil, m is the degradation parameter, N is the number of load cycles, t is the solution time and T is the period of loading. The values of m is dependent on cyclic shear strain in soil. Idriss et al. (1987) reported the values of degradation parameter (m) for cyclic shear strain amplitude (γ) as shown in Figure 2. In the analysis, the average strain in the soil (γ_{avg}) around laterally loaded pile is considered for the estimation of m from Figure 2. The γ_{avg} is estimated is given by (Lombardi et al. 2013),

$$\gamma_{avg} = 2.6\frac{\Delta}{D} \qquad (2)$$

where Δ and D are the lateral deflection and the outer diameter of the monopile respectively. At the first step, the dynamic analysis is carried out considering initial soil stiffness which is estimated from API (2011) based *p-y* curves. The γ_{avg} in the soil spring is estimated based on the deflection in each soil spring for the applied load at each time step. The degradation parameter (m) is estimated from the values of γ_{avg} and the degradation factor δ is estimated from Eq. (1). Subsequently, degraded stiffness is assigned in each spring after N cycles of loading. Note that, N load cycles is calculated from the solution time (t) and time period of loading (T) as indicated in Eq. (1).

VALIDATION OF THE PROPOSED MODEL

The numerical model is developed based on the parameters used in the experiment considering degraded shear modulus of soil. The cross section of tower and monopile are modeled as equivalent solid section. The RNA mass is modeled as point mass at the top of tower. The numerical results are validated with numerical model considering two cases: (i) fundamental frequency (Figure 3a) and (ii) a time series of deflection measured at the pile head at soil surface with the number of cycles (Figure 3b). The fundamental frequency varying with number of cycles obtained from experiment is in good agreement with the numerical model. The comparison of time series of deflection measured from experimental result and numerical model is reasonably good.

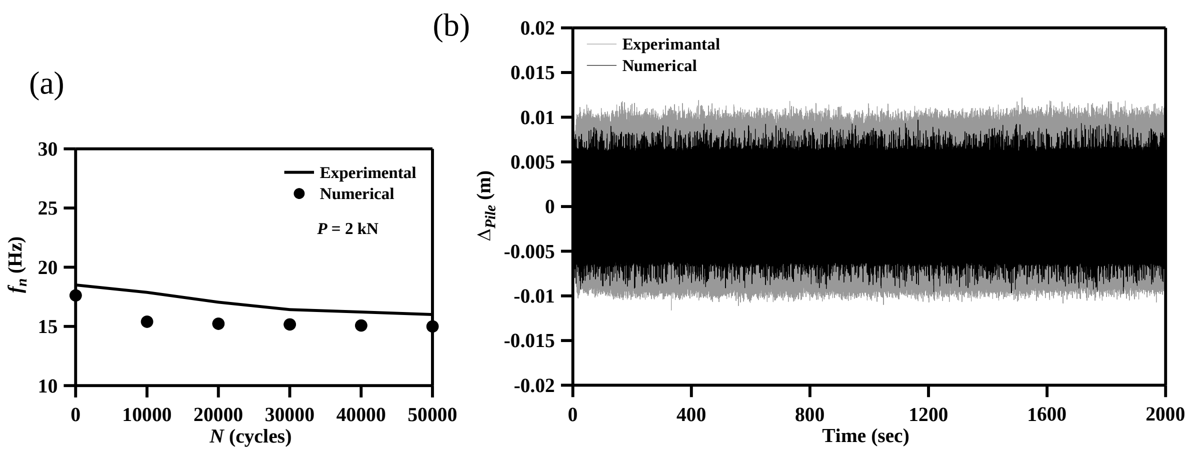

Figure 3. Observed and predicted (a) fundamental frequency and (b) lateral deflection of model OWT, when *P* = 2 kN and loading frequency = 5 Hz

RESULTS AND DISCUSSION

Numerical model is solved in COMSOL Multiphysics® (COMSOL, 2013) finite element program using API based soil *p-y* springs and proposed degradation model. The numerical analysis is carried out replicating the experimental model and a 5 MW OWT structure. The maximum rotation of monopile at ground level is determined both for model structure and real OWT after application of 10000, 20000, 30000, 40000 and 50000 cycles of loading. Loading for model OWT is considered to be same frequency and amplitude that of the model tests. Wind and wave loads were estimated based on DNV-OS-J101 (2010) for 5 MW OWT which are not presented due to brevity. The frequency of wind thrust at hub height is 0.25 Hz and the frequency of wave load is 0.1 Hz. Response is compared between proposed degradation model and *p-y* based model. The maximum rotation of monopile at mudline ($\theta_{pile,\ max}$) for different load cycles is presented in Figure 4. After 50000 cycles of loading, $\theta_{pile,\ max}$ is found to be increased up to 20% and 46% from the initial values for model scale experiment and proposed degradation model respectively. It is to be noted that $\theta_{pile,\ max}$ is found to be constant with number of load cycles for API based model.

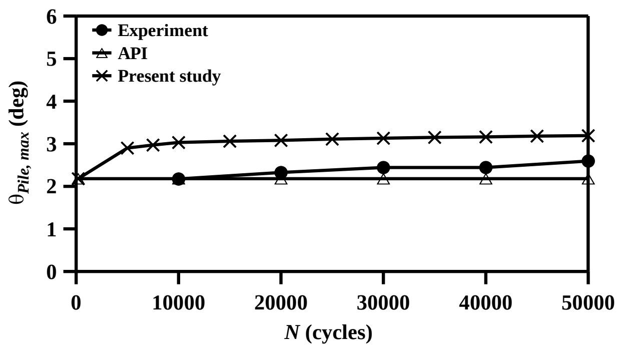

Figure 4. Maximum rotation at monopile head based on API (2011) and present study of model scale OWT.

The rotation of monopile at mudline is obtained from numerical analysis for real 5 OWT structure. Figure 5 illustrates rotation for different load cycles considering the proposed stiffness degradation model and *p-y* based model. It is interesting to note that the rotation is unaffected by the increased load cycles in case of *p-y* based model. However, the rotation is increased up to 47% after 2500 cycles considering proposed degradation model. Figure 6 shows the maximum rotation of monopile at mudline ($\theta_{pile,\ max}$) for different load cycles. It is observed that the rotation is increased by 25% and 78% for 5000 and 25000 cycles respectively from the initial $\theta_{pile,\ max}$. The $\theta_{pile,\ max}$ is found to be constant after 25000 load cycles. It is interesting to note that $\theta_{pile,\ max}$ does not change with load cycles in case of API based model.

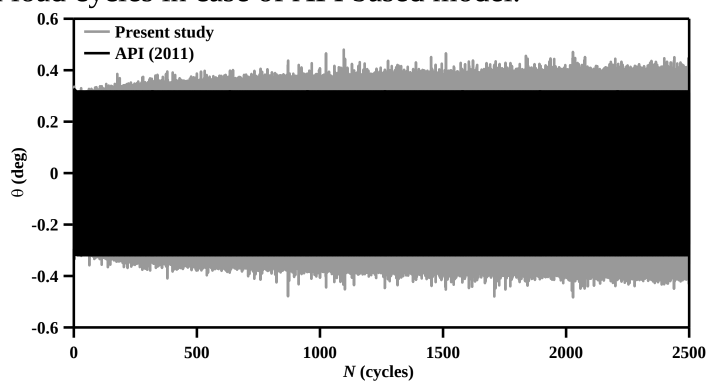

Figure 5. Rotation in a time series at monopile head based on API (2011) and present study of prototype OWT.

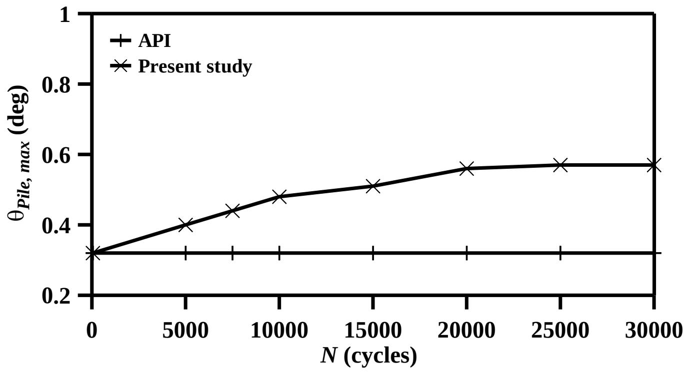

Figure 6. Maximum rotation at monopile head based on API (2011) and present study of prototype OWT.

CONCLUSIONS

This study shows limitations of API based *p-y* curve for the prediction of responses of monopile supported offshore wind turbine in clayey soil. A Winkler based soil-pile interaction model is proposed incorporating the stiffness degradation effect with number of load cycles. The proposed model is also calibrated with experimental results on model scale OWT in clay. The results shows that the maximum rotation of monopile at mudline increases with the application of load cycles whereas the rotation is found to be unaffected considering API based foundation model. It may be concluded that the API based cyclic *p-y* curves may underestimate the design of foundation of OWT structure.

REFERENCES

Achmus, M., Kuo, Y. and Rahman, K.A. (2009). “Behavior of monopile foundations under cyclic lateral load.” *Computers and Geotechnics*, 36, 725-735.

Andersen, L. V., Vahdatirad, M. J., Sichani, M. T. and Sorensen, J. D. (2012). “Natural frequencies of wind turbines on monopile foundations in clayey soils—a probabilistic approach.” *Computer Geotechnics*, 43, 1–11.

API (2011). American Petroleum Institute. *Petroleum and natural gas industries-specific requirements for offshore structures*. Part 4 – geotechnical and foundation design considerations.

Bekken, L. (2009). *Lateral behavior of large diameter offshore monopile foundations for wind turbines*. Thesis Report, Delft University of Technology, The Netherlands.

Bhattacharya, S. and Adhikari, S. (2011). “Experimental validation os soil-structure interaction of offshore wind turbines.” *Soil Dynamics and Earthquake Engineering*, 31, 8.5-816.

Bhattacharya, S., Lombardi, D. and Wood, D. M. (2011). “Similitude relationships for physical modelling of monopile-supported offshore wind turbines.” *International Journal of Physical Modelling in Geotechnics*, 11, 58-68.

Bhattacharya, S. (2014). “Challenges in design of foundations for offshore wind turbines.” *Engineering & Technology Reference*. DOI: 10.1049/etr.2014.0041.

Carswell, W., Arwade, S. R., DeGroot, D.J., and Lackner, M. A. (2015). “Soil-structure reliability of offshore wind turbine monopile foundations.” *Wind Energy*, 18 (3), 483 – 498.

COMSOL multiphysics user guide, Version 4.3b Edition, *COMSOL AB*, U.S., 2013.

Damgaard, M., Ibsen, L. B., Andersen, L. V. and Andersen, J. K. F. (2013). "Cross-wind modal properties of offshore wind turbines identified by full scale testing." *Journal of Wind Engineering and Industrial Aerodynamics*, 116, 94 - 108.

DNV-OS-J101. (2010). *Design of offshore wind turbine structures*. DET NORSKE VERITAS.

Feld, T. (2001). *Suction Buckets, a new innovative foundation concept, applied to Offshore Wind Turbines*. Ph.D. Thesis, Aalborg University, Denmark.

Guo, Z., Yu, L., Wang, L., Bhattacharya, S., Nikitas, G. and Xing, Y. (2015). "Model tests on the long-term dynamic performance of offshore wind turbines founded on monopoles in sand." *Journal of Offshore Mechanics and Arctic Engineering*, 137, 1-11.

GWEC (2011). *Indian Wind Energy Outlook 2011*. Global Wind Energy Council, Brussels, Belgium.

Idriss I. M., Dobry R. and Singh R. D. (1978). "Nonlinear behaviour of soft clays during cyclic loading." *Proc. ASCE*, 104, 1427–1447.

LeBlanc, C. (2009). *Design of offshore wind turbine support structures — selected topics in the field of geotechnical engineering*. PhD Thesis. Aalborg University.

Lesny, K., Wiemann, J. and Richwien, W. (2004). *Evaluation of pile diameter effects on soil-pile stiffness*. University of Duisburg-Essen, Institute for Soil Mechanics and Foundation Engineering, Essen, Germany.

Li, Z., Haigh, S. K. and Bolton, M. D. (2010). "The response of pile groups under cyclic lateral loads." *International Journal of Physical Modelling in Geotechnics*, 47–57.

Lombardi, D., Bhattacharya, S. and Wood, D.M. (2013). "Dynamic soil-structure interaction of monopile supported wind turbines in cohesive soil." *Soil Dynamics and Earthquake Engineering*, 49, 165-180.

Martinez-Chaluisant, V. (2011). *Static and dynamic response of monopiles for offshore wind turbines*. M.Sc. Thesis, University of Wisconsin-Madison, U.S.A.

Mostafa, Y. E. and El Naggar, M. H. (2004). "Response of fixed offshore platforms to wave and current loading including soil-structure interaction." *Soil dynamics and earthquake engineering*, 24, 357-368.

MACHINE FOUNDATIONS: A REVIEW OF FAILURES

Priya Jose[1], Ravi S. Jakka[2] and Ashok D. Pandey[3]

[1]M.Tech Student, Department of Earthquake Engineering, Indian Institute of Technology, P.O. Box 247667, Roorkee, email: priyajosevithayathil@gmail.com
[2]Associate Professor, Department of Earthquake Engineering, Indian Institute of Technology, P.O. Box 247667, Roorkee, email: rsjakka@gmail.com
[3]Assistant Professor, Department of Earthquake Engineering, Indian Institute of Technology, P.O. Box 247667, Roorkee, email: adpanfeq@gmail.com

ABSTRACT

Foundation failures are relatively uncommon where these support static loads. However, the potential for failure is greatly increased where foundations support machinery or equipment which applies dynamic excitation. The term ‘failure’, when applied to machine foundations does not necessarily infer damage to the foundation block itself; nor unacceptable static deformation; it more often relates to unacceptable levels of vibration resulting from inadequate design or functioning of the machine in a manner not accounted for in design. Abnormally high machine foundation oscillations are a serious concern for any enterprise since they cause excessive wear and bearing, damage to machine components and supply pipes, loosening of fasteners, electrical and electronic malfunctions in the equipment, damage of foundation structures and undesirable soil deformations. The paper reviews case studies where foundations have failed due to intolerable vibrations and various aspects of analyzing; diagnostics and monitoring of these vibrations are described.

INTRODUCTION

Machine foundations are special type of foundations built for supporting machines, machine tools and heavy equipments which have wide range of speeds, loads and operating conditions. These foundations are subjected to dynamic loads in addition to static loads due to the weight of machine and foundation. Thus they require special attention of a foundation engineer. The basic philosophy behind design of machine foundations is that: a) the dynamic forces of machines are transmitted through the foundation to the soil in such a way that all kinds of damaging effects are removed and the amplitudes of vibration of the machine as well as that of foundation are well within the specified limits, b) foundation should be structurally safe to resist all static and dynamic forces generated by the machine. The amplitude of motion of a machine at its operating frequency is the most important parameter to be determined in designing machine foundation. High amplitudes can cause either serviceability and malfunctioning problems reducing people’s comfort, or safety problems with danger of failure. When excessive motions of an existing foundation obstruct the operation of the supported machinery, analysis is necessary to understand the causes of the problem and hence to guide appropriate remedial action. The paper reviews various vibration problems grouped under different types of machine foundations and the different schemes by which the foundations were revived.

CASE STUDIES ON BLOCK FOUNDATIONS

Compressor Foundation Subjected to High Horizontal Vibrations (Wang, 1984)

Foundations under 3 compressors rested on clay base. The horizontal vibration velocity reached 8.96 mm/s exceeding the permissible limit, affecting normal production and work in neighboring offices. The author was asked to rectify the problem without interrupting production. Firstly, two foundations (N-1 and N-2) were tested under horizontal forced vibration. Test results are shown in Figure 1. From the figure, the natural frequency was found to be 14.2 Hz for N-1 and 14 Hz for N-2.

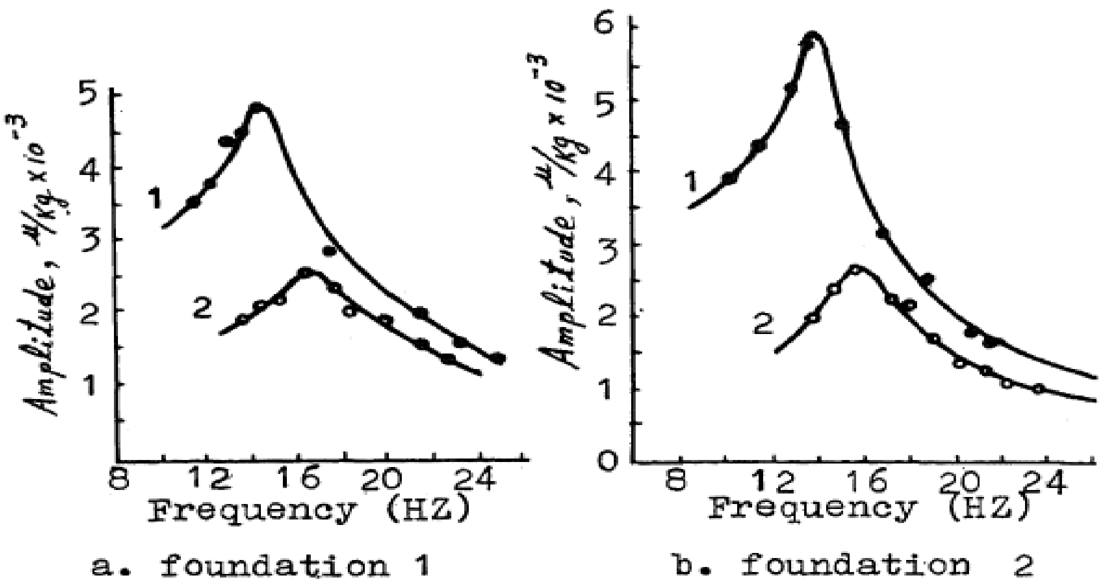

Figure 1. Response of amplitude under horizontal exciting force: (1) Before treatment (2) After treatment (Wang, 1984)

The secondary exciting frequency being 13 Hz, the ratio of operating frequency of machine to natural frequency of the system was 0.92 – 0.93, clearly indicating resonant vibrations. Various treatment schemes were available. Since the foundations were lying close to one another, it would be helpful to connect the foundations so as to increase the rigidity as a whole. Thus combined foundation was employed; base plates of foundations were combined using a reinforced concrete ground beam as shown in Figure 2. to increase elastic resistance, damping ratio and resonance frequency of base.

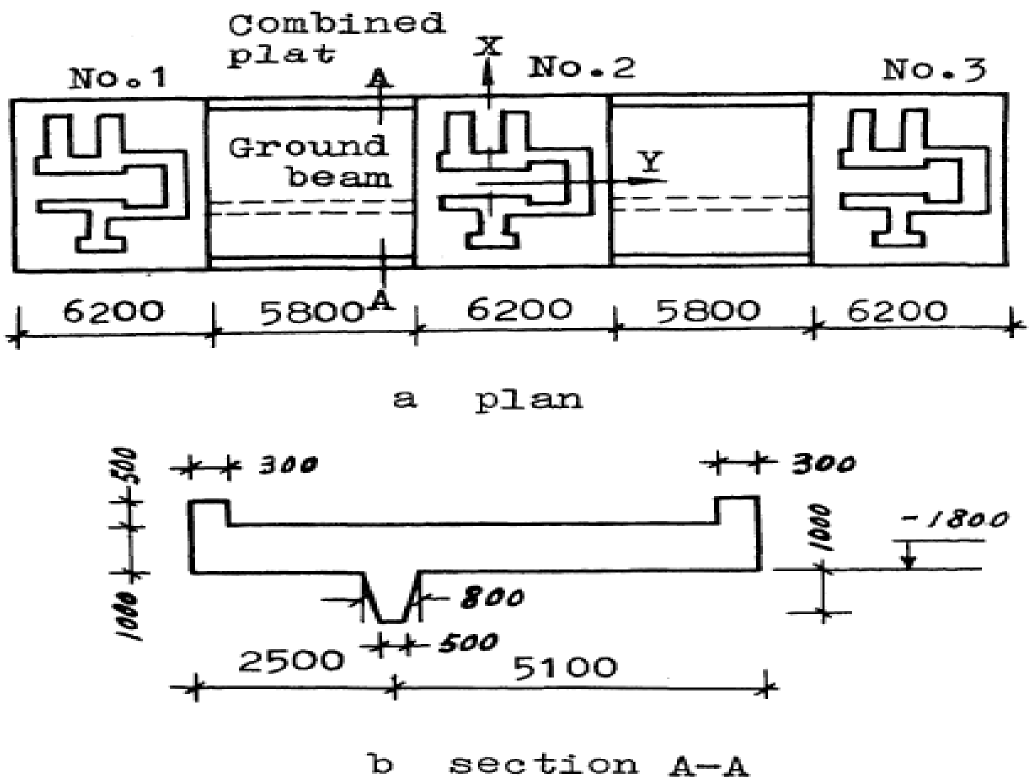

Figure 2. Diagrams of combined foundations (Wang, 1984)

A forced horizontal vibration test was repeated after hardening of ground beams, results of which are given in Figure 1. It can be seen that the amplitude of vibrations has significantly decreased and the frequency of N-1 increased from 14.2 to 17 Hz while that of N-2 from 14 to 16 Hz. This can be attributed to increase in stiffness of base with an increase in mass participating in vibration.

Analysis of Compressor Station before Completion of Work (Kvasnicka et al., 1988)

A compressor station consisted of eight compressors. Measurements were taken before the whole station was completed and only 3 compressors were in operation. Analyses were performed considering three soil profiles:-

a) Soil profile modeled as clay stratum (G= 50 MN/m^2) over sand half space (G=100 MN/m^2).
b) Foundation on half space with G= 100 MN/m^2 (thus neglecting the clay sub layer).
c) Foundation stratum with average modulus G=80 MN/m^2 over half space with sand properties (G= 100 MN/m^2).

The calculated amplitudes of vibrations for the above soil profiles are given in Table 1.

Table 1. Calculated amplitudes of vibrations at corners of foundation (Kvasnicka et al., 1988)

Case	Longitudinal (μm)	Vertical (μm)	Radial(μm)
a)	1,1	4,2	23,2
b)	0,6	2,3	5,9
c)	0,8	2,7	11,3

From the table, the amplitudes were found to be high when clay was direct foundation supporting soil. Therefore it was decided to replace clay above ground water level with one meter thick densified gravel layer. After treatment, measurements were taken in the middle (M) and at corners (C) of the foundation for three compressor foundations as shown in Table 2. Substituting clay by gravel layer has significantly lowered the amplitudes. This accounts to the increased stiffness of soil supporting the foundation.

Table 2. Measured values of amplitudes (Kvasnicka et al., 1988)

		Longitudinal (μm)	Vertical (μm)	Radial (μm)
C1	(M)	0,4	0,8	1,8
	(C)	0,4	1,25	1,33
C2	(M)	0,9	1,2	2,19
	(C)	0,9	1,2	2,5
C3	(M)	1,2	1,7	2,5

Compressor Foundation Producing Excessive Vibrations (Arya et al., 1978)

During the operation of a four stage BPCL air compressor in the oxygen plant of Central forge plant of M/s BHEL, Haridwar excessive vibrations occurred necessitating check in the design of foundations of the air compressor. Natural frequencies and amplitudes in different modes were computed using the linear elastic weightless spring method from the given design data. Amplitudes of vibration of the compressor foundation were also determined by measuring in horizontal and vertical direction at different locations. From the computed results, it was found that the natural frequency in yawing mode coincided with the operating frequency and the vertical frequency was only slightly different from the operating frequency. The higher natural frequency due to combined rocking and sliding approached the second harmonic. Both the observed and computed amplitudes were much higher than the permissible amplitude. The foundation was therefore considered inadequate. It was suggested to adopt appropriate remedial measures such as attachment of special slabs to reduce the vibration amplitudes.

CASE STUDIES ON HAMMER FOUNDATIONS

Intolerable Vibrations due to Hammer Foundation (Svinkin, 1993)

Five storey apartment building was situated at a distance of 500 m from the vibration isolated foundation under a forge hammer. Measured vibrations of the building were intolerable when the natural frequency of the foundation was 3.1 Hz. For diminishing intolerable resonance building vibrations, it is necessary either to reinforce building structures or change the frequency of the vibration isolated foundation. Changing the frequency of block vibrations is much simpler and more economical than the first measure. This can be accomplished by decreasing vibroisolator stiffness by eliminating a part of them from work. Since springs are accounted from condition of strength, it is possible to diminish only dashpot amount. Thus the frequency of the foundation was decreased to a value of 2.9 Hz by eliminating a few dashpots. Buildings usually have narrow resonance range and a small change in the frequency of block vibrations gives good result.

High Oscillations of a Hammer Foundation in Turkey (Arsoy, 2008)

Unwanted vibrations were arising from a forging facility in Turkey, causing trouble to surrounding facilities within a radius of 300 meters. The solution lies in reducing vibrations at source or employing active or passive vibration barriers. A vibration barrier at other structures could not be requested. Effectiveness of vibration isolation employing open or filled trenches was questionable for the site. Therefore it was not considered. The best solution was to increase the stiffness of soil using piles as foundation support. However, the owner wanted cost effective rapid solution of unwanted vibrations. The short term solution opted was to use reverse vibration absorber approach by reducing the foundation amplitude by allowing the machine to have higher amplitudes; the machine acted as a vibration isolator block by protecting foundation from vibrations. This was carried out by reducing the springs between the foundation and the machine. The disadvantages were absorbed by taking additional measures on the lifeline connections of the machine.

CASE STUDIES ON FRAMED FOUNDATIONS

Sudden Rise in Vibrations of Foundation under Cone Crusher (Svinkin, 1993)

Two cone crushers were mounted on two separate identical framed foundations. The vibrations of these crusher foundations were in tolerable limits for long time. However, the vibration of one foundation surged all of a sudden and the amplitude reached 1 mm. Such vibration level was inadmissible and could be attributed to changes in any part of machine-foundation-soil system. Steps were undertaken to diagnose the vibration problem. Impulse loads cannot be suddenly increased and the unbalanced forces can only increase gradually. Crusher as a source of vibrations was ruled out for these reasons. The crusher foundation didn’t have any visible damage and cracks and therefore it was not responsible for high vibrations. The soil below crusher foundation was limestone with sandy and clayey interlayer’s. Crushing being wet process production, water penetrated and reversed the soil properties. Changes in soil moisture resulted in low stiffness of soil, causing a change in the frequency of the system and correspondingly the amplitudes of motion. The viable solution was to reduce the moisture content by pumping out water.

Excessive Horizontal Vibrations of Foundation under Centrifugal Pumps

On initial installation of 3600 RPM horizontal centrifugal pumps in petroleum refinery, the pumps were found to exhibit high levels of horizontal vibrations. Suspecting a resonance condition, ‘bump test’ was performed in the horizontal direction on the pump bearing. The horizontal natural frequency of the pump bearing was found to be of same order from the test.

Thus resonance was confirmed as the cause for excessive vibrations. The best solution to solve a resonance problem is to separate the natural frequency from the exciting force frequency. This can be done by changing the natural frequency by increasing or decreasing mass or stiffness, or by increasing or decreasing exciting force frequency. However, these changes are not possible or cost-effective. Another possible solution is to install a dynamic absorber (auxiliary mass vibration neutralizer). The dynamic absorber is usually a spring-mass system installed in series with the resonant system to create an out of phase exciting force to effectively curb the initial excitation force. In this case, plant engineering opted for dynamic absorber approach to solve the problem.

CASE STUDY ON MAT FOUNDATION

Offset Printing Press Subjected to High Levels of Vibration (Vlad, 2010)

An offset printing press was installed in a steel industrial building in Romania. Some undesirable transverse vibrations began to occur when the speed of operation was increased. After a detailed instrumental investigation and evaluation, the source of occurred vibrations was found to be the printing press itself. During operation, ink is distributed to the printing plates by rollers which rotate about an axis transverse to the longitudinal direction of the press. This transverse excitation produced by ink distributing rollers was very close to the Eigen frequency of the first swaying mode of the ensemble. Thus the performance of ink rollers paved way for excessive vibrations. The solution proposed was to change the inking roller gears so that they wouldn't reach a frequency ratio greater than 0.6. This case study showed how at higher speeds, an unbalanced force can cause undesirable vibrations.

CONCLUSIONS

The effects of excessive vibrations range from annoyance for local population and disturbance of working conditions for sensitive devices, to diminution of structure serviceability and durability. Therefore there is an increasing need to analyze, monitor, diagnose and retrieve machine foundations from intolerable vibrations. Various schemes are available for remedying vibration problems.

- Firstly, the machine is checked for unbalance. **Balancing** is done by minimizing eccentricities in rotary parts or by applying a counter-force/moment.
- **Structural measures** like increasing base area or mass of the foundation, attaching a slab to the foundation, and using auxiliary spring-mass system are resorted to achieve largest possible difference between natural frequency and operational frequency of machine, i.e. during resonance.
- **Stabilization of soils** results in an increase in the rigidity of base and consequently reduces vibrations.
- Effective isolation can be achieved by **proper location** of vibration causing machinery. For example, foundations on sound, deep-seated bedrock will experience smaller vibration amplitudes than foundations on weathered materials or soils subjected to same excitation.
- Transmission of waves generated by machine foundations can be minimized by placing a suitable **wave barrier** in the ground before the structure. Open trenches, in-filled concrete or bentonite trenches, sheet pile walls, concrete core walls or row of piles can be effective wave barriers.

The solution therefore lies in identifying the cause for vibrations and taking remedial action in the concerned direction.

REFERENCES

Arsoy, S. (2008). "Mitigation of adverse vibrations in nearby structures arising from a large forge hammer", 6thInternational Conference on Case Histories in Geotechnical Engineering, Arlington, VA, 1-4.

Arya, A.S., Puri, V.K., and Gupta, M.K. (1978). "Evaluation of the performance of the foundations of BCPL air compressor at central foundry forge plant BHEL Hardwar", Report No. EQ 78-9, School of Research and Training in Earthquake Engineering, University of Roorkee, 1- 15.

Bhatia, K.G. (2006). "Machine foundation design – a state of the art", Journal of Structural Engineering, 33, 69-80.

Bhatia, K.G. (2008). "Foundations for Industrial Machines", D-CAD Publishers, New Delhi.

Fox, R. "Dynamic absorbers for solving resonance problems", Entek IRD International Cooperation, Houston.

Jain, A., and Soni, D.K. (2007). "Foundation vibration isolation methods", 3rd WSEAS International Conference on Applied and Theoretical Mechanics, Spain, 163-167.

Kvasnicka, P., Ivsic, T., and Klricenko, A. (1988). "Analysis and measurement of foundation vibrations at two compressor stations in yugoslavia", 2nd International Conference on Case Histories in Geotechnical Engineering, St. Louis, Missouri, 819 - 823.

Prakash, S. (1981). "Soil dynamics", McGraw-Hill Book Company, New Delhi.

Srinivasalu. P., and Vaidyanathan, C.V. (1976). "Handbook of machine foundations", TATA McGraw-HILL Publishing Company Ltd, New Delhi.

Svinkin, M.R. (1993). "Analyzing man-made vibrations, diagnostics and monitoring", 3rd International Conference on Case Histories in Geotechnical Engineering, St. Louis, Missouri, 663 - 670.

Vlad, I. (2010). "Machine foundations and blast engineering vibrations case studies", 5th International Conferences on Recent Advances in Geotechnical Earthquake Engineering and Soil Dynamics, San Diego, California, 1- 25.

Wang, X. (1984). "A case study on decreasing vibration of machine foundations and structures", 1st International Conference on Case Histories in Geotechnical Engineering, 787 - 790.

Failure Analysis of Semi-elliptical Tunnel in Soft Ground

K.S.Ram[1], D.K.Singh[1], A.L.Murmu[1], A Mandal[2]

[1]PhD Scholar, Civil Engineering Department, VNIT, Nagpur.
[2]Associate Professor, Civil Engineering Department, VNIT, Nagpur.

ABSTRACT

This study investigates the potential causes and extent of squeezing for a tunnel, which is supported by steel-rib backfill support system constructed as a part of Udhampur Srinagar Baramulla Rail Link (USBRL) project at the Himalayan region in Jammu & Kashmir, India. The semi-elliptical tunnel with 8 segmented steel ribs is constructed in soft ground conditions containing soft clay which had undergone tunnel failure, mainly due to squeezing at various sections. Finite element method is adopted for modelling the tunnel to study the behavior of tunnel support system. Field observations indicated the failure at crown level, while finite element analysis has shown the maximum deformations developed at the side walls as well as top of the crown. This has been investigated and it is concluded that the failure at the centre of side wall is mainly due to joint deflection of the steel-rib segments, while the squeezing potential is affected by the flexible support system provided and high overburden pressure due to soft ground. It is suggested to provide a flexible support system with high energy absorbing capacity SFRS with increasing the flexural strength by providing high quality steel bars for better performance of the tunnel. Interpretation of deformations by regular monitoring of excavation process is mandatory take further necessary measures, if required.

INTRODUCTION

The Udhampur-Srinagar-Baramulla Rail Link (USBRL) project is one of the significant project is under construction in the state of Jammu & Kashmir, India linking the Kashmir valley goes through the great Himalayas region. This project is constructed under Northern Railway Corporation limited and the tunnel alignment considered in this paper is T42-43 from chainage Ch.93/300 to Ch. 94/663.219km as shown in Figure 1. Failure of underground structures frequently faced during construction of tunnel is discussed in this paper.

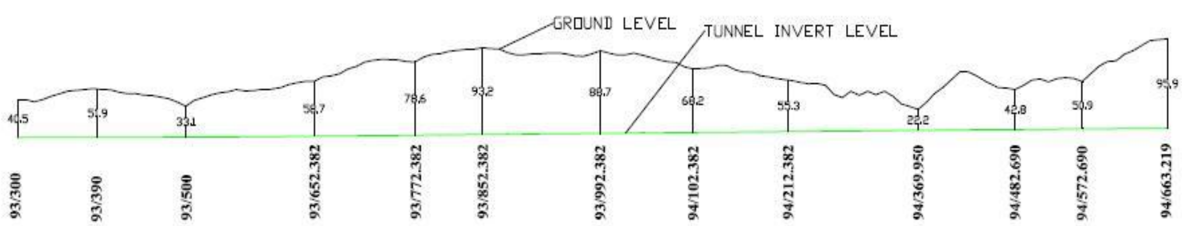

Figure 1. Longitudinal section of Tunnel T42-43 from Ch.93/300 to Ch. 94/663.219km

GEOLOGY OF THE AREA

The Himalayas possess young rock formations, consists mainly of sedimentary rocks. These rocks are weak and are highly sheared in nature. Most commonly sand stone, silt stone and weak clay stone are encountered. These rocks are highly jointed and belong to class-III to class-V as RMR classification system. Further, the deposits in natural drains are made of loose conglomerates, which creates problem during tunnelling. The provision of support system will be based on the Ground conditions (i.e., squeezing/non-squeezing) [2]. The Claystone present in this area comprised of montmorillonite upto 50%, also certain proportions of kaolinite and illite [4]. Claystone with all these minerals have swelling properties as reported by [3].

SQUEEZING OF WEAK ROCK MASS

Tunnelling in rock comprised of swelling clay is a special challenge, since the gradual deformations are predominant over time even after the completion of excavation which is a time-dependent behaviour [8]. These deformations are generally constrained by support members resulting in the failure of these members if their strength is insufficient [8]. Therefore, it is important to estimate potential tunnel problems as early as possible [10]. To predict squeezing, load cell, contact pressure cells and tape extensometers are installed at various locations [2]. As shallow buried conditions, weak rock always have complex mechanical properties and also uneven ground lead to the uneven distribution of loads [9]. The tunnel construction throughout this area are affected by squeezing of rock at many locations with high rock cover resulting in the buckling of wall support ribs and tunnel roof support is damaged as shown in Figure 2 [4 ,5].

Figure 2. Failure of steel ribs at crown portion

TUNNEL CONSTRUCTION METHODOLOGY

The tunnel is elliptical shaped with excavated width of 7.2m. The longitudinal section along the tunnel is shown in Figure 1. It can be observed from Figure 1 that maximum rock cover above the tunnel is 96m at the chainage Ch. 94/663.219km. The conventional method of drill and blast was used for tunnelling. The tunnel advanced rate of 2.0-2.25m was considered during normal geological conditions and 0.5-1.0m during adverse geological conditions. The distance between heading and benching was maintained upto 10m. The steel rib supports of ISMB 150 @ 0.5m spacing centre to centre with backfill of M10 concrete were installed in heading as well as in benching. In heading the supports were resting on the haunch. The gaps between steel ribs were covered by precast lagging of 50mm. Then the gap in between steel ribs and shotcrete is filled with the backfill of M10 grade concrete. Rock bolts having length 1.2m of resin grouted were installed in competent rocks and cement grouted self-drilling anchors of 6m were installed in weak rocks. When the excavation of entire tunnel is completed then the lining of 300mm thickness is applied, M25 grade concrete is used. For good geological conditions single layer reinforcement mesh is used, whereas for poor geological conditions and near tunnel portals double layer of reinforcement mesh is used. The steel rods of diameter 10mm and c/c spacing 10cm is used to make the reinforcement mesh.

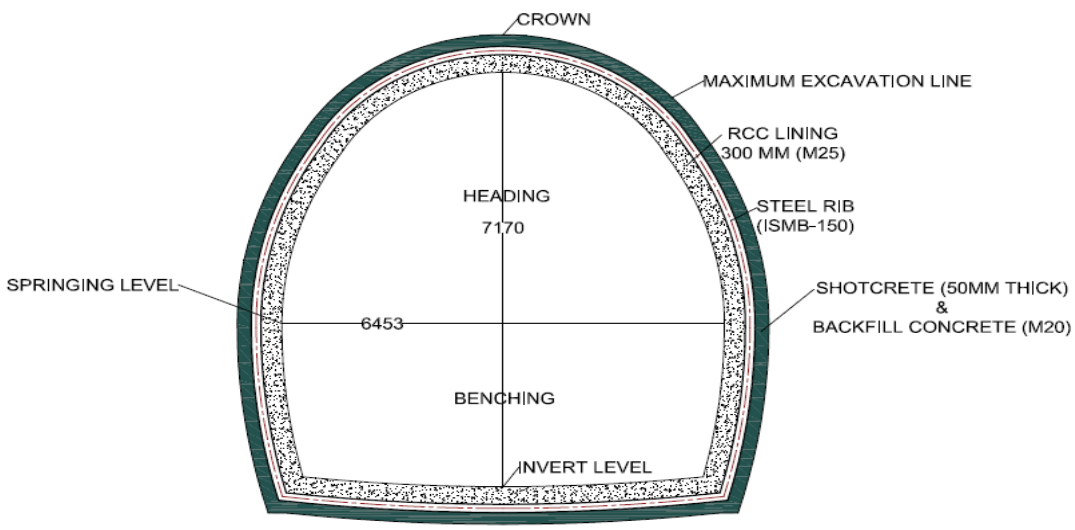

Figure 3. Semi-elliptical shape of section

FAILURE MECHANISM

Continued deformation of tunnel wall resulted in collapse of the steel rib support system of heading and side wall of tunnel at various locations. These high order deformations due to swelling of claystone had become major concern for the stability of the tunnel. Also tunnel deformations are observed at all sides mainly at the centre portion of the walls. To control these tunnel support failure problems, support system for the tunnel is assessed using numerical technique to propose appropriate remedial measures.

NUMERICAL MODELLING

In the present study, the semi-elliptical tunnel cross-section is considered for analysis with different overburden depths along the alignment of the proposed railway-line. The dimensions of the tunnel are considered based on the proposed plan. All the material properties of insitu Rockmass, Steel ribs and lining, used in this study are given in Table 1. The tunnel has been analysed for the effect of gravity.

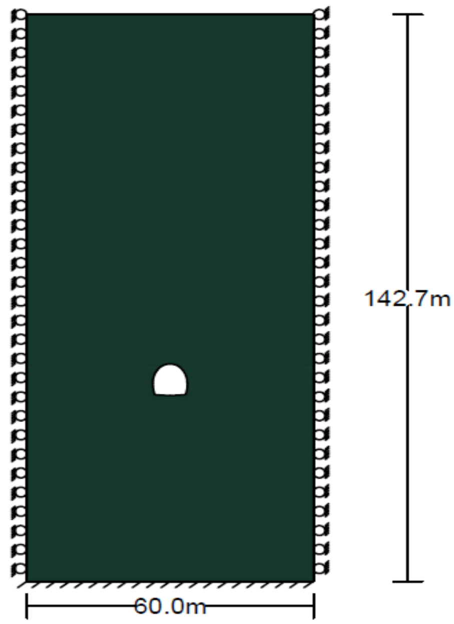

Figure 4. Dimensions and boundaries of the model for numerical analysis.

Table 1. Material Properties

Sl.no	Density, KN/m^3	Young's modulus, KN/m^2	Poisson ratio	Cohesion, KN/m^2	Angle of internal friction
Rock mass	21	30000	0.3	40	25
Steel Ribs	78.5	210×10^6	0.295	-	-
Concrete Lining	25	25×10^6	0.15	-	-

2D non-linear finite element model have been developed using ABAQUS software to simulate the coupled behavior of Tunnel-Ground system. Rockmass has been modelled using plane-strain linear quadrilateral (CPE4R) in dry conditions and 4-node plane strain quadrilateral, bilinear displacement, bilinear pore pressure (CPE4P) for simulating pore pressure analysis. An elasto-plastic constitutive model considering Mohr-Coulomb failure criterion with zero dilatancy following non-associated flow rule has been used for

Rockmass modelling [6]. The tunnel components i.e. Steel-ribs have been modelled using 2-noded beam element (B22) available in ABAQUS element library. The interaction between tunnel and rock is assumed to follow coulomb-friction model. The coefficient of friction is assumed as 0.4. The contact is allowed for separation after the initiation of tensile forces. The boundary conditions are applied in such a way that all the movements are restrained at base (i.e., both horizontal, vertical displacements are zero) and only horizontal displacements are restrained for left and right boundaries. Also, for saturated condition initial pore-water pressure is defined as zero at the location of the ground-water table l.

The response of tunnel support system has been studied in terms of deformations and stresses. In this analysis the insitu stresses are calculated by assuming k as 1 where, k denotes the ratio of horizontal to the vertical stress.

RESULTS AND DISCUSSION

Static analysis have been performed for two different cases i.e., prior to and after construction of lining, considering different overburden depths and ground water conditions coupled with surrounding rock mass. The results indicate that the deformations before provision of lining are much greater than anticipated. The actual ground conditions i.e. with a ground water table of 20m below the overburden is simulated, which gives a maximum deformation of 61cm at the side wall of the steel-rib and varied with overburden depth with a minimum deformation of 7cm. At many locations the deformations are predominant as the longitudinal section (Figure 1) shows the average overburden depth in the tunnel alignment is 40m. Movement of tunnel is also predominant at the crown level with a deformation of 40cm.

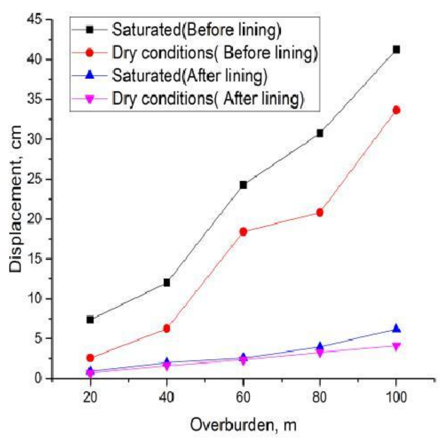

5(a) Displacement at crown level

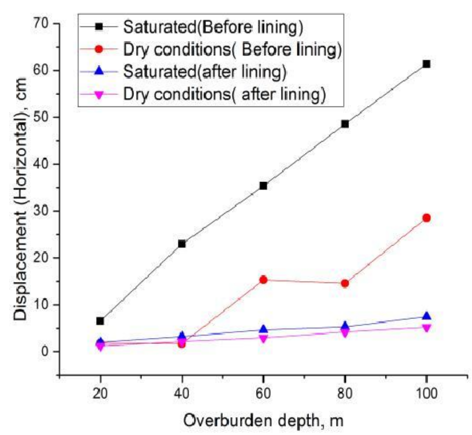

5(b) Horizontal displacement at centre of side-walls

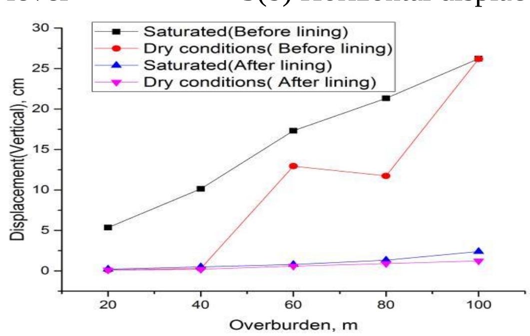

5(c) Vertical displacement at centre of side-walls

Figure 5. Variation of Displacement with overburden depth at Crown and side wall

Comparative analysis is carried out for saturated and dry conditions at overburden depths of 20, 40, 60, 80 and 100m. Significant deformations of ground and steel-ribs in both directions are observed, even in dry conditions. The side walls are affected more due to squeezing of rocks as compared to crown. This is due to the bending moments at the joints are 175 KN-m/m for existing joint condition forming a weak link in the support system and as a result failure at the joint had taken place with predominant deformations. If the joints are replaced with fixed conditions the bending moments are not released so that deformations are reduced to 25cm. After the provision of lining of 0.3m thick the deformations are gradually decreased as shown in the Figure 5 (a)-(c). But, there is a possibility of formation of cracks on the concrete lining due to the existing deformations of steel-ribs. High stresses are developed at the crown level as shown in figure 6 (a)-(b) and also around the tunnel there is a significant distribution of stresses, therefore the rock bolts is provided as long as possible to minimise the stress distribution around the tunnel.

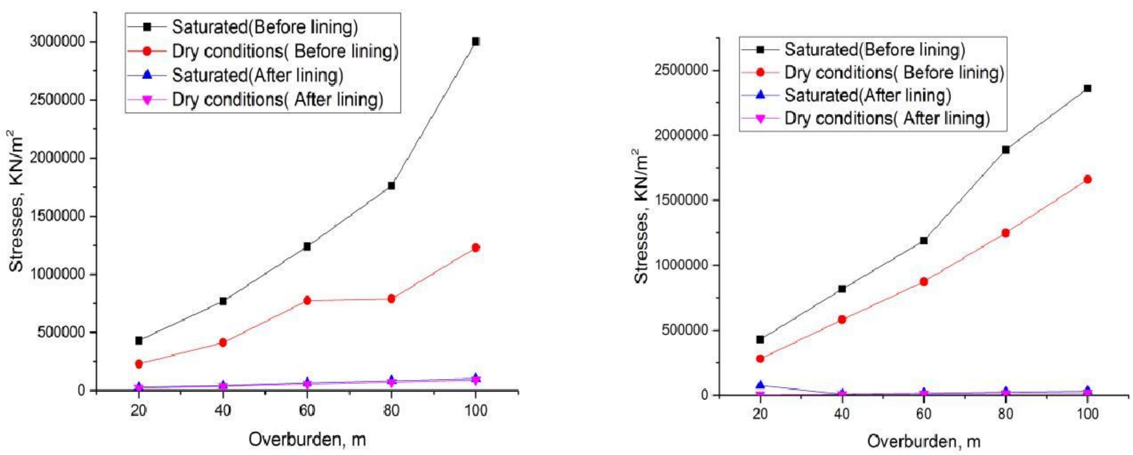

(a) Stresses at crown level (b) Stresses at centre of side-walls

Figure 6. Variation of Stresses with overburden depth at Crown and side wall.

Therefore, to prevent cracking in concrete lining rectification of deformed steel ribs is essential with high energy absorbing capacity SFRS. Also, flexural strength of SFRS can be increased by providing high quality steel bars. For the stability of the Side walls there is a need for heavy steel I sections at the joints to reduce the bending moments at the joints. It is suggested to provide a flexible support system with appropriate provisions for better performance of the tunnel. Interpretation of deformations by regular monitoring of excavation process is mandatory take further necessary measures, if required.

CONCLUSIONS

A numerical study on coupled behavior of Rock mass-tunnel system has been presented. The cause for failure of support system of Tunnel T42-43 at different locations of the of Udhampur-Baramula section has been studied through a comparative analysis, the following conclusions are made

- The field observations had indicated the failure at the top of the crown level at various locations, which is due to the squeezing of the surrounding Rockmass as it is mainly composed of swelling clay minerals.

- It is also observed that with the increase of the overburden, the deformations are predominantly increased at the crown level which led to the failure of the tunnel support system at the top of the crown level.

- Analysis had shown that the horizontal deformations of the steel-ribs at the side wall are higher due to the attracting maximum bending moments at the joints which had formed as a weakest link for the tunnel support system leading to failure.

- The stresses developed after concrete lining of 0.3m thick had been lowered and also does not affect the stability of the tunnel, but there is a probability of formation of cracks in the lining due to existing deformations.

ACKNOWLEDGEMENT

Authors are thankful to Northern Railway, India for providing suitable data for the study. The research work presented here was supported by the Institute Fellowship to the first author from the Ministry of Human Resource Development, Government of India. This support is gratefully acknowledged.

REFERENCES

Evert Hoek and Paul Marinos, (2000). “Predicting tunnel squeezing problems in weak heterogeneous rock masses”. Tunnels and Tunnelling International Part 1 and Part 2.

Dhiraj Raj, Yogendra Singh, (2016), “Pseudostatic Analysis of a Coupled Building-Foundation-Slope System for Seismic and Gravity Actions”. New frontiers in Civil Infrastructure, ASCE Geo-China 2016: pp. 99-107.

J. Donovan Jacobs, (1975), “Some Tunnelling failures and what they have taught”, 4th Conference on Hazards in Tunnelling and on false work, institution of civil engineers, 1975, Proceedings, London.

M. Verman, B. Singh, J. L. Jethwa and M. N. Viladkar, (1995).“Determination of Support Reaction Curve for Steel-Supported Tunnels”. Tunnelling and Underground Space TJ~mIogy, VoL 10, No. 2, pp. 217-224.

Malan DF (2002). “Simulating the time-dependent behavior of excavations in hard rock”. Rock Mechanics and Rock Engineering 35(4):225-254.

Mielenz, R. C., and King, M. E., (2008), “Physical mechanical properties and engineering performance of clays”, in Park, J.A., and Turner, M. D., eds., Clays and clay technology: National Conference on Clays and Clay Technology, 1 st, Berkeley, California, July 21-25, 1952, Proceedings, California Division of Mines Bulletin 169, pp. 196-254.

O. Aydan , T. Akagi , and T. Kawamoto,(1996). “The Squeezing Potential of Rock Around Tunnels: Theory and Prediction with Examples Taken from Japan”. Rock Mechanics and Rock Engineering, 29 (3), 125 143.

R.K. Goel, Anil Swarup, (2008). "Case history of Tunnelling through Claystone. Sixth International Conference on Case Histories in Geotechnical Engineering, Proceedings, Paper 4.

Sharma, P. and Chopra, R. (2006), "Case Study of Railway Tunnel No. 1 on Udhampur-Katra Section, Seminar on Tunnels and Underground Structures", J. of the Indian National Group of the International Association for Bridge &Structural Engineering, Vol. 36, No. 3, Aug-Sept. 2006, New Delhi, India, pp. III47-III56.

YANG Xiao-li, WANG Jin-ming, (2008). "Stress dilatancy analysis of shallow tunnels subjected to unsymmetrical pressure". J. Cent. South Univ. Technol. 15(s2): 028−033.

IDENTIFICATION OF HETEROGENEITIES IN LATERITIC SOILS

Vidyaranya B[1], Anbazhagan P[2], Divyesh R [2] and Athul Prabhakaran[2]

[1]Engineering Manager, L&T, Mumbai, India; e-mail: vidyaranya.bandi@gmail.com.

[2]Department of Civil Engineering, Indian Institute of Science, Bangalore, India; e-mail: anbu@civil.iisc.ernet.in.

[2]Department of Civil Engineering, Indian Institute of Science, Bangalore, India; e-mail: rohit.divyesh@gmail.com.

[2]Department of Civil Engineering, Indian Institute of Science, Bangalore, India; e-mail: apbpkn@gmail.com.

ABSTRACT

Lateritic soils are widely spread across the southern and central parts of India. Formed due to tropical weathering, the physical and chemical properties of lateritic soils vary over a wide range and stark differences are observed even within a given deposit, along horizontal and vertical directions. Lateritic formations usually have soft sediments (lithomargic clays) entrapped between the hard to medium soft lateritic rock which are leached due to the ingress of water during rainy seasons creating hollow sections or cavities which span over large lengths, which may cause excessive settlement to structures founded on such soils. However the macroscopic behavior of such soils has been studied due to their usage as construction materials, literature on the performance of insitu lateritic soils is sparse. Potential soft soil locations which are susceptible to cavity formation need to be identified and treated well in advance to minimize potential geotechnical failures in such soils. Though excavations in past reported number of cavities in lateritic soil and formation of sink holes in region, very limited attempts were made to map scientifically and treat them well in advance for important projects. This study presents an investigation to map heterogeneities in the subsurface profile of a project site in southern Peninsular India. The area of survey was approximately 400,000 sq.m and detailed geophysical surveys were carried out *viz.* Ground Penetrating Radar (GPR) and Multichannel Analysis Surface Wave (MASW) as per ASTM D6432-11 recommendations. 100 MHz and 500 MHz (for confirmative survey) Ground Coupled Antennae were used, with an interline spacing of 2.5 m for the GPR survey to detect changes in the macroscale dielectric properties of the subsurface. With the generated radargrams, heterogeneities in subsurface are identified through changes in the nature of the obtained waveforms. Based on such GPR radargrams observed along multiple parallel survey lines, doubtful locations were identified and detailed GPR cross surveys with reduced spacing between lines and MASW survey were carried out. Suspected cavity locations based on at least two geophysical surveys are investigated by drilling boreholes, which are used as an inlet to fill/close the cavity. This paper highlights a case study of a geophysical investigation at a large scale project and methodology involved in the identification of cavities in lateritic deposits, through integrated geophysical surveys.

Keywords: *Lateritic soils, Cavities, GPR survey, MASW, Electrical Resistivity*

INTRODUCTION

Since 1800's the terminology regarding laterite has been changed over and again. Lateritic soils have a typical taxonomy as they do not fall under the general classification of rocks like igneous, sedimentary or metamorphic rocks but more type of a sedimentary residual product. The laterites of Angadipuram in Kerala, India are considered as national geological monument as it was here were name the 'laterite' was devised from a Latin word "later" which means brick by English surgeon Francis Buchanan in 1807. Buchanan reported this material as full of cavities and voids, soft enough for excavation and can be easily carved into blocks by any iron instruments, but on drying it becomes as hard as brick and is further resistant to action of air and water (Aginam et al. 2015). Past 19th century laterite has been defined by many researchers in various manners like Alexander and Cady, (1962) have described laterite as highly eroded material with prolific amount of aluminum or iron oxides. Laterites are either hard or capable of hardening on exposure to wetting and drying. This terminology was regarding genesis and induration of laterite. Lohnes and Demirel, (1973) slightly modified Alexander and Cady's definition by claiming that laterite was sufficiently indurated that it could not be easily excavated by shovel or spade. In the Malabar region of Kerala, India laterite bricks have been widely used since past centuries for construction of residential structures, forts, churches, temples and other infrastructure. Removal of laterite cover for mining and bricks have proved to be beneficial alternately by clearing the area for cultivation also it was observed to increase the ground water recharge (Kasthurba et al. 2007).

Vermaat and Bentley (1954) studied the Ceylon (Sri Lanka) laterite while no significant study has been done to highlight the sinkhole formation phenomenon in Malabar (Indian) laterite. Typical laterite lithology had a mottled zone consisting of red honeycomb like structure having voids filled with yellowish or pinkish to white kaolinite clay overlying a crust layer. It is found that with depth the honeycombing framework became lighter and the size of the cavities or voids increased. The material filled in the voids remained soft on exposure to dryness and could be washed away. Kay (1972) and Robertson (1979) studied the sinkhole and pseudokarst caves in the lateritic origins of Australia. They credited the sinkhole formation to the subsidence into cavities formed by water flow in the underlying rock. Grimes and Spate (2008) studied the Australian laterite karst and found that the laterites are formed due to intensive chemical weathering of rock minerals over a long period of time. It is observed that caves with a hard surface on the top could form if the piping was localized. Grimes and Spate (2008) found the dissolution of Australian Mullaman lateritic beds to form sinkholes or caverns needed a few favorable conditions like biogenic reactions that is disintegration caused due to bacteria, fluctuating water level that is consecutive wetting and drying season and at the last rising of alkaline water from the limestones beneath during high water table conditions which facilitate dissolution of siliceous strata above. Geophysical methods like ground penetrating radar and seismic refraction have been widely used in subsurface identification of heterogeneities and sinkholes in karst and lateritic terrains in past decades. Ground penetrating radar is effective in the identification of fractures and karstic features at shallow depths (El-Qady et al. 2005). Anirudhan, (2014) observed that in lateritic deposits seismic refraction technique can be used in addition to point testing methods for identification of solution cavities.

The mineral composition of laterites in the Malabar region may vary from Ceylon to Australian Mullaman beds but the intensive weathering process and favorable conditions which help in sinkhole formation are much similar to all of the three places. As the Malabar region enjoys two rainy seasons the southwest monsoon and the northeast monsoon, which provides enough rainfall along with plenty of sunlight there is a constant fluctuation of the water table which assists in creation of piping condition. Cavities are identified in the study area under consideration. It is observed that most of the cavities are in irregular shape and identified due to sudden subsidence of the top hard surface. The ground surface above some of the cavity locations are so hard that they didn't collapse under moving loads of trucks and bulldozers. In view of the importance of structure, it was recommended to carry out detailed geophysical surveys of complete area for subsurface lithology. The literature study reveals that the lateritic profiles are highly heterogeneous in nature with properties varying significantly, it is recommended to use an integrated geophysical approach which shall cover large areas in short duration and provide a continuous subsurface lithological profile.

STUDY AREA

The paper presents a project site in the southern peninsular India, which is well known for its humid equatorial tropical climate with mean daily temperature ranging from 16° C to 35° C. The average annual rainfall is reported as 3438 mm. The laterite formations are found over origin rock types like charnockite, leptynite, anorthosite and gabbro, mainly near the coastal regions. The main bedrock found under the study area is charnockite and granite gneiss. Because of the weathering process it is highly heterogeneous and stratified in nature as seen in Figure 1. The laterites of these regions are found to be acidic, which is caused due to high rainfall and leaching of alkaline material.

INTEGRATED SUBSURFACE INVESTIGATION

Two geophysical methods, namely ground penetrating radar (GPR) survey and multichannel analysis of surface waves (MASW) were performed over the study area.

GROUND PENETRATING RADAR (GPR) SURVEY

GPR is a quick, non-destructive, non-invasive geophysical subsurface imaging technique which uses high frequency (10 MHz to 3 GHz) propagating electromagnetic waves to identify the changes in shallow subsurface strata by observing changes in electromagnetic properties. The electromagnetic properties like dielectric permittivity, conductivity and magnetic permeability in geological formation are dependent on subsurface material, water content and bulk density (ASTM D6432-11). GPR consists of four main components, transmitter, receiver, display unit and control unit. The transmitting antenna radiates a high frequency electromagnetic signal into the ground. When the propagating electromagnetic waves encounter change in electromagnetic properties, they get refracted, diffracted and reflected from the boundary of the subsurface material. The reflected signal is then received by the receiving antenna, recorded as a function of two way travel time for display and further processing. In the present study, Mala ProEx 100 MHz and 500 MHz (center frequency) continuous wave, ground coupled, shielded dipole antenna GPR were used for subsurface investigation.

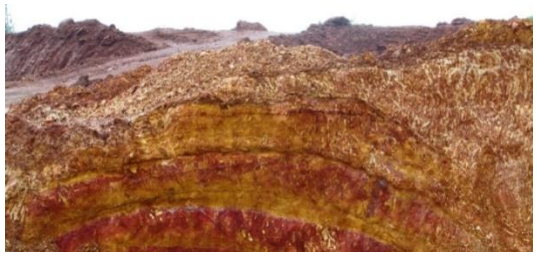

Figure 1. Soil stratification of a cut-section in laterite deposit.

The maximum penetration depth for Mala ProEx 100 MHz antenna is around 25 m and for 500 MHz is around 4 – 5 m which depends on the ground conditions like soil type, moisture content, salt content, etc. The preliminary survey was conducted over the identified areas of the construction site by 100 MHz frequency antenna longitudinally along the length at a regular interval of 2.5 m. The line lengths of the survey are marked for the full length. The distance traversed by the GPR equipment is measured by a standard distance measuring wheel attached to the antenna. 500 MHz antenna was used for the confirmative survey to obtain high resolution 2D images of the subsurface. The survey data at the site is recorded as radargrams and processed using RadExplorer (Mala GeoScience) software. Signal processing steps like DC Removal (removing constant component of the signal), time adjustment (time-zero correction due to gap between transmitter and receiver), background removal (removing horizontal banding in profiles due to system and surrounding electromagnetic noise), band-pass filter (increasing signal to noise ratio), amplitude correction (gain control) and time-depth conversion (using dielectric permittivity or wave velocity value) are applied to the radargrams. The average depth of penetration is observed to be around 5 to 6 m below ground level.

SEISMIC SURVEY

The seismic survey helps in determining the geotechnical properties of subsurface material by means of measuring their reaction to elastic or seismic action or disturbance. There are three types of seismic surveys, namely reflection, refraction and surface-wave. The surface wave survey method is the most convenient way to determine the elastic properties of shallow subsurface material as the depth-variation of shear wave, Vs is a governing factor among other elastic properties like density and depth-variation of P and S-wave velocities from which the dispersion property of surface waves is determined.

In the current study the seismic survey was performed by Multichannel Analysis of Surface Waves (MASW). The MASW survey was performed using 12 or 24 channel seismograph with 4.5 Hz OYO geophones. The seismic wave for this survey was generated from an active source by hitting a 7 kg sledge hammer on a 300 mm x 300 mm size metal plate with 5 shots. A typical view of the MASW survey conducted at the site can be seen in Figure 2. These waves were recorded by geode with 12 or 24 receivers placed at an offset of 1 m. The shot – offset distance for each line was kept at 5 m. The recorded surface wave data were used to extract dispersion curve and calculate the variation of shear wave velocity with depth using the inversion technique.

Figure 2. MASW survey being carried out at site

RESULTS AND DISCUSSIONS

This study tries to demonstrate that in case of areas consisting of laterite deposits, which are prone formation of cavities, an integrated geophysical investigation approach is required to obtain more detailed information of the subsurface lithology. As the soil in the study area mainly consists of laterite soil, the GPR profiles get influenced due to attenuation of radar signals due to presence of clay content and high moisture content. The average penetration depth of the radar wavelets is limited up to 7 m for 100 MHz antenna and 3.0 m for 500 MHz. Two geophysical surveys, GPR survey and MASW survey were performed over the study area. The results from three typical locations conducted by both the surveys are presented in the following sections.

LOCATION 1

An open cavity was idewntified location 1. The cavity had formed just 0.7 m below the ground surface and was of irregular shape (Fig. 3). It was observed that the top surface of the cavity was hard enough for a small car to stand over it. Figures 4 (b) and (c) show the radargram image for 100 MHz antenna while Figures 4 (d) and (e) show the radargram image for 500 MHz antenna.

Figure 3. Survey conducted by 100 MHz ground penetrating radar over the known cavity (Location 1).

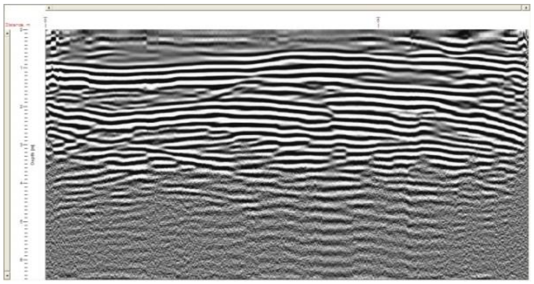

(a)

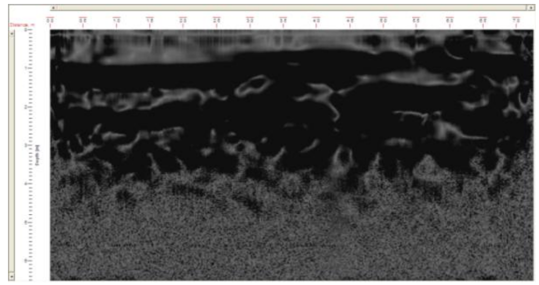

(b)

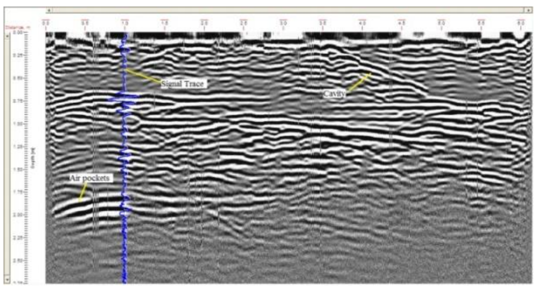

(c)

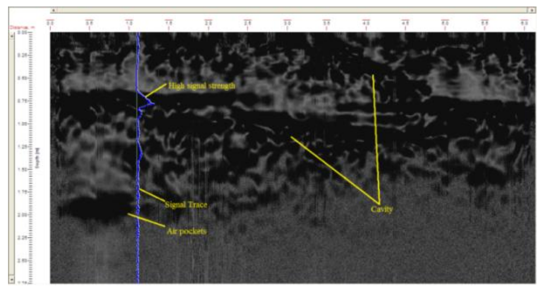

(d)

Figure 4. (a) and (b) 2D processed radargram and signal strength strength envelop for 100 MHz antenna, repectively, (c) and (d) 2D processed radargram and signal strength strength envelop for 500 MHz antenna, repectively over cavity location.

It can be easily observed from the images that the radargram with 500 MHz antenna had a higher resolution and details as compared to 100 MHz antenna. Figures 4 (b) and (d) show the respective 2D radargram for both the antennas which shows higher reflections at the interface of cavity structure and air pockets. Figures 4 (c) and (e), which represent the reflection strength of the electromagnetic (EM) signal in the subsurface, the strength of the signal is higher (darker) in air filled zone. On observing the signal trace in the radargram, it can be ascertained that a peak is observed in the signal amplitude as the signal strength and energy increases in air/water filled voids/cavity area.

LOCATIONS 2 AND 3

The GPR survey with 100 MHz antenna was conducted over the granular sub base (GSB) layer at Location 2 and Locations 3 over plain cement concrete pavement (PCC). From the GPR survey an anomaly was observed at a depth of 2.5 to 3 m in both the locations. MASW survey was carried out at these locations to confirm the presence of the cavity/sinkhole to obtain the shear wave velocity of the subsurface. Figures 5 and 6 ((a) & (b)) show the 2D radargram of and signal strength envelop for survey line at locations 2 & 3 respectively, while Figures 5 and 6 (c) represent the 2D shear wave velocity profile obtained from the MASW survey at the respective locations. In Figures 5 and 6 (a) hyperbolic reflections can be observed at around 3 m depth, which represents the EM wave reflections over air filled cavity. Figure 5 and 6 (b) represent the reflection strength of the electromagentic signal is higher (darker) in air filled or porous zone. Similarly to location 1, a peak is observed in the signal amplitude in signal trace in the cavity area as the signal strength and energy increases in air/water filled voids. The anomaly observed in radargram was confirmed to 2D shear wave velocity profile (Figure 5 and 6 (c)) by identifying the low velocity zone which resembles a loose or porous area.

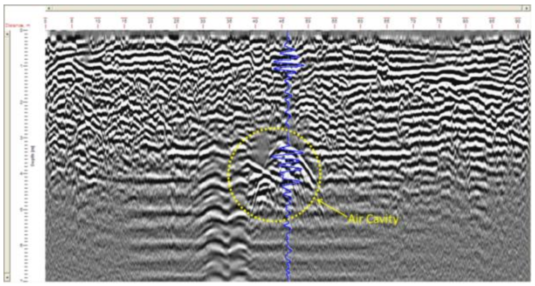

(a)

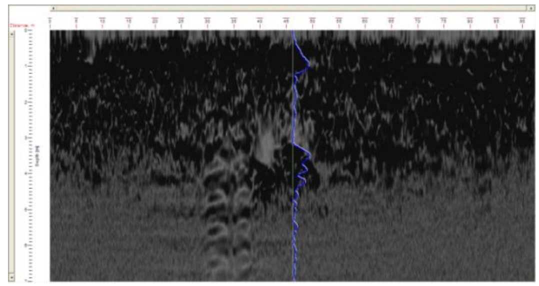

(b)

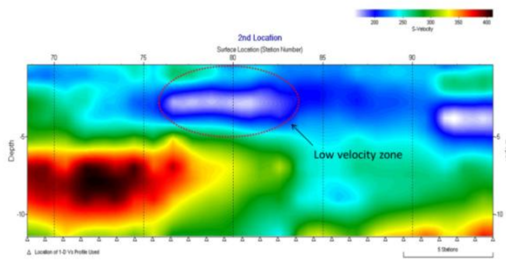

(c)

Figure 5. (a) 2D processed radargram and (b) 2D strength envelop for GPR survey (c) 2D MASW shear wave velocity profile over the unknown cavity location at location 2.

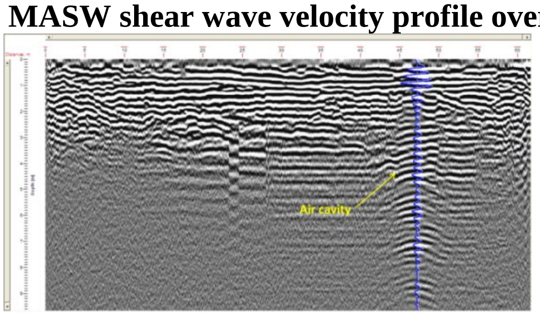

(a)

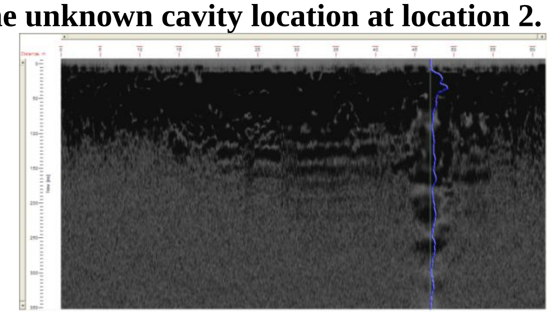

(b)

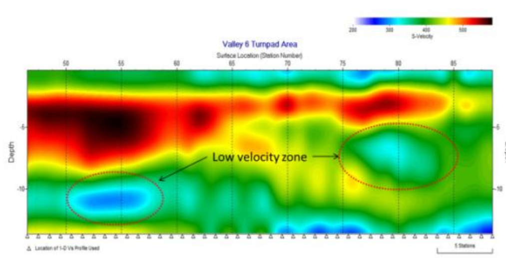

(c)

Figure 6. (a) 2D processed radargram and (b) 2D strength envelop for GPR survey (c) 2D MASW shear wave velocity profile over unknown cavity at Location 3

REMEDIAL MEASURES

Cavities and soft soil locations identified by Geophysical survey locations, which are physically validated and treated so as not to cause any future failure. The locations of the identified cavities are identified and marked at site. Boreholes of 100 mm dia are drilled up to the suggested depth, covering the complete area. Change in strata at heterogeneity/cavity level is recorded on the basis of the drilling time and ease of penetration. The drilled boreholes are grouted with free flowing concrete to plug the cavity and avoid any ingress of water in the future. In case the flow of concrete continues and demand, excess amount than the estimated amount based on GPR data. The locations are excavated and backfilled in layers with good earth up to ground level.

CONCLUSION

The objective of this study was to investigate the formation and location of cavities in lateritic soils. It is widely known from the literature study and visible proofs that laterite soils have a honeycomb like structure with small cavities. These cavities tend to increase in size and wash off under continuous variation of the water table. To identify the cavities a forensic subsurface investigation was conducted using integrated geophysical techniques. Two geophysical methods, namely GPR and MASW are used to collect subsurface data for identifying cavities. A first GPR survey was conducted to identify anomalies and then MASW survey was performed for confirmation of presence of cavity.

As the reflections of EM wave from air filled cavity are distinct from signals obtained from normal soils, they generate readily distinguishable anomalies. Based on the signal trace it was easy to identify the position of the cavity as the amplitude of the signal increases in air or water filled cavity. The processed data highlighted the hyperbolic signature due to the presence of cavity at a depth of 3 m. Also, some anomalous zones like small air pockets are highlighted which represent the karstic features of lateritic deposits. It is recommended to use higher frequency GPR for near surface or shallow investigation as it provides higher resolution Also from the MASW survey, the presence of cavity was confirmed by low velocity zones surrounded by high velocity zones in the shear wave velocity profile.

The results obtained from the survey helped in identifying cavity locations which helped in taking necessary precautions. The study recommends preliminary geophysical investigation by integrated approach along with geotechnical investigation to arrive at detailed profiling of the subsurface for large scale projects. Mitigation measures and timely monitoring need to be carried to avoid formation of cavities in the future.

REFERENCES

Aginam C.H, Nwakaire Chidozie, Nwajuaku A.I (2015), Engineering Properties of Lateritic Soils from Anambra Central Zone, Nigeria. International Journal of Soft Computing and Engineering (IJSCE) ISSN: 2231-2307, Vol. 4 Issue-6.

Alexander Lyle T. and Cady J G (1962) Genesis and Hardening of Laterite in Soils. Technical Bulletin No. 1282 United States Department of Agriculture.

Anirudhan I V. (2014), Significance of case studies in geotechnical engineering, Proceedings of Indian Geotechnical Conference IGC-2014 December 18-20, 2014, Kakinada, India

Gad El-Qady, Mahfooz Hafez, Mohamed A. Abdalla, and Keisuke Ushijima (2005), Imaging subsurface cavities using geoelectric tomography and ground-penetrating radar. Journal of Cave and Karst Studies, v. 67, no. 3: 174–181.

Grimes K. and Spate A. (2008), Laterite Karst ACKMA Journal, Vol.73: 49-52.

Kasthurba A.K., Manu Santhanam and M.S. Mathews (2007), Investigation of laterite stones for building purpose from Malabar region, Kerala state, SW India – Part 1: Field studies and profile characterization. Construction and Building Materials 21: 73–82.

Kay, J.R. (1972) Inspection of ‘Mystery Holes’, South Kolan, Bundaberg area. Unpublished report held by the Geological Survey of Qld as File 2-14-0: 5

Lohnes R. A and. Demirel T. (1973) Strength and Structure of laterites and lateritic soils. Engineering Geology. 7: 13-33.

Robertson, A.D (1979), Origin of the 'Mystery Craters' of South Kolan, Bundaberg area. Qld. Govt. Mining J., 80: 448-449.

Vermaat J. G and C. F. Bentley (1955), The age and channeling of Ceylon laterite. Soil Science Volume 79 No. 4.

OBSERVATIONS DURING RECENT EARTHQUAKES AND DEVELOPMENTS IN LIQUEFACTION ANALYSIS

Vijay K. Puri[1], Shamsher Prakash[2], Sanjeev Kumar[3] and Prabir K. Kolay[4]

[1]Professor, Civil and Environment Engineering, SIU, Carbondale, IL 62901; puri@engr.siu.edu
[2]Professor Emeritus, Civil Engineering, Missouri University of Science and Technology, Rolla, Missouri, 65409; prakash@mst.edu
[3]Professor and Chair, Civil and Environment Engineering, SIU, Carbondale, IL 62901; kumars@siu.edu
[4]Associate Professor, Civil and Environment Engineering, SIU, Carbondale, IL 62901; pkolay@siu.edu

ABSTRACT

Liquefaction has occurred during many earthquakes, Alaska 1964, Niigata 1964, Tangshan 1976, Loma Prieta 1985, Kobe 1995, Chi-Chi Taiwan 1999, Turkey 1999, Haiti 2010, Mexicali 2010 and several others. The extensive liquefaction of loose saturated sands during the Niigata earthquake provided a field verification of the liquefaction phenomenon and triggered research investigations on liquefaction. It was mostly believed as a necessary consequence that only cohesionless soils are prone to liquefaction and silts and clay do not liquefy. The observations during the Tangshan earthquake and damage during Andaprazi (1999) earthquake and others later on suggested that silts and low plasticity clays may also liquefy. The observations on performance of soils during earthquakes has, thus, contributed to better understanding of the phenomenon of liquefaction in different types of soils and development of methods for prediction of susceptibility of soils to liquefaction.

INTRODUCTION

The concepts of forensic geotechnical engineering have been practiced all along in geotechnical area. The observations on performance of geotechnical structures and failures, back analysis to determine what went wrong and to avoid failure in future have been the back bone of geotechnical profession. Developments in geotechnical earthquake engineering, especially in the area of liquefaction present an outstanding example of application of principles of forensics.

Liquefaction has occurred during most earthquakes e.g., Niigata 1964, Tangshan 1976, Loma Prieta 1985, Kobe 1995, Chi-Chi Taiwan 1999, Turkey 1999, Haiti 2010, Mexicali 2010 and others. Observations on performance of soils and structures during these and other earthquakes provide a useful tool to evaluate the design and analysis techniques and refine them for realistic design in future. This is highly relevant in case of developments in the area of geotechnical earthquake engineering in general and liquefaction phenomenon in particular. The performance of structures during the Niigata earthquake (1964) in Japan and the nature of damage suffered by them clearly brought out the fact that soil and soil foundation interaction play a significant role in controlling their performance. Also, the extensive liquefaction of loose saturated sands during the Niigata earthquake provided a field verification of the liquefaction phenomenon. Several other earthquakes in Japan also induced liquefaction. It was mostly believed as a necessary consequence that only cohesionless soils are prone to liquefaction and silts and clay do not liquefy. The Tangshan earthquake (1976) in China provided evidence of liquefaction in low plasticity silts. The authors of this paper had conducted laboratory investigations on undisturbed and reconstituted samples of silts and observed that silts meeting certain criteria can liquefy and develop high pore water pressures and undergo large deformations. Several other investigators also conducted research on liquefaction aspects of fine-grained soils and proposed criteria for liquefaction, some of which were quite confusing. Thus the controversy continued. Some people suggested criteria based on percent of fines in soil and others based on plasticity of soil. It was observed in Aadapazri during the Koceli (1999) earthquake that soils with PI < 12 underwent liquefaction, soils with PI between 12 and 18 were moderately prone to liquefaction and soils with PI > 18 were not prone to liquefaction. An intense earthquake (M 6.4) in western Iran, about 225 km west of Tehran (2002) with soil mostly clay, showed clear traces of sand boiling, softening of soil, and consequent deformations were observed particularly at certain locations. The soil had a liquid limit of 38%, a plasticity index of 18%, and fine fraction of 44%. These properties would indicate a non-liquefiable soil according to the commonly used criteria. Analysis of cyclic triaxial test data suggested that the clayey sand deposit likely developed high residual excess pore pressures and significant shear strains during the earthquake and thus likely contributed to the observed lateral deformations.

Based on these observations and more recent studies, it is believed that soils may be classified into those that will exhibit sand-like behavior and are likely to liquefy or into soils that exhibit clay-like behavior and are not likely to liquefy. Special investigations may be needed in other cases. Thus the observations during the earthquakes, coupled with laboratory data have resulted in a better understanding of liquefaction of fine-grained soils.

RESEARCH ON LIQUEFACTION

The research on liquefaction following the damage caused by the Alaska (1964) and the Niigata (1964) earthquakes was devoted to sands and included the following:

(a) Investigation of sites damaged by earthquakes.
(b) Laboratory tests using undrained cyclic triaxial and cyclic simple shear devices.
(c) Vibration or shake table tests.
(d) Field tests such Standard Penetration Tests (SPT) and Cone Penetration Tests (CPT), and Shear Wave Velocity test.
(e) Numerical analysis.

LIQUEFACTION OF SANDS

The laboratory studies helped identify the factors governing liquefaction of soils. Seed and Lee (1966) reported the first comprehensive data on liquefaction of sand using the cyclic triaxial test. Peacock and Seed (1968) used oscillatory shear device to study liquefaction in sand and a comparison was made of the shear stresses causing liquefaction in sand in the cyclic triaxial and the cyclic simple shear tests. It was observed that cyclic stresses causing liquefaction in loose saturated sands under cyclic simple shear conditions were only about 35% of the cyclic stresses required to cause liquefaction under cyclic triaxial conditions. Since field conditions are more realistically reproduced in cyclic simple shear tests but the cyclic triaxial tests are relatively easier to perform, therefore correction factors were proposed to correlate the cyclic triaxial data with the cyclic simple shear data. This resulted in the well-known ‘simplified procedures’ for liquefaction analysis of sand deposits. The sample size used in the cyclic triaxial and cyclic simple shear device being small, it was pointed out by Finn (1972) that testing large samples using shake table may better represent the liquefaction of field deposits. The results of the shake table studies showed a general qualitative agreement with data obtained from cyclic triaxial and cyclic simple shear tests. Limited studies on liquefaction of undisturbed samples of sand were also attempted and it was found that the natural undisturbed samples were more resistant to liquefaction compared to laboratory made samples at the same relative density due to aging effects and strength increase in sand due to development of bond between sand particles. Because of difficulty in procuring undisturbed sand samples and the associated cost of performing such tests, they cannot be routinely used for liquefaction analysis. The same argument applies to shake table tests. This lead to the search for a field test which could be used for ascertaining liquefaction susceptibility at a site. The standard penetration test which is routinely used for sub-soil exploration showed promise for estimating the liquefaction also. Standard penetration data was collected for sites which had experienced major earthquakes and where liquefaction had or had not occurred (Seed et al., 1985). The SPT value $(N_1)_{60}$ has been adopted by the profession as an index for liquefaction of saturated sand deposits. As more data became available, the charts for cyclic stress ratio vs $(N_1)_{60}$ were updated to account for cases clean sands (<5% fines) and for sands with 10.5 or 35 % fines. The cyclic stress ratio charts vs $(N_1)_{60}$ are for a magnitude 7.5 earthquake. For earthquakes with other magnitudes, the use of magnitude scaling factor (MSF) proposed by Seed et al., (1985). Also, liquefaction potential is seen to decrease with an increase in the fine content in sand, Seed (1987) suggested the use of effective SPT value to account for the effect of fines in sand. The effective SPT value modifies the observed penetration resistance to equivalent clean sand penetration resistance and may be obtained as follows:

$$(N_1)_{60eff} = (N_1)_{60} + \Delta(N_1)_{60}$$

In which $(N_1)_{60}$ = Observed SPT value, $(N_1)_{60eff}$ = Effective standard penetration resistance or equivalent clean sand penetration resistance and $\Delta(N_1)_{60}$ = Correction for silt content.

Another approach known as the ‘cyclic strain approach’ has also been proposed to determine the likelihood of liquefaction by estimating the shear strain induced in the soil due to seismic loading and comparing it with the threshold strain required to develop liquefaction. The typical value the threshold strain is about 0.01 % (Dobry, 2010). The tip resistance from cone penetration tests (CPT) can also be used as a riteria for liquefaction (Mitchell and Tseng, 1990). CPT has the advantage over SPT in its ability to detect thin seams of loose soil. Shear wave velocity has been as a useful indicator for liquefaction. Stokoe et al. (1988) have used the cyclic strain approach and equivalent linear ground response analysis to investigate the relationship between peak ground acceleration for stiff soil site and shear wave velocity and correlated the data with conditions under which liquefaction may or may not occur. Tokimatsu et al. (1991) used laboratory tests to develop plots correlating the cyclic stress ratios required to produce cyclic strain amplitude of 2.5% in given number of cycles as a function of shear wave velocity.

Remarkable progress has been made in the ability to estimate liquefaction potential of a site having sand deposits by using laboratory investigations or from simple in-situ tests such as standard penetration values (N_1 or $(N_1)_{60}$), cone penetration data, shear wave velocity measurements and the experience during the past earthquakes. If a proposed site is found prone to liquefaction, remedial measures can be taken at the design stage resulting in mitigation of the geo-hazard.

LIQUEFACTION OF FINE GRAINED SOILS

Fine soils such as silts, clayey silts and sands with fines and silty soils were generally considered non-liquefiable till the early eighties. This concept, however, changed after observations following the Haicheng (1975) and Tangshan (1976) earthquakes. The soils that liquefied during Tangshan earthquake had clay fraction less than 20%, liquid limit between 21-35%, plasticity index between 4% and 14% and water content more than 90% of their liquid limit. Kishida (1969) reported liquefaction of soils with upto 70% fines and 10% clay fraction during Mino-Owar, Tohankai and Fukui earthquakes. Tohno and Yasuda (1981) reported that soils with fines up to 90% and clay content of 18% exhibited liquefaction during Tokachi –Oki earthquake of 1968. Soils with up to 48% fines and 18% clay content were found to have liquefied during the Hokkaido Nansai–Oki earthquake of 1993. Gold mine tailings liquefied during the Oshima-Kinkai earthquake in Japan (Ishihara, 1993). These tailings had silt sized particles and liquid limit of 31%, plasticity index of 10% and water content of 37%.

Seed et al. (1983) suggested that some soils with fines may be susceptible to liquefaction. Such soils (based on Chinese criteria) appear to have the following characteristics:

Percent finer than 0.005 mm (5 microns) <15%
Liquid limit < 35%
Water content > 90%

The authors conducted studies on liquefaction of low plasticity silts using naturally occurring and laboratory prepared soils and conducting dynamic triaxial tests. Most significant results of these studies were that the nature of fines rather than their percentage has a significant influence in determining the susceptibility of silts to liquefaction (Puri,1984). The effect of nature of fines can be best defined in terms of plasticity index of the soil rather than their percentage. It was observed that the cyclic stress ratio causing liquefaction in a given number of cycles increases with the increase in plasticity index. It was also observed that the cyclic loading of plastic silts can result in pore pressure build up which may become equal to the initial effective confining pressure resulting in development of the initial state of liquefaction for PI < 10.

MORE RESEARCH ON EFFECT OF FINES ON LIQEFACTION

There are several research findings worth mentioning on the effect of fines on liquefaction potential of soils some of which appear to be somewhat conflicting.

1. Seed et al. (1985) have recommended that for sands containing less than 5% fines, the effect of fines may be neglected. For sands containing more than 5% fines, the liquefaction potential decreases. Neglecting the effect of fines should therefore be expected to lead to

conservative estimates of liquefaction potential. However, this suggestion is not based on experimental or field data.

2. Ishihara and Koseki (1989) had suggested that low plasticity fines (PI < 4) do not influence the liquefaction potential. However, they did not consider the effect of the void ratio in their analysis.

3. Finn (1991) made an observation about the effect of fines in sand in developing equivalent clean sand behavior. If the void ratio of silty sand and clean sand is the same the liquefaction resistance decreases. If the comparison is made at the same $(N_1)_{60,}$ the effect of fines is to increase the liquefaction resistance. If comparison is made using the "the same void ratio in and skeleton" as the criteria, then there is no effect on the cyclic strength provided the fines can be accommodated within the sand voids.

4. Ishihara (1993) mentioned that in soils in which the fines content is sufficient to separate the coarser particles, the nature of the fines controls the behavior. Low plasticity or non-plastic silts and silty sands may be highly susceptible to liquefaction. This will be the case when PI is less than about 10. For soils with moderately plastic fines (fines content more than about 15% and $8 \leq PI \leq 15$), the liquefaction behavior may be uncertain and may need further investigation.

5. Seed et al. (2001) observed that there is significant controversy and confusion regarding the liquefaction potential of silty soils (and silty /clayey soils), and also coarser, gravelly soils and rockfills.
6. Andrews and Martin (2000) have provided general criteria about liquefaction susceptibility of soils with fines which use clay content and liquid limit of soil.

7. Bray et al. (2004) and Boulanger and Idriss (2005) and Idriss and Boulanger (2008) have suggested that soils with more than 50% fines may show sand like or clay like behavior under cyclic loading. Clay like behavior should be expected for silts (ML and MH) and for clays (CL and CH) if their PI ≥ 7. Sand like behavior should be expected if their PI is < 7.

8. Bray et al. (2004) and Plito (2001) have suggested that the plasticity index rather than percent of clay size particles as a criterion for assessing the susceptibility of fine grained soils to liquefaction.

9. Bray et al. (2004) found that soils that were observed to have liquefied in Aadapazari during the Koceli (1999) earthquake did not typically meet the Chinese criteria for liquefaction susceptible fine grained soils. During their investigation they found that soils with PI < 12 underwent liquefaction, soils with PI between 12 and 18 were moderately prone to liquefaction and soils with PI > 18 were not prone to liquefaction at the effective confining pressures used in the experiments.

10. Wang et al. (2007) investigated the liquefaction susceptibility of saturated loess (silty soil) and fine sand obtained from an airport site near Lanzhou, China. This loess had PI varying

from 7.2 to 9. Their studies indicated that this loess was more susceptible to liquefaction than fine sand.

11. Towhata (2008) has mentioned that it was previously thought that soils with fines are more resistant to liquefaction. However, he has also mentioned that the fines employed in those studies meant silts and clays that were cohesive in nature and fine materials without cohesion may still be vulnerable. It is the opinion of the authors based on the data presented here that the soils with low plasticity (PI < about 7) may liquefy or develop large deformations under cyclic loading.

12. Ghalandarzadeh et al. (2007) investigated liquefaction behavior of clayey sand from a site where large sand boiling, softening and large deformations had been observed in Iran due to an earthquake of magnitude 6.4. The soil had a liquid limit of 38%, PI =18%, and fine fraction (finer than 75 microns) of 44%. They performed cyclic triaxial tests. The analysis of data indicated that the clayey sand deposit likely developed high residual excess pore water pressures and significant shear strains during the earthquake and experienced liquefaction.

13. Thevanaygam (2010) has observed that at the same void ratio, the cyclic resistance of sand decreases with an increase in silt (non-plastic) content upto a certain threshold value of fines content (fc_{th}); thereafter the cyclic resistance increases with further increase in silt content. Silt content affects the inter-grain contact density of soil compared to that of sand at the same void ratio. When this is taken into account, sand and silty sand show similar liquefaction resistance at same equivalent void ratio $(e_c)_{eq}$. Result shows that at the same equivalent void ratio, the number of cycles inducing 5% strain is almost the same for clean sand (OS-00), sand with 15% silt (OS-15) and sand with 25% silt (OS-25).

The liquefaction of fine grained soils has certainly received the attention of researchers and progress has been made in this direction in the last 30 years and substantial progress has been made in this decade. The laboratory studies have attempted to verify or provide explanation of the behavior observed during earthquakes in silty or clayey soils. Presently in 2016 there is no well-defined index to ascertain the liquefaction potential of fine grained soils like SPT or CPT as in case of sands. From geo-hazard mitigation point of view lot more needs to be done. At a site in a seismic zone where silts and clays with low plasticity (PI < about 7-10) exist, careful investigations should conducted ascertain the likely hood of liquefaction.
Recently, Boulanger and Idriss (2012) have provided probability based equations for estimation of cyclic resistance ratio (CRR) and $(N_1)_{60}$ or standardized CPT values.

CONCLUSIONS

Progress in liquefaction research and procedures of analysis has been strongly influenced by the observations on liquefaction related damage following the major earthquakes. These observations also provided a field verification of this hazardous phenomenon of liquefaction. Most of the efforts were devoted to liquefaction of sands since major earthquakes occurred in alluvial deposits. When evidence became available about liquefaction of fine plastic soils in (1976) research to determine liquefaction susceptibility of fine grained soils started in early eighties. There are many conflicting opinions still there about liquefaction of fine grained soils. It is obvious that it is still not possible to evaluate the likelihood of liquefaction of silts or silty clays with the same confidence as for clean sands without additional investigations. For mitigating liquefaction related geo-hazard during future earthquakes it is of utmost importance that a geotechnical engineer should be able to ascertain the likelihood of a site for liquefaction susceptibility be it sands, silts or clays of low plasticity.

REFERENCES

Andrews, D. C. A. and Martin G. R. (2000), "Criteria for Liquefaction of Silty Soils", Proc. 12th WCEE, Auckland, New Zealand.

Boulanger, R. W. and Idriss, I. M. (2005), "New Criteria for Distinguishing between Silts and Clays that are Susceptible to Liquefaction versus Cyclic Failure", 25th. Annual USSD Conference, Salt Lake City, Utah, June 6-10, pp. 357-366.

Boulanger, R. W. and Idriss, I. M. (2012), "Probabilistic Standard Penetration Based Liquefaction Triggering Procedures", Journal of Geotechnical and Geo-Environmental Engineering, ASCE, Vol. 138, No. 10, pp. 1185-1195.

Bray, J. D., Sancio, R. B., Reimer, M. F. and Durgunoglu, T. (2004), "Liquefaction Susceptibility of Fine-grained Soils", Proc. 11th Int. Conf. on Soil Dynamics and Earthquake Engineering and 3rd Inter. Conf. on Earthquake Geotech. Engrg., Berkeley, CA, Jan. 7-9, Vol. 1, pp. 655-662.

Dobry, R. (2010), "Comparison Between Clean Sand Liquefaction Charts Based on Penetration Resistance and Shear Wave Velocity", 5th International Conference on Recent Developments in Geotechnical Earthquake engineering and Soil Dynamics, San Diego, CA, USA.

Finn, W. D. L. (1991), "Assessment of Liquefaction Potential and Post Liquefaction Behavior of Earth Structures: Developments 1981-1991", Proc. Second International Conference on Recent Advances in Geotechnical Earthquake Engineering and soil Dynamics, St. Louis, March 11-15, Vol. 2, pp. 1883-1850.

Finn, W.D.L. (1972), "Soil-Dynamics-liquefaction of Sands", Proc. First International Conference on Microzonation, Vol. 1, pp. 87-111, Seattle.

Ghalandarzadeh, A., Ghahremani, M. and Konagai, K. (2007), "Investigation on the Liquefaction of a Clayey–-Sandy Soil during Changureh Earthquake", 4th International Conference on Earthquake Geotechnical Engineering, March 25-28, CD-ROM, Thessaloniki, Greece.

Idriss, I. M. and Boulanger, R. W. (2008) "Soil Liquefaction during Earthquakes", EERI, MNO-12.

Ishihara, K. (1993), "Liquefaction of Natural Deposits During Earthquakes", Proc. 11th ICSMFE, San Francisco, 1, 321-376, Vol. 2, pp. 683-692.

Ishihara, K., and Koseki, J. (1989), "Cyclic Shear Strength of Fines-Containing Sands". Earthquake and Geotechnical. Engrg., Japanese Society of Soil Mechanics and Foundation Engineering, Tokyo, pp. 101-106.

Kishida, H. (1969), "Characteristics of Liquefied Sands during Mino-Owari, Tohnankai, and Fukui Earthquakes". Soils and Foundations, Vol. 9, No. 1, pp. 75-92.

Mitchell, J. K., and Tseng, D. J. (1990), "Assessment of Liquefaction Potential by Cone Penetration Resistance", Proceeding, H. Bolton Seed Memorial Symposium, Berkeley, CA, Editor: J. M. Duncan, Vol. 2, pp. 335-350.

Peacock, W. H. and Seed, H. B. (1968), "Sand Liquefaction Under Cyclic Loading Simple Shear Conditions", Journal of Soil Mechanics and Foundation division, ASCE, Vol. 94, No. 3, pp. 689-708.

Plito, C. (2001), "Plasticity Based Liquefaction Criteria", Proc. 4th Int. Conf. on Recent Adv. in Geotech. Earth. Engrg. and Soil Dynamics, San Diego, USA.

Puri, V. K. (1984), "Liquefaction Behavior and Dynamic Properties of Loessial (Silty) Soils", PhD Dissertation, UMR (Now MST), Rolla, USA.

Seed H. B., Tokimatsu, K., Harder, L. F., and Chung, R. (1985), "Influence of SPT Procedures in Soil Liquefaction Resistance Evaluations" J. Geotechnical Engg., ASCE, Vol. 111, No.12, pp. 861-878.

Seed, H. B. (1987), "Design Problems in Soil Liquefaction", Journal of Geotechnical Engineering, ASCE, Vol. 113, No. 8, pp. 827-845.

Seed, H. B., and Lee, K. L. (1966), "Liquefaction of saturated sands during cyclic loading" Journal of the Soil Mechanics and Foundations Division, Vol. 92, No. 6, pp. 105-134.

Seed, H. B., Idriss, I. M. and Arango, I. (1983), "Evaluation of Liquefaction Potential using Field Performance Data" Journal of Geotechnical Engg, ASCE, Vol. 109, No. 3, pp. 458-482.

Seed, R. B., Cetin, K. O., Moss, R. E. S., Kammerer, A. M., Wu, J., Pestana, J. M. and Riemer, M. F. (2001), "Recent Advances in Soil Liquefaction Engineering and Seismic Site Response Evaluation", Proc. 4th Int. Conf. on Recent Adv. in Geotech. Earth. Engrg. and Soil Dynamics, San Diego, USA.

Stokoe. K. H., Roesset, J.M. Bierschwale, J. G. and Aouad, M. (1988), "Liquefaction Potential of sand from Shear Wave Velocity", Proceedings, 9th World Conference on Earthquake Engineering, Tokyo, Vol. 3, pp. 213-218, Tokyo.

Thevanayagam, S. (2010), "Liquefaction, Screeng and remediation of Silty Soils", Fifth International Conference on Geotechnical Earthquake Engineering and Soil Dynamics and Symposium Honoring professor I.M. Idriss, May 24-29, CD Rom, San Diego.

Tokimatsu, K., Kuwayama, S. and Tamura, S. (1991), "Liquefaction Potential Evaluation Based on Rayleigh Wave Investigation and Comparison with Field Behavior", Proceedings 2nd International Conference on Recent Advances on Geotechnical Earthquake Engineering and Soil Dynamics, Saint Louis, Missouri, USA, Vol. 1, pp. 357-354.

Towhata, I. (2008), "Geotechnical Earthquake Engineering", Springer Series in Geomechanics and Geoengineering.

Wang, J., Yuan, Z. and Li, L. (2007), "Study on Liquefaction of Loess Site", 4th International Conference on Earthquake Geotechnical Engineering, CD-ROM, March 25-28, Thessaloniki, Greece,

Effect of Variation of Geotechnical Properties on Stability of Retaining Walls: a Case Study in Japan

Anasua GuhaRay, Ph.D., A.M. ASCE[1] and Dilip Kumar Baidya, Ph.D.[2]

[1]Assistant Professor, Department of Civil Engineering, BITS-Pilani Hyderabad, Secunderabad – 500078, India; Email: anasua08@gmail.com
[2]Professor, Department of Civil Engineering, IIT Kharagpur, West Bengal – 721302, India; Email: baidya@civil.iitkgp.ernet.in

ABSTRACT

In the present paper, the effects of variation of geotechnical properties on stability of a series of 54 retaining walls in Hodogaya Ward and Naka Ward of the Yokohama municipality area in Japan are analyzed for various earthquake conditions. The probabilistic and sensitivity analysis are carried out by Monte Carlo Simulation and *F*-test analysis respectively. It is observed that most of the retaining walls have probability of failure (P_f) between 40-60% for overturning and 10-40% for sliding modes of failure. A range of probabilistic risk factors (R_f), which simultaneously identifies the effects of P_f and also the sensitivity of geotechnical random variables on different failure modes, is proposed for different earthquake conditions. It is observed that internal angle of friction of the backfill is less sensitive to P_f compared to cohesion (c_2) of foundation soil. For PGA > 400 cm/s^2 and variation of c_2> 10%, walls having height more than 3m require a base width almost twice the height of the wall. The proposed procedure in this study can be applied in the design of retaining walls in other parts of Tokyo area as well, for similar subsurface and backfill conditions.

INTRODUCTION

Uncertainty is evident in almost every field of engineering, and geotechnical engineering is no exception. Natural soils are heterogeneous and anisotropic due to their composition and complex depositional processes. The increasing frequency of landslides and failures of earth structures and their adverse impact have led the geotechnical engineers to recognize the importance of probabilistic approaches for analysis of geotechnical structures. Conventional design of geotechnical structures is based on limit equilibrium methods (*LEM*) and on the concept of Factor of Safety (*FS*). This method holds good only when the input parameters, namely, engineering properties of soil, location of ground water table and loading conditions etc., required for design can be accurately assessed. But variation of site data from the estimated value is more common than the exception. The concept of reliability analysis is a well-established mathematical approach to account for these uncertainties of field variables.

A number of approaches are developed through years for assessing reliability of geotechnical structures in terms of reliability index (β) and probability of failure (P_f) (Harr, 1984; Kulhawy, 1992; Duncan, 2000; Hasofer and Lind, 1974; Baecher and Christian, 2003). A few approaches for evaluating sensitivity of random variables on overall failures of structures have also been reported in past research works (Frey and Patil, 2002; Saltelli et al., 1999). In geotechnical engineering, the differential analysis method (local method) for sensitivity analysis has been applied (Babu and Basha, 2008a, 2008b) to estimate the sensitivity of geotechnical random variables on failure probabilities of different structures.

Previous research works indicate that the use of partial safety factors for different geotechnical variables results economises the design compared to applying a lumped factor of safety to the structure as a whole. However, the uncertain nature of soil properties may vary these partial safety factors depending upon the amount of uncertainties, which may result in under-estimation or over-estimation of various parameters/ element dimensions. Limited approaches are available in literature to generalize this "partial factor of safety" based upon variations of different geotechnical random variables. Quite a number of different approaches are available to determine the failure probability (P_f) for variation of the random variables and assess the severity of random variables on different modes of failure. Contrarily, design approach incorporating both the effects has not yet been adequately addressed. The present study adopts a design methodology, which combines the failure probability (P_f) for variation of random variables and sensitivity of random variables (S) on different modes of failure, thereby producing more efficient and economical design.

Guharay *et al.* (2015), Guharay and Baidya (2016) formulated a new factor called the probabilistic risk factor (R_f) by combining mathematically the probability of failure (P_f) of different potential failure modes and sensitivity (S) of geotechnical random variables on each of these failure modes. The authors have applied this probabilistic risk factor based approach to a number of typical geotechnical earth structures such as cantilever retaining wall (GuhaRay *et al.*, 2014), gravity retaining wall (GuhaRay and Baidya, 2012) and sheet pile walls (GuhaRay and Baidya, 2015). The primary objective of the present paper is to apply the above methodology to failure of a series of 54 gravity retaining walls subjected to earthquake loading in Tokyo Metropolitan and Yokohama Municipality area in Tokyo, Japan. The present paper extensively studies the effect of variation of geotechnical random variables on failure and recommends widths required for safe working of the retaining walls based on different wall heights and earthquake conditions.

FORMULATION OF PROBABILISTIC RISK FACTOR

For the probabilistic analysis of the geotechnical structures, the performance function is defined as $g_i(x) = (FS)_i - 1$, where i = different failure modes. $g_i(x) < 0$ implies failure conditions. In the present study, P_f is determined by Monte Carlo Simulation by coding the limit equilibrium equations in MATLAB R2015a (The Mathworks, Inc., Naticks, MA, US) by generating 50,000 data points. A convergence study is carried out to fix the number of data points. For sensitivity analysis, the ANOVA F-test (Saltelli *et al*., 1999) is used to quantify the sensitivity of the input geotechnical parameters on the output performance function. The probabilistic risk factor (R_f) is calculated by mathematically combining probability of failure and sensitivity. If i and j represent the random variables and the number of failure modes respectively, then for each random variable, R_f may be defined as the product of the normalized failure probability (P_f') and sensitivity (S'):

$$R_f(i) = 1 + \sum_{j=1}^{n} P_f'(j) \times S'(i)$$

The original values of the random variables, when modified by these R_f values, yields corrected values of the random variables, which have variations included into them. The reader can refer the work of GuhaRay and Baidya (2012, 2014) and GuhaRay *et al.* (2014) for better understanding of the computational procedure. The computational procedure has not been discussed elaborately in this paper in order to avoid repetition.

CASE STUDY

In the present study, a series of 15 gravity retaining walls located in southern parts of Ota Ward in Tokyo Metropolitan and 39 walls in Hodogaya Ward and Naka Ward of Yokohama Municipality in Japan (Gautam and Kanda, 2009) are considered for analysis. These areas consist of little sloppy and fragile ground condition. Gautam and Kanda (2009) reported that most of the retaining walls have P_f varying from 40-60% for overturning and 10-40% for sliding. The soil properties are reported in Table 1 and the basic configuration of the retaining wall is shown in Fig. 1.

Table 1 ***Soil Properties***

	Backfill Soil	**Foundation Soil**
Type of Soil	Dry Sandy Soil	Cohesive Soil
Unit Weight (kN/m^3)	18	*
Internal Friction Angle (°)	30	*
Cohesion (kN/m^2)	-	30 – 40

*Footnote: *not reported*

During the field survey, it was reported that almost all the walls have similar arrangements in the exposed face (Gautam and Kanda, 2009). The range of heights (h) of the retaining walls was considered from the field survey. The length and thickness of the base were estimated to be 2/3rd of h and at least 20cm respectively. Length from toe to column of wall was taken to be h/8, subjected to a minimum value of 20cm. The walls are analysed against two external modes of failure viz. sliding and overturning by Mononobe-Okabe Method (Mononobe and Matsuo, 1929; Okabe, 1926). It is observed that cohesion c affects only the sliding mode of failure. P_f is negligible for overturning mode of failure when PGA is less than 300 cm/s^2. For PGA above 400 cm/s^2, P_f =1 for overturning mode of failure. Hence, it may be concluded that for PGA < 300 cm/s^2, overturning mode of failure does not contribute significantly to the total P_f and c is the governing geotechnical parameter. But φ affects both sliding and overturning mode of failure. For PGA > 400 cm/s^2, overturning contributes primarily on total P_f and φ becomes the dominating parameter.

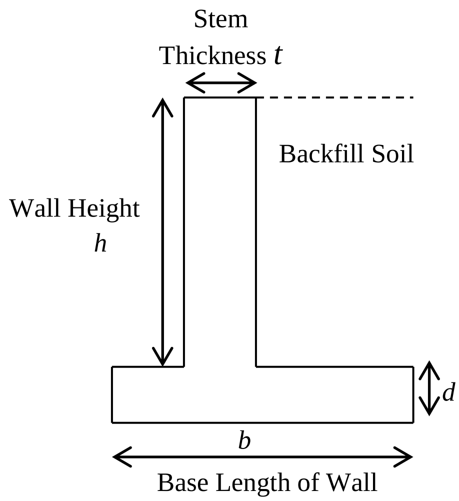

Figure. 1 Basic Configuration of Retaining Wall

Table 2 tabulates the *FS* and P_f for 54 retaining walls for different magnitudes of earthquake for sliding mode of failure. The results presented in Table 1 differ marginally from that reported by Gautam and Kanda (2009) because the later used First Order second Moment Method for analysis, while Monte Carlo Simulation is used in the present study. For example, for Ota ward, upto PGA 400 cm/s^2, total number of failures reported by the cited reference is 10, while that in the present study is 15.

Table 2 *FS* and P_f of 54 retaining walls for different PGA values (Sliding Mode of Failure)

Ret. Wall No.	*h* (m)	*L* (m)	*t* (m)	PGA= 100cm/s^2		PGA= 200cm/s^2		PGA= 300cm/s^2		PGA= 400cm/s^2		PGA= 500cm/s^2	
				FS	P_f	*FS*	P_f	*FS*	P_f	*FS*	P_f	*FS*	P_f
Retaining Walls of Hodogaya and Naka Ward													
Y11	2.75	1.93	0.2	2.322	0	1.605	0	1.198	0.074	0.927	0.768	0.715	0.995
Y14	2.25	1.49	0.21	2.593	0	1.788	0	1.333	0.010	1.029	0.462	0.792	0.961
Y15	2.00	1.32	0.24	2.78	0	1.913	0	1.424	0.003	1.098	0.285	0.844	0.899
Y16	1.50	0.99	0.18	3.33	0	2.289	0	1.7	0	1.308	0.042	1.000	0.549
Y17	1.25	0.83	0.18	3.769	0	2.585	0	1.917	0	1.472	0.006	1.124	0.268
Y18	1.50	0.99	0.22	3.331	0	2.286	0	1.697	0.000	1.305	0.043	0.999	0.549
Y19	2.00	1.32	0.2	2.778	0	1.914	0	1.425	0.003	1.099	0.287	0.844	0.905
Y20	2.75	1.93	0.2	2.322	0	1.605	0	1.198	0.074	0.927	0.768	0.715	0.995
YA1	1.75	1.23	0.2	3.015	0	2.075	0	1.543	0.000	1.188	0.132	0.911	0.774
Y22	3.50	2.45	0.3	2.066	0	1.429	0.00003	1.068	0.309	0.828	0.956	0.642	0.999
Y23	3.60	2.7	0.25	2.036	0	1.409	0	1.054	0.352	0.818	0.963	0.634	0.999
Y24	2.75	1.82	0.2	2.322	0	1.605	0	1.198	0.074	0.927	0.768	0.715	0.995
Y25	2.30	1.52	0.21	2.561	0	1.766	0	1.317	0.013	1.017	0.502	0.783	0.967
Y26	3.00	2.25	0.21	2.221	0	1.536	0	1.147	0.133	0.888	0.858	0.687	0.998
Y112	1.50	0.99	0.2	3.33	0	2.287	0	1.699	0.000	1.306	0.434	1.000	0.540
Y113	2.75	1.82	0.2	2.322	0	1.605	0	1.198	0.074	0.927	0.768	0.715	0.995
Y29	1.60	1.06	0.22	3.193	0	2.194	0	1.629	0.000	1.254	0.070	0.960	0.656
YA2	3.25	2.44	0.2	2.134	0	1.477	0	1.104	0.212	0.856	0.919	0.662	0.999
Y33	2.50	1.65	0.2	2.444	0	1.687	0	1.259	0.031	0.973	0.631	0.750	0.986
Y34	2.50	1.65	0.22	2.445	0	1.688	0	1.259	0.029	0.973	0.628	0.750	0.986
YA3	2.25	1.49	0.21	2.593	0	1.788	0	1.333	0.009	1.029	0.462	0.792	0.961
YA4	2.25	1.49	0.21	2.593	0	1.788	0	1.333	0.009	1.029	0.462	0.792	0.961
YA5	2.35	1.55	0.21	2.53	0	1.745	0	1.301	0.017	1.005	0.531	0.774	0.973
Y50	2.20	1.45	0.18	2.625	0	1.811	0	1.35	0.009	1.042	0.429	0.802	0.952

Y51	1.75	1.16	0.2	3.015	0	2.075	0	1.543	0.000	1.188	0.132	0.911	0.774
Y52	2.00	1.32	0.2	2.778	0	1.914	0	1.425	0.003	1.099	0.287	0.844	0.905
Y58	1.80	1.19	0.2	2.963	0	2.039	0	1.517	0.001	1.168	0.160	0.896	0.804
Y61	2.75	1.82	0.22	2.323	0	1.605	0	1.198	0.071	0.927	0.769	0.715	0.994
Y62	2.25	1.49	0.22	2.594	0	1.788	0	1.332	0.010	1.029	0.464	0.792	0.961
Y63	2.00	1.40	0.2	3.015	0	2.075	0	1.543	0.000	1.188	0.132	0.911	0.774
Y64	3.50	2.45	0.2	2.06	0	1.427	0	1.067	0.309	0.828	0.956	0.641	0.999
Y65	3.50	2.45	0.2	2.06	0	1.427	0	1.067	0.309	0.828	0.956	0.641	0.999
Y66	1.00	0.66	0.2	4.42	0	3.02	0	2.235	0	1.713	0.000	1.305	0.067
Y67	1.50	0.99	0.2	3.33	0	2.287	0	1.699	0.000	1.306	0.434	1.000	0.547
Y68	2.00	1.32	0.2	3.015	0	2.075	0	1.543	0.000	1.188	0.132	0.911	0.774
Y70	2.50	1.65	0.3	2.45	0	1.688	0	1.258	0.032	0.972	0.629	0.75	0.987
Y73	4.25	3.19	0.2	1.89	0	1.311	0.00037	0.982	0.618	0.763	0.994	0.593	1.000
Y86	2.85	1.88	0.28	2.284	0	1.577	0	1.177	0.092	0.91	0.808	0.703	0.997
Y87	2.75	1.82	0.2	2.322	0	1.605	0	1.198	0.074	0.927	0.768	0.715	0.995
Retaining Walls of Ota Ward													
C11	1.25	0.83	0.18	3.769	0	2.585	0	1.917	0	1.472	0.006	1.124	0.268
C12	2.10	1.39	0.22	2.7	0	1.86	0	1.385	0.005	1.069	0.365	0.822	1.000
C13	3.50	2.45	0.22	2.061	0	1.427	0	1.067	0.312	0.828	0.312	0.641	0.999
C15	1.65	1.09	0.2	3.13	0	2.152	0	1.6	0.000	1.231	0.088	0.943	0.694
C16	1.75	1.16	0.2	3.015	0	2.075	0	1.543	0.000	1.188	0.132	0.911	0.774
C17	1.75	1.16	0.2	3.015	0	2.075	0	1.543	0.000	1.188	0.132	0.911	0.774
C18	4.00	2.8	0.22	1.941	0	1.345	0.0001	1.007	0.522	0.782	0.987	0.607	1.000
C21	2.50	1.65	0.22	2.445	0	1.688	0	1.259	0.029	0.973	0.628	0.75	0.986
C23	2.25	1.49	0.2	2.593	0	1.788	0	1.333	0.010	1.029	0.461	0.792	0.959
C26	3.75	2.89	0.25	1.999	0	1.384	0.0007	1.035	0.421	0.803	0.976	0.623	0.999
C27	4.15	3.11	0.3	1.915	0	1.326	0.0001	0.993	0.5767	0.771	0.992	0.599	1.000
C30	3.75	2.63	0.22	1.997	0	1.383	0.0007	1.035	0.4175	0.803	0.973	0.623	0.999
C36	3.25	2.28	0.2	2.134	0	1.477	0	1.104	0.2119	0.856	0.919	0.662	0.999
C37	3.00	1.98	0.3	2.227	0	1.537	0	1.147	0.1303	0.888	0.863	0.687	0.998
C40	2.50	1.65	0.2	2.444	0	1.687	0	1.259	0.0312	0.973	0.631	0.75	0.986

It can be observed from Table 2, that the failure has initiated from PGA = 300 cm/s^2. P_f is within the range of 10^{-3} (which is considered to be safe according to US Army corps of Engineers, 2001) for PGA upto 200 cm/s^2. For PGA = 300 cm/s^2, 16 walls out of 54 is safe against sliding i.e. have $P_f < 0.001$, while only 52 out of 54 has $FS > 1$. In other words, from deterministic analysis, 52 out of 54 walls is safe, while the variation of c is considered, 16 out of 54 is safe (for $P_f < 0.001$). For PGA = 400 cm/s^2, 1 out of 54 walls is safe against sliding i.e. have $P_f < 0.001$, while 28 out of 54 has $FS > 1$. For PGA = 500 cm/s^2, no wall is safe against sliding i.e. all 54 walls have $P_f > 0.001$, while 6 out of 54 has $FS > 1$. Tables 3a and b show the number of failure cases for the two different wards for *COV* of c = 25%.

Table 3a Failure Distribution in Hodogaya and Naka Ward (for *COV* of c = 25%)

PGA (cm/s^2)	100	200	300	400	500
No. of walls with $FS < 1$	0	0	1	16	34
No. of walls with $P_f > 0.001$	0	0	27	38	39

Table 3b Failure Distribution in Ota Ward (for *COV* of c = 25%)

PGA (cm/s^2)	100	200	300	400	500
No. of walls with $FS < 1$	0	0	1	9	14
No. of walls with $P_f > 0.001$	0	0	11	15	15

Hence, variation in cohesion plays significant role in safety of the structure when PGA exceeds 200 cm/s^2. Hence, the breadth (b) of the retaining walls needs to be increased, keeping in mind the variation of cohesion value at that place, in order to maintain safety against PGA > 200cm/s^2. So instead of using b = 2/3rd*h for all cases, it is recommended to increase the heel length L_h, keeping "a" and "L_t" constant (b_{min} = 2/3rd *h).

Tables 4a and b shows the R_f values for c and φ respectively for different intensities of earthquake. From Table 4a, it is seen that the R_f value for c is 1 for PGA < 200 cm/s^2 for all heights of retaining walls, while it increases with increase in PGA values. On the other hand, from Table 4b, it is seen that R_f value for φ is 1 for PGA < 300 cm/s^2 for all heights of retaining walls. These R_f values are incorporated in design and design recommendations for breadth of the retaining walls for variations of c and different intensities of earthquake are presented in Table 5. These values may be directly implemented in design, for known height of the retaining wall and earthquake intensity. From Table 5, it is evident that the retaining walls are safe for PGA < 200 cm/s^2. But if the earthquake intensity exceeds 200 cm/s^2, the retaining wall has to be redesigned to ensure safety. Thus, apart from indicating the P_f of each retaining wall, the present risk factor based design approach helps to identify the breadth required for different retaining walls based on their heights, variation of geotechnical random variables and different earthquake intensities.

Table 4a Risk Factors (R_f) for c with variation of c, h and PGA

Ht. of Wall *h* (m)	PGA<100 cm/s^2		PGA=100 – 200 cm/s^2		PGA=200 – 300 cm/s^2		PGA=300 – 400 cm/s^2		PGA=400 – 500 cm/s^2	
	COV of *c*									
	<10 %	10-25%	<10%	10-25%	<10%	10-25%	<10%	10-25%	<10 %	10-25%
<1.5	1.0	1.0	1.0	1.0	1.0	1.0	1.25	1.75	1.4	1.85
1.5-2.0	1.0	1.0	1.0	1.0	1.0	1.3	1.25	1.75	1.4	1.85
2.0-2.5	1.0	1.0	1.0	1.0	1.0	1.3	1.25	1.75	1.4	1.85
2.5-3.0	1.0	1.0	1.0	1.0	1.0	1.3	1.25	1.75	1.4	1.85
3.0-3.5	1.0	1.0	1.0	1.0	1.1	1.3	1.25	1.75	1.4	1.85
3.5-4.0	1.0	1.0	1.0	1.0	1.1	1.3	1.25	1.75	1.4	1.85
4.0-4.5	1.0	1.0	1.0	1.0	1.1	1.3	1.25	1.75	1.4	1.85
4.5-5.0	1.0	1.0	1.0	1.0	1.1	1.3	1.25	1.75	1.4	1.85

Table 4b Risk Factors (R_f) for φ with variation of c, h and PGA

Ht. of Wall *h* (m)	PGA<100 cm/s^2		PGA=100 – 200 cm/s^2		PGA=200 – 300 cm/s^2		PGA=300 – 400 cm/s^2		PGA=400 – 500 cm/s^2	
	COV of φ									
	<10%	10-25%	<10%	10-25%	<10%	10-25%	<10%	10-25%	<10%	10-25%
<1.5	1.0	1.0	1.0	1.0	1.0	1.0	1.95	2.0	2.0	2.0
1.5-2.0	1.0	1.0	1.0	1.0	1.0	1.0	1.95	2.0	2.0	2.0
2.0-2.5	1.0	1.0	1.0	1.0	1.0	1.0	1.95	2.0	2.0	2.0
2.5-3.0	1.0	1.0	1.0	1.0	1.0	1.0	1.95	2.0	2.0	2.0
3.0-3.5	1.0	1.0	1.0	1.0	1.0	1.0	1.95	2.0	2.0	2.0
3.5-4.0	1.0	1.0	1.0	1.0	1.0	1.0	1.95	2.0	2.0	2.0
4.0-4.5	1.0	1.0	1.0	1.0	1.0	1.0	1.95	2.0	2.0	2.0
4.5-5.0	1.0	1.0	1.0	1.0	1.0	1.0	1.95	2.0	2.0	2.0

Table 5 Breadth of wall (*b*) for variation of *c*, *h* and PGA

Ht. of Wall *h* (m)	Original Breadth (m)	PGA<100 cm/s^2		PGA=100 – 200 cm/s^2		PGA=200 – 300 cm/s^2		PGA=300 – 400 cm/s^2		PGA=400 – 500 cm/s^2	
		COV* of *c									
		<10 %	**10-25%**	**<10 %**	**10-25%**	**<10%**	**10-25%**	**<10%**	**10-25%**	**<10%**	**10-25%**
<1.5	1.0	1.0	1.0	1.0	1.0	1.0	1.0	1.2	1.45	1.6	3.15
1.5-2.0	1.3	1.3	1.3	1.3	1.3	1.3	1.4	1.65	2.5	3.25	6.5
2.0-2.5	1.65	1.65	1.65	1.65	1.65	1.65	2.15	2.5	3.5	6.15	-
2.5-3.0	2.0	2.0	2.0	2.0	2.0	2.0	2.85	3.75	7.0	-	-
3.0-3.5	2.3	2.3	2.3	2.3	2.3	2.75	3.85	5.25	-	-	-
3.5-4.0	2.65	2.65	2.65	2.65	2.65	3.5	4.75	7.25	-	-	-
4.0-4.5	3.0	3.0	3.0	3.0	3.0	4.3	5.75	-	-	-	-
4.5-5.0	3.3	3.3	3.3	3.3	3.3	5.15	6.85	-	-	-	-

CONCLUSIONS

In the present study, the probabilistic risk factor based approach is applied to a series of retaining walls and design recommendations are provided for their safe functioning corresponding to different intensities of earthquake. It is observed that the cohesion of the foundation soil is the dominating factor in failure of the retaining walls for peak ground acceleration (PGA) less than 300 cm/s^2, while the internal angle of friction plays a significant role in stability when PGA exceeds 300 cm/s^2. Seismic reliability analysis also indicates that for variation of cohesion upto 25%, the walls are for PGA upto 200 cm/s^2. For PGA > 400 cm/s^2 and variation of c_2> 10%, walls having height more than 3m require a base width almost twice the height of the wall. The proposed procedure in this study can be applied in the design of retaining walls in other parts of Tokyo area as well, for similar subsurface and backfill conditions.

REFERENCES

Babu, G.L.S. and Basha, B.M. (2008a). “Optimum Design of Cantilever Sheet Pile Walls using Inverse Reliability Approach.” Computers and Geotechnics, 35(2), 134-143.

Babu, G.L.S. and Basha, B.M. (2008b). “Optimum Design of Cantilever Retaining Walls using Target Reliability Approach.” International Journal of Geomechanics, 8 (4), 240-252.

Baecher, G.B. and Christian, J.T. (2003) Reliability and Statistics in Geotechnical Engineering, Wiley, New York.

Becker, D.E. (1996b). “Limit State Design for Foundations. Part II: Development for National Building Code of Canada.” Can. Geotech. J., 33(6), 984-1007.

Duncan, J.M. (2000). “Factors of Safety and Reliability in Geotechnical Engineering.” J. Geotech. Geoenviron. Eng., ASCE, 126(4), 307-316.

Frey, H. and Patil, S. (2002). “Identification and Review of Sensitivity Analysis Methods.” Risk Analysis, 22, 553-578.

Gautam, T.P. and Kanda J. (2009). "Probability of Failure of Concrete Retaining Walls due to Earthquakes in Kanto Area, Tokyo." 2009 Portland GSA Annual Meeting (18-21st October 2009), 27 (7).

GuhaRay, A. and Baidya, D.K. (2012). "Reliability coupled Sensitivity based Design Approach for Gravity Retaining Walls." Journal of the Institution of Engineer (India): Series A, (ISSN: 2250 -2149) Springer, 93(3), 193-201; DOI 10.1007/s40030-013-0023-1.

GuhaRay, A., Ghosh, S. and Baidya, D.K. (2014). "Risk Factor based Design of Cantilever Retaining Walls." Geotechnical and Geological Engineering, An International Journal (ISSN: 0960 -3182), Springer, Netherlands; 32(1), 179-189; DOI 10.1007/s10706-013-9702-y.

GuhaRay, A. and Baidya, D.K. (2015). "Reliability based Analysis of Cantilever Sheet Pile Walls backfilled with different soil types using Finite Element Approach." International Journal of Geomechanics, ASCE, doi 10.1061/(ASCE)GM.1943-5622.0000475, 06015001, 1-11.

GuhaRay, A. and Baidya, D.K. (2016). "Reliability coupled Sensitivity based Seismic Analysis of Gravity Retaining Wall using Pseudo-Static Approach." International Journal of Geotechnical and Geoenvironmental Engineering, ASCE doi: 10.1061/(ASCE)GT.1943-5606.0001467, 142 (6), 04016010 – 1-13.

Harr, M. E. (1984). "Reliability-based design in civil engineering." 1984 Henry M. Shaw Lecture, Dept. of Civil Engineering, North Carolina State University, Raleigh, N.C.

Hasofer, A.M. and Lind, N.C. (1974). "A extract and invariant first order reliability format." Journal of Engg. Mech., ASCE, 100(EM-1), 111-121.

Kulhawy, F.H. (1992). "On the evaluation of soil properties." ASCE Geotech. Spec. Publ. No. 31, 95–115.

Saltelli, A., Tarantola, S., and Chan, K.P.S. (1999). "A quantitative model independent method for global sensitivity analysis of model output." Technometrics, 41, 39–56.

Stabilization of Slope at Cabo Hill, Goa, India – A Case Study

S.D. Anitha Kumari[1,3], B.R. Venkatesh [1,2], M.V.Deepthi[1]

[1] Ramaiah University of Applied Sciences, Bangalore-560057
[2] Director (Retd.), Geological Survey of India
[3]Corresponding author Email: anithakumari.ce.et@msruas.ac.in

ABSTRACT

Forensic Engineering is an important discipline relating to the application of Engineering principles in investigation of failures and suggesting remedial measures. In this regard, a case study of the slope stability studies carried out by the Geological Survey of India on the Cabo Hill in Goa, is presented. Raj Bhavan, the official residence of the Governor of Goa, is located on Cabo Hill at a height of 40m above the sea level. Cabo Hill consists of laterites that occur as capping over the parent rock and the duricrusts developed over the lateritic profile occupy the top surface. The four centuries old Raj Bhavan constructed by the Portugese is a two-storied monumental structure constructed with 0.7m thick walls comprising of laterite blocks in mud mortar. The hill slope was reported to have been undergoing a gradual distress due to natural processes over several decades with cracks appearing at the pavement as well as the rocky floor. The initial studies made by the Central Building Research Institute attributed distress to ground subsidence and concluded the structure as unsafe. Some protective measures by constructing Buttress walls, Retaining walls, Sea-walls etc., by the State Public Works Department in the 1960s, did not yield desired stability and the slope continued to exhibit distress in the form of deepening of cracks and related tilting of parts of the structure, indicating downward slope movement. In view of above, the Geological Survey of India (GSI) took up a detailed investigation on the slope distress and identified the causative factor as sliding along a shear plane. GSI recommended installation of pre-stressed cable anchors at crucial centers, besides RCC grid blocks, micro-piles etc. The work was executed by ITD Cementation India ltd.

INTRODUCTION

The Cabo Hill is essentially a lateritic hill housing Raj Bhavan-the official residence of His Excellency, the Governor of Goa. The hill has an elevation of 40m. The Raj Bhavan shown in Fig 1 is reported to have been constructed 400 years ago. It is said that the western and northwestern slopes close to Raj Bhavan, facing the Arabian Sea was experiencing slope distress over a past few decades. The effect of slope distress was manifested as development of cracks in the pavements, and on the floor of the verandah and the rear part of Raj Bhavan building. The Cabo Hill housing the Raj Bhavan, forms a cape facing the Arabian sea in the State headquarters – Panaji. Cabo Hill forms part of the Survey of India Topo-sheet 48E/15.

Figure 1 Raj Bhavan on Cabo Hill top

STUDY AREA

Fig 2 shows the study area. The hill trends NW-SE bounded by Mandovi River in the North, Zuari River in the South and Arabian Sea in the West. The crest housing Raj Bhavan is convex in its profile.

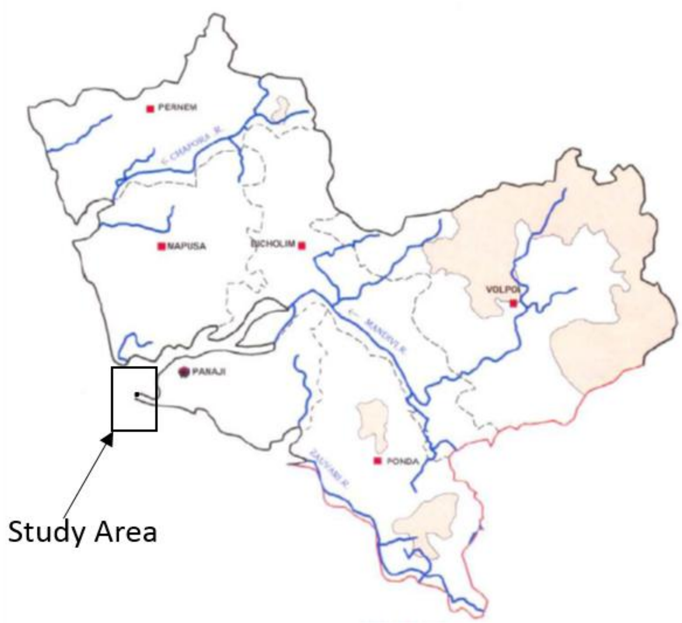

Figure 2 Study area

Geology

Goa situated at the west coast of India, forms a part of Precambrian shield of India, in which the Precambrian Greenschist Supra-crustal rocks overlie a basement consisting of Gneissic rock (Peninsular Gneiss) intruded by Mafic to Ultramafic Dykes and Granites. The geological map of Goa is shown in Fig 3. Late Cretaceous Basaltic rocks (Deccan Traps) occur at the northeastern periphery of Goa (Fig. 4a). Laterite occur as a capping over most of the rocks along the coastal stretches in the state as shown in Fig 4a. A 10m wide Dolerite dyke trending NW-SE characterized by vertical joints is reported close to the Cabo Hill part facing the sea. The dyke at the Cabo Hill is also reported to have a laterite cover. The lateritic profile is rather thick around 60m and the geological studies around the area have indicated the presence of rocks such as Schists, Quartzite, meta-Basalt, Greywacke, Phyllite, Siltstone/Shale intruded by Dolerite and vein-Quartz. Drilling at selected spots have revealed the presence of unaltered rocks at a depth of -42m, trending NNW-SSE with a northerly dip varying between 35° and 70°(Panduranga et al, 2008).

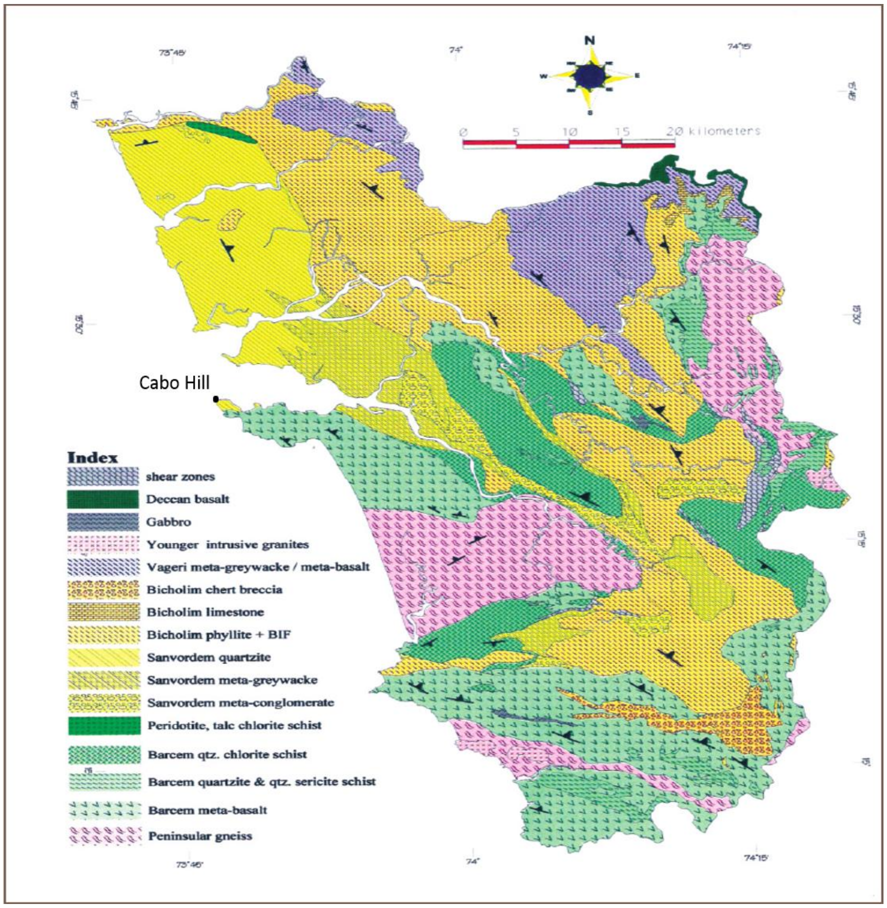

Figure 3 Geological map of Goa (Maruti et al, 2010)

The Cabo Hill comprises of lateritic material (Fig. 4b). Laterite represents a type of rock rich in iron and aluminum and is commonly considered to have formed in hot and wet tropical areas. The laterites have a typical profile and are in general rusty-red in colour on account of high iron oxide content. This rock develops by intensive and prolonged weathering of the underlying parent rock under specific climatic conditions.

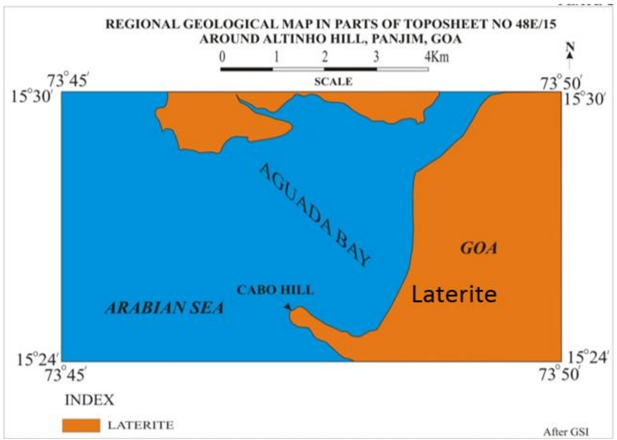

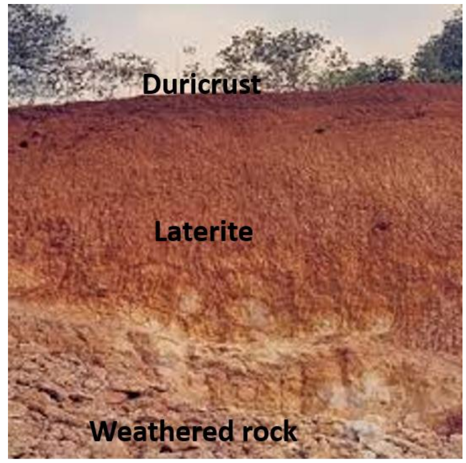

Figure 4(a) Laterite occurrence along the Coastal stretch (b) General laterite profile

The laterite at the site contains a very hard and ferruginous duricrust at the top. The duricrust is a hard crust that forms at the surface of a lateritic profile, which hinders water infiltration and the emergence of seedlings. In the vicinity of Raj Bhavan are also seen fairly steep escarpments that are essentially controlled by joints. At the middle part of the Cabo Hill slope, dislodged blocks are present as debris or a scree.

SLOPE DISTRESS CHARACTERISTICS

The western and northwestern slopes of Cabo Hills are reported to have been undergoing distress over a long period. The south and south eastern slopes that were once stabilized also continued to show distress. Cracks were seen developed on asphalted pavement behind the Raj Bhavan. Small concentric cracks at the Crown were noticed on the asphalted pavements in front of Chapel. The parapet wall constructed around the edge of the steep slope adjacent to Raj Bhavan had developed cracks at many places indicative of horizontal and lateral movement. Five sets of parallel cracks trending in NNW direction were also present at the staircase leading to Grotto – a small Chapel. In addition to it five sets of joints exposed in the laterite was open, showing clear displacement along horizontal and vertical directions.

Steeper slope angles at the higher reaches of the slope, poor shear strength of the subsoil, excessive loading over the steep slope coupled with heavy infiltration of rainwater and sewerage water in an already unstable mass at the crown part were reported to have been responsible in making the subsurface susceptible for continuous distress along the rupture zone. In addition, the scree present at the mid slope part reflects its derivation due to instability effect of the top part of the hill. The material is assorted comprising lateritic, silty clay, saprolite and weathered materials. These materials are found to overlie the fresh and unaltered rocks at depth.

BACKGROUND INFORMATION

Prior to GSI taking up investigation in 2002, M/s Descon Engineering consultants, Bombay had carried out geotechnical investigation between 1969 and 1971, over the slope instability issue, then had suggested grouting and a curtain of rotary drilled anchor piles along the margins of the pavement. Later M/s Central Water Power and Research Station (CWPRS), Pune while investigating the cause of slope failure during 1988-89, found out a zone of tension at the bottom of the lateritic formation leading to development of cracks at its capping. M/s Central Building Research Institute (CBRI), Roorkee in their structural engineering and geological investigations in 1996 recommended some of measures like RCC piling, construction of new toe wall, stitching of cracks on the surface of laterite cap and cantilever support for the first floor verandah to address the problem.

Even though the above recommendations were followed, instability continued to occur affecting the slopes especially the western and northwestern slopes. Subsequently the Geological Survey of India (GSI) took up the investigation following the request of Govt. of Goa and suggested remedial measures (Panduranga et al, 2008).

CAUSES OF SLOPE DISTRESS

The Geological Survey of India (GSI) commenced geotechnical investigation at the portion of the distressed slope in 2002 (Panduranga et al, 2008). A geotechnical map prepared on scale 1:500 showed the weak zones and distribution of scree and debris, duricrust, paleo-scars, cracks as well as appropriate borehole locations. Based on the investigations coupled with borehole analysis, the remedial measures suggested include pre-stressed anchor cables at selected weak zones, vertical and horizontal piles, retaining walls, weep holes etc. The geotechnical map of the Cabo Hill (after GSI) is shown in Fig 5.

When the GSI took up the investigation, cracks had already developed even on the pavement which was asphalted later, parapet wall, corner of verandah and the staircase of Grotto (a chapel at the Cabo Hill), buttress, cladding wall and seawall. This led to a conclusion that the protective measures carried out earlier were not effective. Even the south and south-eastern part, near Grotto, happened to be the continuation of the part of the slope that were once stabilized, found to experience distress. Besides the cracks in the building, five sets of joint planes within the laterite were open indicating clear dislocation.

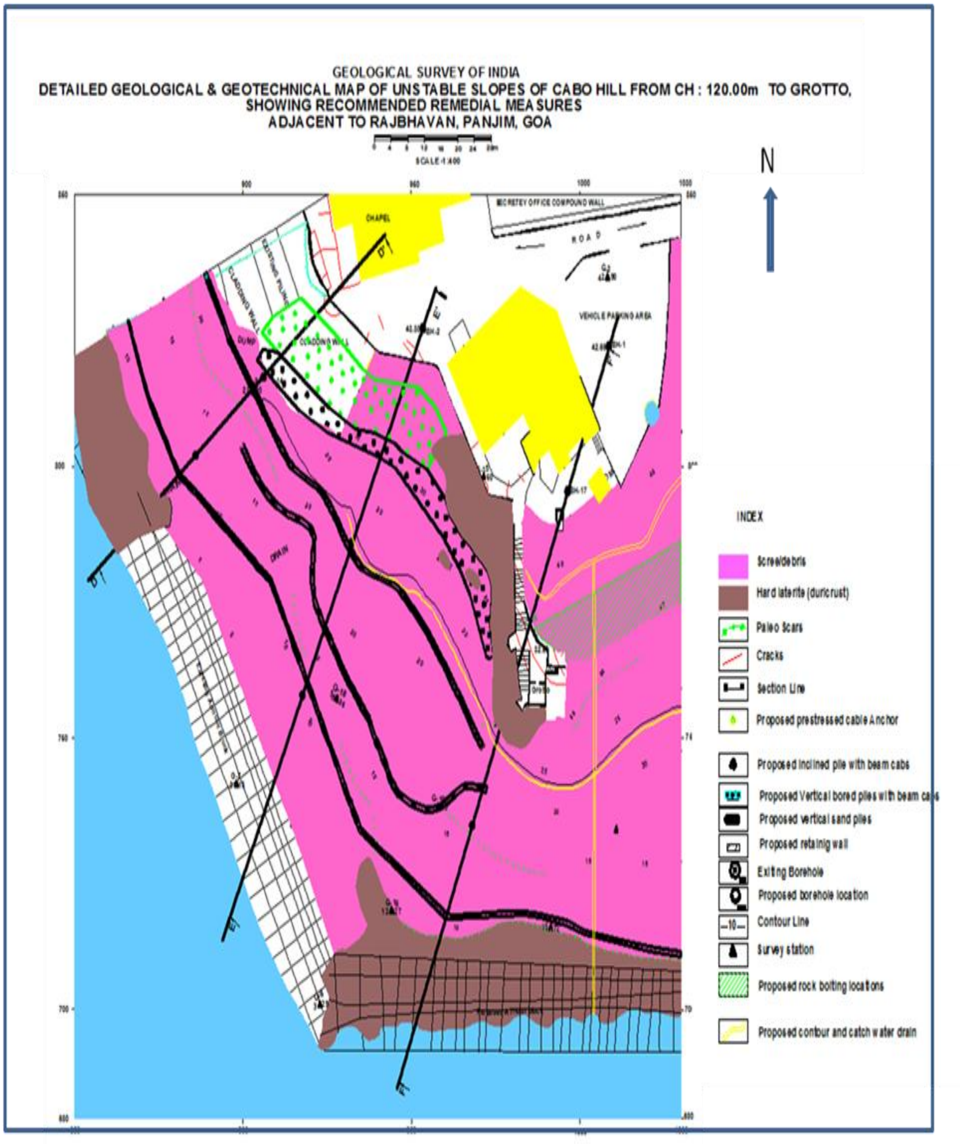

Figure 5 Geotechnical Map of Cabo Hill (After GSI)

Later, GSI took up a detailed geotechnical investigation to find out the cause and suggested remedial measures at the request of Govt. of Goa. GSI carried out drilling up to a maximum of 40m in selected locations and collected undisturbed samples from various horizons and the samples were subjected to geotechnical analysis enabling construction of a critical slip circle. In-situ tests were also carried out by Standard Penetration Tests (SPT) (Maruti et al, 2010). The geotechnical parameters determined on undisturbed samples included particle size distribution, specific gravity, bulk density, natural moisture content, porosity, compressive strength, cohesion and angle of internal friction values. The critical slip circle of the distressed slopes was constructed duly integrating the various geotechnical parameters and the engineering properties of the sub-soil. Later in the year 2009, the geotechnical data obtained by studying the borehole samples were utilized in carrying out stability analysis at the request of Govt. of Goa and revised the measures for stabilization.

The study has revealed that many geological and man-made factors responsible for the distress. These factors can be summarized as:

- The rock has well defined joints that are fairly wide and vulnerable for failures
- The presence of incompetent material between the lateritic duricrust and fresh rock
- Angle of slope is relatively steep in relation to cohesion and angle of internal friction values of sub soil
- Toe cutting or erosion by wave action
- Disproportionate increase in constructional load
- Improper drainage
- Unscientific waste disposal affecting the fractures and joint planes in the laterites enabling water infiltration

SUGGESTED MEASURES

On the basis of geotechnical studies taking into account the slip circle, slope morphometry, geotechnical properties of material forming the slope, the following measures were recommended by GSI for various segments of the slope.

Upper part of the slope

The upper part of the slope is stabilized by using pre-stressed cable to tie up the fractured, hard lateritic media into a monolith and fixing to the intact part of the duricrust. Cable anchors were planned at different levels between 3 and 40 m R.L over a length of 20 m at an inclination of 20° at a spacing of 2 m at each row. Apart from arresting the mobility of the distressed blocks, anchors are expected to arrest further development of any tensional cracks resulting in subsequent distressing. This measure improves the mechanical behaviour of the fractured hard duricrust of the laterite. Also grouting was done for the cladding wall and for the sealing of ground cracks as shown in Fig. 6. In addition to this, vertical piles are laid and rock bolting (Fig 7) was also done to prevent the widening of the rock joints in laterite.

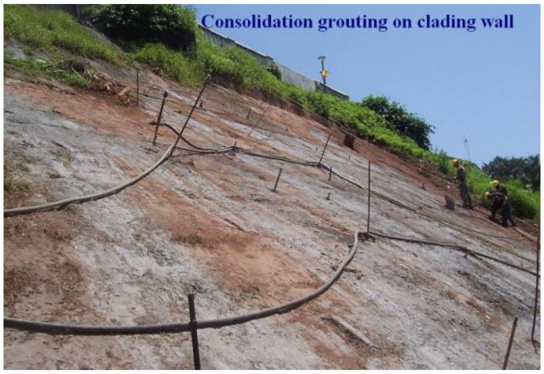

Figure 6 Grouting over the cladding wall

Figure 7 Drilling for Rock bolting

The provision of intermediate shear interceptors at the foot of the steep slope also helps to stabilize the slope. These shear interceptors are inclined bored piles with beam caps.

Middle part of the slope

The middle part of the slope is stabilized by installing shear interceptors of 15m length as vertical micro piles for achieving desired shear resistance to the creeping mass. Also a row of vertical sand piles on the mid slope was provided to release the possible pore water/ ground water pressure from the slope-forming media. The progressive creep of the slope material can be countered by making the slope gentle and by providing surface drainage. Accordingly GSI had recommended grading of mid-slope into terraces utilizing boulder sausages. The boulder sausages were to be provided with weep holes to drain subsurface water and also to overcome pore pressure. Turfing or terrace gardening was done over the treated soil to create a geo-green blanket for aesthetics as well as stability.

Toe part of the slope

The toe part of the slope is stabilized by the construction of retaining walls with effective weep holes and graded filtering. As an effective shore protection work, armour block claddings were recommended all along the shoreline of the unstable slope to protect the toe of the distressed slope from scouring.

Once the remedial measures are adopted, GSI suggested certain measures to monitor the distressed unstable slopes of Cabo Hill. They include the slope movement monitoring, settlement observations, measurement of pore water pressure and monitoring of ground cracks.

Execution of Civil Works

M/s ITD Cementation India carried out the work for the Govt. of Goa in two phases, duly implementing the recommendations of GSI. The first phase of work commenced in 2006 and the later phase was in 2011 at the cost of Rs. 4.45 crore and Rs. 10.73 crore respectively. The second phase could commence only after ensuring that desired stability was achieved from the operations in the first phase. The sponsoring governmental agency was the Water Resources Department (WRD). The main task for the Company was to arrest the sliding which is known to have been occurring along a definite shear plane in the weak rock and the toe of the slip surface extended till the bottom of the slope.

As per the recommendation of GSI, rock anchors were used on a specific grid pattern arrangement. Micro piles were installed to act as shear interceptors. Grouting was done to fill voids and crevices. An important task of stitching the moving rock mass with a rigid and stable rock mass of the Cabo Hill was achieved by using 15 m pre-stressed rock anchors at 4-m staggered spacing (Fig. 8). It was ensured that the rock anchors extended beyond the pre-identified failure surfaces. Also a network of RCC grid beams was utilized as a bearing surface to facilitate pre-stressing and to distribute the pre-stress over a larger area (Fig. 9). Shotcreting (Fig. 10) and rock bolting was also carried out as per the recommendations.

Figure 8 Rock bolting

Figure 9 RCC Grid

Figure 10 Before shotcreting

Vertical and raker micro-piles were utilized to act as shear interceptors (Fig.11). Weep holes were also positioned at selected places in the retaining walls to effectively counter the effect of water saturation. Later, the treated slopes were given an aesthetic look by turfing and terrace gardening (Fig. 12).

Figure 11 Vertical piling in progress

Figure 12 Turfing

As per ITD cementation, the entire work was very challenging as it was carried out on the slope that was showing signs of instability. The slope's surface was strewn with boulders of various sizes, along with vegetal growth and matured jungle, much of which could not be removed due to environmental concerns, which inhibited movement, installation of equipment, supply of material, erection of scaffoldings and platform for drilling. Boulders had to be disintegrated to facilitate slope profiling. Drilling and anchoring were problematic as numerous cavities and crevices that were encountered had to be punctuated with consolidation grouting to fill them up before drilling operations. Besides, an existing buttressed retaining wall along the slope showed signs of disequilibrium and was dangerously poised while the work was in progress. Hence the wall had to be removed right from its foundation and the hollow portion was grouted.

Field monitoring through instrumentation

GSI had recommended field monitoring through instrumentation to monitor stability conditions at the hill slope. Accordingly, M/s ITD Cementation India (www.itdcem.co.in) installed inclinometers at selected spots as shown in Fig. 13.

Fig. 14 shows the settlement gauges fixed to accurately measure deformation in soil and rock. Piezometers were also placed at selected spots to measure pore water pressure.

Figure 13 Inclinometer **Figure 14 Settlement gauge**

CONCLUSIONS

Forensic Engineering is a field where scientific methodology is applied to investigate the failure of materials, components, products and structures and obviously poses a great challenge for the Engineers and Scientists. The stability of Cabo Hill slope in Goa presents one of the classic case history in the field of Forensic Engineering in India. The Cabo Hill is a lateritic hillock facing the Arabian sea and is situated in Panaji. Raj Bhavan, the official residence of His Excellency, the Governor of Goa, is housed atop the hillock at an elevation of 40 above MSL. The 400 year old building had been experiencing continued distress since a few decades. The remedial measures following investigations earlier failed to stabilize the slopes and safeguard the structure. Subsequently investigation to arrest slope failure was taken up by GSI. Based on drilling and in situ testing by SPT methods as well as a detailed geotechnical analyses on the undisturbed borehole samples collected at various levels, certain remedial measures to stabilize the distressed slope were suggested. Currently, the slopes are being monitored for the stability with the help of various instruments installed at the site since 2011.

ACKNOWLEDGEMENT

Special thanks are due to K.V.Maruthi and K.V.Chandran – Officers of the Geological Survey of India for having very well explained the geotechnical investigation carried out by the Department as well as M/s ITD Cementation India Ltd., during the earlier inspection visit and also for having spared some of the images captured during the investigation. The authors are indebted to the authorities of the Geological Survey of India for extending facilities for library consultation

REFERENCES

Mascarenhas, A. and Kalavampara, G. (2009). “Natural Resources of Goa: A Geological Perspective”. A Geological Society of Goa Publication.

Maruthi, K. V., Mishra, A. K. and Chandran, K. V. (2010). “A Report on the geotechnical evaluation of subsurface exploration of unstable slope of south and south eastern part of Cabo hills (grotto), adjacent to Raj Bhavan, Panjim, Goa” F.S 2009-10. www.gsi.gov.in

Panduranga,R., Dharuman, R. and Mishra, A.K. (2008). “Geotechnical evaluation of the unstable slopes of Cabohill, adjacent to Raj Bhavan, Panaji, Goa”.

ITD – Major Projects. www.itdcem.co.in

http://www.constructionworld.in/News.aspx?news=Grounded-in-his-passion

www.isegindia.org/pdfs/Abstract_Seminar_Hyderabad

Numerical Evaluation of the Bearing capacity and displacement of in-situ Piles compared with PDA tests results

Jalili M., Ph.D.,[1] Alirahimi Y., MSc.,[2] Nikkhah Shahmirzadi, M.,[3]

[1] Assistant Professor, Civil Engineering Department, Technical & Engineering Faculty, Semnan Branch, Islamic Azad University, Semnan , Iran, Email: m.jalili@semnaniau.ac.ir

[2] MSc Graduated, Civil Engineering Department, Technical & Engineering Faculty, Semnan Branch, Islamic Azad University, Semnan , Iran, Email: alirahimiyaser@yahoo.com

[3] Assistant Professor, Civil Engineering Department, Technical & Engineering Faculty, Semnan Branch, Islamic Azad University, Semnan , Iran, Email: m.nikkhah@ semnaniau.ac.ir

ABSTRACT

Nowadays, using deep foundations in different structures and subsurface conditions is inevitable. Precise evaluation of pile bearing capacity, as one of the mostly used foundation, will diminish material and energy consumption, so it is a step toward sustainable development. Full-scale static loading test, is not applicable for large number of piles, therefore bearing capacity may be underestimated. Therefore PDA test which is based on the wave propagation theory was used since the early nineteenth. In this study, measured bearing capacity, displacement and wave velocity of field test, which are output of the CAPWAP program, have been compared with the same parameters, calculated by finite element and finite difference programs modeling results, and empirical formulas. In addition to the static assessment, by simulation of hammer impact force to dynamic load and considering damping factor of 5%, changes in some of the above-mentioned parameters have been investigated. The results indicated that measured static end bearing capacity by Finite Difference modeling in Flac2D is 20% more than CAPWAP results, in finite element program (PLAXIS) this error was limited to 45%.among the empirical pile driving formula, modified ENR with modification factor of 16%(F.S=6) is in correlation with the literature. Skin bearing capacity in numerical software is about 55% less than CAPAWAP result due to setting end of the piles in a very dense clayey soil which cannot mobilize skin friction completely and absolute dependency to the interface layer parameters. By using equations such as β method, not acceptable correlation with CAPWAP results was obtained. Also in dynamic assessment by numerical method, the skin friction was 15% overestimated. Acceptable correlation especially in static end-bearing capacity was observed. In term of transferred energy to the pile head, the stiffness of soil-pile interface has an important effect in pile displacement as a result of the increasing the applied energy, more than 40 kN-m.

Keywords: Pile bearing capacity, soil-pile interface, PDA test, numerical modeling.

INTRODUCTION

Noticeable part of safety and stability of structures is related to their foundations. Due to high construction cost of deep foundation (sometimes half of the total project cost), optimum structural design in compliance with sustainable development should be considered. many studies are available in the literature on the basis of static and dynamic load test or in–situ tests such as SPT and CPT(e.g. Eslami et al.,2013[1];Fellenius,2008[2]:Feizee and Fakharian,2008[3]) Despite of great progress in geotechnical science during recent decades, determination of exact pile bearing capacity is a big deal. Due to various factors, affecting physical and mechanical property of soils, modeling of such a situation is complicated. Therefore many researchers tried to find theoretical or empirical formulas to assess bearing capacity. In addition to provide a proper behavioral model, soil geotechnical parameters is another obstacle which leads to underestimate of pile bearing capacity. Dynamic tests, to assess bearing capacity as a part of dynamic methods, is based on foundation response under dynamic loads. Dynamic methods are included dynamic formula, WEAP analysis (Wave Equation Analysis Program), pile dynamic analysis (PDA) and CAPWAP method. Through dynamical impact we can use mass-spring-dashpot model and by solving one dimensional wave propagation theory, based on embedment depth of pile, we can calculate static bearing capacity. Using newton's impact law which was based on simultaneous energy transition from top to bottom of the pile, lead to dynamic formula to determine bearing capacity of piles. Newton's law in this case was an improper idea, so all effort to enhance dynamic formula was interrupted. Issacs (1931) was the first person who shows after impact to the pile head, a longitudinal wave will be generated, so the soil- pile-hammer system should be modeled by one dimensional wave propagation theory. Complicated mathematical wave equations, lead to find a numerical solution based on finite difference to evaluate pile displacement. Smith (1960) performed a vast investigation on effective parameters to model the soil-pile- hammer system ,in this method, designation of hammer efficiency and soil parameters in different depth was a controversial issue. due to the mentioned uncertainties, the pile dynamic analysis (PDA)test was dedicated.in this test by attaching sensors to the pile head, we can measure the force and velocity of the wave initiated in the pile due to hammer impact. Since this tool exerts high magnitude of dynamic loads to produce a certain range of penetration, it's also referred as "High strain dynamic pile testing" .the PDA output data will be analyzed by two methods in order to evaluate the pile bearing capacity: the CASE method and the CAPWAP software. CASE method is consisting of simple equations that can predict the static bearing capacity of piles during the tests. The CAPWAP software is programmed to analyze the PDA data accurately.in this software the pile and soil are divided into smaller elements and the static and dynamic properties are modeled through a series of spring and dash –pots. the total static bearing capacity, skin friction and static load-settlement diagram can be obtained from CAPWAP analysis .the good agreement between CAPWAP results and static load test have been observed in the litrature.in this study the pile bearing capacity and pile displacement of two in-situ piles, constructed in south pars gas field development phase19 calculated from finite and difference elements methods have been compared with PDA test results[4] and empirical pile driving formula the correlation factors have been obtained.

MATERIAL AND METHODS

PDA test procedure

The pile driving analyzer-PDA records, analyzes and saves the strain and the accelerations induced at the pile head .the system PAX as the most modern version of PDA can record up to eight channels (4strain channels and 4 acceleration channels), though most of the time 2 channels of strain and 2channels of acceleration seem to provide enough accuracy needed in practice. The procedure of the pile dynamic test is as follows.

The pile head must be prepared for installation of the gauges .for cast-in-place concrete piles, the pile head must be reconstructed above ground level .The gauges have to be installed at a distance of 1.5 to 3 times from the pile diameter from the pile head.in this regard the role bolts are installed in the concrete at certain points located by the engineer.

The sensors are attached to the pile using small bolts before attaching the gauges to the piles; the allowable error must be evaluated. After the calibration process and ensuring the approved performance of the instruments, the main cable is separated from PDA and gauges are installed on the piles. the gauges must be located at opposite position and it is recommended that their distance be 1.5 to 3 times from the pile diameter from the pile head top.it should be noted that their distance from neutral axis must remain the same to minimize the effect of misaligned impacts of very large local stress.

Some of the parameters which are entered into PDA are the pile length, cross section dimension depth of embedment, hammer weight or type and gauges position, wave speed in pile and elastic modulus.

The equipment for applying dynamic force to a cast-in-place piles could be a free fall hammer .the hammer energy must be capable of mobilizing the full bearing capacity of the pile to achieve the ultimate bearing capacity .besides, the properties of the pile head material must ensure decent energy transfer from the hammer to the pile .if this condition is not met, the data obtained by the test is the bearing capacity which is lower than the ultimate bearing capacity. the drop hammer of the company is weighs 12 tons which is modifiable to the maximum of 15 tons. The 12 tons hammer is capable of activating of bearing capacity of up to 900-1200 tons. The designation and manufacture of the hammer is in a way that energy lost is kept to the lowest.

The remaining procedure is as follows:

-the force and velocity waves recording
-end of driving and test procedure-exit from the program
-dismantling of the gauges from the pile head
-PDA data results analysis by the CAPWAP software

In this study, finite element software (PLAXIS 2D) and finite difference software (FlAC 2D,3D) have been used.

The strength and elastic parameters of the soil for the modeling is required. The required parameters have extracted from the site geotechnical report as shown in table1

Table1-strengh and geotechnical parameters for modeling

No	Pile	Φ	υ	C(kPa)	E(kg/cm^2)
1	B1-12	35	0.3	10	1000
2	E1	36	0.3	10	1000

Geotechnical condition

According to soil strata, [5] one pile is totally submerged and the main part of another pile is under the ground water surface. Regarding the soil layers which are a combination of sand and gravel, we neglect consolidation settlement and the effective parameters on bearing capacity (unit weight) should be revised (1100 kg/m^3). Another important parameters in modeling, is the strength parameters of interface layer which the following formula have been used:

$c_i = (2/3\sim1)\ c$

$\emptyset_i = tan^{-1}(2/3tan\emptyset)$

Software Verification

In order to software verification, a 0.66m diameter and 22m length pile have been modeled in an undrained clayey soil, and the bearing capacity have compared with theoretical formula.

Hammer impact simulation as a dynamic load

For impact modeling, FLAC 2D have been used.in this method, impact is applied to the pile head in 50 ms, as a dynamic load using PAN(2002).As the enclosed area by the curve is the applied energy to the pile head, the maximum force should be chosen to meet the required energy.

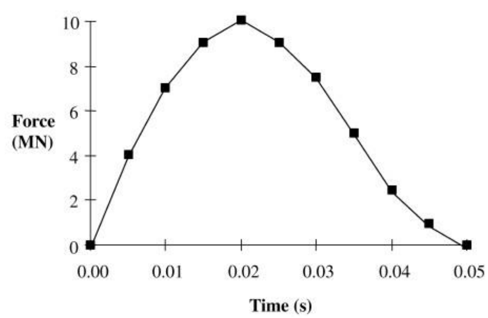

Figure 1. Dynamic load applied to the pile

Figure 2. View of sensor attachment and hammer installation

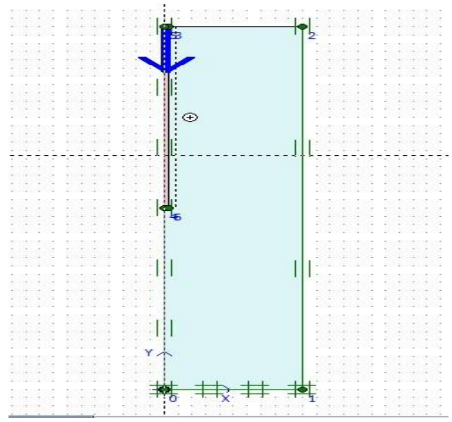

Figure 3. Provided model in PLAXIS software

Empirical pile driving formula

The PDA test results have been compared with three major empirical pile driving formula such as modified ENR, Gate and olson and flaate.

Results and discussion

PDA test results

Figure 4 shows bearing capacity and displacement for pile in PDA test results.Table2 shows bearing capacity and allowable compression capacity using safety factor of 2 in PDA test results.

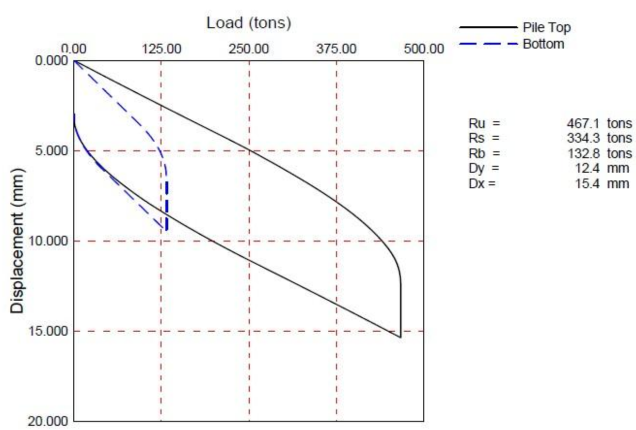

Figure 4. Bearing capacity and pile displacement (PDA results)

Table 2. Bearing capacity and transferred energy

Pile Name	Drop Height (cm)	SET Per Blow (mm)	Energy Transferred to the Pile (ton-m)	Total Capacity (ton)	Skin Friction (ton)	End Bearing (ton)	Allowable Compression Capacity (ton)
B1-12	125	3	11.29	467	334.3	132.8	234
E1	125	3	13.56	554	416.7	137.4	277

Modeling and end-bearing capacity of piles in Numerical evaluation and empirical formula

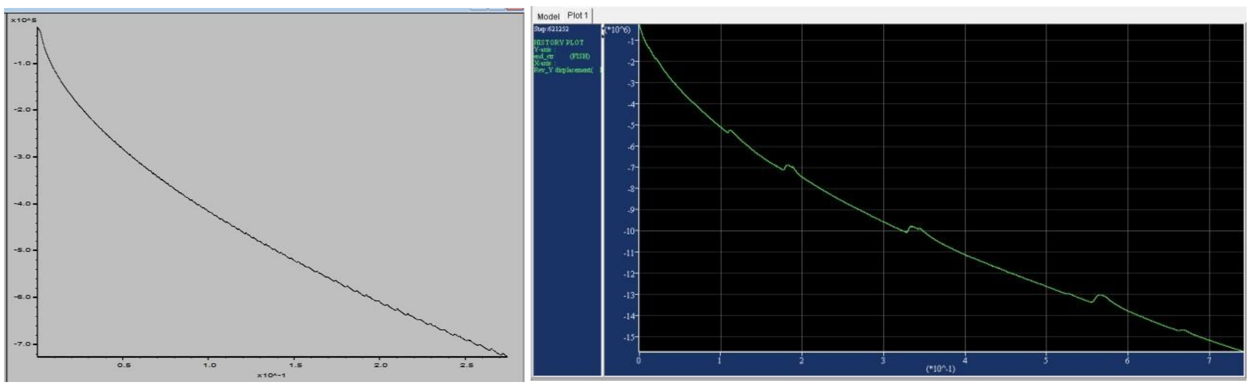

Figure 5. Load –settlement curve for FLAC3D, PLAXIS

As it can be seen, no specific yielding point for the pile is on hand .the more pile settlement, the more end load.by supposing symmetric settlement of about 10 cm, the ultimate end-bearing is calculates according to Fig. 5.

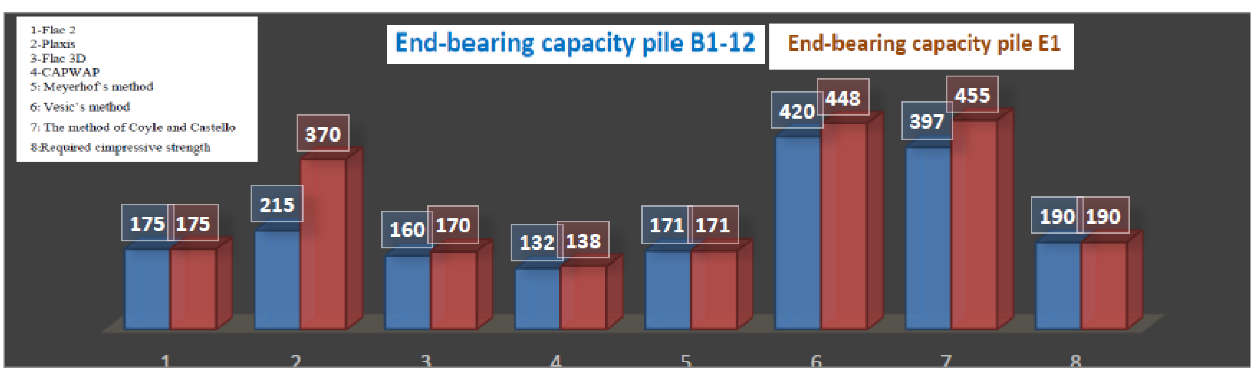

Figure 6. End bearing capacity by 8 different method in two piles(ton)

Sensitive analysis on boundary dimensions in FLAC3D

Fine mesh dimension will cause long analysis time.in opposite way, coarse one, will lead to considerable error.by three different mesh dimensions and studying load-settlement curve, no Considerable different was observed.

Bearing capacity based on pile driving formula

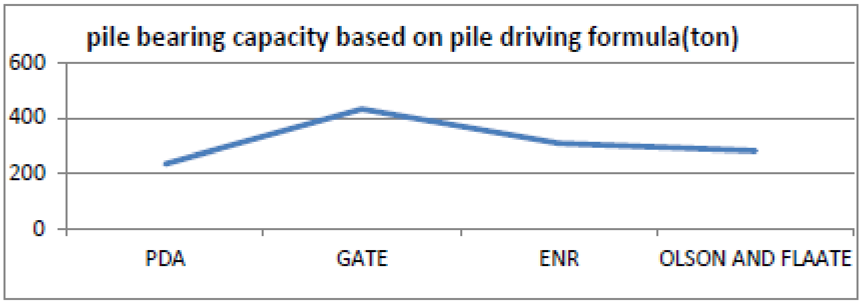

Figure 7. Pile bearing capacity based on pile driving formula on pile B1-12

Dynamic evaluation of bearing capacity and pile displacement

In terms of hammer impact simulation, the wave velocity, stress, displacement changes and bearing capacity have been investigated.by studying above mentioned parameters, we can conclude that in transferred energy more than 40 kNm no correlation by PDA test results, will be found.

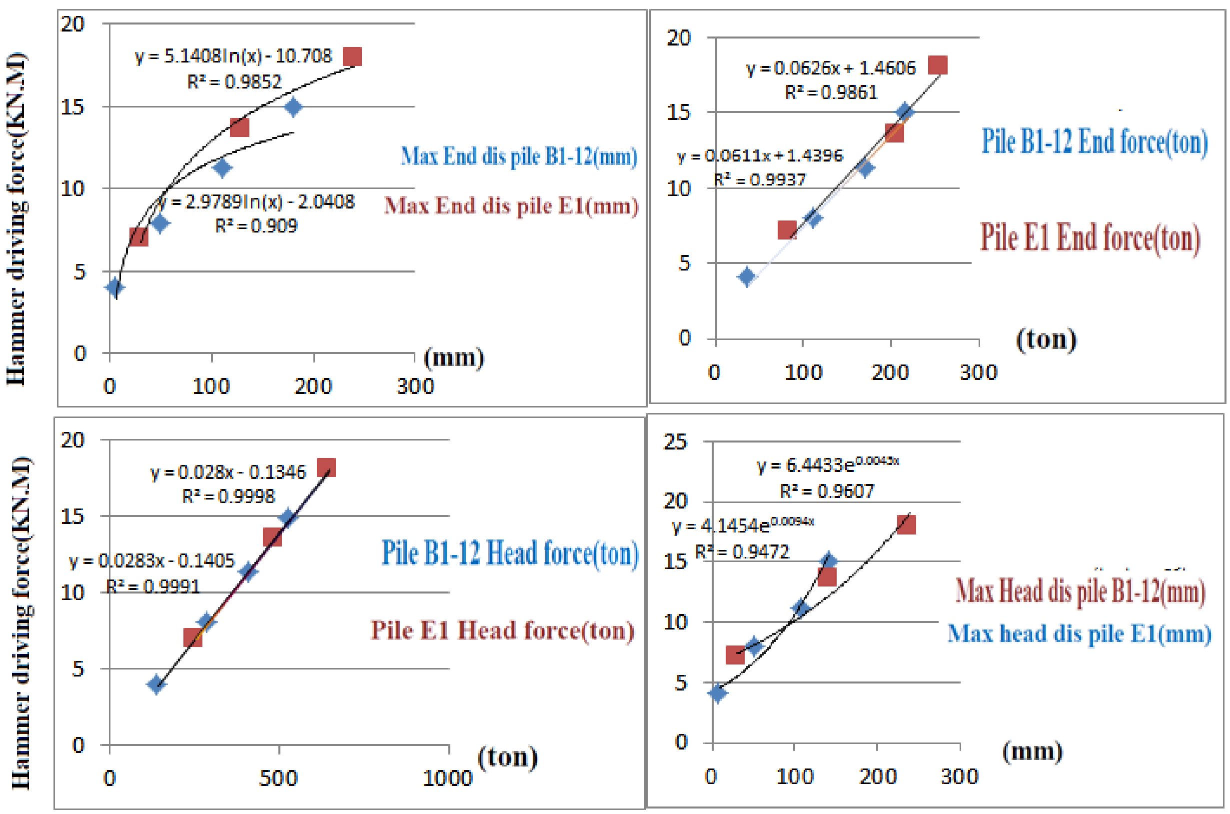

Figure 8. Maximum force and displacement in pile head and end ,in terms of applied dynamic load

Regarding the above diagram, it is obvious that, maximum displacement in numerical modeling is in contrast with PDA results. For example in BH-95related to pile B1-12, maximum displacement under 11.3 t.m energy is 15 mm according to CAPAWAP results. But for FLAC2D, maximum displacement is 10 cm.so the effect of pile end and skin on displacement will be investigated. First by increasing the cohesion to 150 kpa in 20 m length of the pile, the skin effect will be observed. According to Fig.9.maximum displacement equal to 18 mm will be measured.

To study the effect of pile end cohesion, the cohesion after 20 m of pile length will be 150 kpa and the interface strength parameters which show the skin friction, will be null.in this case the displacement is equal to 8cm.

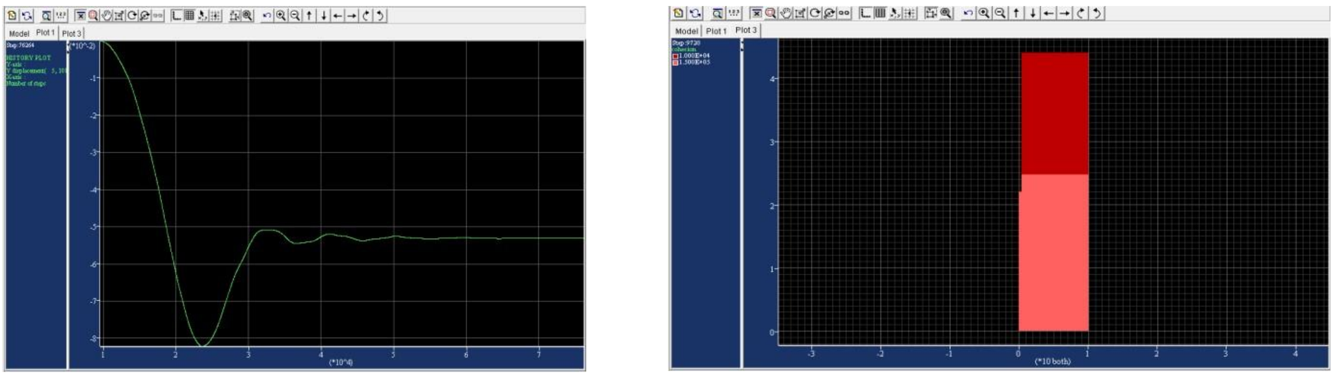

Figure 9. Effect of end pile cohesion on pile displacement

We found that the interface layer parameters has a great effect on pile displacement, and by increasing the interface layer stiffness, the displacement will be reduced.by increasing the interface layer stiffness, from $5*10^{6}$ N/m to $1*10^{8}$ N/m, the displacement will be reduced from 3cm to 7 mm.

CONCLUSION

1-Skin friction bearing capacity calculated from numerical models, is 130, 150 tons in BH-95,BH-96 respectively ,which is almost40% of values measured from CAPWAP test results.

The main reason for this inconsistency is absolute dependency of skin friction to interface layer parameters and setting end of the pile, in a very dense layer, which due to no displacement, cannot mobilize total bearing capacity.

2-in terms of end bearing capacity in numerical model(both finite element and difference) , theoretical formula and PDA test ,results are in a good agreement .among mentioned methods,FLAC3D has the most consistency(78% CAPWAP results) and the vesic's methods has the worse one due to unreliable shape factor.

3-using methods such as β,α to assess the proper performance of numerical software, especially in skin friction, indicated that considerable error in comparison with PDA test results, still exist.

4-by comparing pile driving formula, Modified ENR with correction actor of (16%)F.s=6,has the most agreement with PDA test results, then we can name olson and flaate ,then Gate formula.

5-in dynamic evaluation of bearing capacity, using hammer impact simulation, we found that , end bearing capacity in piles, using PDA will led to20% underestimate than finite difference methods(FLAC2D).in terms of skin friction ,the results of FLAC 2D,is 60%underestimate than PDA results due to abovementioned reasons.

6-in term of pile displacement, inBH-95(, PDA test results, maximum displacement in end and head of the pile is 9.3 and 15.4 mm respectively. but in numerical software in range of 4 t. m transferred energy, displacement is 6,9 mm.by increasing applied energy to 11/3 t. m, which is the applied energy in sites, end and head displacement increased rapidly to 100 ,110 mm.

7-in pile E1,in PDA test results ,the maximum displacement of end and head of the pile is 7.5 and 15.6 mm respectively.in another hand by increasing the energy till 7 t.m end and head displacement will increase to 3 and 3.5 mm. then by increasing energy to the applied energy in sites,(13.56 t.m)displacement in end and head will increase to 14 , 13.5 cm.

8-inconsistency between displacement in PDA and Numerical model made us to investigate the effect of end and skin of the pile, the results showed that, by increasing cohesion of skin from 10kpa to 150 kpa . Maximum displacement will be 18 mm ,which is in good agreement with PDA test results. For assessment of pile end ,we assign 150 kpa cohesion to the length more than 20 m, the displacement will be 8 cm which have no agreement with PDA results.so the great influence of pile skin stiffness was revealed.

9- End and head force generation in piles shows linear relation with correlation factor of R=0.98.the most agreement with PDA test results for pile head will take place in 8t.m energy and 7t,m energy for pile end.

10- by increasing applies energy, pile head and end displacement will increase rapidly due to great effect of interface layer parameters on pile displacement, the best compliance will occur in 4 t.m energy transfer.

REFERENCES

Eslami, A., Tajvidi, I, and Karimpour-Fard, M (2013).”Efficiency of methods for determining pile axial capacity-applied to 70 cases histories in Persian gulf northern shore”, International journal of Civil Engineering, Vol 11,No, 2, pp.174-183

Fellenius,BH. (2008). “Effective stress analysis and set-up for shaft capacityof piles in clay”.ASCE Geo-institute Geo-Congress New Orlans,March 9-12,”Honoring john Schmertmann – “From research to practice in Geotechnical Engineering”,ASCE Geotechnical Special Publication ,Edited by J.E.Laier , D.K. Crapps,and M.H. Hussein,GPS180,PP 384-406.

Feizee,S.M. and Fakharian,K.(2008).”Verification of a signal matching analysis of pile driving using a finite difference based continuum numerical method”, International journal of civil engineering .Vol.6,No.3,pp. 174-183.

Geotechnical report on Phase 19 South Pars Offshore Facilities.

Pile dynamic load test report NO.2, South pars gad field development-Phase 19-Offshore Facilities Flare Cause Way Area. Provided by Irsa Bon Saz Alborz.

Analysis of Rain Fall Induced Landslides Using Catastrophe Theory

S Bala Padmaja[1], G V Narasimha Reddy[2], and E Saibaba Reddy[3]

[1]Research Scholar, Department of Civil Engineering, JNTUH College of Engineering, Hyderabad-500085; e-mail: s.balapadmaja@gmail.com
[2]Associate Professor, Department of Civil Engineering, JNTUH College of Engineering, Hyderabad-500085; e-mail: gvnreddy@jntuh.ac.in
[3]Professor & Vice Chancellor, VSS University of Technology, Sambalpur, Odisha-768018
e-mail: esreddy1101@gmail.com

ABSTRACT

Most of the landslides are catastrophic in nature. Rainfall is a major triggering factor of landslides that claim the lives of many and leads to economic loss in a particular region. It will be more appropriate to consider the soil displacement aspect rather than shear strength alone in the analysis of slope stability. In this paper, for the analysis of landslide evolution process, a nonlinear cusp catastrophe theory is used. The condition similar to cusp catastrophe model is been developed by assuming the planar failure slope model, which is composed of different soils with different strengths. The stability of the slope depends on various parameters such as the displacement of soil wedge, the length of soil along failure plane and stiffness ratio of the soil media. The effect of each parameter on stability of the slope is analyzed and found that using this approach the occurrence of landslides can be predicted most effectively.

INTRODUCTION

Landslide due to rainfall during monsoon season is a very common phenomenon. Different conventional methods are in use to analyze the slope stability but the rainfall triggered landslide failure mechanism is remaining as a open issue. The cusp catastrophe theory (Rene Thom, 1972), is applied for a certain catastrophic landslide, which has features like sudden changes, hysteresis and bimodal behavior. The factors that influence stability of a slope and rainfall induced landslides relationships change over time (Polemio M & Petrucci O, 2000). A nonlinear dynamical model, like cusp catastrophe is suggested for such catastrophic failures, which are discontinuous. According to Qin et al. (2001b), it was observed that the behavior of external environmental factors (rainfall, climate, earthquakes etc.) and soil along the slope are complexly nonlinear. Slope stability due to rainfall should be analyzed as a dynamic problem involving environmental factors instead of a static problem as conventional methods (H.Rahardjo et. al 2002). In rock mass stability analysis, the application of catastrophe theory is vastly carried out (Jiang-Teng et al., 2005, Zhang Jixun et al., 2014). Cusp catastrophe model reflects the real situation of a landslide (Yang et al., 2008) when compared to the conventional models. The depth of sliding surface and the time of shallow landslide can be determined approximately by rainfall infiltration models (A S Muntohar et al. 2010).The effect of local precipitation and human activity on intensity of landslides is studied using this theory (Yun Tao et al., 2013) by providing a new approach to predict landslide. Based on the Qin et al. (2001b) governing equations, which describes the evolution of landslides, are used for different types of soils in the present study.

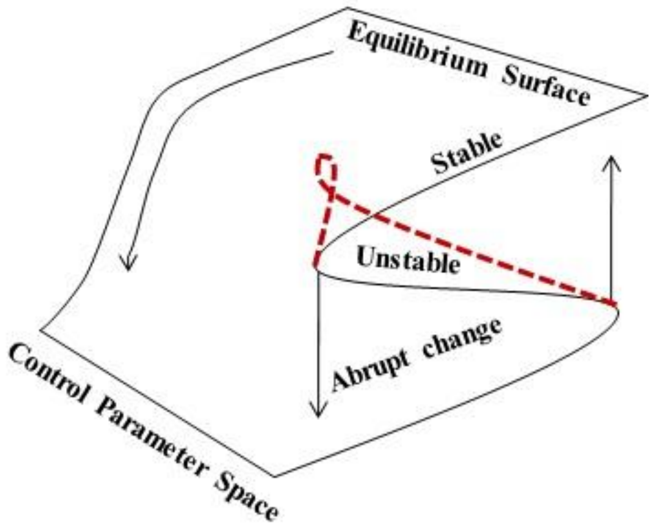

Figure 1. Cusp catastrophe mathematical model

CUSP CATASTROPHE MODEL

According to Qin et al. (2001b, 2006), using cusp catastrophe the condition leading to a landslide can be derived by obtaining overall potential energy for a mechanical model with planar failure plane. Assuming that the planar failure plane is comprised of two different soil media with varying shear strengths such as elasto-brittle and elasto-plastic soils. The overall potential energy can be written as follows

$$P = l_s \int_0^u G_s \frac{u}{h}\, e^{-(\alpha \frac{u}{u_o})} du + \frac{1}{2}\frac{G_e\, l_e}{h} u^2 - mgu \sin\beta$$

where G_{ep} is the initial shear modulus; G_e is the shear modulus; u is displacement; u_o is the displacement value at peak stress (Fig. 3); α is the displacement factor; l_{ep} and l_e are lengths of the sliding surface for the elasto-plastic medium and elasto-brittle medium respectively; h is the thickness of the intercalation, β is the failure slope angle and mg is the weight of the rock mass.

$$x^3 + ax + b = 0$$

The above equation is the standard cusp catastrophe model of the equilibrium surface, with a and b as its control parameters and x is state variable.

$$x = \frac{(u-u_1)}{u_1}, a = \frac{3(k-1)}{2}, b = \frac{3(1+k-k\xi)}{2}, \xi = \frac{mghsin\beta}{G_e l_e u_1}$$

Stiffness ratio is defined as the ratio of stiffness of elastic medium to the stiffness of strain softening medium.

$$\text{Stiffness ratio, } k = \frac{G_e l_e}{G_{ep}\, l_{ep} e^{-(\alpha \frac{u}{u_o})}}$$

Control parameters a and b can be related to human activity and rain precipitation respectively. The catastrophe occurs only when $a \leq 0$ and $b<0$ i.e., for stiffness ratio ($k \leq 1$). Which implies that if $a>0$ then the slope is in a very stable state and catastrophic failure doesn't take place. Stiffness ratio is based on geometry and material property of the system. The condition leading to the catastrophic failure is dependent on the internal characteristics of the slope system. Stiffness ratio, which is also based on the displacement aspect along the failure-sliding plane, describes the stability of the slope.

RESULTS AND DISCUSSIONS

The effect of various parameters such as lengths ratio (l_e/l_{ep}) and displacement factor (α) on k is analyzed. Hence, parametric study has been carried out to know the effect of various parameters on stability of the slope.

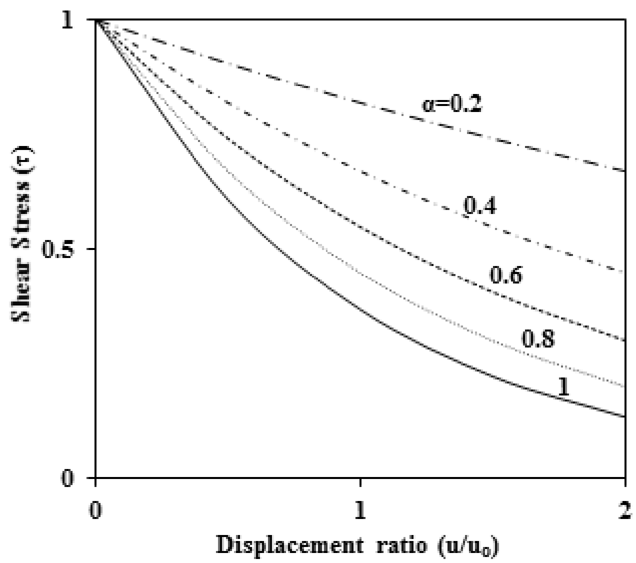

Figure 2. Shear stress (τ) versus Displacement ratio (u/u_o)

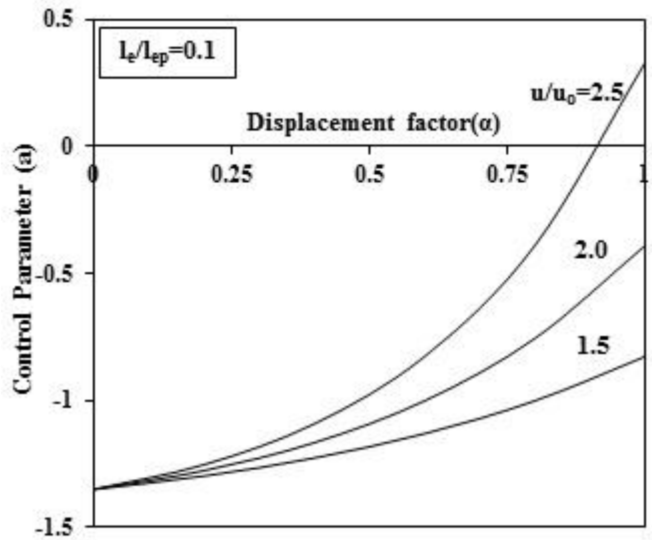

Figure 3. Variation of control parameter (a) with different α values

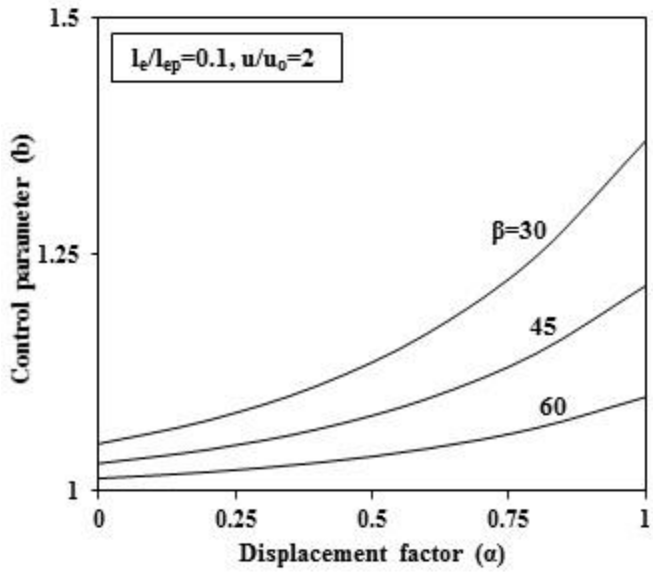

Figure 4. Variation of control parameter (b) with different α values

Fig. 2 shows the variation of shear stress with displacement ratio (u/u_o) with varying displacement factor (α). It is understood that the shear stress decreases nonlinearly with increase in displacement ratio. The shear stress also decreases with increasing α. The displacement factor (α) varies based on the porosity and the moisture content of the soils along the failure-sliding plane. In Fig.3, variation of control parameter (a) with displacement factor (α) for varying displacement ratio (u/u_o) is as shown. Control parameter 'a' increases nonlinearly as the displacement factor (α) increase. The increase in 'a' with increase in u/u_o indicates that the slope is more prone to sliding or failure. The displacement ratio (u/u_o) depends upon the type of soil and nature of its density. If the soil is in loose state, the u/u_o will be relatively more when compared to dense state.

Fig. 4, shows the variation of the control parameter 'b' with displacement factor (α) for varying failure slope angle (β). Control parameter 'b' is increasing with the increase in displacement factor and decreases with in failure slope angle (β). The rainfall-induced landslides are mainly due to the rate of precipitation, which effects the failure slope angle and stiffness ratio. The increase in β value decreases the control parameter 'b' and thus decreases the stability of the slope.

In Fig. 5, shows the variation of stiffness ratio with displacement factor for varying lengths ratio. Stiffness ratio (k) decreases with increase in displacement factor and increase with lengths ratio (l_e/l_{ep}) resulting in stable slopes. The lengths ratio may vary due to the intensity of rainfall, degree of saturation and permeability of soil along the failure-sliding plane.

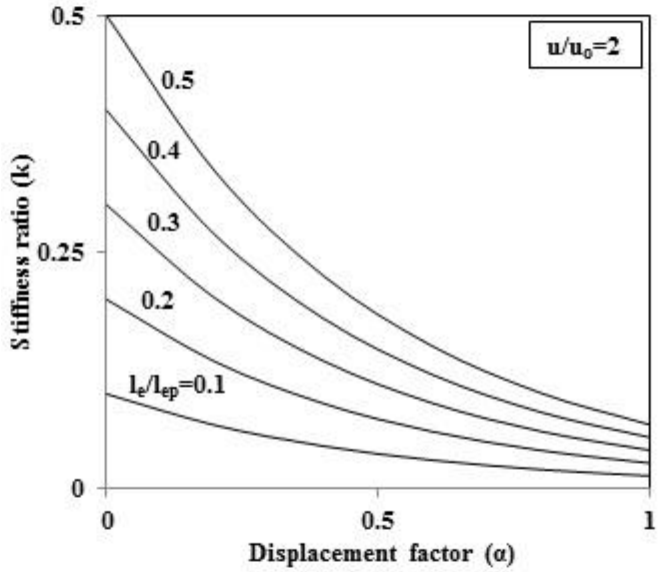

Figure 5. Stiffness ratio with respect to displacement factor for varying lengths ratio

CONCLUSION

- It is observed that, the displacement criterion is more relevant to field conditions to determine the instability mechanism of the planar sliding slope.
- The shear stress varies linearly with u/u_o upto, α= 0.2 and with increase in α it increases nonlinearly.
- The increase in control parameter 'a' increases the displacement ratio, u/u_o from 1.5 to 2.5 which results in unstable slopes.
- The control parameter 'b' effects the displacement factor (α) nonlinearly with decreasing failure slope angle (β).
- The stiffness ratio increases with increase in l_e/l_{ep} ratio (0.1 to 0.5) and displacement factor (α- 0.1 to 1)). As stiffness ratio is increasing, the stability of slope structure also increases gradually.

REFERENCES

Chau, K.T., 1995. Landslides modeled as bifurcations of creeping slope with nonlinear friction law. International Journal of Solids Structures. 32 (23), 3451-3464.

H.Rahardjo ., E.C Leong & R.B. Rezaur. Studies of rainfall induced slope failures. Proceedings of the National Seminar, Slope 2002, Indonesia. 15-29.

Jiang-Teng., Ping, CAO. 2005. Cusp catastrophe model of instability of pillar in asymmetric mining. Applied mathematics and mechanics, vol. 26, No. 28, August 2005. ISSN 0253-4827.

Lan, L., 1993 A general limit equilibrium model for three dimensional slope stability analysis. Canadian Geotechnical Journal.30, 905-919.

Qin, S.Q., 1999. A theory on instability of planar sliding slope –Stiffness effect instability theory. Slope stability engineering, Yagi, Rotterdam, ISBN9058090795, 207-211.

Qin, S.Q., Jiao, J.J., Wang, S.J., 2000. The predictable time scale of landslide. Bulletin of Engineering Geology and the Environment, in Traffic University Press, Chengdu, 307-312.

Qin, S.Q., Jiao, J.J., Wang, S.J., 2001a. A cusp catastrophe model of instability of slip buckling slope. Rock Mechanics and Rock Engineering 34, 119–134.

Qin, S.Q., Jiao, J.J., Wang, S.J., Long, H., 2001b. A nonlinear catastrophe model of instability of planar-slip slope and chaotic dynamical mechanisms of its evolutionary process. International Journal of Solids and Structures 38, 8093–8109.

Robert Gilmore, 1993. Catastrophe Theory for Scientists and Engineers, Dover Publications Inc., New York.

Yang, K., Shi, C., Wang, J.F, 2008. Applying catastrophe theory to slope reliability analysis. Boundaries of Rock Mechanics, Taylor & Francis, London, ISBN 978-0-415-46934-0

Yun Tao, Jie Cao, Jinming Hu, Zhicheng Dai, 2013. A cusp catastrophe model of mid long term landslide evolution over low latitude highlands of China. Journal of Geomorphology 187 (2013) 80-85.

Zhang Jixun, Shu Jiaqing, Zhang Haibo, Ren Xuhua, and Qi Jiang, 2014. Study on Rock Mass Stability Criterion Based on Catastrophe Theory. Hindawi, Volume 2015, Article ID 850604, 7 pages http://dx.doi.org/10.1155/2015/850604

Investigation on Causes of Failure and Design of Remedial Measures of Pile Foundation Supporting Transmission Line Tower.

Manojit Samanta[1], Ajay Dwivedi[2], Piyush Mohanty[3], Anindya Pain[4] & Mahesh Sharma[5]

[1]CSIR-CBRI, Roorkee -247667, Uttrakhand, e-mail: manojit_samanta@rediffmail.com
[2]CSIR-CBRI, Roorkee -247667, Uttrakhand, e-mail: ajaydwivedi@gmail.com
[3]CSIR-CBRI, Roorkee -247667, Uttrakhand, e-mail: pyushmohanty@gmail.com
[4]CSIR-CBRI, Roorkee -247667, Uttrakhand, e-mail: pain_anindya@yahoo.co.in
[5]CSIR-CBRI, Roorkee -247667, Uttrakhand, e-mail: mahesh3.ce@gmail.com

ABSTRACT

The deficiencies in cast in-situ pile are detrimental for long term satisfactory performance of the foundation. The general deficiency found in these piles are reduction in area, discontinuity in pile length, shorter length of pile, quality of concrete and reinforcement. The cast in-situ pile foundation are invariably used as foundation system of power transmission lines towers. One such transmission line was investigated between Mahilpur-Jamsher in Punjab, consist of 143 number of towers, among which 56 number of towers are supported by bored cast in-situ underream pile under each leg. These pile have following design parameters: diameter 400 mm, length 3800 mm, depth 3500 mm from the top and diameter of the underream 2.5 times the shaft diameter. One such tower of this transmission line was uprooted along with the pile foundation. Present study investigates the probable reason (s) of failure of pile foundation through the low strain integrity test. A total of 224 numbers of piles were tested and 34 % of piles were found to be defective. Remedial measures in the form of additional piles were suggested for defective pile (s) based on the pile integrity test results, subsoil profile of the site and the load carrying capacity of the foundation system.

INTRODUCTION

The use of cast-in-situ/bored piles in sub-structure have always been a great concern for geotechnical engineers. Due to deficiencies in quality of concrete and as-built length for new as well as in-service piles, their use as foundation system below the transmission line tower have always been apprehensive. For satisfactory long tern performance of this piles foundation, their geometry and parameters conceived during design should be ensured during construction stage. For quality assessment of the in-service piles, low strain integrity tests are used successfully. The integrity test of existing or in-service piles helps in ensuring the length, discontinuity in geometry of pile (necking, cracking and void) and quality assessment of concrete (Ni et al. 2006 & 2008). The advantages and disadvantages of different nondestructive testing method for piles and their application in field problems for determining the defects and exact length of the piles were carried out by Paikowsky and Chernauskas (2003). Prakash et al. (2003) applied low strain pile integrity test to determine the quality of concrete, shape and length of existing in-service pile below transmission line tower.

A failure in foundation system of Mahilpur-Jamsher transmission line in Punjab was occurred in the year of 2013. One of the towers of this line was uprooted in storm, causing total disruption of power supply of Punjab (Figure 1). The transmission line is about 47 km in length and consists of 143 numbers of towers. The design and drawings of the transmission tower foundation suggested that it is supported by underream piles as well isolated footing system. The transmission line was commissioned in the year of 1994-95. The objective of the project was to investigate the cause (s) of the failure and a suggestion of strengthening/remedial measure to the existing in-service pile foundation. Low strain pile integrity test was carried out to assess the existing conditions and as-built length of the existing piles. The present study discusses the use of the pile integrity test for ascertaining the deficiencies in the piles and strengthening/remedial measures for in-service pile at present conditions.

Figure 1. Uprooted pile foundation with tower

Sub-Soil Condition

The Mahilpur-Jamsher transmission line was commissioned more than 22 years back, the details related to sub-soil investigation carried out at the time of commissioning was not available. In general, this line passes through the cultivated agriculture land in most places. To establish the sub-soil strata of the stretch, geotechnical investigation was carried out at 14 different locations where change in sub-strata was noticed. The investigation work includes drilling of 14 nos. borehole upto 9 m depth and laboratory investigations on disturbed and undisturbed samples. Also, Standard Penetration Test (SPT) were carried out in the boreholes as per IS 2131 (1981). Investigation revealed, the sub soil strata predominantly of silt/ silty sand in top few meters followed by sandy strata. At other locations, the silty sand strata started from the top itself. The laboratory investigations carried out on the UDS and DS samples collected during drilling of borehole reveals that the sub-soil strata are similar in general and consist of predominantly coarse silt/ silty sand /poorly graded sand layers. The observed standard penetration value ‘N’ varies in the range of 4 to15 for a depth of 9 m. The observed N values indicate strata of low compactness. In general, the water table was found to be at a depth of 1.5 m- 4.5 m below NGL. Figure 2 shows the typical borelog with SPT ‘N’ value. These soil properties were used to estimate the capacity of the existing piles.

Depth (m) B.L.	Type of Soil	Bore Hole Log	L.L. %	P.I. %	Bulk Density (kN/m³)	W %	Grain Size Distribution % Grav.	% Sand	% Silt	% Clay	C (kN/m²)	Ø	Cc	e	'N' Value	Graphical Representation of 'N'
1.5	Silt (ML)		25	03	15.91	2.71	-	10	90	-	4.5	25°	0.10	0.73	04	
3.0															04	
3.4	Silt (ML)		26	04	16.43	3.79	-	08	92	-	5.0	24°	0.11	0.70		
4.5															04	
6.0	Silt (ML)		26	04	16.98	4.38	-	08	92	-	5.0	24°	0.11	0.67	10	
7.5															12	
9.0															14	

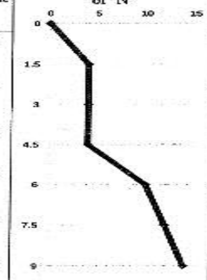

Figure 2. Typical borelog with SPT values

Design Details

Each transmission line tower consists of four leg. Under each leg, one 400 mm in diameter and 3500 mm in length (below NGL), single under reamed pile was provided. Overall length of the pile is 3800 mm and bulb is at a depth of 3500 mm from top of the pile with diameter to pile shaft ratio of 2.5. M15 grade of concrete was used in the piles. The main reinforcement consists of 3-16 mm and 3-20 mm tor steel bars and rings of 6 mm diameter M.S. bars are provided @ 250 mm c/c.

FIELD INVESTIGATIONS

Visual inspection of individual transmission tower foundation was carried out before the low strain integrity test for examining the present conditions and simultaneously, the diameter of the piles with surrounding conditions were also recorded (Figure3). The visual inspection of the physical conditions were then used to decide the stress wave velocity of the pile foundation.

Figure 3. Present condition of the in-service piles

Field procedure

The low strain integrity tests have been conducted on the pile heads (about 300 mm above NGL) under each individual leg of all the towers. Each pile head was cleaned of any earth, loose particles of concrete and dust. The integrity test was conducted by striking the pile head with a small manual hammer in the axial direction. The wave response consisting of reflections from the locations in variation of pile section such as increase or decrease in the cross-section, cracks, necking or inclusion from the pile toe are picked up by an accelerometer placed on pile head close to the hammer blow. At each pile, at least a set of 3 signals were taken to obtain repetitive and good representative signals. Impact of hammer blow was given at two to three locations on pile head to assess the overall condition. To arrive at the most appropriate stress wave velocity and corresponding lengths for proper assessment of structural condition of piles, the maximum stress wave velocity has been taken as 3600 m/s considering grade of concrete, its method of mixing along with its placement and aging. The lower limit for the same was considered as 2400 m/s. These records are stored on the computer for subsequent processing and analysis.

Figure 4. Pile integrity test in progress

RESULT OF INTEGRITY TESTS

Structural condition assessment of piles

Close examination of the failed piles reveals that the pile have improper bulb formation and shorter as-built length than design one. The integrity test results obtained in the field were post-processed subsequently, keeping in mind the observations made during field tests such as soil data, construction of piles and other common features associated with these type of piles. Other features such as projection of pile 300 mm above NGL, variation in soil strata due to cultivation and bracings joints with piles at about 600 mm below the pile top etc. were also considered in final assessment of structural condition of piles. More weightage in the final assessment was given to the shape and length of pile rather than the variations in stress wave velocity which is indicative of average concrete strength over the entire length of pile. This helps in creation of six scale category for the assessed piles vis-à-vis; 'Good', 'Satisfactory', 'Fair', 'Fairly Poor' 'Poor' and 'Very Poor' which are discussed below:

Good - The piles whose signals showed local variations in the sections or reflection of any common features resulting due to sub-soil variations and the other features as mentioned above with proper bulb formation as well as length more than or equal to 3.6 m from test level as shown in Figure 5.

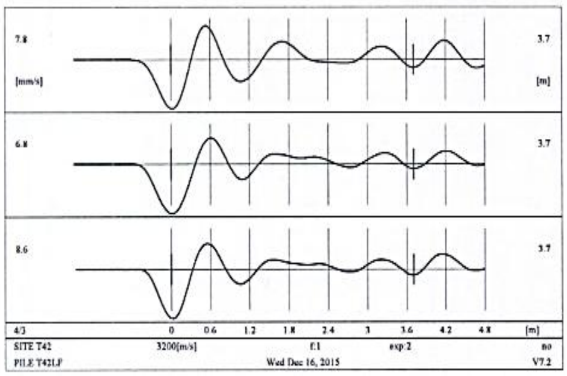

Figure 5. Reflectogram considered as good

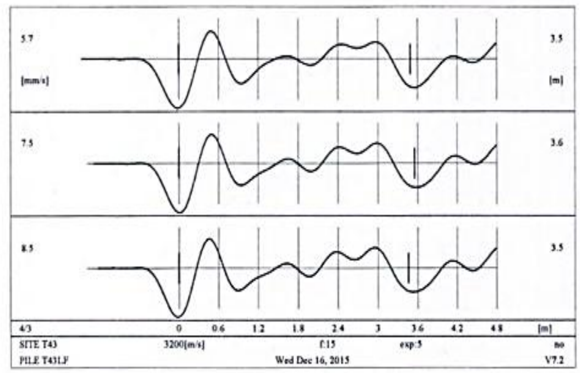

Figure 6. Reflectogram considered as satisfactory

Satisfactory - The piles whose signal showed minor variations in section, increase/enlargement in section above the designed bulb formation level with bulb formation fairly clear and length in between 3.4 m - 3.5 m from the test level as shown in Figure 6. In these cases also, it is expected that the performance of pile shall not be affcted under load.

Fair – The pile whose signal reveals length in between 3.2 m to 3.4 m from test level with reflections of bulb formation fairly clear; irregular/variations (enlargements) in sections as shown in Figure 7. In these cases also, it is expected that the performance of pile shall be affcted marginally (10% to 15%) under load.

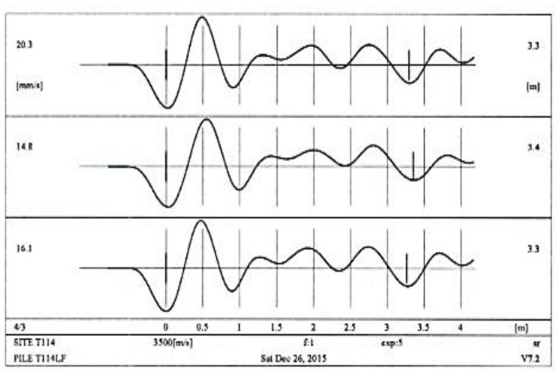

Figure 7. Reflectogram considered as poor

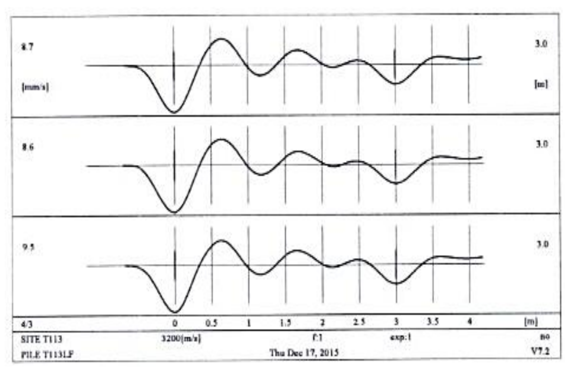

Figure 8. Reflectogram considered as fairly poor

Fairly Poor – The piles whose signal reveals length in the range of 3.1 m - 3.2 m form test level with reflections of bulb formations not very clear, irregular variations in sections as shown in Figure 8. In these cases, it is expected that the performance of the pile shall be affected under loads.

Poor – The piles whoose signal reveals length less than 3.0 m with no clear reflection of bulb formations, only minor incraese in sections at bulb locations, variations in sections as shown in

Figure 9. In these cases, it is expected that the performance of the piles shall considerably affected under load.

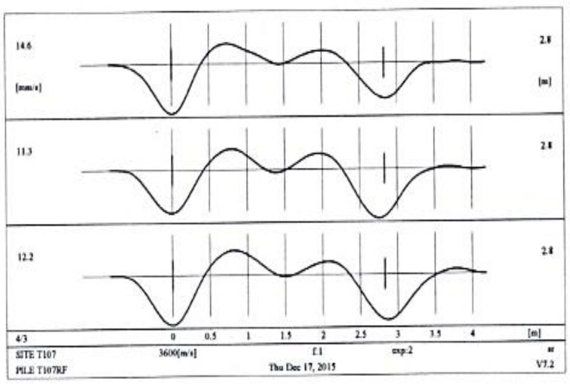

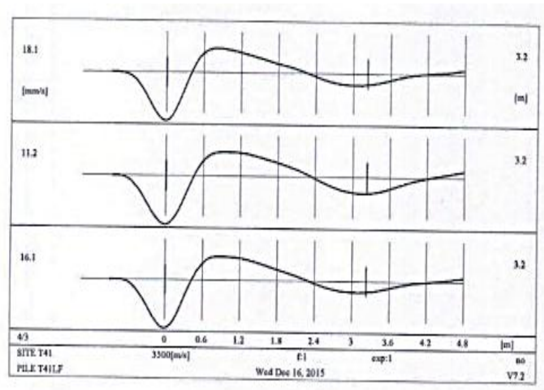

Figure 9. Reflectogram considered as poor Figure 10. Reflectogram considered as very poor

Very Poor – The piles whoose signal reveals significantly less than the designed length with no reflection of bulb formation, defective shaft, almost no increase in section as shown in Fig.10. In this case, it is expected that the performance of piles are greatly affected under loads.

Statistics of stress wave velocity & structural conditions of pile

The statistics of structural condition (Figure 11) of piles show that the out of 224 numbers of underreamed pile tested 15 piles (7%), 57 piles (25%), 75 piles (34%), 50 piles (22%), 9 piles (4%) and 18 piles (8%) fall under the category of Good, Satisfactory, Fairly Poor, Poor and Very Poor respectively.

The statistics of stress wave variation (Figure 11) reveals that out of 224 underream pile tested, 18 piles (8%) with the stress wave velocity 2400 -2800 m/s shows the quality of the concrete is poor to fair; 94 piles (42%) with the stress wave velocity 2800 -3200 m/s show the quality of the concrete is satisfactory; 142 piles (63 %) with the stress wave velocity 3200-3600 m/s shows concrete is of good quality.

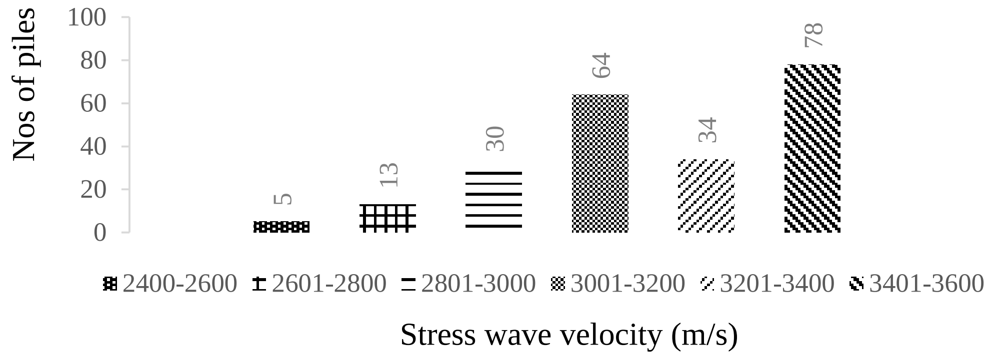

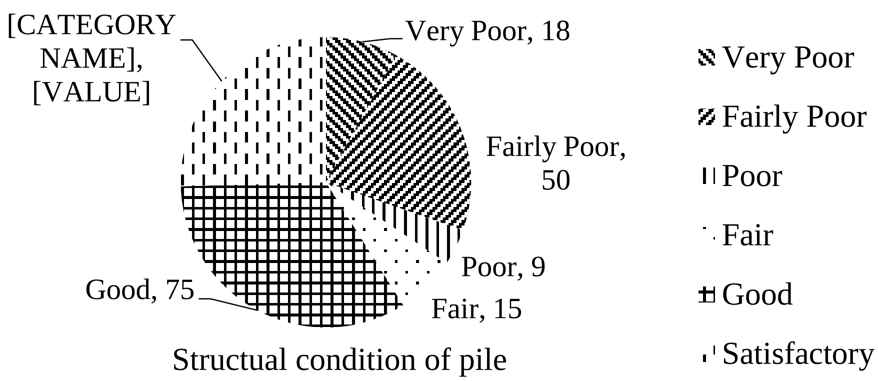

Figure 11. Stress wave velocity & structual condition of underream pile below existing tower

Capacity of piles in existing condition

The design of piles under the tower is mainly governed by the uplift (pullout) loads. Hence, the pile capacity have been asseseed under uplift condition and then checked against vertical and lateral load. In view of the difficulties in assessing capcity of each individual pile considering the actual variations in shape as observed, the capacities have been assessed with the following variations in pile shape and length for the piles corresponding to various catergories of strcutural conditions as already described above. The shaft daimeter (D) is taken as 400 mm while diameter of bulb was taken as 2.5D (100%), 2.125D (75%), 1.75D (50%), 1.375D (25%) & 1D (0%) respectively.The length of piles were taken as 3.5 m, 3.0 m & 2.5 m for the various categories of piles in Good to Very Poor conditions. The results show that the piles falling in the group 'Fairly Poor' 'Poor' and 'Very Poor' requires 40%, 58% and 78% capacity augementation in existing condition to support the towers.

REMEDIAL MEASURES SUGGESTED

The remedial measures to be provided for the piles falling under the structural condition categories,'Fairly Poor', 'Poor', and 'Very Poor' to achieve the additional capacities. The details of remedial measures using additional piles suggested is presented below in Figure 12.

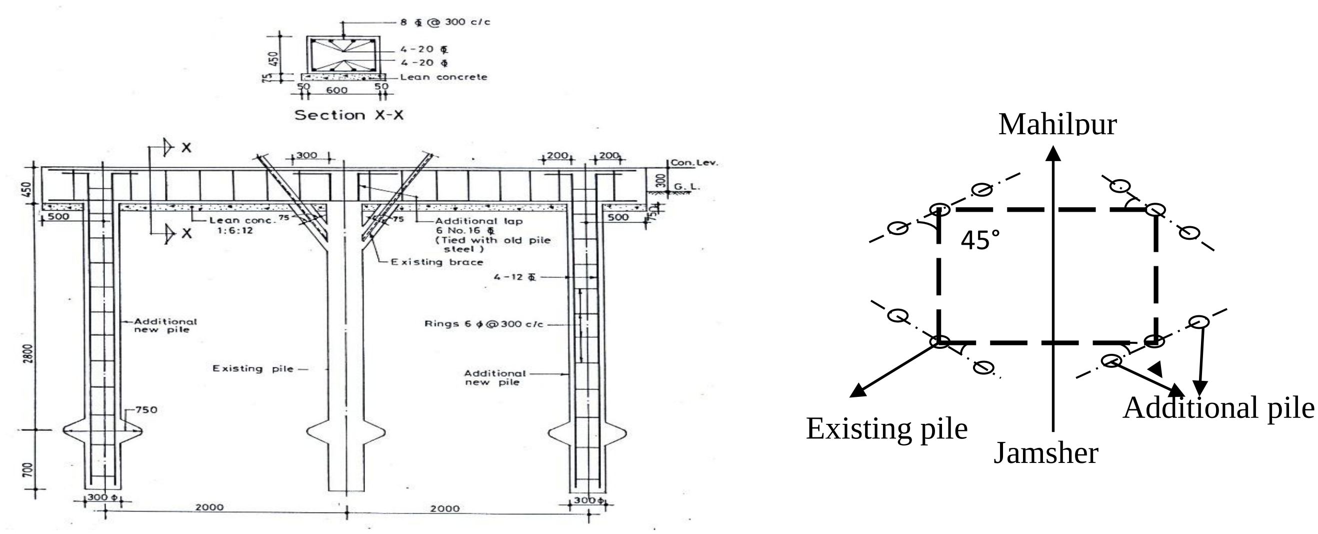

Figure 12. Remedial measures for strengthening foundation system under existing tower

CONCLUSIONS

Low strain pile integrity test was carried out to investigate the present condition of the in-service piles. The as built length and geometry of the underream pile foundation supporting transmission line tower can be estimated through the integrity test. Variation in section along the length of the pile with improper bulb formation can be predicted by pile integrity testing. For the present case study, among 224 number of piles tested, 34% piles needs capacity augmentation in the present condition to support the tansmission line tower. Installation of additional piles with due care ensuring the length and geometry will strengthen the existing piles in present conditons and will ensure the long term satisfactory performance of the tower foundations.

REFERENCES

Chandra Prakash, Rastogi, P.C., and Sharma, A.K. (2003) ‘Assessment of shape and quality of bored concrete piles by integrity testing’ Indian Geotechnical Journal Vol 23 (2).

Indian Standard 14893 (2001) ‘Non-destructive integrity testing of piles (NDT) -Guidelines’

Paikowsky, S. G., and Chernauskas, L. R., (2003) ‘Review of deep foundations integrity testing techniques and case histories’ BSCES-Geo-Institute Deep Foundation Seminar, P30

Ni, S.H., Lehmann, L., Charng, J.J., and Lo, K.F. 2006. Low-strain integrity testing of drilled pileswith high slenderness ratio. Computers and Geotechnics, 33(6–7): 283–93.

Ni, S.H., Lo, K.F., Lehmann, L., and Huang, Y.H. 2008. Time–frequency analyses of pile-integrity testing using wavelet transform. Computers and Geotechnics, 35(4): 600–607.

Analysis of Ground Distress Along a Busy Highway – A Case Study from Mumbai, India

Dasaka Murty[1], Vidyadhar Vengurlekar[2], Dharamveer Singh[3] and Salil Upasham[4]

[1]Associate Professor, Department of Civil Engineering, IIT Bombay, Mumbai, INDIA Email: dasaka@civil.iitb.ac.in

[2]Principal Engineer, NJS Engineers India Pvt. Ltd., Mumbai, INDIA Email: vidveng@icloud.com

[3]Assistant Professor, Department of Civil Engineering, IIT Bombay, Mumbai, INDIA Email: dvsingh@civil.iitb.ac.in

[4]Chief Engineer, Sewage Project, Brihanmumbai Municipal Corporation, Mumbai, INDIA Email: dychespnpd@gmail.com

Abstract

Ground heaving is one of the major causes of damages to highways and other roads, leading to loss of human life and economic losses. Chembur-Sewri highway is one of the busiest roads in Mumbai, adjoining the Wadala Truck Terminal, and constructed on a reclaimed land. Part of the Phase I of Mumbai's elevated Monorail, first of its kind in independent India, runs along this highway. Construction of monorail project was started in 2009, and is made open to public in 2014. Substantial ground heaving/settlement has been observed over a distance of 6 km along this highway, noticeably adjacent to the supporting pillars of the monorail, after its construction. This highway is made of concrete pavement, and ground distress is observed to increase with time, posing serious threat to the public safety. The ground water table is very close to the ground surface, and soil profiles in the close vicinity exhibit very low SPT 'N' values. A strip of 1 m width on either side of the pillar along the highway is highly disturbed and poses serious threat to the users. The aim of the present study is understanding the causes of ground distress, through systematic study of the ground profiles, and geotechnical properties of the subsoil. Based on the present analysis, it can be concluded that the consolidation of thick soft to medium stiff clay layer is mainly responsible for the differential settlement of the pavement. Keeping in mind the subsoil and traffic conditions on this stretch of the highway, a hybrid ground improvement strategy, involving installation of stone columns penetrating through the clay layers, overlying a well-designed in-filled geocell reinforced soil layer, can be adopted at the site, which can prevent further settlement of the pavement.

Introduction

Substantial volume change resulting in ground heaving or ground subsidence is one of the major causes of damages to highways and other roads, leading to poor ride quality, frequent disruptions to traffic, traffic diversions, economic losses, and loss of life (Chen et al. 2009, Chen et al. 2012,. Chembur-Sewri 6-lane highway is one of the busiest roads in Mumbai, adjoining the Wadala Truck Terminal, and constructed on a reclaimed land. Part of the Phase I of Mumbai's elevated Monorail, first of its kind in independent India, runs along this highway. Construction of monorail project was started in 2009, and is made open to public in 2014. This highway is made of concrete pavement. Substantial ground distress, in the form of differential settlement of the pavement, has been observed over a distance of 6 km along this highway, noticeably around each pillar of the monorail, after its construction, as shown in Figure 1. It is reported that this distress was smaller in magnitude initially and has been increasing with time, posing serious threat to the public safety, as several accidents have been reported in the last couple of years. Figure 1 also shows severe cracking of the pavement in addition to large differential settlement at several locations of the highway. To date, the monorail system is not affected by this uncontrolled volume changes, and a hazard may not be ruled out in near future, if the reasons for this distress is not understood properly and controlled forever. Such failure can be averted if through and systematic study of the ground profiles, geotechnical properties of the subsoil is done before planning and construction of any major structures. From the observed ground features, one of the following two causes for the ground distress can be thought of. They are (i) continuous settlement of the pavement due to consolidation of clay deposit, except in the zone surrounding each monorail pillar, which is supported by a strong piled raft foundation; and (ii) pavement distress due to ground heaving around each monorail pillar, probably due to buoyancy effect. If the second possibility is true, it should also be reflected in the upheaval (uplift) of the monorail pillar.

Figure 1: Pavement distress along Wadala-Sewri highway

History of the study area and details of subsoil

The typical soil profile along the highway stretch consists of 0-3 m of fill material underlain by soft marine clay deposits of soft to medium stiff consistency extended up to 11 m below the existing ground surface, followed by basalt rock of varying degrees of weathering. The typical borehole profile at the site is shown in Figure 2. There is a high degree of variability in the soil profiles and estimated geotechnical properties all-over the study area. The SPT-N values of the marine clay deposit vary in the range of 1-5 m, whereas for the top 3 m layer, SPT-N values vary in the range of 6-15 m. The particle size distribution analysis reveals that 86-97% clay content in the clay layer, whereas 66-90% of the fill material is coarse grained soil, predominantly of sand. The liquid and plastic limits of the clay layer typically vary in the range of 63-88% and 30-35%, with plasticity index in the range of 30-53%. The data on organic content and swelling characteristics of the marine clay deposit is not available. Part of this area is covered with salt pans and frequently inundated with sea water during the high-tides. The ground water table is very high and at times reaches very close to ground surface, especially during the monsoon. Based on the data collected from reliable sources, there is no history of ground improvement adopted at this site.

Co-ordinate: 19.029072°N 72.877532°E
R.L.: 100
Location: Chembur-Sewri Road
Dia of Borehole: 100/Nx
Depth of GWT: 1.0m

Bore Hole No: BH 1
Depth of Bore Hole: 24.0 m
Depth of Casing: 15.50
Date of Commencement: 20/08/2010
Date of Completion: 26/08/2010

Scale m	Depth m	R.L. m	Log	Description	Sample No.	Type	Depth (m) From	Depth (m) To	SPT 'N' Value 15	15	15	15	N	CR %	RQD %	P.R. m/hr	Remarks/ Other Tests
1				Fill up Soil (GM-GC)													
2																	GWT
3					1	SPT-1	2.0	2.30	9	20			R				
					2	SPT-2	3.0	3.38	10	13	8/ 27		R				
4	4.0	96.0		[4 m]													
5				Grey Soil Marine Clay (CH)	4	SPT-3	4.0	4.60	2	2	3	3	5				
6					5	SPT-4	5.0	5.60	2	2	3	4	5				
					9	UDS	6.0	6.60									
7	7.0	93.0		[3 m]													
8				Grey Medium Stiff to Stiff Marine Clay (CH)	6	SPT-5	7.0	7.60	2	3	3	4	6				
					7	SPT-6	8.0	8.60	3	3	3	7	6				
9					8	SPT-7	9.0	9.60	4	3	4	6	7				
10.5	10.6	89.4		[3.6 m]	9	SPT-8	10.0	10.6	4	4	4	6	8				
11				Completely Weathered Rock		DR1	11.0	11.5						14	Nil		Small Pieces
						DR2	11.5	12.0						Nil	Nil		Small Pieces
12						DR3	12.0	12.5						Nil	Nil		Small Pieces
						DR4	12.5	13.0						Nil	Nil		Small Pieces
13						DR5	13.0	13.5						Nil	Nil		Small Pieces
						DR6	13.5	14.0						Nil	Nil		Small Pieces
14						DR7	14.0	14.5						Nil	Nil		Small Pieces
						DR8	14.5	15.0						Nil	Nil		Small Pieces
15	15.0	85.0		[4.4 m]		DR9	15.0	15.5						Nil	Nil		Small Pieces

DS: Disturbed sample
USD: Undisturbed sample
SPT: Standard Penetration Test
WS: Wash Sample
CR: Core Recovery
RQD: Rock Quality Designation
PR: Rate of Penetration in Rock
VST: Vane Shear Test
K: Permeability of Soil/Rock
PT: Packer Permeability tests
DR: Drill Run
GWT: Ground Water Table

Figure 2. Typical borelog profile at the affected site (MCGM, 2015)

Forensic investigation of pavement distress

From the limited information available, the pillars of monorail are supported by piled raft foundations, wherein each pile was extended below 16 m and terminated in weathered rock strata. In view of the possible normally consolidated state of the clay, and no visible signs of upheaval of the monorail pillars, it can be safely concluded that the distress in the pavement is, in fact, due to the consolidation of the clay and subsequent settlement of the pavement, except around the monorail pillars, which is firmly supported.

Remedial measures

In order to prevent further settlements of the subgrade due to consolidation of the soft marine clay deposit, the ground should be substantially improved. Pre-consolidation of the clay deposit is a simple and effective method, and can be achieved by using prefabricated vertical drains with surcharge preloading. However, after installation of the PVD and placing the required surcharge, the ground should be left unattended for a minimum period of 3-6 months to achieve majority of the consolidation. However, owing to heavy and continuous vehicular traffic on the highway, being only access to some of the important establishments, such as Wadala truck terminal, Wadala RTO, and remote possibility of closing the highway even for a small duration, the conventional ground improvement techniques, such as surcharge preloading, sand columns, PVD assisted consolidation, vacuum consolidation, to accelerate the consolidation of the clay layer, may not be suitable at this site. Instead, one of the following alternative ground improvement strategies can be adopted at the site: (i) installation of stone columns extending into the poor subsoil, which can improve the load carrying capacity of the soft soil layer, and subsequently reduce the settlement due to working loads; (ii) placing in-filled geocell layer in base course or above the subgrade of the pavement, which can distribute the traffic loading on a wider area, and significantly reduce the intensity of vertical stresses transferred to the clay layer; (iii) compaction grouting extending into the poor subsoil; or (iv) a combination of stone columns underlying a reinforced in-filled geocell layer. In case of stone columns, a substantial loading needs to be applied on the stone columns and the surrounding area, in the form of embankment loading, in order to allow the stone columns to bulge and mobilize maximum passive resistance from the surrounding soft soil. Placing an additional fill of minimum 1-2 m over the stone columns to enhance the load carrying capacity of the reinforced ground, and substantially reduce the settlements under working loads, may not be possible in this project, and on the other hand increasing the replacement ratio of the stone columns, the control the settlements of the soft soil, proves very costly. In view of the above limitation, the more amenable alternative to improve the ground is to place a well-designed geocell reinforced soil layer overlying the stone columns. The geocell reinforced soil layer acts as a reinforcement layer, and dissipates the traffic loads on a wider area, and prevent overstressing of the soft clay layer. This hybrid reinforcing technique, involving both stone columns and geocell reinforced soil bed, can be effective in controlling the settlement of the pavement, and may prove economical. However, further studies are warranted to critically examine the geotechnical properties of the clay layer, and optimize the ground improvement strategy, in terms of choosing the spacing and depth of the stone columns, and type and thickness of the geocell reinforced soil bed overlying the stone columns.

Conclusions

Pavement distress due to substantial volume changes of the subsoil is one of the major causes of damages to highways and other roads. In the present study a forensic study has been carried out to identify the likely causes of distress to a 6 km highway stretch in Mumbai, India, and understand the most viable ground improvement strategy to prevent further settlement of the pavement. The following are some of the major conclusions from the study.

Consolidation of thick soft to medium stiff clay layer is mainly responsible for the differential settlement of the pavement.

Conventional ground improvement techniques, such as surcharge induced preloading, sand columns or PVD assisted preloading is not feasible to preconsolidate the soft clay layer in the present study, mainly due to heavy and continuous traffic at the affected area.

A hybrid ground improvement strategy, involving installation of stone columns penetrating through the clay layers, overlying a well-designed in-filled geocell reinforced soil layer, can be a viable option for the site, which can prevent further settlement of the pavement.

References

Chen, D-H, Si, Z., Saribudak, M. (2009). Roadway heaving caused by high organic matter, Journal of Performance of Constructed Facilities, ASCE, Vol.23(2), pp. 100-108.

Chen, D-H, Scullion, T., Hong, F., and Lee, J. (2012). Pavement swelling and heaving at state highway 6, Journal of Performance of Constructed Facilities, ASCE, Vol.26(3), pp. 335-344.

MCGM (2015). Detailed design report: Design of Sewerage System for F/North & M/West Wards, NJS Engineers India Ltd., India, submitted to the Municipal Corporation of Greater Mumbai.

NUMERICAL INVESTIGATION OF A FULL SCALE REINFORCED SOIL WALL – A CASE STUDY

Pavan Kumar. P.V,[1] Shantanu Patra,[2] and Vikrant Patel[3]

[1] Postgraduate Student, Department of Civil Engineering, NIT Rourkela, Rourkela, 769008, India, e-mail: pvpavan416@gmail.com
[2] Assistant Professor, Department of Civil Engineering, NIT Rourkela, Rourkela, 769008, India, e-mail: patrashantanu@nitrkl.ac.in
[3] Postgraduate Student, Department of Civil Engineering, NIT Rourkela, Rourkela, 769008, India, e-mail: vikrant.patel89@gmail.com

ABSTRACT

Reinforced soil walls (RSW) are gaining popularity as sustainable and cost effective alternatives to the concrete and masonry earth retaining structures. Limit equilibrium methods are usually used in checking the stability of these walls for its simplicity but most of these methods are empirical in nature and do not consider proper soil reinforcement interaction. Numerical analysis may offer as a useful tool in the design of reinforced soil walls however, it is still not widespread because of lack of guidance and proper training. In this paper, a case study has been considered in which a full scale soil wall is constructed and they are loaded to stress levels well beyond the working condition. A numerical analysis has been carried out using a commercially available software PLAXIS 2D to study the performance of a full scale wall at different construction stages and at the end of the construction. The backfill soil was modeled by Mohr-Coulomb constitutive relationship and the reinforcement as a tension member. The maximum reinforcement tensions at each level and the displacement of the wall facing were computed and the results are compared with the measured values. The present analysis shows a good matching with the measured values and helps to infuse confidence to the practitioner.

INTRODUCTION

For the production of cost effective reinforced soil walls, the prediction of loads and their distribution in reinforcement are necessary. This affects the strength, spacing of the reinforcement and the reinforcement length required to resists the pullout. The reinforcement loads are developed due to the active earth pressure state in the soil mass which is calculate using the peak friction angle of the soil (AASHTO 2002). Based on the reinforcement spacing this active earth pressure is distributed to reinforcement layers. Empirical methods are available to calculate the reinforcement loads (Allen et al. 2003). The reinforced soil wall mentioned here is constructed in Royal Military College of Canada (RMC) retaining wall test facility. A total of 11 full-scale walls has been constructed which are of a 3.6m height and with the same backfill material. Out of these 11 walls, 2 are considered for this paper and analyzed using a commercially available software PLAXIS 2D. The difference between these two walls is the reinforcement type, the 1st wall is built with polypropylene geogrid and the 2nd wall is built with Modified geogrid where the reinforcement stiffness is lesser.

It has been reported from Bathurst et al. (2006, 2007) that the walls which are having stiff modular block facing shows fewer deformations and reinforcement load levels compare to the walls with flexibly wrapped face construction, reported that the facing column acted as a structural member to carry earth loads.

Hatami and Bathurst (2006) investigated the segmental retaining wall using FLAC numerical model. In this study, the influence of compaction and reinforcement type on the end of construction and the surcharge loading response is reported.

The geosynthetic reinforcement loads for walls with the cohesionless backfill soils were almost three times lower than values predicted using the AASHTO (2002) simplified method. In addition, the reinforcement loads are uniform with the depth predicted Bathurst et al. (2008).

FINITE ELEMENT MODEL (PLAXIS 2D)

Plaxis 2D is a special purpose two-dimensional finite element computer program used to perform deformation and stability analyses for various types of geotechnical applications. Real situations may be modelled by either a plane strain or an axisymmetric model. The wall considered here is modelled by assuming a plane strain condition.

The model is a 15 noded triangular element which provides an accurate calculation of stresses and the failure loads. The 15-node triangle provides a fourth order interpolation for displacements and the numerical integration involves Gauss points (stress points).. During the finite element calculation, displacements are calculated at the nodes and the stresses and strains are calculated at individual Gaussian integration points (stress points).

The wall is fixed horizontally along the right vertical border, fixed horizontally and vertically at the bottom of concrete foundation. Avery fine mesh was used for the wall model, which divides the whole system into triangular elements, while calculation.

CONFIGURATION OF THE WALL

The two walls considered in this paper are full-scale modular block walls constructed in the RMC test facility. The walls are of a 3.6m height and reinforced with polypropylene geogrid reinforcement. Wall 1 and wall 2 are nominally identical walls. Figure 1 shows the geometry of the wall having six layers of geogrid reinforcement with a spacing of (S_v) 0.6m and the batter angle (inclination of the wall with respect to vertical) is 8^0. The geogrid is having a length of 2.52m measured from the front of the facing column. The facing blocks are solid masonry blocks having a size of 300mmx200mmx150mm (LxBxH) and having a mass of 20kg.

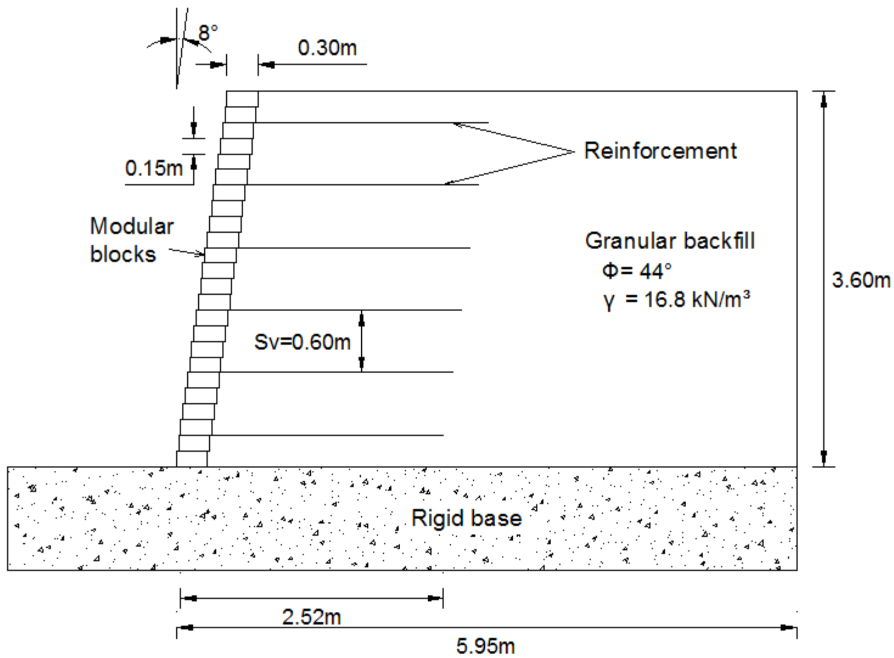

Figure 1. Geometry of the GRS wall

PROPERTIES OF SOIL AND THE REINFORCEMENT

The soil is modelled as a mohr-coulomb model which involves five input parameters i.e. E and μ for soil elasticity, φ and c for soil plasticity and ψ as an angle of dilatancy. Table 1 shows the different properties of the backfill soil (Bathurst et al. 2009).

The walls 1 and 2 are reinforced with polypropylene geogrids with global reinforcement stiffness of 477 and 238 kN/m^2 respectively (Bathurst et al. 2009). The reinforcement is modelled as an elastic material.

Table 1: Properties of the backfill soil

Property	Value
Peak plane-strain friction angle, φ (degrees)	44
Cohesion, c (kPa)	0.1
Dilatancy, ψ (degrees)	14
Bulk unit weight, γ (kN/m^3)	16.8
Youngs modulus, E (kPa)	20000
Poisons ratio, μ	0.3

RESULTS

Wall Facing Displacement:

The analysis has been carried out in PLAXIS 2D, based on that the wall facing displacements and the reinforcement loads are found out. The Figures 2(a) and 2(b) shows the wall facing displacement profile for wall 1 and for wall 2 at the end of construction and at a surcharge load of 50 kPa.

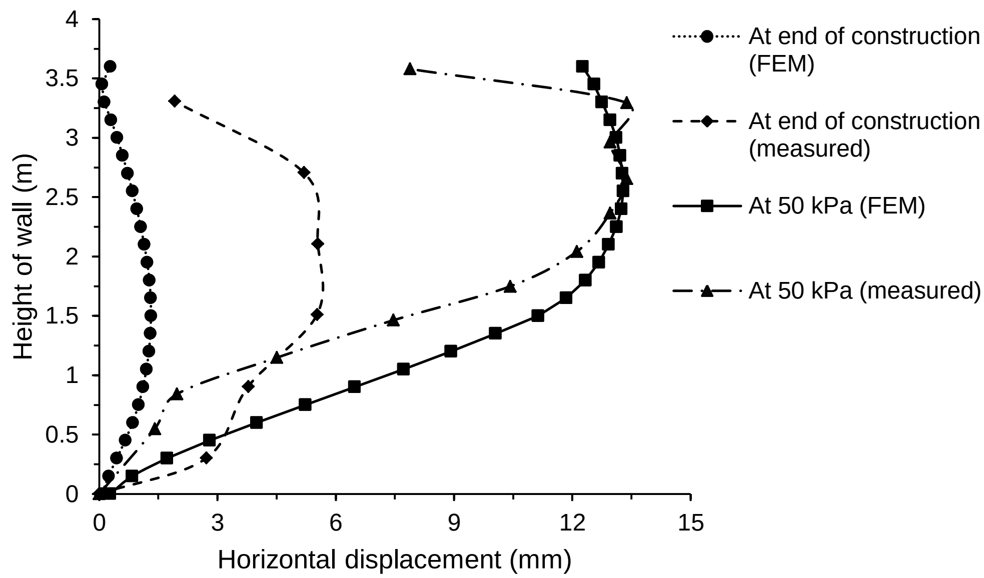

Figure 2(a). Wall facing displacement for wall 1

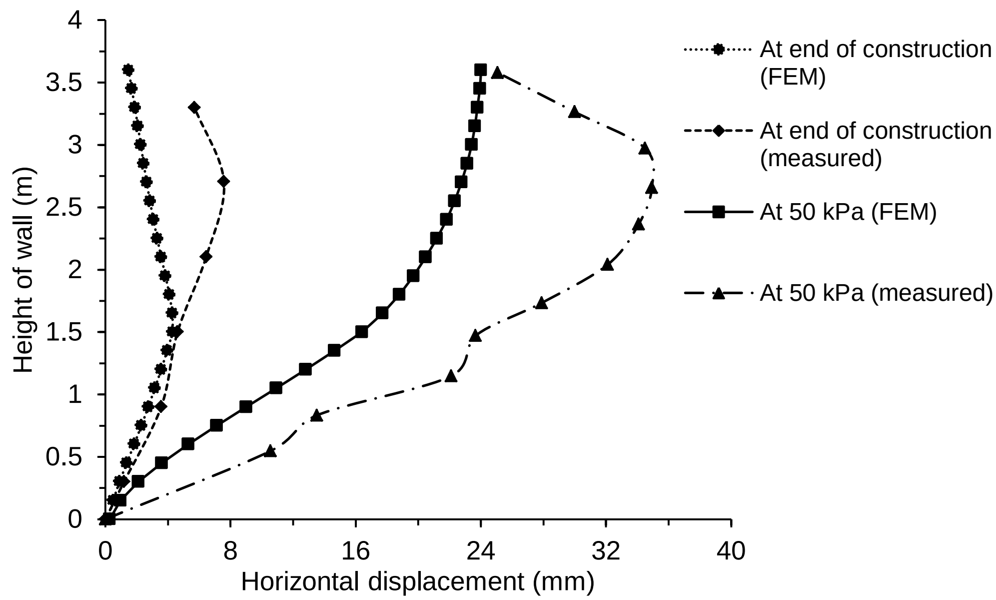

Figure 2(b). Wall facing displacement for wall 2

It is observed from the results that the maximum wall displacements are higher for measured values than the calculated values.

Reinforcement Loads:

The reinforcement loads predicted using AASHTO (2002) simplified method, calculated loads and the measured values has been compared. For Wall 1 the reinforcement loads at the end of construction and at a surcharge level of 50 kPa are shown in Figure 3(a) and 3(b) respectively and for wall 2 in Figure 4(a) and 4(b).

Wall 1

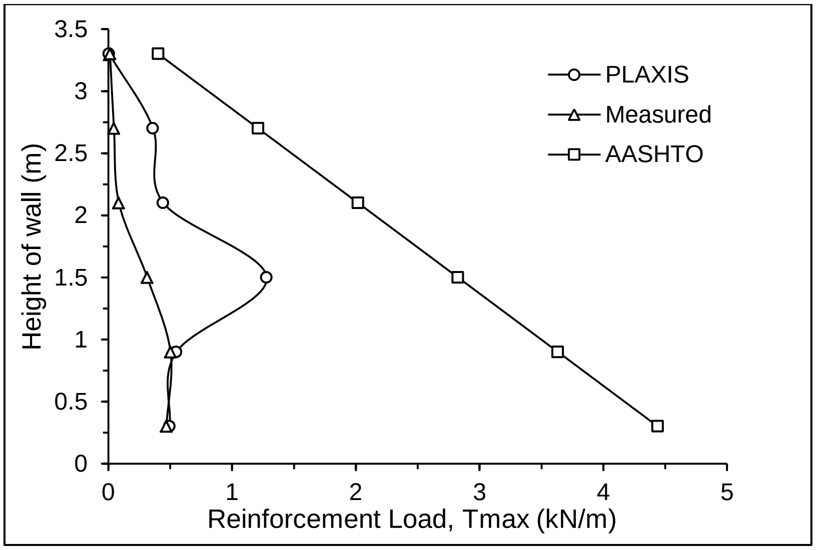

Figure 3(a). Reinforcement loads at the end of construction

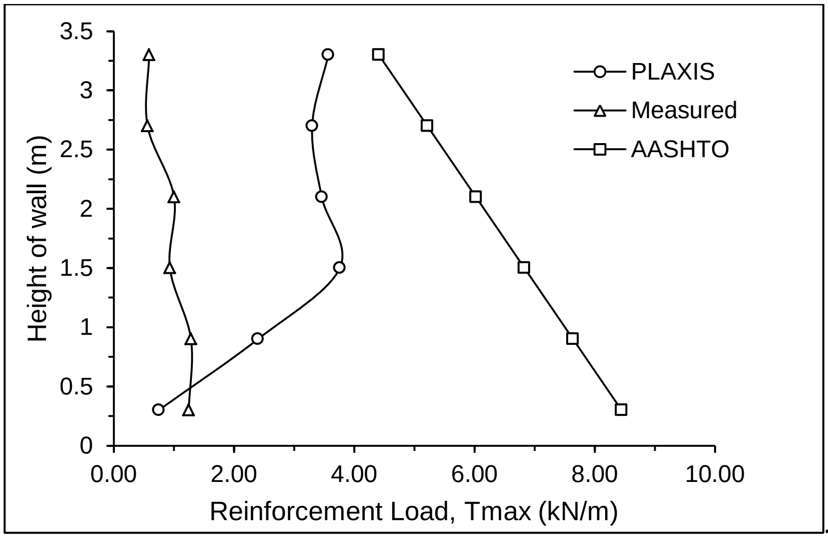

Figure 3(b). Reinforcement loads at 50kPa surcharge

Wall 2

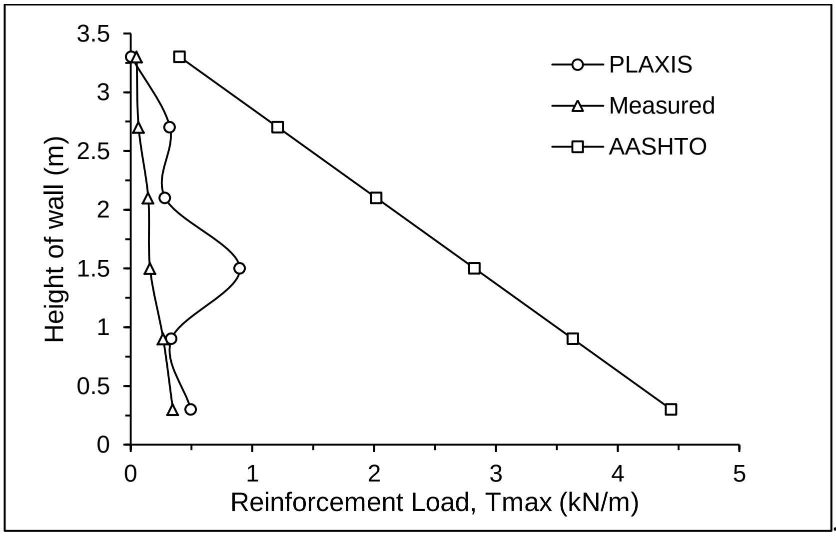

Figure 4(a). Reinforcement loads at the end of construction

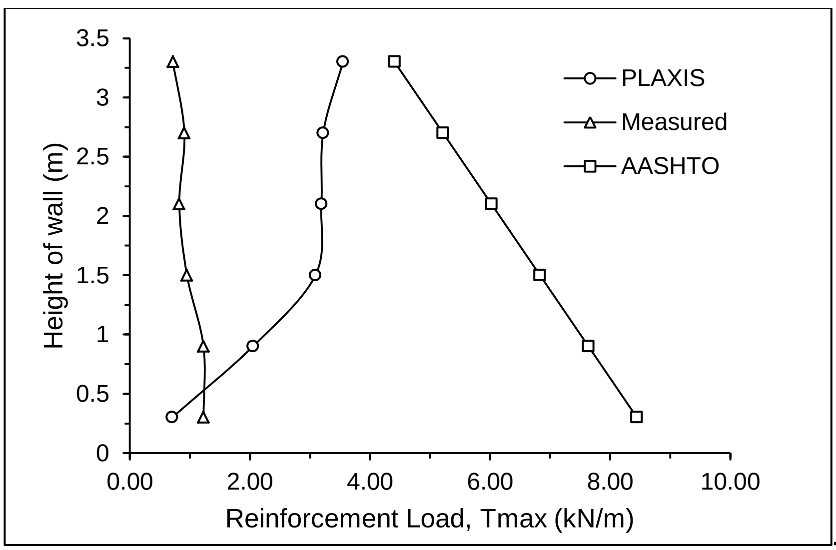

Figure 4(b). Reinforcement loads at 50kPa surcharge

CONCLUSIONS

The analysis is carried for the walls which are having different reinforcement stiffness and at same spacing. The wall is constructed on a rigid concrete foundation. The following conclusions are drawn from the study.

a) The reinforcement load obtained from the FEM analysis is in between the measured and the load obtained by AASHTO (2002) method.
b) The calculated reinforcement loads are matching with the measured loads at the end of the construction.
c) The measured facing wall displacements are higher at end of construction and at surcharge of 50 kPa compared to FEM values.

d) The facing wall displacements are almost twice for wall 2 than that of wall 1 which is having higher reinforcement stiffness.

REFERENCES

AASHTO (2002). *Standard Specifications for Highway Bridges*, 17th edn, American Association of State Highway and Transportation Officials (AASHTO), Washington, DC.

Allen, T. M., Bathurst, R. J., Holtz, R. D., Walters, D. L. & Lee, W. F. (2003). A new working stress method for prediction of reinforcement loads in geosynthetic walls. *Canadian Geotechnical Journal*, 40, No. 5, 976–994.

Bathurst, R. J., Vlachopoulos, N., Walters, D. L., Burgess, P. G. & Allen, T. M. (2006). The influence of facing rigidity on the performance of two geosynthetic reinforced soil retaining walls. *Canadian Geotechnical Journal*, 43, No. 12, 1225–1237.

Bathurst, R. J., Vlachopoulos, N., Walters, D. L., Burgess, P. G. & Allen, T. M. (2007). Reply to the discussions on ‘The influence of facing rigidity on the performance of two geosynthetic reinforced soil retaining walls’. *Canadian Geotechnical Journal*, 44, No. 12, 1484–1490.

Bathurst, R. J., Miyata, Y., Nernheim, A. & Allen, T. M. (2008). Refinement of K-stiffness Method for geosynthetic reinforced soil walls. *Geosynthetics International*, 15, No. 4, 269–295.

Behaviour of rigid retaining wall with relief shelves with cohesive backfill

V. B. Chauhan[1] and S. M. Dasaka[2]

[1]Research Scholar, Department of Civil Engineering, Indian Institute of Technology Bombay, Mumbai 400076, India; email: chauhan.vinaybhushan@gmail.com
[2]Associate Professor, Department of Civil Engineering, Indian Institute of Technology Bombay, Mumbai 400076, India; email: dasaka@civil.iitb.ac.in

ABSTRACT

Present study attempts to investigate the possible reasons behind the failure of a cantilever retaining wall with relief shelves, which is located in the heart of Hyderabad city, India. The height of the failed retaining wall ranges from 10 to 13.9 m and retains a firm to stiff cohesive backfill, and constructed with 5 relief shelves. After few years of construction, a portion of retaining wall of about 20 m length had collapsed and adjoining 20 m length had severely distressed, immediately after the end of a monsoon. From the preliminary post-failure investigation, it is noted that quality of concrete used in construction was satisfactory, and the construction joints were intact. To get more insight about the causes of failure, numerical analysis of retaining wall with relief shelves is carried out in undrained condition of saturated cohesive backfill, as the wall had failed just after monsoon. From the preliminary analysis, it is noted that, though the lateral thrust on the retaining wall in the presence of relief shelves is reduced up to 18%, use of inappropriate magnitude and distribution of lateral earth pressure in the design calculations might have attributed to the failure of the wall.

INTRODUCTION

A retaining wall is a structure, which is designed and constructed to resist the lateral pressure of soil, to support vertical or near vertical backfills. There have been situations where high retaining walls are required to resist the lateral earth pressure. Reinforced soil walls may be a possible solution for such cases, but for construction of such walls, a well graded granular material is preferable due to its higher shear resistance and good soil reinforcement interaction, where undrained conditions would prevail. So, availability of a suitable backfill material is a prerequisite for its suitability in reinforced soil wall construction. One alternative to tackle such issues is to reduce the lateral thrust on the wall, which would obviously reduce the sectional dimensions of the wall and cost of the project.

A pressure relief shelf is a thin horizontal cantilever platform of finite width, extending into the backfill at right angles, throughout the length of the retaining wall, constructed monolithically with the stem of the retaining wall. Number of such shelves is constructed at regular spacing along the height of the wall.

A few researchers previously proposed this technique with limited theoretical studies but without systematic analysis and proper validation, and demonstrated that provision of relief shelves can reduce lateral earth pressure on retaining walls and subsequently increase the stability of the retaining (Jumikis 1964; Chaudhuri et al. 1973; Banerjee 1977 and Bowles 1997). Chaudhuri et al. (1973) demonstrated the benefit of single relief shelf on the reduction of total lateral thrust on a cantilever wall, through stability analysis of wedges as well as small-scale physical model tests. Through small scale model tests, it was showed that wall with relief shelf can retain larger height of sand just prior to the incipient overturning compared to wall without relief shelf (Chaudhuri et al. 1973). Through a series of model tests on instrumented wall, Yoo et al. (2012) and Moon et al. (2013) showed that distribution of lateral earth pressure on the retaining with relief shelves is a compound function of width and position of relief shelf on wall. Similarly, through the finding of model tests, it is noted that when the relief shelf is located below a certain depth, it could not contribute much to the lateral earth pressure reduction in upper part of wall (Liu et al. 2011). Also some recommendations were laid for optimum ratio of location to width of relief shelf for possible distribution of lateral earth pressure on upper part of wall. Analogous to proposed lateral earth pressure below the relief shelf (Jumikis 1964; Chaudhuri et al. 1973 and Bowles 1997), zero earth pressure is reported just below the relief shelf from the findings of model study of pile-supported cantilever retaining wall with single relief shelf (Liu et al. 2013). To study the effectiveness of various width and location of one/two relief shelves, authors have also investigated lateral earth pressure on the retaining with relief shelves by conducting a physical model test in laboratory for 0.6m high instrumented wall with relief shelves (at different positions with varying width) and noted that provision of relief shelf contributes to the reduction of earth pressure on the wall and make the design economical (Chauhan and Dasaka 2016 and Khan et al. 2016).

A case study of failure of a 10-13.9 m high cantilever retaining wall with relief shelves located in Hyderabad, India, had been reported. The above structure had failed after few years of construction, and cracks on the stem of retaining wall just below one of the relief shelves were noted, as shown in Fig. 1. The forensic studies reveal that quality of concrete

Figure 1. Cantilever retaining wall with relief shelves in Hyderabad, India.

used in the wall construction was very satisfactory, and construction defects were completely ruled out. To get more insight into the causes of failure, Chauhan et al. (2016) conducted numerical analysis of retaining wall with pressure relief shelves considering cohesionless backfill. It was reported that larger width of relief shelves, i.e. 2.5 m, used in the above study, might have significantly increased the stresses in the stem of retaining wall just below the relief shelves, leading to unanticipated high tensile and compressive stress on the faces of stem of wall just below one of the relief shelves. These unanticipated stresses might have been neglected in the designs, resulting in failure/distress of retaining wall. As the wall had failed just after monsoon, so poor drainage and earth pressure generated due to saturated backfill may be a probable reason to failure. In order to investigate the possible reason behind the failure of wall, this study is extended with saturated cohesive backfill material in undrained analysis.

The present study is aimed at understanding the behaviour of such walls having cohesive backfill and ascertain the effectiveness of relief shelves to reduce lateral thrust and getting proper insight into the associated mechanisms involved in the failure of wall.

INVESTIGATION OF FAILURE OF A RIGID RETAINING WALL WITH RELIEF SHELVES

Failed retaining wall at Hyderabad, India, with relief shelves has been analysed in FLAC^{3D}. Sectional dimensions of the wall (Fig. 2b) were obtained from the forensic report available with the client (Chauhan et al. 2016). As the soil (backfill and foundation) and wall properties are not available to the authors, so an acceptable range of material properties were taken from Singh and Babu (2010) and Chauhan et al. (2016) respectively, as shown in Table 1.

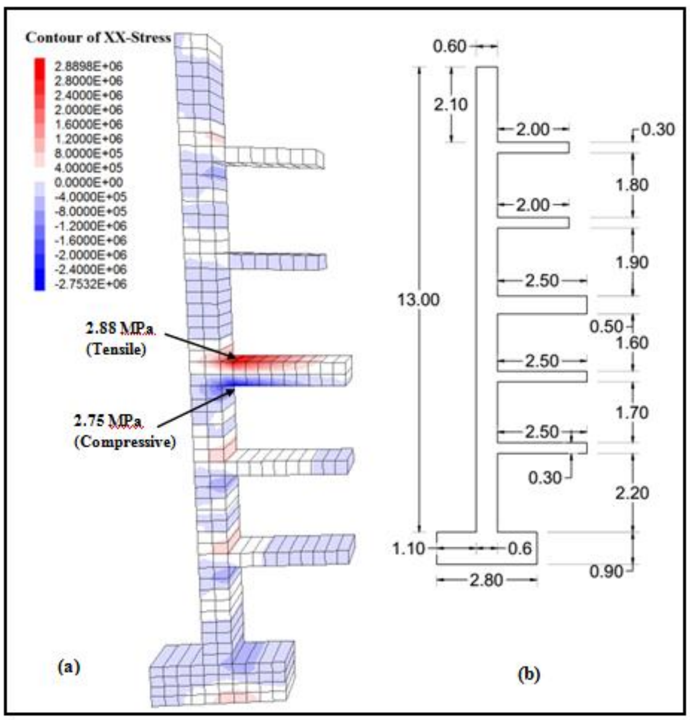

Figure 2. Cantilever retaining wall with relief shelves, Hyderabad (a) result of numerical analysis (b) sectional dimensions (m).

From the numerical analysis, it is found that retaining wall has failed and an attempt is made to capture the progressive failure of wall to understand the reason behind the inception of failure. It is found that due to use of high width of relief shelves, third relief shelf from the backfill surface is severely stressed at the wall and relief shelf junction due to very high bending stresses at the junction (Fig. 2a), due to which wall portion above to this relief shelf has displaced significantly compared to lower part of wall stems (Fig. 3a).

Table 1. Material properties (Chauhan et al. 2016 and Singh and Babu 2010)

Property	Backfill and Foundation soil	Retaining wall
Bulk unit weight (kN/m^3)	19.0	25.0
Modulus of elasticity (kN/m^2)	3×10^4	2.9×10^7
Poisson's ratio	0.3	0.15
Friction angle (degrees)	27.5	--
Cohesion (kN/m^2)	10	--

Also a sign of succeeding displacement started at the relief shelf next below it. Due to this wall movement, a subsequent phase of movement in backfill can be observed in Fig. 3b and 3c. Also a stress reversal of generated stresses on faces of wall (contrary to conventional rigid retaining cantilever walls) is observed near the wall stem junction similar to that observed in the study of same wall with unsaturated cohesionless backfill (Chauhan et al. 2016). It is noteworthy that displacement at wall-shelf junction (Fig. 3a) is similar to failure of wall and crack below one of relief shelf (Fig. 1)**.** These unanticipated stresses might have been ignored during the design of the retaining wall, which resulted cracking of the stem of retaining wall.

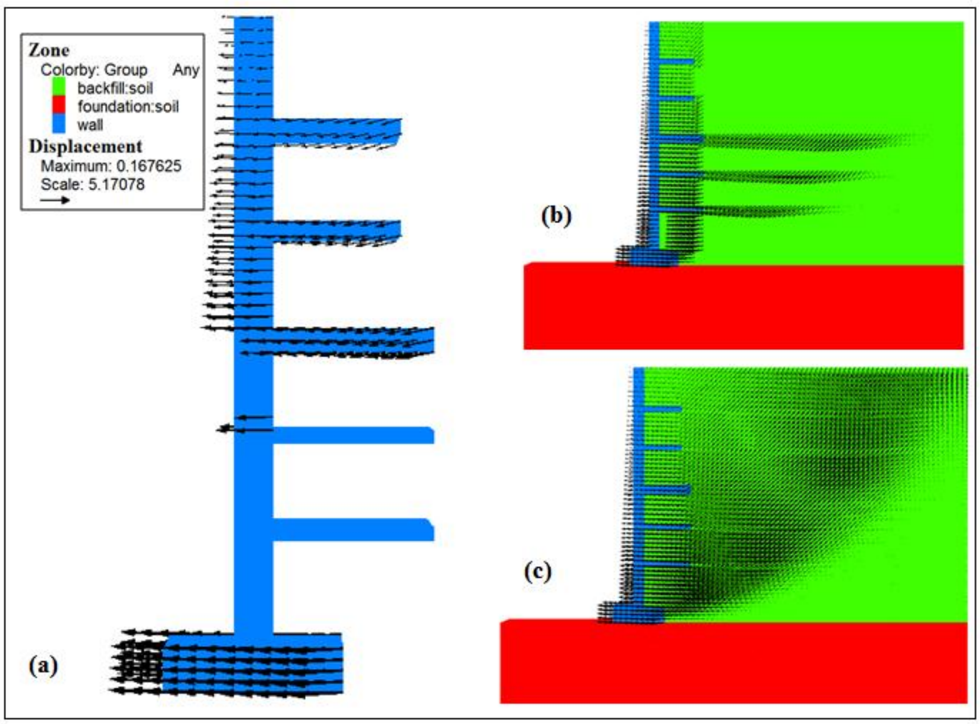

Figure 3. Cantilever retaining wall with relief shelves, Hyderabad (a) displacement of wall started (b) progressive displacement in backfill system (c) overall failure of wall system.

MODELLING OF RETAINING WALL WITH RELIEF SHELVES

To provide a possible solution for the failed retaining wall with relief shelves with cohesive backfill, a cantilever retaining wall having a height of 14.2 m has been chosen for the present study (Fig. 4). Five cantilever relief shelves of same widths are provided at different heights of the wall (Chauhan et al. 2016). Cohesive soil has been selected as backfill and foundation soil (same as shown in Table 1). Width of relief shelf is varied from 0.6 m to 1.5 m to examine the reduction of lateral earth pressure and total thrust. Length of wall is considered as 1.0 m for analysis. Conventional retaining wall without relief shelves (Fig. 5a) is hereafter referred to as RS 0.0. Retaining wall with relief shelves is shown in Fig. 5b, where B represents width of relief shelf which is varied as 0.6 m, 0.9 m, 1.2 m and 1.5 m, having thickness of 0.3 m and referred to as RS 0.6, RS 0.9, RS 1.2 and RS 1.5.

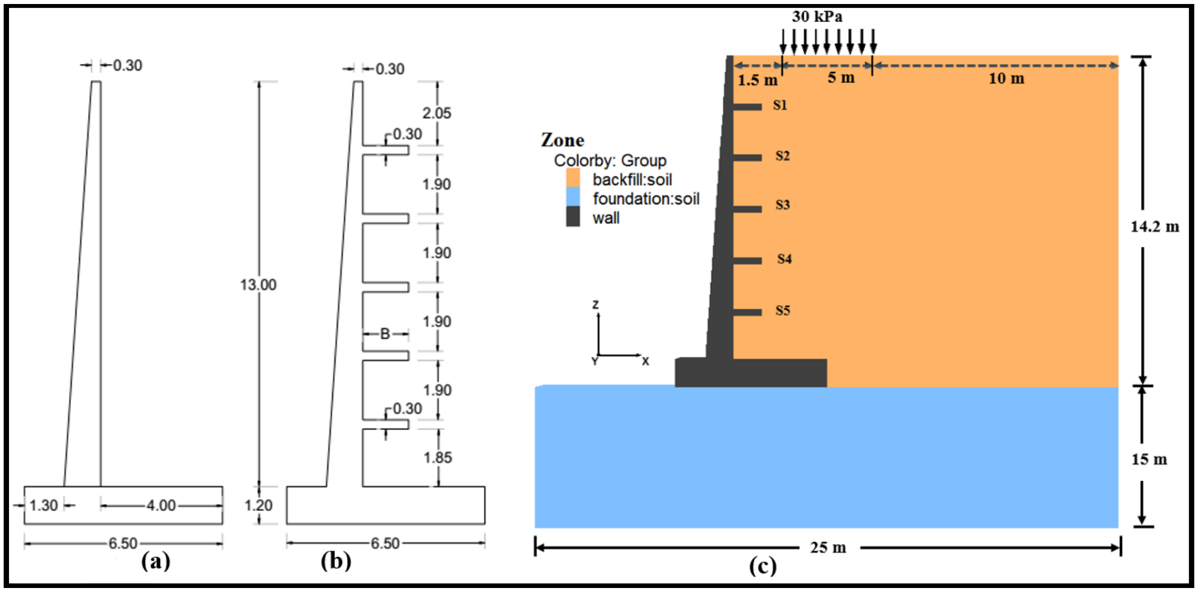

Figure 5. Sectional dimensions of retaining wall (a) without relief shelf and (b) with relief shelves (Chauhan et al. 2016) and (c) numerical grid of rigid retaining wall with relief shelves (not to scale).

The rigid wall is modelled as elastic material and backfill material is modelled as an elasto-plastic material following Mohr-Coulomb failure criterion. Material properties considered in the analysis are shown in Table 1. Fig. 5 shows the numerical grid considered to simulate the rigid retaining wall having static surcharge of 30 kPa. Fixed boundary condition at bottom of foundation and roller boundary condition at vertical end of soils are chosen to represent field conditions. Numerical model described above is validated with the experimental findings of Ertugrul and Trandafir (2011) and discussed in Chauhan et al. (2016).

RESULTS AND DISCUSSION

In the present analysis, rigid retaining walls with five relief shelves provided at different heights of wall having equal widths are analysed with FLAC^{3D}. The lateral earth pressure distribution, contact pressure below base slab, total lateral thrust and deflection of relief shelves are analysed and discussed below.

Contact pressure below base slab

Variation of contact pressure below base slab for all retaining walls considered in the present study is shown in Fig. 6. Contact pressure is marginally lower in case of walls with shelves. With increase in width of relief shelf, contact pressure below the base slab has reduced by maximum 2% only.

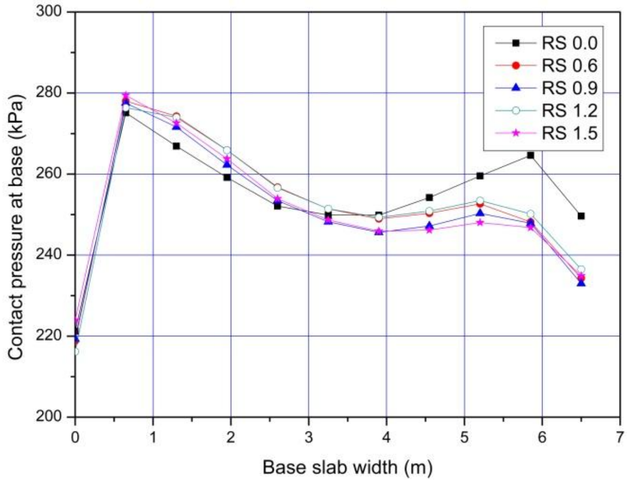

Figure 6. Contact pressure below the base for various retaining walls.

Lateral earth pressure and total thrust on the retaining wall

Distribution of earth pressure on all walls with and without relief shelves have been studied and shown in Fig. 8. Provision of five relief shelves has divided the whole retaining wall into six small segments.

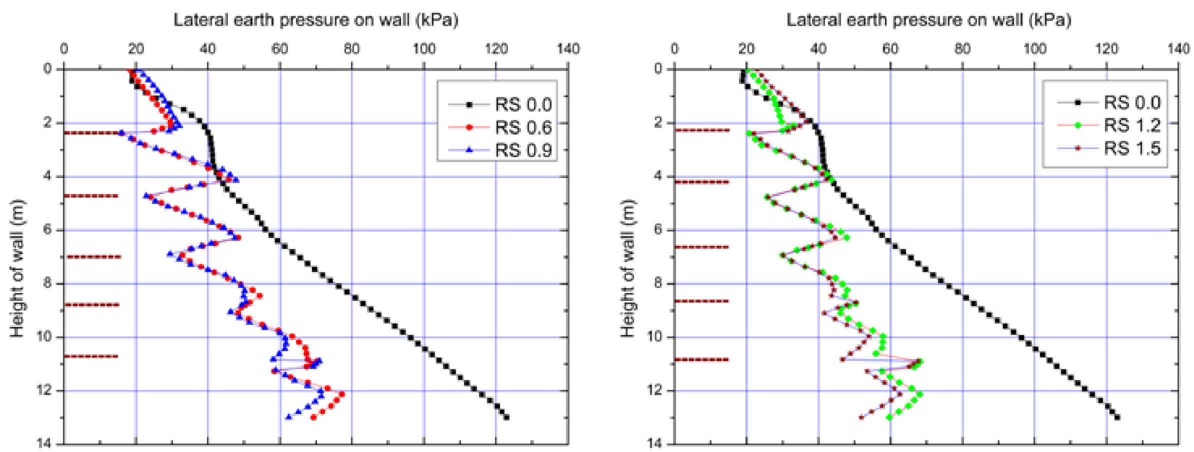

Figure 7. Lateral earth pressure on the wall for rigid retaining wall with relief shelves.

Table 2. Total thrust and reduction in thrust on retaining walls

Wall type	RS 0.0	RS 0.6	RS 0.9	RS 1.2	RS 1.5
Total thrust (kN/m)	19074	17013	16858	15609	16123
% Reduction in thrust	-------	10.8	11.6	18.2	15.5

From Fig. 7, it can be observed that lateral earth pressure (total stress analysis) in top first segment has not changed with width of relief shelf which is in line with Liu et al. (2011), which suggests that relief shelf does not much participate in reduction of earth pressure in upper wall section. In lower portions of wall, earth pressure reduced with increase in width of relief shelf, which can be attributed to the fact that a great portion of overburden and surcharge is carried by uppermost relief shelf. Total thrust from above earth pressure distribution is calculated and shown in Table 2. A noteworthy amount of total thrust reduction is obtained by provision of relief shelves. A range of 11-18% of total thrust reduction is achieved by provision of relief shelves having saturated cohesive backfill with static surcharge of 30kPa.

Lateral displacement of retaining walls and deflection of relief shelves

A typical displacement of wall away from backfill has been shown in Fig. 8. It can be seen that provision of relief shelves to the wall has marginally reduced the maximum lateral displacement of the wall from 25.2 mm (wall without relief shelf) to 24.9-24.2 mm (walls with relief shelf).

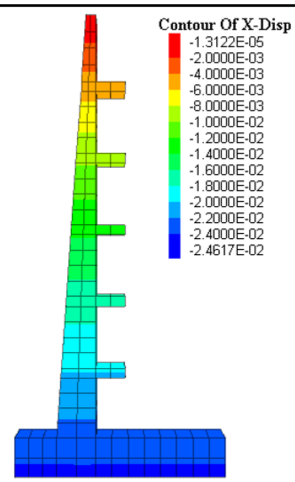

Wall Type	Maximum wall displacement (mm)
RS 0.0	25.2
RS 0.6	24.9
RS 0.9	24.6
RS 1.2	24.3
RS 1.5	24.2

Figure 8. Contour of lateral displacement of RS 0.9 and summary of maximum displacement of rigid retaining wall with relief shelves

With increase in width of relief shelf, maximum displacement of retaining walls has been reduced, which is due to the reduction of total thrust on wall and increased weight of wall due to relief shelves.

Maximum deflection of all relief shelves from top to bottom are compared and summarized in Table 3. The notations S1, S2, S3, S4 and S5 represent the relief shelves from top to bottom of retaining wall. Deflection of relief shelves from top to bottom of wall has reduced and found minimum for bottommost relief shelf for all retaining walls with relief shelves. Deflection of relief shelves has significantly increased where the width of relief shelf is greater than 1.2 m.

Table 3. Maximum deflection (mm) of relief shelves for various retaining walls

Relief Shelf	RS 0.6	RS 0.9	RS 1.2	RS 1.5
S1	1.39	2.10	2.93	3.45
S2	1.17	1.94	2.52	3.26
S3	1.02	1.56	2.23	2.84
S4	0.83	1.31	1.85	2.34
S5	0.78	1.20	1.73	2.02

This observation would restrict maximum width of relief shelves to 1.2 m. Larger widths of relief shelves lead to excessive deflection due to its own weight, which may further increase due to creep. Among all the cases of retaining wall with relief shelves, RS 1.2 provides maximum benefit, without leading to excessive deflection of relief shelves.

CONCLUSIONS

The study involves comprehensive finite difference numerical analysis to examine the possible reason of failure of retaining wall with relief shelves. It is found that use of larger width of relief shelves has significantly increased bending stress in relief shelf as well as on the faces of stem of wall just the relief shelves. This unanticipated stresses might have been neglected in the designs, resulting in failure/distress of retaining wall. From the present study, it is noted that this technique of reducing earth pressure on retaining walls may prove economical. Among all the cases of retaining wall with relief shelves, RS 1.2 proves viable, without leading to excessive deflection of relief shelves. The following conclusions are drawn from the present study.

1. Retaining walls with relief shelves can considerably reduce the total thrust on wall with even cohesive backfill. For the present study under prescribed surcharge, a total reduction is thrust is noted in range of 11-18%.
2. Among all walls considered in the present study, using relief shelves of width 1.2 m will be effective without leading to excessive deflection of relief shelves.
3. Deflection of relief shelf is proportional to the width of relief shelf, and it also decreases from top shelf to bottom shelf for a given retaining wall with relief shelves.

REFERENCES

Bowles, J.E. (1997). Foundation analysis and design, 5th Edition, McGraw-Hill, Singapore.

Chaudhuri, P.R., Garg, A.K., Rao, M.V.B., Sharma, R.N., Satija, P.D. (1973). "Design of retaining wall with relieving shelves", IRC J. 35(2), 289 - 325.

Chauhan, V.B. and Dasaka, S.M. (2016). "Reduction of Lateral Earth Pressure Acting on Non-yielding Retaining Wall using Relief Shelves" Proc. Int. Geot. Engg. Conf. on Sustainability in Geot. Eng. Practices Related Urban Issues, Mumbai, India. Paper ID-34

Chauhan, V.B., Dasaka, S.M., Gade, V.K. (2016). "Investigation of failure of a rigid retaining wall with relief shelves". Jap. Geot. Society, 10.3208/JGSSP.TC302-02.

Ertugrul, O. L. and Trandafir, A.C. (2011). "Reduction of lateral earth forces acting on rigid non-yielding retaining walls by EPS geofoam inclusions", J. Mater. Civil Eng., 23(12), 1711-1718.

Jumikis, A.R. (1964). Mechanics of soils, D. Van Nostrand Company Inc, Princeton NJ.

Khan R., Chauhan V.B. and Dasaka S.M. (2016). "Reduction of lateral earth pressure on retaining wall using relief shelf: A numerical study", Int. conf. soil env., Bangalore, India, Paper no-117.

Liu, G., Hu, R., Pan, X., Liu Y. (2011): Model tests on earth pressure of upper part wall of sheet pile wall with relieving platform Rock and Soil Mechanics, 32(2), 103-110.

Liu, G., Hu, R., Pan, X., Liu Y. (2013): Model tests on mechanical behaviors of sheet pile wall with relieving platform. Chinese J. Geotech. Eng., 35(1), 94-99.

Singh, V.P. and Babu, G.L.S. (2010). "2D Numerical Simulations of Soil Nail Walls", Geot. and Geol. Engg., 10.1007/s10706-009-9292-x.

Discrete Piles as a Measure to Control the Slope Instability Issues in Urban Areas – A case study from Mumbai, India

George Tharakan Idiculla[1] and Satyanarayana Murty Dasaka [2]

[1]Research Scholar, Department of Civil Engineering, Indian Institute of Technology Bombay, Pin: 400076, Mumbai; e-mail: 25.george@gmail.com
[2]Associate Professor, Department of Civil Engineering, Indian Institute of Technology Bombay, Pin: 400076, Mumbai; e-mail: dasaka@civil.iitb.ac.in

ABSTRACT

Slope failures or landslides often result in extensive damages to the property lying on the slopes or in the close proximity, and may cause loss of human life. Recently, several cracks were observed along the stem of retaining structures protecting a very old and important structure located in one of the prime locations in Mumbai, India. This structure had been lying on a slope of 30 meters height and sloping at angle varying from 50 to 70 degree with horizontal. This structure has been classified as a heritage structure. The cracks developed are most probably due to the soil movement occurred over a period of time. Three boreholes were dug on the site, and the borehole data shows that the top layer soil comprises of filled up soil and gravels up to 1 meter depth and beneath that, sandy clay with small boulders were noted up to around 11 meters. As the site is very sensitive, a detailed site investigation, to map critical slip surface is not viable. A close look at the borehole logs suggest the presence of clay with small rock fragments up to 11 meters depth which in all likelihood, causes the slope instability, especially in rainy season. Considering the project location, topography and soil stratification, the implementation of staggered discrete piles of 15 meters length would be a viable solution to restrict further movement of the slope, and present distress to the main structure. The proposed solution is numerically analysed and discussed in the study. A detailed description on the selection of embedment depth, spacing and diameter of piles, and its location on the slope is analysed as well.

INTRODUCTION

Several ground improvement techniques had been developed for stabilizing slopes in the past few decades. However, the determination of the most critical failure surface of a slope is still a challenging task for geotechnical engineers, in view of the non-homogeneity of soil, layered soil deposits, etc. More recently, laterally loaded piles are successfully used to mitigate the slope instability issues. The piles embedded on slopes will serve as an effective reinforcement to the slope, and enhances the factor of safety against shear failure. The successful use of this method has been described by several researchers (for example, Esu and D'Elina 1974; Ito and Matsui 1975; Sommer 1977; Nethero 1982; Morgenstern 1982; Ito et al. 1982; Gudehus and Schwarz 1985; Reese et al. 1992; Rollins and Rollins 1992; Poulos 1995). Sharafi and Sojoudi 2016, carried out both experimental and numerical studies of pile-stabilized slopes under surface load conditions. The design aspects of the pile and pile groups used for slope stability were mentioned by Poulous 1995; Hassiotis et al. 1997; Kourkoulis et al. 2011; Mujah et al. 2013. Numerical studies conducted by Kourkoulis et al. (2011) focused on implementation of staggered piles for slope stability. For staggered piles, the rear (trailing) pile is not positioned directly behind the front piles, but at mid-distance between the front piles (Figure 1). This arrangement diminishes the shadow effect and imparts increased resistance to soil movements. The multiple soil arching effects that can develop for this configuration will in turn increase the resistance to the soil movement (Chen and Poulos 1993; Bransby and Springman 1999; Chen and Martin 2002).

Recently, several cracks were observed on the retaining structures adjacent to a very important structure located in Mumbai, India, resting on a slope of 30 meters height and of sloping angle varying from 50 to 70 degree with horizontal. The cracks would indicate the possibility of a very gentle soil movement. The further movement of slope can lead to failure of the existing slope and thereby causing a threat to the existing buildings located on the slope. The slope was numerically modelled in Plaxis-3D to simulate the existing ground conditions and soil properties. Staggered piles are proposed as a ground improvement technique, and safety factors and location of critical failure surfaces on the slopes are obtained for various combinations of arrangement of staggered piles.

SIMULATION OF IN-SITU CONDITIONS

Soil Profile

The plot is situated on a hilly terrain with sloping angle of 50˚ to 70˚ to horizontal, with a level difference of around 30.00 meters between upstream ground level and downstream ground level. Three boreholes were dug at the site as part of the ground investigation. Based on the soil investigation, it is noted that the top layer of slope comprises of filled up soil with silty clay and gravels up to 1.00 m depth. The presence of sandy clay with small boulders/rock fragments are noted up to 10.40 to 11.00 m depth from existing ground level, underlain by a weathered rock deposit.

Soil Properties

For the analysis, length of the model (perpendicular to the cross-section of slope) is considered as 25 meters and its height as 30 meters, which comprise of three subsequent layers (clayey silt with gravels, silty sandy clay and weathered rock). Surcharge loadings of 25 kPa, 12.5 kPa and 10 kPa are provided on the top surface of the slope to simulate the actual loading due to existing buildings. Figure 2 shows the geometry of the slope model and properties considered for different layers are listed in Table 1. Embedded pile is composed of beam elements that can be placed in arbitrary direction in the sub-soil and that interacts with the sub-soil by means of special interface elements. The interaction may involve skin resistance as well as base resistance. Although an embedded pile does not occupy volume in modelling, a particular volume around the pile (elastic zone) is assumed in which plastic soil behavior is excluded. The size of this (equivalent) zone is based on the pile diameter, and corresponding embedded pile material data set. The installation effects of piles are not considered in the analysis.

Table 1 Soil properties considered for numerical modelling

	Clayey silt with gravels	**Silty sandy clay**	**Weathered rock**
Depth from the surface	0 m (top layer)	1.5 to 2.5 m	6 to 10 m
Constitutive model used	Mohr- Coulomb	Mohr-Coulomb	Mohr-Coulomb

Cohesion, C (kPa)	29 kPa	32 kPa	37 kPa
Angle of internal friction, Φ	32°	33°	35°
Bulk unit weight, γ_{bulk} (kN/m^3)	17.62	19	22
Saturated unit weight, γ_{sat} (kN/m^3)	19	21.5	23
Young's modulus, E (kPa)	3.2x10^4	3.5x10^4	4.7x10^7
Poisson's ratio, ν	0.35	0.25	0.25

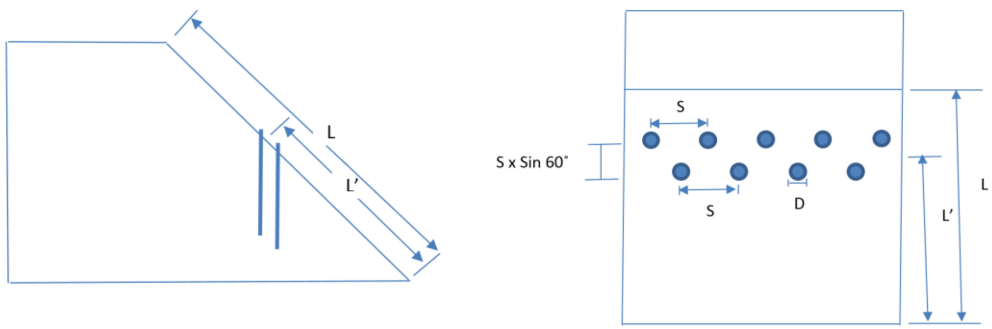

(a) (b)

Figure 1 Staggered arrangement of piles on slope
(a) Cross-sectional view (b) Top view

METHODOLOGY

Modelled slope is checked for the factor of safety and the critical failure surface is determined. The critical slip circle for the natural slope, without ground improvement, is shown in Figure 3. To increase the resisting force against sliding, laterally loaded staggered piles are installed on the sloping surface, which act as reinforcement. Analyses are done on plies placed at different locations. Other parameters like diameter of pile and its centre-to-centre spacing are varied and analysed to obtain an optimized solution of ground improvement. Phi-C reduction method is used for the analysis of factor of safety. The parameters, cohesion (C) and tan Φ and are reduced during calculation, until failure of the slope occurs. The properties of reinforced concrete piles used for the slope stabilization are given in Table 2. Considering the soil and rock properties as well as the obtained critical slip circle for the existing slope, the length of pile is taken as 15 meters. Figure 4 shows the Finite Element Meshing for the slope. Layer of silty sandy clay beneath the top soil layer is hidden in the figure to show the arrangement of staggered piles embedded on the slope.

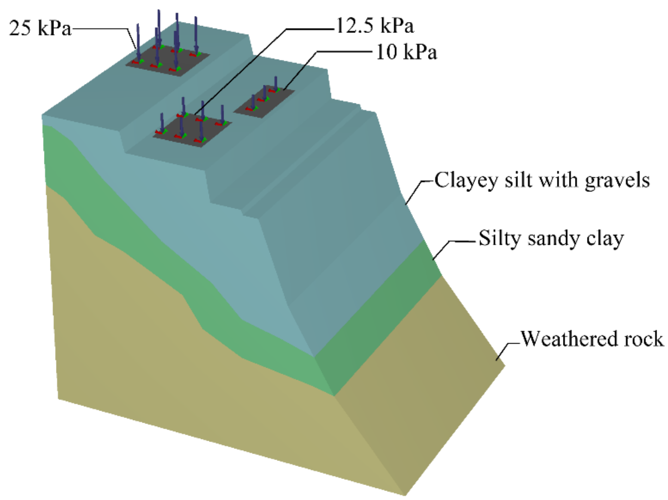

Figure 2 Geometry of slope model used in the analysis

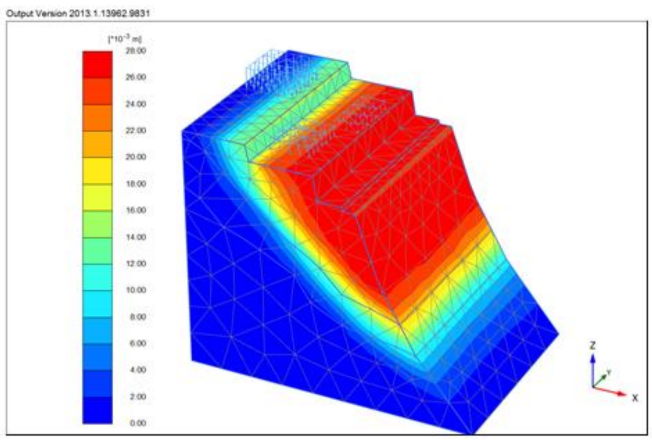

Figure 3 Output window of the safety analysis for the slope without staggered piles

Table 2 Properties of piles considered

Unit weight, γ (kN/m^3)	25
Young's modulus, E (kPa)	2.57 x 10^7
Material	Steel Reinforced Concrete
Diameters, D (m)	0.3, 0.5
Center-to-center spacing of piles, S (m)	3D, 4D, 5D
Length of the pile (m)	15

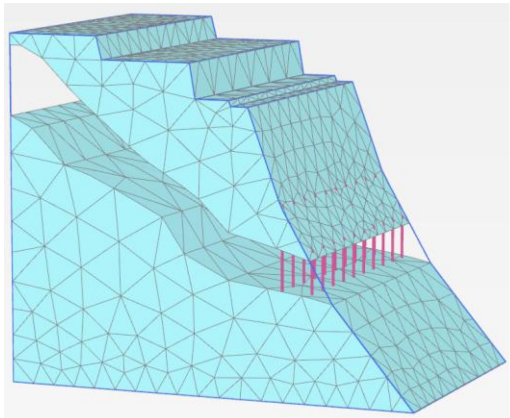

Figure 4 Finite Element Mesh used for safety analysis
(Interlayer is hidden to show the embedded piles)

RESULTS AND DISCUSSION

Factor of safety against sliding for the existing slope (unreinforced slope) is found to be 1.256, and the corresponding critical slip surface is shown in Figure 3. Different locations considered for the embedment of piles are L'/L = 0.4, 0.5, 0.6 and 0.8, where L' is the distance to the midway between two rows of staggered piles measured from the toe of the slope and L is the slanting length of the slope, as shown in Figure 1. Reinforced concrete piles of 0.3 m and 0.5 m diameters (D) are modelled. For each case different center-to-center spacing (3D, 4D, 5D) are considered in the analysis. Comparative studies are conducted and an optimum location, diameter and spacing of staggered piles are suggested considering the site conditions and practical aspects. The factor of safety of the reinforced slope can be found as a function of pile diameter (D), center-to-center distance between the piles (S) and the location of the pile. The effects of these parameters on the factor of safety of the slope can be expressed conveniently by plots; (i) factor of safety versus L'/L ratio (Figure 5) and (ii) factor of safety versus S/D ratio (Figure 6).

Variation of Factor of Safety with location of staggered piles

Figure 5 illustrates the variation of Factor of Safety with the location of staggered pile group. Sharafi and Sujoudi (2016) conducted experimental and numerical studies for homogeneous slope and observed that the factor of safety will be maximum when the piles are embedded at midway between the toe and the crest (L'/L= 0.5). Many other researchers have also reported the same. However, the results for this site specific analysis shows that the maximum factor of safety is observed for the case of L'/L = 0.4. As the location of staggered pile group is shifted from L'/L = 0.4 to L'/L = 0.5, it has been observed in all the cases that the factor of safety decreases from its maximum value by around 10% and 18% for 0.3 and 0.5 diameter piles, respectively. Factor of safety increases and again falls down as the location of staggered pile group shifts from the center to the crest of the slope (i.e. the change in L'/L value from 0.5 to 0.6 and finally to 0.8). This variation is more evident in the case of piles having diameter 0.5 m. The results shows that the percentage of variations is same for all center-to-center spacings.

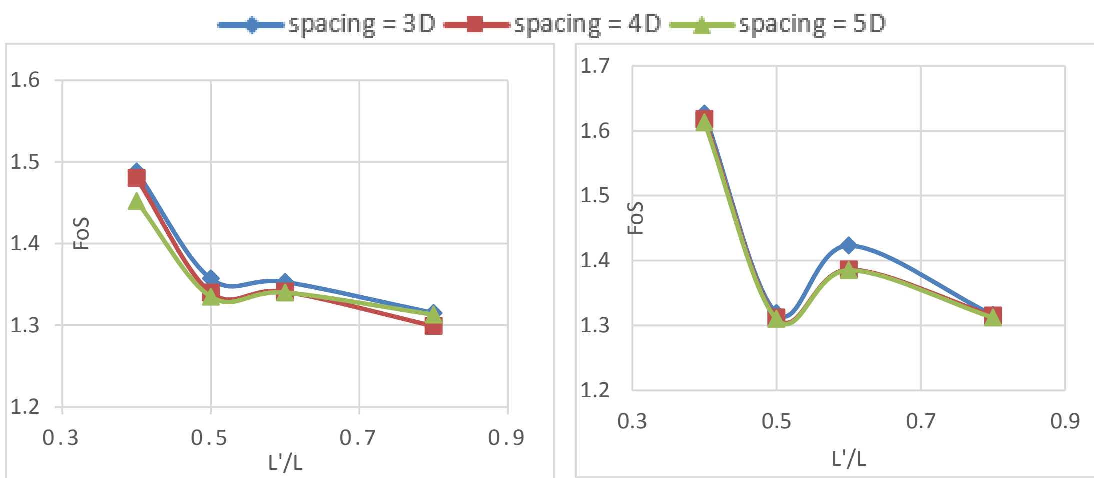

(a) (b)

Figure 5 Factor of Safety v/s Location of pile group (L'/L):
(a) **for pile diameter 0.3 m (b) for pile diameter 0.5 m**

Variation of Factor of Safety with center-to-center spacing (S)

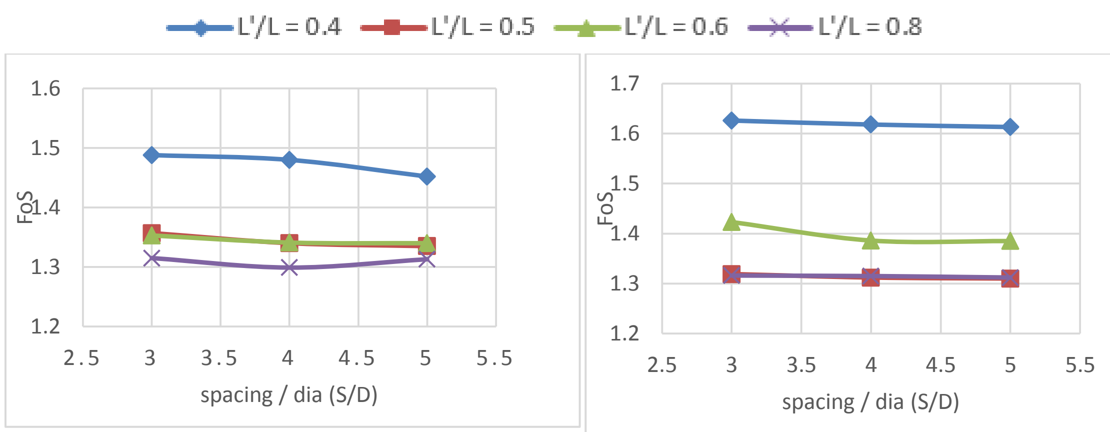

(a) (b)

Figure 6 Factor of Safety v/s S/D:
(a) for pile diameter 0.3 m (b) for pile diameter 0.5 m

Figure 6 shows the variation of factor of safety with the spacing between piles. All the results shows that the factor of safety decreases slightly as the spacing increases from 3D to 5D. The results can be considered as site specific as they mainly depend on the profile and properties of soil and weathered rock layers considered. Though, few researchers observed the optimum location of pile group for slope stability as the midway between crest and toe, the maximum value of factor of safety observed for this case study is L'/L = 0.4. This can be due to the high embedment depths of piles into the weathered rock strata. A noticeable decline in the factor of safety is observed as the location is changed from L'/L = 0.4 to L'/L = 0.5. However, the factor of safety again increases when the piles are located between L'/L = 0.5 to L'/L = 0, and beyond this zone, the factor of safety continuously reduces to a minimum value as the location of staggered piles approaches the crest. Moreover, the reduction in factor of safety is observed as the center-to-center spacing between piles increases.

The maximum value of factor of safety observed among all the combinations considered in the present study is for staggered piles of 0.5 m diameter with a spacing of 3D, at location L'/L = 0.4. However, Kourkoulis et al. (2011) emphasized an optimum centre-to-centre spacing, S, as 4D, as it has the largest spacing required to produce soil arching between piles, so that the soil between piles will be adequately retained. In view of the above recommendation, and keeping the practical difficulty in implementing 3D spacing in this particular case, it can be concluded that the optimum solution is to provide staggered piles of 0.5 m diameter with 4D center-to-center spacing at location L'/L = 0.4.

CONCLUSIONS

The threat due to slope instability near an important building located near the top portion of an existing slope in Mumbai, India, was analysed. The need of reinforcement of the slope was confirmed by numerical modelling using PLAXIS 3D, and numerical analyses are carried out to obtain the optimum location, diameter and center-to-center spacing of piles in staggered arrangement. The results confirm that optimum solution is to provide staggered piles of 0.5 m diameter with 4D center-to-center spacing at location L'/L = 0.4.

REFERENCES

Broms, B. B., (1964). "Lateral Resistance of Piles in Cohesionless Soils" *Journal of the Soil Mechanics and Foundations Division*, ASCE 90 (SM3): 123-156.

Chen, L., and Poulos, H. G., (1993). "Analysis of pile-soil interaction under lateral loading using infinite and finite elements." *Computers and Geotechniques*, 15:189-220.

Esu, F. and D'Elina, B. (1974). "Interazione terrreno-struttura in un palo sollecitato dauna frana tip colata." *Rev. Ital. di Geot.*, 111:27-38.

Gudehus, G., and Schwarz, W. (1985). "Stabilization of creeping slopes by dowels." *Proceedings , 11th International Conference on Soil Mechanics and Foundation Engineering, San Fransisco*, Vol 3: 1697-1700.

Hassiotis, S., Chameau, J. L., and Gunaratne, M (1997). "Design Method for Stabilization of Slopes with Piles." *Journal of Geotechnical and Geoenvironmental Engineering.*

Ito, T., and Matsui, T. (1975). "Methods to estimate lateral force acting on stabilising piles." *Soils and Foundations.* 18(4): 43-59.

Kourkoulis, R., Gelagoti, F., Anastasopoulos, I., and Gazetas, G. (2011). "Slope Stabilizing Piles and Pile Groups: Parametric Study and Design Insights." *Journal of Geotechnical and Geoenvironmental Engineering*, ASCE.

Mujah, D., Ahmad, F., Hazarika, H., and Watanabe, N., (2013). "The Design Method of Slope Stabilizing Piles: A Review." *International Journal of Current Engineering and Technology*, ISSN.

Nethero, M. F. (1982). "Slide control by drilled pier walls. In Application of walls to landslide control problems." Edited by Reeeves, R. B., *American Society of Civil Engineers*, pp: 61-76.

Poulous, H. G (1995). "Design of Reinforcing piles to Increase Slope Stability." *Canadian Geotechnical Journal.* 32: 808-818.

Rollins, K. M., and Rollins, R. L. (1992). "Landslide stabilisation using drilled shaft walls." Edited by Geddes, J. D. *Ground movements and structures.* vol 4,pp: 755-770.

Sharafi, H. and Sojoudi, Y. (2016). "Experimental and Numerical Study of Pile-Stabilized Slopes Under Surface Load Conditions" *International Journal of Civil Engineering.*

Sommer, H. (1977). "Creeping slope in a stiff clay." *Proceedings Special Session No. 10, 9th International Conference on Soil Mechanics and Foundation Engineering, Tokyo.* pp: 113-118.

Remedial Measures for Upheaval of PQC Panels Adjacent to Piers of Monorail in Mumbai

P.S. Prasad[1], U.K. Guru Vittal[2], K. Sitaramanjaneyulu[3] and M. R. Madhav[4]

[1]Senior Scientist, CSIR – Central Road Research Institute, CRRI (PO), New Delhi – 110025, India ; PH: +91 9013471432; email: pulikanti@gmail.com

[2]Head & Chief scientist, CSIR – Central Road Research Institute, CRRI (PO), New Delhi – 110025, India ; PH: +91 9868858380; email: vittal.crri@gmail.com

[3]Senior Principal Scientist, CSIR – Central Road Research Institute, CRRI (PO), New Delhi – 110025, India; PH: +91 9899257418; email: ksitaramcrri@yahoo.co.in

[4] Professor Emeritus, JNT University, Hyderabad, India - 500034: PH: +91 9866228583: email: madhavmr@gmail.com

ABSTRACT

Mumbai city has several modes of public transport system including 'Monorail'. The Wadala Depot to Chembur is an elevated monorail system which is supported by pier, pile cap and piles. Monorail piers have been positioned in the median portion of cement concrete roads. Since the sub-soil comprises of marine clay in these two roads, stone columns (0.9 m diameter at a spacing of 2.5 m c/c in a triangular patter) were installed before constructing the cement concrete pavement. In the year 2015 the cement concrete pavement near the monorail piers in Sion-Koliwada Connector road and Anik-Wadala Road as well as in front of Wadala Monorail Station is severely distressed in the form of level displacement (which appears as upheaval) and cracking, while the concrete panels away from the piers are intact. This paper presents detailed geotechnical investigation, probable reasons for displacement /settlements in PQC slabs and design of remedial measures.

INTRODUCTION

Many of the metro capital cities in India have been constructed in the coastal / river delta regions. As a result, sub-soil in such cities happens to be soft marine clay. Due to growth in population and increasing demand for better mobility, city development authorities are building flyovers, metro trains and monorails in such cities. Constructing elevated metro or monorail corridor is often cheaper and much easier than construction in the underground. The India's first Monorail project is implemented in Mumbai and is being executed by the Mumbai Metropolitan Region Development Authority (MMRDA). The detailed project report (DPR) for Mumbai monorail project from Jacob circle to Chembur was prepared in the year 2008. Construction work started in the year 2009 and the first operational line from Wadala Depot to Chembur (approximately 8.5 km in length) was opened to the public in February 2014. In this stretch, Monorail alignment starting from Wadala Depot passes through Sion-Koliwada connector road, then to Anik-Wadala road (Northern connector road - Main road) and takes a turn towards Mysore Colony (Figure 1). The Sion-Koliwada Connector road and road in front of Wadala Monorail station are six lane divided cement concrete roads with a median in between. The thickness of PQC is about 300 mm, below which dry lean concrete (DLC) bed has been provided. GSB layer has been sand-witched between DLC and fill up soil. Since the sub-soil comprises of marine clay in these two roads, stone columns (0.9 m diameter at a spacing of 2.5 m c/c in a triangular patter) were installed before constructing the cement concrete pavement. Near Wadala station and monorail depot, the alignment is adjacent to a creek. In the year 2015 the cement concrete pavement near the monorail piers in Sion-Koliwada connector road and Anik-Wadala road as well as in front of Wadala Monorail Station roads are severely distressed in the form of level displacement (which appears as upheaval) and cracking as shown in Figures 2a and 2b respectively, while the concrete panels away from the piers are intact. The problem of level displacement (upheaval) of slabs near monorail pier and subsequent cracking in such panels can be seen from Wadala Monorail Station upto about Pier No 80 on Anik-Wadala Road (North Connector road) until the alignment takes a turn towards Mysore Colony Station.

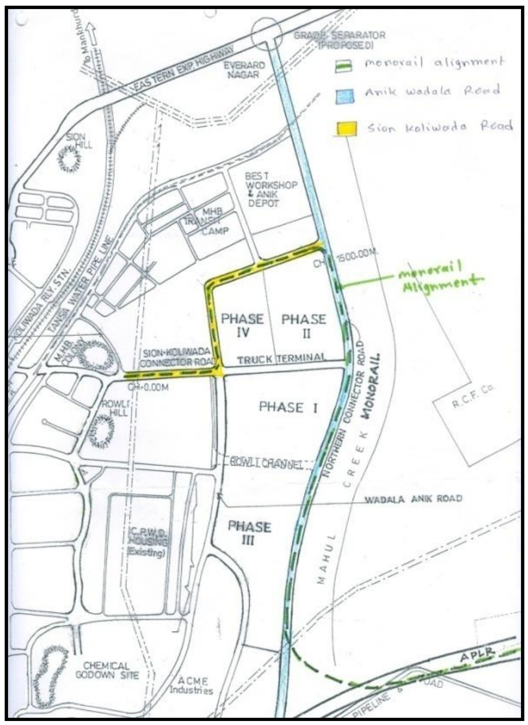

Figure 1 Plan of Monorail Alignment from Wadala Station to Mysore Colony Station

FIELD AND LABORATORY INVESTIGATIONS

Selection of bore holes

The sub-soil investigations were carried out by M/s Soiltech (India) Pvt. Ltd, Pune at five boreholes in the median portion of the road stretch. These borehole locations are presented in Table 1 and locations are marked in Figure 3. The locations of bore holes have been distributed in such a way so as to cover the entire alignment of the proposed stretch of Monorail project.

Figure 2a Distress and Cracking of PQC slabs around Monorail pillars (Anik-Wadala Road)

Figure 2b Distress in PQC slabs around Monorail pillars (Sion-Koliwada Road)

Table - 1 Location of Bore Holes

Bore Hole No	Located Between Piers Nos	Remarks
BH – 1	32 - 33	Main road (Anik - Wadala Road, near IMAX Cinema)
BH – 2	24 - 25	Sion - Koliwada road (Behind Wadala Monorail station)
BH – 3	19 - 20	Sion - Koliwada road (Behind Wadala monorail station)
BH – 4	76 - 77	Main Road (Anik - Wadala road)
BH – 5	1L 36a - 37	Wadala Monorail station

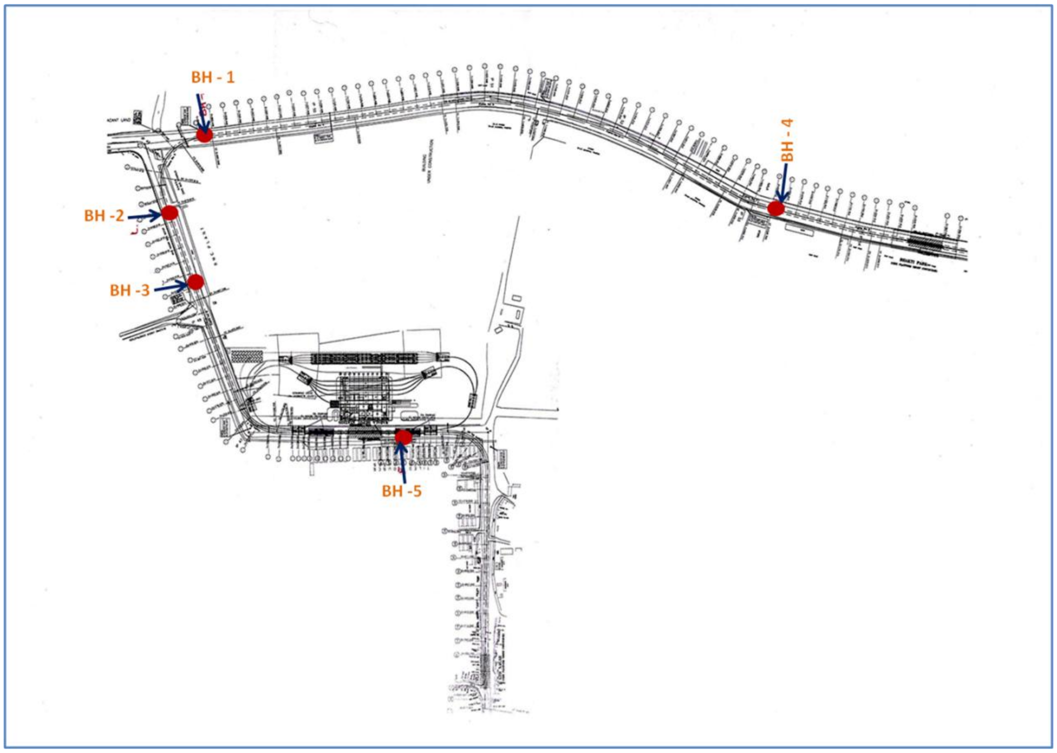

Figure 3 Location of boreholes along the Wadala – Chembur Monorail alignment

Soil profile

The typical bore-log details have been provided in Figure 4. Details of sub-soil layers are presented below:

- ***Fill Material***

  The sub-soil below road pavement has fill material of thickness varying from 3.00 m to 4.50 m. In BH 4, thickness of fill material is about 7.0 m. Fill material comprises of a mixture of soil, boulders and waste refuse materials. Fill material can be classified as Gravelly Clay / Sandy Clay / Sand. This layer is having a good SPT value (>15).

- ***Marine Clay***

  All the boreholes have stiff to very stiff marine clay varying from 5.50 m to 10.0 m thickness except BH 2. In BH 2, soft marine clay of about 7 m thickness was noticed. This soft marine clay is having low SPT value (2 – 5) and high compressibility.

Ground Water

Depth of ground water table in the boreholes varied from 2.5 m to 2.8 m from present finished road top level.

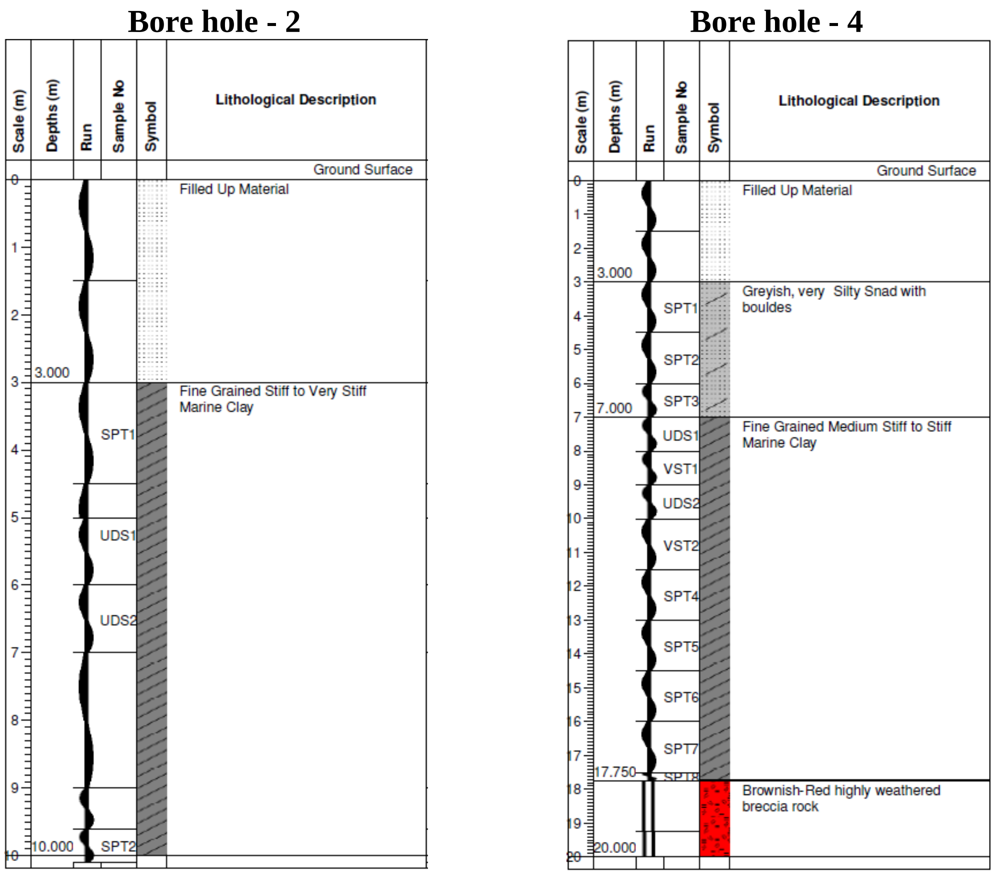

Figure 4. Typical bore-log details

Laboratory Investigations

Two typical undisturbed samples (Sample - 1 is very soft marine clay and sample - 2 is very stiff marine clay) collected from boreholes were tested and their geotechnical properties are presented in Table 2.

Table 2 Geotechnical properties of clay samples

Geotechnical properties	Sample - 1	Sample - 2
Specific gravity (Gs)	2.70	2.69
In-situ moisture content (%)	73	50
Liquid limit (%)	120	110
Plastic Limit (%)	41	41
Plasticity Index (%)	79	69
Shear Strength (kPa)	22	35
Sensitivity	1.22	1.12

SETTLEMENT ANALYSIS

The bore-log data locations selected for analysis is shown in Map 1. To determine the compressibility characteristics of soils, one dimensional consolidation test have been carried out on undisturbed soil samples collected at selected depths and the results are presented in Table 3.

Map1: Bore-log locations selected for settlement analysis

Table 3 consolidation characteristics of soil samples

Property	Sample - 1	Sample - 2
Initial Void ratio (e_0)	1.973	1.438
Compression Index (C_c)	0.59	0.38
Bulk density (kN/m^3)	15.6	16.6

The settlement analysis has been carried based on data from table 3 and bore-log data from DPR reports (RITES Ltd) and latest bore-log data from Soiltech (India) Pvt. Ltd, Pune. The other data considered for settlement analysis as follows

Average density of pavement layers - 20 kN/m^3
Dead load + Live load due to pavement - 24 kN/m^3
Water table is 1 m below the existing road top level.
Terzahgi's equation for settlement calculation due to one dimensional consolidation

$$S_c = \sum_{i=1}^{n} \frac{C_{ci} H_{oi}}{1+e_{oi}} \log\left(\frac{\sigma'_{vfi}}{\sigma'_{voi}}\right) \qquad \text{----------------------------------} (1)$$

Where S_c = total settlement

C_{ci} = Compression index of respective layer
H_{oi} = Thickness of respective layer
E_{oi} = Initial void ratio of respective layer
$\sigma_{v'fi}$ = final vertical effective stress of respective layer
$\sigma_{v'oi}$ = Initial vertical effective stress of respective layer

The results of settlement calculations for various borehole locations are presented in Table 4a and 4b.

PROBABLE REASONS FOR DISPLACEMENT / SETTLEMENTS IN PQC SLABS

Based on the field study, other technical data provided by MMRDA and laboratory studies the following observations can be made:

- The Monorail structure (Pear, Pile cap and Piles) is intact and the structure has been designed for a settlement ≤10 mm.
- Since monorail operations are going on unhindered, this indicates no differential settlement of monorail track.
- Before construction of existing concrete pavement in Sion-Koliwada Connector road, ground improvement using stone columns was undertaken. The design of stone column was verified and it was found to be conforming to IS 15284 (part 1) - 2003.
- It may also be noted that, provision of stone columns accelerates the rate of settlement. Also, stone columns help in reducing the total settlement, but they cannot completely eliminate consolidation settlements (IS 15284 (part 1) - 2003).
- Difference in elevation between PQC panels located just adjacent to monorail piers (0.5 m) and panels away from piers (9.5 m away from median) was obtained through levelling by MMRDA in October 2010 and February 2015. This level difference as reported varies from 250 to 550 mm at different chainages in this stretch.
- Analyzing these aspects, it emerges that soft marine sub-soil found in this stretch has undergone consolidation settlement due to load imposed by fill soil and pavement. The monorail piers and pier cap did not settle since they have been rested on piles which rest on hard stratum (Basalt Rock). As a result, PQC slabs which are resting on monorail pier pile caps stayed at their original position while all other slabs away from piers gradually settled. Hence, it appears as though PQC slabs near Monorail piers have suffered upheaval.
- By considering the level differences already recorded (settlements) in the field and the settlements calculated based on sub-soil properties, it can be seen that about 85 per cent of the degree of consolidation has already occurred in the field. Hence, it is expected that further settlements / increase in level differences between PQC slabs near the pier and PQC slabs away from pier would be minimal.

Table 4a: Settlement of the existing road along the monorail alignment

Bore Hole No	Thickness of			Settlement of (mm)		Total settlement (mm)	Remarks
	Fill (m)	Soft clay(m)	Stiff clay (m)	Soft clay (m)	Stiff clay (m)		
1	3	6	0	0.325	0.000	325.1	Bore hole locations are shown in map1.
2	4	3.5	3	0.187	0.102	289.4	

3	3	8.5	0	0.418	0.000	417.9	Bore-log data taken from DPR reports (FUGRO Geotech Pvt. Ltd, Navi Mumbai, India).
4	3	6	2.5	0.325	0.081	406.6	
5	3	7	2	0.364	0.063	427.0	
6	0.5	6.5	3	0.486	0.117	603.4	
7	4.5	4.5	2	0.219	0.064	282.8	
8	3	6	4.5	0.325	0.137	462.2	
9	2.6	6.4	4.5	0.358	0.138	496.1	
10	4.5	4.5	7.5	0.219	0.202	420.6	
11	4.5	6	5	0.277	0.134	411.0	
12	2	10	0	0.518	0.000	517.7	
13	3	9	1.5	0.434	0.043	477.2	
14	4.5	7.5	2	0.329	0.054	383.3	
15	1.5	7.5	0	0.459	0.000	459.1	
16	4.5	5.5	0	0.258	0.000	258.1	
17	4.7	5.8	0	0.264	0.000	264.1	
18	3	9	1	0.434	0.029	463.4	
19	3	7.5	1.5	0.383	0.046	429.3	
20	4.5	6	0.5	0.277	0.015	292.1	
21	4.5	6.5	0	0.295	0.000	294.7	
22	4.5	6	0.5	0.277	0.015	292.1	
23	4.5	6	0.5	0.277	0.015	292.1	
24	4.5	6	0.5	0.277	0.015	292.1	
25	3	6	1	0.325	0.034	359.5	
26	4.5	6	0	0.277	0.000	276.7	
27	4.5	7.5	0	0.329	0.000	328.9	
28	4.5	7.5	0	0.329	0.000	328.9	
29	3	9	0.5	0.434	0.015	449.2	
30	6	7.5	0	0.288	0.000	288.4	
31	4.5	9	0	0.376	0.000	376.2	
32	4.5	9	0	0.376	0.000	376.2	
33	6	6	1.5	0.241	0.040	281.2	
34	7.5	3	3.5	0.116	0.092	208.3	
35	6	6	1	0.241	0.027	268.2	

Table 4b: Settlement of the existing road along the monorail alignment (Contd..)

Bore Hole No	Thickness of			Settlement of (mm)		Total settlement (mm)	Remarks
	Fill (m)	Soft clay(m)	Stiff clay (m)	Soft clay (m)	Stiff clay (m)		
36	4.5	6	4.5	0.277	0.123	399.3	Bore hole locations are shown in map1. Bore-log data taken from DPR reports (FUGRO Geotech Pvt. Ltd, Navi
37	4.5	6	4.5	0.277	0.123	399.3	
38	7.5	6.5	3.5	0.228	0.079	307.5	
38	6	3	6	0.132	0.163	295.7	

40	4.5	11	0	0.433	0.000	432.8	Mumbai, India)
41	4	6.5	1.5	0.310	0.045	355.0	
42	4.5	6	4.5	0.277	0.123	399.3	
-	3.5	4	9	0.222	0.255	476.9	Anik – wadala
-	3	8	4.1	0.401	0.114	514.5	Anik – wadala
-	2.3	3.7	2.6	0.244	0.105	348.7	near Bakti park
-	2.3	3.65	3.05	0.241	0.121	362.3	Anik – wadala
-	2.35	3.6	2.05	0.237	0.085	321.7	Anik to Mysore colony
-	2.1	8.4	0	0.458	0.000	458.4	Madhuban
-	2.2	12.5	0	0.578	0.000	578.0	Bakti Park
-	4.5	0	5.5	0.000	0.205	204.6	between pier 32 - 33
-	3	7	0	0.364	0.000	364.4	between pier 24 - 25
-	3	0	7	0.000	0.285	284.8	between pier 19 - 20
-	7	0	10.5	0.000	0.271	271.2	between pier 76 - 77

DESIGN OF REMEDIAL MEASURES

The existing level difference between the concrete slabs near the monorail piers and the slabs away from piers has created a safety hazard for traffic movement. All most all slabs near the pier show distress in the form of multiple cracks. Hence, such slabs need to be replaced immediately. For replacing these slabs, various options like reconstruction of PQC slabs, Interlocking Concrete Block Pavement and Flexible pavement are available. It may be noted from tables 4a and 4b that, at different locations the amount of settlement / level difference is varying but after repairs, the road top level for repaired locations and existing slabs should match. This means that thickness of pavement to be reconstructed after dismantling distressed PQC slabs near the piers varies. Further, there should not be any drainage problems due to percolation of water from repaired locations. Looking into these aspects, it is recommended that the PQC slabs which are severely affected near the piers and away from the piers should be dismantled and the whole pavement can be reconstructed using flexible pavement. The thickness of pavement in such case can be designed based on IRC: 37-2012. Since the sub-soil comprises of marine clay and subgarde is made of selected soil (filled up soil), there would be significant difference between the CBRs of the selected subgrade and foundation soils. As per IRC: 37 - 2012, in such a scenario, effective CBR is to be considered for pavement design. Assuming CBR of soft marine clay as 2 per cent, CBR value of filled up material to be 6 per cent, the effective CBR for subgrade would be 5 per cent.

The design of flexible pavement has been carried out based on IRC: 37- 2102. Data assumed for the design is as follows:

Effective CBR of the subgrade = 5 %
Traffic in terms of million standard axles considered for the Main road (Anik - Wadala Road) = 150 msa
The traffic in terms of million standard axles considered for Sion - Koliwada road (Wadala monorail station and behind the station) = 30 msa

To prevent differential settlement and to improve the bearing capacity and drainage of fill material, non-woven geotextile and bi-axial geogrid of ultimate tensile strength 100 kN/m are proposed to be used.

Based on the above data the proposed pavement cross sections of the road for long term measures (reconstruction of affected stretch) is given in Figure 5 and Figure 6 for Anik - Wadla road and Wadala station to main roads respectively. Finally the proposed cross section road level should be matched with existing finished road top levels of the other lane which is stable and not showing any sign of distress. The typical sketch shows the finished road level after implementation of remedial measures is indicated in figure 7.

Construction Procedure

The identified PQC slabs which have developed distress and other pavement layer below the PQC slabs should be removed and the soil should be excavated up to a depth of 780 mm for Anik - Wadala Road (Northern connector road) and 740 mm for Wadala station to Main road (Wadala station and Sion – Koliwada road behind the Wadala Monorail station). The depth mentioned here is from the existing finished road top level (FRL).

- The loose soil in the excavated pit should be compacted by a vibratory roller / plate compactor
- Non woven geotextile layer should be cut to required dimensions and placed inside the excavated portion. The geogrid and geotextile should conform to Section 700 of MORTH Specifications for Road and Bridge Works (Fifth revision - 2013).
- The sand layer should be spread on the top of the geotextile layer and compacted using plate vibrator. Sand should conform IS 383 (Grading Zone III or coarser).
- The construction sequence of different pavement layers as shown in Fig 5 and 6 should be taken up sequentially.
- The pavement layers (GSB, WMM, DBM and BC) shall be constructed as per MoRTH (Ministry of Road Transport and Highways) Specifications for Road and Bridge Works (Fifth revision - 2013).

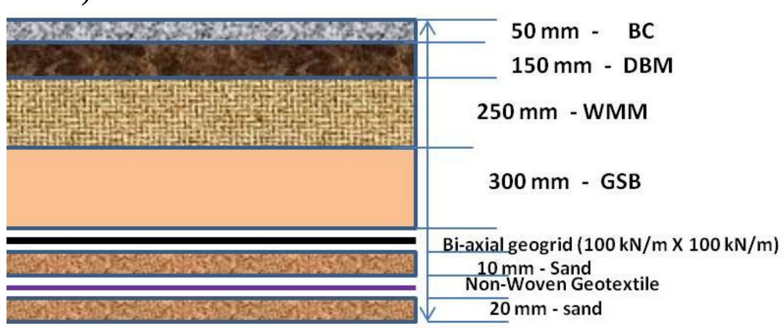

Figure 5 Proposed cross section for Anik - Wadala road (Northern connector road)

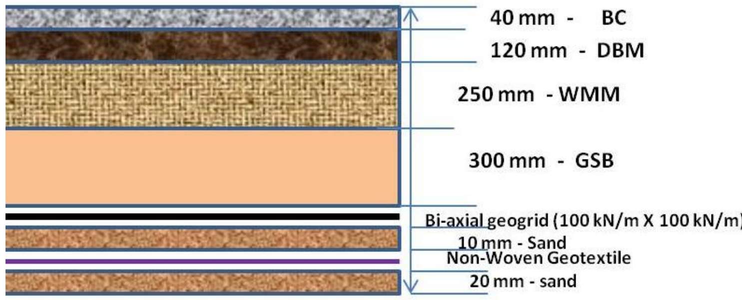

Figure 6 Proposed cross section from Wadala station to Main road(Wadala station and Sion – Koliwada road behind the Wadala Monorail station)

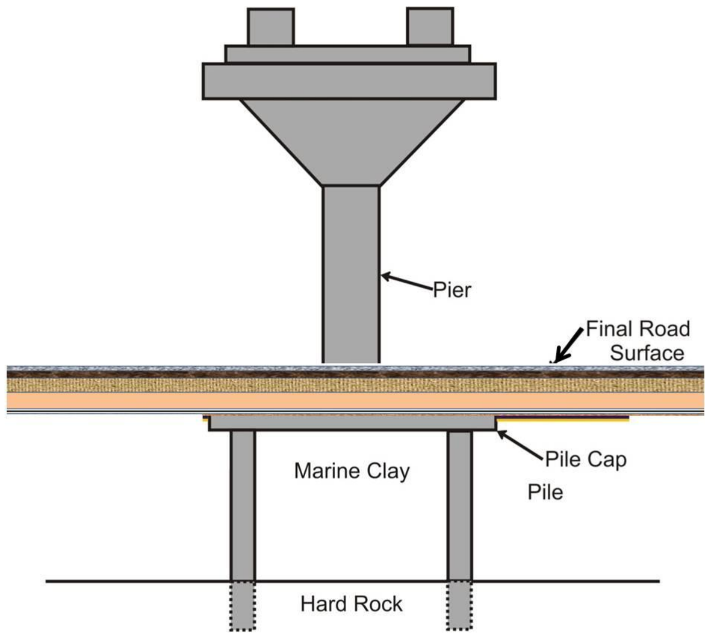

Figure 7 Typical sketch showing the FRL after implementation of remedial measures

CONCLUSIONS

The cement concrete pavement near the monorail piers is severely distressed and cracked, while the concrete panels away from the piers are intact. From the settlement analysis it was observed that the distress and cracking of cement concrete pavement is due to consolidation (settlement) of soft marine clay sub-soil.

The observed level difference (from surveying) between the concrete slabs near the monorail piers and the slabs away from piers (varies from 250 to 550 mm) are matching with the current settlement analysis.

It was noted from observed settlements in the field and the settlements estimated based on sub-soil properties, about 85 per cent of the degree of consolidation has already been occurred in the field. Hence, further settlements would be minimal.

Since the sub-soil comprises of soft marine clay and subgarde is made of filled up soil, effective CBR is considered for pavement design. The design of flexible pavement has been carried out based on IRC: 37- 2102.

To prevent differential settlement and to improve the bearing capacity bi-axial geogrid are proposed as a basal reinforcement.

ACKNOWLEDGEMENTS

The work reported in this paper was taken up by CSIR - CRRI at the request of Mumbai Metropolitan Region Development Authority (MMRDA). Authors are thankful to MMRDA for sponsoring this study. The cooperation and help extended by several officers of MMRDA to CRRI team is gratefully acknowledged. Authors are thankful to Prof. Satish Chandra, Director, CSIR - CRRI for his kind permission to publish this paper.

REFERENCES

CSIR – CRRI report (2015). “Design of remedial measures for upheaval of PQC panels adjacent to piers of monorail in Mumbai”, New Delhi.

IRC: 37 (2012). “Tentative guidelines for design of flexible pavements”

IS 383 (1970). "Specification for coarse and fine aggregates from natural sources for concrete (Second revision)"

IS 15284 (2003). Design and construction for ground improvement-Guidelines. Part 1: Stone columns. 267-290.

MoRTH (Ministry of Road Transport and Highways)(2013). “Specifications for Road and Bridge Works (Fifth revision)”

Response Modification Factor for Soil Structure Interaction of Multistoried Buildings: Myths and Facts

Aly K. Author, M.Tech.,[1] Antony Balan, Co-Author, Ph.D.,[2] V Mustafa, Co-Author, Ph.D.,[3]

[1] Research Scholar, Karunya University, Coimbatore, T N and Executive Engineer, Local self Govt. Dept. Kerala , India. alykothur@yahoo.co.in
[2] Former Professor, Karunya University, Coimbatore, T N and Former Chairman Central water Commission, India. thadicaran@hotmail.com
[3] Professor , Department of Civil Engineering, National Institute of Technology, Calicut, Kerala, India. mustafa@nitc.ac.in

ABSTRACT

In the seismic evaluation and risk assessment of existing as well as proposed multistoried buildings, the strength reduction factor had an important role, especially in highly seismic area. The strength reduction in multi storied buildings will be determined by the difference between the ultimate shear force at the tip of the foundation and the seismic force at the bottom. SRF were not well defined by various authors and contribute in different way without uniformity among various researchers. It is also noticed that researchers are sticking on their own definitions to verify their results in the academic world. The typical values given in codes of developed countries can't be applied to developing countries irrespective of ground motion, site conditions, ductility demand etc. The various codes provide values for strength reduction factor depending on type of structure, namely moment resisting frames with or without shear wall/ load bearing, steel, Rcc/Masonry structure. More over it is further to be noted that the structural engineers presumes that the foundations are rigid and heavy whereas geotechnical engineers in vice versa. International codes ATC, FEMA,UBC,IBC and Current codes {IS1893(PART1&2)} etc emphasize the need for evaluating SSI if the structure is resting on other than rocky or rock like material having SPT -N value less than 50. In this paper, the need for seismic assessment, performance evaluation and hazard mitigation using SRF along with inconsistencies of structural and geotechnical engineers are discussed. It is worthwhile to notice that India is not yet having any codes on response reduction factor for SSI. However the forensic geotechnical engineering principles can be wisely utilized for evaluation, testing and control of technical and legal aspects of seismic assessment and Damage analysis of multistoried buildings.

KEY WORDS: Seismic Evaluation, Multistoried Buildings, Strength Reduction Factor (SRF), International Codes, Soil Structure Interaction

INTRODUCTION

Current seismic provisions allow nonlinear response of building structures in the event of strong ground motions due to economic factors. As a matter of such a design approach, strength reduction factor ($R\mu$) which is the ratio of elastic base shear to the one required for a target ductility level are used in seismic design codes. Most of the seismic design codes currently applied in structural design do not take into consideration the soil structure phenomenon. It has been known for many years that soil structure interaction affects the elastic strength demand of structures because of the longer period and higher damping ratio of interacting system compared to the fixed base case. However, soil structure interaction effects on inelastic displacement ratios and strength reduction factors ,especially for multi storey structures have not been the topic of comprehensive researches, yet. Strength reduction factors have been the topic of several investigations so far. The first well known studies on strength reduction factors were conducted by Veletsos and Newmark and Newmark and Hall. They proposed formulas for strength reduction factors as functions of structural period and displacement ductility to be used in the short-, medium- and long period regions. Alternative formulas were proposed by Lai and Biggs and Riddell et al. The first study that considered the effects of soil conditions on the strength reduction factors was conducted by Elghadamsi and Mohraz . Another study which considered the site effects on the strength reduction factors was conducted by Nassar and Krawinkler, also considering the effects of yield level, strain hardening ratio and the type of inelastic material behavior. More recently, Miranda studied the influence of local site conditions on strength reduction factors, using a group of 124 ground motions classified into three groups as; ground motions recorded on rock, alluvium and very soft soil. During last decade, soil-structure interaction effects on strength reduction factors have been the topic. Many earthquake prone countries in the world have significant amount of existing deficient buildings to be evaluated for seismic actions. Although nonlinear methods are more preferable for assessment of existing buildings, most of the practicing engineers are unfamiliar to these methods. Therefore, linear methods seem to be in use in the near future for assessment of great number of deficient existing buildings in a reasonable time. In linear methods, nonlinear behavior is taken into account by a single parameter: strength reduction factor (R).

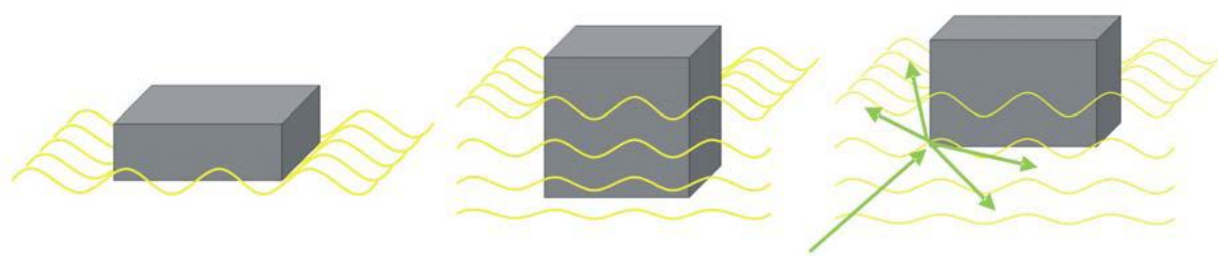

Figure 1: Averaging effect (Left), Decreasing motion amplitude with depth (centre), Wave scattering at the corners (right)

SOIL-STRUCTURE MODEL

The soil-foundation element is modeled by an equivalent linear discrete model based on the cone model with frequency-dependent coefficients and equivalent linear elastic properties (Wolf, 1994). Cone model based on the one-dimensional wave propagation theory represents circular rigid foundation with mass and area moment of inertia resting on a homogeneous half-space. The simplified cone model can be used with sufficient accuracy in engineering practice (Wolf, 1994). A typical MDOF soil-structure system and the corresponding E-SDOF system are shown in Fig. 2.The sway and rocking DOFs are defined for translational and rotational motions of the foundation, while the vertical and torsion movement of the foundation are neglected. The stiffness and energy dissipation of the supporting soil are modeled by springs and dashpot, respectively.Soil material damping is assumed as commonly used viscous damping so that more intricacies in time-domain analysis are avoided. All coefficients of springs and dashpots for sway and rocking motions used to define the soil-foundation model in Fig. 2

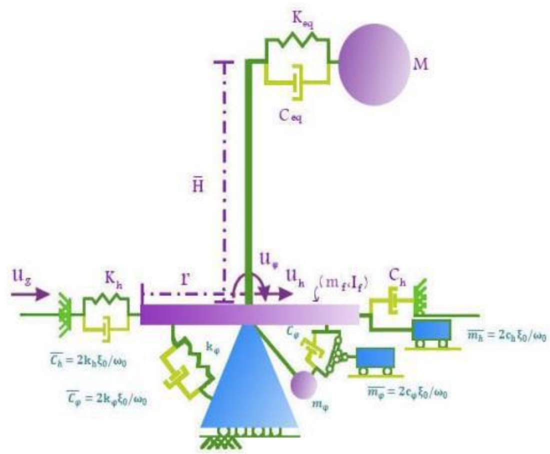

Fig.2a

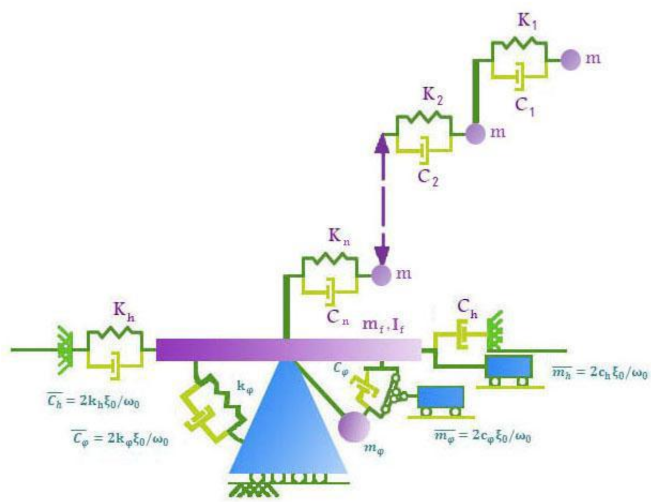

Fig. 2b

Figure 2: Soil-structure models for sway and rocking motions (a) E-SDOF system (b) Typical MDOF system

TERMINOLOGY: In design codes the considered seismic force used to dimensioning the structural elements is multiplied by several coefficients, in order to simplify the design process. One of them is the reduction factor. In the following are presented different ways to evaluate the values for the behavior factor in some seismic design codes. The behavior factor of the response is computed as a product of three factors. Where *RS* is the strength reduction factor, *R*μ- the ductility reduction factor, *R*ξ − the damping reduction factor. In the ATC-19 meeting from 1995 the damping reduction factor was not taken into consideration being replaced by the redundancy reduction factor, *RR* The values of the strength reduction factor are determined by

a) the strength characteristics of the materials;

b) the use of the response spectrum in the seismic computations;

c) column design to the seismic action on two directions; along one is applied 100% of the seismic force, and along the orthogonal one only 30% of the seismic force

Table 1

The Strength Reduction Factor for Reinforced Concrete Structures

Structural type	RS
Rc structures medium and high in elevation	1.6…4.6
Rc structures with irregularities in elevation	2.0…3.0

The strength reduction factor *RS*, is computed as the difference between the seismic force at the bottom *Vb*, and the ultimate shear force at the bottom *Vu.* The values of this factor, depending on the height of the structure, are presented in Table 1

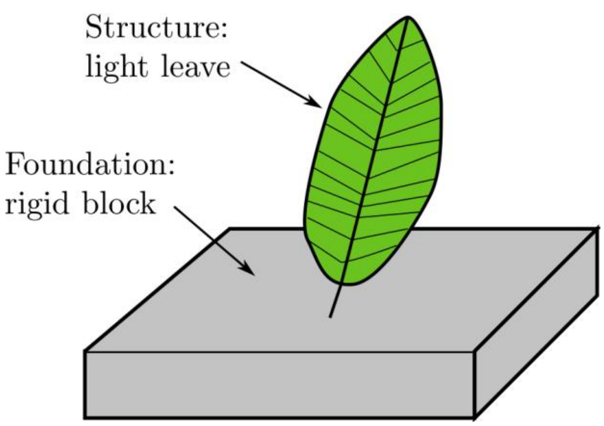

Fig 3 structural engineer's point of view

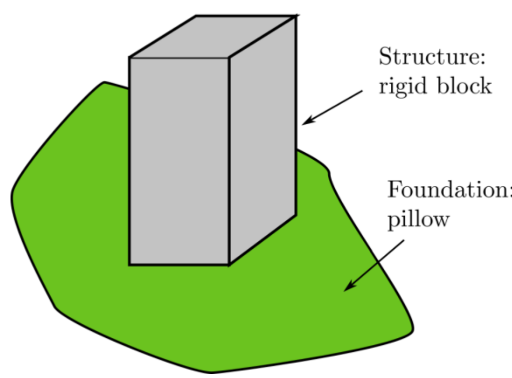

Fig 4 Geotechnical engineer's point of view

BEARING CAPACITY FOR SHALLOW FOUNDATIONS

Once the forces transmitted to the soil by the foundation are determined, the design engineer must check that these forces can be safely supported: the foundation must not experience a bearing capacity failure nor excessive permanent displacements. At this point a major difference appears between static, permanently acting loads, and seismic loads. In the first instance excessive loads generate a general foundation failure whereas seismic loads, which by nature vary in time, may induce only permanent irrecoverable displacements. Failure can therefore no longer be defined as a situation in which the safety factor becomes less than unity; it must rather be defined with reference to excessive permanent displacements which impede the proper functioning of the structure. Although this definition seems rather simple and the methodology has been successfully applied to dam engineering (Newmark, 1965), its implementation in a code format is far from an easy task. One of the difficulties is to define what are acceptable displacements of the structure in relation to the required performance. Another difficulty obviously lies in the uncertainty linked to the estimation of permanent displacements.

FUNDAMENTAL REQUIREMENT OF CODE APPROACHES

As an example of code documentation Eurocode 8 states that "The stability against seismic bearing capacity failure taking into account load inclination and eccentricity arising from the inertia forces of the structure as well as the possible effects of the inertia forces in the supporting soil itself can be checked with the general expression and criteria provided in annex F. The rise of pore water pressure under cyclic loading should be considered either in the form of undrained strength or as pore pressure in effective stress analysis. For important structures, non linear soil behavior should be considered in determining possible permanent deformation during earthquakes."More specifically, in most seismic codes the design engineer is required to check the following general inequality :

$Sd \leq Rd$ (1) where Sd is the seismic design action and Rd the system design resistance.

The design action represents the set of forces acting on the foundations. For the bearing capacity problem, they are composed of the normal force Nsd , shear force Vsd , overturning moment Msd and soil inertia forces F developed in the soil. The actions Nsd, Vsd, and Msd arise from the inertial soil-structure interaction. The inertia force, $F = \rho a$ (ρ mass density, a acceleration), arises from the site response analysis and kinematic interaction. The term design action is used to reflect that these forces must take into account the actual forces transmitted to the foundation i.e. including any behavior and over-strength factors used in inelastic design. The design resistance represents the bearing capacity of the foundation; it is a function of the soil strength, soil-foundation interface strength and system geometry (for instance foundation width and length). Obviously, inequality) must include some safety factors. One way is to introduce partial safety factors, as in Eurocode 8. This is not the only possibility and some other codes, like the New Zealand one, choose the Load and Resistance Factored Method (LRFD) and factor the loads and resistance (Pender,1999). The Eurocode approach is preferred because it gives more insight in the philosophy of safety; on the other hand it requires more experimental data and numerical analyses to calibrate the partial safety factors. With the introduction of partial safety factors inequality is modified as follows:

$$Sd(\nu f, \text{actions}) \leq Rd(\underline{\text{Strength parameters}}, \text{Geometry})$$
$$\nu rd \qquad\qquad \nu m$$

where "actions" represent the design action and "strength" the material strength (soil cohesion and /or friction angle, soil-foundation friction coefficient); νF is the load factor applied to the design action: νF is larger than one for unfavorable actions and smaller than 1.0 for favorable ones; γm is the material safety factor used to reflect the variability and uncertainty in the determination of the soil strength. In Eurocode 8, the following values are used: 1.4 on the undrained shear strength and cohesion and 1.25 on the tangent of the soil friction angle or interface friction coefficient; γRd is a model factor. It acts like the inverse of a strength reduction factor applied to the resistance in an LRFD code. This factor reflects the fact, that to evaluate the system resistance some approximations must be made: a theoretical framework must be developed to compute the resistance and like any model it involves simplifications, and assumptions which deviate from reality. It will be seen later on that the model factor is essential and can be used with benefit to differentiate a static problem from a seismic one.

INCONSISTENCIES BETWEEN GEOTECHNICAL & STRUCTURAL ENGINEERS

Clear lines of communication between geotechnical and structural consultants is a key component of a successful foundation design. Poor communication can lead to misunderstandings and poor design outcomes i.e. overly conservative foundation designs, or worse, unsatisfactory foundation performance. Often it is found that geotechnical and structural engineers have different performance objectives in mind, or simply do not clearly understand what each discipline contributes or is able to contribute to the design process, or what actually matters for design. A common source of misunderstanding between geotechnical and structural consultants is the differing terminology used to describe design parameters. Table 2 illustrates some common examples.

Another example of potentially misleading terms is present in B1/VM4 where Section 3.3.2 (entitled 'Ultimate bearing strength') covers the topic of bearing capacity. Although the units of both are pressure (force/area), the strength and capacity of a soil mass are very different properties that should not be confused. Furthermore, there is more than one type of strength that can be determined for a soil sample and there are several different capacity definitions e.g. gross, net, total, effective, ultimate, safe, allowable, and presumed. In some cases the differing terminologies are easy to translate; in other situations it can be less clear. The authors know of more than one occasion when a structural engineer has inadvertently used the ultimate geotechnical capacity to size a foundation element. There is a clear need to develop a common set of terms that can be used by both structural and geotechnical consultants to design foundation systems. This could be included in future Building Code compliance document revisions or as a Technical Memo. A course could be run to cover these issues to provide important Continuing Professional Development.

CAPACITY DESIGN

Another aspect of building design that is not well understood by all parties is application of over strength design actions associated with "capacity" design. Capacity design is a design process whereby distinct elements of a structural system are chosen, and suitably designed and detailed for energy dissipation during a major earthquake. All other structural elements are then protected against actions that could cause failure. This is done by providing those elements with a greater strength than that corresponding to the development of the energy dissipating mechanisms selected for the building (Paulay & Priestley 1992). When capacity design principles are used, the over strength design actions on foundation elements, Ro, can be calculated as:

$$Ro = \acute{\O}oRu$$

Table 2

Terminology used to describe common design parameters NZS 1170 Terminology	**Common alternative wording or interpretations of the NZS1170 terms**
ULS design action, Rv	Fully factored loads, ultimate design loads
Nominal capacity (5th percentile), Rn	Unfactored capacity, ultimate capacity, ultimate strength, ultimate geotechnical capacity
ULS design capacity, vRn	Design capacity, allowable ultimate capacity, geotechnical limit state design strength, allowable capacity
Over strength design action, Ro Strength reduction factor, R SLS design action, Rs	Over strength load vSFR, Factor of safety Un factored loads, SLS design load

where Ro = over strength factor and Ru = ULS design action. For a simple cantilever reinforced concrete shear structure the over strength factor, Ro, for used for the foundation design is calculated as:

$$\acute{Ø}o = \acute{Ø}(o,fy)Mn/Mu$$

where Ro,fy = material over strength factor which accounts for the difference between the 5th percentile material strengths and the “maximum-feasible” strengths which are higher due to strain hardening and other related factors (refer NZS 3101); Mn = the nominal flexural capacity of the wall calculated using 5th percentile strengths; and Mu = ULS design bending moment for the element. For conventional reinforced concrete walls with G300 reinforcing steel Ro,fy = 1.25. In typical design situations Ro typically lies in a range of between 1.5 to 2.5. It is worth noting that the material over strength factors, Ro, fy, used by structural engineers have been determined by means of a statistical analysis. This means that in practice, like other ULS design load cases (i.e. wind), foundation systems may experience loads that are greater than that determined using capacity design. Following submissions to, and reporting by, the Canterbury Earthquake Royal Commission, SESOC is developing structural design guidance including advice and recommendations on foundation design, including, for example, that designers should no longer use the higher strength reduction factors permitted in B1/VM4 for load combinations involving earthquake over strength design action

PERFORMANCE EVALUATION

Performance evaluation of the investigated buildings is conducted using recently published Turkish Earthquake Code (2006). Three levels, Immediate Occupancy (IO), Life Safety (LS), and Collapse Prevention (CP) are considered as specified in this code and several other international guidelines such as FEMA-356, ATC-40. Criteria given in the code for three performance levels are listed below.

PERFORMANCE LEVEL / PERFORMANCE CRITERIA

Immediate Occupancy (IO)

1. There shall not be any column or shear walls beyond IO level.
2. The ratio of beams in IO-LS region shall not exceed 10% in any story.
3. There shall not be any beams beyond LS.

Life Safety (LS)

1. In any story, the shear carried by columns or shear walls in LS-CP region shall not exceed 20% of story shear. This ratio can be taken as 40% for roof story.
2. In any story, the shear carried by columns or shear walls yielded at both ends shall not exceed 30% of story shear.
3. The ratio of beams in LS-CP region shall not exceed 20% in any story.

Collapse Prevention (CP)

1. In any story, the shear carried by columns or shear walls beyond CP region shall not exceed 20% of story shear. This ratio can be taken as 40% for roof story.
2. In any story, the shear carried by columns or shear walls yielded at both ends shall not exceed 30% of story shear.
3. The ratio of beams beyond CP region shall not exceed 20% in any story.

Figure 4: Shear failure typical of poor construction of a beam-column joint (Galli, 2005)

APPENDIX: Classification of Damage According to EMS 98

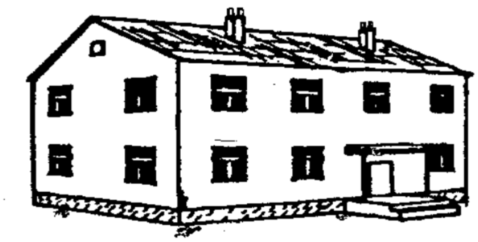	**Grade 1: Negligible to slight damage** **(no structural damage,** **slight non-structural damage)** Hair-line cracks in very few walls. Fall of small pieces of plaster only. Fall of loose stones from upper parts of buildings in very few cases.
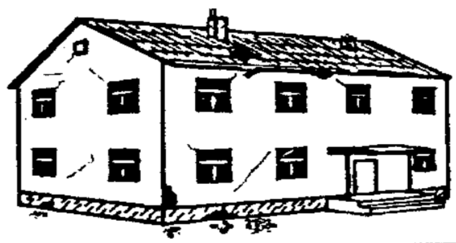	**Grade 2: Moderate damage** **(slight structural damage, moderate non-structural damage)** Cracks in many walls. Fall of fairly large pieces of plaster. Partial collapse of chimneys.
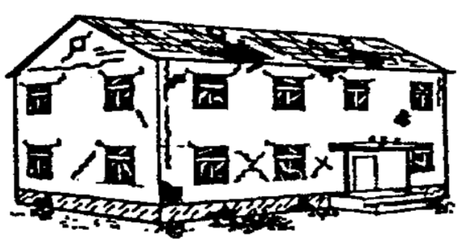	**Grade 3: Substantial to heavy damage** **(moderate structural damage,** **heavy non-structural damage)** Large and extensive cracks in most walls. Roof tiles detach. Chimneys fracture at the roof line; failure of individual non-structural elements (partitions, gable walls).
	**Grade 4: Very heavy damage** **(heavy structural damage,** **very heavy non-structural damage)** Serious failure of walls; partial structural failure of roofs and floors.
	**Grade 5: Destruction** **(very heavy structural damage)** Total or near total collapse.

A1.1 Classification of Damage to Masonry Buildings

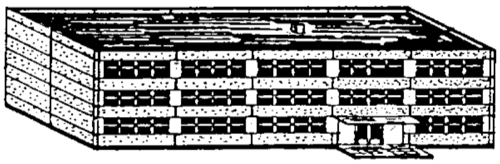	**Grade 1: Negligible to slight damage** **(no structural damage,** **slight non-structural damage)** Fine cracks in plaster over frame members or in walls at the base. Fine cracks in partitions and infills.
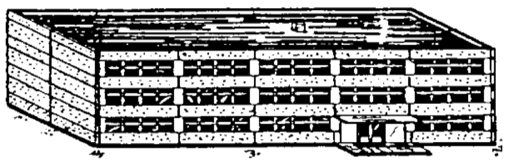	**Grade 2: Moderate damage** **(slight structural damage,** **moderate non-structural damage)** Cracks in columns and beams of frames and in structural walls. Cracks in partition and infill walls; fall of brittle cladding and plaster. Falling mortar from the joints of wall panels.
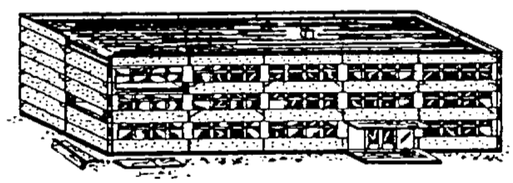	**Grade 3: Substantial to heavy damage** **(moderate structural damage,** **heavy non-structural damage)** Cracks in columns and beam column joints of frames at the base and at joints of coupled walls. Spalling of conrete cover, buckling of reinforced rods. Large cracks in partition and infill walls, failure of individual infill panels.
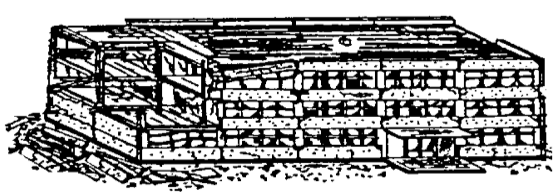	**Grade 4: Very heavy damage** **(heavy structural damage,** **very heavy non-structural damage)** Large cracks in structural elements with compression failure of concrete and fracture of rebars; bond failure of beam reinforced bars; tilting of columns. Collapse of a few columns or of a single upper floor.
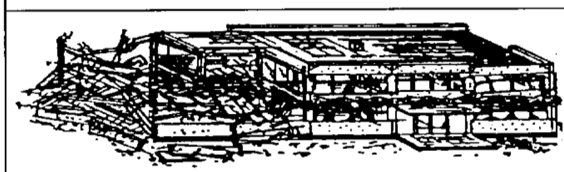	**Grade 5: Destruction** **(very heavy structural damage)** Collapse of ground floor or parts (e. g. wings) of buildings.

Figure A1.2: Classification of Damage to RCC Buildings [EMS 98]

CONCLUSION

Non uniformity in definition, design standards, and code provisions for various countries increases the demand for International uniform soil structure interaction code, like International Uniform Building Code. The inconsistency among structural and geotechnical engineers would be solved at the root level with top priority. The gap developed between different study and research groups may be controlled and monitored by making use of Forensic Geotechnical Engineering principles. Countries like India need to develop Standards to response modification (strength reduction factor) factor for ssi of bridges, vaults and under tunnels, towers etc, with special emphasis for high rise buildings.

REFERENCES

Alain Pecker1 and Michael j. Pender2 “Earthquake Resistant Design of Foundations:New Construction” 1Géodynamique & Structure, Bagneux, France.2 Department of Civil and Resource Engineering, University of Auckland, New Zealand

B. Ganjavi & H. Hao, “Ductility Reduction Factor for Multi-degree-of-freedom systems with soil-structure interaction”, School of Civil and Resource Engineering, The University of Western Australia, 35 Stirling Highway, Crawley, WA 6009, Australia

H. J. Shah, Dr. Sudhir K Jain, Document No .IITK-GSDMA-eq26-v3.0 Final Report A - Earthquake Codes iitk-gsdma Project on Building Codes, “Design Example of a Six Storey Building”, Department of Applied Mechanics, M. S. University of Baroda, Vadodara, Department of Civil Engineering, Indian Institute of Technology, Kanpur

H.M. Rajashekhar Swamy, Krishnamoorthy, D.L. Prabakhara, S.S. Bhavikatti, “Relevance of Interface Elements in Soil Structure Interaction Analysis of Three Dimensional and Multiscale Structure on Foundation”,Prof. and Head, ced, rymec, Bellary-58310 e-mail-swamyraja2005@gmail.com, Prof., ced, mit, Manipal , Principal and Director, scem, Addyar, Mangalore, Prof. Emeritus, BVB college of Engg., Hubli.

Hayri B Ozmen1 and Mehmet Inel 2 The 14th World Conference on Earthquake Engineering October 12-17, 2008, Beijing, China “Evaluation of Strength Reduction Factor for Existing Mid-Rise Rc Buildings” 1 Graduate Student, Dept. of Civil Engineering, Pamukkale University, Denizli. Turkey. Email: hbozmen@pau.edu.tr 2 Assoc. Professor, Dept. of Civil Engineering , Pamukkale University, Denizli. Turkey. Email: minel@pau.edu.tr

IS 1893(Part1):2002 “Indian Standard Criteria for Earthquake Resistant Design of Structures – General Provisions and Buildings (Fifth Revision)”

Muberra Eser Aydemir , “Soil Structure Interaction Effects on Multistorey R/C Structures”, International Journal of Electronics; Mechanical and Mechatronics Engineering vol.2

Stephane Grange, “Simplified modeling strategies for soil-structure interaction problems: The macro-element concept”, Associate Professor, Universite Joseph Fourier/Laboratoire 3sr – Grenoble, stephane.grange@ujf grenoble.fr, October the 5th,2013, Alert Doctoral School, Aussois

Stuart Oliver & John Hare “Soil Structure Interaction Starts With Engineers” Holmes Consulting Group, Christchurch, New Zealand. Nick Harwood Coffey Geotechnics, Christchurch, New Zealand 2013 NZSEE Conference

Forensic Investigation of the Failure of a Marginally Stable Hill Slope

Priyanka Talukdar [1], Ruplekha Bora [2] and Arindam Dey [3]

[1]Department of Civil engineering, IIT Guwahati, email: priyanka.talukdar@iitg.ernet.in
[2]Gammon India Ltd., Kolkata, email: ruplekhabora888@gmail.com
[3]Department of Civil Engineering, IIT Guwahati, email: arindamdeyiitk@gmail.com

ABSTRACT

This paper presents the forensic study of the failure of an existing naturally stable stratified hill-slope, destabilized by seepage and sequential anthropogenic construction activities. The slope, located in the Umrangso region in the Dima Hasao district in the state of Assam, India, was initially in a stable state before any human intervention. However, the site had been chosen to establish various industrial manufacturing units which resulted in a massive mass movement of the slope where deformations were observed nearly approaching the toe of the slope with the progressive stages of construction. Concrete retaining walls constructed to arrest the mass movement did not serve the purpose of protecting the slope, rather added more weight leading to further destabilization of the slope. A forensic geotechnical investigation has been carried with the aid of field and laboratory investigations and subsequently aided by the development of a finite-element based numerical model. Field visits indicated multiple reasons related to the triggering event of the slide, namely (i) absence of any stability check prior to the construction accompanied by no post-construction consequential stability analysis, (ii) heavy monsoon with torrential downpour leading to heavy infiltration, seepage and surface runoff leading to the softening the slope material, and (iii) Adopting stabilization and mitigation techniques without any sound engineering basis. The primary objective of the forensic investigation has been to precisely identify the triggering events and the mechanisms of subsequent destabilization which occurred at the site. This paper illustrates the development of a FE model to simulate the real-field scenario of the progressive construction and slope failure. The analysis had been carried out for both dry and saturated conditions of the slope. Each stage of the numerical model has been validated with the field observation and based on a vivid investigation of the outcome of the analyses the triggering mechanisms for the slope failure have been successfully identified.

KEYWORDS: Forensic investigation, Hill-slope instability, Triggering mechanism, Deformation-based failure, Finite element analysis

INTRODUCTION

Natural hill slopes are subjected to varied conditions of criticality, which are the consequences of either some natural or various human activities. Slope disasters induced by harsh natural conditions such as steep topography, fragile geology, heavy rainfall, river flood and earthquakes inducing mass movements in the form of creep, landslide, subsidence, etc. are a common phenomenon in all natural hill slopes. Amongst all, rain water infiltration or fluctuations in the level of ground water can affect and initiate the disturbance by seepage related activities which is one of the prime concerns. In addition to this, the hill slopes are being used today, in a large scale for the set up of various industries and factories and this results in a lot of construction activities in these slopes. These loading and unloading activities can create a lot of instability problems in hill slopes. Stabilization of unstable slopes can present many challenges to the engineer. To reduce some of the uncertainty, it is critical that the engineer have a clear understanding of the problem prior to the development of a design for the slope stabilization.

Studies have been carried out to find out the relationship between the triggering mechanisms, which initiates the slope instability and the causal factors which are the long term triggers, that finally results in slope failure. Sultan *et al.* (2004) had analyzed different slope failures events from different parts of the Costa target areas, which reflect diverse triggering mechanisms. The study was aimed at identifying the geotechnical response of the sediment to different external mechanisms (earthquake, rapid sedimentation and gas hydrate melting) and to establish the relation between these external mechanisms and the consequent changes in the in-situ stress state and the physical, mechanical, and elastic properties of the sediment. Saxena (2008) reviewed an extensive distress settlement of an office building resulting in visible cracks in the interior of the building in west central Florida as a first case history. In the second one, a forensic geotechnical investigation was undertaken to identify the causative factors of the slope failure and to address its extent of damage. Ering *et al.* (2015) conducted a forensic analysis of Malin landslide in India which resulted in the burial of a village of about 40 houses in western India. The investigation showed that slope failure occurred due to loss of suction between the rock and soil interface; however, heavy rainfall was identified as the triggering mechanism for the mass movement. The slope stability issues related with rainfall induced slope failures were investigated by Collins *et al.* (2004) highlighting the negative and positive pore water pressures coupled with infinite slope analysis method to present a predictive formulation of slope failure that occurred as a result of rainfall. The effects of hydraulic characteristics, initial relative degree of saturation, methods to consider boundary condition, rainfall intensity and duration of water pressure in slopes were investigated by finite element analysis with shear strength reduction technique proposed by Cai *et al.* (2004).

In this paper, a real field study of a naturally marginally stable stratified hill slope destabilized by seepage and sequential anthropogenic construction activities has been carried out. The main objective of this paper is to understand the triggering processes and the subsequent failure mechanism that led to the deformation collapse of the slope. This knowledge would further help in developing the stabilization technique to be adopted for the site.

SITE CONDITIONS

The failure mechanism of the hill slope investigated in this study is located at 25^0 31'04" (N) and $92^0$47'19.3" (E) in Umrangso region in the Dima Hasao district of Assam, India. The terrain in the area is hilly with a maximum temperature of 39.9^0C and minimum temperature of 6.0^0C, with a relative humidity ranging between 60% and 85%. The average annual rainfall of the area is 1672.0 mm and it lies in seismic zone V. The location map of the study area and the specific site in the area used in this study are shown in Fig.1 and Fig.2 respectively.

Figure 1. Location of the study area (http://www.mapsofindia.com/)

Figure 2. Location of the site (http://www.mapcoordinates.net/)

Site characteristics

The field investigation of the area under study approximately presents an idea about the soil stratification present at the site. The top 5 to 6 meters of soil layer is covered by thick stiff to very stiff, silty clay/clayey silt (CI-SC) soil, followed by 1 to 2 meters of thick hard, silty clay/ clayey silt soil beneath it. At the bottom, below the top soil layers, moderately weathered fine grained rock is present. Umrangso is a water scarce region. However, the standing water level was observed to be at a depth of 4m to 6m from the site investigations.

SEQUENCE OF DISTRESS

The site had been chosen to establish various industrial manufacturing units. All the units of the establishment are located on hill-slope with or without any benching. In the vicinity of one of the industrial units, the site (comprising of a slope of height ~55m and lateral extent ~220m) experienced a massive mass movement of soil as a result of the various stages of construction. Significant deformations of large lateral extent were observed which nearly approached the toe of the hill slope.

The sequence of distress was observed based on the site visits and preliminary enquiry at the site. The first slip was observed during July 2015. The foundation columns of the workshop building constructed on the hill slope were exposed due to the erosion of soil mass, resulting from the rainfall and subsequent landslide. The exposed columns of the workshop building were observed to be in distress condition as evident from the cracks in the walls of the building as shown in Fig. 3 and Fig. 4. As a preliminary preventive measure, rubble masonry retaining wall-I was constructed with subsequent backfilling during July-August 2015.

Figure 3. Cracks in the walls of the workshop building

Figure 4. Exposed building columns due to soil movement

Figure 5. Cracks in the floors of the colony building

Figure 6. Cracking in retaining wall-I

Further, during the period of September-October 2015, due to the continued land movement, moderate-to-severe distress was recorded in the buildings of a nearby colony area as shown in Fig. 5. This movement also resulted in the distortions, cracking, and disintegration of the retaining wall-I shown below in Fig. 6. In order to prevent further distress, rubble masonry retaining wall-II was constructed adjacent to the colony area during the month of September-October 2015. However, even with the above preventive measures, the soil movement continued, as a consequence of which retaining walls-III and IV was constructed during October 2015.

FINITE ELEMENT MODELING

Finite element modeling of the slope had been carried out to simulate the real field scenario, as closely as possible, to comprehend the failure triggering mechanisms. The critical slope geometry had been modeled in Geostudio 2007. A scaled-down model has been used wherein the actual horizontal field dimensions have been downscaled by 5, while the vertical dimensions are kept the same as that of the field scenario. Such scaling helps to generate the model stresses and strains at par with that developed in the field while the extent of the deformations in the horizontal directions as obtained from the simulation needs to be multiplied by 5 for obtaining the field extents. The entire soil depth had been classified into four layers among which the top three layers consists of soil varying in stiffness and the bottommost layer consists of impenetrable bedrock. The model of the slope for the present study along with its relevant dimensions is presented in Fig.7.

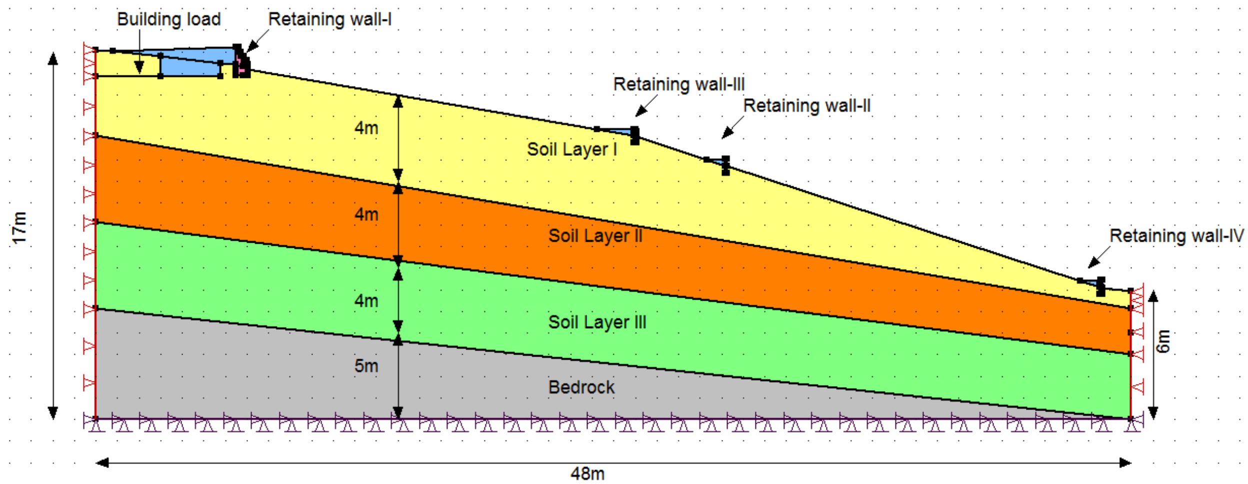

Figure 7. Model slope for the present study

Analyses Methodologies

The entire construction process had been incorporated in this model by considering the various stages of construction, in the same sequence as it was executed in the field. This sequential construction activity was simulated using SIGMA/W module to understand their effects on the progressive destabilization of the slope, and then the corresponding displacement of the slope face and its extent had been studied. In the SIGMA/W analysis after generating the initial stress conditions in the stable slope, the sequential loading and unloading process carried out on the slope in the form of excavation and addition of structures have been modeled stage wise using the load-deformation analysis method. A stress based stability analysis had been performed after every stage of construction with the aid of the SLOPE/W module in GEOSTUDIO 2007 to obtain the corresponding stability values after every stage of construction. The Mohr-Coulomb material model had been assigned for the soil layers in the stability analysis and an impenetrable bed rock had been assigned to the bedrock layer. The entry exit specification had been used to define the slip surfaces in the downstream sections of the slope. The analysis had been carried out for both dry and saturated conditions. The dry state has been analyzed using the total stress parameters and, for the saturated state, effective drained parameters material model had been used. The effect of water had been established at three different levels of the soil by conducting a steady seepage analysis with the SEEP/W module. In the seepage analysis, the fluctuation of water level had been established by using a constant head boundary condition and a 'saturated only' material model had been used for all the soil layers in the slope. The seepage analysis had been assigned as a parent to all other subsequent analysis to incorporate the pore water conditions.

Table 1. Material properties for Case I for Slope/W and Sigma/W analyses

Layer	Material model in Sigma/W	Material model in Slope/W	Cohesion (kPa) c_u	Friction angle φ_u	Cohesion (kPa) c'	Friction angle φ'	E (MPa)	E' (MPa)	Unit weight (kN/m^3)
Soil layer I	Elastic plastic	Mohr Coulomb	18.5	4	12.33	4	4.7	4.2	19
Soil layer II	Elastic plastic	Mohr Coulomb	18.5	4	12.33	4	47.6	42.5	19
Soil layer III	Elastic plastic	Mohr Coulomb	94	4	62.66	4	90.65	81	19

Rock	Linear elastic	Impenetra-ble	-	-	-	-	683	610.4	24.1
Retaining wall	Linear elastic	Impenetra-ble	-	-	-	-	17000	15194	29

Table 2. Material properties for Case II for Slope/W and Sigma/W analyses

Layer	Material model in Sigma/W	Material model (in Slope/W)	Cohesion (kPa) c_u	Friction angle φ_u	Cohesion (kPa) c'	Friction angle φ'	E (MPa)	E' (MPa)	Unit weight (kN/m^3)
Soil layer I	Elastic plastic	Mohr Coulomb	18.5	4	12.33	4	4.7	4.2	19
Soil layer II	Elastic plastic	Mohr Coulomb	94	4	62.66	4	47.6	42.5	19
Soil layer III	Elastic plastic	Mohr Coulomb	94	4	62.66	4	90.65	81	19
Rock	Linear elastic	Impenetra-ble	-	-	-	-	683	610.4	24.116
Retainin g wall	Linear elastic	Impenetra-ble	-	-	-	-	17000	15194	29

Table3: Model parameters for Case I and Case II for SEEP/W analysis

Layer	Material model (in SEEP/W)	Saturated Conductivity (m/sec)	Saturated Volumetric water content (m^3/m^3)
Soil layer I	Saturated Only	3×10^{-8}	0.425
Soil layer II	Saturated Only	3×10^{-8}	0.425
Soil layer III	Saturated Only	3×10^{-8}	0.425
Rock	Saturated Only	2×10^{-10}	0.087
Retaining wall	Saturated Only	3×10^{-13}	0.33

Material Properties

The various properties pertaining to the real field slope used in the modeling had been collected based on the different field and laboratory geotechnical investigations. To account for the possible soil stratification, two different cases had been analyzed and studied by varying the strength parameters of the soil layers, aptly by varying the cohesion values that prevail in the real field. The material properties used in the modeling for analyzing both the cases had been presented in Table 1 and Table 2. The model parameters used in SEEP/W for conducting the saturated analysis for both the cases had been shown in Table 3.

RESULTS AND DISCUSSIONS

Stability Analysis using FE method

The static analysis using the FE formulation enables to conduct a stage-wise stability analysis using SIGMA/W. After generating the stress conditions in SIGMA/W, it is incorporated in SLOPE/W to obtain FE based stability values. The finite element based FoS values for all the different stages of construction during dry and saturated conditions are presented in Table 4 for Case I and in Table 5 for Case II. Any complete set of analysis comprises of the various stages of analysis involved in the sequential anthropogenic constructions in the site, namely: (1) In-situ analysis to assess the stability of the virgin slope before human intervention (2) Excavation of foundation of building (3) Imposition of building load at the site due to the construction of the building (4) Filling back and embedment of the shallow footings (Stages 3 and 4 are simultaneously done in the field) (5) Excavation of the foundation of the retaining wall R1 (6) Construction of R1 and simultaneous back-filing (7) Excavation of the foundation of the retaining wall R2 (8) Construction of R2 and simultaneous back-filing (9) Excavation of the foundation of the retaining wall R3 (10) Construction of R3 and simultaneous back-filing.

Stability analysis of the two different slope geometries (as defined by Case I and Case II) has been carried out for both dry and saturated conditions. Analysis of dry slope represented the hill-slope stability in the dry seasons, while the analyses with saturated slopes has been carried out with varying locations of the water table depicting the effect of varying intensities of rainfall during the monsoon periods. For any individual analyses under saturated conditions, the water table is considered at the top surface of any individual soil layer, defined by a constant head boundary condition during the seepage analysis. These analyses aids in understanding the stability of the hill-slope under different conditions, and forensically help to develop the idea whether the slope failure was triggered by the percolating or seeping water due to monsoon rainfall. Simulations with various heights of water table, when validated with the field observations, help in understanding the possible location of the in-situ water table.

From the stability values enumerated in Table 4, it is observed that the considered slope geometry is marginally stable under dry conditions, and does not manifest massive slope failure. When saturated, the stability reduces substantially due to the incorporation of the water table at different locations. However, the stability value tends to increase, as obvious, when the water table is considered at deeper locations. From the low stability values illustrated in Table 4, it can be stated that Case I slope geometry tended to be unstable right from the in-situ stage when water table was considered into the analyses. This signifies that the slope would have failed during the intense rainfall season even without any anthropogenic activities. This observation is in contrary to the site observation which shows no record of slope failure before any construction activity. Hence, it was concluded that consideration of all soil layers to have low in-situ strength parameters proved to be an exaggeration and is not possibly representing the field scenario.

Table 4. Stability values for Case I for both dry and saturated conditions

Sl. No.	**Stage of construction**	**Dry**	**Water level at a ht. of 17m (W_1)**	**Water level at a ht. of 13m (W_2)**	**Water level at a ht. of 9m (W_3)**
		FoS Values	**FoS Values**	**FoS Values**	**FoS Values**
1	In-situ	1.416	0.920	1.029	1.054
2	Building foundation excavation	1.388	0.952	1.025	1.053
3	Imposition of building load	1.038	0.489	0.609	0.854
4	Filling back of foundation	1.078	0.975	0.976	0.88
5	Excavation for R1	1.076	0.989	0.975	0.875
6	Construction and backfilling of R1	1.064	1.038	1.038	0.919
7	Excavation for R2	1.087	1.146	1.077	0.935
8	Construction and backfilling of R2	1.083	1.151	1.097	0.936
9	Excavation for R3	1.071	1.080	1.083	0.931
10	Construction and backfilling of R3	1.081	1.066	1.060	0.924

Table 5: Stability values for Case II for both dry and saturated conditions

Sl. No.	Stage of construction	**Dry**	**Water level at a ht. of 17m (W_1)**	**Water level at a ht. of 13m (W_2)**	**Water level at a ht. of 9m (W_3)**
		FoS Values	**FoS Values**	**FoS Values**	**FoS Values**

1	In-situ	2.112	1.411	1.588	1.511
2	Building foundation excavation	2.1	1.373	1.577	1.513
3	Imposition of building load	0.976	0.821	0.793	0.769
4	Filling back of foundation	0.967	0.850	0.802	0.774
5	Excavation for R1	1.015	0.875	0.825	0.805
6	Construction and backfilling of R1	0.985	0.838	0.798	0.785
7	Excavation for R2	1.373	0.817	1.065	1.025
8	Construction and backfilling of R2	1.344	0.752	0.967	1.007
9	Excavation for R3	1.288	1.029	1.035	0.975
10	Construction and backfilling of R3	1.294	1.024	0.984	0.959

Table 5 illustrates the FoS values as obtained from the analyses of Case II slope geometry. It is observed that under dry conditions, the slope geometry is stable until the building is constructed. Taking evasive measures by constructing retaining walls R1 an R2 would have sufficiently stabilized the slope. However, such scenario was not observed in the field, as construction of retaining walls R1, R2 and R3 did not have significant stabilization effects. When analyzed for saturated conditions, it is clearly observed that slope illustrated significant failure. Moreover, as observed in the field, construction of R1, R2 and R3 had no effect on the improvement of stability of the slope. Hence, it can be clearly stated that the Case II slope geometry is a very good idealization of the stratification existing in the field. The results of the stability analyses also gets cross validated by the field observation that the major mass movement in the site was observed after the monsoon season and after the construction of the building. The sequence of distress as mentioned earlier in the paper was also observed to be simulated by the analysis. Most importantly, analyses of Case II slope geometry revealed that the construction of the sequence of retaining walls did not improve the stability issues of the moving slope, as observed in the field as well. This suggests that Case II slope geometry is apt in representing the in-situ site characteristics.

Deformation and seepage characteristics of the slope in dry and saturated conditions

The displacement characteristics along the face of the slope for the critical stages of construction pertaining to the probable existing soil stratification in the field (Case II) is shown in Fig. 8 to Fig. 12 for dry and saturated conditions, respectively. Results from the analyses showed that for both dry and saturated conditions, the deformations in the first two stages of construction were negligible. The abrupt increase in deformations starts from the addition of the building load and its increment continues till the addition of the first retaining wall R1, after which no significant increase of deformation was observed for the rest of the stages of construction. Therefore, it can be clearly pointed out that the Stages 3-6 of the various construction sequences (as illustrated in Table 4 and Table 5) are the main triggering factors leading to the initiation and progression of deformation in the marginally stable hill-slope.

It can be noticed that saturation of the upper soil layers lead to higher degree of destabilization as illustrated from the larger values of displacement of the slope face. It can also be seen that different degrees of saturation result in different extents of deformation in the slope face. Seepage analyses conducted with varying levels of water heads yielded different phreatic surfaces and the water flux along the slope face was determined. The results of the simulations were compared with the field observation in terms of the location of water emanating out of the slope face after the monsoon period. Figure 12 shows the water flux along the slope face for Case II slope geometry fully saturated with water and the phreatic line is at its culmination in comparison to the other cases having different positions of water table. It can be observed that the Validating with the real field scenario the level of saturation with gave the maximum displacement can be adopted. A plot showing the variation of water flux along the face of the slope is shown below in Fig. 12. It can be observed that the water flux attains a negative value beyond a distance of 180 m from the crest of the slope. This signifies that water is emanating out from the slope face through this particular location, which is an outcome of the phreatic line intersecting the slope face at the said location. Visit to the distressed site also revealed water emanating out from the slope face as seeping spring at and around the said location (~ 150-200 m from the slope crest). Thus, it can be conclusively stated that the heavy monsoon season led to the saturation of the most parts of the slope and the rise of the phreatic lie towards the ground surface made the soil comparatively weakened (manifested by lower strength properties), and subsequently leading the massive mass movement of the soil. As shown in Fig. 7, retaining wall (R4) was constructed with the provision of weep-holes accompanied by an adjacent water-carrying nallah (open channel conduit) with the intention of releasing the water seeping through the slope. However, the phreatic line intersecting the slope at a much higher elevation had actually rendered R4 to be a dysfunctional one, and hence, resulted in a massive wetting of the toe of the slope, leading to the observed distress at the site.

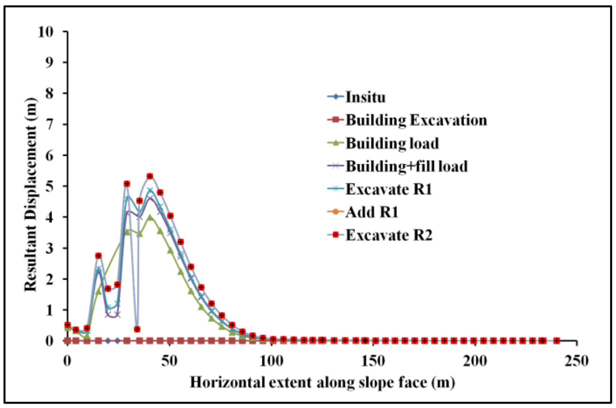

Figure 8. Displacement for the critical stages in dry condition

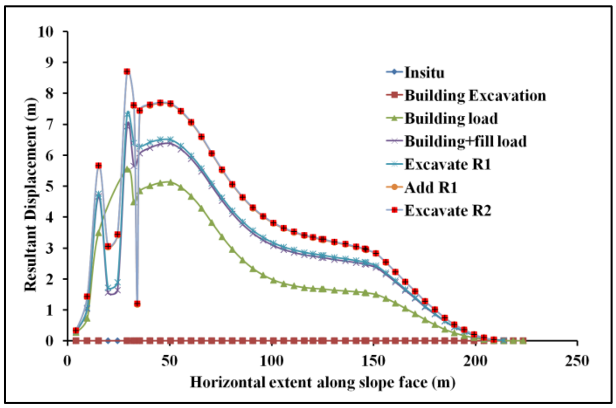

Figure 9. Displacement for the critical stages in saturated condition (*W_1*)

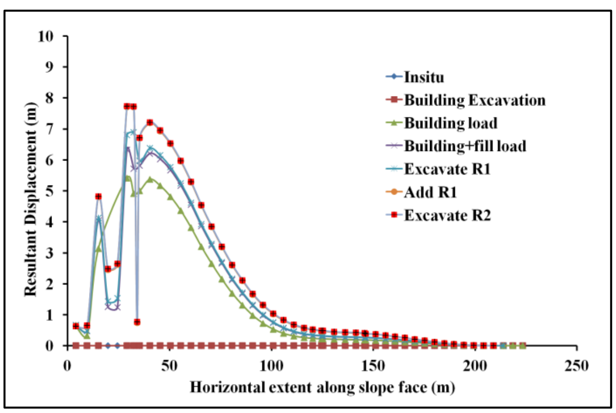

Figure 10. Displacement for the critical stages in saturated condition (*W_2*)

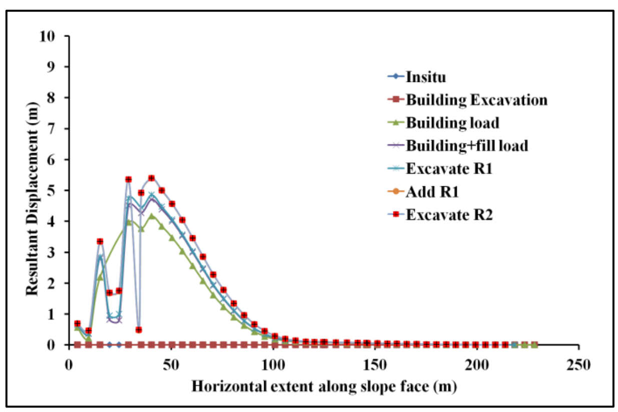

Figure 11. Displacement for the critical stages in saturated condition (*W_3*)

Figures 14 and 15 exhibit the deformation characteristics observed for the two most critical stages of construction (Stage 3 and Stage 6, respectively) with the identified slope geometry, soil stratification and the location of the phreatic surface and its intersection region in the slope. Supplement to Fig. 7, it can be observed from the deformation contours of Fig. 14 that a shallow slope movement with significant deformation extent has taken place at Stage 3 itself, when the building has been constructed. The deformation reached a depth of 4m below the ground surface and laterally extended up to 200 m from the building location towards the downhill of the slope. In order to arrest the movement originated due to the building construction, R1 was constructed with a foundation embedment depth of around 1 m from the ground surface.

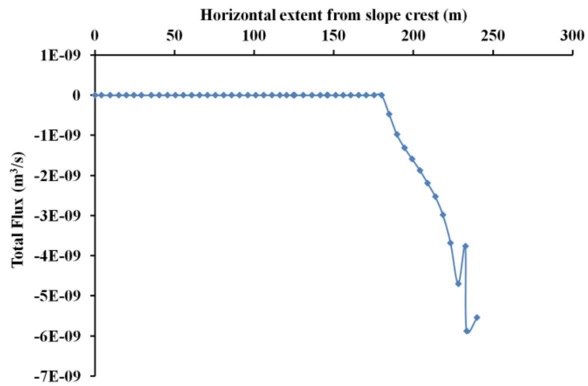

Figure 12: Variation of water flux along the slope face

Figure 13: Water emanating from slope face

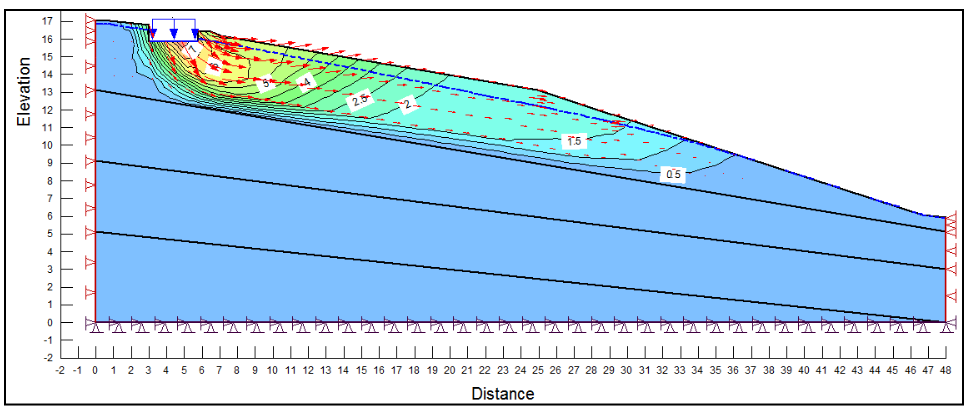

Figure 14. Deformation of the slope (Stage 3)

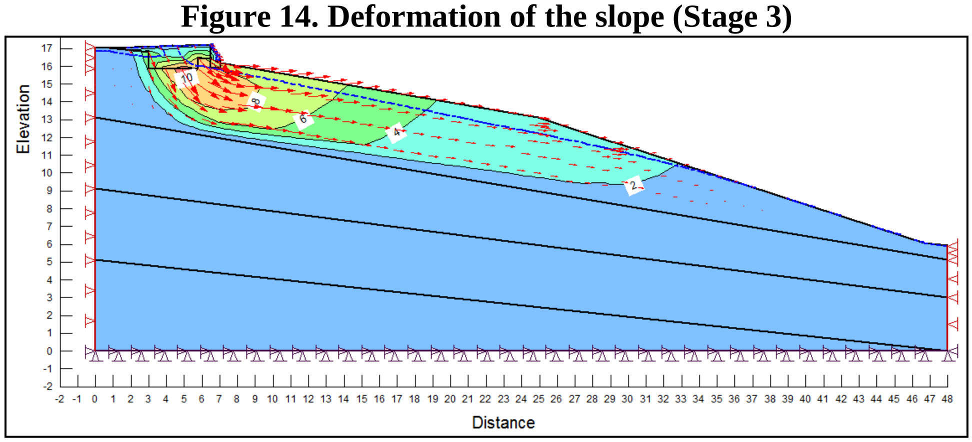

Figure 15. Deformation of the slope (Stage 6)

It can be well understood that this retaining wall, with its backfill, is actually floating on the moving soil mass, and would offer no benefit in arresting the slope movement, which is what exactly happened in the field, where no signs of the arrest of the movement was seen. Rather, after the construction of the retaining wall, large movements were seen even at a distance of 150 m from R1 in the field. Figure 15 exhibits the same in the numerical simulation. The construction of the retaining wall and its subsequent backfilling, in reality, added more load on the moving soil, thus generating additional movement as observed both in the field and in the numerical simulation. The extent of the lateral deformation encompassed the locations of R2 and R3, and hence, their construction was of no additional improvement to the stabilization of the moving slope. The extent of the deformation beyond the retaining walls R2 and R3 reached the colony area and caused a massive damage to the habitation (as shown in Fig. 5 and Fig. 6).

CONCLUSIONS

The main objective of this study was to identify the triggering mechanism of the slope failure of a marginally stable slope located in the North Eastern region of India. In order to attain the objective, with the aid of an obscure knowledge about the stratification from the boreholes in the nearby location, a finite element model of the critical soil geometry had been developed using GEOSTUDIO 2007. Each stage of modeling had been validated with the real field scenario during the subsequent field visits. The results from the analysis indicated that the external stimulus that initiated the slope instability process was the addition of the workshop building load. The seepage of rain water along the slope further aggravated the condition. To prevent the slope failure, construction of the masonary retaining wall-I at a founding depth of 1 m from the ground level, instead of founding it up to the bed rock, did not serve the purpose; rather, it added additional load to the affected slope which caused further slope movement. To prevent this, further two retaining walls were constructed at different locations of the slope, which did no good to protect the slope. The increase in the pore water pressure during the various loading conditions had reduced the strength of the slope leading to its instability. Therefore, the primary objective of this study which was to simulate a real field existing slope and to identify the triggering mechanisms leading to its instability had been achieved. This knowledge can further be used to implement appropriate stabilization techniques which will provide a permanent solution to the slope instability problem of the region.

REFERENCES

Cai, F. and Ugai, K. (2004) "Numerical Analysis of Rainfall Effects on Slope Stability", *International Journal of Geomechanics*, Vol.4, pp. 69-78.

Collins, B.D. and Znidarcic, D. (2004) "Stability analysis of rainfall induced landslides", *Journal of Geotechnical and Geoenvironmental Engineering*, Vol. 130, pp. 362-372.

Ering, P., Kulkarni, R., Kolekar, Y., Dasaka, S.M. and Babu, G.L.S. (2015) "Forensic analysis of Malin Landslide in India", *Proceedings IOP Conference Series: Earth and Environmental Science*, Vol. 26, pp. 1-13.

Saxena, D.S., (2008) "Case studies in Forensic Geotechnical and Foundation Engineering", *International Conference on Case Histories in Geotechnical Engineering*, Paper 2, pp. 1-12.

Sultan, N., Cochonat, P., Canals, M., Cattaneo, A., Dennielou, B., Haflidason, H., Laberg, J.S., Long, D., Mienert, J., Trincardi, F., Urgeles, R., Vorren, T.O. and Wilson, C. (2004) "Triggering mechanisms of slope instability processes and sediment failures on continental margins: a geotechnical approach", *Marine Geology*, Vol. 213, pp. 291-321.

CASE STUDY AND FORENSIC INVESTIGATION OF LANDSLIDE AT MARDOL IN GOA

Leonardo Souza,[1] Aviraj Naik,[1] Praveen Mhaddolkar,[1] and Nisha Naik[2]

[1]PG student – ME Foundation Engineering, Goa College of Engineering, Farmagudi Goa; lrdcs@refiffmail.com
[2]Associate Professor – Civil Engineering Department, Goa College of Engineering, Farmagudi Goa; nisha@gec.ac.in

Keywords: Forensic Investigations, Landslides, Slope Failure

Abstract:

Goa, like the rest of India is undergoing an infrastructure boom. Many infrastructure works are carried out on hill sides in Goa. As a result there is a lot of hill cutting activity going on in Goa. This has caused major landslides in many parts of Goa leading to damage and loss of property and the environment. Forensic analysis of a failure can significantly reduce chances of future slides. The primary purpose of post failure slope and stability analysis is to contribute to the safe and economic planning for disaster aversion. Western Ghats (also known as Sahyadri) is a mountain range that runs along the west coast of India. Most of Goa's soil cover is made up of laterites rich in ferric-aluminium oxides and reddish in colour. Although such laterite composition exhibit good shear strength properties, hills composing of soil possessing low shear strength are also found at some parts of the state. The shear strength parameters of slope material along with slope face, slope angle and height play an important role in governing the stability of a slope. The pore pressure conditions of the slope is also a critical factor. A complete understanding of the nature and causes of slope failures requires a complete investigation into various factors affecting the soil and the slope at the site under consideration. The shear strength parameters of the soils need to be determined using tests. Based on them the forensic study of stability of the slope was determined. The present paper is a forensic analysis of one such landslide occurred alongNH-4A at Mardol, PondaGoa. The landslide is suspected to have occurred due to increase in weight of the sliding soil mass after the area having recently experienced a heavy rainfall. A detailed investigation has been carried out to understand various aspects of failure and possible stabilization techniques to avoid such landslides in future.

INTRODUCTION

The term landslide is used to describe a wide variety of processes that result in the downward and outward movement of slope forming materials composed of rocks, soils, artificial fill or a combination of these (Boop,1991). The material may fall by toppling, sliding, spreading or flowing. Goa has more than 50% of its area under hilly mountainous terrain namely the Sahyadris range and the foothills. These are very old and stable formations compared to the recently formed Himalayas. They face threat due to rapid development and hill cutting for various purposes including infrastructure and mining.

The common sight of relief, swathes of verdant forest, raging fast flowing rivers and rivulets, steep slope and so on characterize the mountain ecosystem of the state of Goa. On the west coast of India, west and north-west slope facets receive maximum rainfall, and are therefore more vulnerable to failure. Considering the fragility, diversity and complexity of the existing geo-environmental setting and the ecosystem, manipulation of natural constant either by nature or man in an unsustainable manner can lead to an irreparable short as well as long term negative side effects and devastation. Forensic analysis of a failure can significantly improve chances of future success.

In most cases the triggering factors are invariably buildup of pore water pressure due to excessive water during monsoons. Landslides triggered by heavy rain have been constant sources of destruction of property and loss of lives. Dormant as well as active slides are a threat to human life and property. Their study and monitoring has become imperative to safeguard against destruction by them. Developmental activities to be sustainable must be confined away from landslides prone and landslide affected locations. So far, disasters caused by landslides, earthquake, flood etc. have not led to large scale human tragedy in Goa in recent memory. However, there is ever increasing human demand of natural resources, especially land for urban development and infrastructure works thereby diverting the attention towards exploring the hills of Goa. The emerging crisis can be minimized by indigenous knowledge based and modern technological interventions prior to start of any construction work.

A landslide occurred in the village of Mardol, in south Goa district at the foot of a hill adjacent to NH4A highway. The proximity of the site to a highway caused a concern and hence was the motivation behind this study. This paper presents a forensic analysis of the landslide at Mardol, Goa. Figure 1(a) shows a google earth image of the location of the site and a photograph taken at the site is shown in Figure 1(b). A forensic investigation of the site includes the following:-

- Google earth image showing location of site.
- Site Survey
- Soil samples
- Stability analysis
- Suggested mitigation measures

(a) (b)

Figure 1: (a) Location of site, (b) Landslide at site.

LANDSLIDE TYPES AND CLASSIFICATION

Various Engineering disciplines have developed classification system to describe natural phenomena. These systems are based on specific repeatable characteristics. In landslide classification, there are great difficulties due to the fact that phenomena are not perfectly repeatable; usually being characterized by different causes, movements and morphology, and involving genetically different materials. For this reason, landslide classifications are based on different discriminating factors, sometimes very subjective. The following table (Table1) shows a schematic landslide classification, which is based on movement type and material of the slope.

Table 1 Types of land slides

<table>
<tr><td colspan="3" rowspan="3">Movement type</td><td colspan="3">Material type</td></tr>
<tr><td rowspan="2">Bedrock</td><td colspan="2">Soil type</td></tr>
<tr><td>Fine</td><td>Coarse</td></tr>
<tr><td>Fall</td><td rowspan="2"></td><td></td><td>Rock fall</td><td>Earth fall</td><td>Debris fall</td></tr>
<tr><td>Topples</td><td></td><td>Rock topple</td><td>Earth topple</td><td>Debris topple</td></tr>
<tr><td>Slides</td><td>Rotational</td><td></td><td>Rock slump</td><td>Earth slump</td><td>Debris slump</td></tr>
<tr><td></td><td rowspan="2">Translational</td><td>Few units</td><td>Earth block slide</td><td>Earth block slide</td><td>Debris block slide</td></tr>
<tr><td></td><td>Many units</td><td>Rock slide</td><td>Earth slide</td><td>Debris slide</td></tr>
<tr><td colspan="3">Lateral spreads</td><td>Rock spread</td><td>Earth spread</td><td>Debris spread</td></tr>
<tr><td colspan="3" rowspan="3">Flows</td><td>Rock flow</td><td>Earth flow</td><td>Debris flow</td></tr>
<tr><td>Rock avalanche</td><td></td><td>Debris avalanche</td></tr>
<tr><td>Deep creep</td><td colspan="2">Soil creep</td></tr>
<tr><td colspan="3">Complex and compound</td><td colspan="3">Combination in time and /or space of two or more principal types of movements</td></tr>
</table>

FACTORS AFFECTING LANDSLIDES

The mountain slope are governed by laws of gravity and with the forces of lubricant like soil and the resistance to motion. The factors affecting these motions can be broadly divided into two groups:

(A) The first one is made up of the criteria utilized in the most widespread classification systems that can generally be easily determined. These are called as the Deterministic Factors.

(B) The second one is formed by those factors that have been utilized in some classifications and can be useful in description only. These are called as the Descriptive Factors.

Types of movement

This is the most important criteria. As the mechanisms of some landslides are often particularly complex, uncertainties and difficulties can arise in the identification of movements. The main movements are falls, slides and flows, but usually topples, lateral spreading and complex movements are added to these.

Material Involved

Rock, earth and debris are the terms generally used to distinguish the material involved in the landslide process. The distinction between earth and debris is usually made by comparing the percentage of coarse grain size fraction. If the weight of the particles with a diameter greater than 2mm is less than 20%, the material will be defined as earth; in the opposite case, it is debris.

Activity

The classification of a landslide based on its activity is particularly relevant in the evaluation of future events. The concept of activity is defined with reference to the spatial and temporal conditions, defining the state, the distribution and the style. The first term describes the information regarding the time in which the movement took place, permitting information to be available on the future evolution, the second term describes, in a general way, where the landslide is moving and the third term indicates how it is moving.

Type of climate

These criteria give particular importance in the genesis of phenomena for which similar geological condition can, in different climatic conditions, lead to totally different morphological evolution. As a consequence, in the description of a landslide, it can be interesting to understand in what type of climate the event occurred.

CAUSE OF LANDSLIDES

The mountain slope are governed by laws of gravity and with the forces of lubricant like water, unstable slope-forming material shall continue to move downwards and cause economic loss in terms of life and property. The landslide trigger mechanism is shown in Figure 2. Landslide with heavy rainfall causes flash floods in the valleys. Landslides or mass movement phenomena in a mountainous state can be attributed to the following causative factors solely or in combination with:

1. Geology of the area.
2. Rainfall.
3. Slope angle and slope formation materials.
4. Hydrological condition of the area

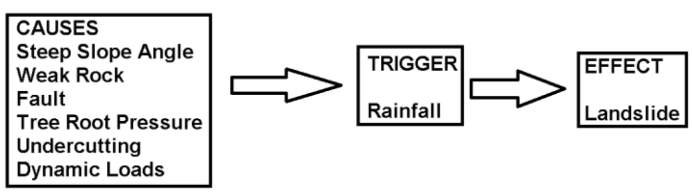

Figure 2: landslide trigger mechanism

Causes may be considered to be the overall factors that made the slope vulnerable to failure, that predispose the slope to becoming unstable whereas, trigger is the single event that finally initiate the landslide. Thus, causes combine to make a slope vulnerable to failure, whilst the trigger finally initiates the movement. Usually, it is relatively easy to determine the trigger after the landslide has occurred (although it is generally very difficult to determine the exact nature of landslide triggers ahead of a movement event). The various causes of landslides are listed as follows:

1. Geological Factors

These include materials which are weak, sensitive, weathered, sheared, jointed or fissured and with adversely oriented discontinuities. The materials also show a wide contrast w.r.t. permeability.

2. Morphological causes

These include slope angle, uplift rebound, fluvial erosion, wave erosion, glacial erosion, erosion of lateral margins, subterranean erosion, slope loading, vegetation change.

3. Physical causes
   Intense rainfall, rapid snow melt, prolonged precipitation, rapid drawdown, earthquake, volcanic eruption, thawing, freeze-thaw cycle, shrink-swell, ground water changes and other mass movements are some of the physical causes of landslides.
4. Human causes
   Human activities like excavation, loading, drawdown, change in use of land, water management, mining, quarrying, vibration and water leakage also add to the possibilities of landslide.

RAINFALL AS A TRIGGER

Considerable efforts have been made to understand the triggers for land sliding in natural sytems, with quite variable results. In the majority of cases, the main trigger of landslides is heavy or prolonged rainfall. Generally, this takes the form of either an exceptional short lived event, such as the passage of a tropical cyclone or even the rainfall associated with a particularly intense thunderstorm or of a long duration rainfall event with lower intensity, such as the cumulative effect of monsoon rainfall in South Asia. This is explained in Figure 3.

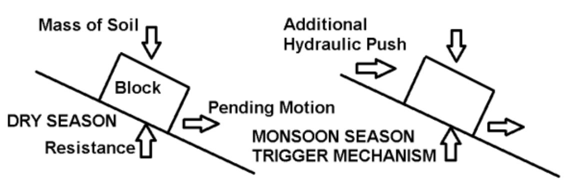

Figure 3:Rainfall as trigger

In the former case, it is usually necessary to have very high rainfall intensities, whereas in the latter the intensity of rainfall may be only moderate- it is the duration and existing pore water pressure conditions that are important. The importance of rainfall as a trigger for landslides cannot be under-estimated. Almost all the landslides in Goa occur after prolonged exposure to monsoon rains and occasionally during or just after cloudburst or precipitation intensity exceeding 135-145 mm in 24 hours. They usually start occurring after August when the soils are fully saturated by the June - July rains.

The Figure 3 illustrates the forces acting on an unstable block on a slope. Movement is driven by shear stress, which is generated by the mass of the block acting under gravity down the slope. Resistance to movement is the result of the normal load. When the slope fills with water, the fluid pressure provides the block with buoyancy, reducing the resistance to movement. In addition for some cases, fluid pressures can act down the slope as a result of groundwater flow to provide a hydraulic push to the landslide that further decreases the stability. In some situations, the presence of high levels of fluid may destabilize the slope through other mechanism, such as:

• Fluidization of debris from earlier events to form debris flows.

• Loss of suction forces in silty materials, leading to generally shallow failures (this may be an important mechanism in residual soils in tropical areas following deforestation).

• Undercutting of the toe of the slope through river erosion or for construction works.

FORENSIC INVESTIGATION TECHNIQUES

The primary purpose of post failure slope and stability analysis is to contribute to the safety of slopes. Proper forensic investigation needs to be carried out using Non Destructive Techniques. The other techniques used are, still-photography, scale object in photograph, land surveying, visual inspection and soil sample followed by lab testing and stability analysis with the aid of slope stability softwares.

Site Conditions

Site conditions play an important part in stability and failure of slope. Slope face and slope angle and height play an important role in governing the stability of slopes. As they increase, chances of failure also increase. The degree of saturation of the slope material is also a major factor. The soil at site was poorly graded clayey sand. Patches of yellowish clayey-sand layers were observed. As the landslide was fresh, the soil was moist and lumps of it could be easily squeezed in hand. Figure 4(a) shows the yellowish clayey sandy layer and Figure 4(b) shows the failure of slope.

(a) (b)

Figure 4: (a) Photo showing yellowish clayey sandy layer, (b) Photo showing failure of slope.

FIELD INVESTIGATIONS

Field investigations have been carried out as per template provided by national Disaster Management Authority (NDMA 2015). A deeper understanding of the nature and causes of these failures requires a detailed investigation into the geology, groundwater conditions, geotechnical characteristics, topography, seismicity and weather patterns at the site under consideration. The shear strength parameters of the soils need to be determined using tests. Based on them the forensic study of stability of the slope was carried out.

Topographical Maps

As the entire area was almost clear of any obstruction a theodolite survey was carried out to locate the significant points and the slope of the ground. The sectional maps were prepared using these. The section is shown in Figure 5.

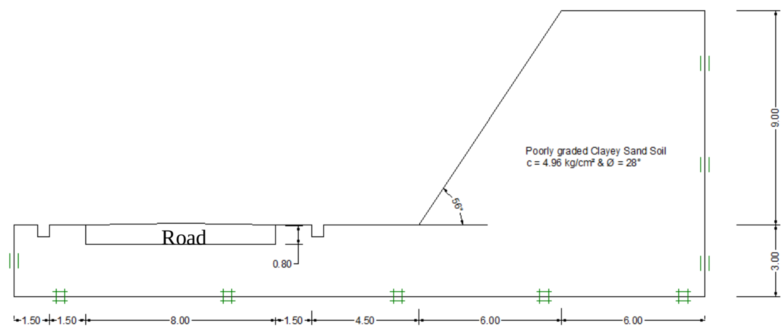

Figure 5 : Section of site (dimensions in meters).

Geomorphology

The site is a hill cutting 9 m high for roadworks as shown. It is west facing and a considerable reduction in vegetation cover on top of slope is seen at location where the landslide has occured.

Metrology

On the west coast of India, in the western ghats region, the west and north-west slope facets receive maximum rainfall, and are therefore more vulnerable to failure. This site being on the west is no exception in facing heavy rainfall. Heavy rains impact the region from June to October. By mid July soil is fully saturated and hence most failures and landslides occur in this season.

Regional Geology

The soil is basically formed of thin layers of red clayey sand interspersed with thick layers of yellowish clayey soil both of which have very weak shear strength. Figure 6, shows the photos resembling regional geology.

Figure 6: photograph of soil layers resembling regional geology.

LABORATORY INVESTIGATIONS

Soil samples were collected and standards laid down in relevant IS codes have been followed for sampling and testing of soil. The values found were used for stability analysis.(4)

Soil Samples

Soil samples were collected from different locations at site. These were kept safe and dry in polyethelene bags in the soil-mechanics laboratory of the Department of Civil Engineering, Goa Engineering College and marked, indicating the soil description, sampling depth and date of sampling. Classification test (natural moisture content, specific gravity, Grain size analysis and Atterberg's limits,) and compaction test (optimum moisture content, Maximum Dry Density)were performed on the samples to determine the geotechnical properties of the samples. The average values have been presented below in Table 2.

Table 2: General Soil Properties

Specific Gravity	Moisture Content	Compaction Test		Atterberg Limits		
		OMC %	MDD g/cc	Liquid limit WL %	Plastic limit wP %	Plasticity index IP %
2.47	22.9	12.13	1.83	27	11.7	15.3

Soil Shear Strength Parameters

Engineering property test for shear strength were performed on the samples A, B and C and the values are indicated in Table 3.

Table 3: Shear Strength Parameters of Soil

c	Ø
4.96 kg/cm^2	28°

STABILITY ANALYSIS

Terzaghi describes failure causes as "internal" and "external" referring to modification in the conditions of the stability of the bodies. Whilst the internal modifications in the material itself which decreases its resistance to shear stress, the external causes generally induce an increase of shear stress, so that block or bodies are no longer stable. It should be noted that the triggering causes induce the movement of the mass. Predisposition to movement due to control factors is determining in landslide evolution. Structural and geological factors, as already described, can determine the development of the movement, inducing the presence of mass in kinematic freedom.

The Bishop's method of slices is used when the slope consists of different soil layers with varying c and Ø values. The soil mass above the failure surface is divided into number of slices and the forces acting on each slice is determined from limit equilibrium method. The equilibrium of the entire mass is determined by summing the forces of individual slices.

Failure Analysis and Results

The current landslide slope site is analysed with a software OptumCEG2 which a finite element program dedicated to geotechnical deformation and stability analysis. The analysis was carried out by limit analysis and considering linear elastic materials of Mohr- Coulomb type. Limit analysis and strength reduction methods were used to get a graphical failure pattern and factor of safety as the output. In limit analysis the fixed loads are kept constant gravity is amplified till failure occurs. The strength Reduction analysis proceeds by computing a strength reduction factor by which the material parameters need to be reduced in order to attain a state of incipient collapse. This reduction factor is taken as the factor of safety [Aniket R. Dessai and Nisha P. Naik, 2016]. The slope was analysed by dividing it into 1000 number of elements. Figure 7 shows the slope model in software. The slope at present condition is having factor of safety of 0.45 which implies that the slope is just stable with present conditions and is highly susceptible to failure with any further loading or increase in pore pressure. Figure 8 shows the software result of slope failure. It is a slip circle failure and this could also be depicted from the site photographs.

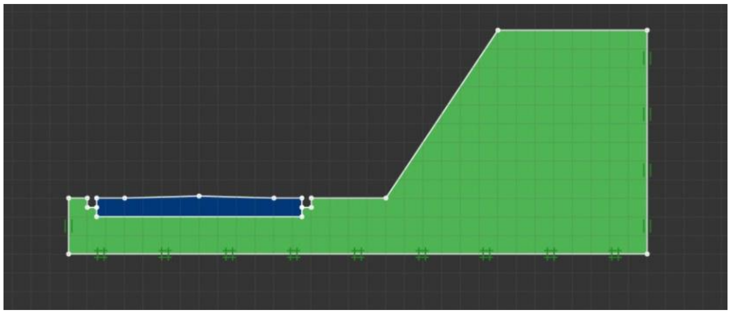

Figure 7 : Model of the slope adopted for analysis

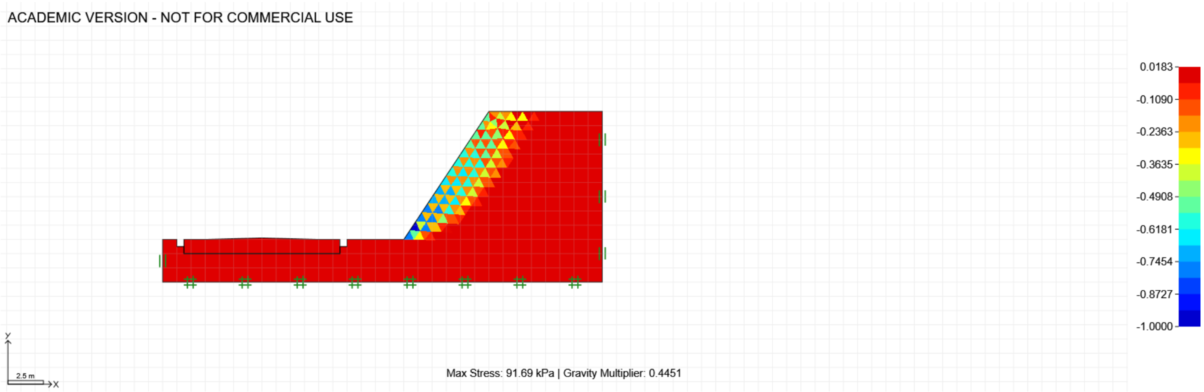

Figure 8 : Slope failure (F.O.S = 0.45)

Cause of this Landslide

As known from stability analysis that the slope is highly vulnerable to further loading or increase of pore pressure, the only possible cause for this landslide can be the continuous heavy rainfall experienced in this region during monsoons. The destruction of natural vegetation along this area has also added to its instability. The slope must have been saturated during rains and thereby increasing its self-weight and eventually leading to collapse.

MITIGATION MEASURES

The purpose of the landslide mitigation is to stop or reduce the landslide movement so that the resulting damages can be minimized (Singh et al 2015). The approaches for mitigating landslide may include:

1. Restrictions of development in landslide prone areas,
2. Modification in geometry of slope, grading, landscaping,
3. Landslide mitigation works, and
4. Warning systems

Benching

Benching results in modification in the geometry of the slope and also decreasing the weight of the earth retained slope. It also helps in decreasing storm water flow and prevent erosion of soil. Figure 9 shows the benching of mardol slope with approx. 1:1 cutting. However in the analysis a horizontal cut of 4.00 meters is taken for a height of 4.50 meters.

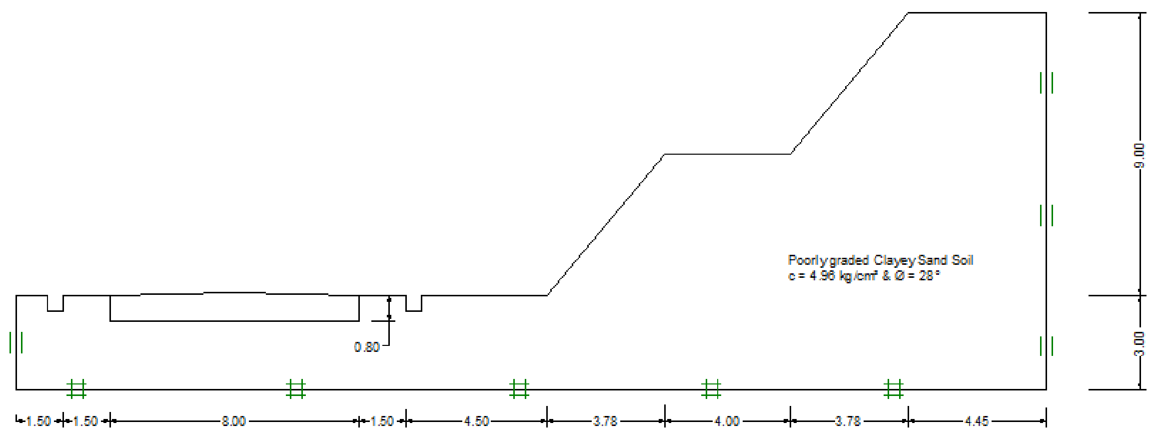

Figure. 9: Proposed benching for Mardol slope (dimensions in meters).

The current analysis of this slope after benching gave a factor of safety of 1.09 which is 42% more than that without benching. The stability result is shown in Figure 10.

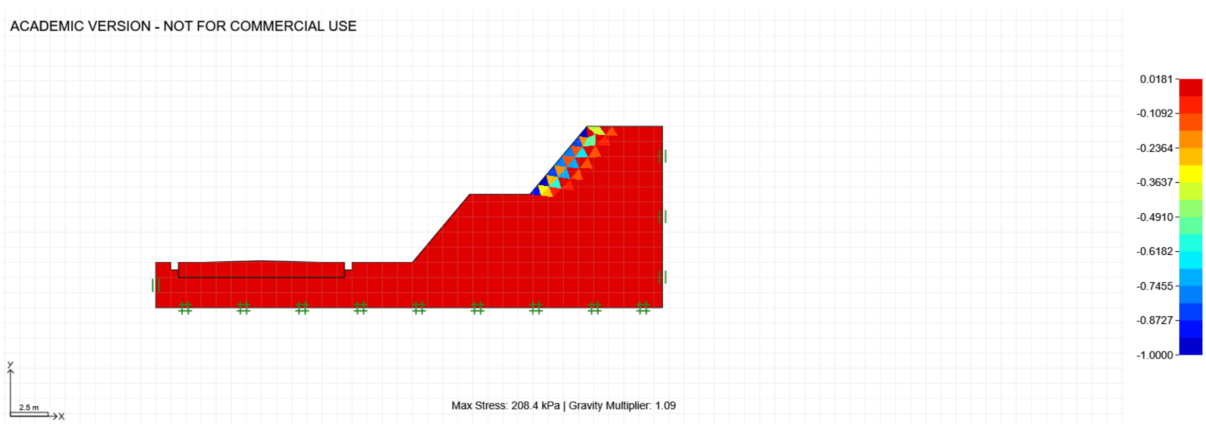

Figure 10: Stability of slope after benching (F.O.S= 1.09)

Installation of nails on unstable hillside

Reinforcement measures generally consist of the introduction of metal elements to increase the shear strength of the rock. As far as the working mechanical of a rock nail is concerned, the strains of the rock induce a stress state is the nail composed of shear and traction stress, due to the roughness of the joint, to their opening and to the direction of the nail, generally non-orthogonal to the joint itself. Soil nailing is providing passive reinforcement of existing ground by installing closely spaced nails i.e. steel bars of required diameter. The nails are then fixed on surface with bearing plate and later if required covered with shotcreting.

The soil nailing for Mardol slope with steel bars of 8.50 meters length and axial strength of 500KN/m with bearing plates of size 280x280x20mm gave a factor of safety of 1.06 (almost same as that obtained on benching). Figure 11 shows the soil nailing section of slope. The stability analysis is shown in Figure 12.

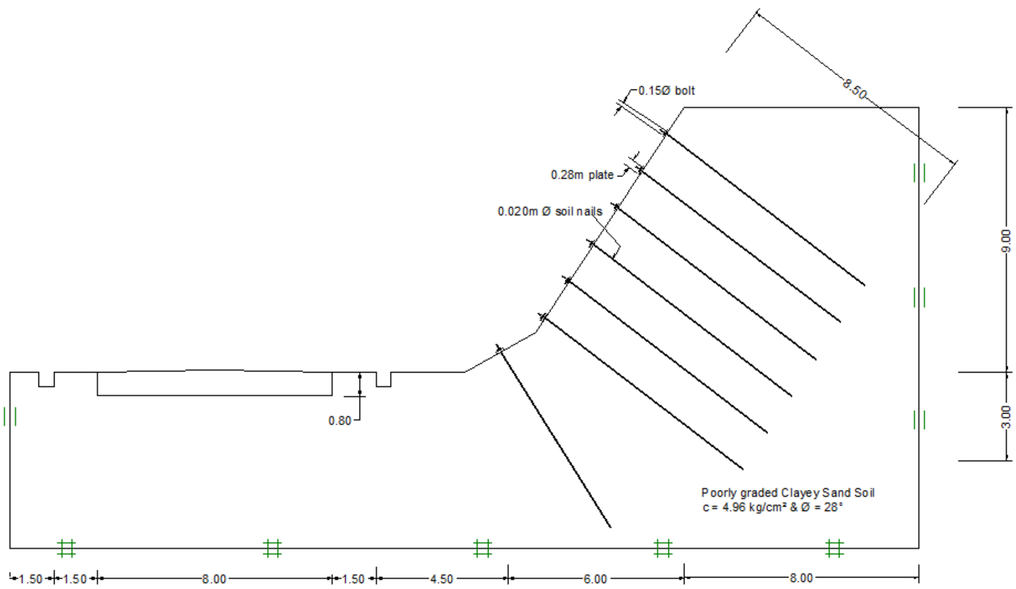

Figure 11: Slope cross-section showing soil nails (dimensions in meters).

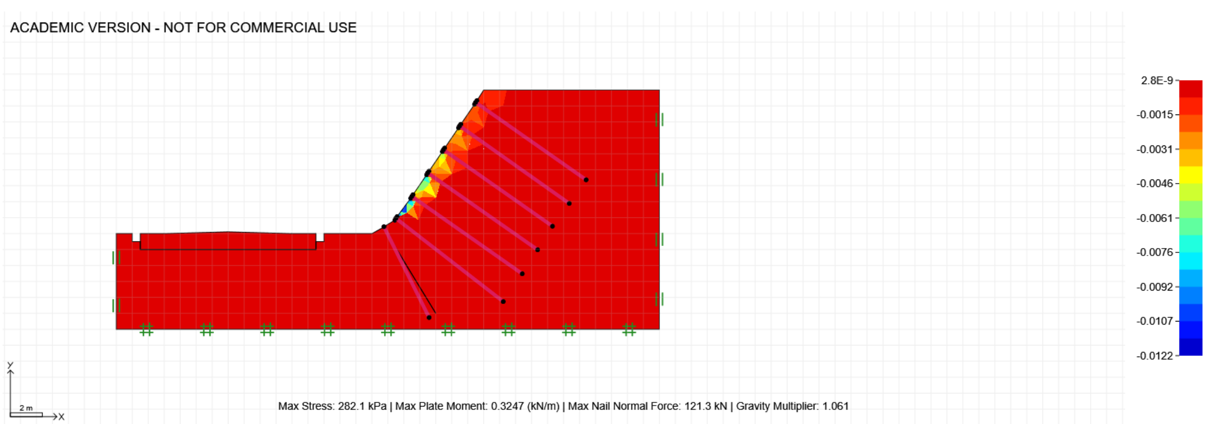

Figure 12: Stability analysis of soil nailed slope

OTHER MITIGATION MEASURES INCLUDE:

Installation of anchors

Anchorage can be classified as active anchorage, in the case in which they are subjected to pre-tensioning, and passive anchorage. Passive anchorage can be used both to nail single unstable blocks and to reinforce large portions of rock. It is, therefore, a specific type of anchorage, not structurally connected to the free length, made up of an element resistant to traction, normally a steel bar of less than 12m, protected against corrosion by a concrete health.

Drainage

The presence of water within a hillside is one of the major factors leading to instability. This can be avoided by;

- Preventing water entering the hillside through open or discontinuity traction cracks.
- Reducing water pressure in the vicinity of potential breakage surfaces through selective shallow and sub-shallow drainage
- Placing drainage in order to reduce water pressure in the immediate vicinity of the hillside.

Vertical Drainage

Vertical drainage is generally associated with sunken pumps which have the task of draining the water and lowering the groundwater level.

Growing Vegetation

Vegetation growth has always been a good method of stabilizing slopes as the trees prevent soil erosion by creating a dense network of roots within. Moreover growing trees is also a sustainable approach towards slope stability. Vetiver grass is a tall, tufted, perennial, scented grass, with a straight stem, long narrow leaves and a lacework root system that is abundant, complex, and extensive. It offers an inexpensive yet effective and eco-friendly tool to combat soil erosion. Vetiver, with its many advantages and very few disadvantages, is a very effective, economical, community-based and environmentally-friendly sustainable bioengineering tool that protects infrastructure and mitigates natural disasters [C. Ghosh]

CONCLUSIONS

More than 50% of the land of Goa comprises of hill regions. Some are strong due to oxidation of rocks while some are weak due to poor geological formations. The hilly region in vicinity of Mardol area comprises of weak clayey sandy soil. Analysis showed us that the slopes in this area are marginally stable with F.O.S of 0.45 and highly susceptible to failure during monsoons or on loading. The stability of current slope was seen to increase by 42% i.e. F.O.S of 1.09 by adopting benching and by 35% i.e. F.O.S of 1.06 on soil nailing. Apart from this other mitigation measures like slope flattening, vegetation cover using Vetiver grass are proposed as they are seen to increase the stability of slopes.

REFRENCES

ABCB (2015).“ Landslides Hazards-Handbook”. Australian Building Codes Board

Aniket R. Dessai andNisha P. Naik(2016). “Stability Analysis of a Vertical Cut at a Factory Site in Goa”Indian Geotechnical Engineering Conference onSustainability in Geotechnical Engineering Practices and Related Urban Issues,Mumbai, India. September 23-24, 2016.

Boop S, (1991). “The Landslide Hazard In India - A Report”. Department of Science and technology, Newdelhi

C. Ghosh, (2016). “Bio-engineering measures for erosion and landslides mitigation byVetiver Grass” Indian Geotechnical Engineering Conference onSustainability in Geotechnical Engineering Practices and Related Urban Issues,Mumbai, India. September 23-24, 2016.

IS: 2720 (1983). “Methods of Test for Soils”.Bureau of Indian Standards, New Delhi, India.

NDMA(2015) National Disaster Management Authority. “Template for detailed project report (DPR) for site specifc landslide risk Mitigation”. NDMA - Government Of India New Delhi.

Singh M, Pandit K, Shaunik D (2015). “Some Aspects Of Geotechnical Investigations At Surbee Landslide, Mussoorie”. Indian Geotechnical Conference College of Engineering Pune, 17-19 December.

Snehabaga R K. (1995). “Design Aids in Soil Mechanics and Foundation Engineering”. Tata McGraw Hill, New Delhi

Sriramkumar.Ca, Saranathan. Eb, Victor Rajamanickam. Ga. and Nadage.B.S(2005).“Landslide Zonation Mapping – Konkan Railway, Ratnagiri Region, Maharashtra”.Konkan Railways, Ratnagiri-415 639.-Commission IV, Working Group IV /022

Taylor D W, (1948). “Elements of Soil Mechanics”. John Whiley& sons NewYork

CASE STUDY AND FORENSIC INVESTIGATION OF FAILURE OF DAM ABOVE KEDARNATH

Leonardo Souza[1], Tanvi Prakash Chanekar[2] and Grishma Sanjay Pandit[3]

[1]Post-Graduate Student, Foundation Engineering, Civil Engineering Department, Goa College of Engineering, Farmagudi, Ponda-Goa, India; lrdcs@rediffmail.com
[2]Post-Graduate Student, Foundation Engineering, Civil Engineering Department, Goa College of Engineering, Farmagudi, Ponda-Goa, India; tanvichanekar@gmail.com
[3]Post-Graduate Student, Foundation Engineering, Civil Engineering Department, Goa College of Engineering, Farmagudi, Ponda-Goa, India; grishmapandit0@gmail.com

Keywords: Forensic Investigations, Failure of Earth Dam structures, Slope Failure

ABSTRACT

Many earthen dams are built on hill sides. Failure of such walls can lead to catastrophic consequences. The effectiveness of a disaster reduction relies on the perception of the disaster itself and proper analysis of the previous experience. From 14 to 17 June 2013, the Indian state of Uttarakhand and adjoining areas received heavy rainfall, which was about 375% more than the benchmark rainfall during a normal monsoon. This caused the melting of Chorabari Glacier at the height of 3800 metres, and eruption of the Mandakini River which led to heavy floods near Gobindghat, Kedar Dome, Rudraprayag district, Uttarakhand, Himachal Pradesh and Western Nepal. Kedarnath, had been obliterated, 608 villages, covering a population of 700,000, in 23 districts of Uttar Pradesh were affected by the flood. Drought in the past year has shown the real pictures of the basins of many dams in India. There is a dangerous levels of silting up reducing both the reservoir capacity and factor of safety. The present average rain fall caused massive flooding all over India. The main result of the Kedernath disaster was a outpouring of silty sediments from the dams along River Mandakini that swallowed up entire villages. Forensic analysis of a failure can significantly improve chances of future success. The present paper is a forensic analysis of failure of dam wall behind Kedarnath temple with respect to danger of silting up of dams and their potential for failures thus help to prevent future such catastrophes in India

INTRODUCTION

An earth or rock fill dam is a geotechnical structure that forms a “barrier” that obstructs the flow of a river. Moraine dams are a special category of earth-rockfill dam naturally formed when glacial debris blocks the path of glacial melt. As they are easily erodible, they need spillways that are designed to safely pass water to the downstream side of the river. They have to have sufficient freeboard to absorb sudden rise in water level caused by snowmelts cloudbursts and floods. Mountain dams tend to get silted up faster as they have greater debris and silt load.

Construction of dams has been known to exist across the Tigris and Euphrates rivers about 5000 years ago. In Tamil Nadu there is a still serviceable dam 1500 years old. The damming of streams and rivers has been integral to human population growth and technological innovation.

Among other things, dams have reduced flood hazard and allowed humans to settle and farm productive alluvial soils on river flood-plains; they have harnessed the power of moving water for commerce and industry; and they have created reservoirs to augment the supply of water during periods of drought. Recently, the risk of natural disasters has increased in the areas below dams as a result of increasing anthropogenic activities (Dhobal, 2013). This trend is likely to increase in the future as human activities will increase. The natural flow paths of the channels get obstructed due to the construction of man-made structures that results in deviation of the flow from its natural course. These are the first to be affected in floods and they are usually either unplanned or illegal in nature.

Dams are categorized generally as earth or concrete dams, depending on the material used to construct it. This paper, discusses failure of an earth dam. Earth dams have their embankments constructed of soil and rock. Properly constructed and maintained earth dams usually have a unending life span. However, improperly constructed and un-maintained dams usually fail as in the present case. A dam failure is a catastrophic type of failure characterized by the sudden, rapid and uncontrolled release of impounded water accompanied by the trapped silt and debris that erode and accumulate additional debris along the way. Major causes of failure of earth dams worldwide include construction flaws, seepage/ piping, overtopping and siltation.(Tandeswara, 1992; ASDSO, 2010) This study shows that siltation and overtopping caused the disaster at Kedarnath.

Sometimes overtopping of a dam could be caused by a poorly designed spillway that is failing to convey excess water away from the dam. Heavy rains from a single tropical storm can cause overtopping as the spillway fails to convey excess flood water thus resulting in the washing away of the dam. The dam above kedarnath did not have a spillway. Excess water usually used to spill out from the back so the need for spillway was never envisioned. The plausible causes of such failure in Kedarnath has been researched by Dobhal et al of the Wadia Institute of Himalayan Geology. (Dobhal, 2013) Dam failure is normally viewed in the context of the risk that is posed to life and property downstream of dams. This is usually so for large dams constructed directly above large population centres. These are capable of causing catastrophic losses. Dam failure can cause loss of life, property damage, cultural and historic losses, environmental losses as well as causing social impacts (Nyoni, 2013)

Case Study cum Forensic Investigation Procedure

Many Earthen Dams are built as part of infrastructure projects in India. They lie mostly on the hillsides and are a potential cause of future danger unless properly constructed and maintained. Failures of one such dam lead to devastating consequences. A disaster reduction plan is essential and its effectiveness relies on the expectation of the disaster itself, previous experience and state of preparedness.

The present case study aims to present the data available in a new light. From the review of the studies carried out by multiple agencies in the area, it is seen that the reasons given for the disaster are inadequate. As a forensic procedure the data was collected from various sources and assimilated and a conclusion was reached that the disaster occurred due to reduced reservoir capacity due to siltation, improper compaction as it was a natural blockage and increase in height without spillway provisions.

We will first study the data available from the source at closest proximity to the site- the Wadia Institute of Himalayan Geology, Dehradun which operate monitoring stations in that area. We will also study the impact of the siltation on the reservoir. From these studies we will draw reasonable conclusion as to the possible plausible cause of the Earthen Dam Failure.

Study area

The Kedarnath temple town (see Fig. 1) is located in Uttrakhand state of India in the western extremity of the Central Himalaya (30 44 6.7 N; 79 04 1 E) in the Mandakini River valley which has a total catchment area of ~67 km2 (up to Rambara), out of which 23% area is covered by glaciers. The Primary deity of Kedarnath is the 'Lord of Kedar Khand' (Shiva) (Wikepedia, 2016). The catchment area is situated in the glacier modified U-shaped valley; the altitude ranges from 2740 to 6578 m asl (above sea level). Such a variation in the altitude provides diverse landscape.

Mandakini River originates from the Chorabari Glacier (3895 m) near Chorabari Lake and joins Saraswati River which originates from Companion glacier at Kedarnath, passing through Rambara and Gaurikund. The Madhu Ganga and Dudh Ganga are the main tributaries that merge into the Mandakini River at Kedarnath town.

The Chorabari Lake (3960 m asl) also known as Gandhi Sarovar Lake is a snow melt and rain fed lake, located about 2 km upstream of Kedarnath town which is approximately 400 m long, 200 m wide having a depth of 15–20 m. The bursting of this lake led to its complete draining within 5–10 min as reported by the watch and ward staff of the Wadia Institute of Himalayan Geology (WIHG) who were present in WIHG camp at Chorabari Glacier on 16 June and early morning of 17 June 2013(Dobhal 2013).

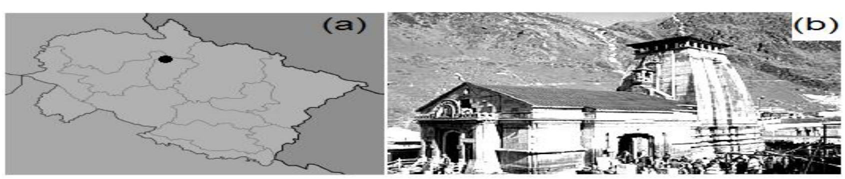

Figure 1(a)Location of Kedarnath in Utrakhand (Wikipedia);(b) Kedarnath Temple

Legend of the Chorabari Lake

The Chorabari lake is a moraine dammed reservoir. It is caused by the natural blockage of a glacial valley by glacial moraine. It causes the resulting sediments to pile up behind the blockage thus creating a reservoir for molten snow, ice and rain. The unstable temple is not directly accessible by road and has to be reached by a 14 kilometers (8.7 mi) uphill trek from Gaurikund. Pony and manchan (porter-carried) service is available to reach the structure. The temple was allegedly built by Pandavas during their journey to heaven and revived by Adi Sankaracharya (the great Hindu reformer) and is one of the twelve Jyotirlingas, the holiest Hindu shrines of Shiva. (Wikepedia, 2016) Kedarnath is an in accessible place even today accessible with great difficulty only six months in a year. With modernization of India’s transport system the rush of pilgrims grew from a trickle in 1900’s to a torrent today. There was an acute shortage of water for consumption. As the area developed, the water from the Snowmelt Rivers was insufficient. The people prayed for divine intervention. It is said that one day as the parched people of Kedarnath prayed to Lord Shiva, and he sent his 'ling' down to dam the valley above Kedarnath and created a lake. Over the years the dammed portion was raised and *used for consumption*. When disaster struck it is claimed that that very giant stone (Ling) that had dammed the valley, tumbled down and came and stood between the temple and the mud flow thus protecting the shrine. A huge rock got stuck behind Kedarnath Temple and protected it from the ravages of the flood. The waters gushed on both the sides of the temple destroying everything in their path. Even eyewitness observed that one large rock got carried to the rear side of Kedarnath Temple, thus causing obstruction to the debris, diverting the flow of river and debris to the sides of the temple avoiding damage. (Wikipedia, 2016) It still stands there today a mute spectator to the destruction caused by mans greed and negligence. Deforestation and denudation of vegetation on the slope to feed the firewood-fuel-needs of the ever growing pilgrim population, hap-hazard development, unsustainable augmentation of reservoir height without provision of proper spillway and design freeboard, (see Fig. 2) and no effort to de-silt the reservoir caused and compounded this disaster.

Plausible Causes of Failure

The standard cause of failure was the cloud burst followed by snowmelt and overtopping. The real reason for over topping was the silted up reservoir. We will discuss both the scenarios here.

Recent climate changes have had significant impact on high-mountain glacial environment. Rapid melting of snow/ice and heavy rainfall has resulted in the formation and expansion of moraine dammed lakes, creating a potential danger from dammed lake outburst floods. The Indian Summer Monsoon is the major source of precipitation (rainfall) in the study area with partial contribution from western disturbances during winter. On 16 and 17 June 2013, heavy rains together with moraine dammed lake (Chorabari Lake) burst caused flooding of Saraswati and Mandakini Rivers in Rudraprayag district of Uttarakhand.

Figure 2 the photo shows the raised part of the dam, the breech at the abutment and the silt accumulated in the dam (WIHG).

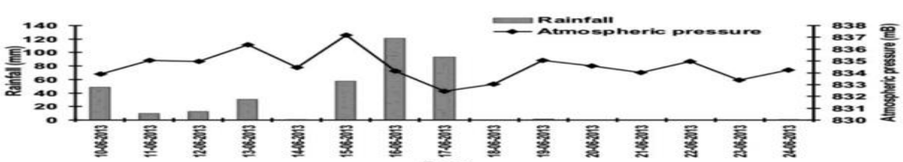

Figure 3 Rain fall and pressure at Ghuttu observatory 38 km from Kedarnath

Prolonged heavy down pour (Figure 3) on 16 and 17 June 2013 resembled 'cloud burst' (except for amount of precipitation of 100 mm/h) type event in the Kedarnath valley and surrounding areas that damaged the banks of River Mandakini for 18 km between Kedarnath and Sonprayag, and completely washed away Gaurikund (1990 m asl), Rambara (2740 m asl) and Kedarnath (3546 m asl) towns. The preliminary results suggest that the following two events caused devastation in the Kedarnath area of the Mandakini River basin.(Dobhal et al 2013). This was widely accepted as the official version as it exonerated all responsibility from any one especially the powers that be. Subsequent Analysis of the disaster was only limited to the overtopping and breech. The actual cause of the rapid overtopping was never discussed. This paper suggests that the silting up of the reservoir by glacial deposits combined with the silt pressure to enhance the impact of the disaster.

Preliminary Devastation Event

On 16 June 2013, at 5:15 p.m., the unprecedented heavy rains fell on the Saraswati River and Dudh Ganga catchment area. This resulted in excessive flooding as the flow across all the channels increased beyond safety limits. The slopes were denuded of vegetation due to active deforestation in that area.

Figure 4: (a) Denuded Slope (Dobhal; May 2012 (b)Devastation of the valley See small house in middle left edge for comparison of size. (Gupta 2013)

There was very active erosion creating deep gulleys and causing excessive water and sediment accumulation in the rivers leading from that area (Fig 4). Subsequently, large volumes of water struck the towns down river which as a result of erosion simultaneously picked huge amount of loose sediment en route. The voluminous muddy water studded with debris from the surrounding regions and glacial moraines moved towards Kedarnath town, washing off all newly constructed structures that lay on and blocked the direct path of the flow - Sankaracharya samadhi, Jalnigam guest house, Bharat Seva Sangh Ashram, etc. the whole upper part of Kedarnath was buried and torn apart and leading to the biggest ever devastation ever witnessed in the region. The WIHG meteorological stations near Chorabari glacier recorded 325 mm rainfall at the base of the glaciers in two days on 15 and 16 June 2013. Due to heavy downpour, the town of Rambara was completely washed away on 16 June evening.

Secondary Devastation Event

The second event occurred on 17 June 2013 at 6:45 a.m., after overflow and collapse of the moraine dammed Chorabari Lake which released large volume of water that caused another flash flood in the Kedarnath town leading to heavy devastation downstream (Gaurikund, Sonprayag, Phata, etc.). Our study shows that the main cause of the Chorabari Lake collapse was torrential rains that the area received between 15 and 17 June 2013.

After the heavy rainfall the right lateral basin of the glacier, which is thickly covered by snow more than 2 meters thick near the upper part of lake during June 2013, rapidly melted due to rainwater allowing large amount of water accumulation in the Gandhi Sarovar lake. There were no outlets in the lake, the water was simply released through narrow passages at the bottom of the lake which were already partly blocked by silt. The sudden water accumulation blocked these passages too. Suddenly millions of gallons of water accumulated in the moraine dammed lake within 3 days, which increased their potential energy and reduced the shear strength of the dam. Ultimately the loose-moraine dam breached causing an enormous devastation in the Kedarnath valley (Figures 5 a,b,c,d & 6)

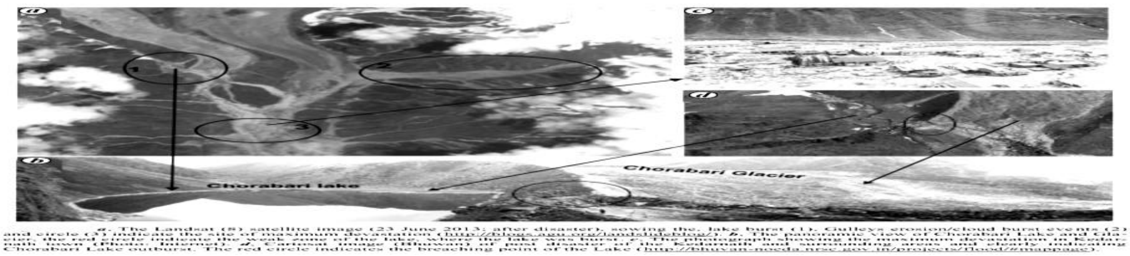

Figure 5: Shows the Devastation at Kedarnath

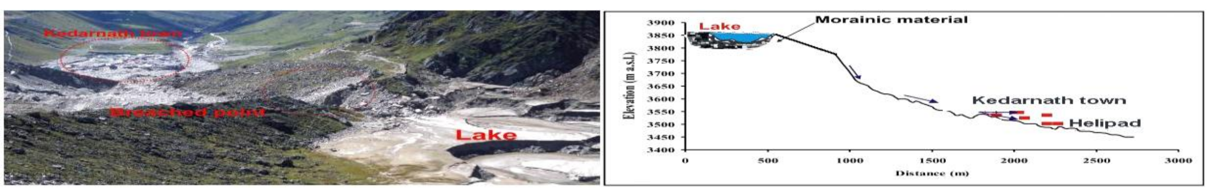

Figure 6: Showing devastation due to silt (Gupta ,2013)

Alternative methods available to prevent dam failure

Many retaining walls are built as part of housing projects on hill sides. Failure of such walls can lead to catastrophic consequences. The effectiveness of a disaster reduction relies on the perception of the disaster itself and previous experience

Analysis by other agencies

Various experts from all over the world studied this disaster; ASI, TERI, IITM, WIHR and many others international and national agencies. There was just too much devastation and too much data floating around. Each analyzed the failure in their own unique way and reached the same conclusion. The danger was caused by excessive runoff, no runoff control (adequate dan storage) and runoff diversion mechanisms and overtopping of the reservoir. But none dared to dwell into why the reservoir overtop. The real reason was simple reduction of capacity due to siltation.

The experts, who were asked by the Archaeological Survey of India (ASI) to examine the condition of the foundation in wake of the floods have arrived at the conclusion that there was no danger to the temple. The IIT Madras experts visited the temple thrice for the purpose. Non-destructive testing instruments that do not disturb the structure of the temple were used by the IIT-team for assessing the health of the structure, foundation and walls. They have submitted their interim report that the temple is stable and there was no major danger (Wikipedia, 2016).

Geologic Study

Geologically, the area north of the Pindari Thrust comprises calc silicate, biotite gneisses, schist and granite pegmatite apatite veins belonging to the Pindari Formation3. Above 3800 m asl altitudes, glacial processes dominate and between 3800-2800 m asl glacio-fluvial processes are dominant; below 2800 m asl mainly the fluvial processes are active.

Geomorphologically Mandakini valley (Figure 7) was formed by the erosional and depositional processes of glacio-fluvial origin. The Kedarnath town is situated on the outwash plane of Chorabari and Companion glaciers. The channels of Mandakini and Saraswati Rivers encircles this outwash plane and meet near the Kedarnath town where the outwash plane ends.

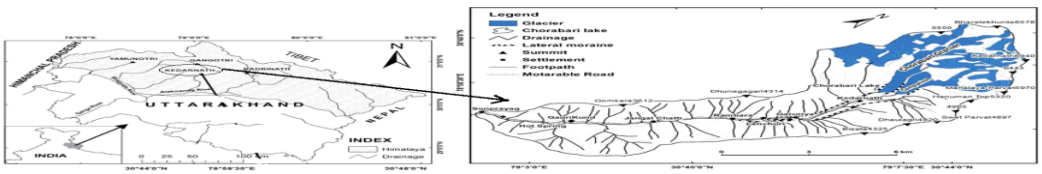

Figure 7: geomorphology of Kedarnath (Gupta ,2013)

These streams cut their banks every year. Overcrowding of the people near the temple led to an artificial change in the course of Sarswati River which now flows just behind the Kedarnath town. This was the major reason for the scale of the disaster.

Desiccation Cracking

The phenomenon of cracking is present in most geotechnical structures and has been of particular interest to civil and mining engineers. Cracks increase by progression as drying increases as shown in the (fig 8). Cracks pose a threat to the integrity of geotechnical structures such as slopes, embankments, dams, tunnels, pavements, foundations, etc. Cracks adversely influence the stability of slopes by:

1. Providing a preferential path to water flow, thereby inducing high pore-water pressures
2. Cracks can form part of the slip surface providing little or no shear strength.
3. Surface cracks formed due to silt deposition on the dam surface have a tendency to progress inwards thus reducing the critical section of the dam.
4. Cracks provide initial route for piping failure
5. Cracks aid in washout during overtopping failure

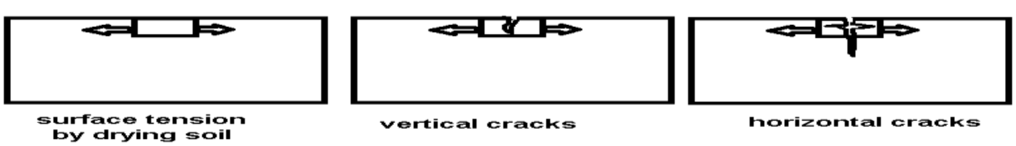

Figure 8: shows Progression of desiccation or shrinkage cracks

Therefore, a clear understanding of the effect of cracks is vital for safe and economical designs of levees, dams and slopes. Traditional design of earth embankments is based on the hypothesis of intact fill, i.e., the presence and occurrence of cracks is disregarded. But under actual conditions, it is unavoidable to prevent cracks formation. Desiccation cracks are formed due to shrinkage of the soil mass as a result of evaporation of water during summer seasons. In the hot summer seasons of India cracking is natural. The phenomenon of desiccation cracking is presumed to increase in future due to global warming, when the range of the extreme temperatures will increase. The total flow increases dramatically with increases in crack size (Figure. 9a)

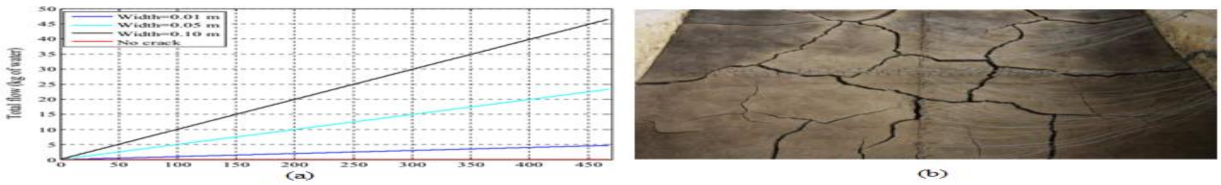

Figure 9: (a) flow v/s cracks (b) Dessication cracks (Khandelwal 2011)

The presence of cracks (fig 9b) makes the soil slopes susceptible to water seepage, erosion, loss of shear strength and consequent failures (Khandelwal 2011)

Loss of storage Capacity of dam: The observed annual percentage loss in gross storage is given in Tables below. The annual percentage loss in gross storage has been worked out as the average based on the data of 239 reservoirs (CWC, 2015). Earlier it was believed that sediment in a reservoir always deposited in the bottom elevations of a reservoir rather than depositing throughout the full range of reservoir depth. It has now fully been established that sediment deposits throughout the depth of reservoir and reduces the capacity of reservoirs at all elevations. The maximum silting takes place at the interface of dam and water.

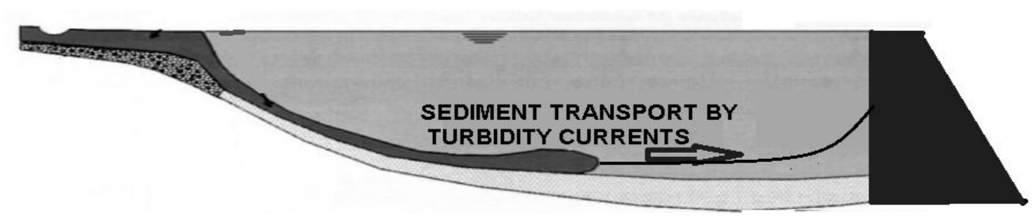

Figure 10: shows transport of sediments in dams

There is an up-wash of bottom sediments against the wall due to back pressure build up and continuity of motion (Figure 10). This causes a bowl shaped bottom that can be seen in various photographs of dried up dams elsewhere in India and internationally too.

In the reservoirs which have small sluicing capacity with respect to normal floods and which have no reservoirs above them, the siltation rate is comparatively high in the first 15-20 years and thereafter it decreases. This is because the obstruction by the dam causes the dips and flanks of the storage basin to fill up with silt in the early years. Besides, the progressive development of deltas above reservoirs helps in trapping some of the silt load (Table 1a & 1b).

These tables show that the reservoir capacity is steadily decreasing. The impact is more on the Himalayan region dams. The silt arrives as a suspension and different particle sizes settle at different rates. The turbidity currents and eddies caused by heat cycle keep much of the silt in suspension. The various sizes and turbulence cause a sub-zones in the reservoir storage zone as shown in the figure below (Figure 11). There is a clear water zone of about one third height, a turbid water zone of one sixth height, a sludge zone of one third height maintained by turbidity currents and the settled sedimentation zone of the balance height. These values are not absolute but vary from dam to dam depending on the properties of the catchment area. They are as seen the tables above (CWC, 2015) the highest for Himalayan region. The values of siltation often record only the bottom zone and ignore the other zones.

Additional Silt Pressures: Normally dams are designed for water pressure on the upstream side. The silt load creates an additional pressure on the water face of the dam. As mentioned earlier the various sizes cause a zonation of the reservoir storage zone. The IS code (IS:6515-1984) gives the following provisions for Consideration of Silt Load. Gravity dams are subjected to earth pressures on the downstream and upstream faces where the foundation trench is to be backfilled. Except in the abutment sections in specific casts and in the junctions of the dam with an earth or rock-fill embankment, earth pressures have usually a minor effect on the stability of the structure and may be ignored. The present procedure is to treat silt as a saturated cohesionless soil having full uplift and whose value of internal friction is not materially changed on account of submergence. Experiments indicate that silt pressure and water pressure exist together in a submerged fill and that the silt pressure on the dam is in proportion of the fill by submergence. Criteria for Design - Horizontal ‘ silt pressure ’ is assumed to be equivalent to that of a fluid with a mass of density of 1360 kg/m^2, and Vertical ‘ silt pressure ’ is determined as if silt equivalent to that of a fluid of mass density of 1 925 kg/m^2. Thus we see that the factors of safety will get considerably reduced due to siltation.

Stability calculation: Himalayan dams as mentioned earlier have a huge silt load almost 3.5 to 5 times that of dams in the rest of India. We will compare the factor of safety for normal dams with no silt load and dams with silt load.

The silt is assumed to be uniformly distributed throughout the height of the water storage during peak rainy season. The following values were adopted for the purpose of calculation.

Height of dam = 15 m; Density of moraine dam =2 Mg/m^3 ; Density of water = 1 Mg/m^3

Density of silty water = 1.75 Mg/m^3

Table 1a: Annual percentage loss of gross, live and dead storage capacity of reservoirs (CWC 2015)

Sl.No.	Description	Minimum	Maximum	Average	Remarks
1	Annual percentage loss of gross storage	0.03	3.38	0.42	Based on average data of 239 reservoirs
2	Annual percentage loss of dead storage	0.007	5.23	0.494	Based on average data of 86 reservoirs
3	Annual percentage loss of live storage	0.003	3.23	0.04	Based on average data of 86 reservoirs

Table 1b: Rate of Siltation of Reservoirs (Region wise) (CWC 2015)

Sl. No.	Region	No. of reservoirs	Median values of rate of siltation	
			Th.cu.m./ sq.km/yr	Ha.m./100 sq.km/year
1	Himalayan Region (Indus, Ganga and Brahmaputra basins)	14	1.581	15.81
2	Indo Gangetic Plains	15	0.752	7.52
3	East flowing rivers upto Godavari (Excluding Ganga)	5	0.678	6.78
4	Decan Peninsular east flowing rivers including Godavari and south Indian rivers	115	0.378	3.78
5	West flowing rivers upto Narmada	53	0.861	8.61
6	Narmada and Tapi Basins	10	0.651	6.51
7	West flowing rivers beyond Tapi and south Indian rivers	31	2.1325	21.325

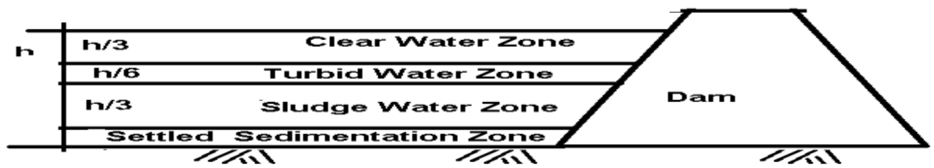

Figure 11: shows different zones in a Dam Storage

The factor of safety against over topping is reservoir volume (reach and depth) dependent. The Chorbari dam was neither designed nor maintained hence there was no safe balance storage volume. We have not calculated the factor of safety against over topping as there was insufficient data available. But as seen in these deliberations siltation reduces the balance storage to zero thus it also reduces the Factor of safety from 1 to nearly zero.

Table 2: Formulas used for calculation of factor of safety

Stability Check	Formula	Notations
Factor of safety against sliding (F_s):	$F_s = \frac{P_r}{P_s}$	P_r = Resisting Force P_s = Horizontal Sliding Force
Factor of safety against overturning (F_o):	$F_o = \frac{M_r}{M_o}$	M_r = Resisting Moment M_o = Overturning Moment
Factor of safety against over topping(F_h)	$F_h = \frac{V_b}{V_f}$	V_f = Volume of Peak Flood Inflow V_b = Balance Storage Capacity Volume

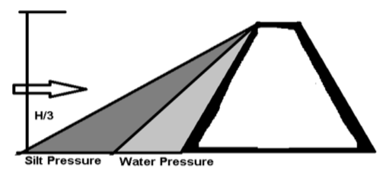

Fig12: schematic Silt pressure diagram

Figure 12: showing schematic silt pressure diagram and table used for stability check for dam

The available commercial software do not adequately provide for silting load on reservoir. The calculations of the factors of safety were hence performed on excel sheets prepared by us. The results are shown below for comparison.

Table 3: of comparison between normal and silt load

Case	F_s (Sliding)	F_s (Over turning)	F_s (Over topping)
normal load	1.5	4.8	0
silt load	1.26	4.39	0

Conclusion

Moraine dams are basically temporary natural earth dams. When these dams are augmented for height without the proper precautions they are in danger of failure. The melting of Chorabari Glacier combined with the cloud burst and the reduced capacity of the dam due to silting up caused a major disaster that was avoidable. The results have shown that there is critical loss of soil when an earth dam fails. The accumulated silt load cascades down the slope carrying with it loose boulders and rock that obliterate everything in their path. Also the bigger the dam, the greater the soil loss and resulting damage. The Government has to take care of these issues in future zoning of such areas.(Dobhal et al 2013) Failure of such dams can lead to catastrophic consequences. The data collected from various sources indicates that the disaster occurred due to reduced reservoir capacity due to siltation, improper compaction as it was a natural blockage and increase in height without spillway provisions. Due to natural formation of the lake there was no proper bondage at the abutment of the moraine with the mountain. This was the weakest spot and was saturated due to the ongoing monsoon season. It was the first to give way during the overtopping caused by reduced reservoir flood absorption capacity due to silting up of the reservoir. The effectiveness of a disaster reduction plans rely on the perception of the disaster itself and what is learnt from such an experience.

References

ASDSO-Association of State Dam Safety Officials(2010) Dam Failures, Dam Incidents (Near Failures) www.damsafety.org

CWC-Central Water Commission APRIL 2015 COMPENDIUM ON SILTING OF RESERVOIRS IN INDIA Central Water Commission, New Delhi.

Dobhal D. P., Gupta A. K., Mehta M., Khandelwal D. D. -, 25 July 2013 - Kedarnath disaster: facts and plausible causes-Wadia Institute of Himalayan Geology, Dehradun 248 001, India -CURRENT SCIENCE, VOL. 105, NO. 2pg 171-174

Gupta A. K et al (2013) - A Report On Kedarnath Devastation- Wadia Institute of Himalayan Geology, Dehradun

IS:6512(1984) Indian Standard- Criteria For Design Of Solid Gravity Dams- Bureau Of Indian Standard-'Smanak Biiava-N. 9 Bahadur Sliah Zafar Hlarg New Delhi 110003-section 5

Kaniraj. S. R IIT Delhi – 1995 – Design Aids in Soil Mechanics and Foundation Engineering. – Tata McGraw Hill, New Delhi

Khandelwal S (2011) Effect Of Desiccation Cracks On Earth Embankments A Thesis Texas A&M University

Nyoni K. -August 2013-Environmental Impacts of Earth Dam Failures and Spillway Malfunctions-Greener Journal of Physical Sciences Vol. 3 (5), pp. 177-186, ISSN: 2276-7851

Thandaveswar B.S. (1992) History of Dam Failures – ppt Lecture Notes- Indian Institute of Technology Madras

Wikipedia,(2016) Kedarnath Temple www.wikipedia.com

Quantification of particle morphology through image based techniques and its importance in forensic studies

Prashanth Vangla, Ph.D., [1]Nimisha Roy, M.Sc. (Engg.), [2] and Gali Madhavi Latha, Professor[3]

[1]Department of Civil Engineering, Indian Institute of science, 560012, Bangalore, India;e-mail: pvangla@civil.iisc.ernet.in
[2] Department of Civil Engineering, Indian Institute of science, 560012, Bangalore, India;e-mail: nimisha.roy9@gmail.com
[3]Department of Civil Engineering, Indian Institute of science, 560012, Bangalore, India;e-mail: madhavi@civil.iisc.ernet.in

ABSTRACT

Recent advancement in digital technology enabled the development of sophisticated methods for understanding the fundamental aspects of particle morphology and facilitated the precise quantification of sphericity, roundness, angularity and roughness of particles. This paper presents new computational methods to quantify the particle morphology using image analysis. These methods overcomes the limitations of existing methods based on image analysis and classify all types of sands with more accuracy. The importance of particle morphology on the interface shear behavior of sand-geosynthetic surfaces is demonstrated through microtopographical analysis of shear induced surface changes in geosynthetics. Results from the investigations showed that angularity of particles is a very influential parameter in controlling the interface shear behavior. These results play key role in understanding shear induced failures in reinforced soil structures and help in forensic investigations of such failures.

INTRODUCTION

The internal stability of reinforced soil structures mainly depends on shear strength of soil-reinforcement interfaces, because these interfaces are weakest zones in the structure (Palmeria, 2009). Shear strength and deformation characteristics of sand–reinforcement interface hugely depend upon the interaction mechanism (sliding, rolling, plowing and interlocking) that develops between them while shearing. Several researchers demonstrated that interaction mechanism between sand and reinforcement largely depends on particle size, shape and surface features of the reinforcement (Jewell et al., 1985; Latha and Murthy, 2007; Fuggle, 2011). If the coefficient of friction is less for an interface, then the predominant mechanism could be sliding or plowing because relatively less force is required to initiate a relative motion against the friction force offered by a particle, which is partially embedded in the surface of geosynthetics. The volume changes in this type of interface are negligible, therefore these are called non-dilative interface systems (Dove et al., 2006). However, if the coefficient of friction is large, the predominant mechanism could be rolling because relatively high friction force is required to push and rotate the particle, which is locked in the surface asperities (Jewell, 1996; Biabani and Indraratna, 2015). In this type of interface volume changes are evident, therefore these are called dilative interface systems. Literature suggests that interface shear behaviour of particulate materials and geosynthetics is significantly influenced by the morphology and surface asperities of reinforcement. Hence, precise characterization of the morphological properties of the particulate material and surface features of geosynthetics are essential for understanding the mechanical behaviour of reinforced structures. Many a times, failure of such structures is governed by microscopic shear mechanisms, which cannot be understood by conventional forensic geotechnical investigations and need advanced image based techniques, which are explained in this paper.

The international conference on Forensic Geoscience: Principles, Techniques and Applications held at the Geological Society of London in 2003 emphasized the importance and usefulness of particle morphology in forensic soil examination (Pye and Croft, 2004). Most often the image of particulate materials captured using microscope and digital image capture system (Ehrlich et al., 1980; Pye and Mazzullo, 1994; Murray, 2004) is used for qualitative and quantitative soil examination to determine the size and morphology. Fourier analysis is most common technique performed on projected images of particulate materials for quantitative measurements (Bowman et al. 2001). However, Fonseca and O'Sullivan (2008) concluded that the approach used by Bowman et al. (2001) to quantify the particle shape using Fourier descriptors is not applicable for general soil characterization.

The use of image analysis and optical methods for thorough understanding of the morphological characteristics of particulate materials (sand) and surface roughness of the geosynthetic surfaces is of growing interest among many researchers (Dove and Frost, 1996; Alshibli and Alsaleh 2004; Vangla and Latha, 2016). Research in particle morphological characterization has gone through several phases, starting from visual characterizations in olden days to the most recent methods based on image analysis. According to Barrett (1980), particle shape comprises of three different multi-scale components- form (macro-scale), roundness (meso-scale) and surface texture (micro-scale), which are independent properties because each one varies widely without necessarily affecting the other two properties. Several researchers have attempted to characterize the shape of sand particles through various methods including projection methods, standard shape comparison methods, functional methods, and fractal methods (Sozer, 2005), which led to the identification of many shape parameters/descriptors. Despite the availability of many methods, no method has been accepted as standard, because of conceptual and practical deficiencies. Wadell's definition (Wadell, 1932) of roundness is the most widely accepted formula as it is more statistically sound as compared to the formulae coined by several other researchers.

This paper presents an accurate computational method based on image analysis to quantify the particle shape and studies on effect of particle shape and size on non-dilative interface systems. The reasons for the variation in peak friction angle at different interfaces are examined through particle shape and surface roughness studies.

PARTICLE MORPHOLOGY BY COMPUTATIONAL METHODS

The process of quantifying particle morphology, viz. roughness, roundness and sphericity, by the proposed method can be realized in three steps. In the first step, filtering techniques are employed on segmented 2D image projections of particles to remove high frequency components of noise and roughness after converting the boundary profile of the image into the frequency domain using Fourier Transforms. This process is also used to quantify roughness of the particle outline. The second stage implements an algorithm developed to identify 'corners' along the particle outline free from micro-scale features and to fit the most appropriate circle in each corner for the quantification of roundness as per Wadell's concept. The third stage deals with the quantification of form or sphericity of the particle using computational geometry.

Roughness

Roughness of a surface is generally computed by measuring the deviations of the surface from its mean plane at a specific scale. However, because of greatly uneven soil particle surfaces, there is generally no functional form to evaluate the mean surface. This problem is addressed in the present study by separating the micro scale features of roughness from the opened up boundary profile of the binary image of the particle, by the use of digital filters to obtain the roughness free profile. The boundary of the particle is obtained by tracing the outline of the binary particle (Figure. 1a)silhouette. The roughness feature comprises of actual particle roughness along with the noise in the image, which is the consequence of aliasing effect by the square pixels tessellation. The open profile of the particle outline, called as raw profile in this study, is obtained by opening the boundary of the particle at a constant interval of 0.0017 radians (0.1 degree) in clockwise direction from its centroid. The raw profile in the spatial domain is transformed into the frequency domain subsequently by the use of Fast Fourier algorithm. The frequency domain comprises different wavelength components of the raw profile corresponding to various aspects of particle shape, viz. roughness corresponding to small wavelength component, roundness corresponding to medium wavelength component and form corresponding to high wavelength component. This information is very useful to suppress or retain the selected wavelength components by applying filters before reconstructing the particle outline for further findings.

To filter out the micro scale features of roughness from the raw profile, a low pass Gaussian regression filter is used in the present study. The input cutoff wavelength corresponding to micro-scale features is decided based on the cutoff amplitudes given as a percentage of the maximum amplitude of intensity in the frequency domain. The cutoff amplitude is established by checking the variations in three key parameters with change in cutoff value for filter, viz. number of corners, ratio of perimeter of cumulative corner length to the perimeter of particle (referred to as perimeter ratio) and the value of roundness according to Wadell's definition. The standard chart particles of Krumbein and Sloss (1951), Powers (1953) and Hawkins (1993) of known range of roundness values and few real particles were used in this investigation to arrive at an appropriate cutoff amplitude for filter. The values of the key parameters are observed to be constant for cutoff amplitude range of 1.1-1.5% for all investigated particles. The values of roundness obtained in this range compared well with the values given in the visual charts. Hence for removing roughness from particle outline, an amplitude cutoff of 1.2% is used in this study.

Having decided the cutoff amplitudes for roughness, the corresponding maximum number of descriptors required to remove these features were read from the frequency spectrum plot. The wavelength of the sinusoid component of the profile corresponding to the number of descriptors read is the cutoff wavelength for the profile. The cutoff wavelengths obtained are used in the second order low pass Gaussian regression filter to filter out the roughness features and obtain the roughness free profile (Figure. 1b). Having established the roughness free profile, root mean squared roughness (R_q) can be computed as:

$$R_q = \sqrt{\frac{\sum_{k=1}^{n}(y_{kr} - y_{ks})^2}{n}} \qquad (1)$$

Wherey_{kr} is the value of the k_{th} coordinate of the raw profile, y_{ks} is the value of the k_{th} coordinate of the smoothened profile, and n is the total number of points in the profile. The R_q is scale dependent value, which increases with the increase in particle size. Therefore to obtain R_q which is free from this scale dependence, it is normalized with length (L) of the particle, which is called as normalized roughness (NR_q), expressed in percentage.

$$NR_q = \frac{R_q}{L} \quad (2)$$

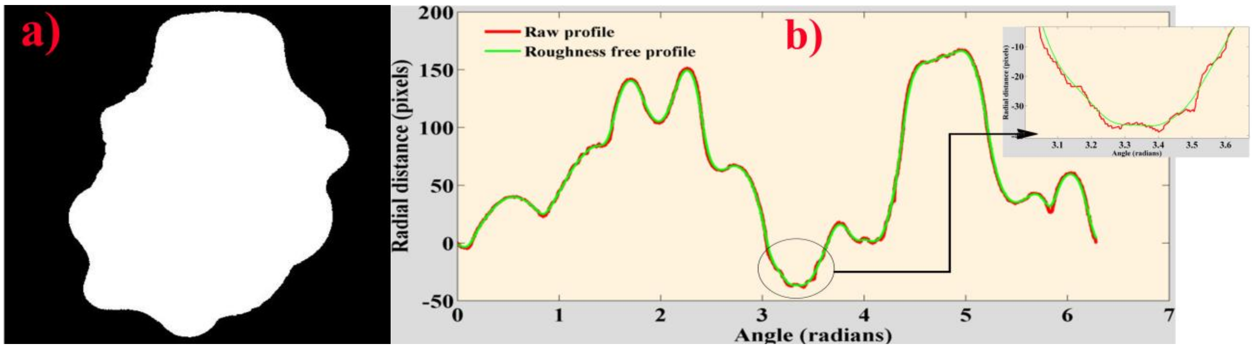

Figure 1. Removing roughness from a particle outline a) binary image of particle b) raw profile and roughness free profile obtained by filtering roughness features at cutoff amplitude of 1.2% of the maximum amplitude of intensity in the frequency domain

Roundness

There are four main steps required to compute roundness as per Wadell (1932) definition after obtaining the smoothened particle outline. In the first step, dominant points along the particle outline are identified using linear polygonal approximation method. The dominant points are a set of fewer key points that contain almost complete information of the particle boundary. An algorithm is written for this purpose, similar to that proposed by Gerken (1994) and Altunbasak et al. (1997) and is implemented in MATLAB. The algorithm involves detecting boundary points at maximum distance (d) from a defined vector, starting from the vector representing the length of the particle, and iterating to obtain vectors formed by joining endpoints of the previous vector and the detected boundary points at maximum distances from it on either side, until d is greater than a predefined threshold value n. The value of n, which depends on the characteristics of the image captured, should be as small as possible so as to not miss the small sharp corners along the particle outline yet high enough to save computational cost. Its value is taken to be a fraction of the maximum dimension of the particle in pixels and it is found after performing numerous computations on various particles of different angularities, that n = 0.09 % of the maximum dimension of the particle is the highest possible value which manages to capture all corners of even the most angular particles. At the end of this iteration, the particle boundary is discretized into small straight lines joining the dominant points as shown in Figure. 2a.

The second step involves identification of corner portions along the particle outline by using the detected dominant points. In a closed boundary, a corner is identified as any concave inward portion of the particle boundary having radius of curvature equal to or less than the radius of curvature of the maximum inscribed circle in accordance with Wadell's definition. A curve is concave inwards if a line joining any two points on the curve always lies inside the curve whereas a concave outwards curve is one in which a line joining any points on the curve always lies outside the curve. The corner detection algorithm detects all continuous set of dominant points that are concave inwards as a whole. The detected corner regions of the particle are shown in Figure. 2b.

In the third step, the maximum inscribed circle is found. For each white pixel inside the boundary of the soil particle, the minimum distance to the nearest black pixel outside the particle boundary is computed, which produces a distance contour map as shown in Figure. 2c. The pixel with the maximum stored distance is the center of the maximum inscribed circle and the stored distance is its radius.

The final step is to fit the best circle in each corner so as to determine its radius of curvature. The radius of curvature is determined at every point of each corner using a modified double derivative formula, to take into account the uneven spacing of discrete points along a closed boundary. Let the first point of the curve be (x_s, y_s), the middle point be (x_m, y_m) at a finite difference k with respect to the first point and at a finite difference h with respect to the end point (x_e, y_e). Considering these points, the double derivative formula can be modified as follows by incorporating the average weightage of h and k (both represent a small change in x).

$$f''(x) = \frac{k\times(y_e-y_m)+h\times(y_s-y_m)}{k\times h\times\left(\frac{h+k}{2}\right)} \quad (3)$$

Where, $h = x_e\text{-}x_m$, $k = x_m\text{-}x_s$.

The above double derivative formula results in many circles at each corner. The best fit circle among these circles is the one, which is tangential to the local maxima of the corner and touches the maximum number of points along the corner boundary as shown in Figure. 2d. Roundness can now be computed using Wadell's definition as follows

$$R = \frac{\sum_{r=1}^{n} D_r}{D_i} \quad (4)$$

Where D_r is the diameter of the r^{th} circle, n is the total number of circles and D_i is the diameter of the inscribed circle. The roundness of the particle in Figure. 2d is computed to be 0.44.

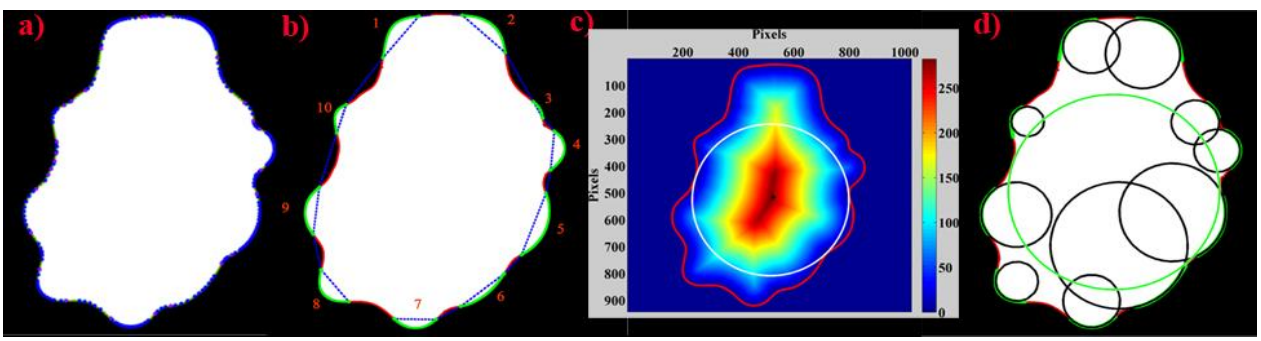

Figure 2. Evaluating roundness of a particle a) detected dominant points from polygonal approximation algorithm b) final corners obtained from corner detection algorithm c) maximum inscribed circle of the particle d) best fit circles for all corners of the particle with the value of roundness

Sphericity

Sphericity is defined in many ways by researchers till date. Zheng and Hryciw (2015) investigated the usefulness and effectiveness of most widely used definitions of sphericity and concluded that sphericity defined as width to length ratio of the particle (S_{wl}) is the most simple and practical definition. The values obtained using this definition were well matching with the visual chart provided by Krumbein and Sloss (1951). Hence, in the present study, the same definition is used for quantifying the sphericity of sand particles. The length and width of the sand particle are determined computationally. The length of the particle (L) is same as the main axis of the particle used in iterative polygonal approximation. The width of the particle is determined in the following way. The coordinates of the boundary points on either side of the main axis at maximum distance from it are stored in an array. A line is drawn parallel to main axis (L) and passing through any one of these points. The perpendicular distance of the other boundary point from the drawn line is the width of the particle 'W'. The length, width and sphericity of the particle is shown in Figure. 3. The values of sphericity are independent of roundness values and the definition yields sphericity values between 0 and 1.

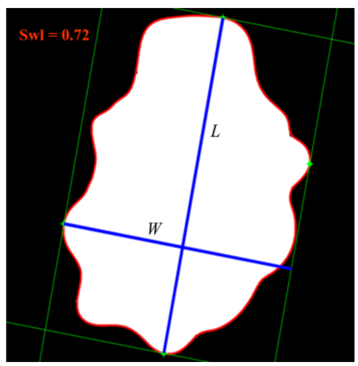

Figure 3. Sphericity of the particle

Shape analysis of real particles

Shape analysis is also carried out on randomly selected particles from four sand groups; Angular coarse sand (ACS), Coarse sand (CS), Medium Sand (MS) and Fine Sand (FS) by the new computational method discussed in above sections. The sands belonging to the category CS, MS and FS are river sands taken from the same source whereas sand belonging to category ACS is quarry sand taken from a different source. SEM images of 30 particles of each type of sand were taken for shape analysis in this study. The values of roundness are nearly same for coarse, medium and fine sands (CS- 0.28, MS- 0.24, FS- 0.26), classifying them as subangular (roundness between 0.25-0.35) as per Powers (1953). Angular coarse sand has average roundness value of 0.18, classifying it as angular (roundness between 0.17-0.25) as per Powers (1953). The average values of sphericity for coarse, medium and fine sands are 0.82, 0.83 and 0.80, whereas angular coarse sand has average sphericity value of 0.74. The reference chart provided by Krumbein and Sloss (1951)classifies CS, MS and FS into the same category of sphericity and roundness, whereas ACS falls into the more angular and less spherical category. Particles from CS, MS and FS have shown almost same average NRq values (CS- 0.05, MS- 0.06, FS- 0.07) whereas ACS particles have exhibited higher average NRq value of 0.10. The obtained values of sphericity, roundness and normalized roughness indicates that CS, MS and FS exhibit similar morphology, whereas ACS is more angular, less spherical and more rough as compared to the other three sands. Figure. 4 shows SEM images of typical sand particles of all four groups used for shape analysis along with their roundness, sphericity and normalized roughness values.

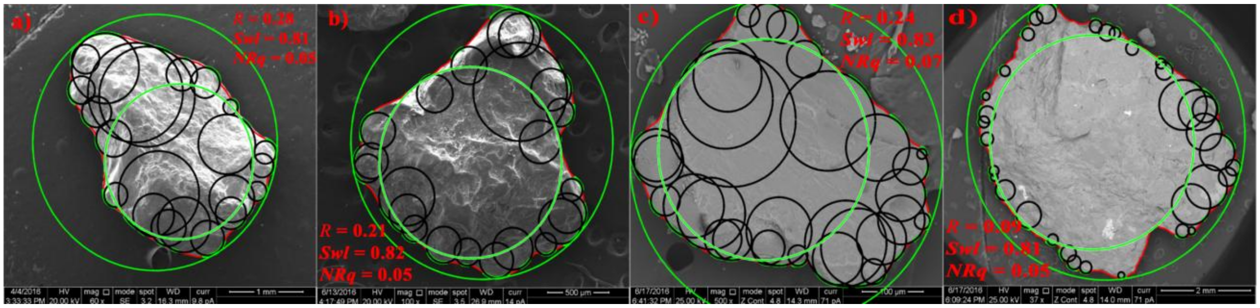

Figure. 4. SEM images of typical sand particles used for shape analysis a) CS b) MS c) FS d) ACS

DIRECT SHEAR TESTS

Initially series of symmetric loading direct shear tests were performed on four sands (ACS, CS, MS and FS) to understand their shear behaviour and to compare with interface shear behaviour of these sands with smooth geomembrane. Symmetric loading test conditions and direct shear test setup used in this study are described in Vangla and Latha (2014, 2015). All direct shear tests were conducted at a relative density of 70% under three normal stresses (22, 37 and 53 kPa). The initial void ratio and the peak and post peak friction angle obtained for these sands are presented in Table 1. One can observe from Table 1that CS, MS and FS have exhibited almost same friction angle. Despite the fact that these three sands have very different particle sizes, they showed almost same friction angles due to their similar morphological characteristics and also because their void ratios were almost same (about 0.7) at a relative density of 70%. Studies by Santamarina and Cho (2001) and Holtz and Kovacs (1981) also suggested that particle size does not affect the peak friction angle of sands of similar morphology if the void ratio is same.

ACS and CS are having same size range and different particle morphology; ACS is more angular compared to CS. However, ACS exhibited low friction angle compared to CS. Literature suggests that the increase in angularity of sands generally results in increase in friction angle.However, the initial void ratio of ACS is 0.93, which is 28% higher compared to CS (0.67) at relative density (RD) of 70% because of the shape of the particles. The higher void ratio of ACS at 70% RD compared to CS resulted a loose state of packing, this caused decreased friction angle. To confirm this aspect, direct shear tests on ACS samples prepared at a higher relative density of 90% are performed; the void ratio corresponding to this RD is 0.85. Friction angle reported from this set of tests was found to be same as the friction angle reported for CS prepared at 70% relative density though the void ratio was 21% more, confirming the effect of angularity in improving the friction angle.

Table 1.Peak and post peak friction angles for sands used in study

Type of sand	Initial void ratio '*e*'	Peak friction angle, degrees	Post peak friction angle, degrees
CS	0.67	40.8	38.9
MS	0.67	40.7	37.2
FS	0.70	40.4	35.9
ACS	0.93	36.5	35.8

INTERFACE DIRECT SHEAR TESTS

Systematic investigations carried out to study the effect of particle shape on the shear behaviour of non-dilative interfaces through a series of symmetric loading direct shear tests and surface roughness studies of the geomembrane. All interface shear tests were conducted under three normal stresses (22, 37 and 53 kPa) at relative density (RD) of 70%.A smooth high density polyethylene geomembrane (GM) of 1.5 mm thickness, which is commercially available and more often used in engineering applications due to its more favorable properties like high tensile strength at low strain, is used in this study.

Some of the earlier studies (e.g. Uesugi and Kishida, 1986;Vaid and Rinne 1995; Zettler et al. 2000; Frost et al. 2012) have brought out the influence of morphological properties of sands, especially their angularity on their interface shear strength with continuum materials. To understand the effect of particle morphology alone two sands ACS and CS having same mean particle size (D_{50}) of 3 mm and similar particle size range (2 mm - 4.75 mm) but distinct in morphological characteristics were selected. The effect of morphology is more pronounced in case of smooth geomembranes than any other continuum materials because sands can easily plow and form deeper grooves to offer higher interface shear resistance.

The peak shear stress envelopes of CS-GM and ACS-GM interfaces under three normal stresses are shown in Figure. 5. The peak and post peak friction angles measured assuming straight line envelopes for ACS-GM are 27.1 and 24.8 degrees respectively. The peak and post peak friction angles for CS-GM are 18.7 and 18.6 degrees respectively. This demonstrations that ACS has shown significantly higher interface shear strength than CS-GM interface despite higher void ratio and lesser peak friction angle at 70% RD compared to CS at same RD. This fact emphasizes that morphology of the particulate materials is highly influential than the initial void ratio or packing of the sand particles in sample. ACS is less rounded, less spherical and rough compared to CS and classified as angular sand and CS is classified as sub-angular based on their sphericity and roundness values. Hence the higher shear resistance of ACS-GM interfaces can be attributed to its higher angularity and roughness. The influence of morphology of the sands on non-dilative interface systems can also be understood in terms of efficiency parameter (*E*) defined as the ratio of Tan δ/Tan ϕ (Koerner 2005) to have relative comparison between the interface friction angle (δ) and sand alone friction angle (ϕ), eliminating the variations due to soil properties. The efficiency parameter calculated for CS is 0.38 and it is 0.69 for ACS. As the particle size distribution for both these sands is same, the increased efficiency can be attributed to the effect of morphology alone.

The reasons for higher shear strength for ACS-GM interface when compared to CS-GM interface was investigated by quantifying the surface changes induced by ACS and CS while shearing using 3D optical profilometer as explained in (Vangla and Latha, 2016). Figure. 6a and Figure. 6b present the 3D images of the surface topography of the GM samples formed due to shearing by ACS and CS respectively at a normal stress of 53 kPa. These figures very clearly show that ACS caused deeper grooves than CS. The 3D quantitative measurement of surface changes is given by areal measurement S_a, the average surface roughness. Average surface roughness (S_a) is the arithmetic average of the absolute values of profile height deviations recorded within the evaluation area and measured from the mean surface area, which is a horizontal plane. Average surface roughness (S_a) values obtained for GM sheared by ACS and CS are 1.09 μm and 0.77 μmrespectively. It is evident from these values and visual observations (Figure. 6) that due to higher angularity of ACS compared to CS induced more surface changes and thus developed higher interface shear resistance than CS.

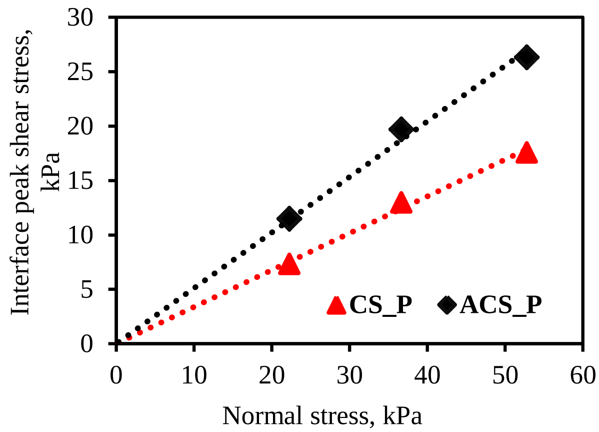

Figure5.Peak shear stress envelopes CS-GM and ACS-GM interfaces

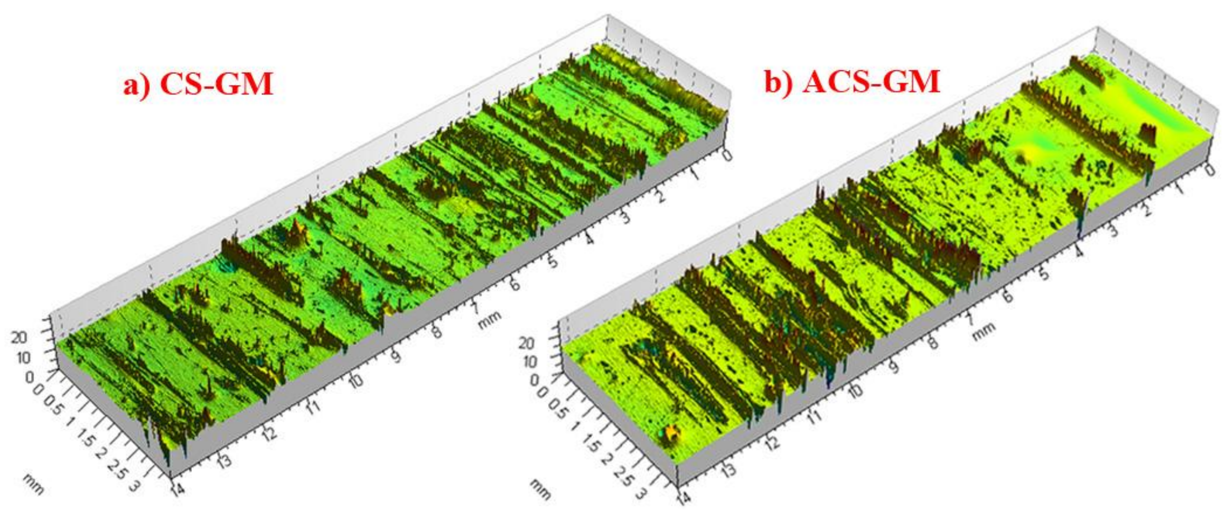

Figure 6.3D images of shear induced surface changes and 2D surface relief profiles of GM samples sheared by a) CS and b) ACS

In case of an interface failure leading to the failure of a reinforced soil structure, the friction mobilized at the interface can be computed by quantifying the surface changes in the geosynthetic material and correlating it to the interface friction through image analysis. These correlations can be established through single particle interface shear tests. The present study provides directions to such future investigations, which could aid the forensic investigations of failed soil-geosynthetic interfaces.

SUMMARY AND CONCLUSIONS

A new computational method is developed for quantifying the shape of sand particles and this method is demonstrated through real sand particles. Effect of sand particle morphology on the shear mechanisms at the sand-geomembrane interfaces is studied through interface shear tests and surface topographical analysis on sheared geomembranes. Results from this study showed that the morphology of sand particles affects the interface friction significantly by governing the microscopic shear mechanisms at the interface, which can be understood through surface roughness studies. These results provide important insights into the interface shear mechanisms, understanding which is very important in forensic investigations of failure of geosynthetic reinforced soil structures.

REFERENCES

Alshibli, K.A. and Alsaleh, M.I. (2004). “Characterizing surface roughness and shape of sands using digital microscopy.” *J. Comput. Civil. Eng.*, 18(1), 36-45.

Altunbasak, Y. and Tekalp, A.M. (1997). “Occlusion-adaptive, content-based mesh design and forward tracking”. *IEEE Trans. Image Process.*,6, 1270-1280.

Athanasopoulos, G.A. (1993). “Effect of particle size on the mechanical behaviour of sand-geotextile composites.” *Geotext and Geomemb.*, 12(3), 255-273.

Bareither, C.A., Edil, T.B., Benson, C.H. and Mickelson, D.M. (2008). “Geological and physical factors affecting the friction angle of compactedsands.*” J. Geotech. Geoenviron. Eng.*134(10), 1476-1489

Barrett, P.J. (1980). “The shape of rock particles, a critical review”. *Sedimentology.*, 27(3), 291-303

Biabani, M.M. and Indraratna, B. (2015). “An evaluation of the interface behaviour of rail subballaststabilised with geogrids and geomembranes”.*Geotext and Geomembr.*, 43(3), 240-249.

Bowman ET, Soga K, and Drummnond, W. (2001). “Particle shape characterization using Fourier descriptor analysis.” *Geotechnique.*, 51(6), 545-554.

Cho, G.-C., Dodds, J., Santamarina, J.C. (2006).“Particle shape effects onpacking density, stiffness, and strength: natural and crushed sands.” *J. Geotech. Geoenviron. Eng.*132(5), 591-602.

Dove, J.E. and Frost, J.D. (1996). “A method for measuring geomembrane surface roughness.” *Geosynth. Int.*, *3*(3),369-392.

Dove, J.E., Bents, D.D., Wang, J. and Gao, B. (2006). “Particle-scale surface interactions of non-dilative interface systems.” *Geotext and Geomembr*, *24*(3), 156-168.

Ehrlich, R., Brown, P.J., Yarus, J.M., and Przygocki, R.S. (1980). “The origin of shape frequency distributions and the relationships between size and shape.” *J. Sediment. Petrol*. 50, 475–483.

Fonseca, J. and O'Sullivan, C. (2008). “A re-evaluation of the Fourier descriptor approach to quantifying sand particle geometry.” *In 4th Int. Symp. on Deformation Characteristics of Geomaterials*, Atlanta, Georgia, USA.

Frost, J.D., Kim, D., and Lee, S. (2012). “Microscale geomembrane-granular material interactions.” *KSCE J. Civ. Eng.* 16 (1), 79-92.

Fuggle, A. R. 2011. “Geomaterial gradation influences on interface shear behavior.”Doctoral dissertation, Georgia Institute of Technology, Atlanta, USA.

Gerken, P. (1994). "Object-based analysis-synthesis coding of image sequences at very low bit-rates". *IEEE Trans. Circuits Syst. Video Technol.*, 4, 228–235.

Göktepe, A.B. and Sezer, A. (2010). "Effect of particle shape on density and permeability of sands." *Proc. Inst. Civil Eng-Geotech Eng.*, 163(6),307-320.

Hawkins, A.E., 1993. The shape of powder-particle outlines. Research Studies Press Ltd., John Wiley and Sons Inc, Chichester, UK, 150.

Holtz, R.D., Kovacs, W.D. (1981). *An Introduction to Geotechnical Engineering*. Prentice-Hall, Inc., Englewood cliffs.

Jewell, R.A., (1996). *Soil reinforcement with geotextiles*. Construction Industry Research and Information Association, London.

Juran, I., Knockenmus, G., Acar, Y.B., Arman, A. (1988). Pull-out response of geotextiles and geogrids (synthesis of available experimental data). *In: Holtz, R.D. (Ed.), Geotechnical Special Publication 18ASCE*, New York, USA, pp. 92-111.

Kabeya, H., Karmokar, A.K., Kamata, Y. and Tsunoda, S. (1993). "Influence of surface roughness of woven geotextiles on interfacial frictional behavior-evaluation through model experiments." *Text. Res. J.*, 63(10), 604-610.

Koerner, R.M. (2005). *Designing with geosynthetics*. (5th Edn.). Prentice Hall, Inc., Engelwood Cliffs, NJ, USA.

Krumbein, W.C. and Sloss, L.L. (1951).*Stratigraphy and sedimentation*. W.H. Freeman and company. San Francisco, USA.

Latha, G.M. and Murthy, V.S. (2007). Effects of reinforcement form on the behavior of geosynthetic reinforced sand. *Geotext and Geomembr.*, 25(1), 23-32.

Murray, R. C. (2004). Forensic geology: yesterday, today and tomorrow. *In: Pye, K. & Croft, D. J. (eds). Forensic Geoscience: Principles, Techniques and Applications*. Geological Society, London, Special Publications, 232, 7-9.

Palmeira, E.M. (2009). Soil-geosynthetic interaction: modelling and analysis. *Geotext. Geomembr.*, 27 (5), 368-390.

Powers, M.C. (1953). A new roundness scale for sedimentary particles. *J. Sediment. Res.*, 23, 117-119.

Pye, K. and Croft, D. J. (eds). (2004). *Forensic Geoscience: Principles, Techniques and Applications*. Geological Society, London, Special Publications, 232.

Pye, K. and Mazzullo, J. (1994) Effects of tropical weathering on quartz grain shape: an example from northern Australia. *J. Sediment. Res.*,64, 500–507.

Rouse, P. C., Fannin, R. J. and Shuttle, D. A. (2008). Influence of roundness on the void ratio and strength of uniform sand. *Géotechnique.*, 58(3), 227–231.

Santamarina, J.C. and Cho, G.C. (2001). Determination of critical state parameters in sandy soils-simple procedure. *Geotech. Test. J. ASTM.*, 24 (2), 185-192.

Sozer. Z.B. 2005. "Two-dimensional characterization of topographies of geomaterial particles and surfaces." Doctoral dissertation, Georgia Institute of Technology, Atlanta, USA.

Uesugi, M. and Kishida, H. (1986)." Influential factors of friction between steel and dry sands." *Soils Found.,* 26 (2), 33-46.

Vaid, Y.P. and Rinne, N. (1995). "Geomembrane coefficients of interface friction." *Geosynth. Int.* 2 (1), 309-325.

Vangla, P., and Latha, G.M. (2016). "Surface topographical analysis of geomembranes and sands using 3D optical profilometer". *Geosynth. int*. DOI:http://dx.doi.org/10.1680/jgein.16.00023.

Vangla, P. and Latha, G.M. (2014). “Image segmentation technique to analyze deformation profiles in different direct shear tests.” *Geotech. Test. J. ASTM.,* 37 (5), 828-839.

Vangla, P. and Latha, G.M. (2015). “Influence of particle size on the friction and interfacial shear strength of sands of similar morphology.” *Int. J. Geosynth. Ground Eng.,* 1(1), 1-12

Wadell, H. (1932). “Volume, shape, and roundness of rock particles”. *J. Geol.*, 40(5),443-451.

Zettler, T.E., Frost, J.D. and DeJong, J.T. (2000). “Shear induced changes in geomembrane surface topogrpahy.” *Geosynth. Int.*, 7(3), 243-267.

Zheng, J. and Hryciw, R. D. (2015). “Traditional soil particle sphericity, roundness and surface roughness by computational geometry.” *Geotechnique*, 65, 494-506.

DIAGNOSTIC ANALYSIS OF DISTRESSED HYDRAULIC STRUCTURES: CASE STUDIES OF GUJARAT, INDIA

Vivek P. Kapadia[1]

[1]*Chief Engineer, Narmada, Water Resources, Water Supply and Kalpasar Department, Government of Gujarat, Block No – 9, New Secretariat, Gandhinagar – 382010 India Email:* *vivekpkapadia@gmail.com*

ABSTRACT

Dams and canals are complex structures which sometimes do not timely manifest the sign of distress and hence the damage to them becomes irreparable or very difficult to repair. Many times that the diagnosis of the fault becomes an issue as the symptoms are strange and hence the repairs can not be done timely. Sometime some aspects which required attention at the time of construction are ignored and therefore they do not perform as per expectations or suddenly manifest signs of distress. Repairs of every dam or canal become a unique case study because of the said reasons. The paper discusses two complex case studies - one of canal and one of dam that exhibited some strange signs which were properly understood and the restoration was done.

Keywords: *canals, dams, distress, diagnosis, repairs*

CASE STUDY – 1 NARMADA MAIN CANAL

Historical Background

Sardar Sarovar Project consists of a dam and reservoir on the Narmada River having its command area of 1.8 million hectare. Its canal network is 76000 Kilometer long. The command area is shown in Figure 1. The main canal of the Sardar Sarovar Project is 458 Kilometer long in the Gujarat reach only. Because of huge length, the design of the embankment has been made as per height of embankment, available soil for the construction and discharge.

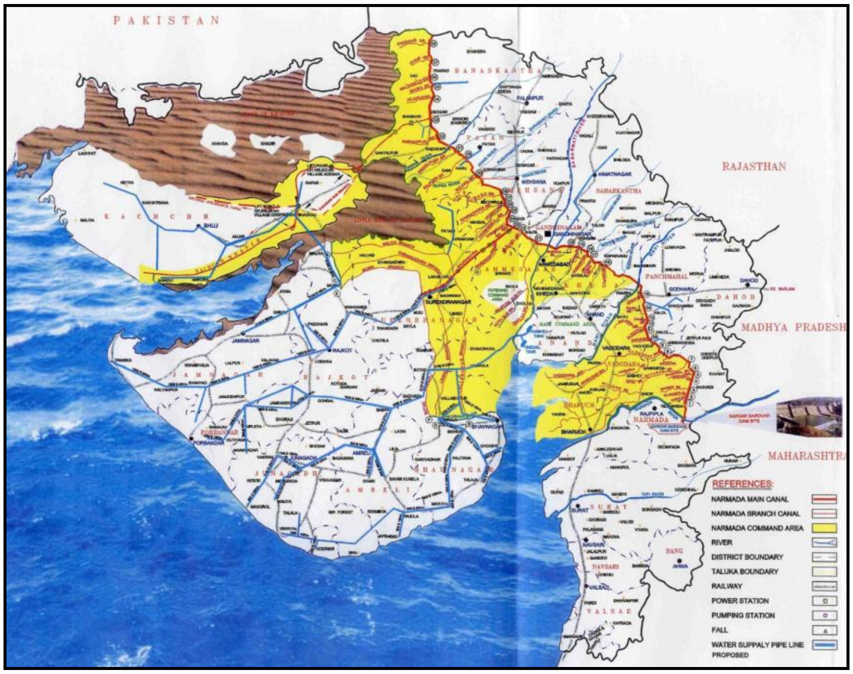

Figure - 1 Command area of Sardar Sarovar Project

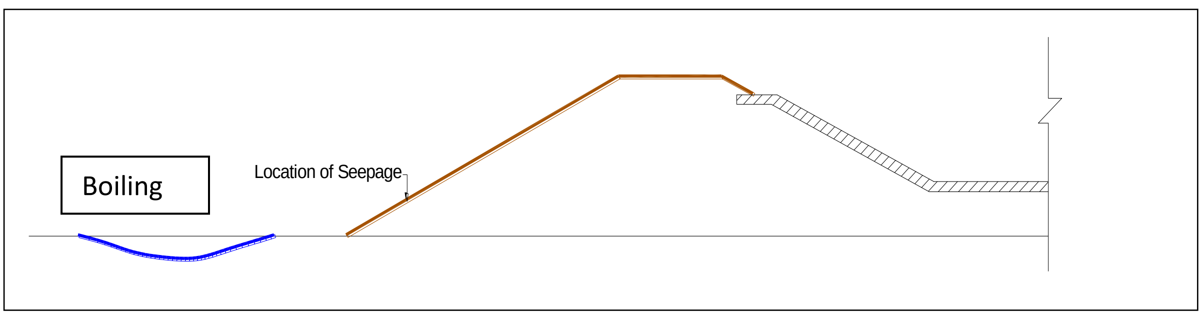

Figure – 2 Conceptual View of Canal Section in Problematic Reach

After construction of the main canal, because of overdependence for the drinking water, it has never been given closure and hence the saturation of embankment has been an issue especially where the embankment is very high. At some locations high groundwater table beneath the canal and at some locations subsurface flow have also manifested some issues. One such location is the upstream side of the Watrak Canal Syphon near Ch.195.00 km which is in heavy banking. The average height of bank is 12.50 m. Water depth in the canal section is 7 meter. Some boiling was observed on left bank at 30 m away from the outer toe of the canal bank during 2001 to 2005. Some seepage was also observed on the outer side of the canal embankment above its toe. This problem was in a length of more than 50 meter.

Investigations, Findings and Solution in Steps

As this problem was very complex and diagnosis was not simple, stepwise analysis of the problem was selected as an approach. The phenomenon was like what is generally experienced in a dam though the canal did not completely resemble a dam. An additional constraint was that the canal flow was not possible to be stopped.

The problem of boiling at some distance from the toe of the canal embankment suggested subsurface flow due to favorable hydraulic gradient. Subsurface flow could not be attributed to the canal flow as the canal was lined and the bed banking was more than 3.5 meter. Some punctures were required to be made in the soil at some distance away from the outer toes of the canal embankments which helped in finding that there was a shallow live aquifer which was not noticed during the construction of the canal. This aquifer might have dried up during the construction period as there were two preceding years lean from rainfall point of view and hence at that time no one could notice anything during the construction. The aquifer was cut due to construction of the canal siphon in the downstream which spread and saturated the surrounding soil above in some years which finally took the form of boiling as the waterway was obstructed. This important finding gave the clue as to why the canal that did not completely resemble a dam manifested a problem that is generally found with dams.

Seepage from the canal embankment above its toe suggested either the phreatic line developed within the canal embankment cutting it across or capillary action developed near the toe from within the ground itself or both together. The said diagnosis was made by considering the loam type of soil from which the canal embankment was constructed. Loam is generally erodible type of soil and phreatic line or capillary action could be easily developed in to due to high permeability when the compaction is not sufficient. Deep rain-cuts on the outer side of the canal embankments were also observed which also suggested erodible soil.

It was planned to provide exit to the subsurface flow by providing a lateral drain somewhat away and establish a steady state of the soil beneath the canal embankment so that crumbling of the foundation resulting in to failure of the embankment could be avoided. This would also stop the capillary action of water in to the canal embankment near the toe if any. The lateral drain which was a collecting drain was extended to a far situated pond for the disposal. This was aimed at releasing the water accumulated in large quantity within the soil beneath the canal embankment. Figure – 3 represents the said arrangement.

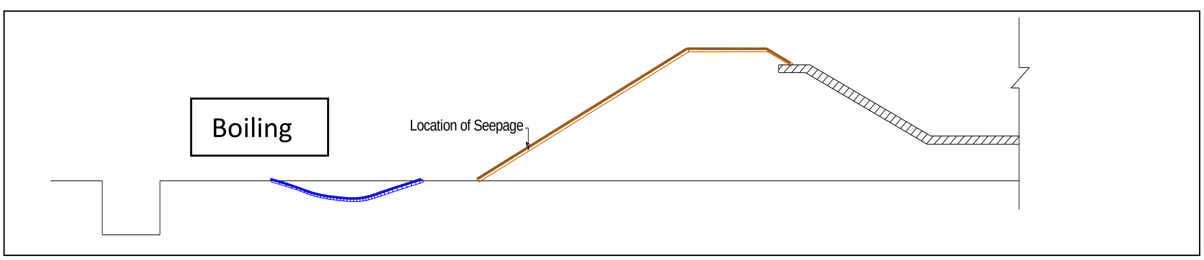

Figure – 3 Initial Stage of Solution

The canal embankment was kept under observation for some days with the aforesaid mechanism working continuously. It was observed that the boiling phenomenon had almost disappeared. It was also observed that seepage from above the toe of the embankment was reduced but was not completely stopped which suggested that the phreatic line had established within the embankment which had an exit above the toe. This state could not be taken lightly.

In order to ensure the phreatic line to be within the width of the embankment, increasing the width of the canal embankment was necessary. Moreover, this could also control the exit gradient within the foundation. It was planned then to provide an additional berm of 5 meter width and 5 meter height to ensure the stability of the embankment in addition to the said two benefits. The additional berm thus constructed resulted in to total disappearance of the boiling phenomenon and the seepage from within the embankment. But the chances of adverse effect of saturated soil already within the embankment and further saturation due to continuous flow in the canal could not be ruled out. In this situation, the solution provided must of a long term nature was the general feeling.

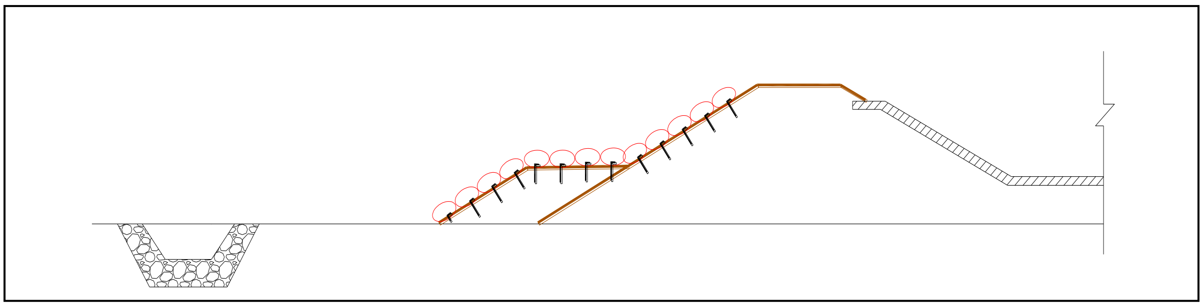

Figure – 4 Conceptual View of Solution

Counter weight through the additional berm was planned to be further improved by providing some additional burden in the form of sand bags which could also function as protection against the rain and the rain-cuts could be avoided. Finally jute textile bags were selected for this purpose which were specially designed in the form of long rolls. They were filled up with cement soil in 1:9 ratio and were nailed on the outer slope of the canal embankment. This was aimed at avoiding rolling down of the jute rolls. The objective was to prove an anti-erosion surface on the outer slope of the embankment and to add extra burden to provide more stability. In course of time the jute might be disintegrated but would have vegetation on it which would provide good drainage facility in addition to protection against rain-cuts. The lateral drain was then provided with a trapezoidal section with inner side having dry pitching which could easily collect the water without any destabilization. Figure – 4 represents the conceptual view of the solution.

The said solution was provided between Ch.195.225 KM and Ch. 195.375 KM was carried out during June-2005 to August-2005. The extra length of the solution on both – upstream and downstream of the problematic reach was keeping in view the chances of spreading of subsurface flow. The solution has been found working well and till date there is no problem in the said length of the canal.

CASE STUDY – 2 GORATHIYA DAM

Introduction

One minor irrigation dam – Gorathiya has been situated in Sabarkantha district i.e. in North Gujarat in India. Its construction was completed only before 10 years. It has been constructed across river Meshwo. Its Gross Storage Capacity has been 146 Million Cubic Feet. Its catchment area is 371 square Kilometers and the designed flood at the dam site with 1 in 50 year frequency is 3774 cubic meter per second. The storage is small but the spillover capacity is large. Length of the spillway section is 101.80 meter. The concrete gravity dam has been provided 9 vertical gates. Hydraulic jump type stilling basin has been provided in the downstream for energy dissipation. Upstream and downstream keys were 3.5 meter deep.

The Gorathiya dam manifested some signs of distress in only 2 years from its completion. The downstream glacis slope has been 1:3 whose toe got disintegrated and the reinforcements were pulled out as a sign of distress as shown in Photo-1. The next year the downstream apron got damaged but not in the entire length of the dam, only in the right half of the length i.e. river's half width as shown in Photo-2.

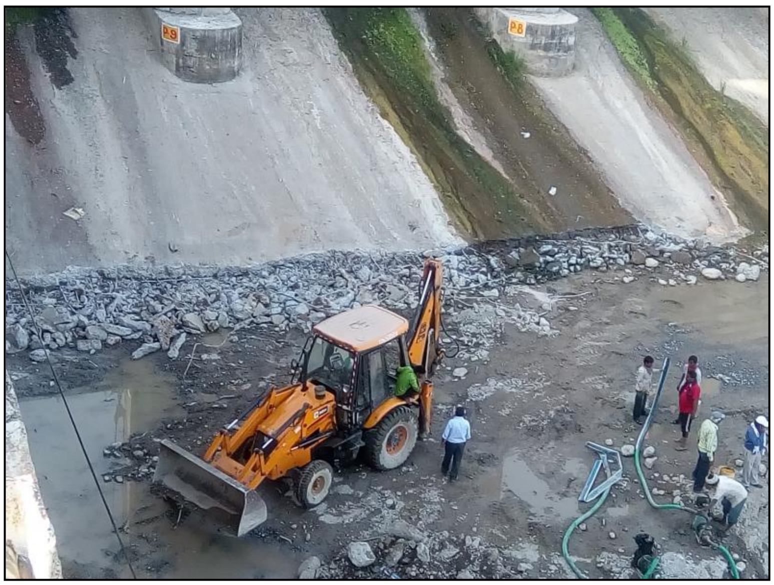

Photo – 1 Pullout of Reinforcement at Toe

Photo – 2 Tope View of Pulled Out Reinforcement at Toe and Damaged Apron

The loose concrete was removed and fresh concreting was done twice but the same problem recurred.

Diagnostic Analysis

Disintegration of concrete at toe of the downstream slope of the dam and pulling out of reinforcement in the entire length at the same location clearly suggested that it was not a construction flaw but it was due to cavity formation during release of water. This was because the glacis with 1:3 slope was insufficient to avoid cavity formation. There should have been a much flatter slope or an ogee. This part of the diagnosis was comparatively easy as it required only inspection and some knowledge of design.

The reason for repeated damage in the half of the length of the apron was difficult to understand. If it were a design flaw, the damage would have been in the entire length of the dam. If it were a poor quality concrete in the apron, repeated failure could not be there as the repairs were done meticulously. The history of site investigation was thoroughly studied to commence with. There was some record that there was originally a basalt mine in the gorge of the river as the river was having good quality basalt in its bed. For preparation of the site, the design included lean concrete filling with large coarse aggregate i.e. plum concrete in the pit. The investigation began with identification of width and depth of the mine. Some other records with geological mapping suggested that the mine was only in the right half width of the river and the depth was about 9 meter. It was not a big mine but only some removal of basalt from this location which was advised to be filled up with plum concrete. The apron was removed and the plum concrete beneath was investigated. It was learnt that the large coarse aggregates were there in place with mechanical locking and no compaction could be done but the cement and sand were in loose form and hence there was substantial amount of water beneath the apron in the voids of the aggregates. The dam was full up to crest level i.e. approximately 6 meter from the bed of the river. This gave a clue that the filling of the pit was aimed at plugging it but either the concrete was not allowed to set properly or the casting was not done properly and hence the concrete was not in a solid form and hence the voids between the large coarse aggregates were filled up with water which was not the groundwater; it was the water from the reservoir in the upstream of the dam. The water started flowing out after some hours which corroborated the said finding. This condition was extremely dangerous as at any time the subsurface flow could result in to undermining the foundation and collapse of the concrete dam itself.

The reason for damage to the apron in the right half length of the dam was then understood. When the gates were opened and water was released, the impact of the water fall was supposed to be taken up by the apron which required a solid foundation beneath which actually was not there and hence the concrete apron used to settle which caused sagging resulting in to damage at the bottom and top – bottom damage was not visible but the top was. Every time the gates were operated and the apron was found badly damaged due to this situation.

The diagnostic analysis required experience and insight in to the behavior of the dam, spillway, flow of water and its kinetics and of structural behavior of reinforced concrete.

Restoration

The objective of filling the pit with plum concrete was to plug the waterway beneath the apron so as to check the hydraulic path beneath the foundation. Keeping in view the same, plum concrete up to 1.5 meter of depth from the bottom of the apron was removed to see the condition of the plum concrete which was tremendously risky but was somehow done by taking necessary risk. Albeit, a precaution was taken in the form of a temporary plugging of subsurface waterway beneath the toe of the downstream slope. Cement and sand were mixed in 1:4 proportion with high water cement ratio and it was poured up on the loose material so as to allow it to creep inside the dump of aggregates in the pit and plug it. It was allowed to properly set. Then the initial layer of 1.5 meter which was removed was recast with high cement level and polymers so as to ensure a high strength concrete as the foundation. It was a concrete with normal coarse aggregate so as to ensure proper strength and compaction.

Photo – 3 Construction of Cut-off under Abutment

The apron was to be recast but it was decided to go for a 5 meter downstream cut-off to ensure checking the hydraulic path from the foundation. Additional cut-off was provided with the new apron. The right side abutment was also found vulnerable and hence the shuttering was made at its foundation after opening it and additional cut-off was also constructed there as shown in Photo-3. A peripheral cut-off was thus provided as shown in Photo-4. Entire construction activity required constant dewatering. Rapid hardening agents were added to concrete to ensure early setting of the concrete to reduce the construction time as the risk was very high.

Photo – 4 Construction of Peripheral Cut-off

Removed portion of concrete apron in half of the length of the dam was provided with horizontal and vertical drainage embedded in to the concrete and the new construction of apron was done with properly compacted polymer concrete with reinforcement mesh at the top. These reinforcements were welded with the reinforcements which were pulled out at the toe of the downstream slope of the dam. The concrete was cast for the apron such that at the toe of the dam was made a curved fillet to avoid pullout during the cavity formation. Strong foundation and strong apron with peripheral key checked the hydraulic path beneath the foundation and also assured impact resistance against the fall of water.

Photo – 5 Post-Repair Performance of Dam

It is learnt that generally the concrete apron provided to dissipate energy in the downstream of the dam is subjected to pitting or erosion in many cases. This is because the impact of water is very high and the design engineers provide strong concrete to resist the impact but the property actually required is surface hardness rather than strength. Hardness is tried to be attained by increasing strength in most of the designs but it is found that over some value of strength, much increase in strength is required to have little increase in hardness and hence it is not a cost-effective proposition. Here was used special construction chemical to provide surface hardness on the top of the apron just as it is done with the floor of the factory which requires high impact resistance.

Finally to provide a proper hydraulic condition to the water flowing down, the river channel in the downstream of the dam was retrenched. The entire repairs got completed in a time of four months.

The solution worked out was tested soon i.e. monsoon 2016 and there was full discharge released from the gates twice as shown in Photo-5 and it was found that the performance was as per expectations.

CONCLUSION

Problems in civil engineering are very complex and understanding the real cause of the problem is the most important aspect. A small aspect ignored at the construction stage may lead to difficult problems. The diagnostic part in designing the solution of such problems is the most important as that is the key to address the real issue and it needs experience and insight as mostly the findings can be reached by way of using judgmental and intuitive decisions. Therefore, sometime the diagnosis is required to be done stage-wise along with step by step implementation of solution. The solution of such problems may involve several activities to be executed with proper sequence and proper materials.

Geotechnical perspectives of Failure cases in Head walls of Hume pipe culverts and their Forensic Investigations

Amit Srivastava[1] and Dharmendra Kumar Srivastava[2]

[1]Associate Professor, Department of Civil & Environmental Engineering, The NorthCap University, Gurgaon, Haryana – 122017. Email: amitsrivastava@ncuindia.edu
[2]Research Scholar, Department of Civil & Environmental Engineering, The NorthCap University, Gurgaon, Haryana – 122017. Email: srivastava.dk2009@gmail.com

Abstract:
The present study discuss and highlights the geotechnical aspects of failure cases observed in the head wall of Hume pipe culverts constructed at various locations on a bypass as apart work of ''Four Laning & strengthening of a national highway in Haryana state''. Systematic Forensic investigation of the observed cracks developed in a head wall of Hume pipe culvert suggested construction as well as design deficiencies. From geotechnical perspectives, various aspects of failure, such as, suitability of soil as foundation material, inadequate compaction of the foundation soil, consolidation process and amount of settlement etc. were studied. Observed performance and development of crack at the location of stress concentration in the head wall were also verified through numerical analysis using finite element based numerical tool PLAXIS 2D. Upon investigation, it has been found that inadequate compaction of soil below headwall foundation was the primary reason for excessive settlement and development of stress (tension) concentration at the top of the Hume pipe culvert that finally lead to the development of cracks. Also, the construction of the head wall was taken in a hasty manner and not much enough time was given for the PCC layer to stabilize and gain strength through enough curing. Apart from that the PCC layer below the headwall was missing and head wall was directly laid on the unprepared ground.

Keywords: *Forensic, Geotechnical, numerical, compaction, consolidation, construction*

Introduction

Forensic Geotechnical Engineering is a process which involves engineering, legal and scientific investigations and methods to detect the reasons of failure and process of development of sign of distress, failure and collapse in a structure, which may be caused due to geotechnical reasons. Several case studies (Cassidy et al 2008, Ken Ho et al 2009, Svinkin 2013, Ramesh et al 2016, which have been taken up earlier for such forensic investigation in various aspects and reason of failure cases and its remedial measures which have been found very effective with regards to economy and legalistic scrutiny also fall in same purview. In majority of case studies, it has been reported that the standard procedures which are adopted in routine testing, design and analysis are not adequate rather the test parameters, design parameters and basis of analysis will have to be in similar condition encountered at site. The scope for forensic investigation covers the following: (i) To investigate the initial reasons behind failure and establish an initial theory of failure, (ii) collection of the evidences in support of theory adopted for failure, (iii) selection of suitable testing methods and techniques to prove the evidence collection in support of failure scientifically, and (iv) To reach out at the conclusion of final reason of failure and derive the basic cause of failure based on the analysis of evidence.

General procedures of forensic engineering investigation

Normally, investigations are carried out into four stages, i.e., the early stage, evidence collection stage, analysis and confirmation of failure assumption (hypothesis) and conclusion stage.

Early stage of investigation:

The investigation process maybe started based on assumed initial failure theory or hypothesis. After establishing the initial failure hypothesis, investigation approach to collect evidences and confirmation of failure hypothesis must be planned. The testing techniques and associated equipment useful in evidence collection are identified during this stage.

Evidence collection stage:

Reaching the failure site as soon as possible after the failure happened to avoid any disturbance to the evidence. Early start of site investigation is very useful and necessary in investigation approach which comprises of visual inspection, eyewitness interviews and sample collection. By visual inspection, investigators can observe the failure scene and wreckage and take its photographs which may provide the main evidence of failure. By eyewitness interviews-eyewitness often provide the valuable evidence and feedback to investigators which are helpful in deciding the actual modes and sequence of failure. Collecting the samples is an important step in the evidence collection stage for analysis.

Analysis and confirmation of failure hypothesis

There are three approaches of analysis and confirmation of failure hypothesis by carrying out testing methods, analytical methods and expert's interviews.

i) The testing methods consist of field testing and laboratory testing. Field testing involves a series of non-destructive testing and destructive testing carried out at site to check the actual behavior of the structure. Laboratory testing involves some specific tests that are normally destructive tests to check specific properties of certain components of structure.
ii) Analytical or numerical methods comprises of design check and computational analysis. Design check includes the review of relevant documents related to the failure. Computational analysis is an approach by using computer engineering software to compute and analyze the case study.
iii) A supplementary approach to analyze the failure hypothesis is by means of expert's interviews. Normally an expert's opinion can be very valuable to the investigators to understand the cause of the failure.

Conclusion stage

Last stage is the conclusion stage when all the analysis work has been done and failure hypothesis is confirmed.

Following Fig. 1 depicts the systemic approach for the forensic investigation which is followed in the present case study, i.e., failure analysis of Hume pipe culvert head wall.

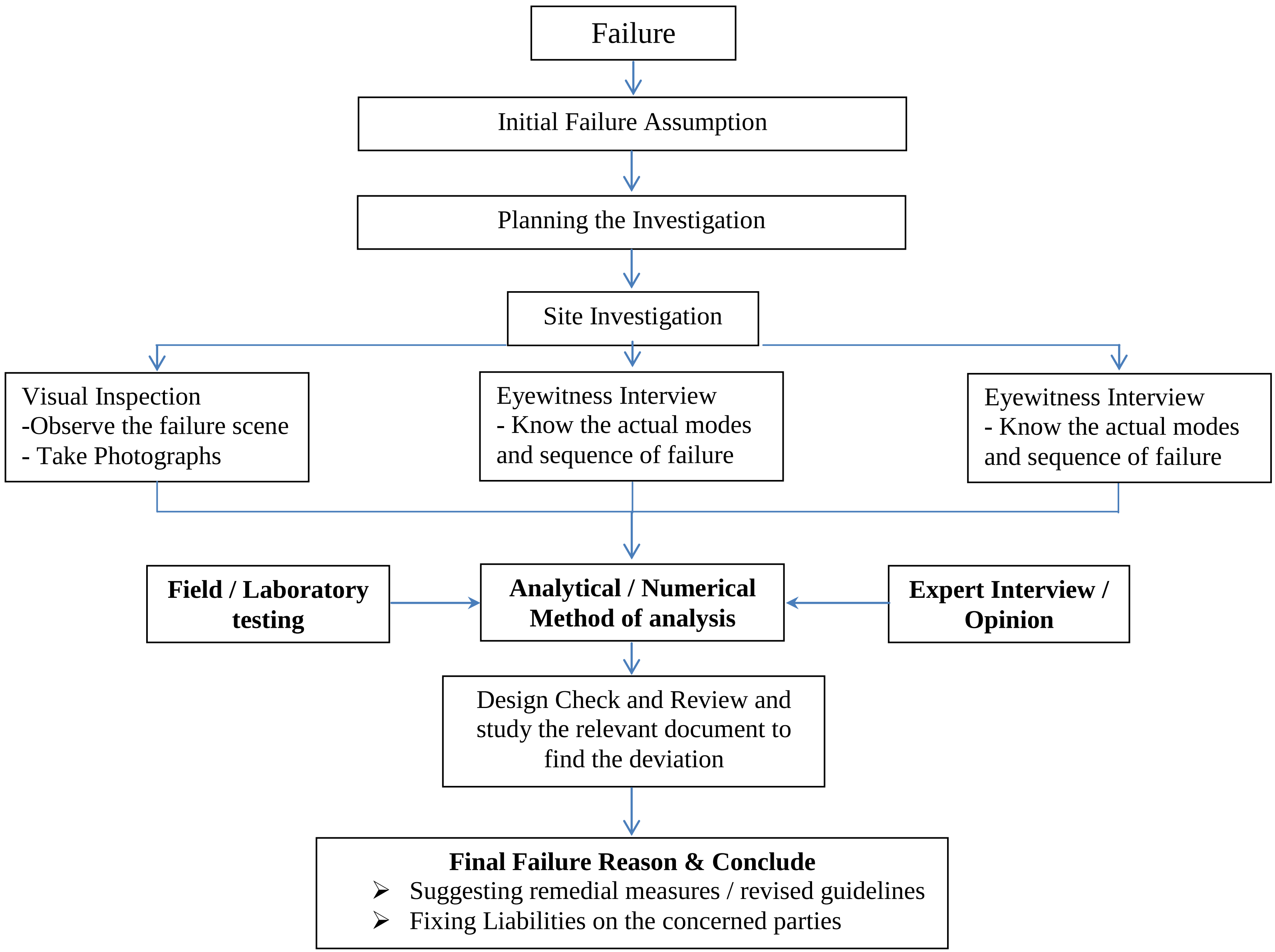

Figure 1 Investigation methodology and Flow chart for Forensic Investigation

Problem statement

1200 mm diameter Hume pipe culvert was proposed on a bypass as a part work of "Four Laning & strengthening of one of the national highways (NH)". Main function of provision of hume pipe culvert is for cross drainage of accumulated water from one side (U/S) to another side (D/S). Headwall is a part of HPC, generally, constructed to confine the road laterally at two ends of culvert and also serve as a retaining wall as protection against the scouring or undermining of fill or a flow diverting device. As per information and records, the construction of these culvert started in the month of June 2016 and was completed by the mid of July 2016. Soon after the construction, cracks were visible in the month of August 2016 during inspection. Similar observations were made at several other locations and severity of these cracks was on increase and with time, gradually, the crack was mostly 5mm to 10mm wide within a span of one month (Fig 2). This cause a serious concern to the concerned parties involved.

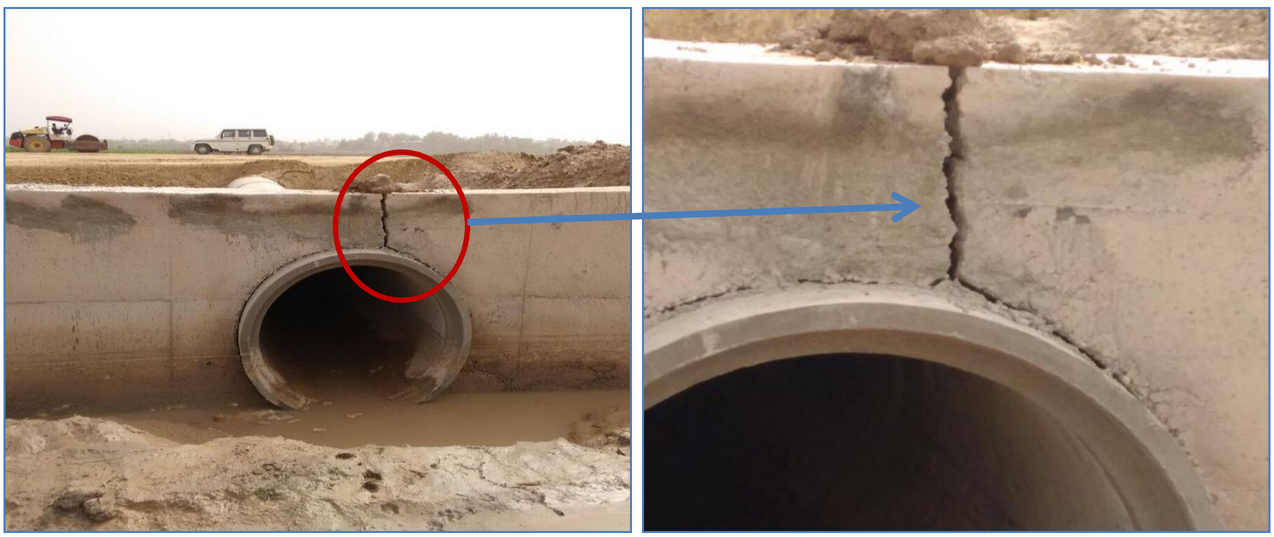

Figure 2 Crack development in the head wall of a typical Hume pipe culvert

Fig 3 shows typical geometrical details of Hume pipe culvert.

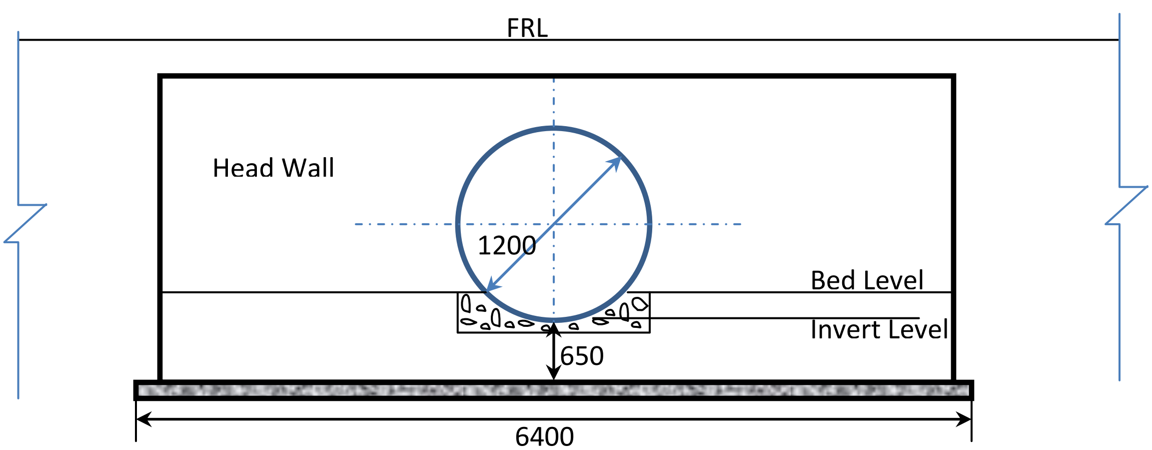

Figure 3 Typical Geometrical details of Hume pipe

Construction procedure for Head wall

Construction of HPC follows the sequence of activities like preparation of bed of foundation soil, such as, leveling and compaction of bed. Compactions are done either with roller or manual. After bed compaction, the foundation concrete (PCC, M-10 grade) of nearly 100mm are placed to support the Hume pipe. Hume Pipes are laid and jointed with each other so that there is no leakage take place (Fig 4). After laying and jointing the pipes, headwalls are constructed on both ends of culvert, serving as a retaining wall as protection against the scouring or undermining of fill or a flow diverting device

Figure 4(a) Laying of Hume pipe culvert

Figure 4(b) casting of raft for head wall

Figure 4(c) casting of raft for Hume pipe culvert

Figure 4(d) Casting of head wall

Normally, it is very rare to show sign of failure on headwall of culvert constructed with concrete or masonry at so early stage. Once cracks are visible at very early stage because of various reasons, the development of crack at a particular position of structure like headwall creates a reason for forensic investigation.

Field Observations and Testing

Settlement of both the head wall and pipe culvert was monitored during and after construction and it was observed that significant amount of settlement was noticed within a month of casting of head wall .It was also noted that there was intermittent rain soon after construction (within 15 days) of culvert and the foundation soil was submerged under water as it can be seen in Fig 2. As per drawing, the top R.L. of Head wall should be kept at 209.370 m (when head wall was casted). Following RLs at different locations of head wall were recorded (Fig 5a) and same has been reported in the following Table 1.

Fig 5(a) Measurement of settlement of head wall and comparison with RLs

Fig 5 (b) collection of soil samples for laboratory testing

Fig 5(c) In situ density measurement using sand replacement method

Fig 5 (d) Investigation for construction deficiency

Table 1 Observation on RLs (meter) of Head wall

Side	Towards Hisar	Center	Towards Sirsa	Average
LHS	209.337	209.272	209.314	209.307
RHS	209.178	209.095	209.148	209.140

It can be noted that RHS of head wall settles more than the LHS of headwall but the settlement is more or less uniform. On the LHS, the amount of differential settlement is 0.065 m and 0.042m on both side of the culvert. Similarly, on the RHS, the amount of differential settlement is 0.083 m and 0.053m on both side of the culvert. This must have caused stress concentration at the location in head wall where cracks are observed. Total amount of settlement from the original RL (209.37 m) of the head wall can be estimated as 0.063 m, i.e., 63 mm (LHS) and 0.230 m, i.e., 230 mm on the RHS.

Failure hypothesis

Based on expert opinion and review of documents, following possibilities of failure were further investigated:

- Swelling and shrinkage characteristics of soil
- Excessive settlement due to improper compaction of foundation bed
- Lateral earth pressure due to filling of material inside
- Possibilities of any construction or design deficiencies

Swelling and shrinkage characteristic

Soil samples were collected from the both side of Hume pipe culvert below head wall (Fig 5b) and its properties like grain size analysis, Atterberg's limit and free swell Index and compaction characteristics have been checked in site laboratory. Following Table 2 summarizes relevant geotechnical properties of the soil sample collected from the site:

Table 2 Geotechnical properties of soil samples collected

Geotechnical Properties	Location – A (LHS)	Location – B (RHS)
% Gravel	10.0	11.5
% Sand	22.5	22.7
% Silt & Clay	77.4	76.1
Liquid Limit	24.8	21.9
Free Swell Index	18.2	19.8
OMC	11.3%	11.3%
MDD	1.88 gm/cc	1.87 gm/cc

Field Density

Field density test by sand replacement test (IS: 2720-Part (XXVIII) was conducted at site near to foundation of headwall by investigating team. Following Table 3 summarizes the results of the analysis of the field density test.

Table 3 results of the field density test and RC values

	Location	Trial - 1	Trial - 2	Trial - 3
Bulk Density	A (LHS) B (RHS)	1.98 1.727	1.95 -	1.97 1.731
In situ moisture	A (LHS) B	9.39 8.88	8.89 -	8.80 9.31
Relative Compaction	A (RHS) B (LHS)	96.5% 91.8%	95.12% -	96.2% 92.1%

It can be noted that the soil was very well compacted on the LHS of the culvert and the RC value achieved was more than 95%. This is the reason LHS of the culvert was not much settled. On the other hand, soil on the RHS of the culvert was poorly compacted and RC value was only 92%. This must have caused excessive settlement of the head wall.

Discussion on field observations and results

- The assumption that foundation of head wall was resting on black cotton soil and because of swelling and shrinkage cracks were developed has not been found correct as fee swell index (FSI) of soil was less than 50. FSI of soil sample of both end of H.P.C. head wall was found around 18% & 19% and liquid limit was also less than specified for unsuitable soil. Hence, soil properly tested & observed does not support the assumption and the soil although had blackish appearance does not possess the swelling and shrinkage properties.

- The assumption of lateral movement of the wall was also not been supported by field observations as there was no lateral displacement noticed in head wall. Also, the space between headwall was not filled and the road way was filled on later stage of road construction after the cracks appeared.

- The hypothesis of improper compaction was also checked and it was found that the RC value achieved in the field was approximately 92%, which was much less than the specified value of 95%. Hence, there was improper compaction at the site. After the construction of head wall, soil settled to due huge pressure of head wall. The amount of settlement can be estimated form the simple calculation as shown below:

  $\Delta H = \Delta e/(1+e_o) \times H_o$

  Δe = change in void ratio = $(e_i - e_f)$

  e_i = initial void ratio and e_f = final void ratio

  Dry unit weight of the in situ soil after compaction = 1.88 × 0.92 = 1.72 gm/cc
  Assuming Gs = 2.65, the initial void ratio is estimated as, 0.54

  Assuming that the soil gets further compacted due to load of head wall and it achieves the maximum dry density, final void ratio is estimated as, 0.41
  Hence, $\Delta e = 0.13$
  The base width of the head wall = 1.25 m. Assuming zone of influence as 2B, the amount of settlement can be estimated as
  $\Delta H = 0.13 \times 1.25 \times 2 / (1+0.54) = 0.211$, i.e., 211 mm

  It can be noted that the total amount of settlement observed on the RHS of the culvert, 230 mm, is very much close to the calculated value of settlement, 211 mm.]

- By eye witness interview, it has been brought to notice that there was no proper compaction below foundation of headwall and the construction of head wall was done in a hasty manner. There was no enough time gap between casting of leveling course (P.C.C.-M15) and raft of headwall. It was also noticed (Fig 5d) that P.C.C. below Hume pipe connecting to raft of head wall was also not laid with proper compaction.

Numerical analysis

Commercially available Finite element tool PLAXIS 2D was used to perform the numerical analysis of the problem. 15-node triangular elements can be used for generating finite element mesh. Soil behavior was modeled as to follow the Mohr-Coulomb failure criterion. Tunnel element was used to the Hume pipe. Concrete Head wall was considered as elastic material with properties of M15 grade. The input properties used for the numerical analysis are summarized in Table 4.

Table 4 Input properties for the numerical analysis

Properties	**values**
Material behavior of foundation soil	Mohr-Coulomb
Elastic modulus of soil	5 MPa
Poison's ratio	0.40
Cohesion	0.1 kPa
Friction angle	28°
EA (plate element for tunnel)	32.25×10^5 kN/m
EI (plate element for tunnel)	60.47×10^2 kN-m^2/m
E (M15 Grade concrete)	$5700\ \sqrt{\square}_{ck}$ (MPa)
Poison's ratio	0.15

Fig 6 shows the step followed in the numerical analysis of the Hume pipe culvert. From results of the analysis, it can be noted that both compressive and tensile stresses are developed in the head wall. Blue shade shows tensile stresses developed and red shades indicates development of compressive stresses in the Head wall. It can be noted that the tensile stresses developed in the head wall is at the location of the crown of Hume pipe where the crack was developed. As we know that concrete cannot take tension, development of tensile stress (53 kN/m^2) has caused severe cracks in the head wall. Based on the study, provision of reinforcement can be suggested at the location of tensile stresses development in the head wall.

Conclusion

The most credible hypothesis regarding this case study i.e. failure of the head wall was found that crack development in headwall has occurred because of lack of proper compaction of soil below foundation of culverts and no time gap between the casting of headwall and its foundation. The preparation of bed foundation was not carefully done and even intermittent rain has made the soil mass saturated which has caused the primary consolidation in 61 days. This has reflected in the form of cracks in headwall.

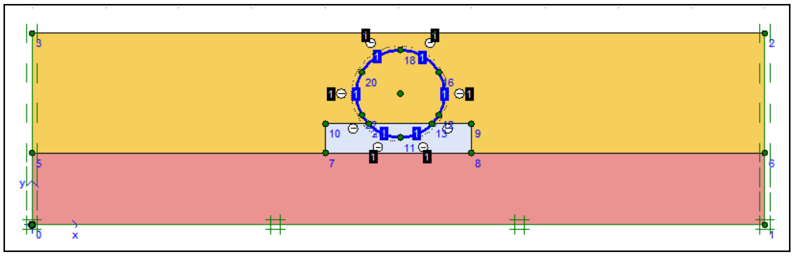

Figure 6(a) Finite Element model for the numerical analysis of Head Wall

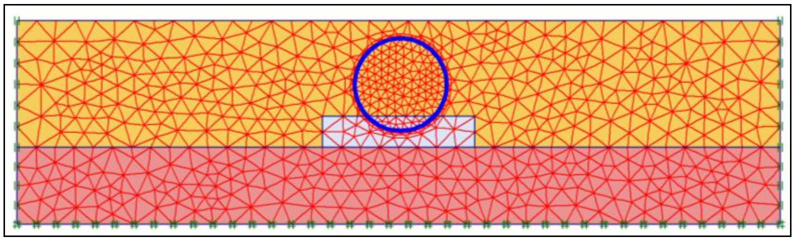

Figure 6(b) 15 Node triangular element for the discretization of model

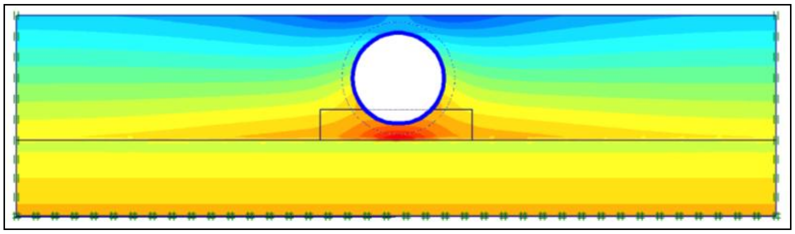

Figure 6 (c) Stress concentration in Head Wall(blue shade for tensile stresses)

References

Cassidy MJ, Uzielli M, Lacasse S (2008) Probability risk assessment of landslides: case study at Finneidfjord, Canadian Geotechnical Journal, Vol. 45, 1250-1267.

Day, RW (2011) Forensic geotechnical and foundation engineering, 2nd Edition, McGraw Hill, NY, 508 p

Ken Ho, Tony Lau, Jonathan Lau (2009). Forensic landslide investigations in Hong Kong, Proceedings of the Institution of Civil Engineers - Civil Engineering, Volume 162, Issue 5 (DOI: http://dx.doi.org/10.1680/cien.2009.162.5.44)

Mark R. Svinkin (2013) Forensic engineering of construction vibrations. Proceedings of the Institution of Civil Engineers - Civil Engineering, Volume 166, Issue 2 (DOI: http://dx.doi.org/10.1680/feng.12.00017)

Ramesh Vandanapu, Joshua R. Omer, Mousa F. Attom (2016). No Access Geotechnical case studies: emphasis on collapsible soil cases, Proceedings of the Institution of Civil Engineers - Civil Engineering, Volume 169, Issue 3 (DOI: http://dx.doi.org/10.1680/jfoen.16.00011).